BEILSTEIN JOURNAL OF ORGANIC CHEMISTRY

Molecular switches and cages

Edited by Dirk Trauner

Imprint

Beilstein Journal of Organic Chemistry
www.bjoc.org
ISSN 1860-5397
Email: journals-support@beilstein-institut.de

The *Beilstein Journal of Organic Chemistry* is published by the Beilstein-Institut zur Förderung der Chemischen Wissenschaften.

Beilstein-Institut zur Förderung der Chemischen Wissenschaften
Trakehner Straße 7–9
60487 Frankfurt am Main
Germany
www.beilstein-institut.de

Beilstein Journal of Organic Chemistry

Molecular switches and cages

Dirk Trauner

Editorial

Open Access

Address:
Department Chemie und Biochemie, Ludwig-Maximilians-Universität München, Butenandtstr. 5–13, 81377 München, Germany

Email:
Dirk Trauner - Dirk.Trauner@lmu.de

Keywords:
molecular switches

Beilstein J. Org. Chem. **2012,** *8,* 870–871.
doi:10.3762/bjoc.8.97

Received: 10 June 2012
Accepted: 11 June 2012
Published: 13 June 2012

This article is part of the Thematic Series "Molecular switches and cages".

Guest Editor: D. Trauner

Molecular switches can toggle between two (or more) stable states encoding different physical features. They allow complex systems to respond to changes in their environment defined by light intensity, pH, temperature or voltage. As such, molecular switches play a key role in biology and information technology and have become important components of advanced materials.

Chemists have developed a large number of synthetic switches, complementing the many types found in nature. Given their prominence in biology, it is not surprisingly that photoswitches, which are actuated by ultraviolet, visible or infrared light, have been an especially productive field of study. Despite their long history, new types of synthetic photoswitches continue to emerge and "old friends", such as azobenzenes are constantly improved and optimized. This is not only true with respect to their photophysical properties but also with regard to their synthetic accessibility. Indeed, as molecular switches are applied in ever-increasing quantities, the efficiency of their syntheses becomes a primary concern, requiring the development of new synthetic methods and strategies. The corresponding results, however, are often buried in the Supporting Information of papers that focus on functional aspects, which does not reflect the relative effort that goes into the design and synthesis of these molecules.

Caged compounds are a subclass of (photo)switches that have special functional features. As opposed to "true" switches, they can only be turned ON and the abatement of their activity depends on secondary processes (such as diffusion from the active zone or, more importantly, re-uptake systems). In terms of their biological application, especially in neurobiology, they are much further developed than reversibly switchable molecules. For instance, two-photon activation, which allows for very precise localization, is fairly well established with caged compounds but in its infancy in the case of reversible photoswitches.

The present Thematic Series of the Beilstein Journal of Organic Chemistry addresses the crucial role that chemistry, and particularly organic chemistry, can play in tuning the functional features of molecular switches and cages. These features include their absorption spectra, conductivity, geometry and bistability, as well as their polarity, solubility, efficacy, or catalytic activity. Photoswitches are covered extensively, ranging from diarylethenes (Pu, Wagenknecht) to dihydro-

azulenes/vinylheptafulvenes (Nielsen) and azobenzenes (Rück-Braun, Hoppmann). Two reviews discuss *cis*-azobenzenes with rapid thermal isomerization kinetics (Velasco), and highlight the azobenzene moiety as one of the smallest light-driven molecular motors conceivable (Merino). Issues of bistability are also addressed in an account on shape-persistent, optically active macrocycles (Pasini). Molecular switches that respond to changes in pH are covered as well (Haberhauer and Aprahamian), reflecting their importance in biology and in materials science. Finally, switching is highlighted as a synthetic strategy for building advanced materials that are useful in photovoltaics (Matile).

Chemists, by nature, like to control things and probably actuate macroscopic switches more often than the average person. We hope that this collection of papers will motivate some of our colleagues to also consider nanoscopic versions of switches (and cages). For those of us who deal with these molecules on a daily basis, this Thematic Series will hopefully provide further inspiration and an impetus to continue work in this fascinating field of research.

Dirk Trauner

Munich, June 2012

Beilstein Journal of Organic Chemistry

The importance of the rotor in hydrazone-based molecular switches

Xin Su[1], Timo Lessing[2] and Ivan Aprahamian[*1]

Letter

Open Access

Address:
[1]Department of Chemistry, Dartmouth College, Hanover, New Hampshire 03755, United States and [2]Department of Chemistry, Heinrich-Heine-Universität Düsseldorf, Universitätsstr. 1, 40225 Düsseldorf, Germany

Email:
Ivan Aprahamian[*] - ivan.aprahamian@dartmouth.edu

* Corresponding author

Keywords:
E/*Z* isomerization; hydrazone; molecular switches; pH activation; structure–property analysis

Beilstein J. Org. Chem. **2012,** *8,* 872–876.
doi:10.3762/bjoc.8.98

Received: 29 February 2012
Accepted: 09 May 2012
Published: 13 June 2012

This article is part of the Thematic Series "Molecular switches and cages".

Guest Editor: D. Trauner

Abstract

The pH-activated *E*/*Z* isomerization of a series of hydrazone-based systems having different functional groups as part of the rotor (R = COMe, CN, Me, H), was studied. The switching efficiency of these systems was compared to that of a hydrazone-based molecular switch (R = COOEt) whose *E*/*Z* isomerization is fully reversible. It was found that the nature of the R group is critical for efficient switching to occur; the R group should be a moderate H-bond acceptor in order to (i) provide enough driving force for the rotor to move upon protonation, and (ii) stabilize the obtained *Z* configuration, to achieve full conversion.

Findings

Nature is full of elegant examples of perfectly designed biological motors and machines [1] that perform delicate and precise tasks. Primitive as they may be, numerous artificial molecular machines [2-6] have been developed that strive to mimic their biological counterparts as far as function is concerned. As part of these efforts, a variety of molecular systems have been developed that can perform different types of motion (e.g., translation, rotation) in response to chemical [7-9], electrochemical [10-13], and photochemical stimuli [14-18]. One of the benefits of artificial molecular switches and machines is that their output can be controlled or fine-tuned by altering their components [19-21]. A relevant example in this context is Feringa's overcrowded alkene-based light-driven rotary switches that can be induced to rotate at different rates by replacing a naphthyl group in the upper-half of the molecule (i.e., the rotor) with a less sterically hindered benzothiophenyl group [20].

Previously, we have shown that hydrazone-based rotary switches can change their configuration (i.e., *E*/*Z* isomerization) as a function of pH [22-24], or upon the addition of a Lewis acid (i.e., Zn^{2+}) [25]. The simplest hydrazone switch (**PPH-1**, Scheme 1) for example, exists mainly as its *E* isomer (**PPH-1-*E***) in solution, as illustrated by the *E*/*Z* isomer ratio of 93:7 in CD_3CN. Protonation of **PPH-1-*E*** with acid results in an intermediate **PPH-1-*E*-H$^+$**, which quickly isomerizes to

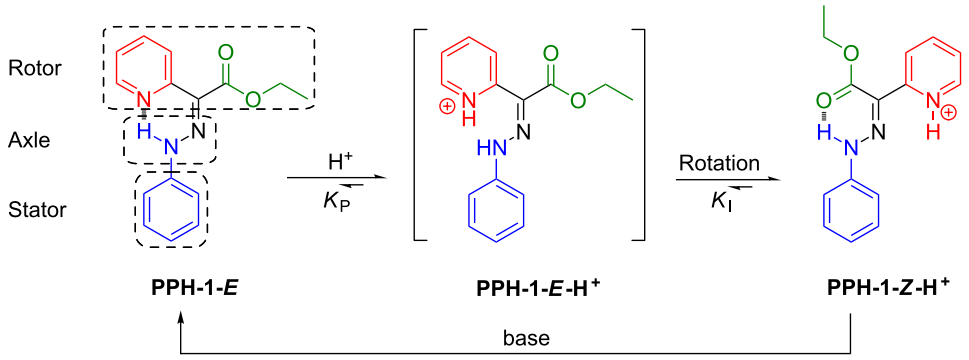

Scheme 1: The acid-activated switching process of **PPH-1**.

PPH-1-*Z*-H$^+$, which is the more stable isomer. During this process, an *E*/*Z* isomerization takes place, which can be fully reversed by the addition of base to the solution.

In order to fine tune the properties of the hydrazone switches, we studied the effect of different R groups in the rotor part (Scheme 2) on the switching cycle. The target hydrazones were

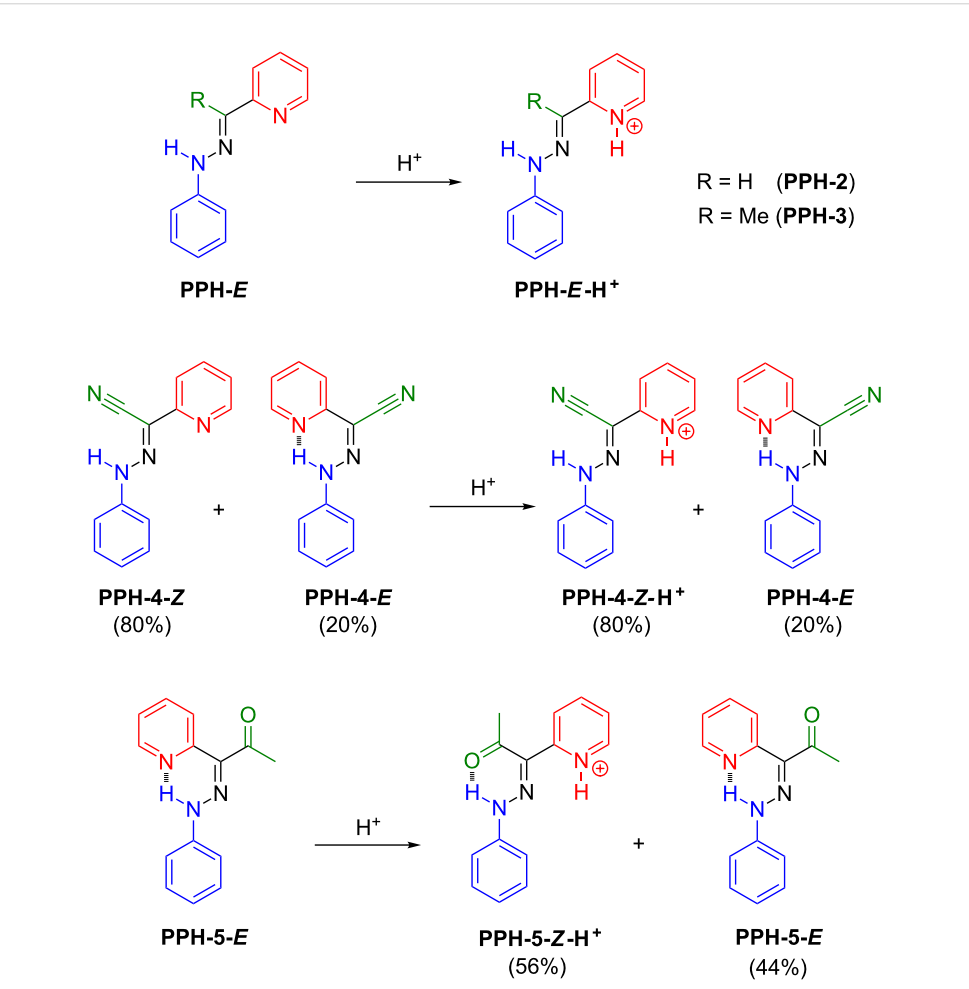

Scheme 2: The hydrazone-based molecular systems that were analysed in this paper, each having different rotors. The stable isomer(s) in solution and their protonation products are shown.

synthesized either by the direct condensation of phenylhydrazine with the corresponding aldehyde (**PPH-2**) or ketone (**PPH-3**), or by Japp–Klingemann reaction (**PPH-4**, **PPH-5**) [26]. The NMR spectroscopy and mass spectrometry characterizations show results consistent with the previously reported data [26].

In certain cases it has been shown that intramolecularly H-bonded hydrazones exist predominantly as the kinetically stable *Z* isomer in solution [27-29]. We were expecting that the intramolecular H-bonds in **PPH-2** and **PPH-3** would drive them to adopt the *Z* configuration in solution as well, leading to a low-field-lying NH signal (12–16 ppm) [22-24]. However, this is not the case with **PPH-2**. The hydrazone N–H proton in **PPH-2** resonates at 8.95 ppm, which clearly shows that it is not H-bonded to the pyridyl nitrogen, indicating that the *E* configuration is the predominant isomer in solution (CD_3CN). The addition of trifluoroacetic acid (TFA) only results in a general downfield shift of the aromatic and the hydrazone N–H proton signals as a result of protonation, which reaches saturation with 3 equiv of TFA. Unlike in **PPH-1**, signals from other species are not observed during the course of protonation, suggesting that the protonation of **PPH-2** with TFA is a fast equilibrium, and that, as expected, it does not cause any isomerization. Similar to **PPH-2**, the ^{1}H NMR spectrum of **PPH-3** shows a signal for the hydrazone N–H proton at 8.24 ppm indicating that it too is in the *E* configuration. The protonation of **PPH-3** with TFA is a fast equilibrium as well, without any indication of rotary motion (i.e., isomerization).

On the other hand, **PPH-4**, in which R is a strong electron-withdrawing group (–CN) shows two sets of signals in the ^{1}H NMR spectrum (CD_3CN), indicating that two isomers, having a 4:1 ratio, coexist in solution. The major isomer shows a hydrazone N–H signal at 9.60 ppm, indicating that it is the *Z* isomer, in which an intramolecular H-bond is not present. On the other hand, the hydrazone N–H signal of the minor isomer resonates at 15.12 ppm, which is characteristic of H-bonded N–H signals, suggesting that the minor isomer is actually the *E* configuration. Such an unusual *E*/*Z* isomer ratio was reported before for similar systems, and it was attributed to kinetic stability of the *Z* isomer, in addition to solvent effects [27-29]. The titration of **PPH-4** with TFA only affects the major isomer (*Z*), while the minor isomer (*E*) remains intact even in the presence of 10 equiv of TFA. The changes in the ^{1}H NMR spectrum of **PPH-4-*Z*** are similar to those of **PPH-2** and **PPH-3**, except for the fact that it requires an excess of TFA (ca. 10 equiv) for the protonation to reach saturation. This observation can be attributed to the strong electron-withdrawing nature of the CN group, which drastically decreases the basicity of the pyridyl nitrogen. Furthermore, since the pyridyl nitrogen in **PPH-4-*E*** is H-bonded to the hydrazone N–H, the basicity of **PPH-4-*E*** becomes even lower, which explains why **PPH-4-*E*** does not become protonated even in the presence of 10 equiv of TFA.

Structurally, **PPH-5** is the closest to **PPH-1**, that is, instead of an acyl ester group, **PPH-5** has an acetyl residue as the R group. The ^{1}H NMR spectrum of **PPH-5** in CD_3CN shows only one set of signals, and a sharp singlet at 14.54 ppm for the hydrazone N–H proton, indicating that it is H-bonded to the pyridyl nitrogen. Since the acetyl group is a less effective H-bond acceptor than ethyl ester, it is reasonable that **PPH-5** exists exclusively in the *E* form in solution. When TFA is added to the solution, a second set of signals arises, which grows as the amount of acid increases. The protonation of the pyridyl ring results in the downfield shift of the aromatic signals, except for proton H1, which shifts from 8.92 to 8.70 ppm as it is no longer affected by the H-bond [22-24]. Moreover, the hydrazone N–H signal shifts to a higher field (13.22 ppm) in congruence with what is observed in **PPH-1** [24]. These changes are consistent with those observed during the acid-activated switching of **PPH-1**, suggesting that **PPH-5** switches from the *E* to the *Z* configuration upon protonation. However, the switching process of **PPH-5** is relatively inefficient as there is still ca. 44% of **PPH-5-*E*** remaining in solution even when 30 equiv of TFA is added.

In order to rationalize the different behaviour of the structurally similar switches, **PPH-1** and **PPH-5**, a quantitative evaluation of the thermodynamic process is necessary. Taking a look at the acid-activated switching process of **PPH-1** (Scheme 1), we can formulate the following equations for the acid-induced *E*/*Z* isomerization:

$$K_P = \frac{[\text{PPH-1-}E\text{-H}^+]}{[\text{PPH-1-}E\text{-H}^+][\text{H}^+]} \quad (1)$$

$$K_I = \frac{[\text{PPH-1-}Z\text{-H}^+]}{[\text{PPH-1-}E\text{-H}^+]} \quad (2)$$

$$K_S = K_P \cdot K_I = \frac{[\text{PPH-1-}Z\text{-H}^+]}{[\text{PPH-1-}E\text{-H}^+][\text{H}^+]} \quad (3)$$

where K_P is the equilibrium constant of the protonation step, K_I is the equilibrium constant for the rotation process, and K_S is the overall equilibrium constant for the switching reaction. The pK_a of **PPH-1** is actually $\log_{10}K_P$, so K_S also equals $10^{[pK_a(\text{PPH-1})]} \cdot K_I$. From the above equations, it becomes clear that K_S can be used as an index to evaluate the feasibility of the

switching process in hydrazone-based switches; the larger the K_S value, the easier the switching process. In the case of **PPH-1** versus **PPH-5**, since the acetyl group is a stronger electron-withdrawing group than the ester group, the basicity (pK_a) of the pyridyl group in **PPH-1** will be higher than in **PPH-5**. Moreover, the ester group is a better H-bond acceptor than the acetyl group, which means that the protonated *Z* configuration of **PPH-1** is more stable than that of **PPH-5**, resulting in a larger K_I for **PPH-1**. Thus, it can be qualitatively deduced that **PPH-1** has a larger K_S than **PPH-5**, suggesting that **PPH-1** is a more ideal system to be used as a molecular switch. This analysis is clearly in line with the acid switching experiments that show that **PPH-1** can be fully switched, whereas **PPH-5** cannot.

Conclusion

In summary, we have synthesized four hydrazone-based systems having different R groups as part of the rotor section. The role of the R group was assessed *vis-à-vis* the switching of the system, and it was found that for the switch to operate effectively it is crucial that (1) the R group be able to offer a second H-bond-accepting site in order to provide enough driving force for the rotor to move; and (2) the R group be a moderate H-bond acceptor, otherwise the isomer generated will not be stable enough to enable full conversion (isomerization).

Supporting Information

Supporting Information File 1

Experimental section and acid titration of the hydrazone compounds.
[http://www.beilstein-journals.org/bjoc/content/supplementary/1860-5397-8-98-S1.pdf]

Acknowledgements

This research was supported by Dartmouth College and the Burke Research Initiation Award. Timo Lessing wishes to thank the German Academic Exchange Service (DAAD) for a RISE worldwide research internship.

References

1. Schilwa, M., Ed. *Molecular Motors;* Wiley-VCH: Weinheim, Germany, 2003.
2. Kelly, T. R.; De Silva, H.; Silva, R. A. *Nature* **1999,** *401,* 150–152. doi:10.1038/43639
3. Leigh, D. A.; Wong, J. K. Y.; Dehez, F.; Zerbetto, F. *Nature* **2003,** *424,* 174–179. doi:10.1038/nature01758
4. Fletcher, S. P.; Dumur, F.; Pollard, M. M.; Feringa, B. L. *Science* **2005,** *310,* 80–82. doi:10.1126/science.1117090
5. Kelly, T. R.; Cai, X.; Damkaci, F.; Panicker, S. B.; Tu, B.; Bushell, S. M.; Cornella, I.; Piggott, M. J.; Salives, R.; Cavero, M.; Zhao, Y.; Jasmin, S. *J. Am. Chem. Soc.* **2007,** *129,* 376–386. doi:10.1021/ja066044a
6. Feringa, B. L. *J. Org. Chem.* **2007,** *72,* 6635–6652. doi:10.1021/jo070394d
7. Badjić, J. D.; Balzani, V.; Credi, A.; Silvi, S.; Stoddart, J. F. *Science* **2004,** *303,* 1845–1849. doi:10.1126/science.1094791
8. Berná, J.; Leigh, D. A.; Lubomska, M.; Mendoza, S. M.; Pérez, E. M.; Rudolf, P.; Teobaldi, G.; Zerbetto, F. *Nat. Mater.* **2005,** *4,* 704–710. doi:10.1038/nmat1455
9. Bonnet, S.; Collin, J.-P.; Koizumi, M.; Mobian, P.; Sauvage, J.-P. *Adv. Mater.* **2006,** *18,* 1239–1250. doi:10.1002/adma.200502394
10. Wang, W.; Kaifer, A. E. *Angew. Chem., Int. Ed.* **2006,** *45,* 7042–7046. doi:10.1002/anie.200602220
11. Nijhuis, C. A.; Ravoo, B. J.; Huskens, J.; Reinhoudt, D. N. *Coord. Chem. Rev.* **2007,** *251,* 1761–1780. doi:10.1016/j.ccr.2007.02.001
12. Juluri, B. K.; Kumar, A. S.; Liu, Y.; Ye, T.; Yang, Y.-W.; Flood, A. H.; Fang, L.; Stoddart, J. F.; Weiss, P. S.; Huang, T. J. *ACS Nano* **2009,** *3,* 291–300. doi:10.1021/nn8002373
13. Parimal, K.; Witlicki, E. H.; Flood, A. H. *Angew. Chem., Int. Ed.* **2010,** *49,* 4628–4632. doi:10.1002/anie.201001003
14. Balzani, V.; Credi, A.; Venturi, M. *Pure Appl. Chem.* **2003,** *75,* 541–547. doi:10.1351/pac200375050541
15. Kottas, G. S.; Clarke, L. I.; Horinek, D.; Michl, J. *Chem. Rev.* **2005,** *105,* 1281–1376. doi:10.1021/cr0300993
16. Eelkema, R.; Pollard, M. M.; Vicario, J.; Katsonis, N.; Ramon, B. S.; Bastiaansen, C. W. M.; Broer, D. J.; Feringa, B. L. *Nature* **2006,** *440,* 163. doi:10.1038/440163a
17. Muraoka, T.; Kinbara, K.; Aida, T. *Nature* **2006,** *440,* 512–515. doi:10.1038/nature04635
18. Russew, M.-M.; Hecht, S. *Adv. Mater.* **2010,** *22,* 3348–3360. doi:10.1002/adma.200904102
19. Kulago, A. A.; Mes, E. M.; Klok, M.; Meetsma, A.; Brouwer, A. M.; Feringa, B. L. *J. Org. Chem.* **2010,** *75,* 666–679. doi:10.1021/jo902207x
20. Landaluce, T. F.; London, G.; Pollard, M. M.; Rudolf, P.; Feringa, B. L. *J. Org. Chem.* **2010,** *75,* 5323–5325. doi:10.1021/jo1006976
21. Lubbe, A. S.; Ruangsupapichat, N.; Caroli, G.; Feringa, B. L. *J. Org. Chem.* **2011,** *76,* 8599–8610. doi:10.1021/jo201583z
22. Landge, S. M.; Aprahamian, I. *J. Am. Chem. Soc.* **2009,** *131,* 18269–18271. doi:10.1021/ja909149z
23. Su, X.; Aprahamian, I. *Org. Lett.* **2011,** *13,* 30–33. doi:10.1021/ol102422h
24. Landge, S. M.; Tkatchouk, E.; Benítez, D.; Lanfranchi, D. A.; Elhabiri, M.; Goddard, W. A., III; Aprahamian, I. *J. Am. Chem. Soc.* **2011,** *133,* 9812–9823. doi:10.1021/ja200699v
25. Su, X.; Robbins, T. F.; Aprahamian, I. *Angew. Chem., Int. Ed.* **2011,** *50,* 1841–1844. doi:10.1002/anie.201006982
26. Yang, Y.; Su, X.; Carroll, C. N.; Aprahamian, I. *Chem. Sci.* **2012,** *3,* 610–613. doi:10.1039/c1sc00658d
27. Karabatsos, G. J.; Shapiro, B. L.; Vane, F. M.; Fleming, J. S.; Ratka, J. S. *J. Am. Chem. Soc.* **1963,** *85,* 2784–2788. doi:10.1021/ja00901a025
28. Mitchell, A. D.; Nonhebel, D. C. *Tetrahedron Lett.* **1975,** *16,* 3859–3862. doi:10.1016/S0040-4039(00)91297-8
29. Butler, R. N.; Johnson, S. M. *J. Chem. Soc., Perkin Trans. 1* **1984,** 2109–2116. doi:10.1039/P19840002109

Beilstein Journal of Organic Chemistry

meta-Oligoazobiphenyls – synthesis via site-selective Mills reaction and photochemical properties

Raphael Reuter and Hermann A. Wegner*

Full Research Paper

Open Access

Address:
University of Basel, Department of Chemistry, St. Johanns-Ring 19, 4056 Basel, Switzerland

Email:
Hermann A. Wegner* - hermann.wegner@unibas.ch

* Corresponding author

Keywords:
azobenzene; cross-coupling reaction; foldamer; molecular switches; photochromism

Beilstein J. Org. Chem. **2012,** *8,* 877–883.
doi:10.3762/bjoc.8.99

Received: 02 March 2012
Accepted: 09 May 2012
Published: 13 June 2012

This article is part of the Thematic Series "Molecular switches and cages".

Guest Editor: D. Trauner

Abstract

The investigation of multi-photochromic compounds constitutes a great challenge, not only from a synthetic point of view, but also with respect to the analysis of the photochemical properties. In this context we designed a novel strategy to access *meta*-oligoazobiphenyls via site-selective Mills reaction and Suzuki cross-coupling in a highly efficient iterative way. Photochemical examination of the resulting monomeric and oligomeric azo compounds revealed that the overall degree of switching was independent of the connected azo-units. However, one of the azobonds in the bis-azobiphenyl is isomerized preferentially despite the high structural similarity.

Introduction

The possibility to control structures on the molecular level in a reversible manner by using an external stimulus has fascinated scientists for a long time. One of the earliest reports on a molecular entity that can be influenced in this way concerns the azobenzene scaffold. Since this discovery by Hartley in 1937 [1] many more compounds showing such a photochromism have been reported [2]. However, the azobenzene moiety still remains one of the most popular "work horses" in this respect [3-6]. The reason can probably be found in its relatively easy synthetic accessibility combined with its interesting switching behavior. Upon irradiation with UV light the usually more stable *E* isomer can be switched to the *Z* form. If the *Z* isomer is irradiated with visible light or heated it can be converted back to the *E* state. During this isomerization the azobenzene undergoes a drastic length reduction of ~3.5 nm rendering it an ideal candidate for changing spatial arrangements on the molecular level. This change has been featured in a variety of applications [7-9], such as, switchable sensors [10], ion channels [11], catalysts [12], or liquid crystals [13].

In most of these applications, however, only one azobenzene unit is incorporated. One of the reasons is the synthetic chal-

lenge associated with the preparation of such oligomers. Solubility and, especially, selectivity issues have to be addressed. Another reason is the higher complexity of the photochemistry of these multi-photochromic compounds. The number of possible isomers increases exponentially with the number of azo units. Additionally, it has been shown by others [14], as well as by us [15-17], that the direct connection of two azobonds to one aromatic ring alters the switching behavior considerably, such that bis-*ortho*-azobenzenes did not show any photochromicity. Therefore, in recent examples in the literature the azo-units have been dissected by incorporation of biphenyl units. Hecht and co-workers investigated the effect of the electronic coupling in detail and showed that the incorporation of *ortho*-methyl groups on the biphenyl restores the photoisomerization properties (Figure 1) [18,19]. In a related example by Samanta and Woolley a similar compound was presented featuring anchoring groups for biological applications (Figure 1) [20]. In another study the team of Hecht synthesized oligomers separated by alkynyl linkers, demonstrating interesting coil–uncoil phenomena upon irradiation [21]. There are also reports on polymers that contain multiple azobenzene units. In these materials, however, the effect of the individual azobenzene moiety on the whole molecular assembly is not specified [22,23].

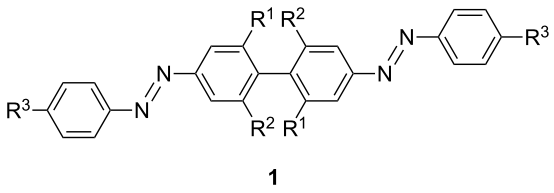

Figure 1: *para*-Substituted bisazobiphenyls **1** investigated by Hecht (R^1, R^2 = H, Me, R^3 = *t*-Bu) and by Woolley and co-workers (R^1 = H, SO_3Na, R^2 = H, R^3 = $NHCOCH_3$).

So far, mainly *para*-connected bisazobiphenyls have been addressed. Synthetic studies on *meta*-bisazobiphenyls were reported early on, in the context of azodyes over 100 years ago [24-26]. The switching properties of this class of compounds have not been examined though. As it has been shown that the connectivity is crucial for the photochemical properties, we set out to study *meta*-connected azobiphenyls. Not only have the photochemical properties been investigated, but also selective synthetic strategies for their preparation have been explored.

Results and Discussion

Synthesis of *meta*-substituted azobiphenyls

In the design of our target molecule, different aspects were considered: One important issue is solubility, which was addressed by incorporating *tert*-butyl-groups on every second ring. Additionally, it was envisioned to attach groups such as an amino functionality, which would open the potential to incorporate our system in, for example, biological settings. As a synthetic strategy it would be highly desirable to be able to build up the oligomer in a modular, protecting-group-free manner. In this respect, we planed a combination of the Mills reaction [27] with Suzuki cross-coupling, which we have successfully employed in previous studies (Figure 2) [28]. A key issue, however, was a site-selective transformation in order to differentiate both ends of the oligomer. The installment of an ester group on one site of the biphenyl unit should steer the critical Mills reactivity not only by steric, but also by electronic factors to the second ring.

One of the building blocks for the synthesis envisioned in Figure 2 is a tetra-substituted phenylderivative, which can be prepared from readily available 4-*tert*-butyltoluene (**3**) (Scheme 1). The first reaction was a nitration at the 2-position. After discouraging results were obtained under classical nitrating conditions employing a H_2SO_4/HNO_3 mixture, the

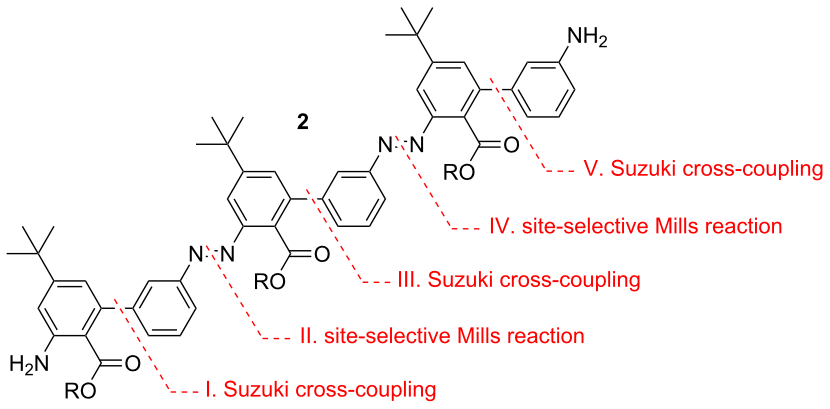

Figure 2: Synthetic strategy for the assembly of *meta*-substituted oligo-azobiphenyls **2**.

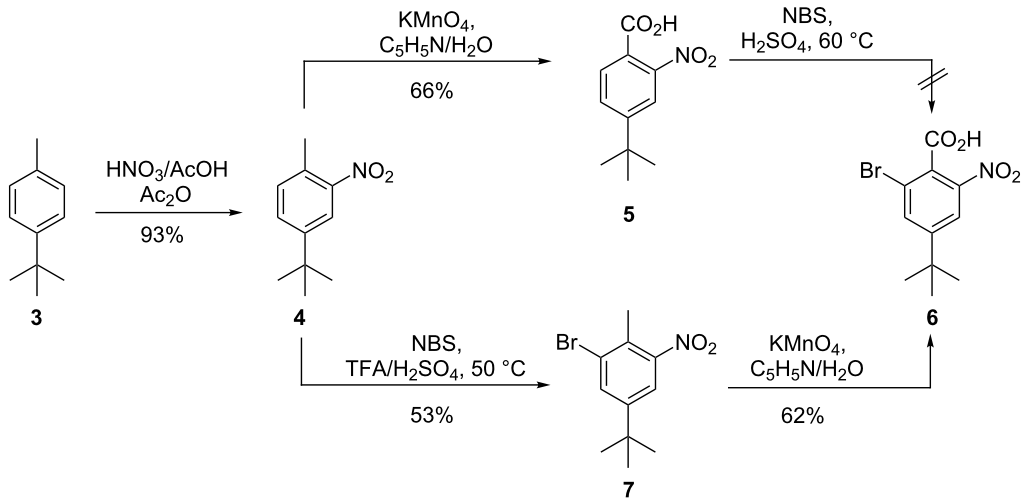

Scheme 1: Synthesis of 2-nitro-4-*tert*-butyl-6-bromobenzoic acid (**6**).

conditions were altered to use a mixture of AcOH/HNO_3 in acetic anhydride as the solvent. In this way the mono nitration product **4** could be obtained in excellent yields. In a first attempt, the intermediate 2-nitro-4-*tert*-butyltoluene (**4**) was oxidized with potassium permanganate in a 1:1 solvent mixture of pyridine/H_2O, to the corresponding benzoic acid **5**. The reaction proceeded with an acceptable yield of 66%. However, the resulting highly deactivated aromatic system **5** did not react even under harsh bromination conditions with NBS in concentrated sulfuric acid. Therefore, the reaction sequence was changed to bromination first, followed then by oxidation of the benzylic position. The bromination proceeded slowly, and after three days of stirring at 50 °C, only 53% of 2-nitro-4-*tert*-butyl-6-bromotoluene (**7**) was obtained. It turned out that the oxidation of this substrate was not as convenient as in the first attempt. Complete conversion of the starting material could not be achieved, even after stirring at 100 °C overnight and by using an excess of 10 equiv of $KMnO_4$. Finally, the desired key compound **6** was isolated in a yield of 62%.

The next two steps in the synthesis of the building blocks were straightforward (Scheme 2) and comprised esterification of the acid **6** with potassium carbonate and methyl iodide in acetone, as well as reduction of the nitro group via a Béchamp reaction to give compound **9**. The amino group was afterwards reacted with *m*CPBA in THF to yield the nitroso derivative **10** in a good yield of 69%.

With all the necessary building blocks in hand, the assembly of oligomer **2** was started with a Suzuki reaction of **9** with 3-aminophenylboronic acid pinacolate (**11**) to prepare biphenyl **12** (Scheme 3). The reaction proceeded in a good yield of 84%. However, pinacol was obtained as a side product and could not be separated by column chromatography. The impure diamine **12** was then subjected to the Mills reaction with one equiv of nitroso compound **10**. The aim was to achieve selectively only one coupling at the less functionalized benzene ring. As expected from the initial design, the deactivation of the second amino group by the ester in the *ortho*-position led to the isolation of the mono-coupled product as the major species in 60%. After this successful Mills reaction step, two more Suzuki reactions and one additional Mills coupling step were required to obtain the bisazobiphenyl **2**. The Suzuki reactions were performed with 3-aminophenylboronic acid (**14**) instead of the

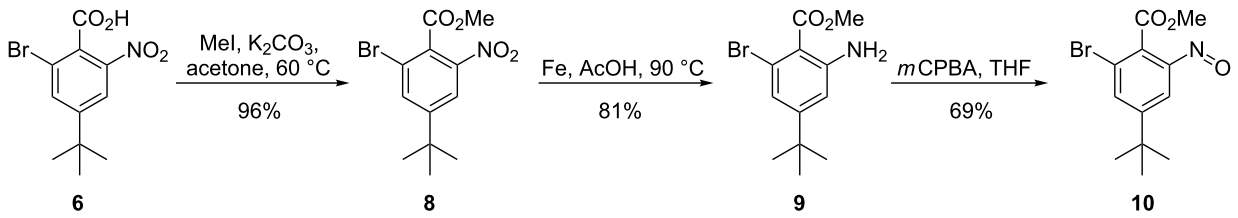

Scheme 2: Preparation of nitroso derivative **10**.

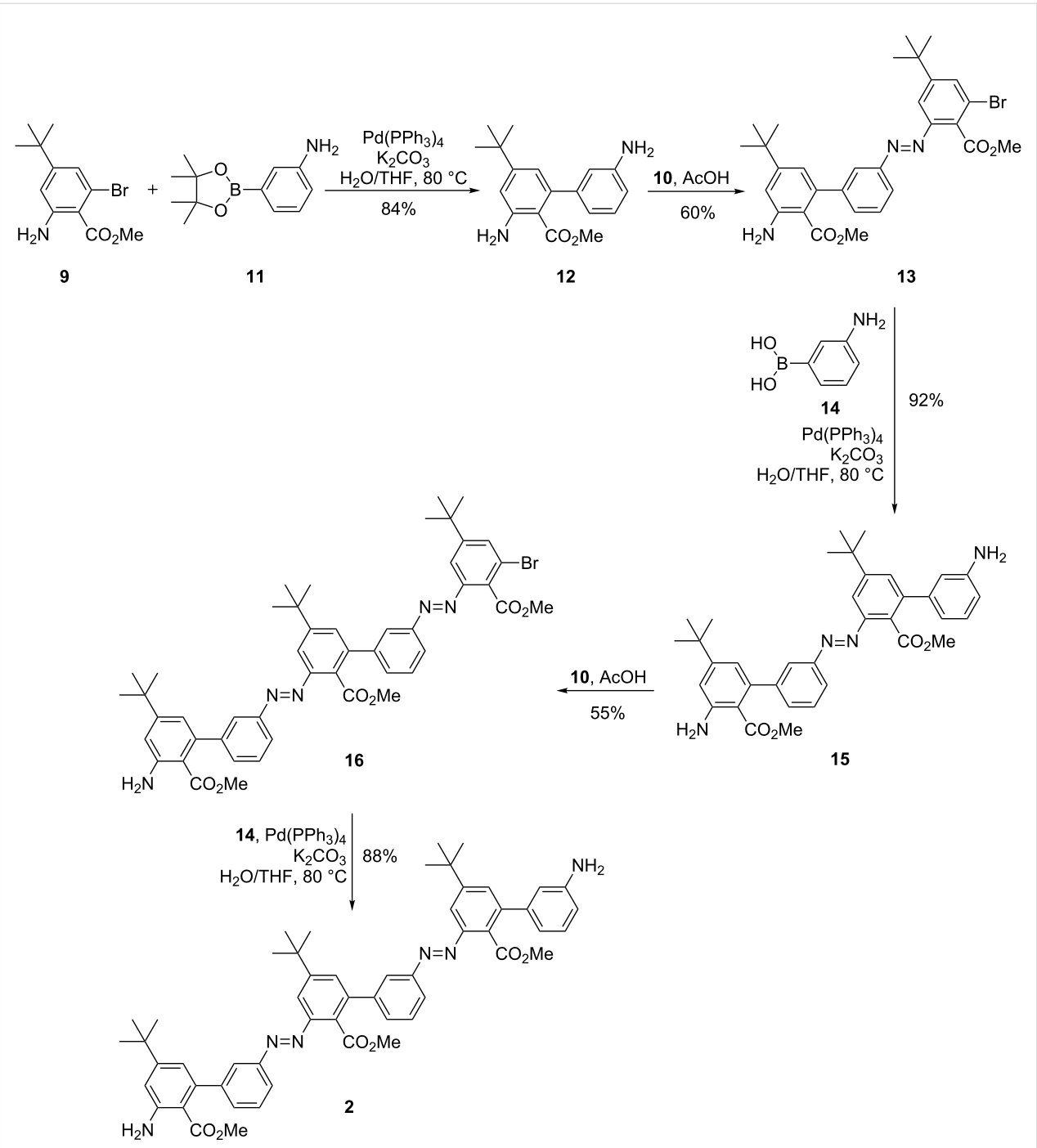

Scheme 3: Assembly of oligomer **2** by Suzuki cross-coupling and site-selective Mills reaction.

pinacolate, to eliminate the difficulties in the purification. The selective Mills reaction was again successful, giving only slightly lower yields.

Isomerization studies

Compounds **13**, **15**, **16** and **2** were analyzed by UV spectroscopy. All of them exhibit the typical behavior of azobenzenes, with a strong absorption at 330 nm for the π–π* transition and a weak absorption at 430 nm for the n–π* transition (Figure 3). For compounds **16** and **2** an increased absorption of the whole spectrum is noted due to the additional chromophore in the molecule. Upon irradiation at 356 nm (8 W hand-held UV lamp, at room temperature) all compounds underwent an *E*→*Z* isomerization, which can be seen as a decrease of the π–π* and

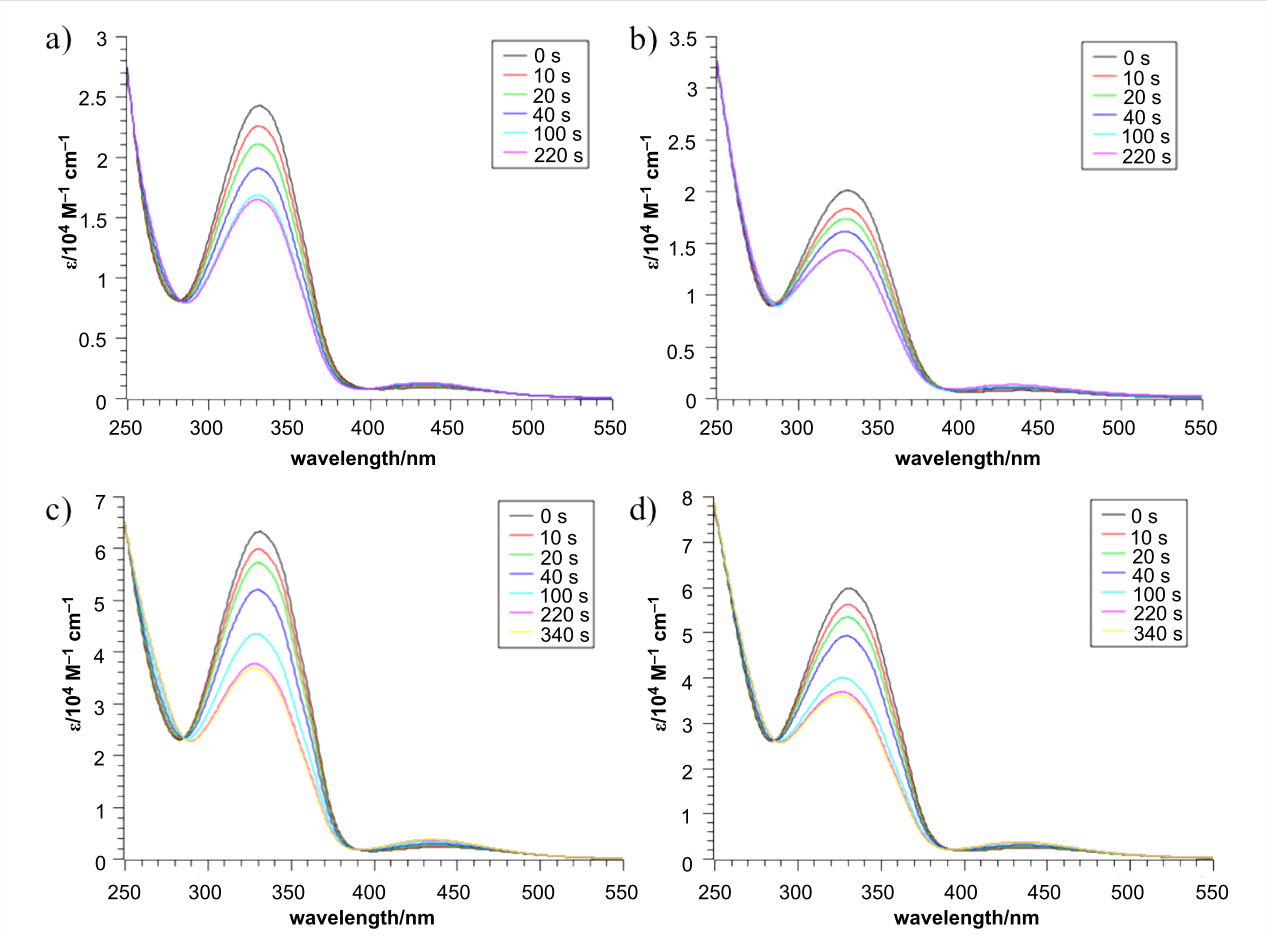

Figure 3: Isomerization studies of compound **13** (a), **15** (b), **16** (c) and **2** (d) (Irradiation at 356 nm in $CHCl_3$).

an increase of the n–π* band. In this respect all compounds display similar characteristics and show a comparable degree of isomerization (Figure 3).

This phenomenon can be easily visualized when the degree of isomerization is plotted against the irradiation time for all four compounds (Figure 4). In the first 100 s all four compounds isomerize at the same rate regardless how many azo units are present. After this time compounds **13** and **15** reach their photostationary state and their isomeric ratio does not change significantly. The bisazocompounds **16** and **2** with their additional azo moiety, however, show a further switching, which plateaus when both of their photochromic azo units have been equilibrated in the photostationary state.

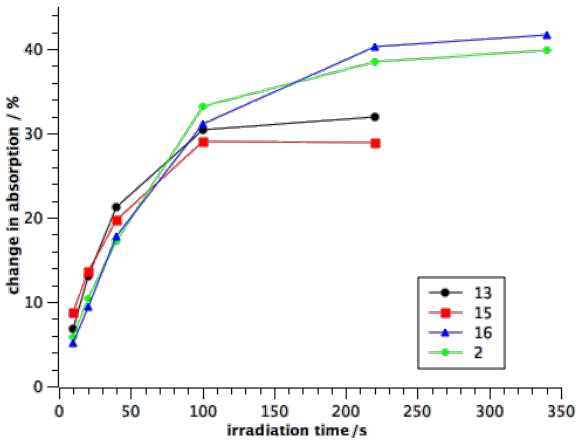

Figure 4: Comparison of the absorption as well as the photostationary state of compounds **13**, **15**, **16**, **2**.

The composition of the photostationary state was investigated for compounds **15** and **2** by NMR spectroscopy. In the case of **15** the ratio of the *E*/*Z* isomers is 1/1.2 in the photostationary state corresponding to a degree of isomerization of ~55%. For **2** the situation is more complicated as, due to the lack of symmetry, four different isomers are possible [(*E*,*E*), (*E*,*Z*), (*Z*,*E*), (*Z*,*Z*); Figure 5]. The ratio in the photostationary state of (*E*,*E*)/(*E*,*Z*)/(*Z*,*E*)/(*Z*,*Z*) is 20/18/36/26, which corresponds also to a similar average isomerization of ~51% per azo unit.

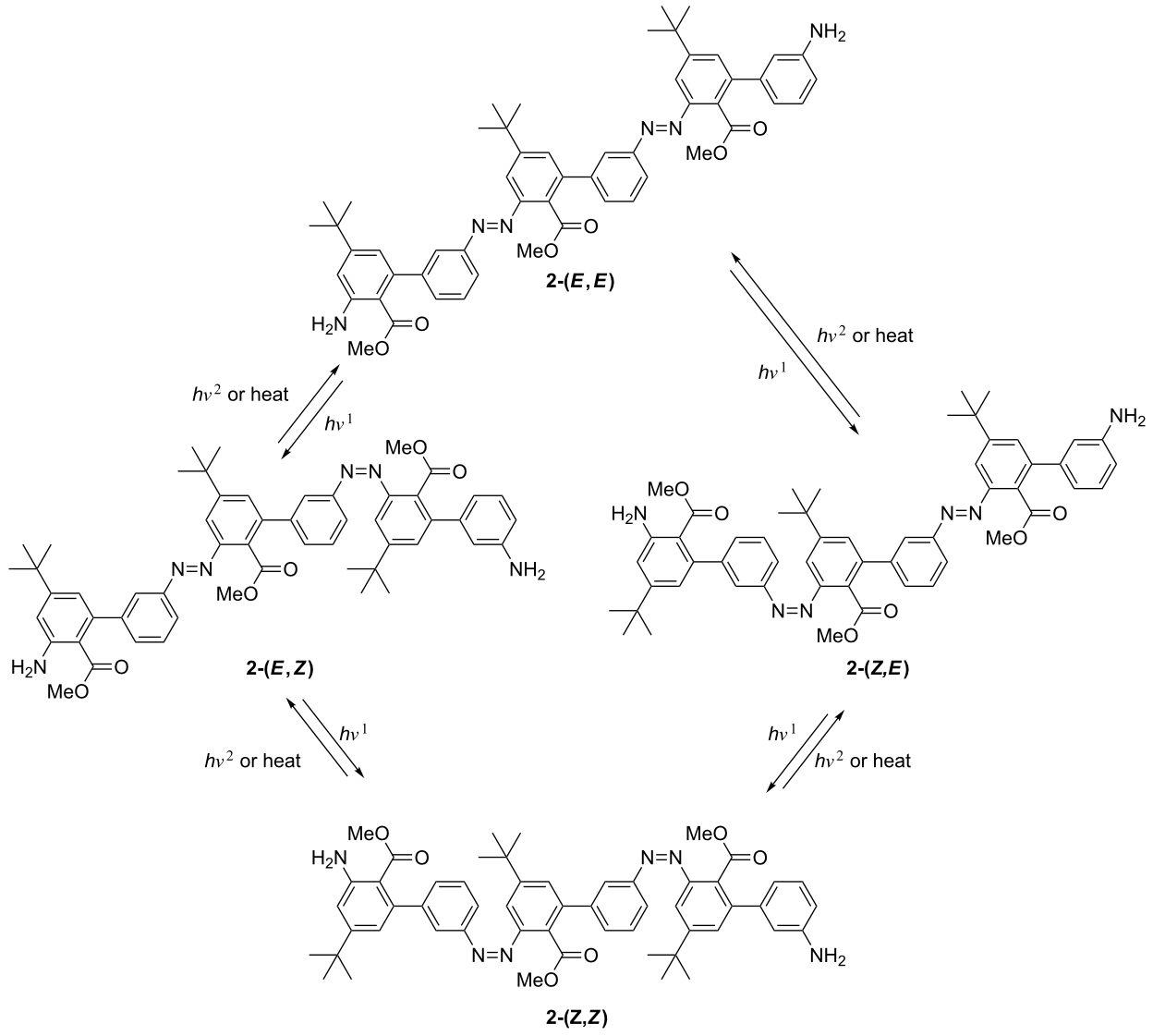

Figure 5: Four different isomers of **2**.

Although it may be expected that the (*E*,*Z*) and the (*Z*,*E*) isomer would be found in equal amounts as their direct chemical environment is very similar, a clear preference for the (*Z*,*E*) isomer can be seen. Therefore, although the overall degree of isomerization seems to be independent if two azo units are connected via a biphenyl unit in *meta*-positions, there seem to be subtle differences that influence the preference as to which azo bond is switched preferentially. Such a property will be highly useful in the design of selective, switchable, functional oligomers.

Conclusion

In summary, a very efficient modular synthetic approach for the preparation of *meta*-oligoazobiphenyls has been developed relying on a site-selective Mills reaction and Suzuki cross-coupling. The switching behavior of the azo units seems to be rather independent from an electronic point of view. However, delicate aspects favor certain isomers, allowing the rational design of selective switchable functional oligomers in the future.

Supporting Information

Supporting Information File 1

Experimental procedures and characterization data.
[http://www.beilstein-journals.org/bjoc/content/supplementary/1860-5397-8-99-S1.pdf]

Acknowledgements

The authors thank the Swiss National Science Foundation and SystemsX.ch for financial support. H.A.W. is indebted to the Fond der Chemischen Industrie for a Liebig fellowship.

References

1. Hartley, G. S. *Nature* **1937,** *140,* 281. doi:10.1038/140281a0
2. Feringa, B. L.; Browne, W. R., Eds. *Molecular Switches,* 2nd ed.; Wiley-VCH: Weinheim, Germany, 2011.
3. Griffiths, J. *Chem. Soc. Rev.* **1972,** *1,* 481–493. doi:10.1039/CS9720100481
4. Beveridge, D. L.; Jaffé, H. H. *J. Am. Chem. Soc.* **1966,** *88,* 1948–1953. doi:10.1021/ja00961a018
5. Kroner, J.; Bock, H. *Chem. Ber.* **1968,** *101,* 1922–1932. doi:10.1002/cber.19681010606
6. Jaffé, H. H.; Yeh, S.-J.; Gardner, R. W. *J. Mol. Spectrosc.* **1958,** *2,* 120–136. doi:10.1016/0022-2852(58)90067-5
7. Feringa, B. L. *Acc. Chem. Res.* **2001,** *34,* 504–513. doi:10.1021/ar0001721
8. Balzani, V.; Credi, A.; Venturi, M. *Molecular Devices and Machines—A Journey into the Nanoworld,* 1st ed.; Wiley-VCH: Weinheim, Germany, 2003. doi:10.1002/3527601600
9. Beharry, A. A.; Woolley, G. A. *Chem. Soc. Rev.* **2011,** *40,* 4422–4437. doi:10.1039/c1cs15023e
10. Shinkai, S.; Nakaji, T.; Nishida, Y.; Ogawa, T.; Manabe, O. *J. Am. Chem. Soc.* **1980,** *102,* 5860–5865. doi:10.1021/ja00538a026
11. Banghart, M.; Borges, K.; Isacoff, E.; Trauner, D.; Kramer, R. H. *Nat. Neurosci.* **2004,** *7,* 1381–1386. doi:10.1038/nn1356
12. Stoll, R. S.; Hecht, S. *Angew. Chem.* **2010,** *122,* 5176–5200. doi:10.1002/ange.201000146
    Angew. Chem., Int. Ed. **2010,** *49,* 5054–5075. doi:10.1002/anie.201000146
13. Ichimura, K. *Chem. Rev.* **2000,** *100,* 1847–1874. doi:10.1021/cr980079e
14. Cisnetti, F.; Ballardini, R.; Credi, A.; Gandolfi, M. T.; Masiero, S.; Negri, F.; Pieraccini, S.; Spada, G. P. *Chem.–Eur. J.* **2004,** *10,* 2011–2021. doi:10.1002/chem.200305590
15. Reuter, R.; Hostettler, N.; Neuburger, M.; Wegner, H. A. *Eur. J. Org. Chem.* **2009,** 5647–5652. doi:10.1002/ejoc.200900861
16. Reuter, R.; Hostettler, N.; Neuburger, M.; Wegner, H. A. *Chimia* **2010,** *64,* 180–183. doi:10.2533/chimia.2010.180
17. Bellotto, S.; Reuter, R.; Heinis, C.; Wegner, H. A. *J. Org. Chem.* **2011,** *76,* 9826–9834. doi:10.1021/jo201996w
18. Bléger, D.; Dokić, J.; Peters, M. V.; Grubert, L.; Saalfrank, P.; Hecht, S. *J. Phys. Chem. B* **2011,** *115,* 9930–9940. doi:10.1021/jp2044114
19. Bléger, D.; Liebig, T.; Thiermann, R.; Maskos, M.; Rabe, J. P.; Hecht, S. *Angew. Chem.* **2011,** *123,* 12767–12771. doi:10.1002/ange.201106879
    Angew. Chem., Int. Ed. **2011,** *50,* 12559–12563. doi:10.1002/anie.201106879
20. Samanta, S.; Woolley, G. A. *ChemBioChem* **2011,** *12,* 1712–1723. doi:10.1002/cbic.201100204
21. Yu, Z.; Hecht, S. *Angew. Chem.* **2011,** *123,* 1678–1681. doi:10.1002/ange.201006084
    Angew. Chem., Int. Ed. **2011,** *50,* 1640–1643. doi:10.1002/anie.201006084
22. Kumar, G. S.; Neckers, D. C. *Chem. Rev.* **1989,** *89,* 1915–1925. doi:10.1021/cr00098a012
23. Natansohn, A.; Rochon, P. *Chem. Rev.* **2002,** *102,* 4139–4176. doi:10.1021/cr970155y
24. Noelting, E.; Fourneaux, E. *Chem. Ber.* **1897,** *30,* 2930–2947. doi:10.1002/cber.18970300398
25. Robertson, P. W.; Brady, O. L. *J. Chem. Soc., Trans.* **1913,** *103,* 1479–1484. doi:10.1039/ct9130301479
26. Musso, H.; Záhorszky, U. I.; Beecken, H.; Gottschalk, E.-M.; Krämer, H. *Chem. Ber.* **1965,** *98,* 3964–3980. doi:10.1002/cber.19650981224
27. Mills, C. *J. Chem. Soc., Trans.* **1895,** *67,* 925–933. doi:10.1039/ct8956700925
28. Reuter, R.; Wegner, H. A. *Chem.–Eur. J.* **2011,** *17,* 2987–2995. doi:10.1002/chem.201002671

License and Terms

Beilstein Journal of Organic Chemistry

Intramolecular bridges formed by photoswitchable click amino acids

Christian Hoppmann*, Ronald Kühne and Michael Beyermann

Letter

Open Access

Address:
Department of Chemical Biology, Leibniz-Institut für Molekulare Pharmakologie, Robert-Rössle-Strasse 10, 13125 Berlin, Germany

Email:
Christian Hoppmann* - hoppmann@fmp-berlin.de

* Corresponding author

Keywords:
azobenzene; helical conformation; isomerization; molecular switches; photoswitchable click amino acid; thiol–ene click

Beilstein J. Org. Chem. **2012,** *8,* 884–889.
doi:10.3762/bjoc.8.100

Received: 29 February 2012
Accepted: 09 May 2012
Published: 13 June 2012

This article is part of the Thematic Series "Molecular switches and cages".

Guest Editor: D. Trauner

Abstract

Photoswitchable click amino acids (PSCaa) are amino acids bearing a side chain consisting of a photoswitchable unit elongated with a functional group that allows for a specific click reaction, such as an alkene that can react with the thiol group of a cysteine residue. An intramolecular click reaction results in the formation of a photoswitchable bridge, which can be used for controlling conformational domains in peptides and proteins. The ability to control conformations as well as the efficiency of the intramolecular bridging depends on the length of the PSCaa side chain and the distance to the cysteine residue to be clicked with. On comparing i,i+4 and i,i+7 spacings of PSCaa and cysteine in a model peptide without a preferred conformation, it was seen that the thiol–ene click reaction takes place efficiently in both cases. Upon induction of an α-helical structure by the addition of trifluoroethanol, the thiol click reaction occurs preferentially with the i,i+4 spacing. Even in the presence of glutathione as an additional thiol the click reaction of the PSCaa occurs intramolecularly with the cysteine rather than with the glutathione, indicating that the click reaction may be used even under reducing conditions occurring in living cells.

Introduction

Photoswitchable bridges that are site-specifically incorporated into proteins allow the conformation and activity of proteins to be modulated by light. In contrast to common bivalent thiol reactive azobenzene switches [1-5], the PSCaa described here (Scheme 1) is an α-amino acid containing, besides an azobenzene unit, a vinyl function that can react specifically with a cysteine within a putative conformational domain of a peptide or a protein by light-induced thiol–ene click reaction [6-9]. The light-induced click reaction of our PSCaa occurs predominantly in the *cis* state that is formed simultaneously due to the photoisomerization at λ = 365 nm.

Recently, the concept of photoswitchable click amino acids has been applied to the polypeptide hormone urocortin, the helical fold of which was regulated by light, showing different biopotencies dependent on the *trans*/*cis* isomeric state of the photocontrollable bridge [6]. In the achievement of an efficient and "clean" thiol–ene click reaction between the vinyl function of

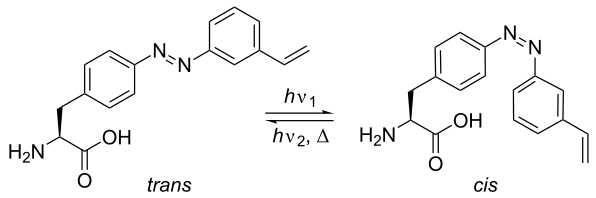

Scheme 1: Photoisomerization of the photoswitchable click amino acid 2-amino-3-(4-((3-vinylphenyl)diazenyl)phenyl)propanoic acid.

PSCaa and the cysteine residue within α-helical structures, the spacing between the two plays a pivotal role. For the i,i+4 spacing we have shown that the thiol–ene click reaction in the model peptide Ac-E-K-E-E-PSC-E-K-K-C-K-E-NH_2 occurs smoothly without a preferred conformation, in aqueous buffered solution (pH 7.5). However, fully recombinant proteins exhibit highly structured domains, which may influence the intramolecular thiol click reaction between the PSCaa and a cysteine residue. Here, we show that the thiol click reaction of the photoswitchable click amino acid (PSCaa) at the i,i+4 position and a cysteine in a helical model peptide, under structure-inducing conditions, is favoured compared to that with PSCaa at the i,i+7 position. Furthermore, in the presence of glutathione (GSH), a naturally occurring thiol in living cells, the click reaction takes place at relatively high GSH concentrations (1 mM) indicating that the thiol click reaction occurs preferentially intramolecularly.

Results and Discussion

Thiol click reaction of PSCaa within α-helical conformations

Before we incorporated PSCaa into the helical model peptide at i,i+4 and i,i+7 positions, we calculated for the *trans* and the *cis* PSCaa the expected end-to-end distances between the C atom of the methyl group and the cysteine S atom of the built-in photocontrollable bridge (Figure 1). The range of distances covered by the *cis* form was found to be between 4 and 11 Å, and between 10 and 14 Å by the *trans* form. Therefore, in α-helical structures the *cis* form of PSCaa is expected to be compatible with an i,i+4 spacing (5.4 Å). Moreover, the different distances covered by the *cis* and the *trans* form of the photocontrollable bridge explain the significant stabilization of the α-helical conformation of the crosslinked peptide **3** (Scheme 2) with i,i+4 spacing in the *cis* form in contrast to the more extended *trans* form, which disturbs an α-helical conformation [6].

To study the effect of i,i+4 or i,i+7 spacings on the efficiency of intramolecular thiol–ene click reactions of the PSCaa with a cysteine in an α-helical structure, we compared the reaction in peptide **1** with i,i+4 and peptide **2** with i,i+7 spacing in the presence of 50% trifluoroethanol (TFE) (Scheme 2). The addition of TFE causes both peptides to adopt an α-helical conformation, while in aqueous buffered solution no preferred conformation of the two peptides was observed (see CD spectra in Supporting Information File 1). Interestingly, the overall helix content of

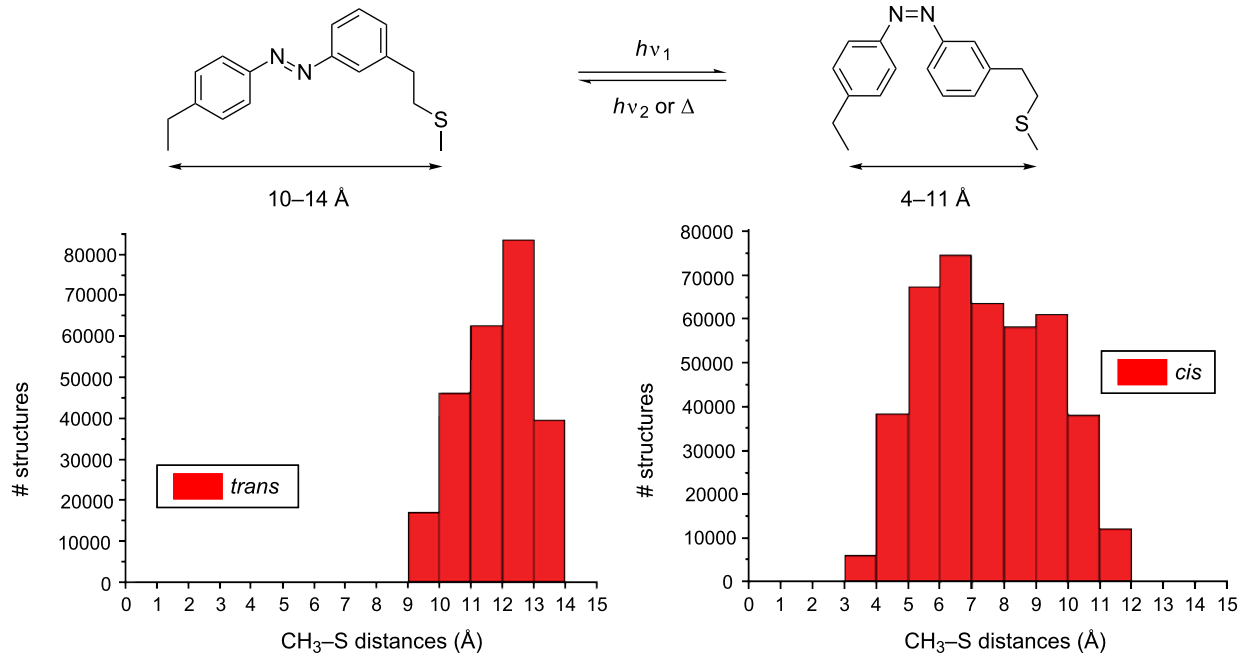

Figure 1: Histogram showing the distribution of end-to-end distances of the *trans* and the *cis* form between the C atom of the methyl group and cysteine S of the built-in photocontrollable bridge.

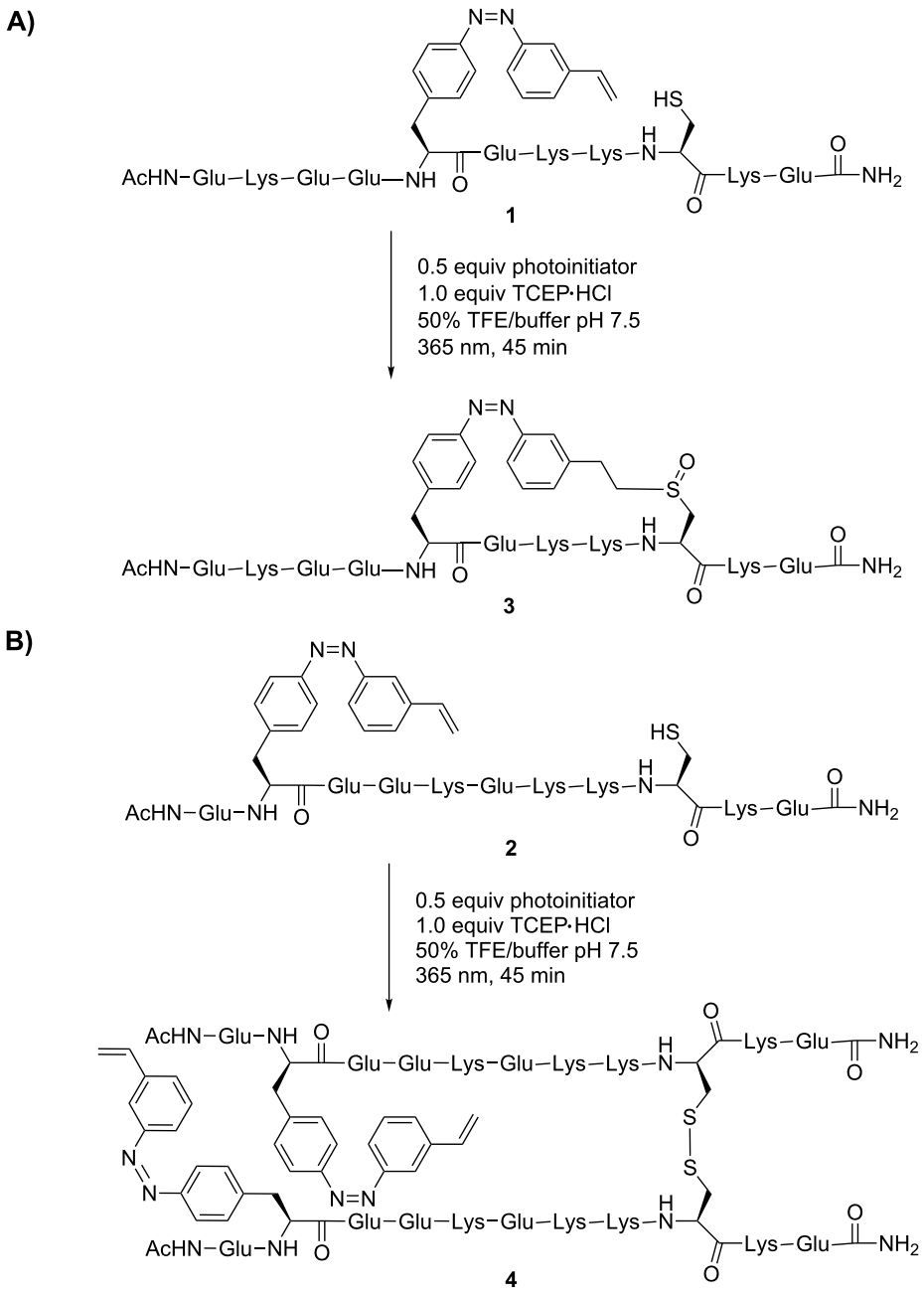

Scheme 2: Thiol–ene click reaction of PSCaa with cysteine within the helical model peptides **1** (i,i+4) and **2** (i,i+7) under structure-inducing conditions in the presence of trifluoroethanol (50%).

peptide **2** is lower (42%) than that of peptide **1** (77%) indicating that the PSCaa positioned at i,i+7 disturbed the α-helical conformation in our model peptide. However, for the herein described investigation the induction of α-helical conformation by adding TFE is sufficient for the study of this effect.

Irradiation of the reaction mixture at λ = 365 nm for 45 min induces not only the thiol–ene click reaction but simultaneously the *trans*-to-*cis* photoisomerization. Under these conditions the formation of the intramolecular bridge resulted in click product **3** with i,i+4 helical spacing, whereas for peptide **2** with i,i+7 spacing only traces of the intramolecular click product were observed. Most notably, for peptide **2** (i,i+7) the predominate formation of the disulfide **4** was detected, indicating that the intramolecular thiol–ene click reaction within i,i+7 helical spacing is inefficient (Scheme 2). In contrast, in aqueous buffered solution, in which both peptides adopted no preferred conformation, the click products of either peptide **1** (i,i+4) or **2**

(i,i+7) were obtained equally. These findings indicate that in α-helical structures, i,i+4 spacing of PSCaa and the cysteine residue preferentially allows the intramolecular thiol click reaction to take place, in contrast to the case of i,i+7 spacing.

Thiol click reaction in presence of glutathione (GSH)

For the formation of intramolecular bridges in proteins, even under conditions in living cells, it is important that the intramolecular thiol–ene click reaction takes place in the presence of endogenous thiols. In most cells the cysteine containing tripeptide glutathione (GSH) is present at millimolar concentrations (0.1 mM–10 mM). Therefore, we investigated the thiol–ene click reaction of PCSaa and cysteine within peptide **1** and **2** in buffered solution (peptide concentration 0.1 mM) in the presence of GSH at different concentrations (10 mM, 5 mM, 1 mM, 0.5 mM, 0.1 mM).

Simply by comparing the intensity of the mass peaks of the intramolecular with that of the intermolecular click product, we found that with decreasing GSH concentration the yield of the intramolecular thiol click reaction increased (Figure 2, data

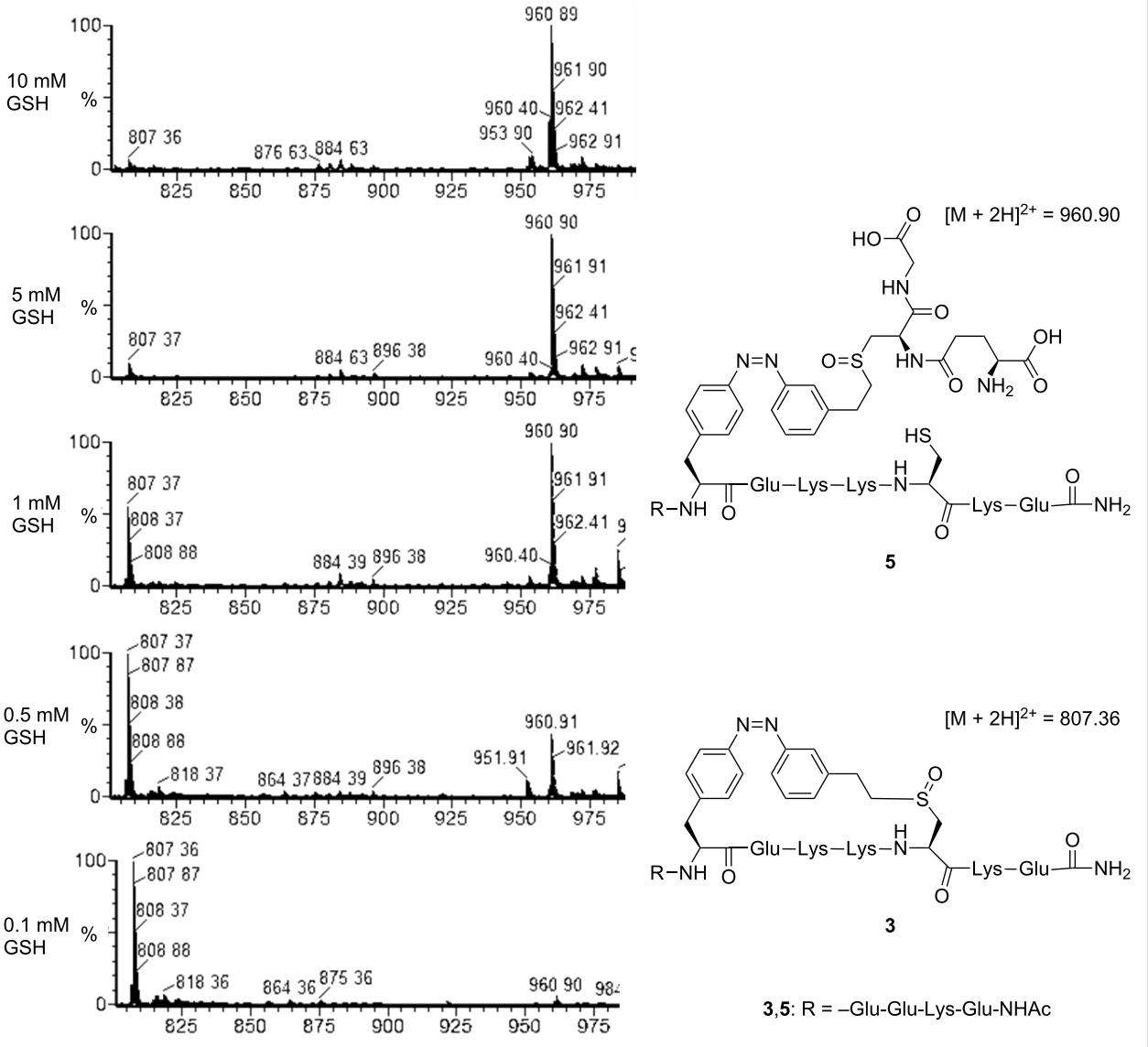

Figure 2: ESI–MS spectra of fractions of the crude reaction solution of the thiol–ene click reaction of peptide **1** (peptide concentration 0.1 mM) in the presence of GSH (10 mM, 5 mM, 1 mM, 0.5 mM, 0.1 mM), showing the intermolecular click product **5** at high GSH concentrations and the intramolecular click product **3** at decreasing GSH concentrations.

shown for peptide **1**). At the highest GSH concentration tested (10 mM), only the intermolecular click product **5** ($[M + 2H]^{2+}$ = 960.90) was detected as the corresponding sulfoxide of the thioether formed in the crosslinked peptide **3**. Already, in the presence of 1 mM GSH the intramolecular thiol click products ($[M + 2H]^{2+}$ = 807.36) of both peptides with i,i+4 and i,i+7 spacings were obtained (for ESI–MS spectra of peptide **2** with i,i+7, see Supporting Information File 1). Our results show that the intramolecular thiol–ene click reaction of PSCaa and cysteine is preferred compared to the intermolecular reaction of PSCaa with glutathione, providing perspectives for an intracellular application of this reaction type within recombinant proteins.

Conclusion

The light-induced thiol–ene click reaction of our PSCaa with cysteine occurs in its *cis* form, which is predominantly formed under the conditions of the inducing light (λ = 365 nm). The distribution of calculated end-to-end distances of the *cis* form (4–11 Å) is compatible with the i,i+4 spacing (5.4 Å) in a helical peptide. Accordingly, the intramolecular click reaction with i,i+4 spacing occurs more efficiently when a helical conformation of the model peptide has been stabilized by the addition of TFE rather than without a preferred conformation in the absence of TFE. Without a preferred peptide conformation, the click reaction proceeds smoothly with both i,i+4 and i,i+7 spacings. Our results indicate that our PSCaa incorporated into helical domains of proteins may allow the formation of photoswitchable bridges for controlling the conformation of biologically important protein domains. The intramolecular click reaction takes place even under reducing conditions, thus lending itself to an application in vivo in combination with protein synthesis with ad hoc evolved orthogonal tRNA/synthease pairs in an ongoing project [10].

Experimental

The photoswitchable click amino acid 2-amino-3-(4-((3-vinylphenyl)diazenyl)phenyl)propanoic acid (PSCaa) and the helical model peptides were synthesized as described in [6]. Thiol–ene coupling was performed at a peptide concentration of 0.1 mM in the presence of the photoinitiator 2-hydroxy-1-[4-(2-hydroxyethoxy)phenyl]-2-methyl-1-propanone (0.5 equiv) and TCEP·HCl (1.0 equiv) in degassed buffered solution containing 50% trifluoroethanol (pH 7.5). The reaction mixture was exposed to λ = 365 (4 mW/cm^2) for 45 min. LC–MS analysis was performed on an ACQUITY UPLC system equipped with a C18 column (3 µm, 2.1 × 30 mm) in combination with an electrospray time-of-flight (ESI–TOF) mass spectrometer (LCT Premier) from Waters. LC conditions: flow 0.2 mL/min, temperature 30 °C, eluent systems: eluent A = 1% acetonitrile in water (0.05% TFA), eluent B = 99% acetonitrile in water (0.05% TFA), linear gradient of 5 to 95% B in 6 min. UV detection was performed at 220 and 358 nm. CD spectra were recorded on a JASCO spectrophotometer (J-720) in a quartz cell of 0.1 cm path length over the range 198–300 nm at 25 °C. Peptide concentration was ~1×10^{-4} M in phosphate buffer pH 7.5. Obtained CD spectra were the average of six accumulations made at 0.1 nm intervals, reported in terms of molar ellipticity per residue ($[\theta]_r$) in deg × cm^2 × dmol^{-1}. The calculation of end-to-end distance changes for each isomer was realized with the Tripos FF method [11-13]. For each isomer 250,000 structures were generated maintaining a threshold of 5 kcal/mol.

Supporting Information

Supporting Information File 1

CD spectra of **1** and **2** and ESI–MS spectra of peptide **2** in the presence of GSH.
[http://www.beilstein-journals.org/bjoc/content/supplementary/1860-5397-8-100-S1.pdf]

References

1. Kumita, J. R.; Smart, O. S.; Woolley, G. A. *Proc. Natl. Acad. Sci. U. S. A.* **2000,** *97,* 3803–3808. doi:10.1073/pnas.97.8.3803
2. Zhang, F.; Timm, K. A.; Arndt, K. M.; Woolley, G. A. *Angew. Chem., Int. Ed.* **2010,** *49,* 3943–3946. doi:10.1002/anie.201000909
   Angew. Chem. **2010,** *122,* 4035–4038. doi:10.1002/ange.201000909
3. Woolley, G. A. *Acc. Chem. Res.* **2005,** *38,* 486–493. doi:10.1021/ar040091v
4. Schierling, B.; Noël, A.-J.; Wende, W.; Hien, L. T.; Volkov, E.; Kubareva, E.; Oretskaya, T.; Kokkinidis, M.; Römpp, A.; Spengler, B.; Pingoud, A. *Proc. Natl. Acad. Sci. U. S. A.* **2010,** *107,* 1361–1366. doi:10.1073/pnas.0909444107
5. Kusebauch, U.; Cadamuro, S. A.; Musiol, H.-J.; Lenz, M. O.; Wachtveitl, J.; Moroder, L.; Renner, C. *Angew. Chem., Int. Ed.* **2006,** *45,* 7015–7018. doi:10.1002/anie.200601432
   Angew. Chem. **2006,** *118,* 7170–7173. doi:10.1002/ange.200601432
6. Hoppmann, C.; Schmieder, P.; Heinrich, N.; Beyermann, M. *ChemBioChem* **2011,** *12,* 2555–2559. doi:10.1002/cbic.201100578
7. Hoyle, C. E.; Bowman, C. N. *Angew. Chem., Int. Ed.* **2010,** *49,* 1540–1573. doi:10.1002/anie.200903924
   Angew. Chem. **2010,** *122,* 1584–1617. doi:10.1002/ange.200903924
8. Aimetti, A. A.; Shoemaker, R. K.; Lin, C.-C.; Anseth, K. S. *Chem. Commun.* **2010,** *46,* 4061–4063. doi:10.1039/c001375g
9. Dondoni, A.; Massi, A.; Nanni, P.; Roda, A. *Chem.–Eur. J.* **2009,** *15,* 11444–11449. doi:10.1002/chem.200901746
10. Wang, Q.; Parrish, A. R.; Wang, L. *Chem. Biol.* **2009,** *16,* 323–336. doi:10.1016/j.chembiol.2009.03.001
11. White, D. N. J. *Comput. Chem. (Oxford, U. K.)* **1977,** *1,* 225–233. doi:10.1016/0097-8485(77)85014-6
12. Dixon, D. A.; Zeroka, D. J.; Wendolowski, J. J.; Wasserman, Z. R. *J. Phys. Chem.* **1985,** *89,* 5334–5336. doi:10.1021/j100271a005
13. Clark, M.; Cramer, R. D., III; Van Opdenbosch, N. *J. Comput. Chem.* **1989,** *10,* 982–1012. doi:10.1002/jcc.540100804

Beilstein Journal of Organic Chemistry

Building photoswitchable 3,4'-AMPB peptides: Probing chemical ligation methods with reducible azobenzene thioesters

Gehad Zeyat and Karola Rück-Braun*

Full Research Paper

Open Access

Address:
Institut für Chemie, Technische Universität Berlin, Strasse des 17. Juni 135, 10623 Berlin, Germany

Email:
Karola Rück-Braun* - karola.rueck-braun@tu-berlin.de

* Corresponding author

Keywords:
acyl transfer auxiliary; azobenzenes; ligation; molecular switches; peptides; redox chemistry

Beilstein J. Org. Chem. **2012,** *8,* 890–896.
doi:10.3762/bjoc.8.101

Received: 28 February 2012
Accepted: 04 May 2012
Published: 18 June 2012

This article is part of the Thematic Series "Molecular switches and cages".

Guest Editor: D. Trauner

Abstract

Photoswitchable peptides were synthesized by using cysteine- and auxiliary-based native chemical ligation reactions. For this purpose, the two regioisomeric azobenzene building blocks 3,4'-AMPB thioester **1b** and 4,4'-AMPB thioester **2b** were employed in the ligation reactions. While 4,4'-AMPB requires the 4,5,6-trimethoxy-2-mercaptobenzyl auxiliary to minimize reduction of the diazene unit, 3,4'-AMPB can be used in combination with the 4,5,6-trimethoxy-2-mercaptobenzyl auxiliary as well as the N^{α}-2-mercaptoethyl auxiliary. Thus, 3,4'-AMPB derivatives/peptides proved to be significantly less prone to reduction by aliphatic and aromatic thiols than were the 4,4'-AMPB compounds.

Introduction

Optical switches not only offer the advantage to elucidate, but also to control biological processes with high spatial and temporal resolution by using light, either in vitro or in vivo [1]. In this context, azobenzenes remain a privileged class of photoswitches, and typical applications based on light-triggered reversible conformational control of cyclic, helical or beta-hairpin peptides have been intensively reviewed [2,3]. Current research in this field focuses on advanced methods and designs for the synthesis of complex azopeptides and azoproteins for ambitious biophysical studies, and also for intracellular applications. In this respect, an increased and predictable stability of azobenzene building blocks under reducing conditions seems to be a prerequisite in light of synthetic challenges, but also when considering the reducing intracellular environment. We recently reported on the synthesis, properties and applications of a series of novel azobenzene ω-amino acids, with a preference for meta-substitution patterns. Our purpose was amongst other things (i) to increase flexibility, and (ii) to suppress resonance effects in order to enhance the stability of the diazene unit [4,5]. Since methods based on native chemical ligation (NCL), e.g., NCL

with N^{α}-acyl transfer auxiliaries, have gained considerable interest in the past two decades [6], we reasoned that a comparative ligation study with the Boc-protected azobenzene ω-amino acids Boc-3,4'-AMPB **1a** and Boc-4,4'-AMPB **2a** may result in an in-depth analysis of the redox-stability of these building blocks under the reducing conditions of thiol-based ligation methods. Generally, native chemical ligation allows the coupling of two unprotected peptides in neutral aqueous solution: a C-terminal thioester peptide and either an N-terminal cysteine peptide or N^{α}-auxiliary-capped peptides. However, for elucidating the complex redox chemistry of the two azobenzene building blocks under the reducing conditions of ligation methods, we solely applied the Boc-protected azobenzene ω-amino acid thioesters **1b** and **2b** instead of a C-terminal thioester peptide. We explored the conventional cysteine-based NCL with Cys-peptide **3**, and also screened the application of the TFA-cleavable 4,5,6-trimethoxy-2-mercaptobenzyl (Tmb) and 1-(2,4-dimethoxyphenyl)-2-mercaptoethyl auxiliaries by using peptides **4** and **5** (Figure 1) [6-8], in order to circumvent the need for the presence of a cysteine at the ligation site.

The peptide motif in peptides **3**, **4** and **5** is based on a specific binding sequence for PDZ recognition [9]. Numerous scaffolding proteins contain multiple PDZ domains for their interaction with PDZ-binding motifs at the C-terminus of transmembrane channels and receptors or other intracellular signaling proteins. Class 1 interactions involve a (S/T)-X-(V/I/L)-COOH sequence motif, and examples for these interactions include the proteins PSD-95, Fas or NHERF 1 [10]. Fas (APO-1/CD95), for example, is a cell surface receptor, belonging to the tumor-necrosis-factor receptor superfamily, which induces apoptosis. Fas-associated phosphatase-1 (FAP-1) is a Fas binding protein, which interacts with 12 to 15 of the C-terminal amino acids of the Fas receptor; however, the necessary and sufficient region for binding consists of the three C-terminal amino acids (SLV) [11-13]. PDZ-domain-containing proteins are superb examples of allosteric systems built up by semirigid domains able to interact by means of flexible regions, and therefore they seem to be ideally suited for biophysical function studies with photoswitchable ligands. For instance, Fas-associated studies in certain cells using the tripeptide SLV suggest that this small peptide alone can induce apoptosis [14,15]. Related peptides containing class I C-terminal sequence motifs, e.g., SKV, are also derived from viral origins [16]. The latter specific binding motif is associated with H5N1 influenza infections. We reasoned that the attachment of a photoswitch next to SXV PDZ-binding motifs would be a powerful strategy for exploring the function of these PDZ-binding peptide ligands in vitro and in vivo. For the synthetic ligation studies presented herein we had to place the ligation junction next to the third amino acid serine of the SKV binding motif. In the case of the conventional NCL, we used cysteine at the ligation site, and for the auxiliary mediated ligations, we decided to introduce auxiliary-glycine-conjugates at the N-terminus, due to the steric limitations of this type of ligation reaction [6-8]. After ligation, the SKV binding motif in the photoswitchable azopeptides should only be accessible in the dark *trans*-azo state (Scheme 1), whereas light switching to the *cis*-azo state should result in unfavorable interactions between the N-terminus, which follows behind the azo-switch, and the side chains that are critical for PDZ recognition (as exemplified in Scheme 1 for the 4,4'-substituted azobenzene system). However, the design presented herein, in combination with an appropriate ligation method, seems also to be applicable to the synthesis and evaluation of photoswitchable protein analogues, for example receptors with the photoswitch placed in the direct neighborhood of the specific C-terminal binding motif.

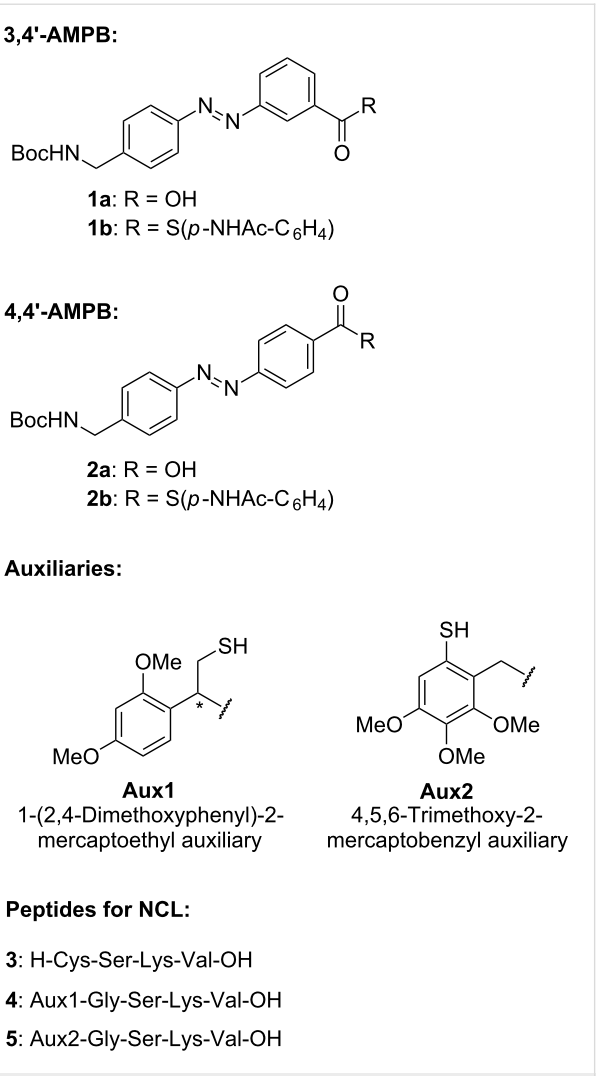

Figure 1: Structures of azobenzene thioesters, N^{α}-ligation auxiliaries and peptides for the application in ligation studies. AMPB = (aminomethylphenylazo)benzoic acid.

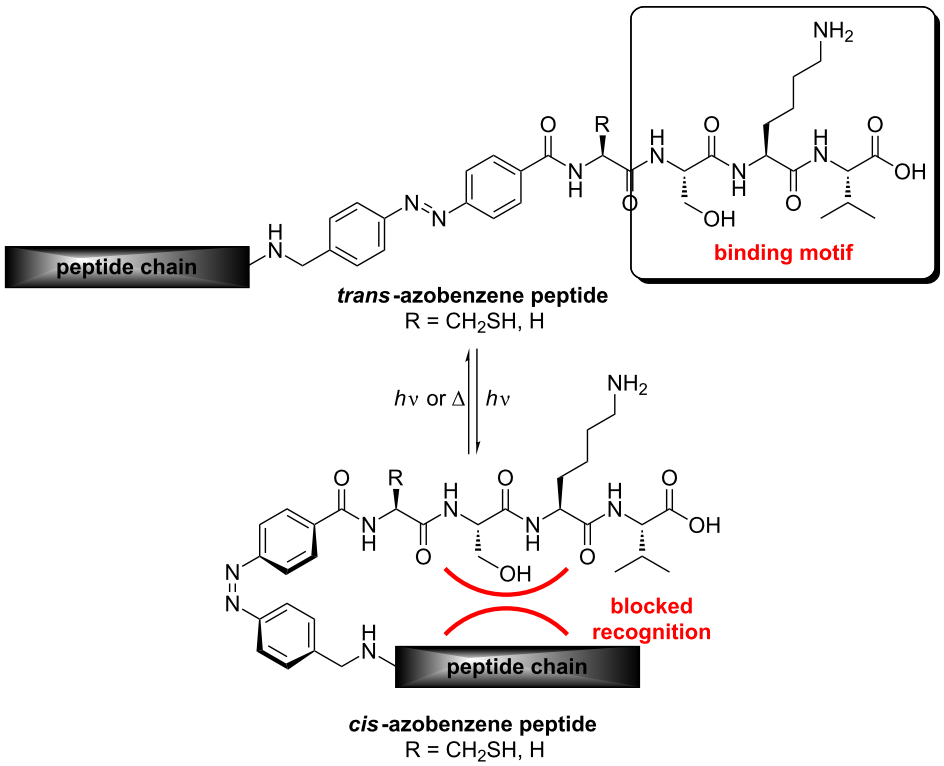

Scheme 1: Structural differences between the *trans*- and the *cis*-state of azopeptides with a SKV PDZ binding motif.

Results and Discussion

The azobenzene ω-amino-acid thioesters **1b** and **2b** were prepared by following and applying literature procedures (Supporting Information File 1) [4,17]. The syntheses of the auxiliary-linked glycine conjugates **7** and **8** were accomplished by using literature protocols developed by Dawson, Offer and MacMillan [7,8] (Figure 2).

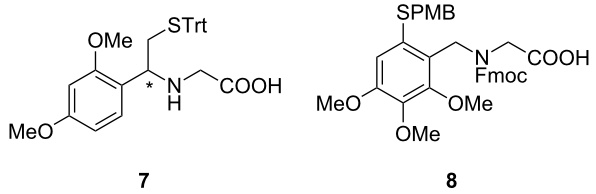

7 **8**

Figure 2: Structure of the glycine-linked auxiliary conjugates **7** and **8**.

The Cys-peptide **3** and the N^{α}-auxiliary peptides **4** and **5** were assembled on Wang resin by manual Fmoc-based peptide synthesis using standard amino-acid building blocks (Scheme 2) [4]. Commercially available preloaded Wang resin was used, and HBTU was applied as the coupling reagent in the presence of DIPEA in NMP. Removal of the temporary Fmoc-protecting group was achieved by using 20% piperidine in NMP. Cleavage

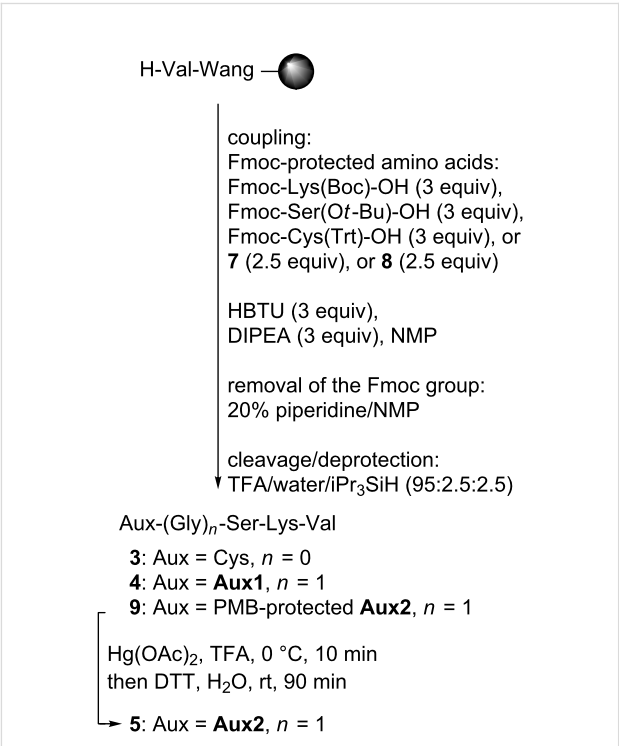

Scheme 2: Solid-phase synthesis of the ligation-mediating peptides **3**–**5**.

from the resin and removal of the permanent *tert*-butyl and trityl protecting groups was carried out with a mixture of trifluoroacetic acid, water and triisopropylsilane. The peptides **3** and **4** were purified by preparative RP-HPLC and isolated in 86% and 56% yield, respectively. Peptide **9** with a protected thiol moiety was treated with $Hg(OAc)_2$ in TFA, followed by DTT according to the literature [8], and the deprotected peptide **5** was purified by preparative RP-HPLC and isolated in 64% yield.

All attempts to ligate azobenzene ω-amino acid thioester **1b** in phosphate buffer in the presence of TCEP·HCl and guanidinium hydrochloride failed, because of the poor solubility of the azobenzene thioester in the aqueous buffer as well as in buffer/NMP mixtures. Therefore, a ligation protocol of Danishefsky et al. was applied using DMF as the solvent [18]. The ligations were realized by reaction of the appropriate peptide **3**, **4** or **5** with an excess of the azobenzene thioester (1.9 equiv), and TCEP·HCl (2.75 equiv) in the presence of Na_2HPO_4 (5.5 equiv, pH 7.3) at room temperature, and the reaction courses were monitored by analytical RP-HPLC (Supporting Information File 1). The ligation reactions were conducted under normal lighting conditions, and therefore small amounts of the *cis*-azobenzene forms of the thioesters **1b**/**2b** and of the ligation products **10**–**15** were detected during HPLC monitoring (Supporting Information File 1). The results of all ligation courses prior to purification by chromatography are summarized in Table 1.

In ligation reactions employing the N-terminal Cys-peptide **3**, nearly complete conversion was determined after five hours, but stirring was nevertheless continued overnight (Table 1, entries 1 and 4). For peptide **5** containing the 4,5,6-trimethoxy-2-mercaptobenzyl auxiliary, complete consumption of the starting material was detected after 23–24 h (Table 1, entries 3 and 6). In ligation reactions employing the N^{α}-2-mercaptoethyl auxiliary peptide **4** reaction times were doubled for complete turnover (Table 1, entries 2 and 5). These results are in accordance with a chemoselective bimolecular thioester exchange prior to the S- to N-acyl transfer through a five-membered transition state for Cys-peptide **3**, a six-membered transition state for 4,5,6-trimethoxy-2-mercaptobenzyl auxiliary peptide **5**, and a sterically more demanding five-membered transition state for racemic N^{α}-2-mercaptoethyl auxiliary peptide **4** [6].

Table 1: Cysteine- and auxiliary-based ligation courses with 3,4'-AMPB thioester **1b** and 4,4'-AMPB thioester **2b**.[a]

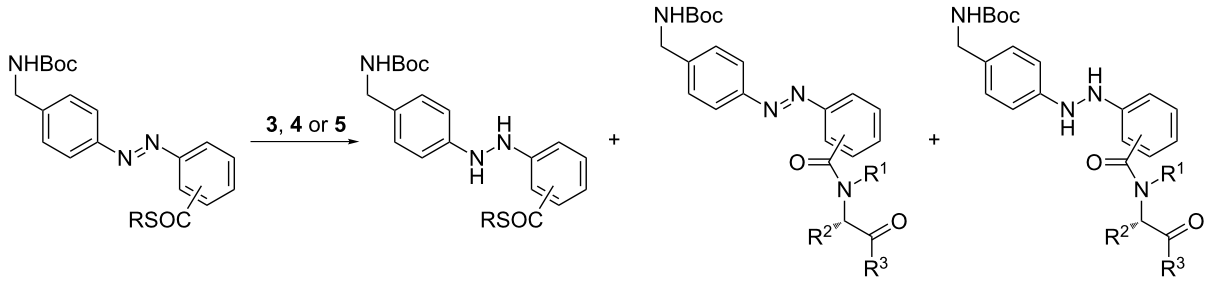

1b: *m*-COSR (3,4'-AMPB)
2b: *p*-COSR (4,4'-AMPB)
R = *p*-C_6H_4(NHAc)

Red-1b: *m*-COSR (3,4'-AMPB)
Red-2b: *p*-COSR (4,4'-AMPB)
R = *p*-C_6H_4(NHAc)

10–15

R^3 = -Ser-Lys-Val-OH

Red-10–Red-15

No.	Thioester	Peptide	Red-**1b**/**2b**[b] [%]	Product	R^1	R^2	Ratio of product/red-product[c]	Yield[d] [%]
1	**1b**	**3**	–	**10**	H	CH_2SH	69:31	62
2	**1b**	**4**	9	**11**	Aux1	H	97:3	43
3	**1b**	**5**	–	**12**	Aux2	H	100:0	38
4	**2b**	**3**	4	**13**	H	CH_2SH	52:48	44
5	**2b**	**4**	14 (12)[e]	**14**	Aux1	H	18:82 (21:79)[e]	43
6	**2b**	**5**	2	**15**	Aux2	H	90:10	45

[a]Reaction conditions: 1.9 equiv of azobenzene thioester **1b** or **2b**, TCEP·HCl (2.75 equiv), Na_2HPO_4 (5.5 equiv), DMF, rt. Peptides **3–5** were employed as the symmetric disulfides and were reduced in situ by TCEP. [b]Conversion of **1b** or **2b** to the hydrazines **Red-1b** or **Red-2b** related to the unreacted excess of **1b** or **2b** in the ligation mixture during HPLC-monitoring after the appropriate reaction time; – : **Red-1b** was not detected. [c]HPLC-based ratio determined by HPLC-monitoring after work-up and lyophilization of the crude ligation mixture. [d]Isolated yield after preparative RP-HPLC. [e]Reinvestigated ratio given in brackets.

During the reaction courses employing Cys-peptide **3** and the 4,5,6-trimethoxy-2-mercaptobenzyl auxiliary peptide **5**, only reduction of the 4,4'-AMPB thioester **2b** to the corresponding hydrazine compound **Red-2b** was observed, in 2–4% yield (Table 1). When using the N^{α}-2-mercaptoethyl auxiliary peptide **4**, reduction of both azobenzene thioesters was detected: Formation of 9% **Red-1b** was observed for the 3,4'-AMPB thioester **1b**, and of 14% **Red-2b** for 4,4'-AMPB thioester **2b**. Obviously, the excess of the azobenzene thioester prohibits reduction of the ligation products. Additional experiments showed that the yields of the ligation products could be improved by dilution of the reaction solutions with water after complete conversion of the peptide starting materials, followed by extraction of the aqueous phase with diethylether and ethyl acetate to remove 4-acetamidothiophenol (Aatp), derived from the thioesters, as well as the excess of the azobenzene thioesters **1b** and **2b**. After lyophilization, analysis of the crude products by RP-HPLC indicated the formation of varying amounts of reduced ligation peptides in five out of six cases. Severe reduction was observed in ligation reactions with Cys-peptide **3** and 3,4'-AMPB thioester **1b**, with a ratio of 69:31 peptide **10**/peptide **Red-10**, as well as 4,4'-AMPB thioester **2b**, with a ratio of 52:48 peptide **13**/peptide **Red-13** (Table 1, entries 1 and 4). Moreover, the N^{α}-2-mercaptoethyl auxiliary peptide **4** in combination with 4,4'-AMPB thioester **2b** gave peptide **14**/peptide **Red14** in an 18:82 ratio (Table 1, entry 5). However, reoxidation of the hydrazine ligation peptides **Red-10**, **Red-13** and **Red-14** to the azobenzene ligation peptides **10**, **13** and **14** was observed after purification by preparative RP-HPLC, and is obviously initiated by oxygen from the air. Finally, the pure ligated azobenzene peptides **10**, **13** and **14** were isolated in yields of 62%, 44% and 43%, respectively. When 3,4'-AMPB thioester **1b** and the N^{α}-2-mercaptoethyl auxiliary peptide **4** were used, the desired peptide **11** and its hydrazine analogue **Red-11** were detected in a ratio of 97:3 by analytical RP-HPLC (Table 1, entry 2), and peptide **11** was isolated in 43% yield after preparative RP-HPLC. In light of the reactivity of the N^{α}-2-mercaptoethyl auxiliary, reduction of the azobenzene ligation peptides derived from peptide **4** can obviously only be avoided by using 3,4'-AMPB thioester **1b**, due to the lower reactivity of the diazene unit in this thioester owing to the meta-substitution pattern.

The ligation reaction of 3,4'-AMPB thioester **1b** with the 4,5,6-trimethoxy-2-mercaptobenzyl auxiliary peptide **5** furnished ligation peptide **12** in 38% yield (Table 1, entry 3). In this case, no hydrazine species **Red-12** were detected at all (Table 1, entry 3). In addition, the ligation reaction of 4,5,6-trimethoxy-2-mercaptobenzyl auxiliary peptide **5** and 4,4'-AMPB thioester **2b** was also successfully accomplished, furnishing a ratio of 90:10 for **15**/**Red-15**, and the pure ligation product **15** was isolated in 45% yield (Table 1, entry 6). Thus, the 4,5,6-trimethoxy-2-mercaptobenzyl auxiliary applied in peptide **5** seems to be of general use for both azobenzene systems **1b** and **2b**, with a manageable tendency toward reduction in the case of the 4,4'-AMPB thioester **2b**.

The reduction sensitivity observed for the 4,4'-AMPB-derived thioester **2b** and its ligation peptides, may be rationalized by the following considerations [19,20]: The initial addition of a thiol to an electron-poor diazene double bond is a reversible reaction, furnishing a zwitterionic adduct intermediate **A** en route to an *N*-sulfenohydrazodiarene **B**, with a rather labile N–S bond (Scheme 3, reaction 1). Aliphatic thiols readily undergo adduct formation towards the *N*-sulfenohydrazodiarene intermediates **B** because of their higher nucleophilicity. Accordingly, we

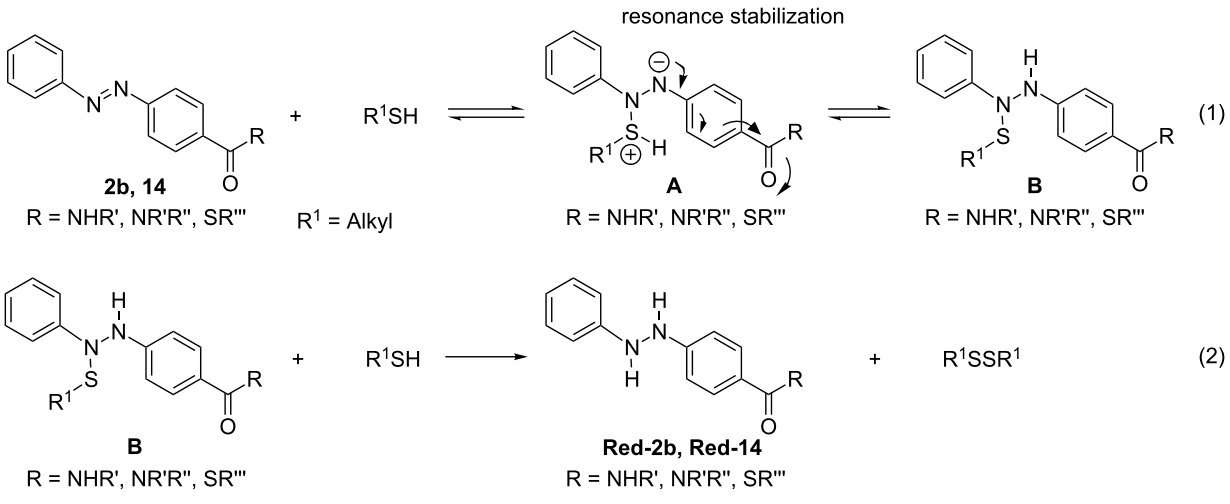

Scheme 3: Reduction of the diazene unit of 4,4'-AMPB thioesters and peptides during aliphatic thiol-based N^{α}-auxiliary ligation strategies.

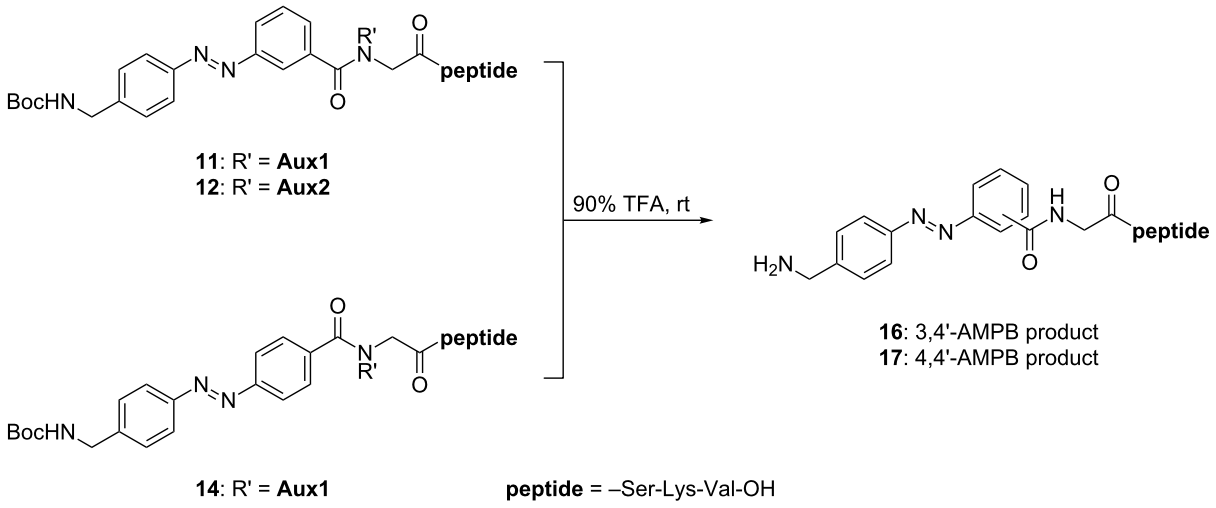

Scheme 4: Synthesis of the azopeptides **16**/**17** by final TFA cleavage of the Boc-protecting groups, and of the auxiliaries **Aux1** and **Aux2** in the ligation peptides **11**, **12** and **14**.

observe a higher tendency toward reduction when applying the aliphatic N^{α}-2-mercaptoethyl auxiliary in comparison to the aromatic 4,5,6-trimethoxy-2-mercaptobenzyl auxiliary. Furthermore, only 4,4'-substituted azobenzene systems, e.g., **2b** and peptide **14**, furnish resonance-stabilized zwitterionic intermediates **A**. Finally, reduction is completed by a nucleophilic attack of the second aliphatic thiol molecule at the *N*-sulfenohydrazodiarene **B**, yielding the symmetric disulfide and the respective hydrazine thioester or hydrazine peptide (Scheme 3, reaction 2). The reduction of diazene units by thiols has been intensively studied in the past for electron-poor azobenzenes or azodicarboxylates, en route to symmetrically and asymmetrically substituted disulfides [21-23].

The final cleavage of the Boc-protecting group, the N^{α}-2-mercaptoethyl auxiliary and the 4,5,6-trimethoxy-2-mercaptobenzyl auxiliary in the 3,4'-AMPB ligation peptides **12** and **14** was successfully achieved with 90% TFA under standard conditions furnishing peptide **16** in 94% and 89% yield, respectively, after purification by preparative RP-HPLC (Scheme 4). Similarly, the Boc-protected 4,4'-AMPB ligation peptide **14** derived from the N^{α}-2-mercaptoethyl auxiliary peptide **4** was deprotected and purified yielding peptide **17** in 81% yield.

Conclusion

In conclusion, we have demonstrated the high redox stability of the Boc-protected 3,4'-AMPB thioester **1b** when applying N^{α}-auxiliary ligation methods en route to photoswitchable peptides containing the C-terminal PDZ binding motif SKV. The positioning of the carbonyl group relative to the diazene unit in the 3,4'-AMPB-derived thioester **1b** and its peptides predictably decreases the reactivity towards unwanted redox side-reactions upon application of aliphatic as well as aromatic thiols in N^{α}-auxiliary ligation strategies using peptides **4** and **5**. In stark contrast, the Boc-protected 4,4'-AMPB thioester reproducibly furnished peptide **15** only in combination with the 4,5,6-trimethoxy-2-mercaptobenzyl auxiliary peptide **5** during the ligation course and work-up, whereas the N^{α}-2-mercaptoethyl auxiliary peptide **4** preferentially gave the hydrazine ligation peptide **Red-14** besides the azobenzene ligation peptide **14**. Our future efforts directed towards the synthesis of photoswitchable peptides will focus on water-soluble 3,4'-AMPB building blocks being applicable in native chemical ligation methods in aqueous media.

Supporting Information

Supporting Information File 1

Experimental procedures, characterization data and copies of spectra.
[http://www.beilstein-journals.org/bjoc/content/supplementary/1860-5397-8-101-S1.pdf]

Acknowledgements

We thank the Technische Universität Berlin and the Deutsche Forschungsgemeinschaft (DFG-Cluster of Excellence 314) for financial support.

References

1. Wachtveitl, J.; Zumbusch, A. *ChemBioChem* **2011,** *12,* 1169–1170. doi:10.1002/cbic.201100185
2. Renner, C.; Moroder, L. *ChemBioChem* **2006,** *7,* 868–878. doi:10.1002/cbic.200500531

3. Beharry, A. A.; Wong, L.; Tropepe, V.; Woolley, G. A. *Angew. Chem., Int. Ed.* **2011,** *50,* 1325–1327. doi:10.1002/anie.201006506
   And references cited therein.
4. Rück-Braun, K.; Kempa, S.; Priewisch, B.; Richter, A.; Seedorff, S.; Wallach, L. *Synthesis* **2009,** 4256–4267. doi:10.1055/s-0029-1217074
5. Hoppmann, C.; Schmieder, P.; Domaing, P.; Vogelreiter, G.; Eichhorst, J.; Wiesner, B.; Morano, I.; Rück-Braun, K.; Beyermann, M. *Angew. Chem., Int. Ed.* **2011,** *50,* 7699–7702. doi:10.1002/anie.201101398
6. Offer, J. *Biopolymers* **2010,** *94,* 530–541. doi:10.1002/bip.21455
7. Offer, J.; Boddy, C. N. C.; Dawson, P. E. *J. Am. Chem. Soc.* **2002,** *124,* 4642–4646. doi:10.1021/ja016731w
8. Macmillan, D.; Anderson, D. W. *Org. Lett.* **2004,** *6,* 4659–4662. doi:10.1021/ol048145o
9. Harris, B. Z.; Lim, W. A. *J. Cell Sci.* **2001,** *114,* 3219–3231.
10. Walma, T.; Spronk, C. A. E. M.; Tessari, M.; Aelen, J.; Schepens, J.; Hendriks, W.; Vuister, G. W. *J. Mol. Biol.* **2002,** *316,* 1101–1110. doi:10.1006/jmbi.2002.5402
11. Yanagisawa, J.; Takahashi, M.; Kanki, H.; Yano-Yanagisawa, H.; Tazunoki, T.; Sawa, E.; Nishitoba, T.; Kamishohara, M.; Kobayashi, E.; Kataoka, S.; Sato, T. *J. Biol. Chem.* **1997,** *272,* 8539–8545. doi:10.1074/jbc.272.13.8539
12. Freiss, G.; Chalbos, D. *Anti-Cancer Agents Med. Chem.* **2011,** *11,* 78–88.
13. Subbaiah, V. K.; Kranjec, C.; Thomas, M.; Banks, L. *Biochem. J.* **2011,** *439,* 195–205. doi:10.1042/BJ20110903
14. Ungefroren, H.; Kruse, M.-L.; Trauzold, A.; Roeschmann, S.; Roeder, C.; Arlt, A.; Henne-Bruns, D.; Kalthoff, H. *J. Cell Sci.* **2001,** *114,* 2735–2746.
15. Huang, W.; Zhu, C.; Wang, H.; Horvath, E.; Eklund, E. A. *J. Biol. Chem.* **2008,** *283,* 7921–7935. doi:10.1074/jbc.M706710200
16. Javier, R. T.; Rice, A. P. *J. Virol.* **2011,** *85,* 11544–11556. doi:10.1128/JVI.05410-11
17. Priewisch, B.; Rück-Braun, K. *J. Org. Chem.* **2005,** *70,* 2350–2352. doi:10.1021/jo048544x
18. Wu, B.; Chen, J.; Warren, J. D.; Chen, G.; Hua, Z.; Danishefsky, S. J. *Angew. Chem., Int. Ed.* **2006,** *45,* 4116–4125. doi:10.1002/anie.200600538
19. Linke, K.-H.; Brandt, W.; Göhausen, H. J. *Chem. Ber.* **1973,** *106,* 707–712. doi:10.1002/cber.19731060235
20. Boulègue, C.; Löweneck, M.; Renner, C.; Moroder, L. *ChemBioChem* **2007,** *8,* 591–594. doi:10.1002/cbic.200600495
21. Mukaiyama, T.; Takahashi, K. *Tetrahedron Lett.* **1968,** *9,* 5907–5908. doi:10.1016/S0040-4039(00)75437-2
22. Wünsch, E.; Moroder, L.; Romani, S. *Hoppe-Seyler's Z. Physiol. Chem.* **1982,** *363,* 1461–1464. doi:10.1515/bchm2.1982.363.2.1461
23. Kosower, E. M.; Kanety-Londner, H. *J. Am. Chem. Soc.* **1976,** *98,* 3001–3007. doi:10.1021/ja00426a054

License and Terms

Beilstein Journal of Organic Chemistry

Multistep organic synthesis of modular photosystems

Naomi Sakai* and Stefan Matile*

Review

Open Access

Address:
Department of Organic Chemistry, University of Geneva, Geneva, Switzerland

Email:
Naomi Sakai* - naomi.sakai@unige.ch;
Stefan Matile* - stefan.matile@unige.ch

* Corresponding author

Keywords:
asparagusic acid; charge-transfer cascades; chromophores; disulfide exchange; hydrazone exchange; molecular switches; naphthalenediimides; π-stacks; surface-initiated polymerization

Beilstein J. Org. Chem. **2012,** *8,* 897–904.
doi:10.3762/bjoc.8.102

Received: 18 February 2012
Accepted: 09 May 2012
Published: 19 June 2012

This article is part of the Thematic Series "Molecular switches and cages".

Guest Editor: D. Trauner

Abstract

Quite extensive synthetic achievements vanish in the online supporting information of publications on functional systems. Underappreciated, their value is recognized by experts only. As an example, we here focus in on the recent synthesis of multicomponent photosystems with antiparallel charge-transfer cascades in co-axial hole- and electron-transporting channels. The synthetic steps are described one-by-one, starting with commercial starting materials and moving on to key intermediates, such as asparagusic acid, an intriguing natural product, as well as diphosphonate "feet", and panchromatic naphthalenediimides (NDIs), to finally reach the target molecules. These products are initiators and propagators for self-organizing surface-initiated polymerization (SOSIP), a new method introduced to secure facile access to complex architectures. Chemoorthogonal to the ring-opening disulfide exchange used for SOSIP, hydrazone exchange is then introduced to achieve stack exchange, which is a "switching" technology invented to drill giant holes into SOSIP architectures and fill them with functional π-stacks of free choice.

Introduction

The architecture of photosystem **1** is rather sophisticated, probably as sophisticated as it gets with photosystems today (Figure 1) [1]. It is composed of three co-axial π-stacks that are grown from an indium tin oxide (ITO) surface. With lower frontier molecular orbital (FMO) levels, the "yellow" stacks can transport photogenerated electrons toward the ITO surface along the gradient in their LUMO. With higher FMO levels, the "red" stacks can transport holes along the gradient in their HOMOs in the opposite direction, away from the ITO surface.

The double-channel architecture **1** with antiparallel redox gradients has been referred to as OMARG-SHJ, that is supra-

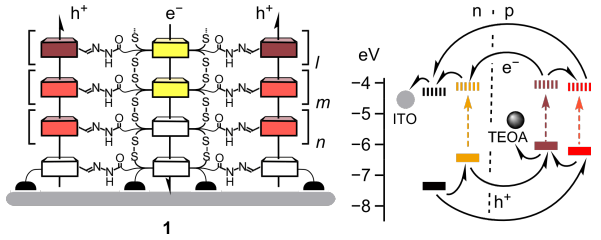

Figure 1: Schematic structure of photosystem **1** on indium tin oxide (ITO, grey) with antiparallel gradients in hole (p, h^+) and electron (n, e^-) transporting coaxial channels. HOMO (solid) and LUMO levels (dashed) of all components (color coded) are indicated in eV against vacuum (−5.1 eV for Fc/Fc^+), including triethanolamine (TEOA), used as mobile hole transporter.

molecular n/p-heterojunctions with oriented multicomponent/color antiparallel redox gradients [2,3]. With n/p contact areas maximized down to the molecular level, photoinduced charge separation (i.e., charge generation) should be as favorable as directional charge translocation (i.e., charge separation) along redox gradients in the molecular channels. With photosystem **1**, these high expectations could finally be tested experimentally [1]. OMARG-SHJs turned out to be best quantified with bimolecular charge recombination efficiencies η_{BR}, that is, losses in photonic energy. Photosystem **1** gave η_{BR} = 22%; gradient-free controls gave η_{BR} = 50%; destructive gradients gave η_{BR} = 76%. These results are very satisfactory. They also confirmed that significant synthetic efforts to build sophisticated functional architectures can be worthwhile. In the original communication, these synthetic efforts completely disappeared in the online supporting information [1]. The fact that results on synthesis are self-explanatory to all and do not require much discussion can be considered as a marvelous illustration of the success of the field. However, to illustrate the frequent lack of appreciation of the synthetic organic chemistry in work on functional systems, the total synthesis of photosystem **1** will be described step-by-step in the following.

Results and Discussion

Synthesis of initiators

Photosystem **1** is constructed from the molecular building blocks **2**–**6** (Schemes 1-3). Initiator **2** is composed of a central naphthalenediimide (NDI) [4-19] to act as a template for the central stack and two peripheral NDIs to act as templates for stack exchange. They are embedded into hydrogen-bonded networks, to assure self-organization, and four geminal diphosphonates [20,21] for tetravalent anchoring on the ITO surface.

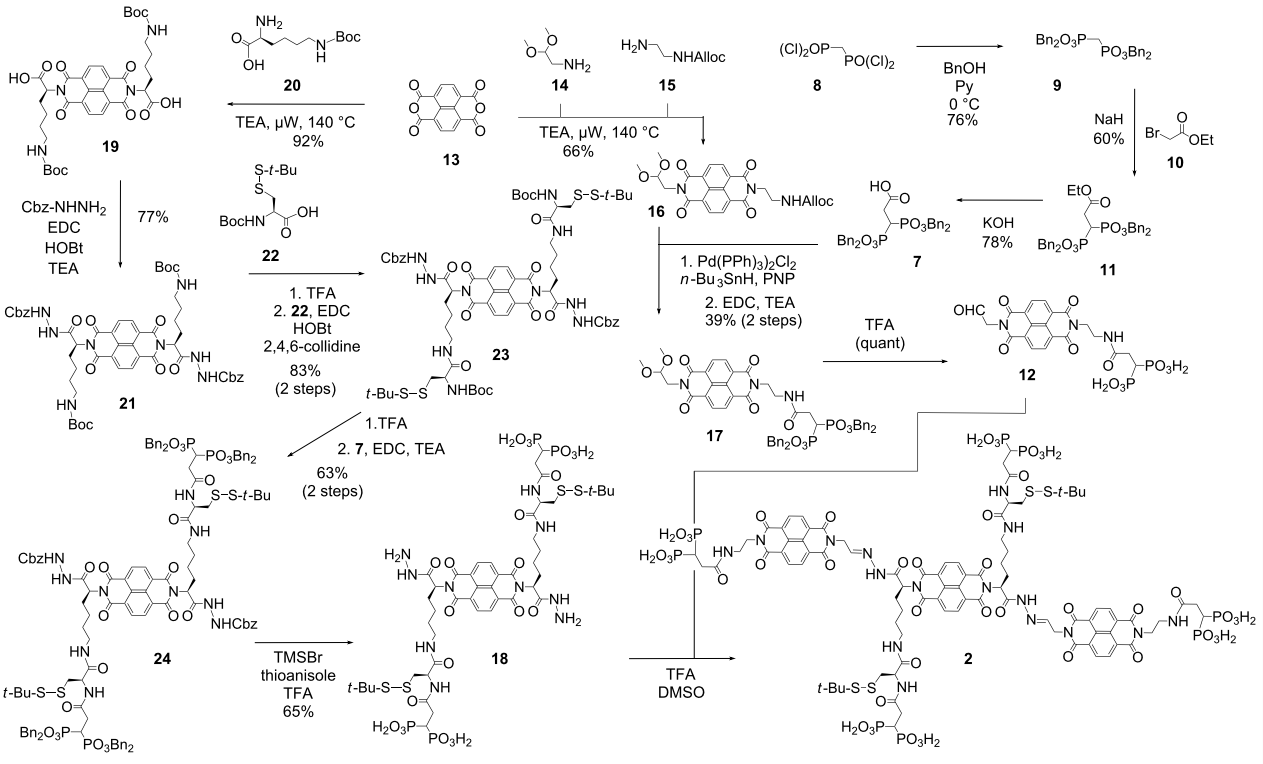

Scheme 1: Synthesis of initiator **2**.

The geminal diphosphonates **7** were synthesized from methylene bis(phosphonic dichloride) **8** (Scheme 1) [20,21]. Conversion with benzyl alcohol and pyridine as a base yielded tetrabenzyl methylene bisphosphonate **9**. Activation with sodium hydride and alkylation with ethyl bromoacetate (**10**) gave ethyl ester **11**, and final ester hydrolysis lead to the desired acid **7**.

The peripheral NDIs **12**, designed to template for stack exchange on initiator **2**, were prepared from naphthalenedianhydride (NDA) **13**. Microwave-assisted imidation [15] with the two amines **14** and **15** at 140 °C gave the mixed diimide **16** in excellent 66% yield together with the symmetric diimide side products. Amines were liberated by palladium-catalyzed Alloc removal and reacted with acid **7**. The obtained amide **17** was deprotected with acid to afford the desired aldehyde **12**.

The central NDI **18** of initiator **2**, designed to initiate and template for SOSIP, was accessible from NDA **13** as well. The synthesis of NDI **19** by microwave-assisted imidation with Boc-protected lysine **20** has been reported before in the literature [15]. Reaction with Cbz-hydrazine gave the Cbz-protected NDI hydrazide **21**. After chemoselective, acid-catalyzed deprotection, the liberated amines were coupled with the Boc-protected cysteine *tert*-butyl disulfide **22**. The obtained amide **23** was treated with TFA for Boc removal and coupled with the geminal diphosphonate foot **7**. Deprotection of both hydrazides and diphosphonates in NDI **24** gave **18**, which was reacted in situ with NDI **12** to yield initiator **2**.

Synthesis of propagators

The synthesis of propagator **3** starts with NDA **13** as well (Scheme 2). Diimidation with Cbz-protected lysine **25** gave the diacid **26**. Activation with EDC, HOBt and TEA was followed by the reaction with *tert*-butyl carbazate under mild conditions. The protected hydrazide **27** was obtained in 59% yield over two steps. The Cbz protecting groups were removed chemoselectively by hydrogenolysis over Pd–C in the presence of acetic acid, and the obtained diamine was reacted with the activated asparagusic acid **28**. Hydrazide deprotection in NDI **29** and in situ hydrazone formation with benzaldehyde **30** gave propagator **3**.

In contrast to propagator **3**, propagator **4** is constructed around a yellow, core-substituted cNDI fluorophore. Nevertheless, the synthesis of this target molecule also starts with NDA **13**. Bromination in the core with dibromocyanuric acid (**31**) afforded an intractable mixture containing the 2,6-dibromo NDA **32** together with lower and higher homologues [16]. However, pure product **33** could be readily isolated from this mixture after transformation of the NDAs into the core-substituted naphthalenetetraesters (cNTEs). Nucleophilic core-substitution with ethanolate gave cNTE **34** as described in the literature [16].

NTE **34** was subjected to basic ester hydrolysis followed by diimidation with lysine **25**. From this point, the synthesis of cNDI propagator **4** was analogous to the synthesis of NDI propagator **3**. Reaction of EDC-activated diacid **35** with *tert*-butyl

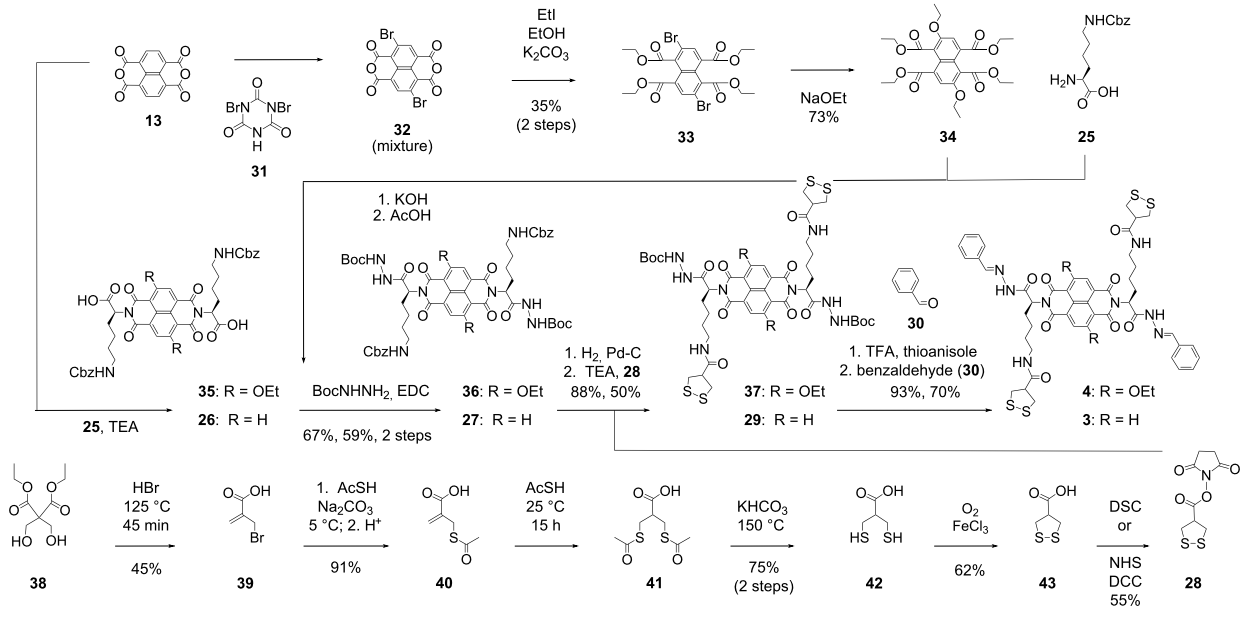

Scheme 2: Synthesis of propagators **3** and **4**.

carbazate followed by deprotection of the obtained cNDI **36** and coupling with activated asparagusic acid **28** gave cNDI **37**. Hydrazide deprotection quenched by benzaldehyde **30** gave the yellow cNDI propagator **4**.

The activated asparagusic acid **28** was prepared by following literature procedures [22-25]. In the first step from bis(hydroxymethyl)malonate **38**, simple nucleophilic substitution is coupled with an ester hydrolysis and a debrominative decarboxylation. Another nucleophilic substitution with thioacetate converted bromide **39** into thioester **40**. Addition of a second thioacetate gave dithioester **41**, which was hydrolyzed with a base. Oxidation of dithiol **42** with molecular oxygen gave asparagusic acid (**43**), which is the natural product that contributes to the characteristic odor of asparagus. Activation with NHS gave the ester **28**, ready for coupling with amines, such as **27** or **36**.

Synthesis of stack exchangers

The synthesis of the red cNDIs **5** and **6** for stack exchange was possible in very few steps starting from available synthetic intermediates (Scheme 3). cNDI **5**, with one bromo and one alkylamino substituent in the core, was prepared from crude dibromo cNDA **32**. Microwave-assisted reaction [15] with amines **14** and **15** gave the mixed cNDI **44** together with the symmetric side products. The obtained mixture of 2,6- and 3,7-regioisomers was not separated throughout the entire synthesis of photosystem **1**. Nucleophilic aromatic substitution with isopropylamine for 10 min at room temperature gave the red cNDI **45**, which was followed by deprotection with acid to give the target aldehyde **5**.

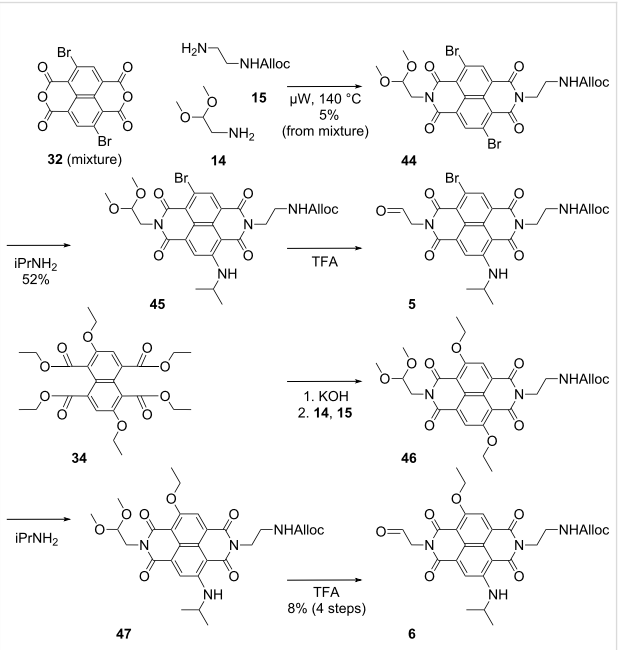

Scheme 3: Synthesis of stack exchangers **5** and **6**. Compounds **5**, **6**, **45** and **47** are mixtures of 2,6- and 3,7-regioisomers.

The more pinkish cNDI **6** was synthesized from the cNTE **34** following the procedure developed for cNDI **5**. Diimide formation with amines **14** and **15** followed by core substitution of the mixed cNDI **46** and deprotection of the red cNDI **47** gave the desired aldehyde **6**.

Self-organizing surface-initiated polymerization

With the five building blocks **2**–**6** in hand, the solid-phase synthesis of photosystem **1** on ITO surfaces could be launched. ITO was first cleaned with RCA solution, that is, a boiling 5:1:1 mixture of water, 24% NH_4OH and 30% H_2O_2, and then rinsed with bidistilled water and EtOH, and dried. Then the ITO was immersed in a 3 mM solution of initiator **2** in DMSO for 2 days. The formation of monolayers of **48** on ITO electrodes was followed by the inhibition of potassium ferricyanide reduction in solution, and by absorption spectroscopy (Scheme 4). The obtained monolayers of **48** were annealed for 1 h in the oven at 120 °C. These conditions are known to improve the covalent bonding between phosphonic acids and the ITO substrate [26].

The disulfide protecting groups on the surface of monolayer **48** were removed with DTT to afford free thiols on the surface of monolayer **49**. For SOSIP [18,19], the concentration of propagators had to be optimized to a critical SOSIP concentration, c_{SOSIP}. Below c_{SOSIP}, ring-opening disulfide-exchange polymerization [27] does not occur, whereas above c_{SOSIP}, the polymerization occurs everywhere, not only on the surface but also in solution. To determine c_{SOSIP}, ITO plates with and without activated initiators were incubated together in the same solution of propagators. The amount of polymers either grown from the ITO surface or deposited on the ITO surface by precipitation during polymerization in solution was determined by absorption spectroscopy. Plots of the absorption of the electrode as a function of the concentration of the propagator in solution revealed both c_{SOSIP}, the critical concentration needed for SOSIP, and c_{SOL}, the critical concentration needed for polymerization in solution. Operational SOSIP was demonstrated with $c_{SOSIP} < c_{SOL}$, and failure of SOSIP with $c_{SOSIP} = c_{SOL}$. Both c_{SOSIP} and c_{SOL} depended strongly on the conditions, i.e., the concentration and nature of the base catalyst, the nature of initiator and propagator, the temperature, the presence of oxygen in the solution and, most importantly, the composition of the solvent mixture used.

For propagator **3**, c_{SOSIP} = 3.5 mM was found in a 1:1 mixture of chloroform and methanol with 100 mM DIPEA as a base catalyst. Incubation of monolayer **49** in this solution gave

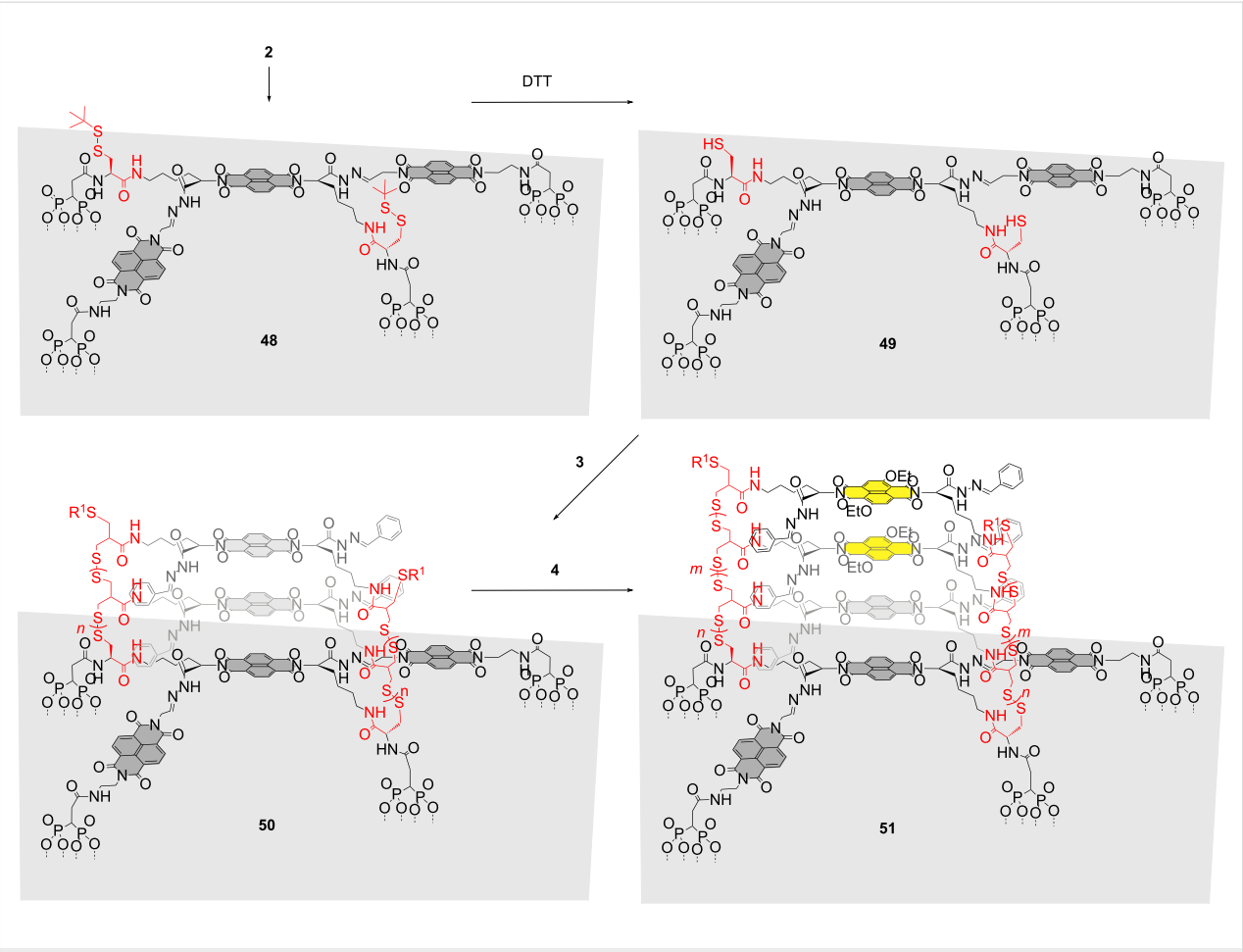

Scheme 4: Synthesis of photosystem **1**, self-organizing surface-initiated polymerization (SOSIP). R^1 = SH (**50**) or oxidized derivative (**51**), grey surface = ITO. Dotted lines from diphosphonate groups indicate the bonds to the ITO surface. The polymer structures are generalized and idealized structures, which are consistent with the experimental results. They will naturally contain defects.

SOSIP architecture **50**. To add the yellow stacks in photosystem **1**, photosystem **50** was incubated with propagator **4** at c_{SOSIP} = 7 mM in chloroform/methanol (1:1) with 100 mM DIPEA. The obtained oriented diblock disulfide polymers **51** were characterized by the absorption of colorless NDIs at 385 nm and the absorption of yellow cNDIs at 470 nm. Assuming regular growth, these absorptions provided a meaningful approximation of the average composition *n* and *m* of the poly(disulfide) [27].

Stack exchange

Stack exchange within the resulting SOSIP photosystem **51** was initiated with excess hydroxylamine (Scheme 5). The chemoorthogonality of disulfide and hydrazone exchange has been demonstrated previously by several groups [28-31]. Benzaldehyde removal as oxime was followed by HPLC. The hydrazide-rich pores produced in the resulting architecture **52** were first filled by reversible covalent capture of the red cNDI aldehyde **5**.

Stack exchange was easily detectable by comparison of the respective maxima in the absorption spectra. Exchange of the benzaldehyde hydrazones in photosystem **51** with NDIs occurred with an excellent 75–95% yield. Moreover, the yield of stack exchange was nearly independent of the thickness of the photosystem. Control experiments revealed that in the case of initiators without extra NDI templates, the yield drops to 40% for thin photosystems and further decreases with increasing thickness to an irrelevant 25%. This significant difference demonstrates the central importance of templated synthesis for successful stack exchange.

To engineer antiparallel gradients into the red stack of photosystem **53**, partial stack exchange was envisioned. A part of the red cNDI stack, *l*, was removed by brief treatment with hydroxylamine. The produced, shallower holes in photosystem **54** were filled with cNDI aldehyde **6**. The desired photosystem **1** with antiparallel redox gradients in coaxial hole- and electron-transporting channels was obtained.

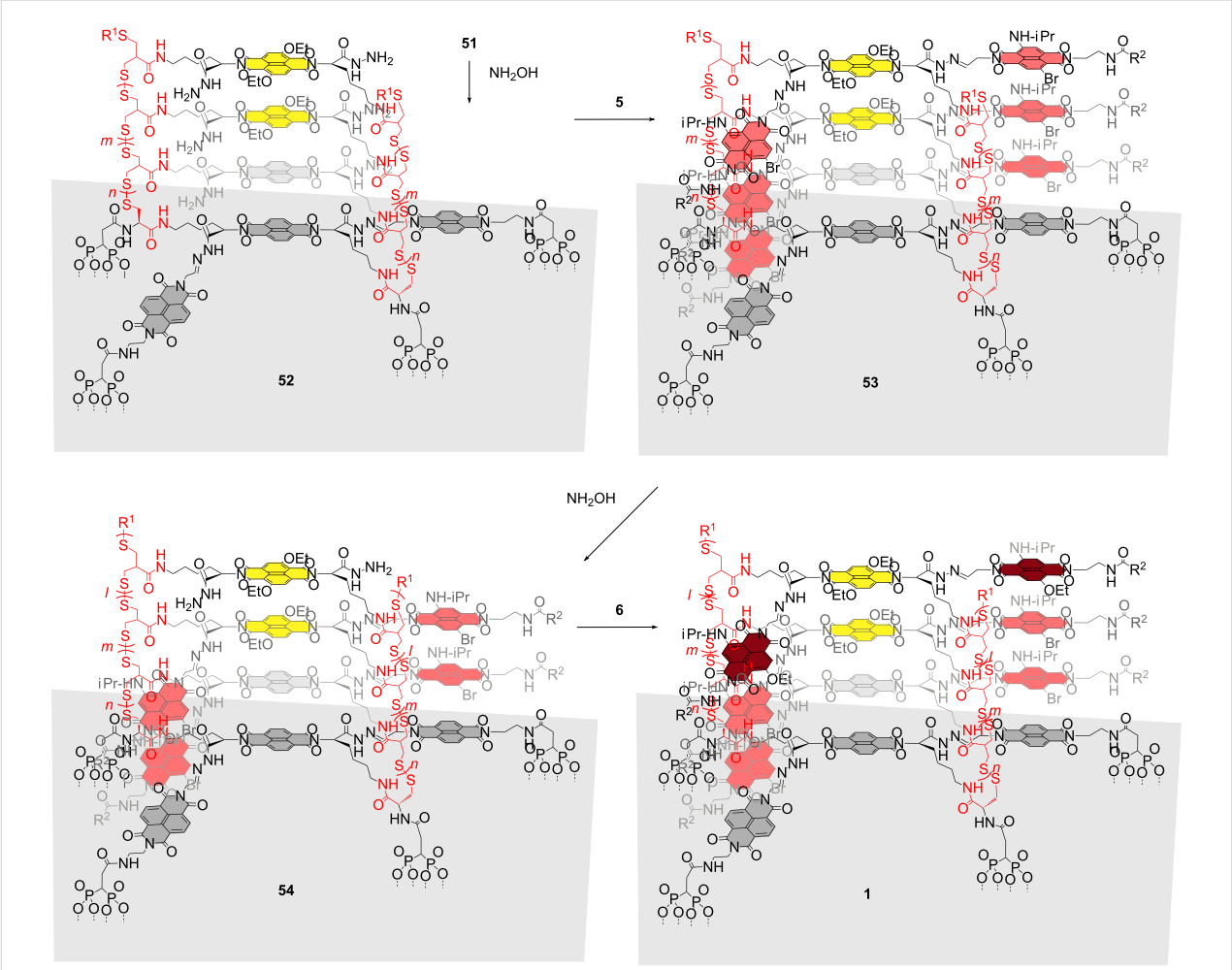

Scheme 5: Synthesis of photosystem **1**, stack exchange. R^1 = SH or oxidized derivative, R^1 = CH_2CHCH_2. **5** and **6** are mixtures of 2,6- and 3,7-regioisomers.

Graphical summary of complex transformations

Both SOSIP and post-SOSIP stack exchange can be quite complicated to follow in complete molecular structures (Scheme 4 and Scheme 5). We thus summarize both processes in schematic form (Scheme 6). To recapitulate briefly from this perspective, we repeat that the solid-phase synthesis begins with the deposition of initiator **2** on ITO. Activation of monolayer **48** with DTT produces monolayer **49** with free thiols on the surface. Recognition of propagators **3** on the surface of **49** places the strained disulfides of asparagusic acid right on top of the activated thiolates on the surface. Covalent capture by ring-opening disulfide exchange generates new thiolates on the surface of the growing photosystem **55** for continuing SOSIP. The obtained ladderphane **50** is then treated with propagator **4**. Ring-opening disulfide exchange SOSIP via intermediates **56** leads to photosystem **51** with a two-component redox gradient in the π-stack.

Post-SOSIP stack exchange is then initiated by benzaldehyde removal as oxime **57**. The giant pores drilled into photosystem **52** are first filled completely with red cNDI **5**. Subsequently, the partial removal of the new stack in photosystem **53** as oxime **58** and covalent capture of **6** in the more shallow pores in photosystem **54** affords the desired double-gradient photosystem **1**.

Conclusion

The objective of this brief highlight was to exemplify the synthetic efforts that are often hidden behind short papers on functional systems. Quite extensive multistep synthesis has been covered, followed by innovative surface-initiated polymerization and chemoorthogonal dynamic covalent chemistry. The excellent properties obtained confirm that significant synthetic efforts to build more sophisticated functional systems can be justified and rewarding. In this research, multistep organic synthesis is the means rather than the end. Therefore, the main difference from research dedicated to synthetic methodology is

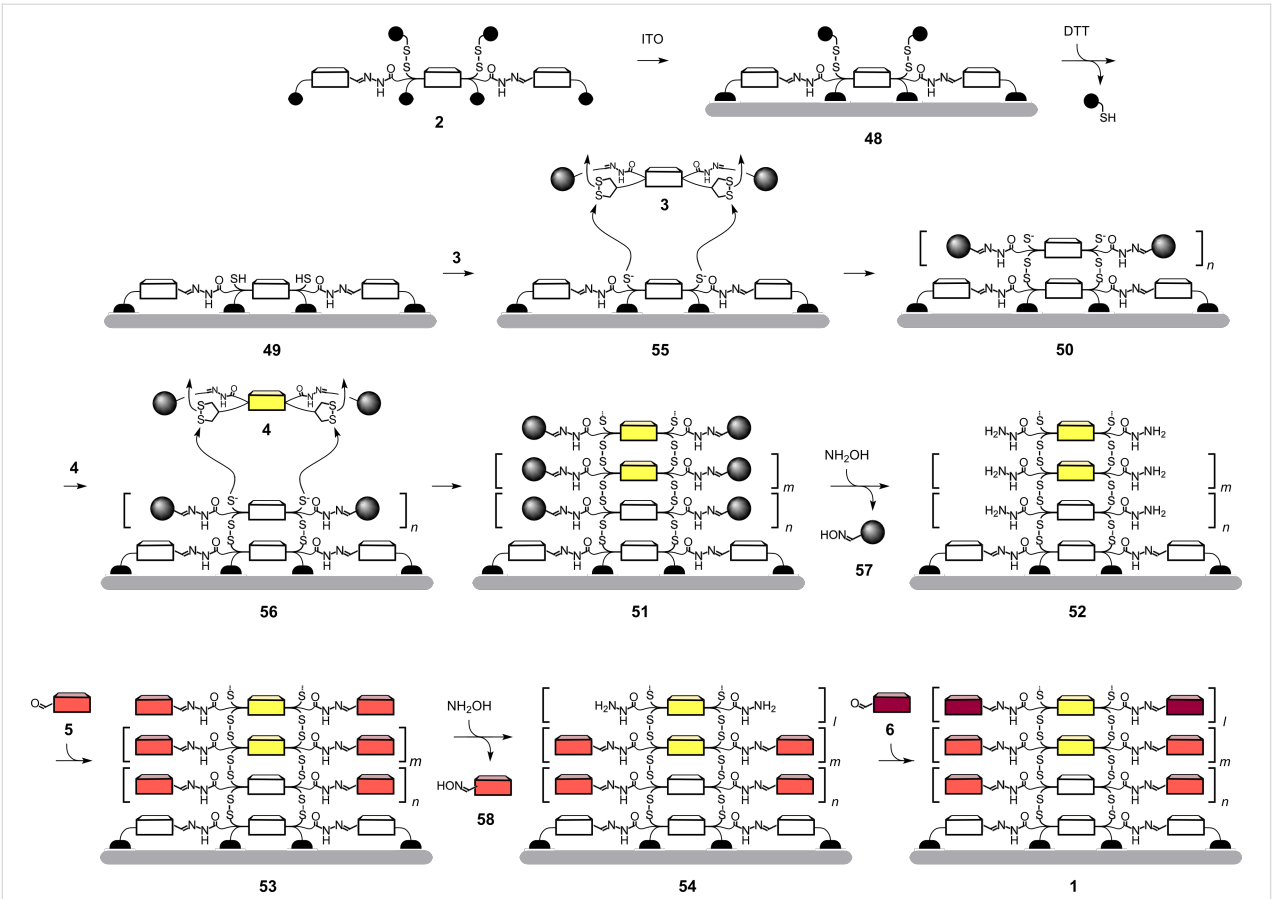

Scheme 6: Schematic overview over SOSIP and stack exchange.

that the individual steps often remain unoptimized as long as the level reached is sufficient to produce large enough amounts of the target molecule without extensive effort and cost. However, the quality, timeliness and beauty of the transformations employed are the same, as is the pleasure of occasional contributions to improve or innovate in the field of organic synthesis.

Acknowledgements

We thank the University of Geneva, the European Research Council (ERC Advanced Investigator), the National Centre of Competence in Research (NCCR) Chemical Biology and the Swiss NSF for financial support.

References

1. Sakai, N.; Matile, S. *J. Am. Chem. Soc.* **2011,** *133,* 18542–18545. doi:10.1021/ja207587x
2. Bhosale, R.; Míšek, J.; Sakai, N.; Matile, S. *Chem. Soc. Rev.* **2010,** *39,* 138–149. doi:10.1039/b906115k
3. Sakai, N.; Bhosale, R.; Emery, D.; Mareda, J.; Matile, S. *J. Am. Chem. Soc.* **2010,** *132,* 6923–6925. doi:10.1021/ja101944r
4. Sakai, N.; Mareda, J.; Vauthey, E.; Matile, S. *Chem. Commun.* **2010,** *46,* 4225–4237. doi:10.1039/c0cc00078g
5. Bhosale, S. V.; Jani, C. H.; Lalander, C. H.; Langford, S. J.; Nerush, I.; Shapter, J. G.; Villamaina, D.; Vauthey, E. *Chem. Commun.* **2011,** *47,* 8226–8228. doi:10.1039/c1cc11318f
6. Hu, Y.; Gao, X.; Di, C.; Yang, X.; Zhang, F.; Liu, Y.; Li, H.; Zhu, D. *Chem. Mater.* **2011,** *23,* 1204–1215. doi:10.1021/cm102850j
7. Gabutti, S.; Knutzen, M.; Neuburger, M.; Schull, G.; Berndt, R.; Mayor, M. *Chem. Commun.* **2008,** 2370–2372. doi:10.1039/b719796a
8. Jones, B. A.; Facchetti, A.; Wasielewski, M. R.; Marks, T. J. *J. Am. Chem. Soc.* **2007,** *129,* 15259–15278. doi:10.1021/ja075242e
9. Molla, M. R.; Das, A.; Ghosh, S. *Chem.–Eur. J.* **2010,** *16,* 10084–10093. doi:10.1002/chem.201000596
10. Nakamura, M.; Okaue, T.; Takada, T.; Yamana, K. *Chem.–Eur. J.* **2012,** *18,* 196–201. doi:10.1002/chem.201102216
11. Guha, S.; Goodson, F. S.; Roy, S.; Corson, L. J.; Gravenmier, C. A.; Saha, S. *J. Am. Chem. Soc.* **2011,** *133,* 15256–15259. doi:10.1021/ja2055726
12. Chaignon, F.; Falkenström, M.; Karlsson, S.; Blart, E.; Odobel, F.; Hammarström, L. *Chem. Commun.* **2007,** 64–66. doi:10.1039/b615085c
13. Alvey, P. M.; Reczek, J. J.; Lynch, V.; Iverson, B. L. *J. Org. Chem.* **2010,** *75,* 7682–7690. doi:10.1021/jo101498b
14. Shukla, D.; Nelson, S. F.; Freeman, D. C.; Rajeswaran, M.; Ahearn, W. G.; Meyer, D. M.; Carey, J. T. *Chem. Mater.* **2008,** *20,* 7486–7491. doi:10.1021/cm802071w
15. Pengo, P.; Pantos, G. D.; Otto, S.; Sanders, J. K. M. *J. Org. Chem.* **2006,** *71,* 7063–7066. doi:10.1021/jo061195h

16. Kishore, R. S. K.; Kel, O.; Banerji, N.; Emery, D.; Bollot, G.; Mareda, J.; Gomez-Casado, A.; Jonkheijm, P.; Huskens, J.; Maroni, P.; Borkovec, M.; Vauthey, E.; Sakai, N.; Matile, S. *J. Am. Chem. Soc.* **2009,** *131,* 11106–11116. doi:10.1021/ja9030648
17. Thalacker, C.; Röger, C.; Würthner, F. *J. Org. Chem.* **2006,** *71,* 8098–8105. doi:10.1021/jo0612269
18. Sakai, N.; Lista, M.; Kel, O.; Sakurai, S.; Emery, D.; Mareda, J.; Vauthey, E.; Matile, S. *J. Am. Chem. Soc.* **2011,** *133,* 15224–15227. doi:10.1021/ja203792n
19. Lista, M.; Areephong, J.; Sakai, N.; Matile, S. *J. Am. Chem. Soc.* **2011,** *133,* 15228–15231. doi:10.1021/ja204020p
20. Page, P. C. B.; McKenzie, M. J.; Gallagher, J. A. *J. Org. Chem.* **2001,** *66,* 3704–3708. doi:10.1021/jo001489h
21. Page, P. C. B.; McKenzie, M. J.; Gallagher, J. A. *Synth. Commun.* **2002,** *32,* 211–218. doi:10.1081/SCC-120002004
22. Singh, R.; Whitesides, G. M. *J. Am. Chem. Soc.* **1990,** *112,* 1190–1197. doi:10.1021/ja00159a046
23. Danehy, J. P.; Elia, V. J. *J. Org. Chem.* **1972,** *37,* 369–373. doi:10.1021/jo00968a008
24. Schotte, L.; Ström, H. *Acta Chem. Scand.* **1956,** *10,* 687–688. doi:10.3891/acta.chem.scand.10-0687
25. Unger, F. M.; Liehl, E. 1,2-dithiolan derivatives, process for their production pharmaceutical compositions containing them and their use. GB Patent Application GB2148296A, May 30, 1985.
26. Paniagua, S. A.; Hotchkiss, P. J.; Jones, S. C.; Marder, S. R.; Mudalige, A.; Marrikar, F. S.; Pemberton, J. E.; Armstrong, N. R. *J. Phys. Chem. C* **2008,** *112,* 7809–7817. doi:10.1021/jp710893k
27. Bang, E.-K.; Lista, M.; Sforazzini, G.; Sakai, N.; Matile, S. *Chem. Sci.* **2012,** *3,* 1752–1763. doi:10.1039/C2SC20098H
28. Rodriguez-Docampo, Z.; Otto, S. *Chem. Commun.* **2008,** 5301–5303. doi:10.1039/B808725C
29. von Delius, M.; Geertsema, E. M.; Leigh, D. A. *Nat. Chem.* **2010,** *2,* 96–101. doi:10.1038/nchem.481
30. Corbett, P. T.; Leclaire, J.; Vial, L.; West, K. R.; Wietor, J.-L.; Sanders, J. K. M.; Otto, S. *Chem. Rev.* **2006,** *106,* 3652–3711. doi:10.1021/cr020452p
31. Skene, W. G.; Lehn, J.-M. P. *Proc. Natl. Acad. Sci. U. S. A.* **2004,** *101,* 8270–8275. doi:10.1073/pnas.0401885101

License and Terms

Beilstein Journal of Organic Chemistry

Diarylethene-modified nucleotides for switching optical properties in DNA

Sebastian Barrois and Hans-Achim Wagenknecht*

Full Research Paper

Open Access

Address:
Karlsruhe Institute of Technology (KIT), Institute for Organic Chemistry, Fritz-Haber-Weg 6, 76131 Karlsruhe, Germany

Email:
Hans-Achim Wagenknecht* - Wagenknecht@kit.edu

* Corresponding author

Keywords:
absorption; cross coupling; molecular switches; oligonucleotide; palladium; photochromism

Beilstein J. Org. Chem. **2012,** *8,* 905–914.
doi:10.3762/bjoc.8.103

Received: 12 March 2012
Accepted: 09 May 2012
Published: 20 June 2012

This article is part of the Thematic Series "Molecular switches and cages".

Guest Editor: D. Trauner

Abstract

Diarylethenes were attached to the 5-position of 2'-deoxyuridine in order to yield three different photochromic nucleosides. All nucleosides were characterized with respect to their absorption and photochromic properties. Based on these results, the most promising photochromic DNA base modification was incorporated into representative oligonucleotides by using automated phosphoramidite chemistry. The switching of optical properties in DNA can be achieved selectively at 310 nm (forward) and 450 nm (backward); both wavelengths are outside the normal nucleic acid absorption range. Moreover, this nucleoside was proven to be photochemically stable and allows switching back and forth several times. These results open the way for the use of diarylethenes as photochromic compounds in DNA-based architectures.

Introduction

The well-defined photoinduced switching of the optical and electronic properties of molecular components represents an increasingly significant goal for the development of new photoreactive nanostructured architectures. Among those architectures, nucleic acids were proven to be an important scaffold for the precise arrangement of all kinds of chromophores inside or along the double helix [1-4]. Nucleic acids are synthesized by building blocks; in this bottom-up approach artificial functionalities, such as photoswitches, can be introduced synthetically by providing the corresponding artificial DNA building block. Among the known and structurally diverse photochromic compounds [5-8], azobenzenes [9], spirobenzopyrans [10] and diarylethenes [11] represent the most promising candidates for introducing photoswitching functionality into biopolymers, and thereby for regulating biological activity [12,13]. Azobenzenes were designed and synthesized as artificial photoswitchable components in nucleic acids and are suitable for the control of a variety of different biological functions. The photoinduced cis–trans isomerization of azobenzene nucleosides can reversibly switch between the formation and dissociation of

DNA duplexes [14-17], photoregulate DNA polymerase reaction [18], photocontrol DNA triplex formation [19], and drive photon-fueled DNA-based nanomachines [20,21].

Concerning the extent of structural change, the cis–trans isomerization of azobenzenes behaves much simpler than the ring opening of spiropyrans to merocyanines. In the latter case not only is a structural change observed but a large change in polarity is yielded additionally [10,22]. It is expected that the ring-closed spiropyran form of this molecular switch does not insert into the base stack due to its twisted structure, but the open merocyanine form could intercalate based on its planarity and polarity. This assumption was experimentally verified by synthetic spiropyrans as noncovalent DNA and RNA binders [23-25]. As expected, ground-state interactions between the noncovalently bound molecular switch and the DNA bases were detected in the case of the merocyanine form by CD spectroscopy, but not in the case of the spiropyran form. Attempts to attach spiropyrans covalently to DNA are rare [26,27] and include our recent approaches to incorporate synthetically the spiropyran chromophore [28], by either DNA building block **1** [29] or by DNA base modifications **2** and **3** [29,30], into oligonucleotides (Scheme 1). Although the spiropyran DNA building blocks **1** and **2** exhibit promising photochromic properties as

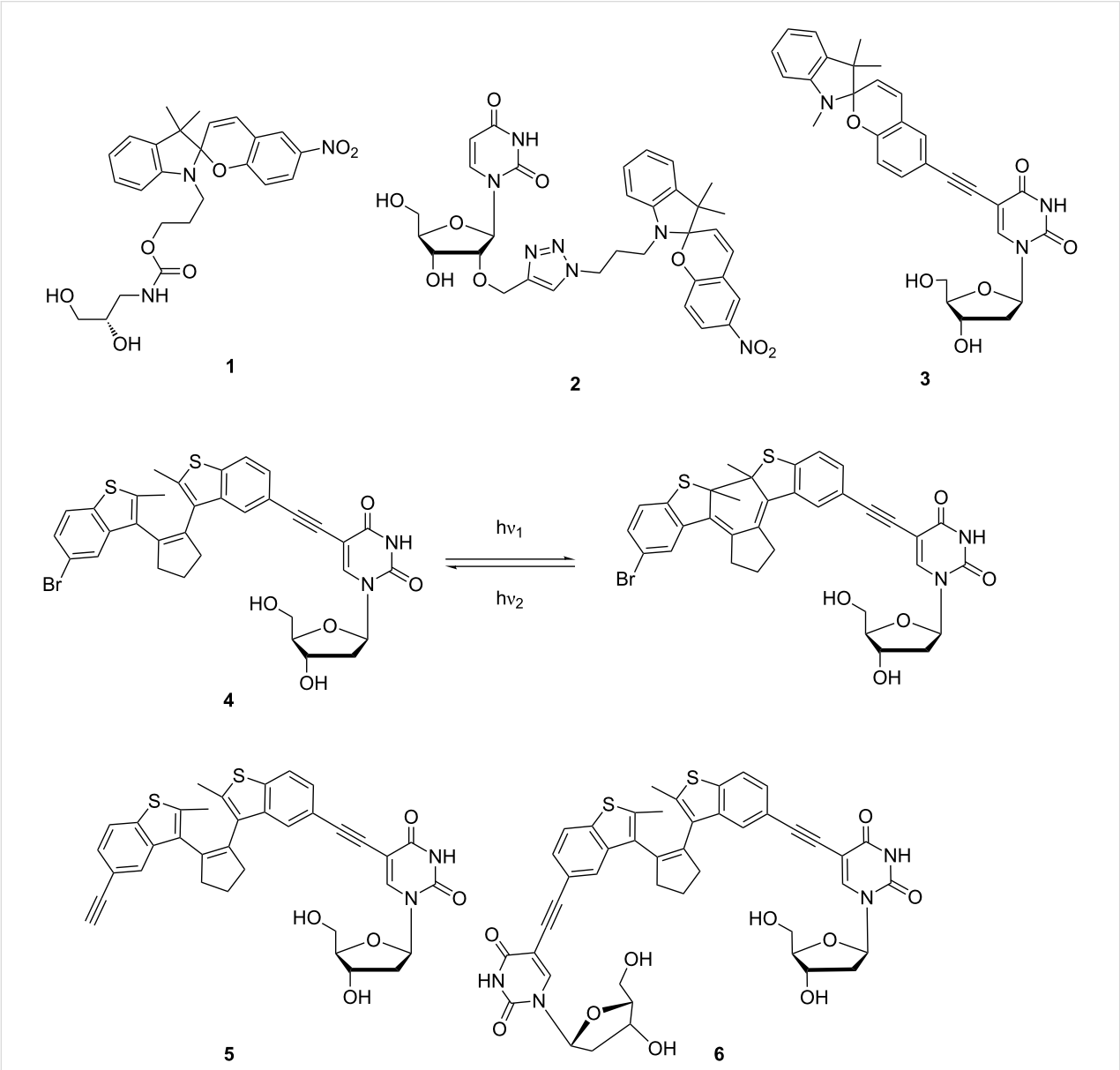

Scheme 1: Spiropyran as DNA base surrogate **1**, DNA base modifications **2** and **3**, and diarylethene-modified nucleosides **4**–**6**. Photoswitching is representatively shown for nucleoside **4**.

nucleosides, it is not worth pursuing this synthetic direction further for the following reasons [30]: (i) It is reported that spiropyrans decompose in aqueous buffer solutions [31], and (according to our experience) the DNA environment does not efficiently prevent this decomposition. (ii) Moreover, we found out that the spiropyran chromophore in the DNA environment loses its photoswitching abilities [29].

The second alternative, diarylethenes, have been applied for switching the binding affinities of proteins and peptides [32] but are still rather unexplored with respect to nucleic acids. The advantage of this type of photoswitch is that back reaction (reopening of the central ring) requires light and cannot be achieved in a thermally induced way. Diarylethenes have been applied in a noncovalent chiroptical photoswitchable DNA complex [33] and combined with 7-deazaadenosine to obtain a nucleosidic diarylethene switch [34]. Recently, we reported, very preliminarily, the preparation and optical properties of nucleoside **4** [30]. Herein, we give a full account and present the detailed synthesis of diarylethene-modified nucleosides **4**, **5** and **6** (Scheme 1), and the characterization of their photochromic behavior. It turned out to be most promising to continue the DNA work with the modified and photochromic nucleoside **4**, which was, thus, incorporated into representative oligonucleotides by using automated phosphoramidite chemistry, and characterized with respect to its photochromism in DNA.

Results and Discussion

Design and synthesis of diarylethene-modified 2'-deoxyuridines **4–6**

The typical way to tether fluorophores to oligonucleotides is to use an alkyl chain linker between the chromophore and DNA base as the point of attachment. The purpose of this conformationally flexible tether is to overcome problems in the enzymatic activity by DNA polymerases in the context of primer-extension (PEX) or PCR studies [35-37]. However, the shortest possible linking of chromophores to oligonucleotides offers potentially interesting optical characteristics, among these being solvatochromism and red-shifted exciplex-type fluorescence [38]. Such absorption and fluorescence readouts are potentially suitable for DNA probing [39-41]. On the other hand, with respect to polymerase-assisted PEX and PCR experiments, an absolutely critical issue regarding the application of single C–C bonds, or ethinyl or phenylene linkers is the question of whether the canonical base-recognition complementarity is effected by the chromophore modification [42,43]. Due to the strongest reactivity the 5-position of pyrimidines (U/T and C) and the 8-position of purines (A and G) are preferred as chromophore modification sites. The assumption, that these points of attachment allow the chromophores to point into the major groove is only partially true, if at all. In particular, large and aromatic chromophores tend to insert into the base stack due to their hydrophobicity by changing the attached nucleoside from the natural anti- to the syn-conformation. The modification of the 8-position of purines clearly forces the nucleoside into the syn-conformation, which interferes with Watson–Crick base pairing. In the case of the pyrimidines the modification at position 5 should not significantly interfere with the preferred anti-conformation of the nucleosidic bond. Thus, the Watson–Crick base pairing of the corresponding modified oligonucleotides should be maintained. Over the past few years we have synthetically attached various chromophores, such as ethynylpyrenes [44,45], BODIPY [46], ethynyl nile red [47,48] and others, to 2'-deoxyuridines for electron transfer studies and for fluorescent probes. To gain greater insight into the counterbase selectivity, we performed PEX experiments with a representative set of chromophore-modified oligonucleotides and found that the DNA-polymerase-catalyzed nucleotide incorporation opposite to attached chromophores at the 5-position of uridine follows Watson–Crick selectivity [49]. In the meantime, DNA polymerases have been evolved that have an increased reactivity for C5-modified deoxyribonucleotides [50]. Hence, it looked most reasonable to attach diarylethenes as photochromic compounds to the 5-position of 2'-deoxyuridine. The nucleoside **4** bears the bromine group, which was introduced initially for synthetic reasons. In the second nucleoside **5** the bromine was replaced by an ethynyl group. The third nucleoside **6** carries two 2'-deoxyuridine moieties and should principally allow connection of the two DNA double helices by the diarylethene linker as a covalent bridge between.

The preparation of all three nucleosides **4** [30], **5** and **6** (Scheme 2) is based on Sonogashira-type cross couplings as key steps [51] to attach the photoactive chromophore to the nucleoside. For the synthesis of the first nucleoside **4** (Scheme 2), commercially available 5-bromobenzothiazole (**7**) is deprotonated with LDA and methylated by methyl iodide in quantitative yield. The resulting 5-bromo-2-methylbenzothiazole (**8**) was converted in a double Friedel–Crafts-type acylation. Treatment with glutaryl chloride in the presence of $AlCl_3$ connects two benzothiazoles **8** and provides **9** in 74% yield. The double McMurry-type reaction, which is performed with Zn and $TiCl_4$, forms the central cyclopentane ring of diarylethene **10**. Subsequently, the ethynyl linker is attached to **10** by treatment with TMS-protected acetylene in a Pd-catalyzed cross-coupling reaction. Careful evaluation of this synthetic step revealed that the best yield (43%) of the mono-ethinylated product **11** is obtained with 2 equiv of TMS-acetylene in the reaction mixture. The competitively formed doubly ethinylated diarylethene **12** is, of course, easier to obtain. In the latter case, a strong excess of TMS-acetylene (10 equiv) helps to increase the yield of prod-

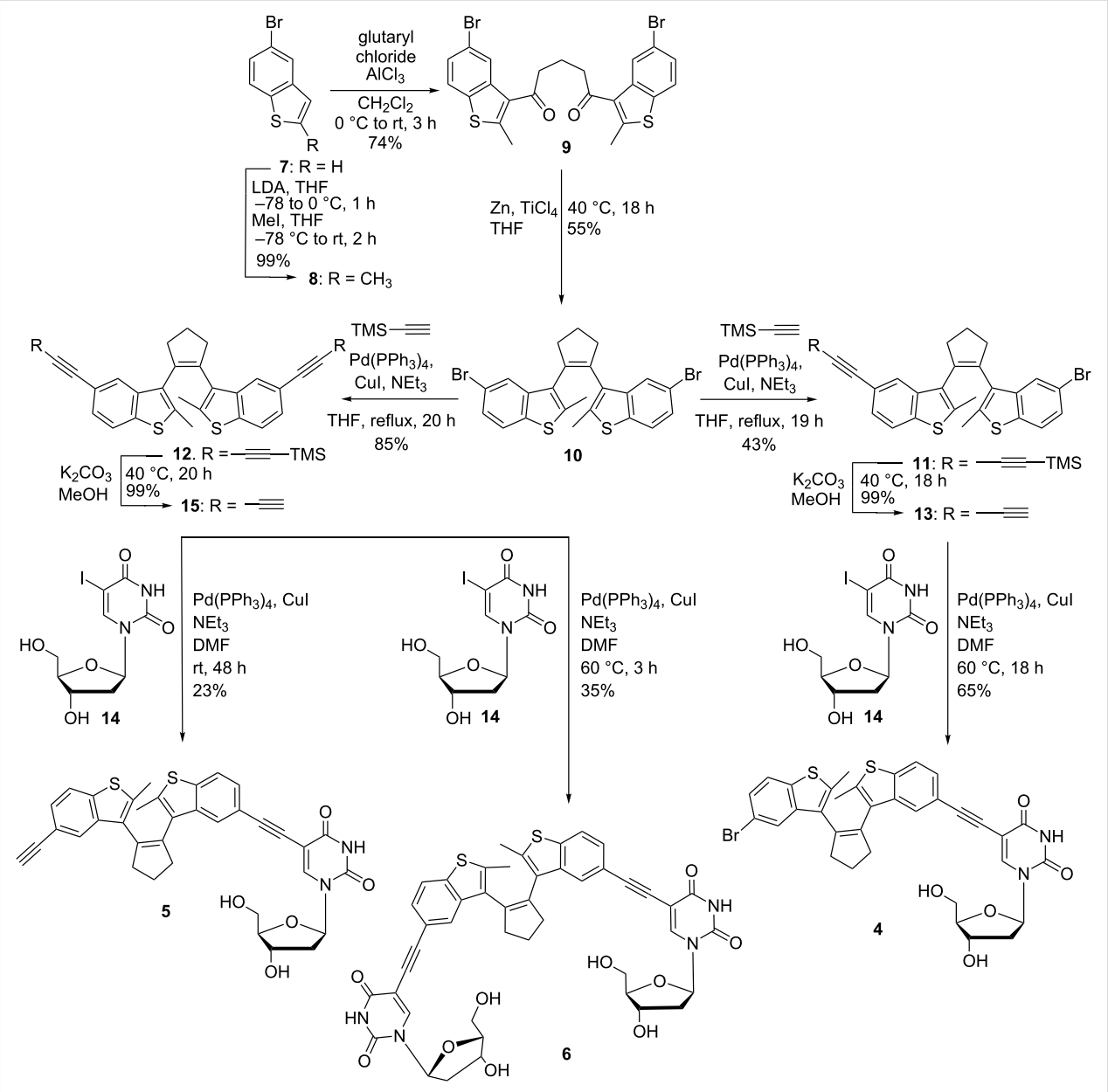

Scheme 2: Synthesis of diarylethene-modified 2'-deoxyuridines **4** [30], **5** and **6**.

uct **12** to 85%. The synthesis of the first diarylethene-modified nucleoside **4** then continues by cleavage of the TMS protecting group of **11** with K_2CO_3 in MeOH. Finally, the synthesis is concluded by the Sonogashira-type coupling of diarylethene **13** to 5-iodo-2'-deoxyuridine (**14**) in 65% yield.

For the second and third modified nucleosides **5** and **6**, the last two synthetic steps are similar to those for nucleoside **4**. Deprotection of **12** gave the doubly ethinylated diarylethene **15** in quantitative yield. The subsequent Sonogashira coupling with **14** at rt gave the mono-nucleosidic product **5** in 23% yield, and at 60 °C the di-nucleosidic product **6** in 35% yield.

Photochromic properties of diarylethene-modified 2'-deoxyuridines 4–6

The photochromic properties of the modified nucleosides **4**–**6** were characterized by UV–vis absorption spectroscopy at rt. All irradiations for photoswitching of the nucleosides were performed by using a 75 W Xe arc lamp equipped with a monochromator for wavelength-selective excitation. The absorption of nucleoside **4** in the pure synthetic form (and presumably open form) shows absorption peaks in the UV range at 242 nm and 310 nm (Figure 1A). It is assumed that the band at 242 nm overlays with the absorption of the uracil moiety. Hence, the absorption side band at 310 nm should allow, at least in prin-

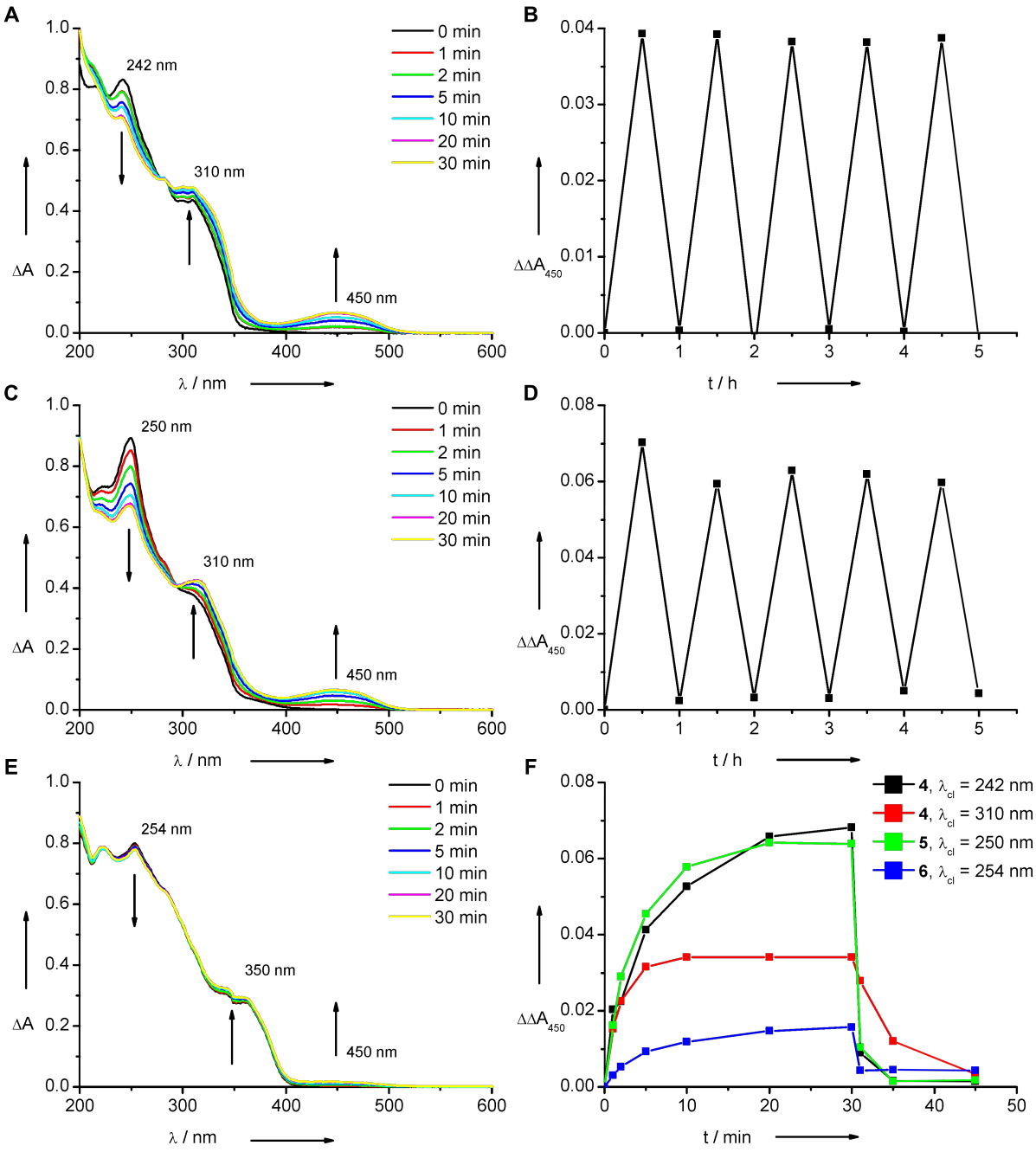

Figure 1: Photoswitching properties of nucleosides **4**–**6** (each 20 mM in MeCN, rt). Top: Irradiation of **4** at 242 nm (**A**, left) and irradiation of **4** alternating at 242 nm and 450 nm (**B**, right). Middle: Irradiation of **5** at 250 nm (**C**, left) and irradiation of **5** alternating at 250 nm and 450 nm (**D**, right). Bottom: Irradiation of **6** at 254 nm (**E**, left) and plots of kinetic traces of absorption changes at 450 nm of all nucleosides **4**–**6** irradiated at the corresponding wavelength until 30 min, then at 450 nm (**F**, right).

cipal, the selective excitation of the switch, outside the nucleic acid absorption range. Accordingly, the photoswitching of **4** was probed at 242 and 310 nm. In fact, by irradiation at either wavelength the closed form of nucleoside **4** is formed with its characteristic band at 450 nm in the visible range. The color of the samples turns yellow. However, the differences in the absorption changes indicate that especially the contribution of the colored closed form of **4** in the photostationary state by excitation at 310 nm is less than at 242 nm (Figure 1F). Hence it can be concluded, that the band at 310 nm can be used indeed to

excite selectively the diarylethene chromophore in nucleic acids, but the yield of the colored form is reduced. In all cases, the photostationary state was reached in 30 min since no additional changes were observed after that time. The absorption bands of the open and closed forms of **4** overlap in the UV range, which makes a detailed analysis of the photostationary state impossible. Irradiation of the sample at 450 nm reopens the diarylethene **4** within a few minutes. The absorption spectra of **4** during all irradiations show an isosbestic point at 275 nm. As expected, the thermally induced opening of the closed chromophore in nucleoside **4** was never observed. The diarylethene nucleoside **4** stays chemically and photochemically stable and can be switched several times to the closed form, and back to the opened form (Figure 1B).

At first glance, the photochromic properties of the second nucleoside (**5**) are very similar to those of **4** (Figure 1C). However, a careful look at the absorption changes performed at 250 nm reveals that the isosbestic point between the closed and the opened form of nucleoside **5** has moved bathochromically from 275 to 300 nm. Moreover, the closed form does not only show an increased absorption in the visible range at 450 nm but also a more significant contribution to the absorption in the UV range at 310 nm. As a result, photoswitching from the opened form of **5** to the closed form at 310 nm cannot be performed in an efficient way. This result is in contrast to that for the first diarylethene-modified nucleoside **4** described above and limits the applicability of nucleoside **5** significantly as a photochromic switch in nucleic acids. The diarylethene **5** can be switched several times back and forth; however, the photochemical stability is slightly reduced compared to nucleoside **4** (Figure 1D).

A rather dramatic change of photochromic properties is observed upon comparison of nucleosides **4** and **5** with the third one (**6**). The synthetically obtained and thereby purely closed form of diarylethene **6** shows absorption at 254 and 350 nm (Figure 1E). Irradiation at 250 nm indeed shows the formation of the colored form at 450 nm, but to a much smaller extent when compared with **4** or **5**. Obviously, the conjugation of the terminal acetylene group of nucleoside **5** to a second 2'-deoxyuridine in **6** affects its photochromism significantly and reduces its photoswitching abilities.

Synthesis and photochromic properties of DNA modified with diarylethene **4**

As mentioned in the introduction, in a bottom-up approach nucleic acids can be modified with artificial functionalities by providing the corresponding synthetic building blocks. Based on the previously described results regarding the photochromic properties of nucleosides **4** [30], **5** and **6** it appeared to be most promising to incorporate synthetically the nucleoside **4** into oligonucleotides. It is the only diarylethene that allows selective excitation at 310 nm, outside of the absorption range of DNA. The preparation of the corresponding phosphoramidite **17** as an artificial DNA building block follows standard procedures (Scheme 3) [30]: Protection of the 5'-OH group of nucleoside **4** by DMT-chloride is followed by phosphitylation of the 3'-OH group of the intermediate **16** yielding phosphoramidite **17**. By automated DNA synthesis on a solid phase we prepared a set of four oligonucleotides in order to report preliminarily the optical properties of **4** in DNA. The sequences were identical except for the base pairs that surround the position of nucleoside **4**. The oligonucleotides were purified by semi-preparative HPLC, identified by mass spectrometry and quantified by their extinction coefficient at 260 nm.

Irradiation of each of the four single-stranded oligonucleotides **DNA1**–**DNA4** at 310 nm yields the characteristic absorption of the closed forms as small and broad bands at ~450 nm, and irradiation at this wavelength drives the reaction back toward the open form of the switch (representatively shown for **DNA2** in Figure 2). The most remarkable result is that of **DNA2** bearing two guanines in the direct vicinity of the diarylethene modification. Guanine is known to interfere with a variety of photophysical properties (mainly fluorescence) in DNA. It is important to mention here that guanine does not influence the photochromic properties of the diarylethene switch **4** as a DNA modification. In fact, the photoswitching behavior of **4** is maintained in all four different DNA environments. The sequence independent photochromic behavior represents an important result for the future application of this type of switch in DNA-based nanostructures. Representatively, we performed switching experiments with the double strand (ds) of the most critical candidate (**DNA2**). The kinetic behavior of the opening and closing of nucleoside **4** cannot be directly compared to ds**DNA2** since the solvents in the two measurements are different. However, the photochromic switching is clearly observable in the absorption spectra (Figure 2A and 2B) and is very similar to that of the single strand. Double-stranded **DNA2**, with the diarylethene switch in the opened form, exhibits a melting temperature of 60.6 °C and shows a high destabilization according to the unmodified double strand (68.0 °C). After irradiation at 310 nm, the melting temperature decreases significantly to 56.8 °C. According to the noncovalently bound diarylethene derivative as chiroptical switch published by Feringa and coworkers [33], the closed form is able to intercalate whereas the open form of the switch binds differently. This could potentially explain the difference in melting temperature for ds**DNA2**, since the intercalated closed form of the diarylethene interferes with stacking to the neighboring bases by the two methyl groups pointing up and down from the chromophore.

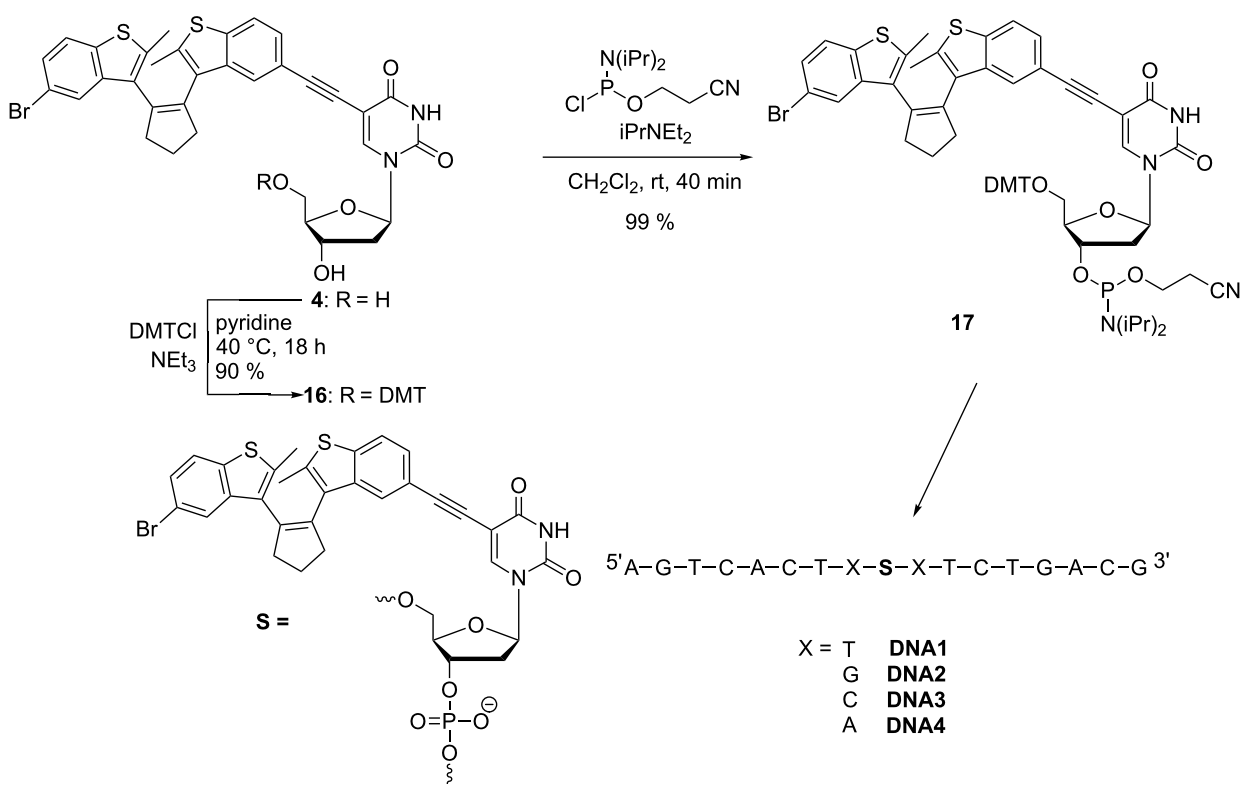

Scheme 3: Synthesis of DNA building block **17** [30] and sequences of diarylethene-modified **DNA1**–**DNA4**.

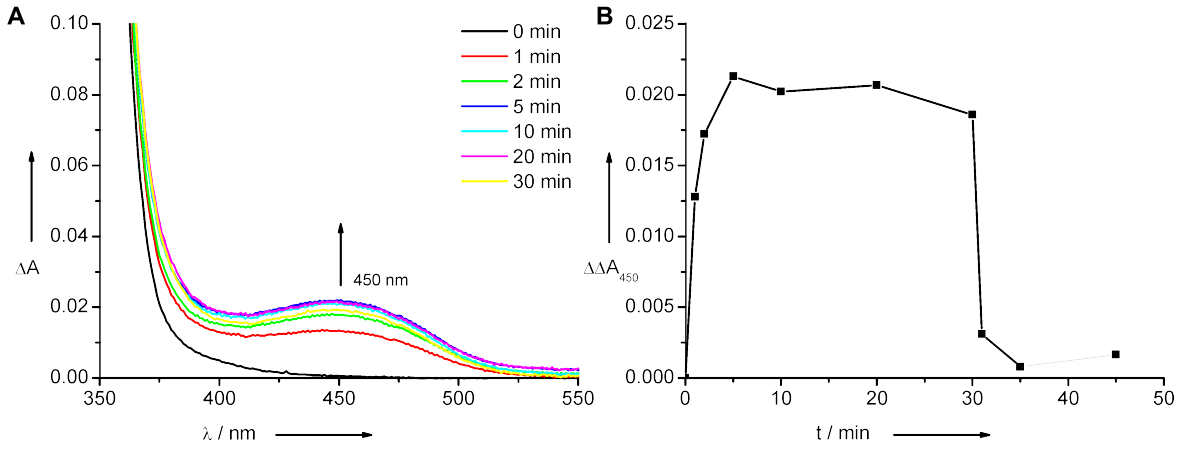

Figure 2: Irradiation of ds**DNA2** at 310 nm (**A**, left) and plot of kinetic trace of absorption changes at 450 nm of ds**DNA2** irradiated at 310 nm until 30 min, then 450 nm (**B**, right).

Conclusion

Three different diarylethene-modified 2‘-deoxyuridines **4**–**6** were prepared by using Sonogashira-type cross couplings as key steps. The photochromic properties of the nucleosides were evaluated and revealed that only nucleoside **4** allows selective excitation at 310 nm, outside the nucleic acid absorption window, to close the diarylethene chromophore. Switching back of the colored form of all three nucleosides **4**–**6** to the corresponding opened forms can be achieved by selective excitation at 450 nm. Moreover, nucleoside **4** was proven to be photochemically stable and, hence, allows switching back and forth several times. Nucleoside **4** was incorporated into oligonucleotides by automated DNA synthesis. It is remarkable that the photochromic properties of **4** are maintained for the corresponding base modification in oligonucleotides and show sequence-independent switching behavior. Our results open the

way for the use of diarylethenes as photochromic compounds in DNA-based architectures and represent one important step further for the design and synthesis of photoreactive and self-assembled nanostructures and materials based on nucleic acids.

Experimental

Materials and methods

Chemicals were purchased from Sigma Aldrich, Fluka, ABCR, Alfa Aesar and Acros. Unmodified oligonucleotides were purchased from Metabion. TLC was performed on Merck silica gel 60 F_{254} coated aluminum foil. Flash chromatography was carried out with silica gel 60 from Aldrich (60–73 μm). Spectroscopic measurements and the melting points were recorded on a Varian Cary 100 spectrometer in quartz-glass cuvettes. Irradiation experiments were performed with a 75 W Xe arc lamp equipped with a monochromator. The synthetic procedures for compounds **4, 8**, **9**, **10**, **11**, **13**, **16** and **17** have been already described in [30].

Compound 12: 10 (617 mg, 1.19 mmol), trimethylsilylacetylene (1.68 mL, 11.90 mmol), dry NEt_3 (0.39 mL, 4.76 mmol), $Pd(PPh_3)_4$ (550 mg, 0.48 mmol) and CuI (91 mg, 0.48 mmol) were dissolved in dry THF (11 mL) under argon. The mixture was degassed and heated under reflux for 20 h. After cooling to rt, the solvent was removed under reduced pressure. The residue was dried in vacuo and purified by flash chromatography on silica gel (hexanes–toluene 100:1) to yield 559 mg **12** (85%) as a white solid. R_f 0.20 (hexanes); ^{1}H NMR (300 MHz, $CDCl_3$) δ 7.72 (s, 2H, H-Ar), 7.56 (d, J = 7.9 Hz, 2H, H-Ar), 7.30 (d, J = 6.9 Hz, 2H, H-Ar), 3.20–2.80 (m, 4H, CH_2), 2.31 (p, J = 6.8 Hz, 2H, CH_2), 1.99 (s, 6H, CH_3), 0.30 (s, 18H, $Si(CH_3)_3$); ^{13}C NMR (75 MHz, $CDCl_3$) δ 139.3 ($C_{quart.}$), 138.7 ($C_{quart.}$), 137.5 ($C_{quart.}$), 137.1 ($C_{quart.}$), 130.2 ($C_{quart.}$), 127.1 ($C_{arom.}$), 126.1 ($C_{arom.}$), 121.9 ($C_{arom.}$), 118.7 ($C_{arom.}$), 106.0 (C≡C), 37.9 (CH_2), 29.9 (C≡C), 24.3 (CH_2), 15.4 (CH_3), 0.3 ($Si(CH_3)_3$); EIMS (70 eV) m/z (%): 552.2 (8) $[M]^+$; HRMS–ESI (m/z): $[M]^+$ calcd for $C_{33}H_{36}S_2Si_2$, 552.1797; found, 552.1794.

Compound 15: 12 (408 mg, 0.74 mmol) was dissolved in dry MeOH (15 mL), and K_2CO_3 (408 mg, 2.95 mmol) was added. The reaction mixture was stirred for 20 h at 40 °C. After cooling to rt, MeOH was removed under reduced pressure. The residue was dried in vacuo and purified by flash chromatography on silica gel (hexanes–toluene 10:1) yielding 299 mg **15** (99%) as a white solid. R_f 0.41 (hexanes–toluene 10:1); ^{1}H NMR (400 MHz, $CDCl_3$) δ 7.75 (s, 2H, H-Ar), 7.57 (s, 2H, H-Ar), 7.31 (s, 2H, H-Ar), 3.08 (s, 2H, C≡CH), 3.01–2.77 (m, 4H, CH_2), 2.28 (p, J = 7.3 Hz, 2H, CH_2), 1.96 (s, 6H, CH_3); ^{13}C NMR (101 MHz, $CDCl_3$) δ 139.3 ($C_{quart.}$), 138.9 ($C_{quart.}$), 137.1 ($C_{quart.}$), 130.0 ($C_{quart.}$), 128.5 ($C_{quart.}$), 126.8 ($C_{arom.}$), 126.4 ($C_{arom.}$), 122.0 ($C_{arom.}$), 117.6 ($C_{arom.}$), 76.4 (C≡C), 37.9 (CH_2), 29.9 (C≡C), 24.2 (CH_2), 15.2 (CH_3); EIMS (70 eV) m/z (%): 408.1 (48) $[M]^+$.

Compound 5: 15 (75 mg, 0.18 mmol), 5-iodo-2'-deoxyuridine (**14**, 65 mg, 0.18 mmol), dry NEt_3 (30 μL, 0.37 mmol), $Pd(PPh_3)_4$ (42 mg, 0.04 mmol) and CuI (7 mg, 0.04 mmol) were dissolved in dry DMF (7 mL). The mixture was degassed and stirred for 48 h at rt. The solvent was removed under reduced pressure and the residue was dried in vacuo and purified by flash chromatography on silica gel (CH_2Cl_2–MeOH 10:1) yielding 27 mg **5** (23%) as a white solid. R_f 0.53 (CH_2Cl_2–MeOH 5:1); ^{1}H NMR (300 MHz, $CDCl_3$) δ 8.01 (s, 1H, NH), 7.82 (s, 1H, C=CH), 7.70 (s, 2H, H-Ar), 7.55 (d, J = 7.8 Hz, 2H, H-Ar), 7.36 (s, 2H, H-Ar), 6.22 (t, J = 6.0 Hz, 1H, 1'-H), 4.62 (s, 1H, 3'-H), 4.16–4.02 (m, 1H, 4'-H), 4.00–3.85 (m, 2H, 5'-H), 3.08 (s, 1H, C≡CH), 3.02–2.72 (m, 4H, CH_2), 2.40 (s, 1H, 2'-H), 2.26 (s, 2H, CH_2), 2.05–1.79 (m, 7H, CH_3, 2'-H); ^{13}C NMR (75 MHz, $CDCl_3$) δ 154.2, 142.7, 141.4, 140.1, 138.9, 138.6, 137.2, 130.0, 127.1, 127.0, 121.6, 118.0, 106.1, 90.4, 88.1, 77.3, 72.8, 64.0, 42.5, 38.5, 24.9, 15.0; MALDI–MS m/z (%): 633.6 (5) $[M]^+$; HRMS–ESI (m/z): $[M + H]^+$ calcd for $C_{36}H_{31}N_2O_5S_2$, 635.1674; found, 635.1681.

Compound 6: 15 (81 mg, 0.20 mmol), 5-iodo-2'-deoxyuridine (**14**, 140 mg, 0.40 mmol), dry NEt_3 (30 μL, 0.40 mmol), $Pd(PPh_3)_4$ (46 mg, 0.04 mmol) and CuI (8 mg, 0.04 mmol) were dissolved in dry DMF (7 mL). The mixture was degassed and stirred for 3 h at 60 °C. After cooling to rt, the solvent was removed under reduced pressure, and the residue was dried in vacuo and purified by flash chromatography on silica gel (CH_2Cl_2–MeOH 15:1) to yield 60 mg **6** (35%) as a white solid. R_f 0.55 (CH_2Cl_2–MeOH 10:1); ^{1}H NMR (400 MHz, DMSO-d_6) δ 8.87 (s, 1H, NH), 8.38 (s, 1H, NH), 7.97 (s, 2H, C=CH), 7.85 (d, J = 9.3 Hz, 2H, H-Ar), 7.80–7.52 (m, 4H, H-Ar), 6.31–6.02 (m, 2H, 1'-H), 5.31 (d, J = 10.7 Hz, 2H, 3'-H), 5.24–5.08 (m, 2H, 4'-H), 4.27 (s, 2H, 5'-H), 3.94–3.83 (m, 2H, 5'-H), 3.79–3.43 (m, 4H, CH_2), 3.17–3.13 (m, 2H, 2'-H), 3.00–2.67 (m, 10H, 2'-H, CH_2, CH_3); ^{13}C NMR (101 MHz, DMSO-d_6) δ 161.4, 153.9, 149.4, 137.5, 136.2, 130.3, 130.0, 129.6, 122.8, 120.1, 117.9, 117.6, 106.9, 99.5, 99.2, 98.3, 88.2, 87.6, 84.8, 70.1, 69.5, 60.9, 60.7, 45.6, 37.5, 29.0, 28.7, 23.4, 22.1, 15.0. MS–FAB m/z (%): 883.4 (25) $[M + Na]^+$; HRMS–ESI (m/z): $[M + H]^+$ calcd for $C_{45}H_{41}N_4O_{10}S_2$, 861.2264; found, 861.2282.

DNA synthesis: Oligonucleotides were prepared with an Expedite 8909 Synthesizer from ABI by using standard phosphoramidite chemistry. Reagents and CPGs were purchased from ABi and Glen research. Modified oligonucleotides were synthesized by a modified protocol. The activator solution

(0.45 M tetrazole in MeCN) was pumped simultaneously with the building block **17** [30] and the coupling time was extended to 35 min, with an intervening step after 17.5 min for washing and refreshing of the activator–**17** solution. After coupling, the vial was washed with MeCN. When the synthesis was complete the trityl-on oligonucleotides were treated with conc. NH_4OH (700 µL, >25%, trace select, Fluka) at 55 °C for 14 h for cleavage from the resin for deprotection. The oligonucleotides were purified by HPLC on a semipreparative RP-18 column (300 Å, Supelco) by using NH_4OAc buffer (pH = 6.5) and MeCN as eluents (0–20% MeCN over 70 min; flow rate: 2.5 mL; UV detection: 260 nm, 310 nm). To cleave the terminal DMT group the oligonucleotides were treated with 80% acetic acid for 1 h at rt. After removal of the solvent, the residue was redissolved in H_2O and the emerging precipitate was removed. The oligonucleotides were lyophilized and quantified by their absorbance in H_2O at 260 nm on a Varian Cary 100 spectrometer, including ε_{260} = 56200 M^{-1} cm^{-1} for modification **S** (Scheme 3). ds**DNA1** was formed by heating to 90 °C (10 min) followed by slow cooling to rt. MALDI–MS **DNA1** *m/z* (%): 5898.9 (100) $[M + DMT]^-$, 5597.3 (99) $[M]^-$, 2949.2 (21) $[M + DMT]^-/2$, 2797.7 (20) $[M]^{2-}/2$; **DNA2** *m/z* (%): 5950.0 (100) $[M + DMT]^-$, 5647.9 (38) $[M]^-$, 2974.6 (17) $[M + DMT]^{2-}/2$, 2823.6 (7) $[M]^{2-}/2$; **DNA3** *m/z* (%): 5869.0 (100) $[M + DMT]^-$, 5666.8 (58) $[M]^-$, 2944.4 (12) $[M + DMT]^{2-}/2$, 2782.6 (12) $[M]^{2-}/2$; **DNA4** *m/z* (%): 5919.9 (100) $[M + DMT]^-$, 5617.7 (34) $[M]^-$, 2957.7 (25) $[M + DMT]^{2-}/2$, 2808.9 (6) $[M]^{2-}/2$. The UV–vis absorption spectra of ss**DNA1**–ss**DNA4** are shown in Figure 3.

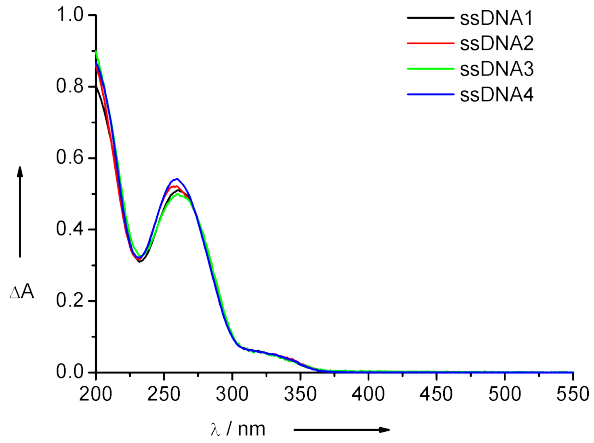

Figure 3: UV–vis absorption spectra of ss**DNA1**–ss**DNA4** (2.5 µM in 50 mM Na–Pi buffer, pH 7, 250 mM NaCl, rt).

Acknowledgements

Financial support by the Deutsche Forschungsgemeinschaft, the University of Regensburg and the Karlsruhe Institute of Technology (KIT) is gratefully acknowledged.

References

1. Malinovskii, V. L.; Wenger, D.; Häner, R. *Chem. Soc. Rev.* **2010,** *39,* 410–422. doi:10.1039/b910030j
2. Ruiz-Carretero, A.; Janssen, P. G. A.; Kaeser, A.; Schenning, A. P. H. J. *Chem. Commun.* **2011,** *47,* 4340–4347. doi:10.1039/c0cc05155a
   See review and references therein.
3. Bandy, T. J.; Brewer, A.; Burns, J. R.; Marth, G.; Nguyen, T.; Stulz, E. *Chem. Soc. Rev.* **2011,** *40,* 138–148. doi:10.1039/b820255a
   See review and references therein.
4. Varghese, R.; Wagenknecht, H.-A. *Chem. Commun.* **2009,** 2615–2624. doi:10.1039/b821728a
   See review and references therein.
5. Raymo, F. M.; Tomasulo, M. *Chem.–Eur. J.* **2006,** *12,* 3186–3193. doi:10.1002/chem.200501178
   See review and references therein.
6. Cusido, J.; Deniz, E.; Raymo, F. M. *Eur. J. Org. Chem.* **2009,** 2031–2045. doi:10.1002/ejoc.200801244
   See review and references therein.
7. Pischel, U. *Angew. Chem., Int. Ed.* **2007,** *46,* 4026–4040. doi:10.1002/anie.200603990
   See review and references therein.
8. Szaciłowski, K. *Chem. Rev.* **2008,** *108,* 3481–3548. doi:10.1021/cr068403q
   See review and references therein.
9. Renner, C.; Moroder, L. *ChemBioChem* **2006,** *7,* 868–878. doi:10.1002/cbic.200500531
   See review and references therein.
10. Berkovic, G.; Krongauz, V.; Weiss, V. *Chem. Rev.* **2000,** *100,* 1741–1754. doi:10.1021/cr9800715
    See review and references therein.
11. Irie, M. *Chem. Rev.* **2000,** *100,* 1685–1716. doi:10.1021/cr980069d
    See review and references therein.
12. Mayer, G.; Heckel, A. *Angew. Chem., Int. Ed.* **2006,** *45,* 4900–4921. doi:10.1002/anie.200600387
    See review and references therein.
13. Fehrentz, T.; Schönberger, M.; Trauner, D. *Angew. Chem., Int. Ed.* **2011,** *50,* 12156–12182. doi:10.1002/anie.201103236
    See review and references therein.
14. Asanuma, H.; Liang, X.; Yoshida, T.; Komiyama, M. *ChemBioChem* **2001,** *2,* 39–44. doi:10.1002/1439-7633(20010105)2:1<39::AID-CBIC39>3.0.CO;2-E
15. Nishioka, H.; Liang, X.; Kashida, H.; Asanuma, H. *Chem. Commun.* **2007,** 4354–4356. doi:10.1039/b708952j
16. Liang, X.; Takenaka, N.; Nishioka, H.; Asanuma, H. *Chem.–Asian J.* **2008,** *3,* 553–560. doi:10.1002/asia.200700384
17. Nishioka, H.; Liang, X.; Asanuma, H. *Chem.–Eur. J.* **2010,** *16,* 2054–2062. doi:10.1002/chem.200902789
18. Yamazawa, A.; Liang, X.; Asanuma, H.; Komiyama, M. *Angew. Chem., Int. Ed.* **2000,** *39,* 2356–2357. doi:10.1002/1521-3773(20000703)39:13<2356::AID-ANIE2356>3.0.CO;2-9
19. Liang, X.; Asanuma, H.; Komiyama, M. *J. Am. Chem. Soc.* **2002,** *124,* 1877–1883. doi:10.1021/ja011988f
20. Liang, X.; Nishioka, H.; Takenaka, N.; Asanuma, H. *ChemBioChem* **2008,** *9,* 702–705. doi:10.1002/cbic.200700649
21. Nishioka, H.; Liang, X.; Kato, T.; Asanuma, H. *Angew. Chem., Int. Ed.* **2012,** *51,* 1165–1168. doi:10.1002/anie.201106093
22. Sakata, T.; Yan, Y.; Marriott, G. *J. Org. Chem.* **2005,** *70,* 2009–2013. doi:10.1021/jo048207o

23. Young, D. D.; Deiters, A. *ChemBioChem* **2008,** *9,* 1225–1228. doi:10.1002/cbic.200800051
24. Andersson, J.; Li, S.; Lincoln, P.; Andréasson, J. *J. Am. Chem. Soc.* **2008,** *130,* 11836–11837. doi:10.1021/ja801968f
25. Hammarson, M.; Andersson, J.; Li, S.; Lincoln, P.; Andréasson, J. *Chem. Commun.* **2010,** *46,* 7130–7132. doi:10.1039/c0cc01682a
26. Asanuma, H.; Shirasuka, K.; Yoshida, T.; Takarada, T.; Liang, X.; Komiyama, M. *Chem. Lett.* **2001,** *30,* 108–109. doi:10.1246/cl.2001.108
27. Zhang, P.; Meng, J. B.; Matsuura, T.; Wang, Y. M. *Chin. Chem. Lett.* **2002,** *13,* 299–302.
28. Beyer, C.; Wagenknecht, H.-A. *J. Org. Chem.* **2010,** *75,* 2752–2755. doi:10.1021/jo100309r
29. Beyer, C.; Wagenknecht, H.-A. *Synlett* **2010,** 1371–1376. doi:10.1055/s-0029-1219924
30. Barrois, S.; Beyer, C.; Wagenknecht, H.-A. *Synlett* **2012,** *23,* 711–716. doi:10.1055/s-0031-1290599
31. Stafforst, T.; Hilvert, D. *Chem. Commun.* **2009,** *3,* 287–288. doi:10.1039/b818050d
32. Vomasta, D.; Högner, C.; Branda, N. R.; König, B. *Angew. Chem., Int. Ed.* **2008,** *47,* 7644–7647. doi:10.1002/anie.200802242
33. Mammana, A.; Carroll, G. T.; Areephong, J.; Feringa, B. L. *J. Phys. Chem. B* **2011,** *115,* 11581–11587. doi:10.1021/jp205893y
34. Singer, M.; Jäschke, A. *J. Am. Chem. Soc.* **2010,** *132,* 8372–8377. doi:10.1021/ja1024782
35. Ranasinghe, R. T.; Brown, T. *Chem. Commun.* **2005,** 5487–5502. doi:10.1039/b509522k
36. Waggoner, A. *Curr. Opin. Chem. Biol.* **2006,** *10,* 62–66. doi:10.1016/j.cbpa.2006.01.005
37. Cobb, A. J. A. *Org. Biomol. Chem.* **2007,** *5,* 3260–3275. doi:10.1039/b709797m
38. Wang, Y.; Haze, O.; Dinnocenzo, J. P.; Farid, S.; Farid, R. S.; Gould, I. R. *J. Org. Chem.* **2007,** *72,* 6970–6981. doi:10.1021/jo071157d
39. Raytchev, M.; Mayer, E.; Amann, N.; Wagenknecht, H.-A.; Fiebig, T. *ChemPhysChem* **2004,** *5,* 706–712. doi:10.1002/cphc.200301205
40. Sinkeldam, R. W.; Greco, N. J.; Tor, Y. *Chem. Rev.* **2010,** *110,* 2579–2619. doi:10.1021/cr900301e
See review and references therein.
41. Sindbert, S.; Kalinin, S.; Nguyen, H.; Kienzler, A.; Clima, L.; Bannwarth, W.; Appel, B.; Müller, S.; Seidel, C. A. M. *J. Am. Chem. Soc.* **2011,** *133,* 2463–2480. doi:10.1021/ja105725e
42. Kool, E. T. *Annu. Rev. Biochem.* **2002,** *71,* 191–219. doi:10.1146/annurev.biochem.71.110601.135453
43. Henry, A. A.; Romesberg, F. E. *Curr. Opin. Biotechnol.* **2005,** *16,* 370–377. doi:10.1016/j.copbio.2005.06.008
44. Rist, M.; Amann, N.; Wagenknecht, H.-A. *Eur. J. Org. Chem.* **2003,** 2498–2504. doi:10.1002/ejoc.200300125
45. Wagner, C.; Rist, M.; Mayer-Enthart, E.; Wagenknecht, H.-A. *Org. Biomol. Chem.* **2005,** *3,* 2062–2063. doi:10.1039/b504079e
46. Ehrenschwender, T.; Wagenknecht, H.-A. *Synthesis* **2008,** 3657–3662. doi:10.1055/s-0028-1083206
47. Varghese, R.; Wagenknecht, H.-A. *Chem.–Eur. J.* **2009,** *15,* 9307–9310. doi:10.1002/chem.200901147
48. Varghese, R.; Wagenknecht, H.-A. *Chem.–Eur. J.* **2010,** *16,* 9040–9046. doi:10.1002/chem.201001136
49. Wanninger-Weiß, C.; Di Pasquale, F.; Ehrenschwender, T.; Marx, A.; Wagenknecht, H.-A. *Chem. Commun.* **2008,** 1443–1445. doi:10.1039/B718002K
50. Staiger, N.; Marx, A. *ChemBioChem* **2010,** *11,* 1963–1966. doi:10.1002/cbic.201000384
51. Sonogashira, K. *J. Organomet. Chem.* **2002,** *653,* 46–49. doi:10.1016/S0022-328X(02)01158-0

License and Terms

Beilstein Journal of Organic Chemistry

On the bromination of the dihydroazulene/vinylheptafulvene photo-/thermoswitch

Virginia Mazzanti[1,2], Martina Cacciarini[1,3], Søren L. Broman[1], Christian R. Parker[1], Magnus Schau-Magnussen[1], Andrew D. Bond[4] and Mogens B. Nielsen[*1]

Full Research Paper

Open Access

Address:
[1]Department of Chemistry, University of Copenhagen, Universitetsparken 5, DK-2100 Copenhagen Ø, Denmark, [2]Sino-Danish Center for Education and Research (SDC), Niels Jensens Vej 2, DK-8000 Aarhus C, Denmark, [3]Department of Chemistry, University of Florence, via della Lastruccia 3-13, I-50019, Sesto F.no, Italy and [4]Department of Physics, Chemistry and Pharmacy, University of Southern Denmark, Campusvej 55, DK-5230 Odense M, Denmark

Email:
Mogens B. Nielsen* - mbn@kiku.dk

* Corresponding author

Keywords:
azulene; bromination; dihydroazulene; molecular switches; photoswitch; vinylheptafulvene

Beilstein J. Org. Chem. **2012,** *8,* 958–966.
doi:10.3762/bjoc.8.108

Received: 28 February 2012
Accepted: 23 May 2012
Published: 27 June 2012

This article is part of the Thematic Series "Molecular switches and cages".

Guest Editor: D. Trauner

Abstract

Background: The dihydroazulene (DHA)/vinylheptafulvene (VHF) system (with two cyano groups at C1) functions as a photo-/thermoswitch. Direct ionic bromination of DHA has previously furnished a regioselective route to a 7,8-dibromide, which by elimination was converted to a 7-bromo-substituted DHA. This compound has served as a central building block for functionalization of the DHA by palladium-catalyzed cross-coupling reactions. The current work explores another bromination protocol for achieving the isomeric 3-bromo-DHA and also explores the outcome of additional bromination of this compound as well as of the known 7-bromo-DHA.

Results: Radical bromination on two different VHFs by using *N*-bromosuccinimide/benzoyl peroxide and light, followed by a ring-closure reaction generated the corresponding 3-bromo-DHAs, as confirmed in one case by X-ray crystallography. According to a ^{1}H NMR spectroscopic study, the ring closure of the brominated VHF seemed to occur readily under the reaction conditions. A subsequent bromination–elimination protocol provided a 3,7-dibromo-DHA. In contrast, treating the known 7-bromo-DHA with bromine generated a very labile species that was converted to a new 3,7-dibromoazulene, i.e., the fully unsaturated species. Azulenes were also found to form from brominated compounds when left standing for a long time in the solid state. Kinetics measurements reveal that the 3-bromo substituent enhances the rate of the thermal conversion of the VHF to DHA, which is opposite to the effect exerted by a bromo substituent in the seven-membered ring.

Conclusion: Two general procedures for functionalizing the DHA core with a bromo substituent (at positions 3 and 7, respectively) are now available with the DHA as starting material.

Introduction

1,8a-Dihydroazulene-1,1-dicarbonitrile (DHA, **1**) is a yellow photochromic compound, which undergoes a light-induced 10-electron retro-electrocyclization to a red-colored vinylheptafulvene (VHF) (Scheme 1) [1-3]. The VHF compound is formed as the s-*cis* conformer, which, however, is in equilibrium with the more stable s-*trans* conformer. The s-*cis* VHF undergoes a thermally induced cyclization to regenerate the original DHA. The significant structural difference between the DHA and VHF forms, as reflected in their different colors and hence electronic properties, renders the system interesting as a light-controlled molecular switch in, for example, molecular electronics. Indeed, light-induced conductance switching was recently observed for a DHA derivative situated in a single-molecule junction [4]. For the further exploration of the DHA/VHF switch in this field, ongoing synthetic efforts are required for the incorporation of functional groups onto the system, especially in a regioselective manner.

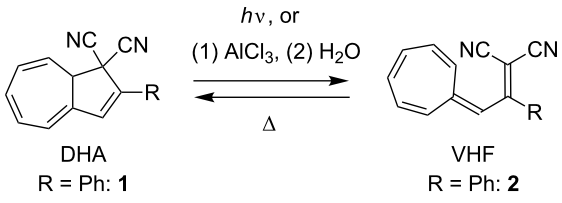

Scheme 1: Dihydroazulene (DHA)/vinylheptafulvene (VHF) photo-/thermoswitch.

We have recently developed an efficient protocol for functionalizing the DHA/VHF **1**/**2** (R = Ph) at position 7 (for numbering, see Figure 1) by a bromination–elimination protocol of **1**, as shown in Scheme 2 [3,5-8]. Elimination of HBr from the intermediate **3** provided the bromo-functionalized DHA **4** that was employed for further cross-coupling reactions. The advantage of this method is that the "parent DHA" **1** can be prepared on a large scale in a few steps [9] and it is hence a convenient building block for further functionalization. Moreover, we have found that the treatment of DHA by aluminum chloride followed by water provided another means of inducing ring-opening of DHA to form VHF (Scheme 1) [10]. This method is

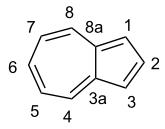

Figure 1: Numbering of azulene.

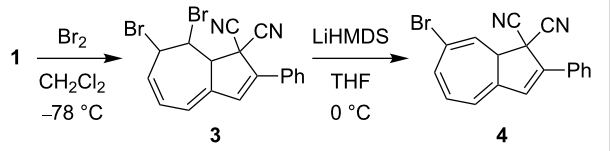

Scheme 2: Bromination–elimination protocol for functionalization of DHA [3,5-8]. HMDS = hexamethyldisilazide.

particularly convenient for making VHF on a preparative scale, which is more tedious when employing a light source. Along this line, we became interested in investigating the possibility of brominating the VHF **2**. It was previously shown by Kuroda and Asao [11] that the related VHF **5** underwent bromination by *N*-bromosuccinimide (NBS) to form the product **6** (Scheme 3), but any thermal conversion of this VHF to a DHA was not described. Here we describe NBS bromination of VHF **2** and isolation of the corresponding 3-bromo-DHA. In addition, the outcome of further bromination of this compound as well as of the 7-bromo-DHA **4** is presented.

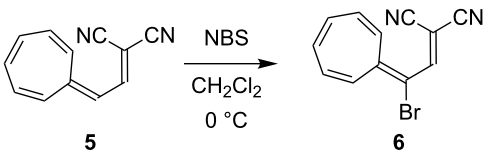

Scheme 3: Bromination of VHF [11]. NBS = *N*-bromosuccinimide.

Results and Discussion

Synthesis

DHA **1** was first opened to VHF **2** by aluminum chloride followed by quenching with water according to a previously described procedure (Scheme 4) [10]. The resulting VHF **2** was then treated with NBS and benzoyl peroxide in benzene and the mixture was subjected to irradiation from a 500 W halogen lamp source, presumably generating the intermediate, but short-lived (see below), species **7**. No structural evidence for **7** was obtained, but after standard work-up, the ring-closed 3-bromo-DHA product **8** was isolated in an overall yield of 46%, suggesting that **7** is indeed formed as an intermediate. The structure of **8** was elucidated by a ^{1}H,^{1}H COSY NMR spectrum (Figure 2) and ultimately confirmed by X-ray crystallographic analysis (Figure 3a). Interestingly, when following the bromination by ^{1}H NMR spectroscopy, signals from the VHF **2** seem absent within 5 min, while instead signals from the DHA **8** quickly emerge (Figure 4). There are, however, some signals

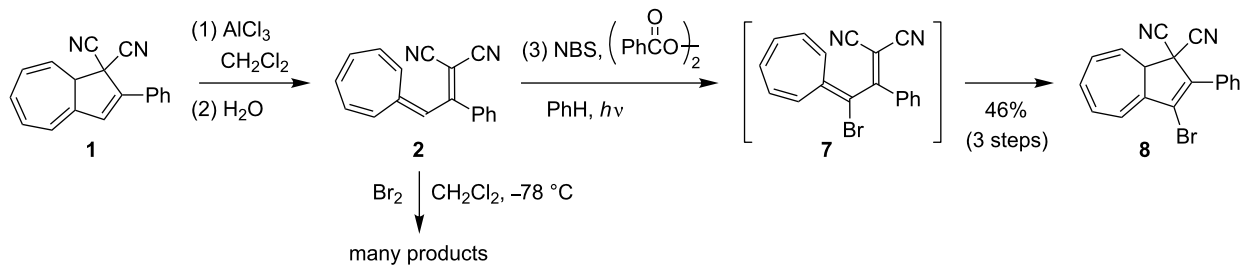

Scheme 4: Radical and ionic brominations of VHF.

around 6.5 and 7.3 ppm (Figure 4c and Figure 4d) from unidentified intermediates, which decrease in intensity after irradiation for longer time. No characteristic signals from the suggested bromo-VHF intermediate **7** were observed, thus it must undergo rapid ring closure to the DHA **8** under the reaction conditions although the mixture is subjected to light.

Interestingly, when the known tolyl derivative **9** [12] (Figure 5) was subjected to the ring opening followed by NBS bromination, the 3-bromo-DHA **10** was formed in almost quantitative yield (estimated yield of 95%) instead of the benzylic bromide product. This compound was, however, difficult to purify without significant loss of material. When subjecting VHF **2** to bromination by Br_2 (Scheme 4), under the same conditions used to regioselectively brominate the corresponding DHA **1**, many products (unidentified) were formed according to NMR spectroscopy. Thus, ionic bromination is not a useful method for the functionalization of the VHF. Gratifyingly, we managed to

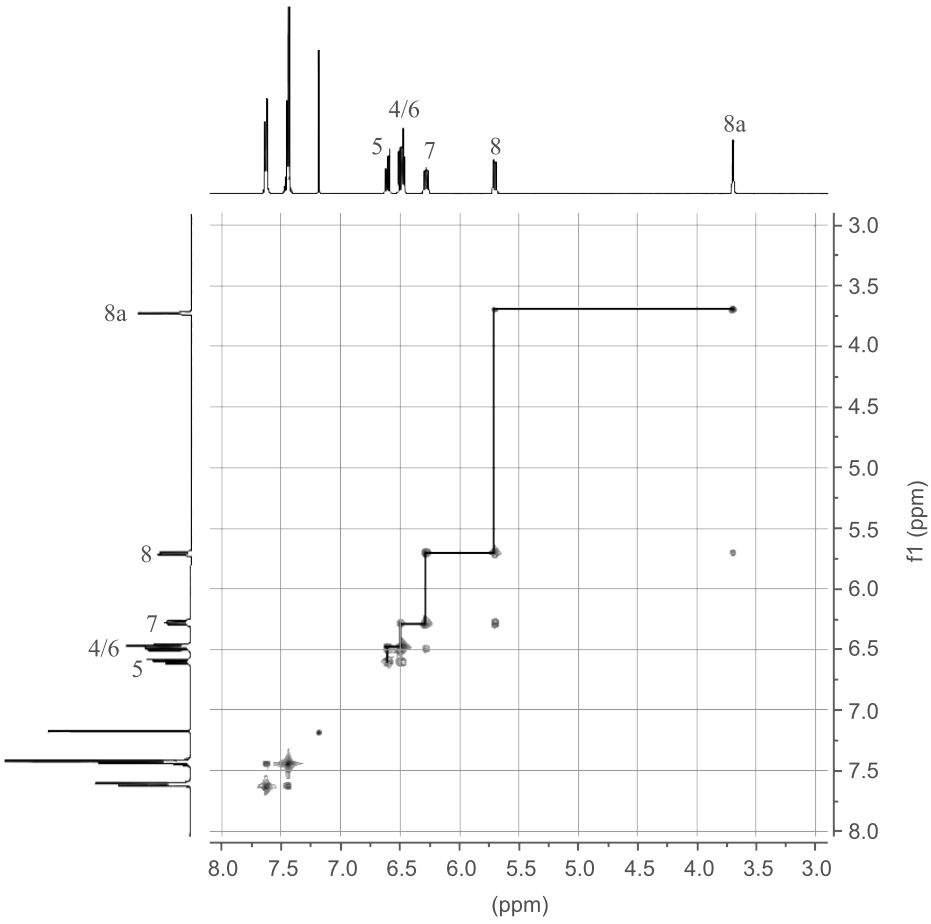

Figure 2: $^1H,^1H$ COSY NMR spectrum of DHA **8** ($CDCl_3$, 500 MHz). For assignments of DHA signals, see numbering in Figure 1.

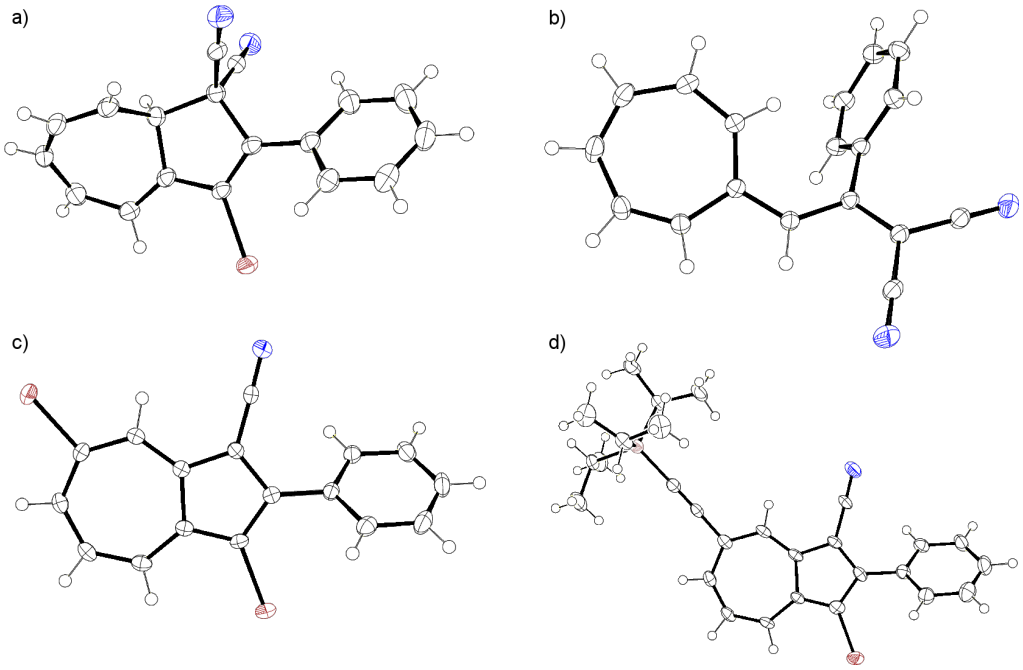

Figure 3: Molecular structures (with displacements ellipsoids at 50% probability for non-H atoms) of (a) DHA **8** (CCDC 868717; crystals were grown from butanone/heptane); (b) VHF **2** (CCDC 866016; crystals were grown from benzene/cyclohexane; benzene cocrystallized with the VHF but has been omitted for clarity); (c) azulene **14** (CCDC 868718; crystals were grown from dichloromethane/heptane); (d) azulene **15** (CCDC 868719; crystals were grown from dichloromethane/heptane).

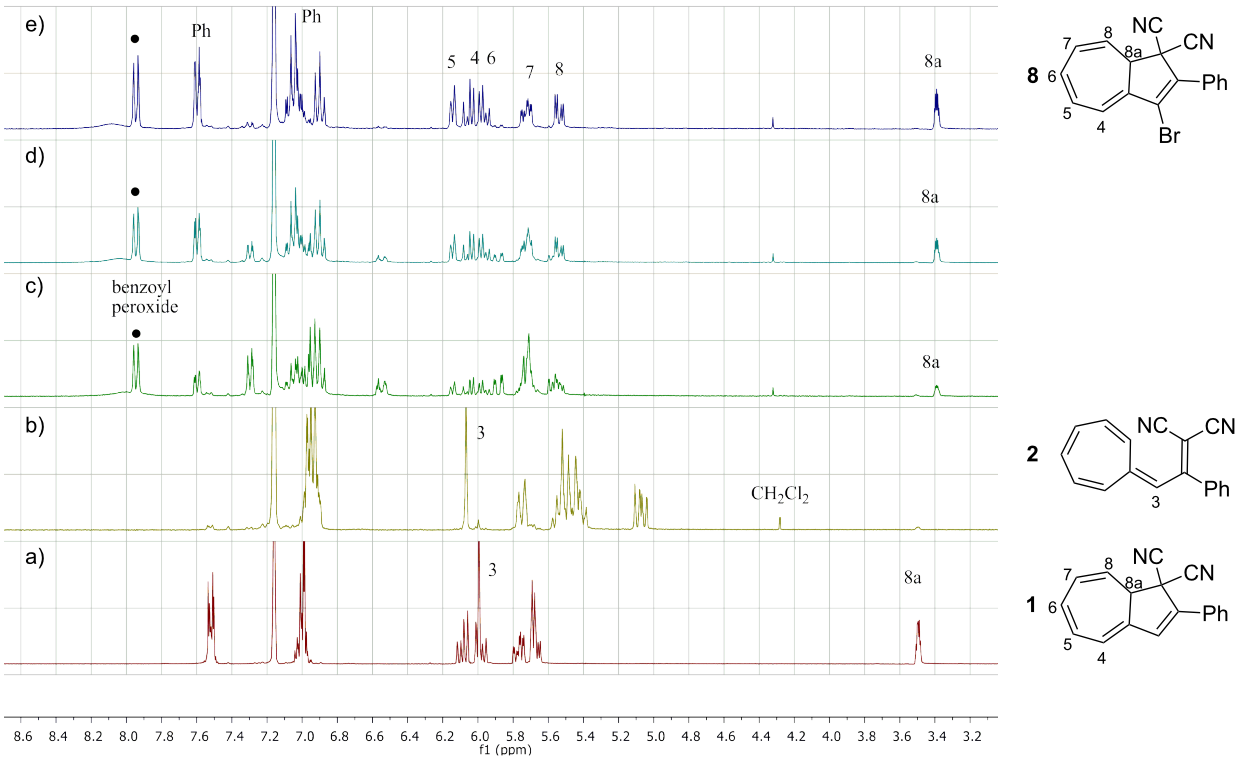

Figure 4: ^{1}H NMR spectra (C_6D_6, 300 MHz) of (a) DHA **1**; (b) VHF **2**; (c–e) VHF **2** after treatment with 2 molar equiv of NBS in the presence of benzoyl peroxide and irradiation for 5, 15, and 35 min, respectively.

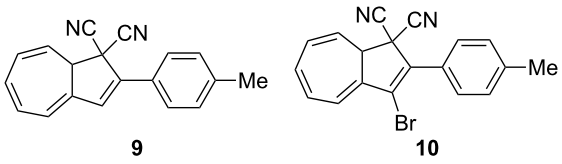

Figure 5: Compound **9** was selectively brominated to furnish the product **10**.

grow crystals suitable for X-ray diffraction studies of the VHF **2** (generated by the $AlCl_3$-induced ring opening of DHA **1** followed by a liquid–liquid extraction) by layering cyclohexane upon a solution of the VHF in benzene and allowing this mixture to crystallize at 5 °C (lower temperatures and nonpolar solvents reduce the rate of the undesired thermal back reaction [9]). The crystal structure of VHF **2** is shown in Figure 3b.

With the objective to generate DHA building blocks with more than one bromo functionality for further reactions, we subjected the 3-bromo-DHA **8** to the ionic bromination–elimination protocol, which, via the intermediate **11**, provided the 3,7-dibromo-substituted DHA **12** (Scheme 5). In an alternative strategy (Scheme 6), we started out with the 7-bromo-DHA **4**. Treatment with bromine at −78 °C generated in this case, however, a very labile intermediate, tentatively assigned to the structure **13**, which underwent ready conversion, without the addition of base, to the azulene **14** together with a complex mixture of other nonisolated products. This product is not surprising, inasmuch as we have previously found that a solution of the related dibromide **3** over time underwent conversion to a mixture of 1-bromo-3-cyano-2-phenylazulene and 1-cyano-2-phenylazulene [5]. The conversion of **13** into azulenes was, however, so fast that we could not perform the controlled elimination of HBr by LiHMDS to generate the corresponding 7-bromo-DHA as we could from **3**. The structure of the azulene **14** was confirmed by X-ray crystallographic analysis (Figure 3c). Functionalized azulenes are themselves interesting in materials chemistry for their optical and redox properties [13].

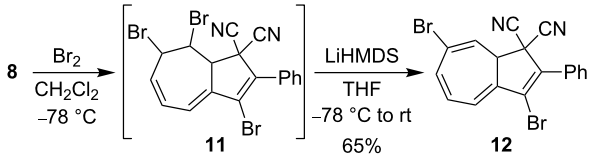

Scheme 5: Synthesis of 3,7-dibromo-DHA.

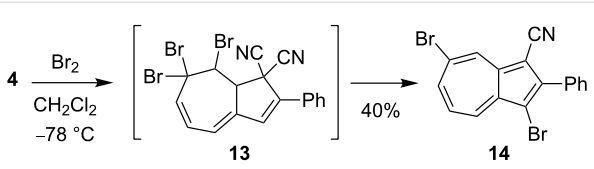

Scheme 6: Synthesis of a 3,7-dibromoazulene.

The two bromo positions of **14** showed very different reactivity. Thus, subjecting **14** to a Sonogashira coupling with triisopropylsilylacetylene by using the $Pd(PPh_3)_2Cl_2$/CuI catalyst system only gave the monocoupled product **15** (Scheme 7), confirmed by X-ray crystal structure analysis (Figure 3d). Moreover, a Suzuki cross-coupling reaction with boronic acid **16** gave the product **17**, albeit in rather low yield (Scheme 7). The substitution was confirmed by NOESY 1D experiments (see Supporting Information File 1).

Finally, we observed that upon storage at room temperature, the dibromide **3** as well as the known tetrabromide **18** [5] slowly turned into a mixture of azulenes, which we isolated and identified as **19**–**22** shown in Scheme 8. While, **19** (X-ray crystal structure is given in [6]), **20** [5], and **21** [5,14,15] are already known, the dibromoazulene **22** is new.

UV–vis absorption and switching studies

The UV–vis absorption spectrum of the 3-bromo-DHA **8** in cyclohexane is shown in Figure 6. The compound exhibits an absorption maximum at 337 nm, which is blue-shifted by 17 nm relative to that of DHA **1** [9]. By irradiation at 337 nm, the

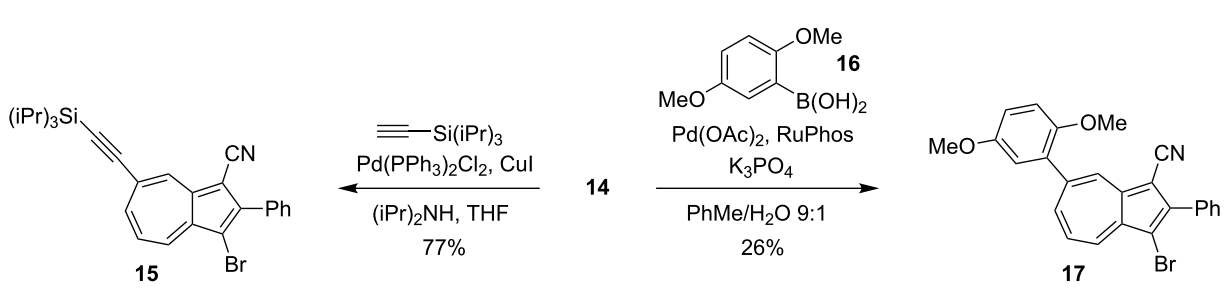

Scheme 7: Regioselective Sonogashira and Suzuki couplings. RuPhos = 2-dicyclohexylphosphino-2',6'-diisopropoxy-1,1'-biphenyl.

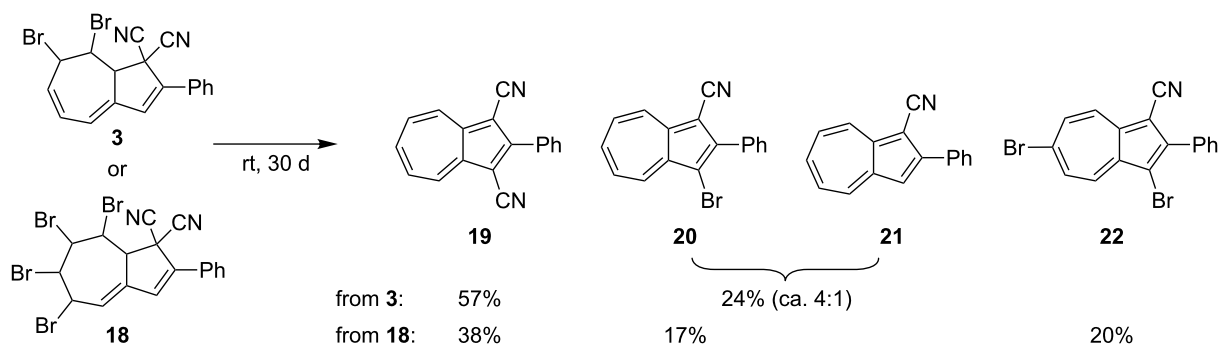

Scheme 8: Slow conversions to azulenes in the solid state.

DHA was gradually converted to the VHF **7** (Figure 6) exhibiting a characteristic absorption maximum at 453 nm (blue-shifted by 7 nm relative to that of VHF **2** [9]). Upon heating of the VHF at 50 °C, a gradual conversion to the DHA was observed. Although both the light-induced DHA-to-VHF conversion and the thermally induced VHF-to-DHA conversion were found to occur with isosbestic points in the absorption spectra, we found that the conversion was not fully reversible. First, the VHF could not be fully converted to DHA (Figure 6, broken curve), and, second, when a second cycle was performed, the final VHF absorption was at a lower intensity than after the first conversion. Nevertheless, the decay of the VHF absorption could be fitted to an exponential decay (see Supporting Information File 1).

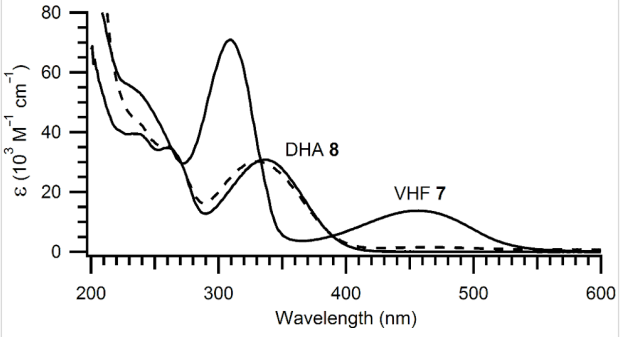

Figure 6: Absorption spectra of DHA **8** and VHF **7** in cyclohexane. The broken curve shows the absorption spectrum after one light–heat cycle (DHA → VHF → DHA).

From this fit, we obtained rough estimates of the rate constant and half-life of $k = 5.1 \times 10^{-4}$ s^{-1} and $t_{1/2} = 27$ min at 50 °C. For comparison, the values for conversion of VHF **2** to DHA **1** in cyclohexane are 8.3×10^{-5} s^{-1} and $t_{1/2} = 139$ min at 50 °C (found from Arrhenius plot, [9]). Thus, the influence of the bromo substituent in **7** is to enhance significantly the rate of the thermal ring closure, which is explained by its inductive electron withdrawal, hence stabilizing a zwitterionic VHF transition state, as previously suggested [9]. In accordance hereto, we have previously found that moving the bromo substituent to the seven-membered ring has the opposite effect; thus, the VHF derived from 7-bromo-DHA **4** underwent ring closure considerably slower than VHF **2** [7]. We are, however, not able to explain the remarkably fast formation of **8** from **7** under the bromination conditions described above, but it may be the result of the slight Lewis acidity under the reaction conditions.

Conclusion

In conclusion, we have developed a method for functionalizing the DHA/VHF photo-/thermoswitch with a bromo substituent at position 3 in the DHA core (product **8**). The synthesis explores the ready conversion of DHA **1** to VHF **2** on a preparative scale by using aluminum chloride followed by NBS bromination. This bromination was found to occur selectively in the presence of a tolyl group (product **10**). The method contrasts the earlier bromination (Br_2)–elimination protocol on DHA for incorporating selectively a bromo substituent at position 7 in the DHA core without proceeding via the VHF as an intermediate. Subjecting the 3-bromo-DHA **8** to this bromination–elimination protocol furnished the 3,7-dibromo-DHA **12**. In contrast, subjecting the 7-bromo-DHA **4** to an additional bromination with Br_2 generated a very labile compound that was readily converted to the fully unsaturated 3,7-dibromo-substituted azulene **14** together with other unidentified products. The instability of intermediate bromide addition products was also reflected by solid-state conversions of di- and tetrabromides to a variety of azulenes. The influence on the thermal VHF-to-DHA conversion exerted by a bromo substituent at position 3 (DHA numbering) is opposite to that of one at position 7; the former substitution enhances the ring closure while the latter retards it. The new bromo-substituted compounds will be interesting for future scaffolding in the quest for advanced photo- and thermoswitches. We note, however, that initial attempts at using the 3-bromo-substituted DHA for Sonogashira or Suzuki couplings

(as previously accomplished for the 7-bromo-substituted DHA) have so far been unsuccessful. It seems that the 3-bromo functionality is not very reactive, which is reflected as well by the regioselective Sonogashira and Suzuki reactions on the 3,7-dibromoazulene **14** reported in this work.

Experimental

General Methods

NMR spectra were measured on 300 or 500 MHz instruments. All chemical shift values in the ^{1}H and ^{13}C NMR spectra are referenced to the solvent (δ_H = 7.26 ppm, δ_C = 77.16 ppm). Thin-layer chromatography (TLC) was carried out on commercially available precoated plates (silica 60) with fluorescence indicator; color change of the spot from yellow (DHA) to red (VHF) upon irradiation by UV light indicated the presence of a DHA. For column chromatographic purification of DHAs, the column was covered by aluminium foil to exclude light; the isolated fractions were also kept in the dark. All melting points are uncorrected. All spectroscopic measurements (including photolysis of DHA to VHF and kinetics studies on the thermal conversion of VHF to DHA) were performed in a cuvette of 1 cm path length. Photoswitching experiments were performed by using a 150 W xenon arc lamp equipped with a monochromator. Elemental analyses were performed at the Department of Chemistry, University of Copenhagen.

3-Bromo-2-phenyl-1,8a-dihydroazulene-1,1-dicarbonitrile (8): To a stirred solution of DHA **1** (300 mg, 1.17 mmol) in CH_2Cl_2 (40 mL) at rt was added $AlCl_3$ (800 mg, 6.01 mmol). Stirring was continued for further 20 min and then the mixture was quenched with water (60 mL). The organic layer was separated, dried over anhydrous Na_2SO_4, filtered, and concentrated under reduced pressure. The resulting red compound was then dissolved in benzene (40 mL) and NBS (700 mg, 3.93 mmol) was added. The solution was stirred under an Ar atmosphere for 10 min and then benzoyl peroxide (13 mg, 0.05 mmol) was added. The solution was irradiated with a 500 W halogen lamp kept at a distance of ca. 1 m from the reaction mixture. After 4 h, the mixture was filtered and washed with water. The organic layer was washed with saturated aqueous $NaHCO_3$ solution (3 × 100 mL), dried over anhydrous Na_2SO_4, and filtered. The solvent was removed under reduced pressure and the crude residue was purified by dry column vacuum chromatography (SiO_2, 60% Et_2O/heptane) affording **8** (180 mg, 46%) as a yellow solid. R_f 0.73 (30% heptane/EtOAc); mp 126 °C; ^{1}H NMR (500 MHz, $CDCl_3$) δ 7.63 (m, 2H), 7.44 (m, 3H), 6.61 (dd, *J* = 11.3, 6.4 Hz, 1H), 6.50 (d, *J* = 6.1 Hz, 1H), 6.49–6.46 (m, 1H), 6.28 (ddd, *J* = 10.1, 6.1, 2.1 Hz, 1H), 5.70 (dd, *J* = 10.1, 4.0 Hz, 1H), 3.70 (m, 1H) ppm; ^{13}C NMR (125 MHz, $CDCl_3$) δ 136.5, 135.8, 131.8, 130.8, 130.4, 130.3, 129.0, 128.8, 128.10, 126.9, 122.1, 119.6, 114.3, 111.9, 48.8, 47.4 ppm; FABMS *m*/*z*: $[M]^+$ 334; Analysis calcd for $C_{18}H_{11}BrN_2$: C, 64.50; H, 3.31; N, 8.36; found: C, 63.90; H, 3.42; N, 7.86.

3-Bromo-2-(4-methylphenyl)-1,8a-dihydroazulene-1,1-dicarbonitrile (10): To a stirred solution of 2-(4-methylphenyl)-1,8a-dihydroazulene-1,1-dicarbonitrile (**9**) (250 mg, 0.97 mmol) in CH_2Cl_2 (30 mL) at rt was added $AlCl_3$ (760 mg, 5.74 mmol). Stirring was continued for a further 10 min and then the mixture was quenched with water (50 mL). The organic layer was separated, dried over Na_2SO_4, filtered, and concentrated under reduced pressure. The residue was then dissolved in benzene (50 mL), and NBS (1.60 g, 9.50 mmol) was added. The solution was stirred under an Ar atmosphere for 10 min and then benzoyl peroxide (3 mg, 0.01 mmol) was added. The solution was irradiated with a 500 W halogen lamp for 2 h. The mixture was filtered and washed with water. The organic layer was washed with saturated aqueous $NaHCO_3$ solution (3 × 150 mL), dried over anhydrous Na_2SO_4, and filtered. The solvent was removed under reduced pressure affording **10** with minor impurities (321 mg, estimated yield of 95%). An analytically pure sample (yellow solid) could be obtained by dry column vacuum chromatography (SiO_2, Et_2O/heptane 3:2). R_f 0.79 (30% ethyl acetate/heptane); mp 115 °C; ^{1}H NMR (500 MHz, $CDCl_3$) δ 7.62 (d, *J* = 8.0 Hz, 2H), 7.32 (d, *J* = 8.0 Hz, 2H), 6.67 (dd, *J* = 11.3, 6.4 Hz, 1H), 6.58–6.49 (m, 2H), 6.34 (ddd, *J* = 10.1, 6.1, 2.1 Hz, 1H), 5.76 (dd, *J* = 10.1, 4.0 Hz, 1H), 3.79–3.72 (m, 1H), 2.43 (s, 3H) ppm; ^{13}C NMR (125 MHz, $CDCl_3$) δ 140.8, 136.6, 136.0, 131.6, 130.3, 129.7, 128.6, 128.1, 127.8, 126.2, 121.8, 119.6, 114.4, 112.0, 48.8, 47.3, 21.5 ppm; EIMS *m*/*z*: $[M]^+$ 348; Analysis calcd for $C_{19}H_{13}BrN_2$: C, 65.35; H, 3.75; N, 8.02; found: C, 65.50; H, 3.54; N, 7.94.

3,7-Dibromo-2-phenyl-1,8a-dihydroazulene-1,1-dicarbonitrile (12): 3-Br-DHA **8** (85 mg, 0.25 mmol) was dissolved in CH_2Cl_2 (5 mL) at −78 °C under a N_2 atmosphere and the mixture was excluded from light. Then a solution of Br_2 in CH_2Cl_2 (0.78 M, 327 μL) was slowly added over 2 min. The mixture was stirred for 30 min at −78 °C and then concentrated in vacuo to yield the crude product **11** as a yellow-brown solid (126 mg, 0.25 mmol). This compound was used without purification for the next step. It was dissolved in dry THF (5 mL) and cooled to −78 °C. Then LiHMDS (0.3 mL, 0.3 mmol, 1 M in toluene) was added dropwise, and the solution was stirred for 2 h, while the temperature was slowly raised to rt. The reaction mixture was diluted with Et_2O (20 mL) and then washed with saturated aqueous NH_4Cl (2 × 50 mL). The organic phase was dried over anhydrous Na_2SO_4 and filtered. The solvent was removed under reduced pressure and the crude residue was purified by dry column vacuum chromatography (SiO_2, 50% Et_2O/heptane) affording **12** (68 mg, 65%) as a pale green solid. Mp 118 °C;

^{1}H NMR (300 MHz, $CDCl_3$) δ 7.78–7.64 (m, 2H), 7.61–7.46 (m, 3H), 6.63 (d, *J* = 3.6 Hz, 2H), 6.52 (dt, *J* = 3.6, 1.7 Hz, 1H), 6.08 (d, *J* = 4.5 Hz, 1H), 3.80 (dd, *J* = 4.5, 1.7 Hz, 1H) ppm; ^{13}C NMR (125 MHz, $CDCl_3$) δ 138.3, 137.9, 133.8, 131.3, 130.7, 130.3, 129.1, 128.7, 126.4, 121.2, 120.4, 120.2, 113.7, 111.5, 49.0, 46.9 ppm; Analysis calcd for $C_{18}H_{10}Br_2N_2$: C, 52.21; H, 2.43; N, 6.76; found: C, 52.58; H, 2.41; N, 6.69.

3,7-Dibromo-2-phenylazulene-1-carbonitrile (14): To a solution of **4** excluded from light (154 mg, 0.46 mmol) (prepared as previously described [12]) in CH_2Cl_2 (4 mL) at −78 °C under a N_2 atmosphere was slowly added a 0.78 M solution of Br_2 (0.59 mL, 0.46 mmol) in CH_2Cl_2. After being stirred for 10 min at −78 °C, the reaction mixture was concentrated in vacuo. Purification by flash column chromatography (SiO_2, 50% CH_2Cl_2/heptane) afforded **14** (71 mg, 40%) as a green solid. Mp 220–223 °C; ^{1}H NMR (500 MHz, $CDCl_3$) δ 8.89 (d, *J* = 2.1 Hz, 1H), 8.52 (d, *J* = 9.9 Hz, 1H), 8.17 (dd, *J* = 10.4, 1.8 Hz, 1H), 7.84 (m, 2H), 7.64–7.49 (m, 3H), 7.38 (t, *J* = 10.4 Hz, 1H) ppm; ^{13}C NMR (125 MHz, $CDCl_3$) δ 152.5, 143.3, 141.7, 139.5, 139.4, 137.2, 132.7, 130.3, 130.0, 128.9, 127.4, 124.4, 116.3, 105.4, 96.1 ppm; GC–MS (*m*/*z*): $[M]^+$ 386.9; HRMS–ESI (*m*/*z*): $[M + H]^+$ calcd for $C_{17}H_{10}Br_2N$, 385.9175; found, 385.9196.

3-Bromo-2-phenyl-7-(triisopropylsilylethynyl)azulene-1-carbonitrile (15): To a mixture of the azulene **14** (18 mg, 0.047 mmol), $Pd(PPh_3)_2Cl_2$ (4 mg) and CuI (2 mg) in argon-degassed THF (4 mL) under an Ar atmosphere were added iPr_2NH (40 μL, 0.283 mmol) and triisopropylsilylacetylene (30 μL, 0.134 mmol). After being stirred for 24 h at rt, additional triisopropylsilylacetylene (50 μL, 0.223 mmol) was added, and the mixture was stirred again for 24 h at rt. Concentration of the reaction mixture in vacuo and purification of the residue by flash column chromatography (50% CH_2Cl_2/heptane) afforded **15** (17.5 mg, 77%) as a green solid. Mp 181–183 °C; ^{1}H NMR (500 MHz, $CDCl_3$) δ 8.72 (d, *J* = 1.5 Hz, 1H), 8.51 (dd, *J* = 9.9, 0.7 Hz, 1H), 8.03 (ddd, *J* = 10.4, 1.5, 1.0 Hz, 1H), 7.86–7.80 (m, 2H), 7.60–7.56 (m, 2H), 7.54–7.51 (m, 1H), 7.51 (t, *J* = 10.2 Hz, 1H), 1.22–1.16 (m, 21H) ppm; ^{13}C NMR (125 MHz, $CDCl_3$) δ 151.9, 143.7, 142.1, 139.4, 139.2, 138.0, 132.9, 130.3, 129.8, 128.8, 127.4, 124.1, 116.5, 108.9, 106.0, 97.6, 95.1, 18.9, 11.5 ppm; HRMS–ESI (*m*/*z*): $[M + H]^+$ calcd for $C_{28}H_{31}BrNSi$, 488.1404; found, 488.1398.

3-Bromo-7-(2',5'-dimethoxyphenyl)-2-phenylazulene-1-carbonitrile (17): To a solution of the azulene **14** (50 mg, 0.129 mmol) and 2,5-dimethoxyphenylboronic acid (**16**) (47 mg, 0.259 mmol) under an Ar atmosphere in an argon-degassed toluene/water 9:1 mixture were added K_3PO_4 (110 mg, 0.517 mmol), $Pd(OAc)_2$ (6 mg, 0.0026 mmol) and RuPhos (2-dicyclohexylphosphino-2',6'-diisopropoxy-1,1'-biphenyl) (24 mg, 0.051 mmol). The mixture was vigorously stirred and heated at 100 °C for 4 d. Purification by flash column chromatography (SiO_2, CH_2Cl_2) afforded **17** (15 mg, 26%) as a blue solid. Mp 169–171 °C; ^{1}H NMR (500 MHz, $CDCl_3$) δ 8.81 (d, *J* = 1.7 Hz, 1H), 8.56 (dd, *J* = 10.0, 0.9 Hz, 1H), 8.00 (ddd, *J* = 10.2, 1.7, 0.9 Hz, 1H), 7.86–7.83 (m, 2H), 7.64 (t, *J* = 10.1 Hz, 1H), 7.60–7.55 (m, 2H), 7.53–7.47 (m, 1H), 7.06–6.88 (m, 3H), 3.85 (s, 3H), 3.80 (s, 3H) ppm; ^{13}C NMR (125 MHz, $CDCl_3$) δ 154.1, 151.0, 150.6, 142.5, 142.4, 139.5, 139.4, 139.3, 137.2, 133.3, 132.9, 130.3, 129.5, 128.8, 127.7, 117.2, 117.1, 114.6, 113.0, 104.2, 96.8, 56.5, 56.1 ppm; HRMS–ESI (*m*/*z*): $[M + H]^+$ calcd for $C_{25}H_{19}BrNO_2$, 444.0594; found, 444.0617.

Solid-state conversion of dibromide **3** into azulenes (**19**–**21**)

The dibromide **3** (416 mg, 1.00 mmol) was stored in the dark at rt in a closed vessel (50 mL) for 30 d. The resulting black solid was dissolved in CH_2Cl_2 and purification by dry column vacuum chromatography (SiO_2, 12.6 cm^2, 0–100% toluene/heptanes, 12.5% steps, then 0–35% CH_2Cl_2 in toluene, 7% steps, 40 mL fractions) gave **19** (119.4 mg, 57%) and an inseparable mixture (ca. 4:1) of **20** and **21** (55.8 mg, 24%) (known compounds: [5,14,15]).

2-Phenylazulene-1,3-dicarbonitrile (19): ^{1}H NMR (500 MHz, $CDCl_3$) δ 8.80 (d, *J* = 9.7 Hz, 2H), 8.08 (t, *J* = 9.7 Hz, 1H), 8.05 (d, *J* = 7.4 Hz, 2H), 7.87 (t, *J* = 9.7 Hz, 2H), 7.62 (t, *J* = 7.4 Hz, 2H), 7.58–7.55 (m, 1 H) ppm; ^{13}C NMR (125 MHz, $CDCl_3$) δ 155.6, 145.4, 141.7, 138.1, 131.8, 131.7, 130.9, 129.7, 129.6, 116.1, 97.0 ppm; for X-ray data, see [6].

Solid-state conversion of tetrabromide **18** into azulenes **19**, **20**, and **22**

The tetrabromide **18** (576 mg, 1.00 mmol) was stored in the dark at rt in a closed vessel (50 mL) for 30 d. The resulting black solid was dissolved in $CHCl_3$ and purification by flash column chromatography (SiO_2, toluene) gave **19** (78.9 mg, 38%) as a pink solid, **20** (50.8 mg, 17%) as a violet solid, and **22** (97.7 mg, 20%) as a green solid. TLC (toluene); R_f 0.06–0.09 (**19**), 0.25–0.30 (**20**), 0.43–0.47 (**22**).

3,6-Dibromo-2-phenylazulene-1-carbonitrile (22): ^{1}H NMR (300 MHz, $CDCl_3$) δ 8.32 (d, *J* = 8.2 Hz, 1H), 8.28 (d, *J* = 8.6 Hz, 1H), 7.94 (dd, *J* = 5.2 Hz, *J* = 1.9 Hz, 1H), 7.90 (dd, *J* = 4.6 Hz, *J* = 1.9 Hz, 1H), 7.81–7.85 (m, 2H), 7.49–7.61 (m, 3H) ppm; ^{13}C NMR (75 MHz, $CDCl_3$) δ 151.3, 142.1, 138.6, 137.9, 136.2, 134.4, 132.8, 132.2, 131.7, 130.2, 129.8, 128.9, 116.2, 106.6, 98.5 ppm; Analysis calcd for $C_{17}H_9Br_2N$: C, 52.75; H, 2.34; N, 3.62; found: C, 52.97; H, 2.03; N, 3.55.

Supporting Information

Supporting Information File 1

1D and 2D NMR spectra of all new compounds. Table of bond lengths for VHF **2** (X-ray crystallographic data). Exponential fit of the decay over time of the VHF **7** absorbance at the longest-wavelength absorption maximum.
[http://www.beilstein-journals.org/bjoc/content/supplementary/1860-5397-8-108-S1.pdf]

Acknowledgements

Financial support from The Sino-Danish Center for Education and Research (SDC) and The Danish Council for Independent Research/Natural Sciences (#10-082088) is acknowledged. Mr. Christian G. Tortzen is gratefully acknowledged with regard to NMR characterizations.

References

1. Daub, J.; Knöchel, T.; Mannschreck, A. *Angew. Chem., Int. Ed. Engl.* **1984,** *23,* 960–961. doi:10.1002/anie.198409601
2. Mrozek, T.; Ajayaghosh, A.; Daub, J. Optoelectronic Molecular Switches Based on Dihydroazulene-Vinylheptafulvene (DHA-VHF). In *Molecular Switches;* Feringa, B. L., Ed.; Wiley-VCH: Weinheim, 2001; pp 63–106. doi:10.1002/3527600329.ch3
3. Nielsen, M. B.; Broman, S. L.; Petersen, M. Å.; Andersson, A. S.; Jensen, T. S.; Kilså, K.; Kadziola, A. *Pure Appl. Chem.* **2010,** *82,* 843–852. doi:10.1351/PAC-CON-09-07-08
4. Lara-Avila, S.; Danilov, A. V.; Kubatkin, S. E.; Broman, S. L.; Parker, C. R.; Nielsen, M. B. *J. Phys. Chem. C* **2011,** *115,* 18372–18377. doi:10.1021/jp205638b
5. Petersen, M. Å.; Kilså, K.; Kadziola, A.; Nielsen, M. B. *Eur. J. Org. Chem.* **2007,** 1415–1418. doi:10.1002/ejoc.200601052
6. Petersen, M. Å.; Broman, S. L.; Kadziola, A.; Kilså, K.; Nielsen, M. B. *Eur. J. Org. Chem.* **2009,** 2733–2736. doi:10.1002/ejoc.200900297
7. Broman, S. L.; Petersen, M. Å.; Tortzen, C. G.; Kadziola, A.; Kilså, K.; Nielsen, M. B. *J. Am. Chem. Soc.* **2010,** *132,* 9165–9174. doi:10.1021/ja103235g
8. Petersen, M. Å.; Broman, S. L.; Kilså, K.; Kadziola, A.; Nielsen, M. B. *Eur. J. Org. Chem.* **2011,** 1033–1039. doi:10.1002/ejoc.201001554
9. Broman, S. L.; Brand, S. L.; Parker, C. R.; Petersen, M. Å.; Tortzen, C. G.; Kadziola, A.; Kilså, K.; Nielsen, M. B. *ARKIVOC* **2011,** *(ix),* 51–67. http://hdl.handle.net/2027/spo.5550190.0012.904
10. Parker, C. R.; Tortzen, C. G.; Broman, S. L.; Schau-Magnussen, M.; Kilså, K.; Nielsen, M. B. *Chem. Commun.* **2011,** *47,* 6102–6104. doi:10.1039/c1cc10804b
11. Kuroda, S.; Asao, T. *Tetrahedron Lett.* **1976,** *17,* 251–254. doi:10.1016/S0040-4039(00)93700-6
12. Daub, J.; Gierisch, S.; Klement, U.; Knöchel, T.; Maas, G.; Seitz, U. *Chem. Ber.* **1986,** *119,* 2631–2646. doi:10.1002/cber.19861190820
13. Ito, S.; Shoji, T.; Morita, N. *Synlett* **2011,** 2279–2298. doi:10.1055/s-0030-1260316
    See for a recent review on synthetic methods for the preparation of functionalized azulenes.
14. Nozoe, T.; Takase, K.; Fukuda, S. *Bull. Chem. Soc. Jpn.* **1971,** *44,* 2210–2213. doi:10.1246/bcsj.44.2210
15. Gierisch, S.; Daub, J. *Chem. Ber.* **1989,** *122,* 69–75. doi:10.1002/cber.19891220112

License and Terms

Beilstein Journal of Organic Chemistry

Synthesis and anion recognition properties of shape-persistent binaphthyl-containing chiral macrocyclic amides

Marco Caricato[1], Nerea Jordana Leza[1], Claudia Gargiulli[2], Giuseppe Gattuso[2], Daniele Dondi[1] and Dario Pasini[*1,3]

Full Research Paper

Open Access

Address:
[1]Department of Chemistry, University of Pavia, Viale Taramelli 10, 27100 Pavia, Italy, [2]Department of Organic and Biological Chemistry, University of Messina, Viale F. Stagno d'Alcontres 31, 98166 Messina, Italy and [3]INSTM Research Unit, Department of Chemistry, University of Pavia, 27100 Pavia, Italy

Email:
Dario Pasini* - dario.pasini@unipv.it

* Corresponding author

Keywords:
amides; anion recognition; chirality; macrocycles; molecular switches; supramolecular chemistry

Beilstein J. Org. Chem. **2012,** *8,* 967–976.
doi:10.3762/bjoc.8.109

Received: 08 March 2012
Accepted: 23 May 2012
Published: 28 June 2012

This article is part of the Thematic Series "Molecular switches and cages".

Guest Editor: D. Trauner

Abstract

We report on the synthesis and characterization of novel shape-persistent, optically active arylamide macrocycles, which can be obtained using a one-pot methodology. Resolved, axially chiral binol scaffolds, which incorporate either methoxy or acetoxy functionalities in the 2,2' positions and carboxylic functionalities in the external 3,3' positions, were used as the source of chirality. Two of these binaphthyls are joined through amidation reactions using rigid diaryl amines of differing shapes, to give homochiral tetraamidic macrocycles. The recognition properties of these supramolecular receptors have been analyzed, and the results indicate a modulation of binding affinities towards dicarboxylate anions, with a drastic change of binding mode depending on the steric and electronic features of the functional groups in the 2,2' positions.

Introduction

Macrocyclic molecules possessing a high degree of shape persistency act as molecular cages, and the scientific interest for such compounds is certainly increasing [1-4]. Support for this statement arises from consideration in two main areas of interest: (a) the recognition properties towards suitable guests are usually enhanced by limiting the number of conformations accessible to the covalent cyclic structure (resulting in preorganization [5]); (b) shape persistency is a requirement for the formation of organic nanotubes by means of supramolecular organization of macrocycles in the third dimension [6-12].

Amide functionalities are hydrogen-bonding tools of widespread use for the conformational stabilization of nanostructures. Noticeable examples can be found in the field of foldamers [13,14] or in the design of assembled architectures functioning as artificial ion-channel mimics [15]. Amide functionalities are also widely used for their hydrogen bonding capability in the context of anion complexation. Several macrocyclic systems capable of effective anion recognition and discrimination have been previously reported [16-18]. Binol (1,1'-binaphthyl-2,2'-diol) based synthons are popular in the recent literature; given their robustness, they are frequently used to impart or transfer chiral information, not only in the field of asymmetric synthesis and catalysis, but also in materials science [19-24].

During the course of our ongoing efforts dealing with the use of binol-based synthons for the production of functional, oriented nanomaterials and chiroptical sensors [25-30], we have reported on the design, synthesis and characterization of a rigid, optically active tetraamidic macrocycle with recognition capabilities towards anions (Figure 1) [31].

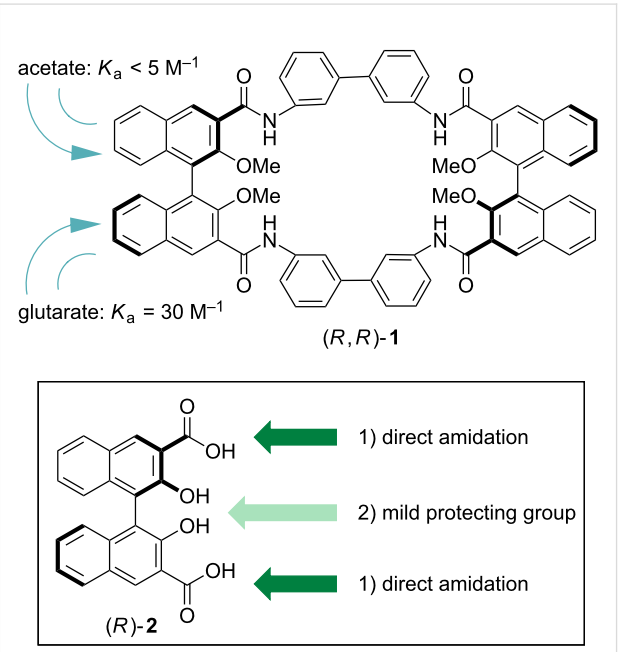

Figure 1: Structure of the macrocycle (*R*,*R*)-**1** (top), and synthetic strategies for the production of novel amide-containing, axially chiral macrocycles (bottom).

In fact, macrocycle (*R*,*R*)-**1** could be obtained efficiently (62% in the macrocyclization step) through a sequential, convergent methodology. It is a 32-membered macrocycle whose cyclic backbone is composed exclusively of sp^2-hybridized carbon and nitrogen atoms. An additional internal rigidification of the macrocyclic cavity is given by the presence of stable, six-membered intramolecular hydrogen bonds between the protected (in the form of methyl ether) phenol moieties in the 2,2' positions and the NH protons of the amide functionalities in the neighboring 3,3' positions of the binaphthyl units. Macrocycle (*R*,*R*)-**1** showed modest binding affinities towards carboxylate anions, yet detectable binding of proper difunctional carboxylates.

We deemed it to be very interesting to increase the availability of hydrogen-bond donors within the macrocycle cavity, and to unlock the hydrogen-bonding capability of the amide NHs to their full potential for anion recognition. The former could in principle be achieved by unmasking the phenolic oxygen atoms in the 2,2' positions of the binaphthyl skeletons. As for the latter, the introduction of another protecting group, sterically and electronically modulating the hydrogen-bond accepting capability of the phenolic oxygen, was needed.

In this paper, we present the exploitation of these strategies, resulting in the synthesis and characterization of three novel binaphthyl-based macrocycles, and the evaluation of their potential as supramolecular receptors for aliphatic bidentate carboxylate anions.

Results and Discussion

Design, synthesis and spectroscopic characterization

Reactions to deprotect the phenolic oxygens, performed directly on (*R*,*R*)-**1** as a substrate and attempted under various reaction conditions, proved completely unsuccessful with degradation of the macrocyclic structure occurring in all cases. On the basis of the introductory considerations mentioned earlier, we set out to exploit two orthogonal synthetic strategies (Figure 1, bottom): (1) A direct amidation of the carboxylic acids in the 3,3' positions, in the presence of the free phenolic oxygens in the 2,2' positions. Literature precedents for such amidation using aromatic amines in the presence of vicinal phenol moieties (which compete since they are comparable in nucleophilicity with aromatic amines) are rare [32,33]. As already reported [31], test reactions on model compounds gave disappointing results. The use of benzylic amines, more nucleophilic than arylamines, and therefore competing less with the phenolic moieties in the 2,2' positions, was envisaged as a potential solution and was therefore actively pursued. (2) The use of milder (with respect to methyl ether) protecting groups for the phenolic functionalities in the 2,2' positions; we focused on the use of compound **3**, bearing acetyl protecting groups, since its synthesis has been reported, and the deprotection of these groups usually occurs under mild basic conditions [34]. Aromatic amines, as in (*R*,*R*)-**1**, could in principle be used.

Preliminary synthetic work was performed on model compounds to test the reaction conditions. Both enantiomerically pure (*R*)-**2** and (*R*)-**3** and racemic (*RS*)-**2** and (*RS*)-**3** were used routinely in the experiments described in the following. Regarding approach (1), direct generation of the carboxylic acid chloride (with $SOCl_2$, or oxalyl chloride and DMF; method i), followed by reaction with benzylamine (**4a**) in the presence of Et_3N as the acid scavenger gave compound **5a** in excellent yields (93%) after purification by column chromatography (Scheme 1). The yield was higher in our hands than the one previously reported [35].

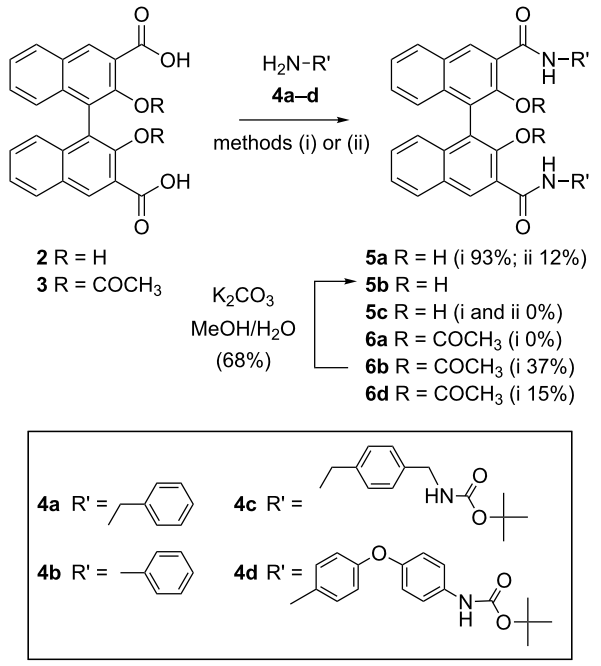

Scheme 1: Reagents and conditions: (i) $SOCl_2$, $CHCl_3$ or $(COCl)_2$, DMF, CH_2Cl_2 then amine, Et_3N, CH_2Cl_2 or (ii) CDI, THF.

Alternative one-pot amidation procedures, performed directly with the aromatic carboxylic acid and the benzylic amine (method ii) using carbonyldiimidazole (CDI) [36], successfully used by us in the past [29], were instead less than satisfactory. Both protocols were applied with commercially available monoprotected benzylic diamine **4c**; in both cases, however, the desired product **5c** could not be isolated. It is likely that the BOC protecting group is not compatible with the presence of the free phenolic groups in our substrates.

Switching to approach (2), when compound **3** was allowed to react with benzylamine (**4a**) or aniline (**4b**), only the aryl derivate **6b** was obtained in good yield. Compound **6b** could be efficiently deprotected under the reported conditions (K_2CO_3/MeOH) to give **5b**. When the monoprotected aryl amine **4d** was allowed to react with compound **3** using the same reaction conditions, however, compound **6d** could not be efficiently synthesized. The low yield obtained in this step discouraged us from pursuing a stepwise methodology for the macrocyclization, which had been used in the case of (*R*,*R*)-**1** [31].

In order to quickly evaluate the potential of acetyl-protected tetraamidic macrocyles as analogues of (*R*,*R*)-**1**, we proceeded to directly cyclize equimolar amounts of optically pure, resolved (*R*)-**3** (via formation of the corresponding diacyl chloride) and commercially available diaryl amines **8** and **9**, under classical high-dilution conditions [13] which were successful for the synthesis of compound **6b**. Indeed, homochiral macrocycles (*R*,*R*)-**10**, (*R*,*R*)-**11** and (*R*,*R*)-**12** could be isolated after extensive purification by column chromatography, although in disappointingly low yields (0–5% isolated yield, Scheme 2).

Furthermore, macrocycle (*R*,*R*)-**13** could not be isolated at all. The low quantities of macrocycles (*R*,*R*)-**10** and (*R*,*R*)-**11** obtained prevented us from exploring the cleavage of the acetyl functionalities.

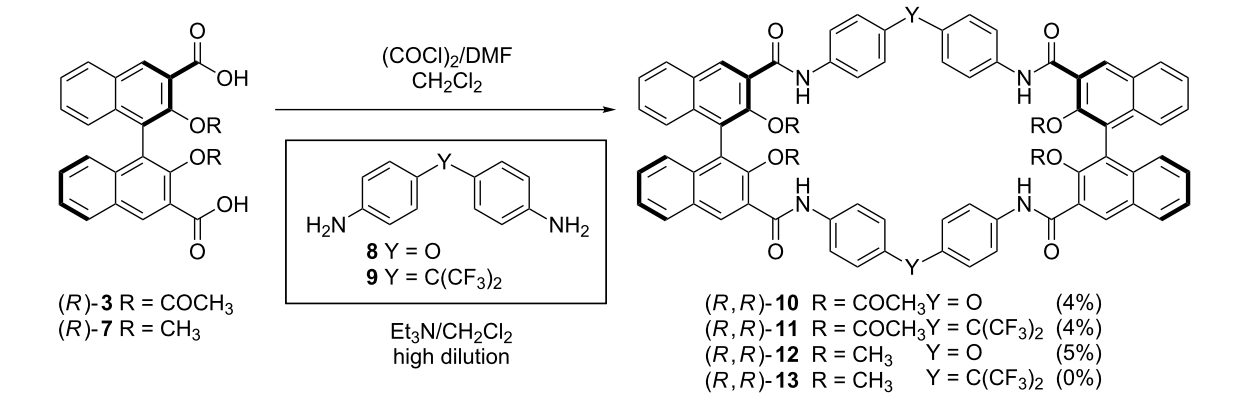

Scheme 2: Structure and synthesis of the macrocycles discussed in this paper.

^{1}H NMR spectra for all compounds were relatively simple (see Experimental and Supporting Information File 1), reflecting the structural symmetry found in precursors (C_2 molecular symmetry) and in homochiral macrocycles **10**–**12** (D_2 molecular symmetry). The peaks for the NH proton resonances of the amide functionalities are sharp in S(6)-type [37] hydrogen-bonded systems, such as those between the NH and the neighboring methoxy groups in (*R*,*R*)-**1** and (*R*,*R*)-**12**. The NH proton resonances, however, could not be assigned either in the series of compounds **5**, or in the acetoxy protected compounds **6** and macrocycles **10**,**11**, as they are broad or below the baseline, so as to indicate unlocked (thus potentially more available to incoming guests), conformationally mobile NH groups (Table 1).

There are also substantial differences in the resonances of the H 4,4' protons of the binaphthyl skeleton, which are usually most sensitive to variations in the substitution pattern (and thus, in the electronic structure) within the naphthyl systems of the binaphthyl units.

The UV–vis spectra of macrocycles (*R*,*R*)-**10** and (*R*,*R*)-**11**, recorded in solvents possessing different solvating and hydrogen-bonding abilities (CH_2Cl_2, EtOH), showed little solvent dependence, with λ_{max} around 230 nm in all cases, and with well-defined shoulders just below 300 nm. Comparison with data available on parent systems [31] reveals that the spectra cannot be explained as the sum of those generated by the two major aromatic chromophoric components (the naphthyl rings of the binaphthyl units and the aryl moieties of the spacing units); electronic communication between them is present (Figure 2).

It is interesting to note how the spectra of macrocycle (*R*,*R*)-**12**, bearing methoxy protected phenols, showed the most bathochromically shifted shoulder, centered at 320 nm (quite different from (*R*,*R*)-**10**). The CD spectra (in EtOH) show activity associated with all active UV chromophores and more marked activity for the macrocycle (*R*,*R*)-**10**, with exciton couplet signals greater in intensity than the ones of the other macrocycles.

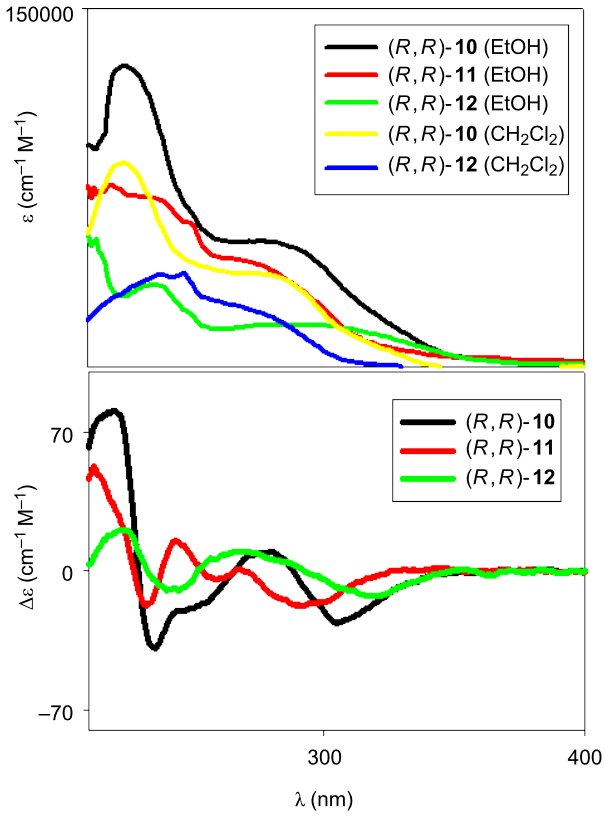

Figure 2: UV and CD (EtOH) spectra of macrocycles (*R*,*R*)-**10**, (*R*,*R*)-**11** and (*R*,*R*)-**12** in the range 220–400 nm.

Table 1: Selected chemical shifts for compounds in $CDCl_3$ (25 °C).[a]

Entry	Compound	NH	Binol-H 4,4'[b]	OCH_3	$COCH_3$	OH
1	**5a**	9.88	8.74	—	—	12.44
2	**5b**	n. d.[c]	8.85	—	—	10.31
4	**6b**	n. d.	8.47	—	1.83	—
5	**6d**	n. d.	8.46	—	1.84	—
6	(*R*,*R*)-**10**	n. d.	8.58	—	1.82	—
7	(*R*,*R*)-**11**	n. d.	8.58	—	1.83	—
8	(*R*,*R*)-**12**	10.45	9.06	3.32	—	—
9	(*R*,*R*)-**1**	10.00	9.00	3.53	—	—

[a]All spectra recorded at 5–10 mM sample concentration. [b]Resonances related to the singlet corresponding to the proton in the 4,4' positions of the binol skeleton. [c]n. d. = broad or not identified.

Molecular modeling

Molecular modeling was performed on the structures of macrocycles (*R*,*R*)-**10**, (*R*,*R*)-**11** and (*R*,*R*)-**12**, and on the hypothetical macrocycle (*R*,*R*)-**13**, in order to have an estimate of macrocyclic cavities, and to gather information on the relative orientation of the functional groups involved in the binding phenomena. Preliminary conformational structures were optimized by using the semiempirical PM3 method [38]. The geometries were then subjected to further refinement by using DFT B3LYP/6-31G(d) methods. In order to locate conformers having the minimum energy, the structures obtained by preliminary optimization were then subjected to molecular dynamics cycles and subsequent reoptimization [28]. The most stable minimized structures of the macrocycles are shown in Figure 3, in which the distances between the four hydrogen atoms of the NH amide groups within each macrocycle are reported (in angstroms).

The two macrocycles bearing aryloxy ether spacers ((*R*,*R*)-**10** and (*R*,*R*)-**12**) have a rectangular overall geometry, probably as a consequence of the imposed dihedral angle of the oxygen atom bridges. In fact, the two trifluoromethyl-containing macrocycles ((*R*,*R*)-**11** and (*R*,*R*)-**13**) have a more square-like geometry, which seems to be associated with the smaller imposed angle of the sp^3-hybridized carbon atom in the spacing units. The dimensions of the macrocycles are essentially identical for the homologous sets of (*R*,*R*)-**11** and (*R*,*R*)-**13** (14 Å × 15.7 Å), and of (*R*,*R*)-**10** and (*R*,*R*)-**12** (12.5 Å × 16.2 Å). In the case of (*R*,*R*)-**1**, the macrocycle cavity is more square-like, with the four amides all at a quite similar distance (ca. 6–7 Å). In the case of **10**–**13**, however, there is a substantial differentiation in distances between the two sets of amide functionalities, those linked to each different binaphthyl unit within the macrocycle. (*R*,*R*)-**11** and (*R*,*R*)-**13** possess slightly less distorted molecular conformations in which a C_2 overall molecular symmetry seems to be retained. In fact, the dihedral angles of the binaphthyl units within the macrocycle are identical in the case of (*R*,*R*)-**11** (76.1°) and of (*R*,*R*)-**13** (79.5°), whereas they differ slightly in the case of the more distorted (*R*,*R*)-**10** (70.8 and 72.6°) and (*R*,*R*)-**12** (85.9 and 85.6°). Molecular modeling does not give clear hints as to why macrocycle (*R*,*R*)-**13** could not be obtained.

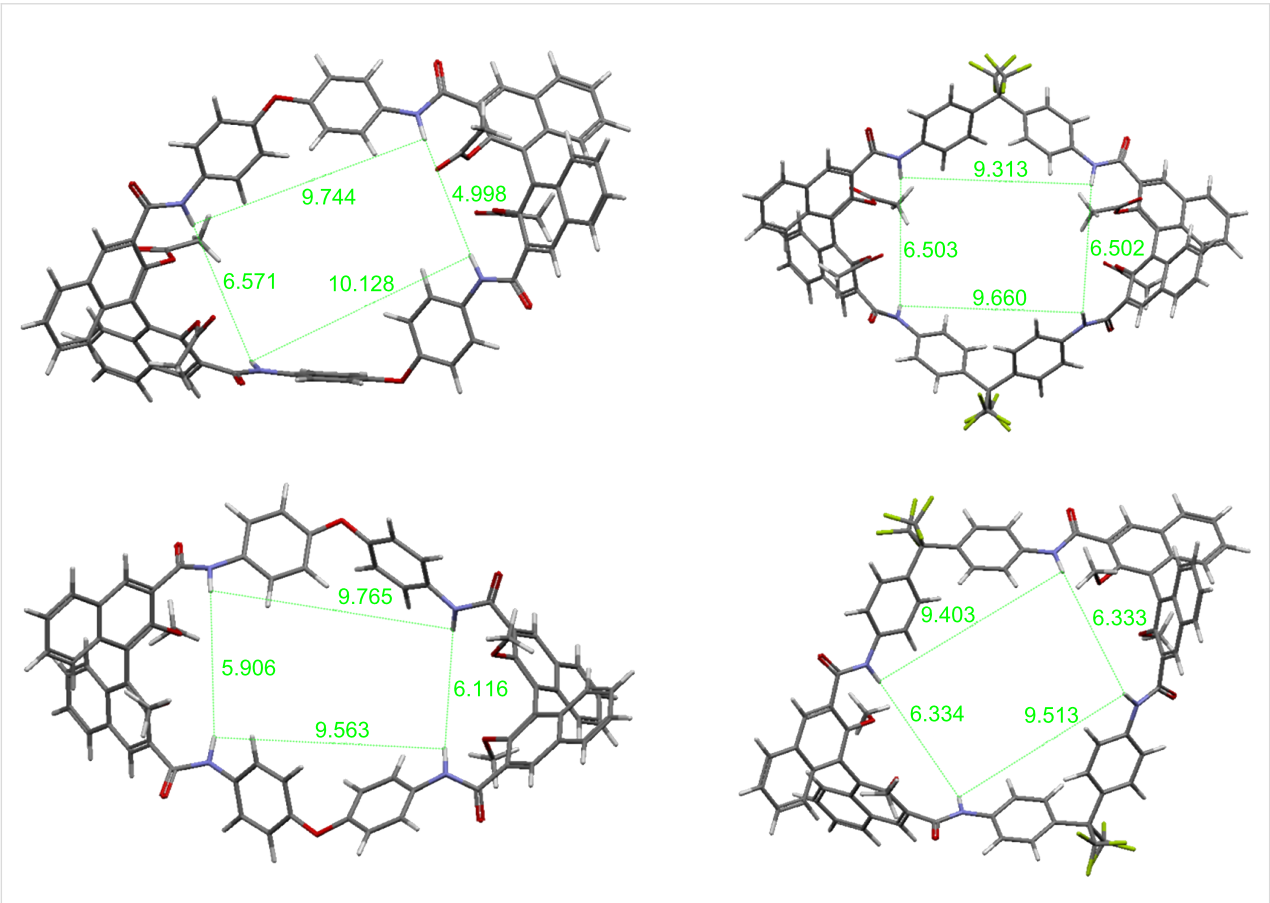

Figure 3: Minimized molecular structures of (from top left to bottom left, clockwise): (*R*,*R*)-**10**, (*R*,*R*)-**11**, (*R*,*R*)-**13** and (*R*,*R*)-**12** (distances between the H atoms of the NH amide groups are given in angstroms).

The shortest distances between the symmetry-related NH groups, shown in Figure 3, are compatible with the insertion of either glutarate or succinate. In fact, the calculated dimensions of the two carboxylates are 5.3 Å for succinate and 6.5 Å for glutarate, considering their fully extended conformation. These data rationalize the preference shown in the case of macrocycle **12** for succinate; in detail, they suggest that the binding mode involves two NH groups linked to the same binaphthyl unit, rather than a complexation mode in which the bidentate guests are extended across the cavities of the macrocycles. These findings also explain why, in the presence of bulkier acetoxy groups on the binaphthyl units, this recognition mechanism in **10** and **11** is suppressed and alternative mechanisms take place (see below).

Complexation studies

^{1}H NMR titration experiments showed that the addition of anionic guests, in the form of their tetrabutylammonium salts, produced progressive chemical-shift variations, along with a broadening of the peaks belonging to the amide NH protons, indicating that these groups were engaged in hydrogen bonding with the carboxylate guests with a fast-exchanging equilibrium on the NMR time scale. Complexation-induced shifts on other resonances of the binaphthyl residues (Figure 4) indicated, as expected, a change of the electronic structure of these units upon complexation; these peaks were used for the calculation of the association constants, by using a 1:1 model equation (see Experimental).

Alternative binding models (i.e., stoichiometries) produced much poorer and hence unacceptable fitting of the titration data. In the case of (*R*,*R*)-**12**, we examined dicarboxylate anions such as glutarate and succinate, in order to have a direct point of comparison with (*R*,*R*)-**1** (Table 2).

Table 2: Binding constants (M^{-1}) for the 1:1 complexes between (*R*,*R*)-**12** or (*R*,*R*)-**1** and dicarboxylate anions in $CDCl_3$.[a]

Entry	Macrocycle	Succinate	Glutarate
1	(*R*,*R*)-**12**	34 ± 3	21 ± 13
2[b]	(*R*,*R*)-**1**	n. d.	30 ± 12

[a]Measured by ^{1}H NMR (500 MHz, 298 K, $CDCl_3$) using tetrabutylammonium salts. [b]Data taken from Ref. [31]; n. d. = not determined.

Succinate was found to bind better than glutarate to macrocycle (*R*,*R*)-**12**, probably as its length is more suited than glutarate to

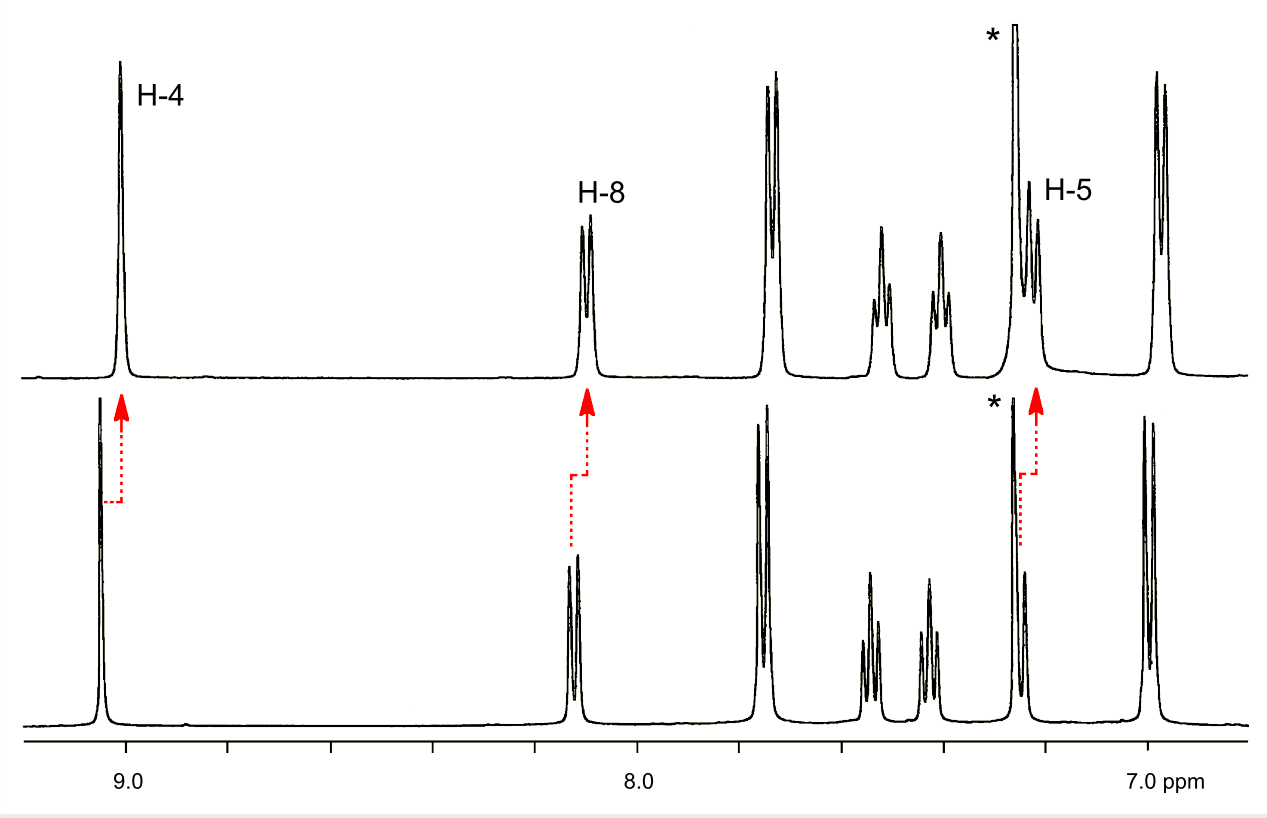

Figure 4: Aromatic region of the ^{1}H NMR ($CDCl_3$, 500 MHz, 25 °C) spectra of macrocycle (*R*,*R*)-**12** (2.8 mM, bottom) and at the end of the titration with tetrabutylammonium succinate ([(*R*)-**7**] = 2.8 mM, $[(CH_2CO_2)_2(Bu_4N)_2]$ = 28 mM, top). Asterisks indicate the residual solvent peaks.

fit into the cavity of **12** by interacting simultaneously with two different NH groups placed on the same binaphthyl residue (see above, molecular modeling), possibly in a cooperative fashion [39].

Similar titrations were carried out on (*R*,*R*)-**10** and (*R,R*)-**11**, bearing acetoxy substituents in the 2,2' positions of the binaphthyl skeletons, which are certainly bulkier than the methoxy substituents present in (*R*,*R*)-**12**. A very different behavior was observed for both macrocycles: The ^{1}H NMR spectra in $CDCl_3$, upon addition of both anionic guests, became very complex, with a complete loss of the initial symmetry. From the preliminary data in our hands, it is clear that there is a slow-exchanging equilibrium on the NMR time scale: the bulkier acetoxy group presumably inhibits a binding mechanism based on a fast host–guest exchange. A slow encapsulation mechanism, with multiple modes of binding of the difunctional anionic guests within the macrocycle, or the formation of aggregates of several macrocyclic units, held by the bifunctional anionic guests binding to a single amide of each macrocycle, cannot be ruled out at the present stage. Further studies are in progress to unravel the behavior of these acetoxy-bearing macrocycles.

Conclusion

We have reported the synthesis and characterization of three novel homochiral macrocycles, built upon resolved 1,1'-binaphthyl scaffolds, which incorporate either methoxy or acetoxy functionalities in the 2,2' positions, and carboxylic functionalities in the external 3,3' positions. After evaluation of the synthetic strategy through test reactions on model compounds, the macrocycles were obtained through one-pot amidation reactions by using two different rigid diarylamines and high-dilution conditions, although in low isolated yields (0–5%). The macrocycle bearing less sterically demanding methoxy substituents is an effective supramolecular receptor for dicarboxylate anions, with a preference for glutarate (K_a = 34 M^{-1} for the 1:1 complex in $CDCl_3$), as measured by ^{1}H NMR spectroscopy. With the acetoxy groups installed within the macrocyclic framework, a drastic change of binding mode occurs, with slow aggregation equilibria on the NMR time scale.

Experimental

General. All commercially available compounds were purchased from commercial sources and used as received. Racemic or (*R*)-**2** [40,41], racemic or (*R*)-**3** [42], **4c** [43], **4d** [44] and (*R*)-**7** [45] were prepared according to literature procedures. THF (Na), CH_2Cl_2 (CaH_2) and $CHCl_3$ (4 Å molecular sieves) were dried before use. Analytical thin-layer chromatography was performed on silica gel, chromophore-loaded, commercially available plates. Flash chromatography was carried out by using silica gel (pore size 60 Å, 230–400 mesh). ^{1}H and ^{13}C NMR spectra were recorded from solutions in $CDCl_3$ on a 200, 300 or 500 MHz spectrometer with the solvent residual proton signal or tetramethylsilane as the standard. The UV–vis spectroscopic studies were recorded by using commercially available spectrophotometers. Mass spectra were recorded by using an electrospray ionization instrument. Optical rotations were measured on a polarimeter with a sodium lamp (λ = 589 nm) and are reported as follows: $[\alpha]_D^{rt}$ (*c* = g (100 mL solution)$^{-1}$). CD spectroscopy was performed by using a spectropolarimeter; spectra were recorded at 25 °C at a scanning speed of 50 nm min^{-1} and were background corrected.

Compound 5a [35]. $SOCl_2$ (1.1 mL) was added to a solution of compound (*RS*)-**2** (250 mg, 0.67 mmol, 1 equiv) in dry $CHCl_3$ (10 mL) and the solution was heated under reflux overnight. Then, the solution was concentrated in vacuo and the crude product was added to a solution of benzylamine cooled to 0 °C (430 mg, 4.00 mmol, 6 equiv) in dry CH_2Cl_2 (10 mL). After being stirred overnight at rt, the reaction mixture was quenched with 1 M HCl (30 mL), extracted with CH_2Cl_2 (3 × 25 mL), and dried (Na_2SO_4). The solution was filtered and concentrated in vacuo to yield pure **5a** (340 mg, 93%). ^{1}H NMR ($CDCl_3$, 300 MHz, 25 °C) δ 12.44 (s, 2H, OH), 9.88 (s, 2H, NH), 8.74 (s, 2H, binaphthyl), 7.91 (d, 2H, binaphthyl), 7.37 (m, 14H, phenyl + binaphthyl), 6.98 (d, 2H, binaphthyl), 4.60 (d, CH_2). Alternative method: A solution of CDI (162 mg, 2.01 mmol, 3 equiv) in THF (12 mL) was added to a solution of (*R*)-**2** (250 mg, 0.668 mmol, 1 equiv) in THF (20 mL). The solution was stirred for 1.5 h at rt, and then a solution of benzylamine (0.146 mL, 1.34 mmol, 2 equiv) in THF (12 mL) was added and the mixture was stirred for 15 h. The reaction mixture was concentrated in vacuo, and the crude product was purified by column chromatography (hexane/AcOEt 9:1) to yield **5a** (44 mg, 12%).

Compound 6b. $(COCl)_2$ (0.137 mL, 1.57 mmol, 8 equiv) and one drop of DMF were added to a solution of compound (*R*)-**3** (90 mg, 0.196 mmol, 1 equiv) and dry CH_2Cl_2 (10 mL). The solution was heated under reflux for 2 h. After 1 h at rt the solution was concentrated in vacuo, the crude product was dissolved in dry CH_2Cl_2 (5 mL), and a solution of **4b** (0.045 mL, 0.49 mmol, 2.5 equiv) and Et_3N (0.082 mL, 0.59 mmol, 3 equiv) in dry CH_2Cl_2 (5 mL) was added. The resulting solution was heated under reflux for 2 h. After cooling, the reaction mixture was quenched with brine (20 mL), extracted with CH_2Cl_2 (3 × 25 mL), and dried (Na_2SO_4). The crude product was purified by column chromatography (hexane/AcOEt 8:2 to 7:3) to yield **6b** (44 mg, 37%). ^{1}H NMR ($CDCl_3$, 300 MHz, 25 °C) δ 8.47 (s, 2H, binaphthyl), 8.10 (s, 2H, binaphthyl), 8.03 (m, 2H, phenyl), 7.60 (m, 6H, binaphthyl + phenyl), 7.37 (m, 4H, binaphthyl), 7.22 (m, 4H, phenyl), 1.83 (s, 6H, –$COCH_3$).

Compound 5b. K_2CO_3 (91 mg, 0.66 mmol, 8 equiv) and H_2O (10 mL) were added to a solution of compound **6b** (44 mg, 0.082 mmol, 1 equiv) and CH_3OH (10 mL). Then, the solution was stirred for 4 h at rt. The reaction mixture was quenched with 1 M HCl, extracted with CH_2Cl_2 and dried (Na_2SO_4). The solution was filtered and concentrated in vacuo and the crude product was purified by column chromatography (hexane/AcOEt 7:3) to yield **5b** (25 mg, 68%). ^{1}H NMR ($CDCl_3$, 300 MHz, 25 °C) δ 10.31 (brs, 2H, OH), 8.85 (s, 2H, binaphthyl), 7.97 (m, 2H, binaphthyl), 7.82 (m, 4H, phenyl), 7.40 (m, 8H, binaphthyl + phenyl), 7.17 (m, 4H, binaphthyl). The data are consistent with those reported in the literature [46].

Compound 6d. $(COCl)_2$ (0.28 mL, 3.21 mmol, 8 equiv) and one drop of DMF were added to a solution of compound **3** (184 mg, 0.402 mmol, 1 equiv) and dry CH_2Cl_2 (15 mL). Then, the solution was heated at reflux for 2 h. After 1 h at rt the solution was concentrated in vacuo and the crude product was dissolved in dry CH_2Cl_2 (10 mL). This solution and a solution of **4d** (300 mg, 1 mmol, 2.5 equiv) in dry CH_2Cl_2 (10 mL) were added dropwise at the same rate over a period of 1 h to a solution of Et_3N (0.279 mL, 2 mmol, 5 equiv) in dry CH_2Cl_2 (10 mL). The resulting solution was heated under reflux for 2 h. After cooling, the reaction mixture was quenched with brine (20 mL), extracted with CH_2Cl_2 (3 × 25 mL) and dried (Na_2SO_4). The crude product was purified by column chromatography (CH_2Cl_2/AcOEt 10:0 to 9:1) to yield **6d** (61 mg, 15%). ^{1}H NMR ($CDCl_3$, 300 MHz, 25 °C) δ 8.46 (s, 2H, binaphthyl), 8.04 (s, 4H, binaphthyl), 7.56 (d, 6H, binaphthyl + phenyl), 7.35 (m, 6H, binaphthyl + phenyl), 6.97 (d, 8H, phenyl), 1.84 (s, 6H, -$COCH_3$), 1.53 (s, 18H, *t*-Bu).

Macrocycle (*R*,*R*)-10. $(COCl)_2$ (0.381 mL, 4.38 mmol, 8 equiv) and one drop of DMF were added to a solution of compound (*R*)-**3** (250 mg, 0.546 mmol, 1 equiv) in dry CH_2Cl_2 (20 mL). The solution was heated under reflux for 2 h. After 1 h at rt the solvent was removed in vacuo and the crude product was dissolved in dry CH_2Cl_2 (35 mL). This solution and a solution of **8** (109 mg, 0.546 mmol, 1 equiv) in dry CH_2Cl_2 (35 mL) were added dropwise at the same rate over a period of 1 h to a solution of Et_3N (0.228 mL, 1.64 mmol, 3 equiv) in dry CH_2Cl_2 (35 mL). The resulting solution was heated under reflux overnight. After cooling, the reaction mixture was quenched with brine (50 mL), extracted with CH_2Cl_2 (3 × 50 mL) and dried (Na_2SO_4). The solution was filtered and concentrated in vacuo, and the crude product was purified by column chromatography (CH_2Cl_2/AcOEt 9:1) to yield (*R*,*R*)-**10** (7 mg, 4%). $[\alpha]_D^{25}$ +101° (*c* 0.001, CH_2Cl_2); ^{1}H NMR ($CDCl_3$, 75 MHz, 25 °C) δ 8.58 (s, 4H, binaphthyl), 8.05 (m, 8H, phenyl), 7.50 (m, 16H, binaphthyl + phenyl), 6.97 (d, 8H, binaphthyl), 1.82 (s, 12H, -$COCH_3$); ^{13}C NMR ($CDCl_3$, 75 MHz, 25 °C) δ 168.7 (O-CqOCH$_3$), 163.5 (O-CqON), 154.6 (Cq), 143.1 (Cq), 133.8 (Cq), 133.3 (CH), 131.2 (Cq) 131.0 (Cq), 129.0 (CH), 128.7 (2CH), 128.0 (Cq), 127.0 (CH), 126.4 (CH), 125.1 (Cq), 121.1 (CH), 119.7 (2CH), 20.4 (COCH$_3$); ESIMS *m*/*z*: 1267.5 ([M + Na]$^+$, 100%).

Macrocycle (*R*,*R*)-11. The title compound was prepared by following the same procedure used for **10** but with diamine **9** used instead of **8**. The crude product was purified by column chromatography (CH_2Cl_2/AcOEt 98:2) to yield (*R*,*R*)-**11** (18 mg, 4%). $[\alpha]_D^{25}$ +56° (*c* 0.0015, CH_2Cl_2); ^{1}H NMR ($CDCl_3$, 75 MHz, 25 °C) δ 8.58 (s, 4H, binaphthyl), 8.25 (s, 4H, phenyl), 8.07 (d, 4H, phenyl), 7.40 (m, 24H, binaphthyl + phenyl), 1.83 (s, 12H, $COCH_3$); ^{13}C NMR ($CDCl_3$, 75 MHz, 25 °C) δ 168.9 (O-CqOCH$_3$), 163.8 (O-CqON), 143.0 (Cq), 138.1 (Cq), 133.9 (Cq), 131.3 (CH), 131.1 (2CH), 130.9 (Cq), 129.6 (Cq), 129.0 (CH), 128.9 (CH), 127.9 (Cq), 127.1 (CH), 126.3 (CH), 125.1 (Cq), 119.2 (2CH), 20.4 (CH_3); ESIMS *m*/*z*: 1535.1 ([M + Na]$^+$, 100%).

Macrocycle (*R*,*R*)-12. The title compound was prepared by following the same procedure used for **10** but with (*R*)-**7** used instead of (*R*)-**3**. The crude product was purified by column chromatography (CH_2Cl_2/AcOEt 99:1) to yield (*R*,*R*)-**12** (6 mg, 5%). $[\alpha]^{25}_D$ +170° (*c* 0.0015, CH_2Cl_2); ^{1}H NMR ($CDCl_3$, 300 MHz, 25 °C) δ 10.44 (s, 4H, NH), 9.07 (s, 4H, binaphthyl), 8.15 (d, 4H, binaphthyl), 7.78 (d, 8H, phenyl), 7.56 (t, 4H, binaphthyl), 7.45 (t, 4H, binaphthyl), 7.27 (d, 4H, binaphthyl), 7.02 (d, 4H, phenyl), 3.33 (s, 12H, O-CH_3); ^{13}C NMR ($CDCl_3$, 75 MHz, 25 °C) δ 162.3 (O-CqON), 154.0 (Cq), 153.5 (Cq), 135.2 (Cq), 134.5 (CH), 133.9 (Cq), 130.4 (Cq), 129.9 (CH), 129.0 (CH), 126.0 (CH), 125.3 (CH+Cq), 124.9 (Cq), 121.0 (2CH), 119.3 (2CH), 62.0 (OCH_3); ESIMS *m*/*z*: 1155.4 ([M + Na]$^+$, 10%).

^{1}H NMR complexation experiments. All spectra were recorded at 500 MHz and at 298 K. K_a values for the complexation of (*R*,*R*)-**12** with (*n*-Bu_4N^+)$_2X^{2-}$ (X^{2-} = $^-O_2C(CH_2)_2CO_2^-$, $^-O_2C(CH_2)_3CO_2^-$) were assessed by nonlinear treatment of the data obtained from ^{1}H NMR titration experiments. Samples were prepared by adding to a 0.5 mL solution of the host (5 mM in $CDCl_3$) successive aliquots of a stock solution of the guest (62.5 mM in $CDCl_3$), up to a final volume of 0.9 mL. Eight values of δ_{obs} for the H-4 resonances were collected by keeping the [host] to [guest] ratio in the (1:0.25)–(1:10) interval. Nonlinear regression analysis of δ_{obs} versus [guest], using the WinEQNMR for Windows software package [47], provided the K_a value.

Molecular modeling. Geometry optimizations for the structures presented were carried out, first by using the semiempir-

ical PM3 method, and then refined at the B3LYP/6-31G(d) level [48]. All calculations were performed at the Cineca supercomputer facility by using the Gaussian 09, Revision C.01 package [49].

Supporting Information

Supporting Information File 1

Additional NMR and MS spectra for the macrocyles, and Cartesian coordinates for the calculated geometries discussed in the paper.
[http://www.beilstein-journals.org/bjoc/content/supplementary/1860-5397-8-109-S1.pdf]

Acknowledgements

Support from the University of Pavia, University of Messina, MIUR (Programs of National Relevant Interest PRIN grants 2004-033354 and 2009-A5Y3N9), the CINECA Supercomputer Center, with computer time granted by the ISCRA NANOCHIR project (HP10CKIGGH), and, in part, from CARIPLO Foundation (2007–2009) and INSTM-Regione Lombardia (2010–2012), is gratefully acknowledged.

References

1. Grave, C.; Schlüter, A. D. *Eur. J. Org. Chem.* **2002,** 3075–3098. doi:10.1002/1099-0690(200209)2002:18<3075::AID-EJOC3075>3.0.CO;2-3
2. Yamaguchi, Y.; Yoshida, Z.-i. *Chem.–Eur. J.* **2003,** *9,* 5430–5440. doi:10.1002/chem.200305099
3. Höger, S. *Chem.–Eur. J.* **2004,** *10,* 1320–1329. doi:10.1002/chem.200305496
4. Zhang, W.; Moore, J. S. *Angew. Chem., Int. Ed.* **2006,** *45,* 4416–4439. doi:10.1002/anie.200503988
5. Hua, Y.; Ramabhadran, R. O.; Karty, J. A.; Raghavachari, K.; Flood, A. H. *Chem. Commun.* **2011,** *47,* 5979–5981. doi:10.1039/c1cc10428d
6. Pasini, D.; Ricci, M. *Curr. Org. Synth.* **2007,** *4,* 59–80. doi:10.2174/157017907779981606
7. Ghadiri, M. R.; Granja, J. R.; Buehler, L. K. *Nature* **1994,** *369,* 301–304. doi:10.1038/369301a0
8. Leclair, S.; Baillargeon, P.; Skouta, R.; Gauthier, D.; Zhao, Y.; Dory, Y. L. *Angew. Chem., Int. Ed.* **2004,** *43,* 349–353. doi:10.1002/anie.200352259
9. Fischer, L.; Decossas, M.; Briand, J.-P.; Didierjean, C.; Guichard, G. *Angew. Chem., Int. Ed.* **2009,** *48,* 1625–1628. doi:10.1002/anie.200804019
10. Pantos, G. D.; Pengo, P.; Sanders, J. K. M. *Angew. Chem., Int. Ed.* **2007,** *46,* 194–197. doi:10.1002/anie.200603348
11. Sakamoto, J.; Schlüter, A. D. *Eur. J. Org. Chem.* **2007,** 2700–2712. doi:10.1002/ejoc.200700118
12. Xu, Y.; Smith, M. D.; Geer, M. F.; Pellechia, P. J.; Brown, J. C.; Wibowo, A. C.; Shimizu, L. S. *J. Am. Chem. Soc.* **2010,** *132,* 5334–5335. doi:10.1021/ja9107066
13. Gong, B. *Acc. Chem. Res.* **2008,** *41,* 1376–1386. doi:10.1021/ar700266f
14. Huc, I. *Eur. J. Org. Chem.* **2004,** 17–29. doi:10.1002/ejoc.200300495
15. Sakai, N.; Mareda, J.; Matile, S. *Acc. Chem. Res.* **2008,** *41,* 1354–1365. doi:10.1021/ar700229r
16. Wenzel, M.; Hiscock, J. R.; Gale, P. A. *Chem. Soc. Rev.* **2012,** *41,* 480–520. doi:10.1039/c1cs15257b
17. Choi, K.; Hamilton, A. D. *J. Am. Chem. Soc.* **2003,** *125,* 10241–10249. doi:10.1021/ja034563x
18. Alfonso, I.; Bolte, M.; Bru, M.; Burguete, M. I.; Luis, S. V.; Rubio, J. *J. Am. Chem. Soc.* **2008,** *130,* 6137–6144. doi:10.1021/ja710132c
19. Pu, L. *Chem. Rev.* **1998,** *98,* 2405–2494. doi:10.1021/cr970463w
20. Brunel, J. M. *Chem. Rev.* **2005,** *105,* 857–898. doi:10.1021/cr040079g
21. Zhu, Y.; Gergel, N.; Majumdar, N.; Harriott, L. R.; Bean, J. C.; Pu, L. *Org. Lett.* **2006,** *8,* 355–358. doi:10.1021/ol0517168
22. Yan, P.; Millard, A. C.; Wei, M.; Loew, L. M. *J. Am. Chem. Soc.* **2006,** *128,* 11030–11031. doi:10.1021/ja0635534
23. Ma, L.; Mihalcik, D. J.; Lin, W. *J. Am. Chem. Soc.* **2009,** *131,* 4610–4612. doi:10.1021/ja809590n
24. Cornelis, D.; Franz, E.; Asselberghs, I.; Clays, K.; Verbiest, T.; Koeckelberghs, G. *J. Am. Chem. Soc.* **2011,** *133,* 1317–1327. doi:10.1021/ja104978t
25. Ricci, M.; Pasini, D. *Org. Biomol. Chem.* **2003,** *1,* 3261–3262. doi:10.1039/b310751p
26. Moletti, A.; Coluccini, C.; Pasini, D.; Taglietti, A. *Dalton Trans.* **2007,** *16,* 1588–1592. doi:10.1039/b700059f
27. Coluccini, C.; Castelluccio, A.; Pasini, D. *J. Org. Chem.* **2008,** *73,* 4237–4240. doi:10.1021/jo800315s
28. Coluccini, C.; Dondi, D.; Caricato, M.; Taglietti, A.; Boiocchi, M.; Pasini, D. *Org. Biomol. Chem.* **2010,** *8,* 1640–1649. doi:10.1039/b920867d
29. Coluccini, C.; Mazzanti, A.; Pasini, D. *Org. Biomol. Chem.* **2010,** *8,* 1807–1815. doi:10.1039/b924400j
30. Caricato, M.; Coluccini, C.; Dondi, D.; Vander Griend, D. A.; Pasini, D. *Org. Biomol. Chem.* **2010,** *8,* 3272–3280. doi:10.1039/c004379f
31. Colombo, S.; Coluccini, C.; Caricato, M.; Gargiulli, C.; Gattuso, G.; Pasini, D. *Tetrahedron* **2010,** *66,* 4206–4211. doi:10.1016/j.tet.2010.03.102
32. Fujita, S.; Momiyama, M.; Kondo, Y.; Kagiyama, N.; Hori, S. H.; Toru, T. *Anal. Chem.* **1994,** *66,* 1347–1353. doi:10.1021/ac00080a022
33. Gramer, C. J.; Raymond, K. N. *Org. Lett.* **2001,** *3,* 2827–2830. doi:10.1021/ol016253u
34. Wuts, P. G. M.; Greene, T. W. *Greene's Protective Groups in Organic Synthesis,* 4th ed.; Wiley, 2006. doi:10.1002/0470053488
35. Yang, W.; Su, W.; Liu, D.; Wang, H.; Shen, J.; Da, C.; Wang, R.; Chan, A. S. C. *Tetrahedron* **2000,** *56,* 3511–3516. doi:10.1016/S0040-4020(00)00260-X
36. Saito, K.; Hirao, T. *Tetrahedron* **2002,** *58,* 7491–7501. doi:10.1016/S0040-4020(02)00828-1
37. Etter, M. C. *Acc. Chem. Res.* **1990,** *23,* 120–126. doi:10.1021/ar00172a005
38. Bhattacharya, S.; Nayak, S. K.; Chattopadhyay, S.; Banerjee, M.; Mukherjee, A. K. *J. Phys. Chem. B* **2003,** *107,* 13022–13028. doi:10.1021/jp0357370
39. Hunter, C. A.; Anderson, H. L. *Angew. Chem., Int. Ed.* **2009,** *48,* 7488–7499. doi:10.1002/anie.200902490
(example for a recent essay on cooperativity).

40. Cram, D. J.; Helgeson, R.; Peacock, S. C.; Kaplan, L. J.; Domeier, L. A.; Moreau, P.; Koga, K.; Mayer, J. M.; Chao, Y.; Siegel, M. G.; Hoffman, D. H.; Sogah, G. D. Y. *J. Org. Chem.* **1978,** *43,* 1930–1946. doi:10.1021/jo00404a019
41. Asakawa, M.; Janssen, H. M.; Meijer, E. W.; Pasini, D.; Stoddart, J. F. *Eur. J. Org. Chem.* **1998,** 983–986. doi:10.1002/(SICI)1099-0690(199806)1998:6<983::AID-EJOC983>3.0.CO;2-W
42. Baret, P.; Beaujolais, V.; Gaude, D.; Coulombeau, C.; Pierre, J.-L. *Chem.–Eur. J.* **1997,** *3,* 969–973. doi:10.1002/chem.19970030619
43. Goodyer, C. L. M.; Chinje, E. C.; Jaffar, M.; Stratford, I. J.; Threadgill, M. D. *Bioorg. Med. Chem.* **2003,** *11,* 4189–4206. doi:10.1016/S0968-0896(03)00451-6
44. Nagle, P. S.; Rodriguez, F.; Kahvedžić, A.; Quinn, S. J.; Rozas, I. *J. Med. Chem.* **2009,** *52,* 7113–7121. doi:10.1021/jm901017t
45. Stock, H. T.; Kellogg, R. M. *J. Org. Chem.* **1996,** *61,* 3093–3105. doi:10.1021/jo952107o
46. Casas, J.; Nájera, C.; Sansano, J. M.; González, J.; Saá, J. M.; Vega, M. *Tetrahedron: Asymmetry* **2001,** *12,* 699–702. doi:10.1016/S0957-4166(01)00107-0
47. Hynes, M. J. *J. Chem. Soc., Dalton Trans.* **1993,** 311–312. doi:10.1039/DT9930000311
48. Hehre, W. J.; Radom, L.; Schleyer, P. R.; Pople, J. A. *Ab Initio Molecular Orbital Theory;* Wiley: New York, 1985.
49. *Gaussian,* Revision C.01; Gaussian, Inc.: Wallingford, CT, 2009.

License and Terms

Beilstein Journal of Organic Chemistry

Toward unidirectional switches: 2-(2-Hydroxyphenyl)pyridine and 2-(2-methoxyphenyl)pyridine derivatives as pH-triggered pivots

Christina Tepper and Gebhard Haberhauer*

Full Research Paper

Open Access

Address:
Institut für Organische Chemie, Fakultät für Chemie, Universität Duisburg-Essen, Universitätsstraße 7, D-45117 Essen, Germany

Email:
Gebhard Haberhauer* - gebhard.haberhauer@uni-due.de

* Corresponding author

Keywords:
CD spectroscopy; chirality; molecular modeling; molecular switches; unidirectional movements

Beilstein J. Org. Chem. **2012,** *8,* 977–985.
doi:10.3762/bjoc.8.110

Received: 29 February 2012
Accepted: 29 May 2012
Published: 29 June 2012

This article is part of the Thematic Series "Molecular switches and cages".

Guest Editor: D. Trauner

Abstract

The pH-induced switching process of 2-(2-hydroxyphenyl)pyridine and 2-(2-methoxyphenyl)pyridine derivatives was investigated with the help of UV spectroscopy. Quantum chemical calculations at the B3LYP/6-31G* level of theory were performed to show that in the case of 2-(2-methoxyphenyl)-3-methylpyridine and 2-(2-hydroxyphenyl)-3-methylpyridine the rotation during the switching process proceeds unidirectionally at the molecular level. If a 2-(2-methoxyphenyl)pyridine derivative is fixed to a chiral cyclopeptidic scaffold, a unidirectional progress of the rotation is achieved macroscopically.

Introduction

A current topic that is rapidly expanding and the subject of extensive research is the design of molecular analogues of mechanical devices that are able to carry out movements powered by external stimuli [1-14]. Numerous examples of switches [15-18], rotors [19-22] and shuttles [23-28] that can be controlled chemically, electrochemically, thermally or by illumination have been described. One of the most challenging aspects in the design of molecular devices is the creation of synthetic molecular motors, which utilize the unidirectional movements of smaller parts thereof and which, thus, should be able to perform a physical task [2]. One important requirement for the construction of a molecular motor is that at least one movement of the motor proceeds unidirectionally. Such a unidirectional movement was already realized for rotations around N–N [29] and C–C [19,20,22,30,31] double bonds, around C–C single bonds [21,32-36], mechanical bonds [37,38] and in metal complexes [39-48]. A system for which unidirectional movement was realized, by making use of two different concepts, is

the 2,2′-bipyridine unit [32,34,35]. Rotation around the C–C bond that connects the two pyridine units is induced by the addition of a metal salt, which leads to the corresponding metal complexes. The back rotation is caused by the removal of the metal ion by the addition of cyclam, which complexes the metal ions better than the 2,2′-biypridine unit does. 2-(2-Hydroxyphenyl)pyridine and 2-(2-methoxyphenyl)pyridine should show a similar behavior (see Scheme 1) and therefore should also be applicable as pivots in molecular switches. While 2,2′-biypridine derivatives have been intensively used for molecular devices [49-56], 2-(2-hydroxyphenyl)pyridine and 2-(2-methoxyphenyl)pyridine derivatives, to our best knowledge, have only been used as ligands for metal complexes, but not for the construction of molecular switches [57-63]. Similar compounds, such the bipyridindiols, were studied as molecular half-subtractors, but they did not work unidirectionally [59]. Here we investigate their usability as pivots, especially for unidirectional rotations.

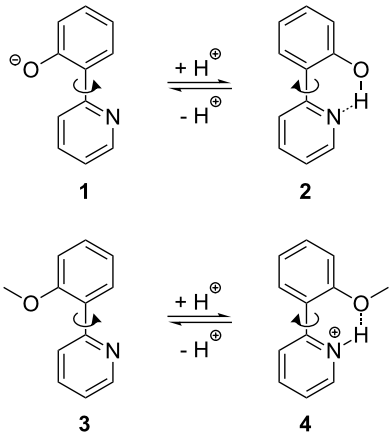

Scheme 1: Principle of the switching mechanism of 2-(2-hydroxyphenyl)pyridine (**2**) and 2-(2-methoxyphenyl)pyridine (**3**).

Results and Discussions

Concept

The switching process for 2-(2-hydroxyphenyl)pyridine (**2**) and 2-(2-methoxyphenyl)pyridine (**3**) should be achieved by the addition of acid and base, respectively. In the case of **2** the dihedral angle $\theta_{N–C–C–C(O)}$, which describes the relative orientation of the two aromatic units to one another, amounts to 0° [62,63]. This conformation is stabilized by the internal hydrogen bridge between the hydroxy group of the phenol and the nitrogen of the pyridine. A deprotonation of **2** to the penolate **1** leads to a rotation around the C–C bond to the most stable conformation of **1**, which has a dihedral angle $\theta_{N–C–C–C(O)}$ of 180°. This conformation allows a maximum conjugation over both aromatic rings and avoids the repulsion between the nitrogen lone pairs and the negatively charged oxygen atom. A similar behavior should be valid for 2-(2-methoxyphenyl)pyridine (**3**): in a neutral or basic environment the conformation showing a dihedral angle $\theta_{N–C–C–C(O)}$ of 180° and thus avoiding the repulsive interaction between the free electron pairs of the nitrogen and the oxygen atoms, should be the more stable one (Scheme 1). A protonation of the nitrogen inverts the relative energies of the two conformers. Due to the internal hydrogen bridge the conformer of **4** having a dihedral angle of 0° is the more stable one.

In order to verify these assumptions, the rotational barriers for **1**–**4** were calculated by using B3LYP and the 6-31G* basis set (Figure 1) [64]. Indeed, for **2** and **4** (red curves), which are able to form internal hydrogen bonds, the conformations with a dihedral angle of 0° are the more stable ones. In the case of **1** and **3** (blue curves), in which the repulsive interaction between the lone pairs is the dominant one, the conformations exhibiting a dihedral angle of about 180° are energetically preferred. A closer look at Figure 1 shows, however, that both systems as such are not suitable for use as a unidirectional pivot. If the phenolate **1** is protonated (grey arrow in Figure 1a), the most-

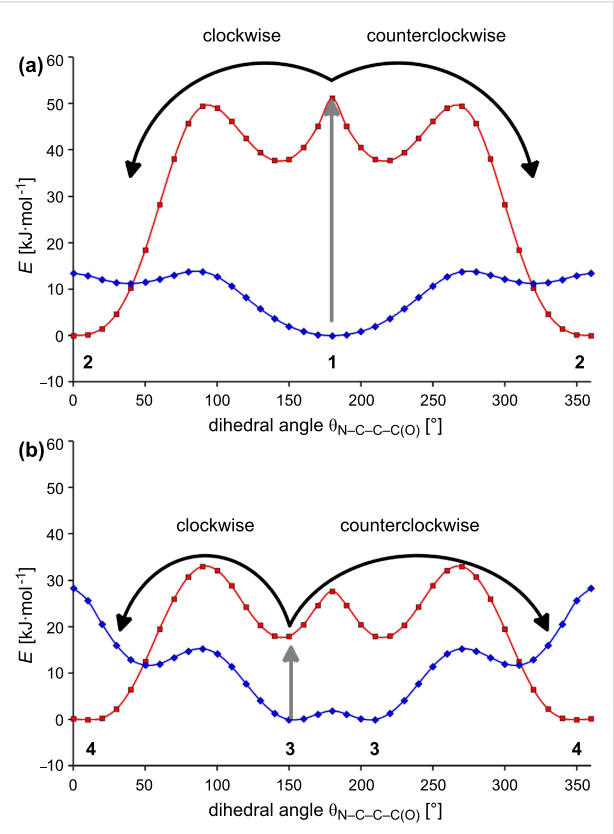

Figure 1: (a) Calculated energy profiles of the pyridine derivatives **1** (blue) and **2** (red) in relation to the dihedral angles $\theta_{N–C–C–C(O)}$ by use of B3LYP/6-31G*. (b) Calculated energy profiles of the pyridine derivatives **3** (blue) and **4** (red) in relation to the dihedral angles $\theta_{N–C–C–C(O)}$ by use of B3LYP/6-31G*.

stable conformation of the phenol **2** can be reached either by a clockwise or a counterclockwise rotation around the C–C single bond (black arrows in Figure 1a). As the transition states for both rotations show equal energies, both processes are equiprobable. The same is true for the protonation of the methoxyphenylpyridine **3** (black arrows in Figure 1b). Thus, protonation of **1** and **3** does not lead to unidirectional rotation at the molecular level.

In order to obtain a switching unit that shows a unidirectional rotation process caused by protonation, the methyl derivatives of **1**–**4**, i.e., **5**–**8** (Scheme 2) were investigated by using quantum chemical calculations at the B3LYP/6-31G* level of theory. Due to the methyl group, all conformations with a dihedral angle $\theta_{N–C–C–C(O)}$ of 180° represent energy maxima, and the minima at dihedral angles of about 130° are pairwise enantiomeric and separated by high energy barriers (Figure 2). Now the rotations around the C–C bonds caused by the protonation of the species **5** and **7** (gray arrows in Figure 2) take place in a unidirectional manner at the molecular level: If for example (*P*)-**5** is protonated, a clockwise rotation to the most stable conformation of **6** is the energetically preferred process (thick black arrow in Figure 2a). The energy barrier for this movement amounts to only a few kJ·mol^{-1}. In contrast, for a counterclockwise rotation, a transition state must be overcome that is more than 45 kJ·mol^{-1} higher in energy (thin black arrow in Figure 2a). Thus, the rotation triggered by the protonation of (*P*)-**5** proceeds unambiguously clockwise. On the other side, a protonation of (*M*)-**5** leads to a unidirectional counterclockwise movement. Even more pronounced is the unidirectionality for the rotation triggered by the protonation of the 3-methylpyridine **7**: If (*P*)-**7** is protonated, the difference between the energy of the rotation barriers for the clockwise and the counterclockwise rotation around the C–C bond between the aromatic units, amounts to more than 55 kJ·mol^{-1}. According to the Boltzmann distribution between the two transition states, the rotation is almost completely (>99.9999%) unidirectional at 298 K.

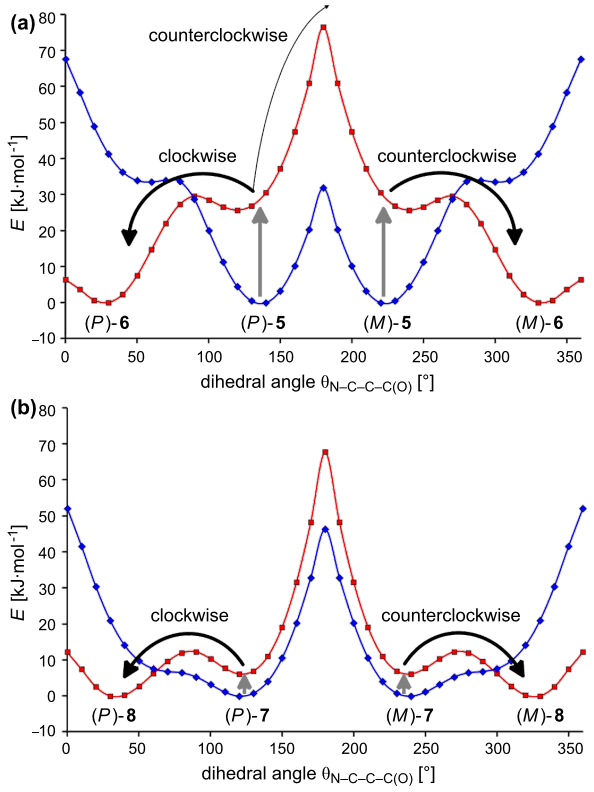

Figure 2: (a) Calculated energy profiles of the 3-methylpyridine derivatives **5** (blue) and **6** (red) in relation to the dihedral angles $\theta_{N–C–C–C(O)}$ by use of B3LYP/6-31G*. (b) Calculated energy profiles of the 3-methylpyridine derivatives **7** (blue) and **8** (red) in relation to the dihedral angles $\theta_{N–C–C–C(O)}$ by use of B3LYP/6-31G*.

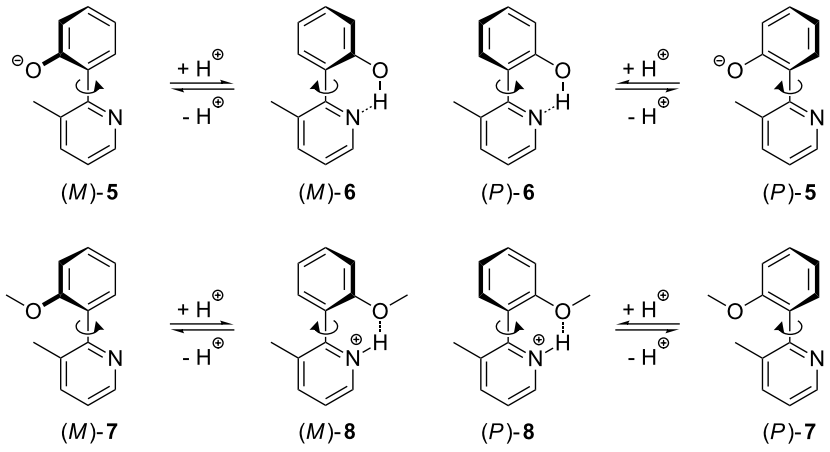

Scheme 2: Principle of the switching mechanism of 2-(2-hydroxyphenyl)-3-methylpyridine (**6**) and 2-(2-methoxyphenyl)-3-methylpyridine (**7**).

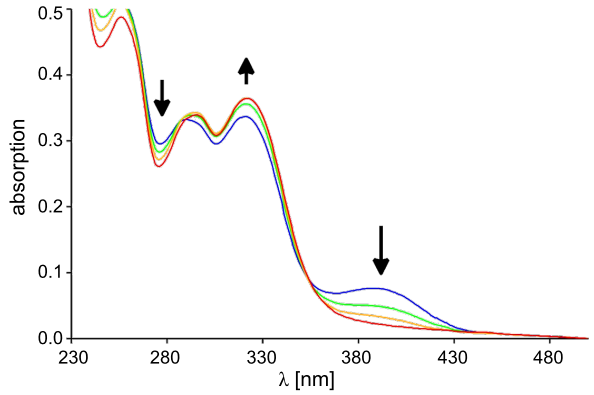

Figure 3: UV spectral change of phenolate **5** (blue) in dichloromethane (c = 5.6 × 10^{-5} M) at 20 °C upon addition of 10 (green), 20 (yellow) and 60 equiv TFA (**6**, red).

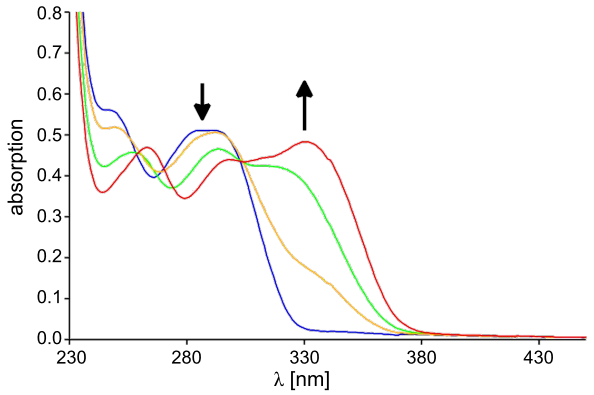

Figure 4: UV spectral change of 3-methylpyridine **7** (blue) in dichloromethane (c = 5.6 × 10^{-5} M) at 20 °C upon addition of 1 (yellow), 2.5 (green) and 20 equiv TFA (**8**, red).

It must be emphasized that the rotation caused by the protonation of **5** and **7** is unidirectional only with respect to a single molecule. In equilibrium, the ratio between the *P* and *M* enantiomers amounts to 1:1. As all *P* enantiomers perform a clockwise rotation and all *M* enantiomers a counterclockwise rotation, the whole process (sum of all single processes) is not unidirectional. One possibility to make the whole process at least partly unidirectional is to transform the enantiomeric conformers with a dihedral angle of about 150° into diastereomers that are different in energy. Due to the energetic gap between the diastereomers there will be an excess of one in solution. As the majority of the switches will now rotate in one direction (e.g., clockwise) and the minority will rotate in the other direction (e.g., counterclockwise), the whole process will now exhibit net unidirectionally (e.g., clockwise).

Proof of the switching process

The switching process can easily be observed by UV spectroscopy. The protonation was accomplished by the addition of several equivalents of trifluoroacetic acid (TFA). If TFA is added to the phenolate **5** (which was previously prepared by the addition of 50 equiv tetrabutylammonium fluoride to **6**) the absorption band at 388 nm disappears and simultaneously the band at 322 nm increases, while the band at 276 nm decreases (Figure 3). The thus obtained spectrum resembles the spectrum of the phenol **6**. Thus the deprotonation–protonation process is reversible. If TFA is added to a solution of **7** in dichloromethane (DCM), a new absorption band at 331 nm appears and the peak at 290 nm decreases (Figure 4). This is nothing else but a bathochromic shift of the band at 290 nm of **7** to higher wavelengths. The addition of tetrabutylammonium fluoride leads to the original spectrum.

The bathochromic shift during the transition from 3-methylpyridine **7** to the protonated species **8** can be explained on the basis of time-dependent density functional theory (TD-DFT) with the B3LYP functional and by employing the 6-31G* basis set. The absorption band at 290 nm for the 3-methylpyridine **7** as well as the absorption band at 331 nm for the protonated 3-methylpyridine **8** are dominated by the transition of an electron from the HOMO to the LUMO (π→π* transition; Figure 5). In both cases the HOMO is represented mainly by the p_π orbitals of the methoxyphenyl unit, whereas in the LUMO the p_π orbitals of the pyridine system prevail. A protonation of the nitrogen atom leads to an energetic decrease of all orbitals. As the HOMO exhibits only a small coefficient at the protonated nitrogen atom, the energetic lowering of the HOMO (Δε = −3.89 eV) caused by the protonation is less pronounced than the one observed for the LUMO (Δε = −5.32 eV). The resulting decrease of the HOMO–LUMO gap is responsible for the

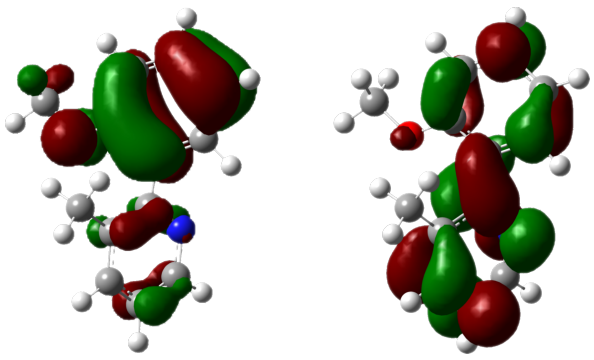

Figure 5: HOMO (left) and LUMO (right) of the 3-methylpyridine **7** calculated by using B3LYP/6-31G*.

bathochromic shift of the energetically lowest π→π* band. A similar explanation can be found for the hypsochromic shift caused by the protonation of the phenolate anion **5**. In summary, both the phenolate **5** and the pyridine **7** can be used as pH-triggered pivots, and according to calculated energy profiles the rotational movements during the switching process proceed in both cases unidirectionally at the molecular level.

Unidirectionality of the switching process

As already mention above, the whole switching process (sum of all molecular processes) becomes unidirectional if the enantiomeric conformers with a dihedral angle of about 150° are transformed into diastereomers that are different in energy. In order to receive diastereomeric derivatives of 2-(2-hydroxyphenyl)-3-methylpyridine (**6**) and 2-(2-methoxyphenyl)-3-methylpyridine (**7**) we intended to insert these units into a chiral macrocycle. Therefore, we used the macrobicyclus **9** in which a bridge consisting of two pyridine units spans over the peptidic clamp **14** (Scheme 3). Due to the chirality of the clamp, the bridge adopts a specific conformation (in this case the *P* conformation). The desired pyridine switches **10** and **12** can easily be synthesized by a Suzuki reaction of the bipyridine **9** with 2-methoxyphenylboronic acid or 2-hydroxyphenylboronic acid, respectively, using tetrakis(triphenylphosphine)palladium(0) and potassium carbonate as a base in dioxane. In the resulting switches **10** and **13** the more stable diastereomeric conformations should be those in which the methoxy group or the negatively charged oxygen atom, respectively, is turned away from the ethylene unit bridging the two pyridine units. In our case that would be the isomers (*M*)-**10** and (*M*)-**13**.

According to full geometry optimization studies in which calculations at the B3LYP/6-31G* level of theory were performed, the *M* isomer of **13** is more stable than the *P* isomer by 4.4 kJ·mol^{-1}. This means that in equilibrium the ratio between the diastereomers amounts to 85:15 in favor of the *M* isomer. In the case of a protonation of the pyridine switch **13** the rotation during the switching process will be in sum unidirectional (in our case counterclockwise). In the case of the methoxyphenylpyridine switch **10** the difference between the *M* and the *P* isomer was calculated with B3LYP/6-31G* to be 2.1 kJ·mol^{-1} in favor of the *M* isomer. According to this calculation the ratio between the diastereomers amounts to 70:30. Unfortunately, there is no hint toward a preference for the *M* conformer of **13** in solution: For example, in the ^{1}H NMR spectrum of **13** signals for only one conformer were found, even at lower temperatures, which means that the diastereomers are rapidly interconverting and the ratio between them cannot be determined by ^{1}H NMR spectroscopy. In the ^{1}H NMR of **10**, the signals of two different conformers are present and the ratio between the conformers is about 60:40. However, it is not possible to determine which isomer is the predominant one from 2D NOESY experiments.

Another possibility to test whether the switches adopt a preferred conformation in solution is through the use of CD spectroscopy. For this purpose, the CD spectrum of **13** in dichloromethane as the solvent was recorded (Figure 6a). Additionally, the CD spectra of (*M*)-**13** and (*P*)-**13** were simulated with the time-dependent density functional theory (TD-DFT) with B3LYP as a functional and by employing the 6-31G* basis set (Figure 6b). TD-DFT calculations were performed at the

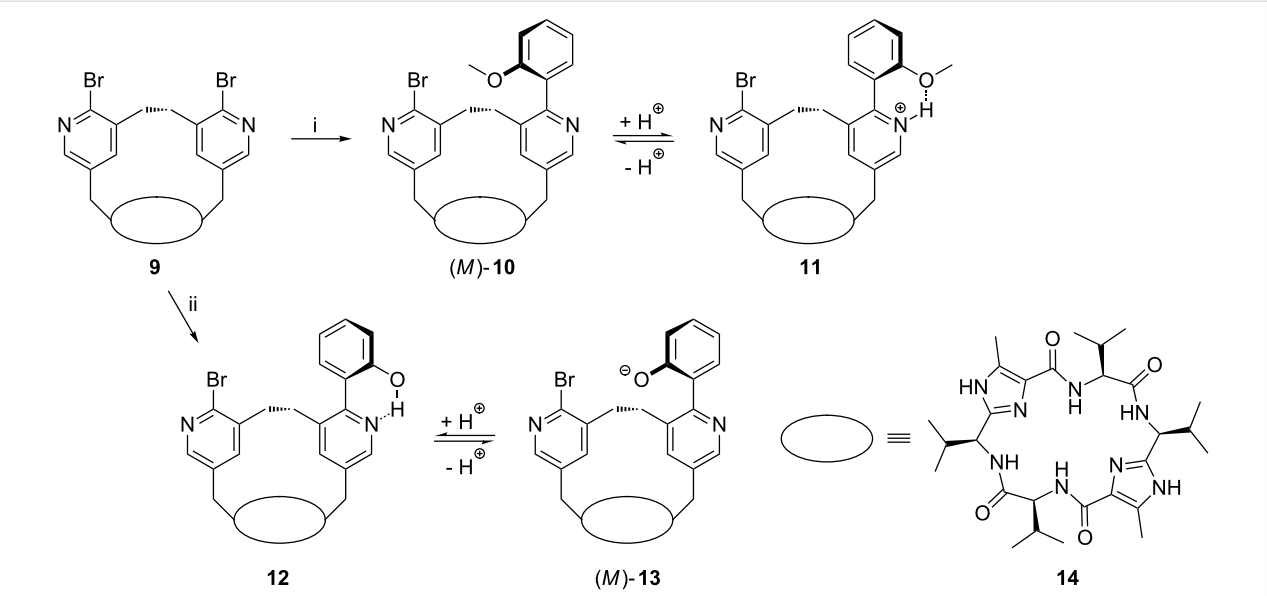

Scheme 3: Synthesis of the methoxyphenylpyridine switch **10** and the hydroxypyridine switch **12**; reaction conditions: (i) 2-methoxyphenylboronic acid, $Pd(PPh_3)_4$, K_2CO_3, H_2O/dioxane, 80 °C, 16%; (ii) 2-hydroxyphenylboronic acid, $Pd(PPh_3)_4$, K_2CO_3, H_2O/dioxane, 80 °C, 29%.

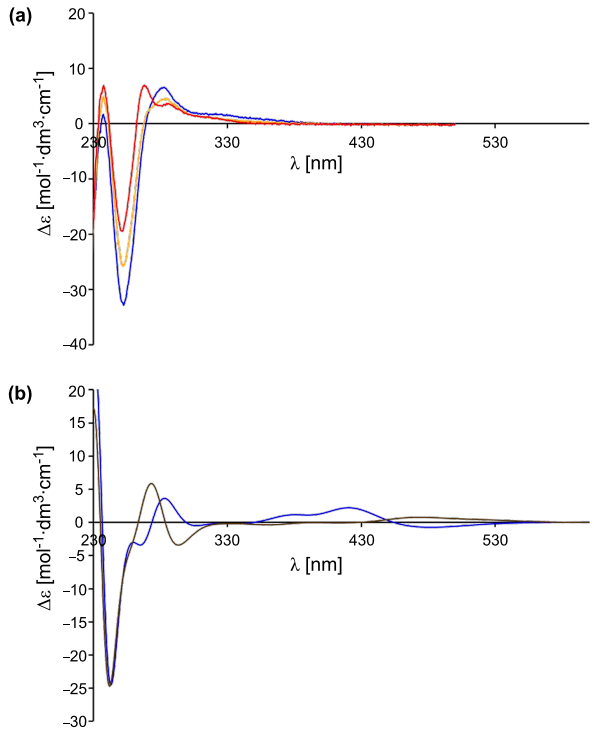

Figure 6: (a) CD spectral change of pyridine switch **13** (blue) in dichloromethane (c = 5.6 × 10^{-5} M) at 20 °C upon addition of 10 (yellow) and 30 equiv TFA (**12**, red). (b) Calculated spectra of (*M*)-**13** (blue) and (*P*)-**13** (brown) by using TD-DFT-B3LYP/6-31G*.

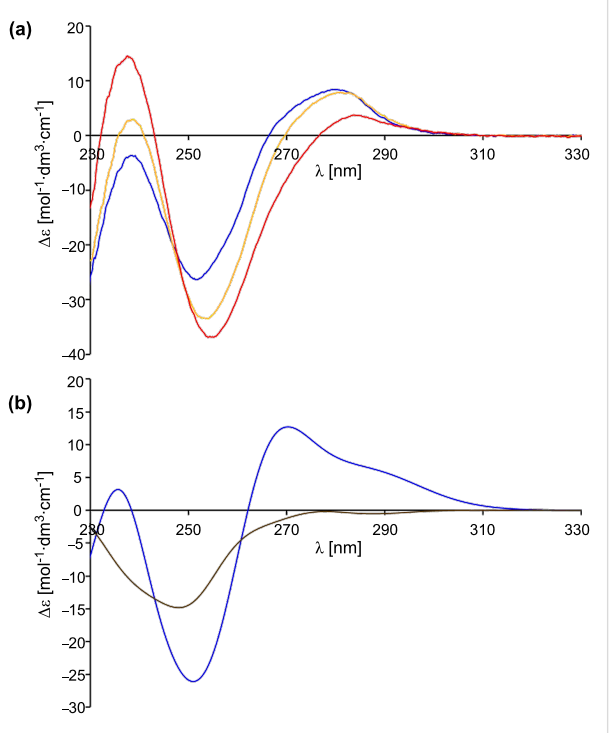

Figure 7: (a) CD spectral change of pyridine switch **10** (blue) in dichloromethane (c = 5.6 × 10^{-5} M) at 20 °C upon addition of 1 (yellow) and 20 equiv TFA (**11**, red). (b) Calculated spectra of (*M*)-**10** (blue) and (*P*)-**10** (brown) by using TD-DFT-B3LYP/6-31G*.

optimized ground-state geometries of (*M*)-**13** and (*P*)-**13**, calculating the energy, oscillator strength and rotatory strength for each of the 200 lowest singlet excitations. The CD spectra were simulated by overlapping Gaussian functions for each transition, for which the width of the band at 1/*e* height was fixed at 0.3 eV, and the resulting intensity of the combined spectrum was scaled to the experimental values. A comparison between the measured spectrum and the calculated spectra shows that apparently neither the *M* nor the *P* isomer of **13** is predominant in solution. Thus, the rotation, which is caused by the protonation of **13** and which can be observed by a hypsochromic shift of the energetic lowest π→π* band in the UV and CD spectrum, does not proceed with net unidirectionally.

Another result is found for the switch **10**: If we compare the simulated spectra of (*M*)-**10** and (*P*)-**10**, using time-dependent density functional theory (TD-DFT-B3LYP/6-31G*; Figure 7b) with the measured spectrum of **10** in DCM (Figure 7a), it becomes evident that the *M* isomer is the prevailing one. The protonation of the methoxyphenylpyridine switch **10** with TFA leads to a bathochromic shift of the energetically lowest π→π* band in the UV and the CD spectrum. As the *M* isomer is present in solution in excess in relation to the *P* isomer, the whole process is unidirectional even if the extent (percentage) of unidirectionality is small.

Conclusion

In sum we were able to show that 2-(2-methoxyphenyl)pyridine and 2-(2-hydroxyphenyl)pyridine derivatives can successfully be used as pivots. According to the calculated energy profiles, the rotation movements during the switching of the corresponding 3-methyl derivatives proceed unidirectionally at the molecular level. In the case of 2-(2-methoxyphenyl)pyridine we were able to construct a chiral switch that shows, in relation to the entire ensemble of the molecules, a unidirectional rotation, although the extent of unidirectionality is small.

Experimental

General remarks: All chemicals were reagent grade and were used as purchased. Reactions were monitored by TLC analysis with silica gel 60 F_{254} thin-layer plates. Flash chromatography was carried out on silica gel 60 (230–400 mesh). ^{1}H and ^{13}C NMR spectra were measured with Bruker Avance DMX 300 and Avance DRX 500 spectrometers. All chemical shifts (δ) are given in ppm. The spectra were referenced to deuterated solvents indicated in brackets in the analytical data. HRMS

spectra were recorded with a Bruker BioTOF III instrument. UV absorption spectra were obtained with Jasco J-815 and V-550 spectrophotometers. CD absorption spectra were recorded with a Jasco J-815 spectrophotometer.

2-(2-Methoxyphenyl)-3-methylpyridine (7): To a solution of 2-bromo-3-methylpyridine (184 mg, 1.07 mmol), 2-methoxyphenylboronic acid (151 mg, 0.99 mmol) and tetrakis(triphenylphosphine)palladium(0) (45 mg, 3.9 mol %) in dioxane (10 mL), a saturated potassium carbonate solution (1 mL) was added. The mixture was purged with argon for 10 min and afterwards heated to 88 °C for 20 h. After cooling to room temperature, water and ethyl acetate were added. The aqueous phase was extracted with ethyl acetate. The organic layers were combined and dried over magnesium sulfate, and the solvent was removed in vacuo. The residue was purified by column chromatography over silica gel (*n*-hexane/AcOEt 1:1). The product was obtained as a colorless solid (77 mg, 39%). ^{1}H NMR (500 MHz, $CDCl_3$) δ 7.74 (dd, $^3J_{H,H}$ = 7.6 Hz, $^4J_{H,H}$ = 1.9 Hz, 1H, H_{ar}), 7.59–7.58 (m, 2H, H_{ar}), 7.37–7.34 (m, 1H, H_{ar}), 7.09–7.06 (m, 2H, H_{ar}), 6.99 (d, $^3J_{H,H}$ = 8.2 Hz, 1H, H_{ar}), 3.84 (s, 3H, OCH_3), 2.63 (s, 3H, PhCH_3) ppm; ^{13}C NMR (125 MHz, $CDCl_3$) δ 157.9, 156.9, 155.4, 135.7, 131.1, 129.6, 129.5, 122.0, 121.2, 121.0, 111.3, 55.6, 24.7 ppm; IR (ATR) $\tilde{\nu}$: 3057, 2938, 2835, 1574, 1492, 1462, 1292, 1269, 1242, 1161, 1123, 1093, 1024, 870, 800, 750 cm^{-1}; UV (CH_2Cl_2) λ_{max}, nm (log ε): 290 (2.97), 285 (2.97), 249 (3.01); HRMS–ESI (*m*/*z*): $[M + H]^+$ calcd for $C_{13}H_{13}NO$, 200.1070; found, 200.1116; $[M + Na]^+$ calcd for $C_{13}H_{12}NONa$, 222.0889; found, 222.0935.

2-(2-Hydroxyphenyl)-3-methylpyridine (6): 2-(2-methoxyphenyl)-3-methylpyridine (**7**) (36 mg, 0.18 mmol) was dissolved in dichloromethane (2 mL) and cooled to −70 °C. Then a 1 M boron tribromide solution in dichloromethane (0.6 mL, 0.60 mmol) was added. The mixture was warmed to room temperature overnight. Subsequently the solution was poured into a dichloromethane/water mixture. The organic layer was separated and dried over magnesium sulfate, and the solvent was removed in vacuo. The product was obtained as a colorless solid (32 mg, 95%). ^{1}H NMR (500 MHz, $CDCl_3$) δ 14.72 (bs, 1H, O*H*), 7.86 (dd, $^3J_{H,H}$ = 8.0 Hz, $^4J_{H,H}$ = 1.6 Hz, 1H, H_{ar}), 7.74–7.73 (m, 2H, H_{ar}), 7.32–7.28 (m, 1H, H_{ar}), 7.11–7.09 (m, 1H, H_{ar}), 7.34 (dd, $^3J_{H,H}$ = 8.2 Hz, $^4J_{H,H}$ = 1.1 Hz, 1H, H_{ar}), 6.92–6.78 (m, 1H, H_{ar}), 2.63 (s, 3H, PhCH_3) ppm; ^{13}C NMR (125 MHz, $CDCl_3$) δ 160.0, 157.1, 155.0, 138.2, 137.4, 126.2, 121.2, 118.7, 118.6, 116.2, 23.7 ppm; IR (ATR) $\tilde{\nu}$: 3053, 2858, 2771, 2559, 2475, 2319, 1596, 1504, 1460, 1403, 1364, 1299, 1259, 1216, 1178, 1159, 1121, 1096, 1051, 989, 926, 883, 811, 746, 680 cm^{-1}; UV (CH_2Cl_2) λ_{max}, nm (log ε): 319 (2.84), 297 (2.80), 256 (2.92); HRMS–ESI (*m*/*z*): $[M + H]^+$ calcd for $C_{12}H_{11}NO$, 186.0913; found, 186.0964; $[M - H]^-$ calcd for $C_{12}H_{10}NO$, 184.0768; found, 184.0815.

Methoxyphenylpyridine switch (10): To a solution of dibromide **9** (20 mg, 0.022 mmol) and tetrakis(triphenylphosphine)palladium(0) (1 mg, 3.9 mol%) in dioxane (3 mL), a saturated potassium carbonate solution (0.2 mL) was added. The mixture was purged with argon for 10 min and afterwards 2-methoxyphenylboronic acid (14 mg, 0.092 mmol) was added and the mixture was heated to 80 °C for 4 h. After cooling to room temperature, water and ethyl acetate were added. The aqueous phase was extracted with ethyl acetate. The organic layers were combined and dried over magnesium sulfate, and the solvent was removed in vacuo. The residue was purified by column chromatography over silica gel (CH_2Cl_2/AcOEt/MeOH 75:25:2) and subsequently by HPLC. The product was obtained as a colorless solid (3.3 mg, 16%). ^{1}H NMR (500 MHz, $CDCl_3$) δ 8.54 (s, 1H, $H_{pyridine}$), 8.14 (s, 1H, $H_{pyridine}$), 7.38–6.93 (m, 8H, H_{phenyl}, N*H*), 5.78 (s, 1H, $H_{pyridine}$), 5.60 (s, 1H, $H_{pyridine}$), 5.48–5.31 (m, 2H, imidazole-CH_2-pyridine), 5.08–5.00 (m, 2H, imidazole-*CH*-NH), 4.92–4.89 (m, 2H, imidazole-CH_2-pyridine), 4.60–4.52 (m, 2H, CO-C*H*-NH), 3.76–3.72 (m, 3H, OCH_3), 2.67–2.44 (m, 4H, CH(CH$_3$)$_2$, CH_2CH_2), 2.38–2.28 (m, 2H, CH(CH$_3$)$_2$), 1.70–1.61 (m, 2H, CH_2CH_2), 2.21–2.06 (m, 6H, imidazole-CH_3), 1.16–1.13 (m, 12H, CH(CH_3)$_2$), 1.00–0.92 (m, 12H, CH(CH_3)$_2$) ppm; ^{13}C NMR (125 MHz, $CDCl_3$) δ 171.11, 162.42, 162.25, 146.48, 146.34, 145.20, 144.90, 142.95, 134.57, 133.20, 131.62, 131.08, 130.53, 130.22, 111.00, 59.06, 55.54, 51.28, 51.10, 45.30, 44.64, 38.30, 34.05, 33.18, 30.92, 19.74, 19.70, 18.91, 18.81, 17.43, 13.34, 10.32, 10.11 ppm; IR (ATR) $\tilde{\nu}$: 3395, 2961, 2929, 2872, 2362, 2324, 1664, 1594, 1497, 1461, 1435, 1389, 1372, 1328, 1269, 1237, 1192, 1154, 1111, 1090, 1052, 1024, 957, 923, 892, 856, 797, 754, 730 cm^{-1}; UV (CH_2Cl_2) λ_{max}, nm (log ε): 295 (2.95); CD (CH_2Cl_2) λ nm (Δε M^{-1}cm^{-1}): 280 (+8.5), 252 (−26.3); HRMS–ESI (*m*/*z*): $[M + H]^+$ calcd for $C_{49}H_{61}{}^{81}BrN_{10}O_5$, 951.4074; found, 951.4129; $[M + Na]^+$ calcd for $C_{49}H_{60}{}^{81}BrN_{10}O_5Na$, 973.3893; found, 973.3977.

Hydroxyphenylpyridine switch (12): To a solution of dibromide **9** (20 mg, 0.022 mmol) and tetrakis(triphenylphosphine)palladium(0) (1 mg, 3.9 mol %) in dioxane (3 mL), a saturated potassium carbonate solution (0.2 mL) was added. The mixture was purged with argon for 10 min and afterwards 2-hydroxyphenylboronic acid (14 mg, 0.102 mmol) was added and the mixture was heated to 80 °C for 9 h. After cooling to room temperature, water and ethyl acetate were added. The aqueous phase was extracted with ethyl acetate. The organic layers were combined and dried over magnesium sulfate, and the solvent was removed in vacuo. The residue was purified by column chromatography over silica gel (CH_2Cl_2/AcOEt/MeOH

75:25:2) and subsequently by HPLC. The product was obtained as a colorless solid (5.9 mg, 29%). ^{1}H NMR (500 MHz, $CDCl_3$) δ 8.48 (s, 1H, $H_{pyridine}$), 8.22 (s, 1H, $H_{pyridine}$), 7.45 (d, $^3J_{H,H}$ = 7.3 Hz, 1H, H_{phenyl}), 7.31–7.28 (m, 3H, H_{phenyl}), N*H*-CH-imidazole), 7.13 (d, $^3J_{H,H}$ = 7.3 Hz, 1H, H_{phenyl}), 7.06 (d, $^3J_{H,H}$ = 8.8 Hz, 2H, N*H*-CH-CO), 6.96–6.91 (m, 1H, H_{phenyl}), 5.92 (s, 1H, $H_{pyridine}$), 5.57 (s, 1H, $H_{pyridine}$), 5.47 (d, 1H, $^2J_{H,H}$ = 17.0 Hz, imidazole-CH_2-pyridine), 5.36 (d, 1H, $^2J_{H,H}$ = 17.7 Hz, imidazole-CH_2-pyridine), 5.07 (d, 1H, $^2J_{H,H}$ = 17.0 Hz, imidazole-CH_2-pyridine), 4.98–4.88 (m, 3H, pyridine-C*H*-NH, imidazol-CH_2-pyridine), 4.56–4.51 (m, 2H, CO-C*H*-NH), 3.19 (td, $^2J_{H,H}$ = 14.2 Hz, $^3J_{H,H}$ = 5.9 Hz, 1H, CH_2CH$_2$), 2.93 (td, $^2J_{H,H}$ = 13.2 Hz, $^3J_{H,H}$ = 5.5 Hz, 1H, CH$_2$CH_2), 2.56–2.43 (m, 2H, C*H*(CH$_3$)$_2$), 2.36–2.27 (m, 2H, C*H*(CH$_3$)$_2$), 2.24 (s, 3H, imidazole-CH_3), 2.12 (s, 3H, imidazole-CH_3), 1.99–1.91 (m, 1H, CH$_2$CH_2), 1.85 (td, $^2J_{H,H}$ = 13.2 Hz, $^3J_{H,H}$ = 4.7 Hz, 1H, CH_2CH$_2$), 1.15–1.14 (m, 12H, CH(CH_3)$_2$), 1.00–0.93 (m, 12H, CH(CH_3)$_2$) ppm; ^{13}C NMR (125 MHz, $CDCl_3$) δ 171.05, 171.01, 162.29, 161.72, 156.33, 146.58, 146.28, 145.43, 143.18, 138.30, 135.53, 135.51, 135.03, 135.02, 133.42, 133.39, 133.13, 131.71, 130.92, 129.99, 129.89, 121.22, 119.52, 117.95, 59.06, 59.05, 58.99, 58.93, 51.21, 51.08, 44.75, 44.26, 37.57, 34.27, 33.23, 33.18, 30.81, 30.77, 19.72, 19.70, 18.91, 18.76, 18.69, 17.42, 17.41, 17.39, 10.19, 10.05 ppm; IR (ATR) $\tilde{\nu}$: 3357, 3280, 2962, 2927, 2872, 2357, 2324, 1660, 1593, 1504, 1455, 1425, 1389, 1372, 1329, 1292, 1250, 1221, 1197, 1153, 1053, 1023, 991, 957, 891, 858, 835, 815, 800, 755, 732, 680 cm^{-1}; UV (CH_2Cl_2) λ_{max}, nm (log ε): 305 nm (2.73); CD (CH_2Cl_2) λ, nm (Δε M^{-1}cm^{-1}): 285 (+3.4), 268 (+6.7), 252 (−16.2); HRMS–ESI (*m*/*z*): [M + H]$^+$ calcd for $C_{48}H_{59}{}^{81}BrN_{10}O_5$, 937.3917; found, 937.3889; [M + Na]$^+$ calcd for $C_{48}H_{58}{}^{81}BrN_{10}O_5$, 959.3737; found, 959.3730.

Acknowledgements

The authors thank the Deutschen Forschungsgemeinschaft (DFG) for financial support.

References

1. Balzani, V.; Credi, A.; Venturi, M. *Molecular Devices and Machines – A Journey into the Nano World;* Wiley-VCH: Weinheim, 2003. doi:10.1002/3527601600
2. Kay, E. R.; Leigh, D. A.; Zerbetto, F. *Angew. Chem., Int. Ed.* **2007,** *46,* 72–191. doi:10.1002/anie.200504313
   Angew. Chem. **2007,** *119,* 72–196. doi:10.1002/ange.200504313
3. Shirai, Y.; Morin, J.-F.; Sasaki, T.; Guerrero, J. M.; Tour, J. M. *Chem. Soc. Rev.* **2006,** *35,* 1043–1055. doi:10.1039/b514700j
4. Leigh, D. A.; Pérez, E. M. Dynamic Chirality: Molecular Shuttles and Motors. In *Supramolecular Chirality;* Crego-Calama, M.; Reinhoudt, D. N., Eds.; Topics in Current Chemistry, Vol. 265; Springer: Berlin, Heidelberg, 2006; pp 185–208. doi:10.1007/128_039
5. Kinbara, K.; Aida, T. *Chem. Rev.* **2005,** *105,* 1377–1400. doi:10.1021/cr030071r
6. Kottas, G. S.; Clarke, L. I.; Horinek, D.; Michl, J. *Chem. Rev.* **2005,** *105,* 1281–1376. doi:10.1021/cr0300993
7. Bustamante, C.; Keller, D.; Oster, G. *Acc. Chem. Res.* **2001,** *34,* 412–420. doi:10.1021/ar0001719
8. Kelly, T. R. *Acc. Chem. Res.* **2001,** *34,* 514–522. doi:10.1021/ar000167x
9. Feringa, B. L. *Acc. Chem. Res.* **2001,** *34,* 504–513. doi:10.1021/ar0001721
10. Shinkai, S.; Ikeda, M.; Sugasaki, A.; Takeuchi, M. *Acc. Chem. Res.* **2001,** *34,* 494–503. doi:10.1021/ar000177y
11. Collin, J.-P.; Dietrich-Buchecker, C.; Gaviña, P.; Jimenez-Molero, M. C.; Sauvage, J. P. *Acc. Chem. Res.* **2001,** *34,* 477–487. doi:10.1021/ar0001766
12. Schalley, C. A.; Beizai, K.; Vögtle, F. *Acc. Chem. Res.* **2001,** *34,* 465–476. doi:10.1021/ar000179i
13. Ballardini, R.; Balzani, V.; Credi, A.; Gandolfi, M. D.; Venturi, M. *Acc. Chem. Res.* **2001,** *34,* 445–455. doi:10.1021/ar000170g
14. Pease, A. R.; Jeppesen, J. O.; Stoddart, J. F.; Luo, Y.; Collier, C. P.; Heath, J. R. *Acc. Chem. Res.* **2001,** *34,* 433–444. doi:10.1021/ar000178q
15. Zhou, Z.; Cao, C.; Yin, Z.; Liu, Q. *Org. Lett.* **2009,** *11,* 1781–1784. doi:10.1021/ol802976h
16. Wang, C.; Zhang, D.; Zhang, G.; Xiang, J.; Zhu, D. *Chem.–Eur. J.* **2008,** *14,* 5680–5686. doi:10.1002/chem.200800216
17. Chatterjee, M. N.; Kay, E. R.; Leigh, D. A. *J. Am. Chem. Soc.* **2006,** *128,* 4058–4073. doi:10.1021/ja057664z
18. Feringa, B. L., Ed. *Molecular Switches;* Wiley-VCH: Weinheim, 2001. doi:10.1002/3527600329
19. Pollard, M. M.; Klok, M.; Pijper, D.; Feringa, B. L. *Adv. Funct. Mater.* **2007,** *17,* 718–729. doi:10.1002/adfm.200601025
20. Pijper, D.; van Delden, R. A.; Meetsma, A.; Feringa, B. L. *J. Am. Chem. Soc.* **2005,** *127,* 17612–17613. doi:10.1021/ja054499e
21. Fletcher, S. P.; Dumur, F.; Pollard, M. M.; Feringa, B. L. *Science* **2005,** *310,* 80–82. doi:10.1126/science.1117090
22. Koumura, N.; Zijlstra, R. W. J.; van Delden, R. A.; Harada, N.; Feringa, B. L. *Nature* **1999,** *401,* 152–155. doi:10.1038/43646
23. Durola, F.; Lux, J.; Sauvage, J.-P. *Chem.–Eur. J.* **2009,** *15,* 4124–4134. doi:10.1002/chem.200802510
24. Rescifina, A.; Zagni, C.; Iannazzo, D.; Merino, P. *Curr. Org. Chem.* **2009,** *13,* 448–481. doi:10.2174/138527209787582222
25. Silvi, S.; Venturi, M.; Credi, A. *J. Mater. Chem.* **2009,** *19,* 2279–2294. doi:10.1039/b818609j
26. Silvi, S.; Constable, E. C.; Housecroft, C. E.; Beves, J. E.; Dunphy, E. L.; Tomasulo, M.; Raymo, F. M.; Credi, A. *Chem.–Eur. J.* **2009,** *15,* 178–185. doi:10.1002/chem.200801645
27. Anelli, P. L.; Spencer, N.; Stoddart, J. F. *J. Am. Chem. Soc.* **1991,** *113,* 5131–5133. doi:10.1021/ja00013a096
28. Lane, A. S.; Leigh, D. A.; Murphy, A. *J. Am. Chem. Soc.* **1997,** *119,* 11092–11093. doi:10.1021/ja971224t
29. Haberhauer, G.; Kallweit, C. *Angew. Chem., Int. Ed.* **2010,** *49,* 2418–2421. doi:10.1002/anie.200906731
    Angew. Chem. **2010,** *122,* 2468–2471. doi:10.1002/ange.200906731
30. Wang, J.; Feringa, B. L. *Science* **2011,** *331,* 1429–1432. doi:10.1126/science.1199844
31. Wang, J.; Hou, L.; Browne, W. R.; Feringa, B. L. *J. Am. Chem. Soc.* **2011,** *133,* 8162–8164. doi:10.1021/ja202882q
32. Haberhauer, G. *Angew. Chem., Int. Ed.* **2011,** *50,* 6415–6418. doi:10.1002/anie.201101501
    Angew. Chem. **2011,** *123,* 6539–6543. doi:10.1002/ange.201101501

33. Tepper, C.; Haberhauer, G. *Chem.–Eur. J.* **2011,** *17,* 8060–8065. doi:10.1002/chem.201003682
34. Ernst, S.; Haberhauer, G. *Chem.–Eur. J.* **2009,** *15,* 13406–13416. doi:10.1002/chem.200901940
35. Haberhauer, G. *Angew. Chem., Int. Ed.* **2008,** *120,* 3691–3694. doi:10.1002/ange.200800062
Angew. Chem., Int. Ed. **2008,** *47,* 3635–3638. doi:10.1002/anie.200800062
36. Kelly, T. R.; De Silva, H.; Silva, R. A. *Nature* **1999,** *401,* 150–152. doi:10.1038/43639
37. Hernández, J. V.; Kay, E. R.; Leigh, D. A. *Science* **2004,** *306,* 1532–1537. doi:10.1126/science.1103949
38. Leigh, D. A.; Wong, J. K. Y.; Dehez, F.; Zerbetto, F. *Nature* **2003,** *424,* 174–179. doi:10.1038/nature01758
39. Vives, G.; Jacquot de Rouville, H.-P.; Carelle, A.; Launay, J.-P.; Rapenne, G. *Chem. Soc. Rev.* **2009,** *38,* 1551–1561. doi:10.1039/b804684k
40. Darbost, U.; Penin, V.; Jeanneau, E.; Félix, C.; Vocanson, F.; Bucher, C.; Royal, G.; Bonnamour, I. *Chem. Commun.* **2009,** 6774–6776. doi:10.1039/b907207a
41. McNitt, K. A.; Parimal, K.; Share, A. I.; Fahrenbach, A. C.; Witlicki, E. H.; Pink, M.; Bediako, D. K.; Plaisier, C. L.; Le, N.; Heeringa, L. P.; Vander Griend, D. A.; Flood, A. H. *J. Am. Chem. Soc.* **2009,** *131,* 1305–1313. doi:10.1021/ja8085593
42. Canary, J. W. *Chem. Soc. Rev.* **2009,** *38,* 747–756. doi:10.1039/b800412a
43. Tanaka, K.; Kinbara, K. *Mol. BioSyst.* **2008,** *4,* 512–514. doi:10.1039/b801621f
44. Kinbara, K.; Muraoka, T.; Aida, T. *Org. Biomol. Chem.* **2008,** *6,* 1871–1876. doi:10.1039/b718982f
45. Muraoka, T.; Kinbara, K.; Aida, T. *Chem. Commun.* **2007,** 1441–1443. doi:10.1039/b618248h
46. Muraoka, T.; Kinbara, K.; Aida, T. *Nature* **2006,** *440,* 512–515. doi:10.1038/nature04635
47. Muraoka, T.; Kinbara, K.; Kobayashi, Y.; Aida, T. *J. Am. Chem. Soc.* **2003,** *125,* 5612–5613. doi:10.1021/ja034994f
48. Zahn, S.; Canary, J. W. *J. Am. Chem. Soc.* **2002,** *124,* 9204–9211. doi:10.1021/ja0120429
49. Zahn, S.; Reckien, W.; Kirchner, B.; Staats, H.; Matthey, J.; Lützen, A. *Chem.–Eur. J.* **2009,** *15,* 2572–2580. doi:10.1002/chem.200801374
50. Jeffery, J. C.; Rice, C. R.; Harding, L. P.; Baylies, C. J.; Riis-Johannessen, T. *Chem.–Eur. J.* **2007,** *13,* 5256–5271. doi:10.1002/chem.200700261
51. Plitt, P.; Gross, D. E.; Lynch, V. M.; Sessler, J. L. *Chem.–Eur. J.* **2007,** *13,* 1374–1381. doi:10.1002/chem.200601514
52. Sauvage, J. P. *Acc. Chem. Res.* **1998,** *31,* 611–619. doi:10.1021/ar960263r
53. Kelly, T. R.; Tellitu, I.; Sestelo, J. P. *Angew. Chem., Int. Ed. Engl.* **1997,** *36,* 1866–1868. doi:10.1002/anie.199718661
Angew. Chem. **1997,** *109,* 1969–1972. doi:10.1002/ange.19971091727
54. König, B.; Hollnagel, H.; Ahrens, B.; Jones, P. G. *Angew. Chem., Int. Ed. Engl.* **1995,** *34,* 2538–2540. doi:10.1002/anie.199525381
Angew. Chem. **1995,** *107,* 2763–2765. doi:10.1002/ange.19951072233
55. Lehn, J. M. *Angew. Chem., Int. Ed. Engl.* **1990,** *29,* 1304–1319. doi:10.1002/anie.199013041
Angew. Chem. **1990,** *102,* 1347–1362. doi:10.1002/ange.19901021117
56. Rebek, J., Jr. *Acc. Chem. Res.* **1984,** *17,* 258–264. doi:10.1021/ar00103a006
57. Zhang, Z.; Bi, H.; Zhang, Y.; Yao, D.; Gao, H.; Fan, Y.; Zhang, H.; Wang, Y.; Wang, Y.; Chen, Z.; Ma, D. *Inorg. Chem.* **2009,** *48,* 7230–7236. doi:10.1021/ic900673s
58. Kim, N. G.; Shin, C. H.; Lee, M. H.; Do, Y. *J. Organomet. Chem.* **2009,** *694,* 1922–1928. doi:10.1016/j.jorganchem.2009.01.035
59. Suresh, M.; Jose, D. A.; Das, A. *Org. Lett.* **2007,** *9,* 441–444. doi:10.1021/ol0628457
60. Rurack, K.; Radeglia, R. *Eur. J. Inorg. Chem.* **2000,** *10,* 2271–2282. doi:10.1002/1099-0682(200010)2000:10<2271::AID-EJIC2271>3.0.CO;2-3
61. LeGourriérec, D.; Kharlanov, V.; Brown, R. G.; Rettig, W. *J. Photochem. Photobiol., A: Chem.* **1998,** *117,* 209–216. doi:10.1016/S1010-6030(98)00328-1
62. Sitkowski, J.; Stefaniak, L.; Kaczmarek, L.; Webb, G. A. *J. Mol. Struct.* **1996,** *385,* 65–67. doi:10.1016/S0022-2860(96)09407-0
63. Kaczmarek, L.; Balicki, R.; Lipkowski, J.; Borowicz, P.; Grabowska, A. *J. Chem. Soc., Perkin Trans. 2* **1994,** 1603–1610. doi:10.1039/p29940001603
64. *Gaussian 03,* Revision C.02; Gaussian, Inc.: Wallingford, CT, 2004.

License and Terms

Beilstein Journal of Organic Chemistry

Recent advances towards azobenzene-based light-driven real-time information-transmitting materials

Jaume García-Amorós and Dolores Velasco*§

Review

Open Access

Address:
Grup de Materials Orgànics, Institut de Nanociència i Nanotecnologia (IN2UB), Departament de Química Orgànica, Universitat de Barcelona, Martí i Franquès 1, E-08028, Barcelona, Spain

Email:
Dolores Velasco* - dvelasco@ub.edu

* Corresponding author
§ tel: + 34 93 403 92 60; fax: + 34 93 339 78 78

Keywords:
kinetics; light-controlled materials; molecular switches; photochromic switches; push–pull azophenols; thermal isomerisation

Beilstein J. Org. Chem. **2012,** *8,* 1003–1017.
doi:10.3762/bjoc.8.113

Received: 01 March 2012
Accepted: 13 June 2012
Published: 04 July 2012

This article is part of the Thematic Series "Molecular switches and cages".

Guest Editor: D. Trauner

Abstract

Photochromic switches that are able to transmit information in a quick fashion have attracted a growing interest within materials science during the last few decades. Although very fast photochromic switching materials working within hundreds of nanoseconds based on other chromophores, such as spiropyranes, have been successfully achieved, reaching such fast relaxation times for azobenzene-based photochromic molecular switches is still a challenge. This review focuses on the most recent achievements on azobenzene-based light-driven real-time information-transmitting systems. Besides, the main relationships between the structural features of the azo-chromophore and the thermal *cis*-to-*trans* isomerisation, the kinetics and mechanism are also discussed as a key point for reaching azoderivatives endowed with fast thermal back-isomerisation kinetics.

Introduction

Nowadays, there is an ever growing interest in molecular switching materials because of the very rapid development of modern technology. This tendency arises from the great applicability of such systems as active data elaboration, storage and communication elements in many devices, such as optical systems for opto-electronics, holographic materials and multicolour displays. Hence, there is a high motivation for the molecular design and study of innovative materials for this purpose. "Molecular switches" denote molecular systems, either small molecules or supramolecular species, that can be reversibly shifted between at least two different states [1]. As a consequence of the molecular change produced by the application of an external input energy, a significant modification of some of the properties of the molecule, e.g., mechanical, magnetic, electrical, optical, etc., is induced. Many diverse organic molecules have been investigated for molecular switching applications. Based on these, monomolecular photochromic [2-4], fluorescence [5,6], chirality [7-9], redox [10] and acid–base [11-13]

switches have been successfully reported during the past few decades. The interconversion between the different states of the molecular switch can be performed by a great variety of environmental stimuli, which can be classified into three main groups: light energy, electrical energy and chemical energy (pH, solvent, the presence of a determined metal or ligand, etc.). Moreover, in some cases, a combination of some of them is required so as to endow the final material with multifunctionality. In comparison with chemical stimulation, both electrochemical and mainly photochemical excitation can be switched back and forward easily and rapidly. On the other hand, the use of light and electricity means that not only the switching of the probe but also the monitoring of the operation can be performed simultaneously. Furthermore, these two external input energies are the easiest to use in macroscopic device engineering. Specifically, light-responsive materials are themselves attractive because light allows a clean, quick and remote operation without the need for direct contact to the material. Photochromism is defined by IUPAC as a "light-induced reversible change of color" [14]. Organic photochromic molecular switches are based on molecules that can be reversibly interconverted, with at least one of the reactions being induced by light excitation, between two forms with different absorption spectra [15]. These two forms differ also in many other physical properties, such as their redox potential, fluorescent intensity, acid/base strength, dielectric constant, dipolar moment, molecular shape, and so on. Traditionally, this type of organic system has been widely used for analytical purposes, but at the present moment, they are widely required for many technical uses, for instance, binary systems for logic gates in computing or signal transmission devices. Many different organic photochromic molecules are known in photochemistry, such as azobenzenes, stilbenes, spiropyranes, fulgides, diarylethenes and chromenes among many others (Figure 1) [16]. The photochromic processes that take place when such compounds are illuminated can be divided in three different classes: *trans–cis–trans* isomerisations, photo-induced ring-closing reactions and photo-tautomerism [17].

Depending on the thermal stability of the photogenerated isomer, photochromic systems can be classified in two categories [18]:

- P-type (photochemically reversible type); these do not revert to the initial isomer even at elevated temperatures (e.g., fulgides and diarylethenes).

- T-type (thermally reversible type); the photogenerated isomer thermally reverts to the initial form (e.g., azobenzenes, stilbenes or spiropyranes).

One of the most used organic chromophores for optical switching applications are certainly azobenzenes. Azobenzene, a photochromic T-type system, exhibits a reversible isomerisation process between its *trans* and *cis* isomers of different stability. In this process, the photoreaction simply causes the rearrangement of the electronic and nuclear structure of the molecule without any bond breaking. Moreover, the totally clean reverse *cis*-to-*trans* conversion also takes place thermally in the dark, spontaneously (Figure 2). It should be also noted

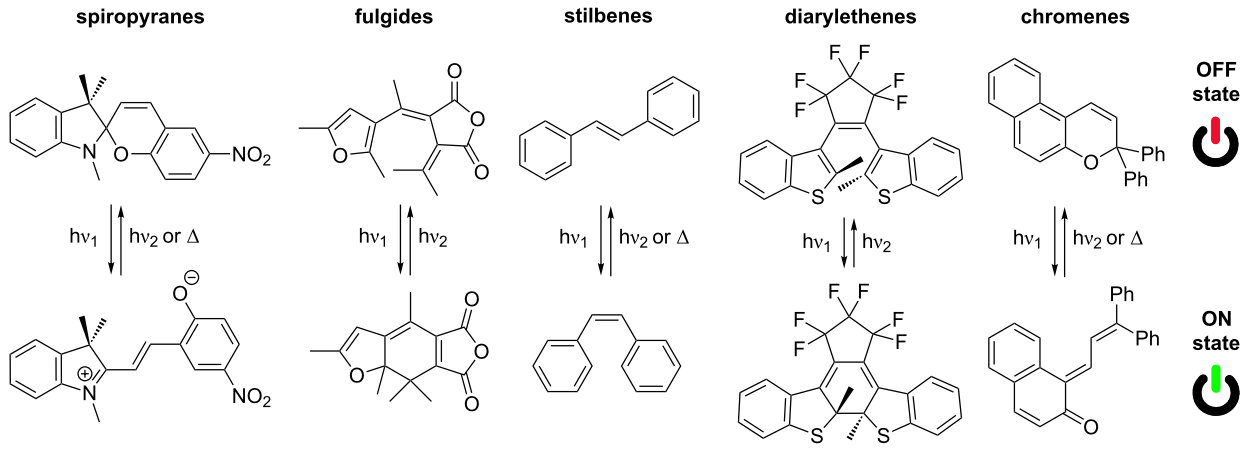

Figure 1: Some important families of photochromic compounds and their photochromic reactions.

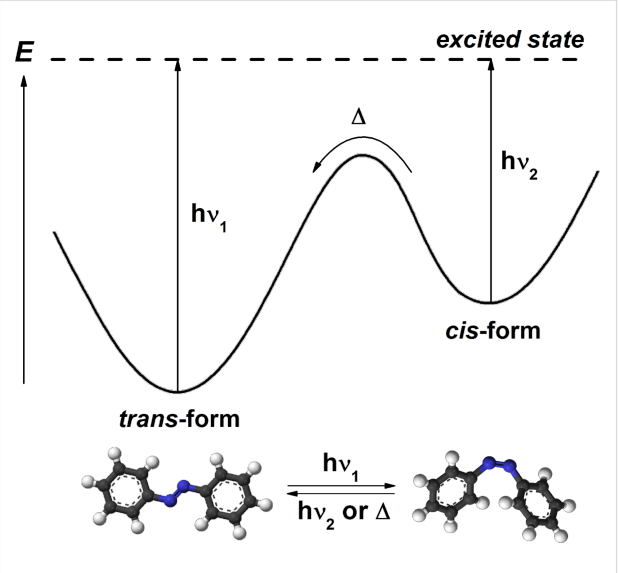

Figure 2: Photochromism of azobenzene derivatives and energetic profile for the switching process.

that if the *cis*-to-*trans* back reaction is induced by visible-light excitation instead of thermally, then the formation of phenyl radicals may occur and dediazotation can be observed [19,20].

Azobenzene-based photochromic systems are under kinetic control; that is, after a photochemical conversion, whose rate depends mainly on the intensity of the excitation beam, the spontaneous thermal back reaction occurs. While the photo-induced *trans*-to-*cis* isomerisation reaction can be performed in a few femtoseconds with a light source that is powerful enough, the rate of the thermal *cis*-to-*trans* back reaction depends greatly on the chemical architecture of the system. It is well known that the appropriate modification of the substitution of the azobenzene core is one of the main factors that allows modulating the thermal relaxation rate of azo-dyes and, therefore, determines the response time of the photochromic molecular switch. The response time of the photochromic switch is a key feature in its overall performance. This parameter is directly related with the thermal isomerisation rate of the photo-sensitive azo-dye in the dark, that is, with the relaxation time of the *cis* isomer of the azo-moiety. Slow thermally back-isomerising azoderivatives are valuable photoactive basic materials for information storage (memory) purposes. A molecular-level memory should be stable and easy to write, and, moreover, its switched form should be stable but readily erasable when necessary. However, for azobenzene-based photochromic switches that can be used in real-time information-transmitting systems as well as optical oscillators, it is essential that the return to the thermodynamically stable *trans* form in the dark occurs as fast as possible, that is, as soon as the optical stimulation is removed the molecule should revert to its initial state. In fact, the information is expected to be transmitted at the molecular scale with response times ultimately within the nanosecond or picosecond range. Even though some chromophores, such as spiropyranes, have been already proved to show very fast thermal back reactions occurring within hundreds of nanoseconds [21-23], reaching such fast relaxation times for azobenzene-based photochromic molecular switches is still a challenge. This aim has attracted a great deal of attention over the past few years due to the potential application of fast photoactive azobenzene-based materials in micropumps and autonomous valves that simulate the beating of the heart; photoactive polymers that mimic cilia movement; and artificial muscles for robotics or molecular rotary motors, among others [24-33]. Moreover, besides photochromic switching, azobenzenes with different isomerisation rates have been successfully applied very recently for both photoelectronic [34-37] and photomagnetic actuating purposes [38].

In this review, we present the efforts made in our research group over the past few years regarding the molecular design of new photosensitive azoderivatives endowed with very fast *cis*-to-*trans* thermal isomerisation processes, with the main aim of transmitting optical information beyond the time scale of microseconds, as well as to produce molecular materials with high oscillation frequencies in their optical properties. In addition, the possible design of such materials in such a way that they would be soluble in water (an environmentally friendly solvent) could be a noteworthy benefit since it opens a new door for further uses of these molecules in both biological and medical applications, such as photochromic ion-channel blockers [39], or allowing the photocontrol of neurotransmitters in the central nervous system [40,41]. Additionally, some of the azobenzene-based photochromic switches reported heretofore require temperatures substantially above 298 K to achieve a rapid thermal isomerisation of the azo-dye [42,43]. This fact limits substantially the usefulness of the final device. In this way, finding new azoderivatives exhibiting fast isomerisation rates at room temperature is a challenging point of research and, consequently, also one of the main topics of the present work. With this purpose in mind, three different types of azoderivatives were designed and studied (Figure 3). Firstly, we investigated such azoderivatives that exhibit a 4-donor-4'-acceptor substitution (*type-I*), that is, bearing a push–pull configuration. Secondly, kinetic studies of different azophenolic systems (*type-II*) will be presented, since these azoderivatives exhibit a fast thermal back reaction due to their capability to establish an azo-hydrazone tautomeric equilibrium. Both *type-I* and *type-II* azoderivatives allowed the transmission of information within a few of milliseconds. Finally, those azo-dyes that combine both phenomena (*type-III*) were tested, registering action speeds down to some tens of microseconds.

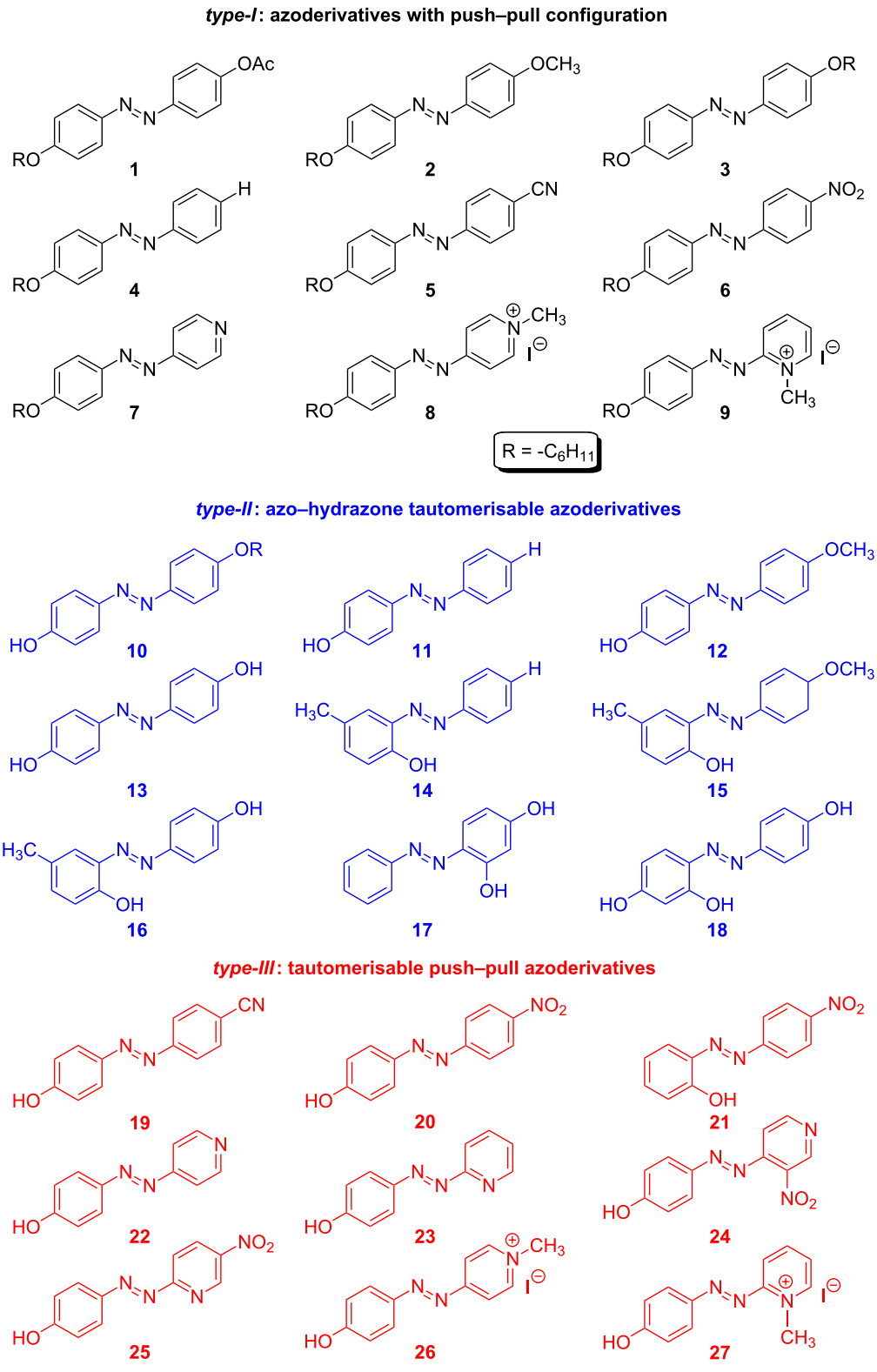

Figure 3: General overview of the different types of azoderivatives presented in this review.

Review

Type-I azoderivatives: photochromic switches acting within the millisecond time scale, based on chromophores with a push–pull configuration

The electronic spectra of the stable *trans* isomer of *type-I* azoderivatives **1**–**4**, display a high-intensity band peaking at ca. 355 nm, corresponding to the $\pi \rightarrow \pi^*$ transition, and a weak broad-band signal at ca. 450 nm, associated with the $n \rightarrow \pi^*$ transition. Upon UV-irradiation, the *trans*-to-*cis* photoisomerisation occurs, producing a decrease in the intensity of the 355 nm band and an increase in the 450 nm signal until the photostationary state is reached, that is, the inverse process of that shown in Figure 4 [44].

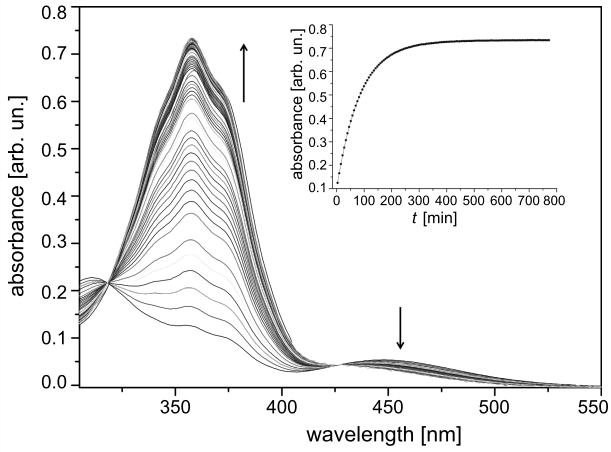

Figure 4: Changes in the electronic spectrum of a **3** *cis*-to-*trans* isomerising ethanol solution at 45 °C (Δt = 360 s, [**3**] = 30 μM). From [44] – Reprinted with permission from *J. Phys. Chem. B.* © 2010, American Chemical Society.

The kinetics of the thermal *cis*-to-*trans* isomerisation process for azo-dyes **1**–**6** were analysed by conventional UV–vis spectroscopy. Since these azoderivatives are not water-soluble, ethanol was used as a solvent instead of water. The unimolecular thermal *cis*-to-*trans* isomerisation process in the dark obeys Equation 1.

$$\Delta A_t = \Delta A_\infty + \Delta A_0 \cdot e^{-t/\tau} \quad (1)$$

where ΔA_t, ΔA_0 and ΔA_∞ correspond to the absorbance change at time t, t = zero and t = infinite, respectively, and τ is the relaxation time of the corresponding *cis* isomer. The relaxation times were derived from plots of the absorbance, ΔA, versus time by fitting Equation 1 to the experimental data, which perfectly described a first-order profile.

Azocompounds **1**–**4** presented very slow thermal *cis*-to-*trans* isomerisation kinetics showing relaxation times for their thermal back reactions from several hours to a few days (Figure 5) [44].

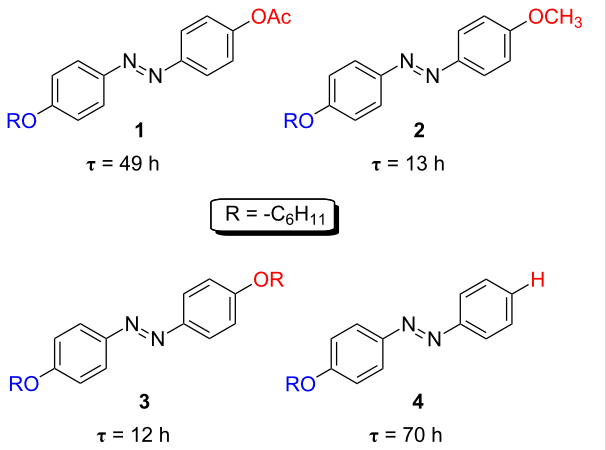

Figure 5: Chemical structure and thermal relaxation time in ethanol at 298 K, τ, for the slow thermally-isomerising *type-I* azoderivatives **1**–**4**.

The rate of the thermal *cis*-to-*trans* back reaction is clearly determined by the intimate mechanism through which the process takes place. This mechanism has attracted much attention for many years and has given rise to controversy. For the process, two different extreme mechanisms have been proposed (Figure 6); one involving a simple rotation around the N–N bond [45,46], and another implying an inversion, in-plane lateral shift, through a linear transition state [47-49]. However, recent advances in both gas phase and in solution point out that some mixed mechanisms, such as the concerted inversion or the inversion-assisted rotation, can also be possible pathways for the *trans*-to-*cis* photoisomerisation of azobenzenes [50-52].

The measurement of the volumes of activation for these processes provides unequivocal evidences regarding the operation of the inversion or rotation isomerisation mechanism [53,54]. The volumes of activation for the thermal *cis*-to-*trans* isomerisation process of azobenzenes **1**–**3** were all close to zero, as expected [44]. These values perfectly correlate with those found in the literature for the azobenzene-bridged crown-ether 3,3'-[1,10-diaza-4,7,13,16-tetraoxa-18-crown-6]-biscarbonylazobenzene, which thermally isomerises by the inversion mechanism, because of its impossibility to evolve through the rotational pathway due to structural restrictions [55]. Therefore, not

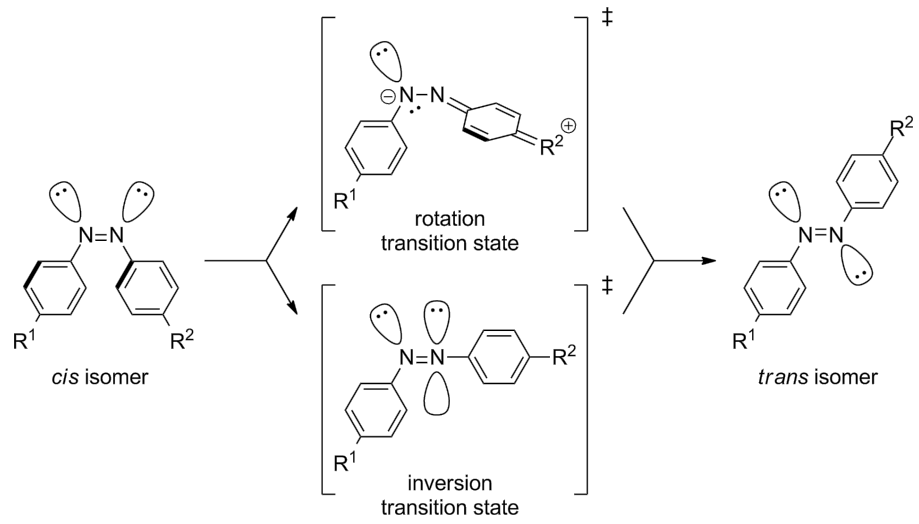

Figure 6: Rotation and inversion mechanisms proposed for the thermal *cis*-to-*trans* isomerisation processes of azobenzenes.

only acetylated (**1**) and alkoxylated (**2** and **3**) azo-dyes, but also the parent nonsubstituted one (**4**), thermally back-isomerise through the inversion mechanism [44]. Both 4-cyano-4'-(5-hexenyloxy)azobenzene (**5**) and 4-(5-hexenyloxy)-4'-nitroazobenzene (**6**) show a gradual increase in the strength of their push–pull electronic distribution as a consequence of the placement of the electron-withdrawing cyano or nitro groups in one of the *para*-positions of the azobenzene core. This structural variation produces a red shift of the $\pi\rightarrow\pi^*$ transition to 375 nm with respect to that of the parent nonsubstituted azo-dye **4** (355 nm). In azoderivatives **5** and especially **6**, their $\pi\rightarrow\pi^*$ transition is very close or directly overlapped with the $n\rightarrow\pi^*$ one, due to an increase in the π orbital energy and a decrease in the energy of the π^* orbital. Subsequently, a clear decrease of the relaxation time from 70 h (compound **4**) to 6 h or 24 min for azoderivatives **5** and **6**, respectively, is detected (Figure 7).

According to the trend observed for azoderivatives **4**, **5** and **6** (Figure 7), the design of a new series of azoderivatives, bearing a pyridine ring (compound **7**) or a pyridinic cation (compounds **8** and **9**) as an electron-withdrawing group, was carried out. This feature allowed the creation of azo-dyes with a much stronger push–pull configuration than the nitro-substituted compound **6** and, thereafter, faster thermal isomerisation rates were obtained. As a consequence, the *trans*-**8** and *trans*-**9** exhibit intense peaks centred at 410 and 400 nm, respectively, corresponding to the allowed $\pi\rightarrow\pi^*$ transition, which is totally overlapped with the $n\rightarrow\pi^*$ one and highly shifted to the visible zone of the electromagnetic spectrum. It should be highlighted that this band is red-shifted by 50–60 nm with respect to that of the non-push–pull pyridine precursor **7**, which exhibits its $\pi\rightarrow\pi^*$ transition at ca. 350 nm, and also 25–35 nm red-shifted from the previously mentioned cyano- or nitro-azobenzene derivatives. This notable red-shift of the absorption wavelength arises from the strong charge transfer from the alkoxy group to the positively-charged nitrogen atom of the pyridinium salt. Figure 8 shows the transient absorption generated upon pulsed laser irradiation of ethanol solutions of azo-dyes **8** and **9** at 298 K. The relaxation times for *cis*-**8** and *cis*-**9** are 2.8 ms and 570 μs, respectively (Figure 9).

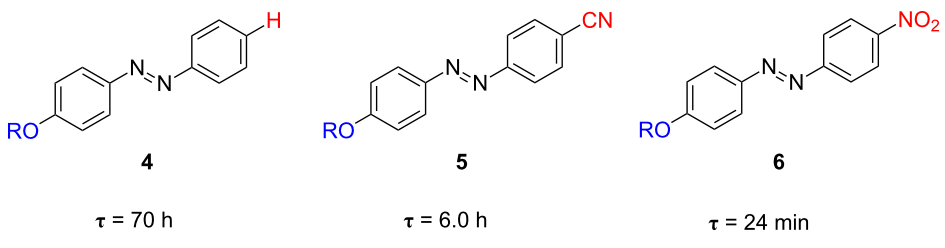

Figure 7: Effect of the presence of the electron-withdrawing cyano and nitro groups on the thermal relaxation time in ethanol at 298 K, τ, for the *type-I* azoderivatives **5** and **6**.

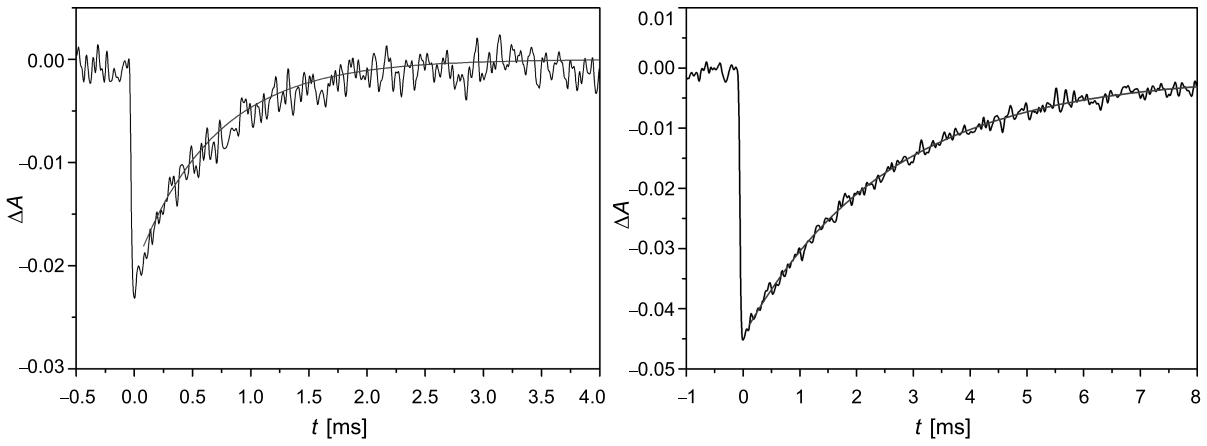

Figure 8: Transient absorption generated by UV irradiation (λ = 355 nm) for azo-dyes **8** (right) and **9** (left) in ethanol at 298 K ([**AZO**] = 20 μM, λ_{obs} = 420 nm for **8** and 405 nm for **9**). From [56] – Reprinted with permission from *Org. Lett.* © 2010, American Chemical Society.

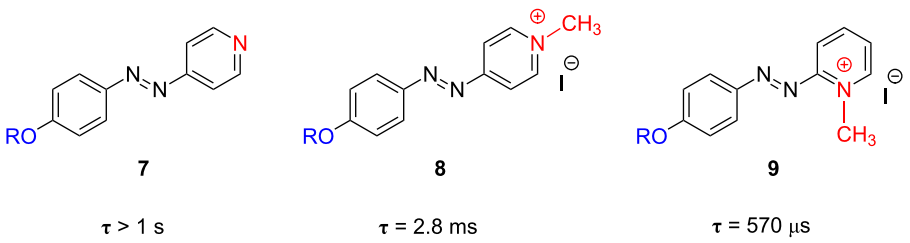

Figure 9: Effect of the presence of a positively charged nitrogen as an electron-withdrawing group on the thermal relaxation time at 298 K, τ, for the *type-I* azoderivatives **8** and **9**.

Figure 10 depicts the proposed mechanism for the thermally-activated *cis*-to-*trans* isomerisation of the *cis* isomers of the push–pull azopyridinium methyl iodide salts **8** and **9**. The strong electron transfer from the alkoxy group to the pyridinium salt produces a partial breaking of the double N–N bond of the azo moiety, thereby facilitating the rotation around this bond to recover the more stable initial *trans* configuration in a quick fashion [56].

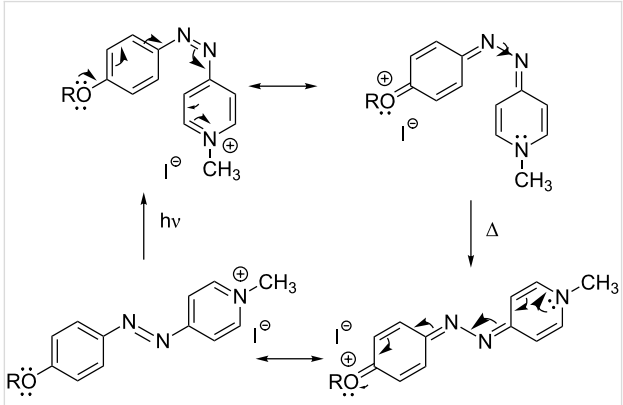

Figure 10: Mechanism proposed for the thermal *cis*-to-*trans* isomerisation process for the push–pull azopyridinium methyl iodide salts **8** and **9**. From [56] – Reprinted with permission from *Org. Lett.* © 2010, American Chemical Society.

Type-II azoderivatives: photochromic switches acting within the milliseconds time scale, based on chromophores able to establish azo-hydrazone tautomeric equilibria

Hydroxy-substituted azobenzenes are a very interesting family of rapidly thermally isomerising azoderivatives, which have been applied successfully not only for light-driven optical switching applications [43], but also as photoactive monomers in elastomers for light-sensitive artificial muscle-like actuators [57]. In 2005, Kojima et al. found that 4-hydroxyazobenzene (**11**), the simplest azophenol, was endowed with a fast thermal *cis*-to-*trans* isomerisation process [58]. In fact, further experiments with this compound demonstrated a relaxation time of 205 ms for its back reaction at room temperature in ethanol [59].

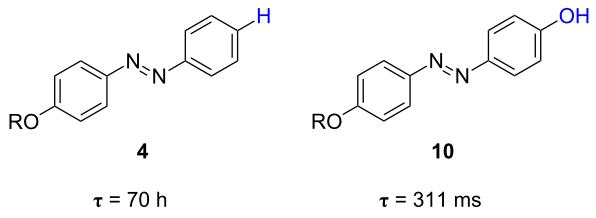

Figure 11: Comparison between the thermal relaxation time at 298 K, τ, for the azoderivative **4** (*type-I*) and the azophenol **10** (*type-II*).

The comparison between the relaxation time for the thermal *cis*-to-*trans* isomerisation of 4-(5-hexenyloxy)azobenzene (**4**) and that of 4-hydroxy-4'-(5-hexenyloxy)azobenzene (**10**) revealed very different behaviours. While the azoderivative **4** exhibits a very slow thermal isomerisation, which can be nicely followed by conventional time-resolved absorption spectroscopy, the thermal back reaction of azophenol **10** must be determined by the laser flash-photolysis technique. Indeed, the thermal *cis*-to-*trans* isomerisation kinetics of *cis*-**10** is up to 8×10^5 times faster than that for the nonsubstituted counterpart **4** (311 ms versus 70 h, respectively, Figure 11). This feature provides evidence for a clear influence of the phenol group on the thermal isomerisation process. The same conclusion can be extracted when comparing the isomerisation kinetics of azophenol **11** with that of azobenzene.

Some insights into the relation between both the chemical structure and the observed kinetic behaviour can be obtained from the study of different *para*-, *ortho*- and *poly*-hydroxy-substituted azobenzenes. There is not only a clear influence of the number and the placement of the hydroxy groups within the azobenzene core, but also of the nature of the solvent used. Both *para*-mono-substituted azophenols **11** and **12** exhibit fast thermal isomerisation kinetics in ethanol at 298 K with relaxation times of 205 and 306 ms, respectively (Figure 12). Remarkably, the relaxation times for these two azocompounds increase in toluene by four orders of magnitude up to 31 and 28 minutes, respectively (Figure 12 and Figure 13). In addition, the analogous *para*-di-substituted azophenol **13** shows a similar behaviour: relaxation times of 33 min and 306 ms in toluene and ethanol, respectively [59].

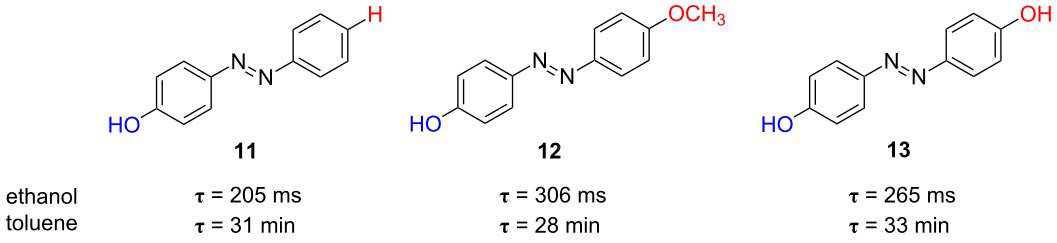

Figure 12: Solvent effect on the thermal relaxation time at 298 K, τ, for the *type-II* azophenols **11**–**13**.

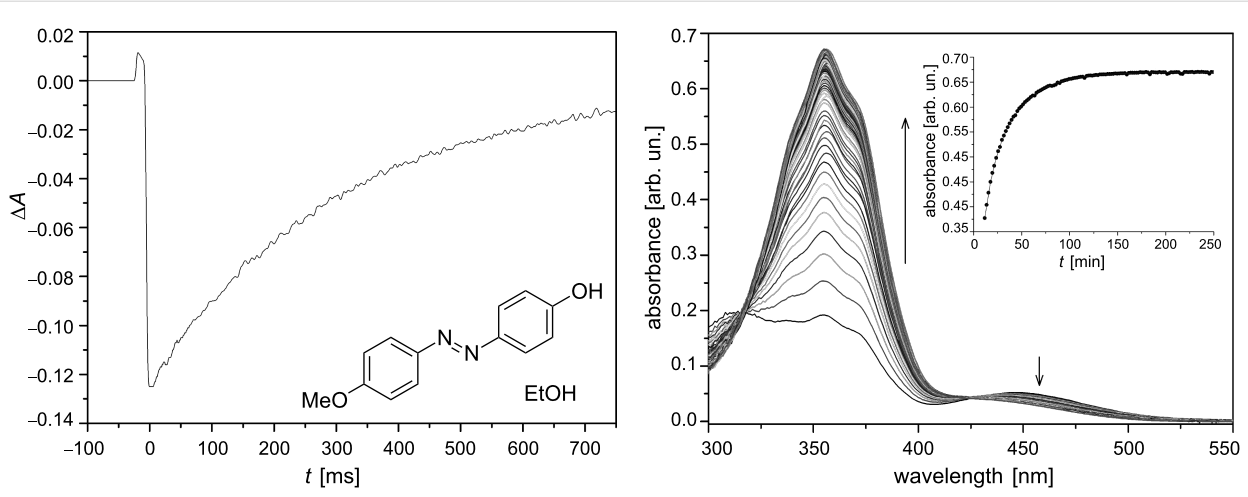

Figure 13: Transient generated by irradiation with UV-light (λ = 355 nm) for the *type-II* azophenol **12** in ethanol (left) and changes in the electronic spectrum of a **12** *cis*-to-*trans* isomerising toluene solution at 298 K (Δ*t* = 120 s, [**12**] = 20 μM). From [59] – Reproduced by permission of the PCCP Owner Societies.

The differential kinetic behaviour detected for azophenols **11**–**13** in toluene and ethanol clearly evidences that the intermolecular interactions established between both the chromophore and the solvent molecules control the rate of the isomerisation process for *type-II* azoderivatives. The formation of intermolecular hydrogen bonds between the nitrogen atom of the azo group and the solvent proton, as well as between the OH group of the azo-dye and the solvent, favours a hydrazone-like electronic distribution with a simple N–N bond, which seems to be the key to the fast thermal isomerisation kinetics observed. In this way, the rotation around the N–N bond facilitates the recovery of the more stable *trans* isomer (Figure 14) [46,59-61].

The completely different kinetic behaviours observed between the alkoxy- and hydroxy-substituted azo-dyes reflect that some alteration in their intimate isomerisation mechanism occurs. The rapid thermal *cis*-to-*trans* isomerisation of the hydroxy-substituted azo-dyes suggests that their back reaction takes place via the rotational pathway, through a polar transition state with a partial breaking of the N–N double bond; however, in the case of the alkoxy-substituted azoderivatives the isomerisation process proceeds by the inversional mechanism (Figure 14).

Ortho-substituted azophenols show much shorter *cis*-relaxation times than their *para*-substituted counterparts in toluene solution, e.g., 31 min for *cis*-**11** versus 650 ms for *cis*-**14** (Figure 15). This can be understood bearing in mind that azocompound **11** should undergo dimerization prior to its isomerisation in toluene. Nevertheless, the formation of an intramolecular hydrogen bond [62] in the *ortho*-substituted compound **14** can take place independently of the solvent; this promotes the hydrazone-like tautomeric form and, therefore, the fast isomerisation process can occur in both protic (ethanol) and nonprotic (toluene) solvents. All three *ortho*-substituted azophenols (**14**–**16**) show slightly slower kinetics in toluene than in ethanol, which can be assumed to be because of the impossibility of the former solvent to establish hydrogen bonding with the azo-dye molecules.

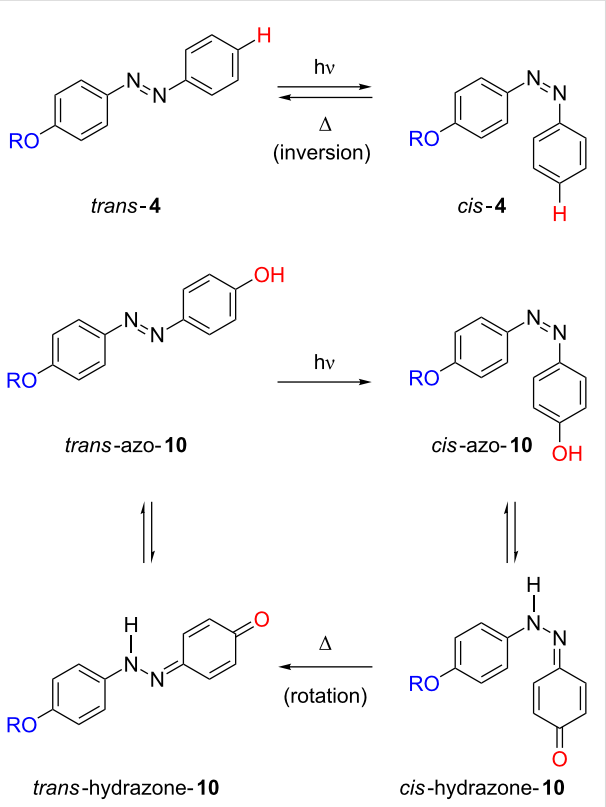

Figure 14: Proposed isomerisation mechanisms for the thermal *cis*-to-*trans* isomerisation of the alkoxy-substituted azoderivative **4** (*type-I*) and the azophenol **10** (*type-II*).

In the wake of these promising results, especially of that of the di-substituted azophenol **16** in ethanol, we devised a possible strategy for decreasing the relaxation time of the photochromic switch by placing two hydroxy groups in the same ring of the azobenzene moiety, to obtain an added effect of the two hydroxy groups. The relaxation time of the *ortho*-*para*-di-substituted azophenol *cis*-**17** was 12 ms in ethanol and 53 ms in toluene, respectively. Indeed, the presence of two hydroxy groups in both *ortho*- and *para*-positions of the same ring of the azobenzene core produces a significant acceleration of the

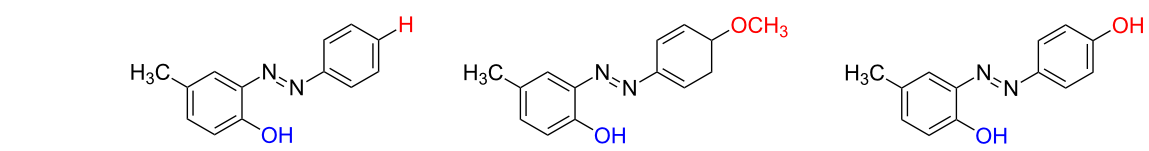

	14	**15**	**16**
ethanol	τ = 399 ms	τ = 302 ms	τ = 175 ms
toluene	τ = 650 ms	τ = 418 ms	τ = 416 ms

Figure 15: Solvent effect on the thermal relaxation time at 298 K, **τ**, for the *type-II ortho*-substituted azophenols **14**–**16**.

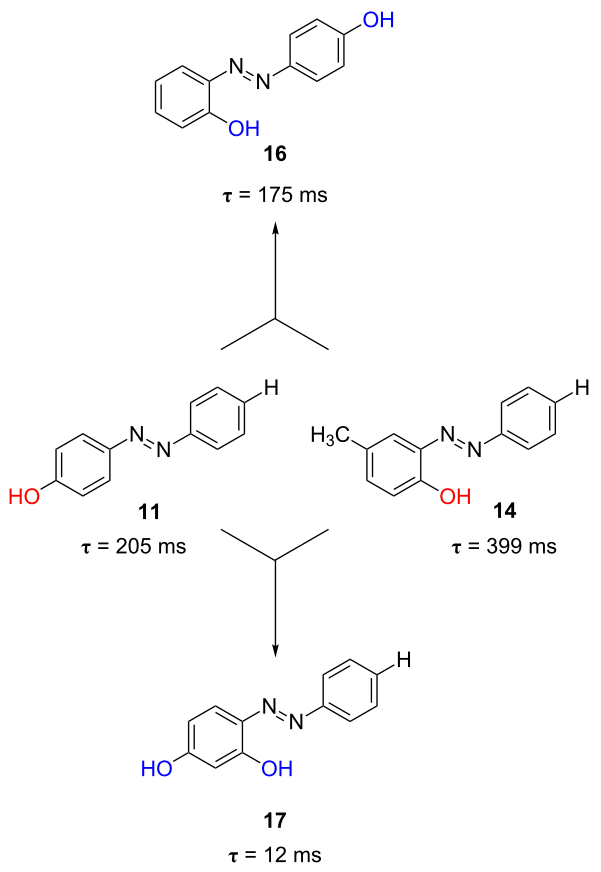

Figure 16: Cooperative effect of the *para*- and *ortho*-hydroxyl groups in azophenol **17**.

process by a cooperative effect. This is not observed when the two hydroxy groups are placed in different rings of the azobenzene molecule (see Figure 16, azophenol **16** versus **17**).

Moreover, the *poly*-hydroxy-substitution of the azobenzene core, such as in 2,4,4'-trihydroxyazobenzene (**18**), considerably decreases the relaxation time down to 6 and 33 milliseconds in ethanol and toluene, respectively, in comparison with its dihydroxy-substituted counterparts **13**, **16** and **17** (Figure 17). Figure 18 shows the transients for the *poly*-substituted azophenol **18** in both ethanol and toluene at 298 K [59]. In fact, the *cis* isomers of both azoderivatives **17** and **18** show the lowest relaxation times of all the azophenol derivatives presented in this section.

Type-III azoderivatives: optical switches acting within the microsecond time scale, based on azo-dyes exhibiting both azo-hydrazone tautomerism and a push–pull electronic distribution

Among all the azoderivatives presented up to now in this review, azopyridinium methyl iodide salts are the fastest ones (azo-dyes **8** and **9**, see *Type-I* azoderivatives) [56]. These azoderivatives exhibit a strong push–pull configuration, which favours the rotational isomerisation mechanism. The relaxation time of *type-I* azoderivatives ranged from several days to hundreds of microseconds. Specifically, azoderivatives **8** and **9** showed relaxation times of 2.8 ms and 570 μs in alcoholic solu-

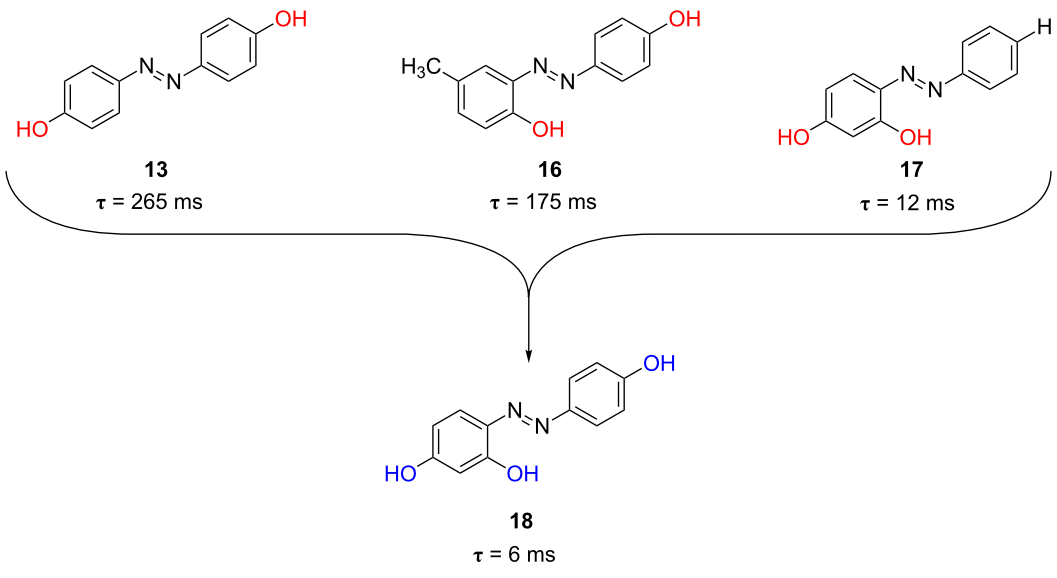

Figure 17: Effect of the *poly*-hydroxylation of the azobenzene core on the thermal relaxation time at 298 K, τ, for the *type-II* azobenzenes: azophenol **18**.

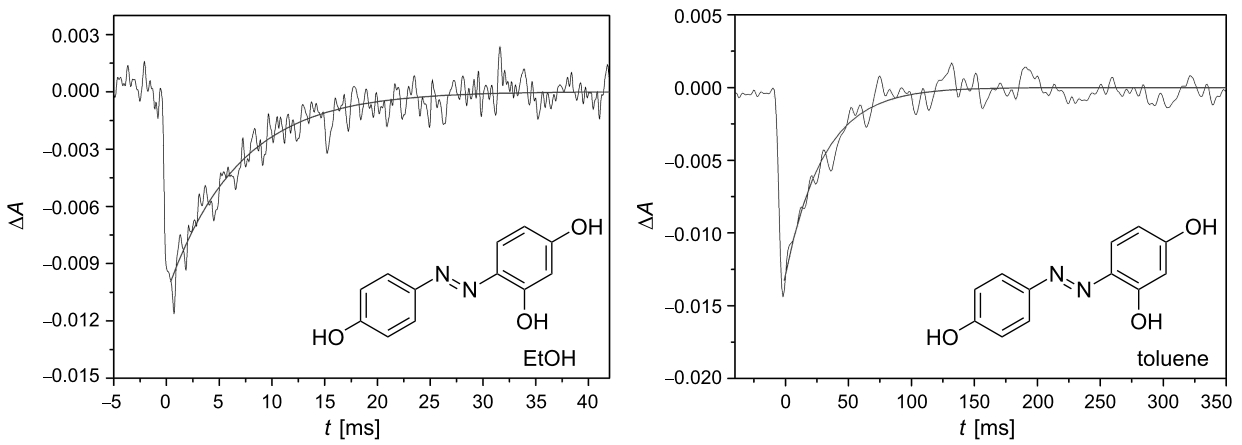

Figure 18: Transients generated by irradiation with UV-light (λ = 355 nm) for the *poly*-substituted azophenol **18** in ethanol (left) and toluene (right) at 298 K. ([**18**] = 20 μM). From [59] – Reproduced by permission of the PCCP Owner Societies.

tions at 298 K, respectively (see Figure 8). As mentioned above, the relaxation time of *type-II* azophenols ranged from 400 ms to 6 ms in ethanol, depending on the position of the phenol groups within the azobenzene core. However, both types of azoderivatives are still too slow for use as light-driven real-time information-transmitting systems or photo-driven optical oscillators.

The combination in the same molecule of both types of rotational-isomerising azo-dyes was suggested to afford very rapidly thermally isomerising azoderivatives [63]. This section collects different families of azoderivatives that combine the two strategies aforementioned: the presence of powerful electron-withdrawing groups, like nitro or pyridinium salts, and the existence of a phenol function in the convenient positions (2' and 4') of the azobenzene core. This feature allows one to obtain highly conjugated systems that extremely favour the thermal isomerisation through the rotational pathway and recovery of the thermodynamically stable *trans* form in a very quick fashion. In this manner, the thermal *cis*-to-*trans* relaxation time for these azoderivatives decreases considerably and, therefore, a further increase in the information transmission capability of the final photochromic switch is observed.

In order to get an idea of the benefits of this strategy it is worth comparing the first the relaxation times of parent azocompounds. Azophenol **11** shows a relaxation time of 205 ms for its thermal isomerisation in ethanol at 298 K (see Figure 12). The introduction of the electron-withdrawing cyano group in the position 4' of the azophenol (compound **19**) caused the relaxation time of the 4'-cyanoazophenol **19** to decrease 10-fold compared to that of the parent azophenol **11** (27 ms versus 205 ms). The relaxation time decreased even further for the 4'-nitroazophenol **20** showing a τ value of 4.6 ms (Figure 19 and Figure 20). Hence, upon going from the azophenol **11** to its push–pull nitro counterpart **20**, the thermal *cis*-to-*trans* isomerisation process becomes faster and, consequently, an increase of the information transmission capability of the photochromic switch is observed.

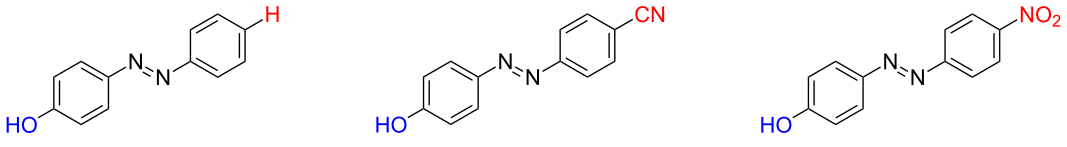

11
τ = 205 ms

19
τ = 27 ms

20
τ = 4.6 ms

Figure 19: Effect of the introduction of electron-withdrawing groups in the position 4' of the azophenol structure on the thermal relaxation time at 298 K in ethanol, τ, for the azoderivatives **11** (*type-II*) and **19** and **20** (*type-III*).

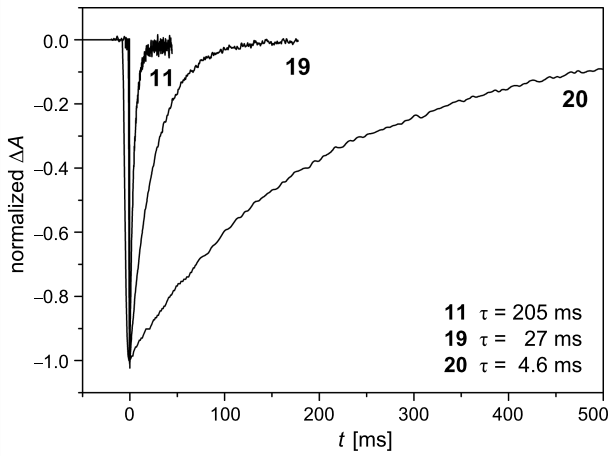

Figure 20: Transient absorptions generated by UV irradiation (λ = 355 nm) of azo-dyes **11** (*type-II*), **19** (*type-III*) and **20** (*type-III*) in ethanol at 298 K ([**AZO**] = 20 μM, λ_{obs} = 370 nm). From [63] – Reproduced by permission of the Royal Society of Chemistry.

The placement of the hydroxy group in the position 2 has been also studied for the *type-III* azophenols. In contrast to that found for the *type-II* azophenols, a notably increase of the relaxation time was detected for the *ortho*-substituted azophenol containing the electron-withdrawing nitro group **21** (τ = 50 ms, Figure 21) with respect to the corresponding non-push–pull counterpart (τ = 399 ms) in ethanol at 298 K. These values are substantially larger than those of the corresponding *para*-hydroxy-substituted azo-dyes **11** (205 ms) and **20** (4.6 ms), respectively (Figure 19).

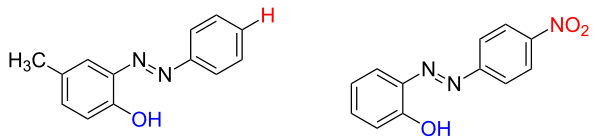

14 τ = 399 ms

21 τ = 50 ms

Figure 21: Effect of the introduction of the hydroxyl group in the position 2' of the push–pull azo-dye on the thermal relaxation time at 298 K in ethanol, τ, for azoderivatives **14** (*type-II*) and **21** (*type-III*).

The substitution of one of the benzene rings of the azo-dye by a pyridine one, a π-electron-deficient heterocycle, has been also considered. In this case, the hydrogen bonding established between ethanol and the pyridine moiety places a positive-charge density over the pyridine nitrogen, which increases susbsequently the push–pull electronic distribution of the azo-dye (compounds **22** and **23**). As observed in Figure 22, the relaxation time of these two azocompounds in ethanol is 49 ms and 14 ms, respectively, substantially shorter than that of the parent

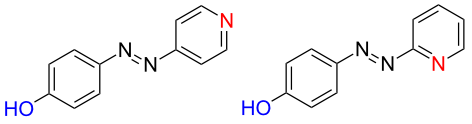

	22	**23**
ethanol	τ = 14 ms	τ = 49 ms
ethanol + PhOH	τ = 1.4 ms	τ = 11 ms

Figure 22: Effect of the substitution of a benzene ring by a pyridine one on the thermal relaxation time in ethanol and effect of 1 equiv phenol added at 298 K, τ, for *type-III* azoderivatives **22** and **23**.

4-hydroxyazobenzene **11** (205 ms), but too large compared to that of the *para*-nitro-substituted azo-dye **20** (4.6 ms).

Additionally, when phenol is added to the ethanol solution, the thermal *cis*-to-*trans* isomerisation kinetics is accelerated. Phenol forms a stable hydrogen bond with the nitrogen atom of pyridine. Indeed, addition of 1 equiv phenol increases the isomerisation rate of azo-dyes **22** and **23** by a factor of 10 and 4.5, respectively (Figure 22). The differential effect can be associated with the major difficulty of the pyridinic nitrogen to establish a hydrogen bond with phenol in the position 2 of the azobenzene core due to steric hindrance.

The introduction of additional nitro groups in the *ortho*- and *para*-positions with respect to the azo function has been also considered (compounds **24** and **25**). These two azoderivatives show relaxation times of 2.9 ms and 1.3 ms in ethanol, respectively, which decrease further down to 1.1 ms and 644 μs in the presence of phenol (Figure 23). This demonstrates that the generation of push–pull systems by the establishment of hydrogen bonds between phenol groups and the pyridinic nitrogen, with the subsequent generation of a deficient electron density in the latter, is a versatile option towards the generation of fast information-transmitting photochromic switches.

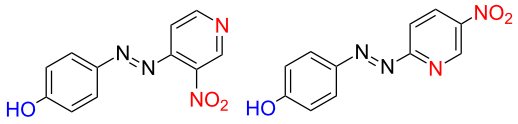

	24	**25**
ethanol	τ = 1.4 ms	τ = 2.9 ms
ethanol + PhOH	τ = 644 μs	τ = 1.1 ms

Figure 23: Influence of the introduction of additional electron-withdrawing nitro groups in the pyridine ring on the thermal relaxation time in ethanol and effect of 1 equiv phenol added at 298 K, τ, for *type-III* azoderivatives **24** and **25**.

Extending the concept even further, azopyridines with a permanent positively charged nitrogen should increase the kinetics and the stability of the final photodriven oscillator. Methylation of the pyridine nitrogen of azo-dyes **22** and **23** was carried out to afford the corresponding pyridinium methyl iodide salts **26** and **27**. Thus, the methyl hydroxy-substituted azopyridinium salts **26** and **27** present relaxation times of only 150 μs and 33 μs, respectively, at room temperature in ethanol (Figure 24). To the best of our knowledge, these are the fastest thermally isomerising azophenol derivatives heretofore reported in the literature [63].

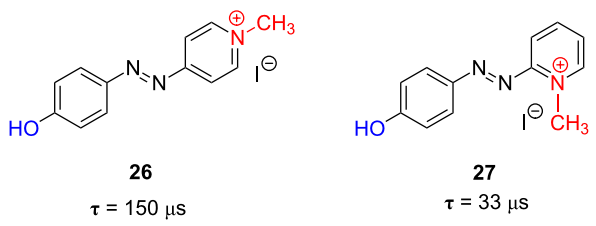

Figure 24: Chemical structure and thermal relaxation time in ethanol at 298 K, τ, for the *type-III* azoderivatives **26** and **27**.

Because of their very fast thermal isomerisation rate, **26** and **27** are the best candidates to be applied as fast information-transmitting photochromic switches. Figure 25 shows the information-transmission capability of azo-dye **26** with time. The repeatability of the different optical oscillators was tested by submitting them to consecutive UV-irradiation–dark cycles. The optical photochromic switches reported show no fatigue (Figure 25).

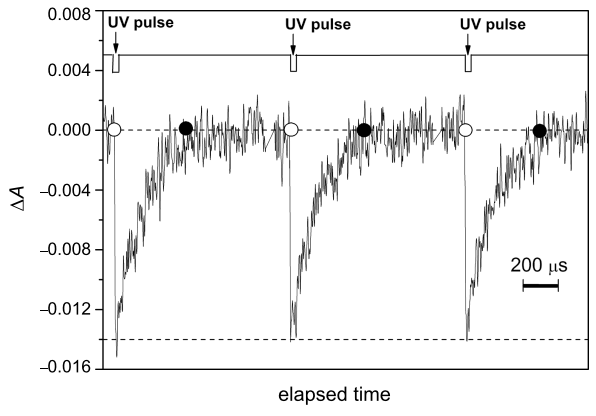

Figure 25: Oscillation of the optical density of an ethanol solution of azo-dye **26** generated by UV-light irradiation (λ = 355 nm, 5 ns pulse width) at 298 K ([**26**] = 20 μM, λ_{obs} = 420 nm). From [63] – Reproduced by permission of the Royal Society of Chemistry.

Conclusion

This review compiles very recently reported advances with regard to rapidly thermally isomerising azoderivatives, which are valuable candidates to be applied as fast information-transmitting photochromic switches. Two structural features should be present in the azobenzene molecule for this purpose: a push–pull electronic distribution together with the existence of a hydroxy group that allows the keto–enol equilibrium to be established. These two factors allow the thermal back isomerisation process of the azo-dye to proceed through the rotational pathway, and, consequently, the thermodynamically stable *trans* form of the azo-dye can be restored in a very quick fashion. Indeed, those azoderivatives that combine both structural factors exhibit an information-transmitting capability within tens of microseconds.

References

1. Sauvage, J.-P., Ed. *Molecular Machines and Motors; Structure and Bonding;* Springer: Berlin, Heidelberg, 2001; Vol. 99. doi:10.1007/3-540-44421-1
2. Gust, D.; Moore, T. A.; Moore, A. L. *Acc. Chem. Res.* **2001,** *34,* 40. doi:10.1021/ar9801301
3. Nakano, A.; Yamazaki, T.; Nishimura, Y.; Yamazaki, I.; Osuka, A. *Chem.–Eur. J.* **2000,** *6,* 3254. doi:10.1002/1521-3765(20000901)6:17<3254::AID-CHEM3254>3.0.CO;2-6
4. Fujiwara, T.; Harada, J.; Ogawa, K. *J. Phys. Chem. B* **2004,** *108,* 4035. doi:10.1021/jp037438g
5. Inada, T.; Uchida, S.; Yokohama, Y. *Chem. Lett.* **1997,** *26,* 321. doi:10.1246/cl.1997.321
6. Tsivgoulis, G. M.; Lehn, J.-M. *Chem.–Eur. J.* **1996,** *2,* 1399. doi:10.1002/chem.19960021112
7. Zhou, Y.; Zhang, D.; Zhang, Y.; Tang, Y.; Zhu, D. *J. Org. Chem.* **2005,** *70,* 6164. doi:10.1021/jo050489k
8. Feringa, B. L.; van Delden, R. A.; Koumura, N.; Geertsema, E. M. *Chem. Rev.* **2000,** *100,* 1789. doi:10.1021/cr9900228
9. Pieraccini, S.; Masiero, S.; Spada, G. P.; Gottarelli, G. *Chem. Commun.* **2003,** 598. doi:10.1039/b211421f
10. Beer, G.; Niederalt, C.; Grimme, S.; Daub, J. *Angew. Chem., Int. Ed.* **2000,** *39,* 3252. doi:10.1002/1521-3773(20000915)39:18<3252::AID-ANIE3252>3.0.CO;2-P
11. Han, M.-J.; Gao, L.-H.; Lü, Y.-Y.; Wang, K.-Z. *J. Phys. Chem. B* **2006,** *110,* 2364. doi:10.1021/jp0548570
12. Badjic, J. D.; Ronconi, C. M.; Stoddart, J. F.; Balzani, V.; Silvi, S.; Credi, A. *J. Am. Chem. Soc.* **2006,** *128,* 1489. doi:10.1021/ja0543954
13. Shiraishi, Y.; Tokitoh, Y.; Nishimura, G.; Hirai, T. *Org. Lett.* **2005,** *7,* 2611. doi:10.1021/ol050735e
14. Bouas-Laurent, H.; Dürr, H. *Pure Appl. Chem.* **2001,** *73,* 639. doi:10.1351/pac200173040639
15. Raymo, F. M.; Tomasulo, M. *Chem.–Eur. J.* **2006,** *12,* 3186. doi:10.1002/chem.200501178
16. Rabek, J. F., Ed. *Photochemistry and Photophysics;* CRC Press: Boca Raton, FL, 1990.
17. Hamon, F.; Djedaini-Pilard, F.; Barbot, F.; Len, C. *Tetrahedron* **2009,** *65,* 10105. doi:10.1016/j.tet.2009.08.063

18. Balzani, V.; Credi, A.; Venturi, M. *Molecular Devices and Machines: Concepts and perspectives for the nanoworld;* Wiley-VCH: Weinheim, 2008.
19. Bozzi, A.; Caronna, T.; Fontana, F.; Marcandalli, B.; Selli, E. *J. Photochem. Photobiol., A: Chem.* **2002,** *152,* 193. doi:10.1016/S1010-6030(02)00245-9
20. Ali, A. M. J.; Al-Saigh, Z. Y. *J. Chem. Technol. Biotechnol.* **2007,** *30,* 440. doi:10.1002/jctb.503300155
21. Deniz, E.; Sortino, S.; Raymo, F. M. *J. Phys. Chem. Lett.* **2010,** *1,* 3506. doi:10.1021/jz101473w
22. Deniz, E.; Ray, S.; Tomasulo, M.; Impellizzeri, S.; Sortino, S.; Raymo, F. M. *J. Phys. Chem. A* **2010,** *114,* 11567. doi:10.1021/jp107116d
23. Deniz, E.; Tomasulo, M.; DeFazio, R. A.; Watson, B. D.; Raymo, F. M. *Phys. Chem. Chem. Phys.* **2010,** *12,* 11630. doi:10.1039/c002285n
24. Camacho-López, M.; Finkelmann, H.; Palffy-Muhoray, P.; Shelley, M. *Nat. Mater.* **2004,** *3,* 307. doi:10.1038/nmat1118
25. Kobatake, S.; Takami, S.; Muto, H.; Ishikawa, T.; Irie, M. *Nature* **2007,** *446,* 778. doi:10.1038/nature05669
26. White, T. J.; Tabiryan, N. V.; Serak, S. V.; Hrozhyk, U. A.; Tondiglia, V. P.; Koerner, H.; Vaia, R. A.; Bunning, T. J. *Soft Matter* **2008,** *4,* 1796. doi:10.1039/b805434g
27. Klok, M.; Boyle, N.; Pryce, M. T.; Meetsma, A.; Browne, W. R.; Feringa, B. L. *J. Am. Chem. Soc.* **2008,** *130,* 10484. doi:10.1021/ja8037245
28. Van Oosten, C. L.; Bastiaansen, C. W. M.; Broer, D. J. *Nat. Mater.* **2009,** *8,* 677. doi:10.1038/nmat2487
29. Koshima, H.; Ojima, N.; Uchimoto, H. *J. Am. Chem. Soc.* **2009,** *131,* 6890. doi:10.1021/ja8098596
30. Horvath, J.; Szalai, I.; Boissonade, J.; De Kepper, P. *Soft Matter* **2011,** *7,* 8462. doi:10.1039/c1sm05226h
31. Lee, K. M.; White, T. J. *Polymers* **2011,** *3,* 1447. doi:10.3390/polym3031447
32. Hrozhyk, U. A.; Serak, S. V.; Tabiryan, N. V.; White, T. J.; Bunning, T. J. *Opt. Mater. Express* **2011,** *1,* 943. doi:10.1364/OME.1.000943
33. Hrozhyk, U. A.; Serak, S. V.; Tabiryan, N. V.; Hoke, L.; Steeves, D. M.; Kimball, B. R. *Opt. Express* **2010,** *18,* 8697. doi:10.1364/OE.18.008697
34. del Valle, M.; Gutiérrez, R.; Tejedor, C.; Cuniberti, G. *Nat. Nanotechnol.* **2007,** *2,* 176. doi:10.1038/nnano.2007.38
35. Ferri, V.; Elbing, M.; Pace, G.; Dickey, M. D.; Zharnikov, M.; Samori, P.; Mayor, M.; Rampi, M. A. *Angew. Chem., Int. Ed.* **2008,** *47,* 3407. doi:10.1002/anie.200705339
36. Lim, S. L.; Li, N.-J.; Lu, J.-M.; Ling, Q.-D.; Zhu, C. X.; Kang, E.-T.; Neoh, K. G. *ACS Appl. Mater. Interfaces* **2009,** *1,* 60. doi:10.1021/am800001e
37. Smaali, K.; Lenfant, S.; Karpe, S.; Oçafrain, M.; Blachard, P.; Deresmes, D.; Godey, S.; Rochefort, A.; Roncali, J.; Vuillaume, D. *ACS Nano* **2010,** *4,* 2411. doi:10.1021/nn100295x
38. Venkataramani, S.; Jana, U.; Dommaschk, M.; Sönnichsen, F. D.; Tuczek, F.; Herges, R. *Science* **2011,** *331,* 445. doi:10.1126/science.1201180
39. Mourot, A.; Keinzler, M. A.; Banghart, M. R.; Fehrentz, T.; Huber, F. M. E.; Stein, M.; Kramer, R. H.; Trauner, D. *ACS Chem. Neurosci.* **2011,** *2,* 536. doi:10.1021/cn200037p
40. Volgraf, M.; Gorostiza, P.; Szobota, S.; Helix, M. R.; Isacoff, E. Y.; Trauner, D. *J. Am. Chem. Soc.* **2007,** *129,* 260. doi:10.1021/ja067269o
41. Gorostiza, P.; Isacoff, E. Y. *Science* **2008,** *322,* 395. doi:10.1126/science.1166022
42. Okano, K.; Shishido, A.; Ikeda, T. *Macromolecules* **2006,** *39,* 145. doi:10.1021/ma0512814
43. Tsutsumi, O.; Ikeda, T. *Mol. Cryst. Liq. Cryst.* **2001,** *368,* 411. doi:10.1080/10587250108029972
44. Garcia-Amorós, J.; Martínez, M.; Finkelmann, H.; Velasco, D. *J. Phys. Chem. B* **2010,** *114,* 1287. doi:10.1021/jp909557h
45. Talaty, E. R.; Fargo, J. C. *Chem. Commun.* **1967,** 65. doi:10.1039/c19670000065
46. Binenboym, J.; Burcat, A.; Lifshitz, A.; Shamir, J. *J. Am. Chem. Soc.* **1966,** *88,* 5039. doi:10.1021/ja00973a058 (And references therein.)
47. Schulte-Frohlinde, D. *Justus Liebigs Ann. Chem.* **1958,** *612,* 138. doi:10.1002/jlac.19586120115
48. Le Fèvre, R. J. W.; Northcott, J. *J. Chem. Soc.* **1953,** 867. doi:10.1039/JR9530000867
49. Jaffé, H. H. *Chem. Rev.* **1953,** *53,* 191. doi:10.1021/cr60165a003
50. Bandara, H. M. D.; Burdette, S. C. *Chem. Soc. Rev.* **2012,** *41,* 1809. doi:10.1039/c1cs15179g
51. Tiberio, G.; Muccioli, L.; Berardi, R.; Zannoni, C. *ChemPhysChem* **2010,** *11,* 1018. doi:10.1002/cphc.200900652
52. Maurer, R. J.; Reuter, K. *J. Chem. Phys.* **2011,** *135,* 224303. doi:10.1063/1.3664305
53. Asano, T. High-pressure kinetics and highly viscous media. In *In High Pressure Chemistry: synthetic, mechanistic, and supercritical applications;* van Eldik, R.; Klärner, F.-G., Eds.; Wiley-VCH: Weinheim, 2002; pp 97–128.
54. Leffler, J. E.; Grundwald, E. *Rates and equilibria of organic reactions as treated by statistical, thermodynamic, and extrathermodynamic methods;* Wiley: New York, 1963.
55. Shinkai, S.; Kusano, Y.; Shigematsu, K.; Manabe, O. *Chem. Lett.* **1980,** *9,* 1303. doi:10.1246/cl.1980.1303
56. Garcia-Amorós, J.; Massad, W. A.; Nonell, S.; Velasco, D. *Org. Lett.* **2010,** *12,* 3514. doi:10.1021/ol1013679
57. Garcia-Amorós, J.; Piñol, A.; Finkelmann, H.; Velasco, D. *Org. Lett.* **2011,** *13,* 2282. doi:10.1021/ol200546q
58. Kojima, M.; Nebashi, S.; Okawa, K.; Kurita, N. *J. Phys. Org. Chem.* **2005,** *18,* 994. doi:10.1002/poc.944
59. Garcia-Amorós, J.; Sánchez-Ferrer, A.; Massad, W. A.; Nonell, S.; Velasco, D. *Phys. Chem. Chem. Phys.* **2010,** *12,* 13238. doi:10.1039/c004340k
60. Kurita, N.; Nebashi, S.; Kojima, M. *Chem. Phys. Lett.* **2005,** *408,* 197. doi:10.1016/j.cplett.2005.04.047
61. Gabor, G.; Frei, Y. F.; Fischer, E. *J. Phys. Chem.* **1968,** *72,* 3266. doi:10.1021/j100855a029
62. Hsieh, B. R.; Desilets, D.; Kazmaier, P. M. *Dyes Pigm.* **1990,** *14,* 165. doi:10.1016/0143-7208(90)87015-U
63. Garcia-Amorós, J.; Nonell, S.; Velasco, D. *Chem. Commun.* **2011,** *47,* 4022. doi:10.1039/c1cc10302d

Beilstein Journal of Organic Chemistry

The effect of the formyl group position upon asymmetric isomeric diarylethenes bearing a naphthalene moiety

Renjie Wang, Shouzhi Pu*§, Gang Liu and Shiqiang Cui

Full Research Paper

Open Access

Address:
Jiangxi Key Laboratory of Organic Chemistry, Jiangxi Science & Technology Normal University, Nanchang 330013, PR China

Email:
Shouzhi Pu* - pushouzhi@tsinghua.org.cn

* Corresponding author
§ Tel.: +86-791-83831996; Fax: +86-791-83831996

Keywords:
chemical diversity; diarylethene; electrochemistry; formyl group; photochromism; substituent position effect

Beilstein J. Org. Chem. **2012,** *8,* 1018–1026.
doi:10.3762/bjoc.8.114

Received: 20 February 2012
Accepted: 19 June 2012
Published: 05 July 2012

This article is part of the Thematic Series "Molecular switches and cages".

Guest Editor: D. Trauner

Abstract

Three new isomeric asymmetric diarylethenes with a naphthyl moiety and a formyl group at the para, meta or ortho position of the terminal benzene ring were synthesized. Their photochromism, fluorescent-switch, and electrochemical properties were investigated. Among these diarylethenes, the one with a formyl group at the ortho position of benzene displayed the largest molar absorption coefficients and fluorescence quantum yield. The cyclization quantum yields of these compounds increased in the order of para < ortho < meta, whereas their cycloreversion quantum yields decreased in the order of meta > para > ortho. Additionally, all of these diarylethenes functioned as effective fluorescent switches in both solution and PMMA films. Cyclic voltammograms proved that the formyl group and its position could effectively modulate the electrochemical behaviors of these diarylethene derivatives.

Introduction

In the past decade, photochromic materials have received much attention because of their applications in potential photoswitchable, molecular devices and optical memory storage systems [1]. Among these materials, the utilization of diarylethene derivatives in molecular electronics, optical memory, and variable-transmission filters has been well documented [1-3]. So far, a huge number of studies concerning the photochromic properties of dithienylethene derivatives have been reported [4-14].

Light is a convenient and powerful trigger to control the reactivity of biomolecules in organisms, exemplified by its use in fluorescent probes, fluorescence imaging, and molecular switches in logic circuits [15-22]. In general, in order to efficiently realize the artificial induction of photosensitivity in biomolecules, the photoactive molecules must possess the following properties: (1) low cytotoxicity, (2) high sensitivity, (3) easy chemical modification. In the past few decades, various types of photochromic molecules, such as fulgides, spiro-

pyranes, azobenzenes, and diarylethenes, have been developed [2,23-31].

Among these compounds, diarylethene is one of the most promising photoswitchable units within the photochromic system, and the successful use of diarylethenes as a fluorescence modulation center to realize a photoswitchable probe for imaging living cells was reported. For example, Zou et al. reported an amphiphilic molecule with hydrophilic and hydrophobic chains on two ends of a rigid diarylethene core. This compound can form stable vesicle nanostructures in aqueous solution, and exhibits excellent switchable fluorescence between open and closed states in the living cells, with low cytotoxicity [32]. Piao et al. developed a multiresponsive fluorescent molecular switch containing terpyridine. This diarylethene can serve as a detector for metal-ion transmembrane transport [33]. Singer et al. explored a novel diarylethene with a 7-deazaadenosine, which led to new research in photochromic nucleosides and molecular recognition properties of nucleic acids with the light sensitivity of diarylethenes [34]. Recently, Wu et al. designed and synthesized a novel diarylethene-containing dithiazolethene, which exhibited a gated photochromic reactivity controlled by complexation/dissociation with BF_3 [35]. All of the above research revealed that the explored novel diarylethenes have versatile applications and are still important and attractive.

Diarylethene derivatives, especially those containing a perfluorocyclopentene bridge are one of the most promising photochromic compounds due to their high fatigue resistance and thermal stability [2,36]. In general, the photochromic reactivity of diarylethenes mainly depends on heteroaryl groups and different electron-donor/acceptor substituents. The formyl group can be modified to form various chemical groups and it can also be connected with different fluorophores via a Schiff base structure. In a previous work, we developed a new class of diarylethenes with a naphthalene group and a thiophene group. The results revealed that these molecules have excellent photochromism with good fatigue resistance and thermal stability [37]. In this study, in order to further elucidate the substituent position effects on the photochromic features of naphthalene-containing diarylethenes, we synthesized three new isomeric diarylethenes with a formyl group at the para, meta, and ortho position on the terminal benzene ring (**1–3**). The photochromic scheme of **1–3** is shown in Scheme 1.

Results and Discussion

The synthesis route for diarylethenes **1o–3o** is shown in Scheme 2. First, the benzaldehydethiophene derivatives **5a–c** were prepared by Suzuki coupling of three bromobenzaldehyde derivatives with a thiopheneboronic acid **4** [38-42]. Second, 1,3-dioxolane-phenylthiophene derivatives **6a–c** were prepared by the reported method [39-41,43]. Then, 1,3-dioxolane-phenylthiophene derivatives **6a–c** were separately lithiated and coupled with (2-methylnaphth-1-yl)perfluorocyclopentene [37] to give the asymmetric diarylethene derivatives **7a–c** [44]. Finally, compounds **1o–3o** were prepared by hydrolyzing compounds **7a–c** in the presence of pyridine and *p*-toluenesulfonic acid in acetone/water. The structures of **1o–3o** were confirmed by elemental analysis, NMR, and IR (Supporting Information File 1).

Photoisomerization of diarylethenes 1–3

Diarylethenes **1**−**3** showed good photochromic properties and could be toggled between their colorless open-ring isomers (**1o**−**3o**) and colored closed-ring isomers (**1c**−**3c**) by alternate irradiation with UV and visible light (λ > 500 nm). As shown in Figure 1A, diarylethene **1o** exhibited a sharp absorption peak at 323 nm (ε, 2.82 × 10^4 L mol^{-1} cm^{-1}) in hexane, which arose from the π→π* transition [45]. Upon irradiation with 297 nm light, the colorless solution of **1o** gradually turned red, and a new absorption band was observed in the visible region centered at 524 nm (ε, 1.40 × 10^4 L mol^{-1} cm^{-1}) due to the formation of the closed-ring isomer **1c**. Alternatively, the red-

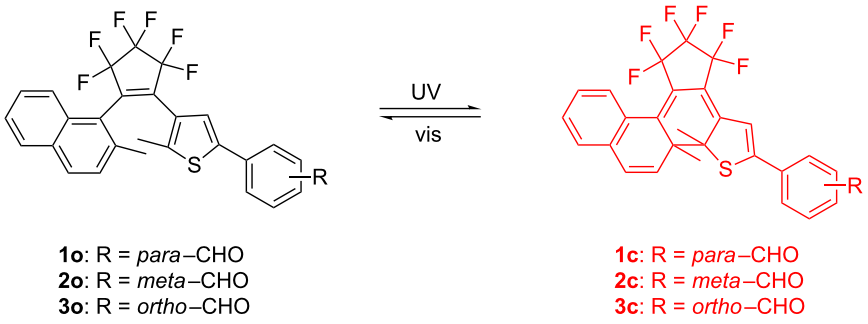

1o: R = *para*–CHO
2o: R = *meta*–CHO
3o: R = *ortho*–CHO

1c: R = *para*–CHO
2c: R = *meta*–CHO
3c: R = *ortho*–CHO

Scheme 1: Photochromism of diarylethenes **1–3**.

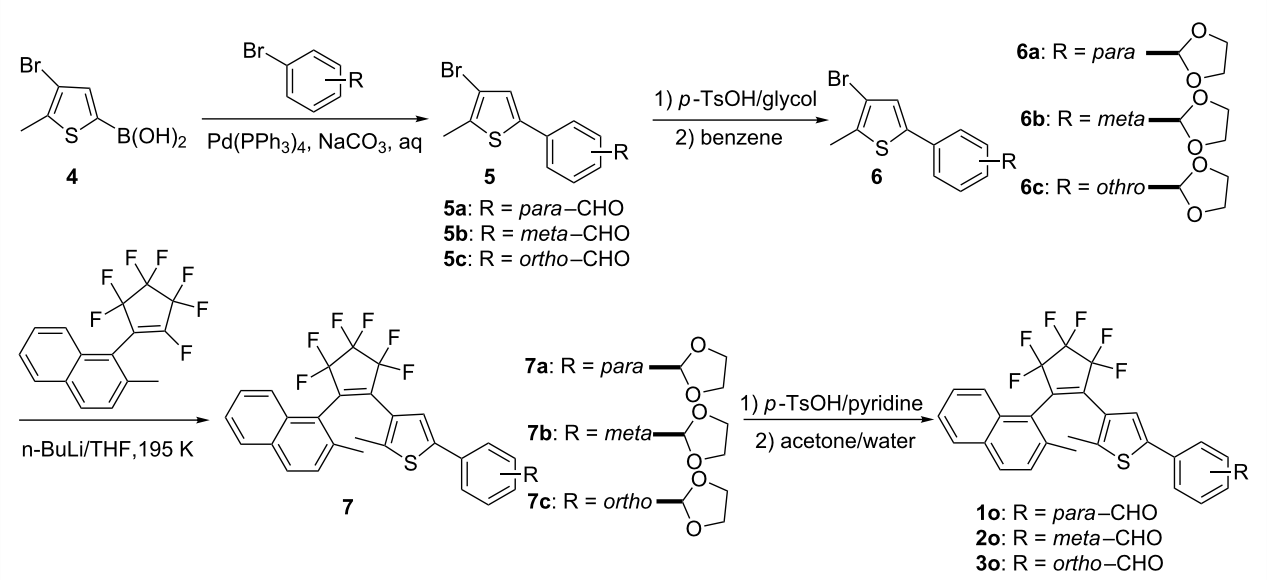

Scheme 2: Synthetic route for diarylethenes **1**–**3**.

colored solution could be bleached to become colorless by re-production of the open-ring isomer **1o** upon irradiation with visible light (λ > 500 nm). In the photostationary state, a clear isosbestic point of diarylethene **1** was observed at 349 nm, which supported the reversible two-component photochromic reaction scheme [46]. Similarly **1o**, compounds **2o** and **3o** also showed good photochromism in hexane (Figure 1B). The colorless solutions of **2o** and **3o** turned pink and magenta due to the formation of the closed-ring isomers **2c** and **3c**, when irradiated with 297 nm light. Their absorption maxima appeared at 512 and 496 nm respectively. The colored solutions of **2c** and **3c** can also be decolorized upon irradiation with visible light (λ > 500 nm), and their isosbestic points were observed at 277 and 268 nm, respectively. The color changes of diarylethenes **1**–**3** by alternating irradiation with UV and visible light (λ > 500 nm) in hexane are shown in Figure 2A.

In PMMA amorphous films, diarylethenes **1**–**3** also showed similar photochromic activity to that in hexane. The absorption maxima of closed-ring isomers of diarylethenes **1c**–**3c** in PMMA films were at longer wavelengths. The values of the absorption maxima of the ring-closed isomers are 14 nm for **1c**, 7 nm for **2c**, and 21 nm for **3c**. The redshift phenomena may be ascribed to a polar effect of the polymer matrix and the stabilization of the molecular arrangement in the solid medium [47,48]. The color changes of diarylethenes **1**–**3** upon alter-

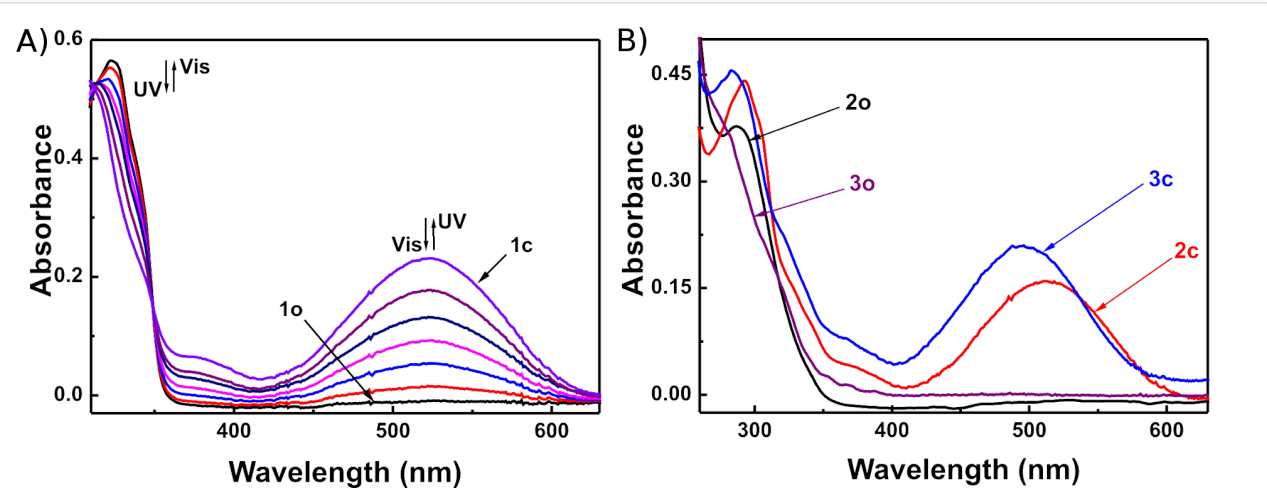

Figure 1: Absorption spectral changes of diarylethenes **1**–**3** by photoirradiation with UV–vis in hexane (2.0×10^{-5} mol/L) at room temperature: (A) **1**; (B) **2** and **3**.

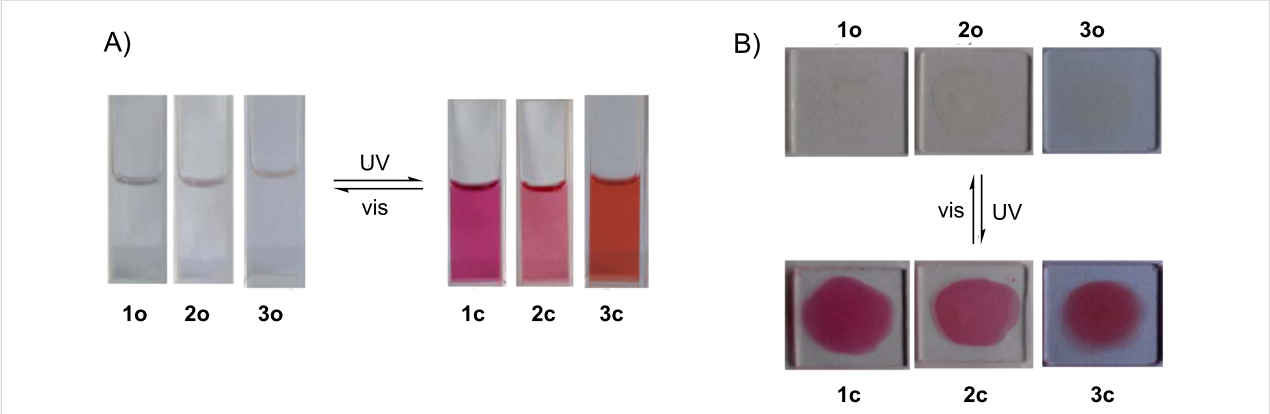

Figure 2: The color changes of diarylethene **1**–**3** by photoirradiation at room temperature: (A) in hexane; (B) in PMMA films.

nating irradiation with UV and visible light in PMMA films are shown in Figure 2B. The photoconversion ratios from open-ring to closed-ring isomers of **1**–**3** were analyzed by HPLC in the photostationary state (Figure 3). It was calculated that their photoconversion ratios in the photostationary state were 82% for **1**, 79% for **2**, and 81% for **3**.

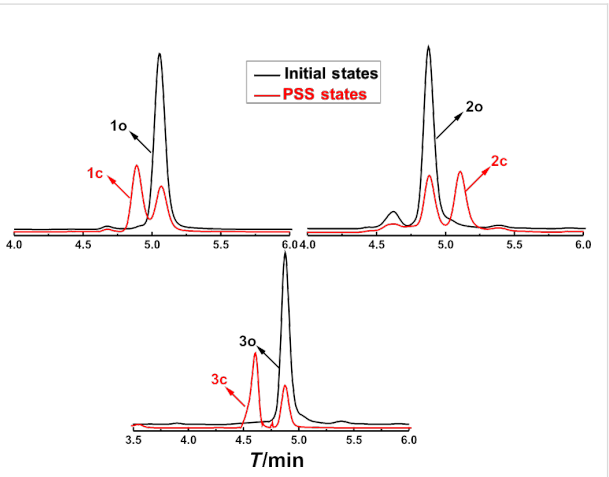

Figure 3: The photoconversion ratios of diarylethenes **1**–**3** in the photostationary state as analyzed by HPLC.

The photochromic features of compounds **1**–**3** are summarized in Table 1. The results indicate that the position of the formyl group at the terminal benzene significantly affects the photochromic properties of these diarylethenes, such as the absorption maxima, molar absorption coefficients, and quantum yields of cyclization and cycloreversion. For the isomeric diarylethenes **1**–**3**, the absorption maxima of both the open-ring and closed-ring isomers exhibited a remarkable hypochromatic shift when the formyl group was moved from the para to the meta, then to the ortho position in both hexane and PMMA films, whereas the molar absorption coefficients of diarylethenes **1**–**3** increased in order of meta < para < ortho substitution by the formyl group in hexane. The results were in agreement with those of the reported diarylethenes containing an electron-withdrawing cyano group [49], but were different from those with an electron-donating methoxy group [14,50,51]. The cycloreversion quantum yields of diarylethenes **1**–**3** increased in the order of ortho ($\Phi_{c\text{-}o}$ = 0.11) < para ($\Phi_{c\text{-}o}$ = 0.12) < meta substitution ($\Phi_{c\text{-}o}$ = 0.15) by the formyl group. However, the cyclization quantum yield of the para-substituted derivative **1** was the largest ($\Phi_{c\text{-}o}$ = 0.35), while that of the meta-substituted derivative **2** was the lowest ($\Phi_{c\text{-}o}$ = 0.21). Compared to the electron-donating methoxy group or electron-withdrawing cyano group [49,50], the position of the electron-

Table 1: Absorption spectral properties of diarylethenes **1**–**3** in hexane (2.0×10^{-5} mol L^{-1}) and in PMMA films (10%, w/w) at room temperature.

compound	$\lambda_{o,max}$/nm[a] (ε/L mol^{-1} cm^{-1})		$\lambda_{c,max}$/nm[b] (ε/L mol^{-1} cm^{-1})		Φ[c]		conversion at PSS in hexane
	hexane	PMMA film	hexane	PMMA film	$\Phi_{o\text{-}c}$	$\Phi_{c\text{-}o}$	
1	323 (2.82×10^4)	326	524 (1.40×10^4)	538	0.35	0.12	82
2	256 (2.75×10^4)	288	512 (1.01×10^4)	519	0.21	0.15	79
3	245 (3.48×10^4)	248	496 (1.57×10^4)	517	0.25	0.11	81

[a]Absorption maxima of ring-open isomers. [b]Absorption maxima of ring-closed isomers. [c]Quantum yields of ring-open ($\Phi_{o\text{-}c}$) and ring-closed isomers ($\Phi_{c\text{-}o}$), respectively.

withdrawing formyl group can effectively modulate the absorption maxima of diarylethenes, which may be a novel strategy for exploring photochromic diarylethenes at shorter wavelengths.

The thermal stabilities of the open-ring and closed-ring isomers of **1**–**3** were tested by storing the compounds at both room temperature in hexane and at 351 K in ethanol. The hexane solutions were kept at room temperature in the dark, and exposed to air for more than two months. No changes in the UV–vis spectra were observed for **1**–**3**. At 351 K, diarylethenes **1**–**3** also showed excellent thermal stability for more than 12 h in ethanol. Fatigue resistance is a critical factor for practical applications in optical devices, and the fatigue resistances of diarylethenes **1**–**3** were examined in both hexane and PMMA films by alternate irradiation with UV and visible light at room temperature [2,52]. As shown in Figure 4, the coloration and decoloration cycle of **1**–**3** can be repeated more than 100 times in hexane with less than 5% degradation of **1c**–**3c**. In PMMA films, **1**–**3** also exhibited excellent photochromic properties after 200 cycles with only ca. 6–10% degradation of **1c**–**3c**. The results showed that all three isomeric diarylethenes **1**–**3** had good fatigue resistance in both hexane and PMMA films.

Fluorescence of diarylethenes 1–3

Fluorescence can be used not only in molecular-scale optoelectronics but also in digital photoswitching [22,53,54]. Like most of reported diarylethenes, diarylethenes **1**–**3** exhibited notable fluorescence in both hexane and PMMA films. Their fluorescence spectra were measured at room temperature with a Hitachi F-4500 spectrophotometer (Figure 5). In hexane, the emission peaks of **1o**–**3o** were observed at 384, 387, and

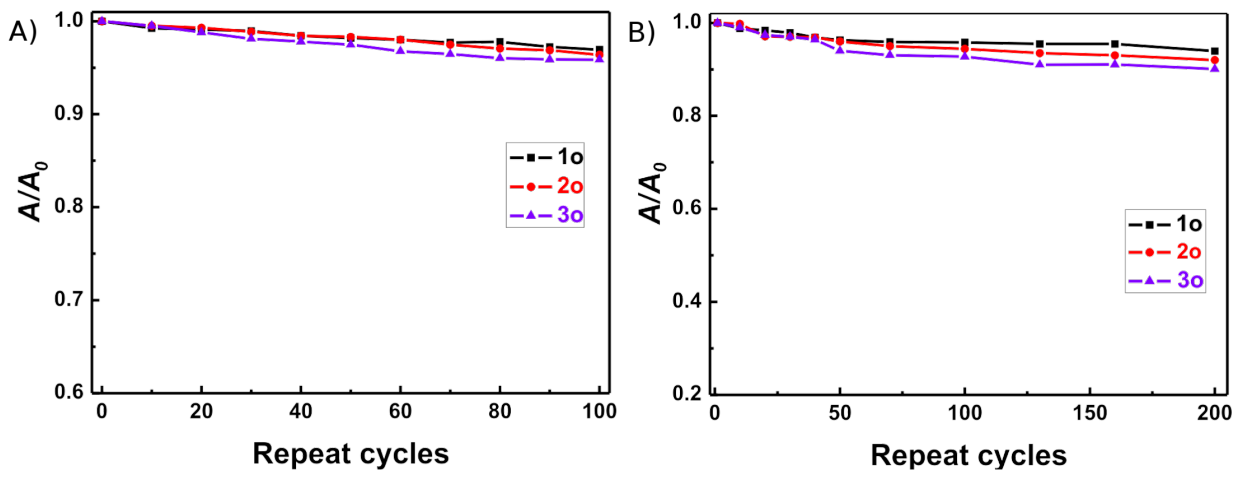

Figure 4: Fatigue resistance of diarylethenes **1**–**3** in hexane in air atmosphere at room temperature: (A) in hexane; (B) in PMMA films. Initial absorbance of the sample was fixed to 1.0.

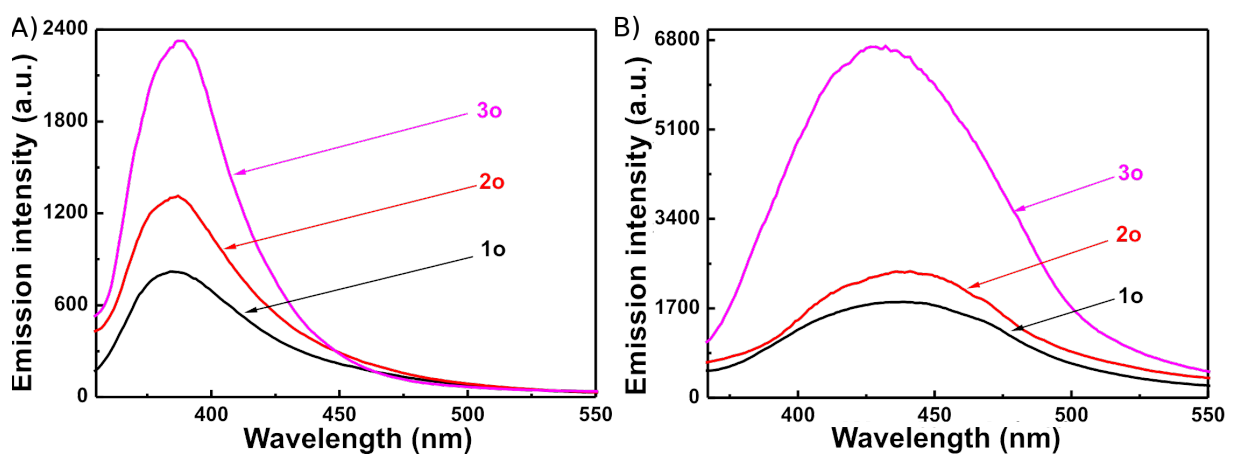

Figure 5: Fluorescence emission spectra of diarylethenes **1–3** at room temperature: (A) in hexane solution (2.0×10^{-5} mol L^{-1}); (B) in PMMA films (10%, w/w).

389 nm, when excited at 307, 315, and 300 nm, whereas those in PMMA films were observed at 438, 441, and 427 nm, when excited at 334, 300, and 300 nm respectively. In comparison with those of **1o**–**3o** in hexane, the fluorescence emission peaks of **1o**–**3o** in PMMA films consistently exhibited a remarkable bathochromic shift. The emission intensity of the ortho-substituted derivative **3o** was the strongest, while that of the para-substituted derivative **1o** was the weakest in both hexane and PMMA films. Compared to the unsubstituted parent diarylethene, 1-(2-methylnaphth-1-yl)-2-[2-methyl-5-phenylthien-3-yl]perfluorocyclopentene (Φ_f = 0.011) [37], the fluorescence emission intensities of diarylethenes **1o** and **2o** were decreased, but that of **3o** was evidently increased. When anthracene was used as the reference, the fluorescence quantum yields of **1o**–**3o** were determined to be 0.012, 0.018, and 0.059, respectively, indicating that the formyl group on the terminal benzene ring could notably enhance the fluorescence quantum yield and remarkably influence the fluorescence emission intensity of diarylethenes with a naphthalene moiety.

Diarylethenes **1**–**3** exhibited an evident fluorescence switching capability upon changing from the open-ring to the closed-ring isomers by photoirradiation in both hexane and PMMA films. When irradiated by UV light, the photocyclization reaction yielded the nonfluorescent closed-ring isomers **1c**–**3c**, resulting in a decrease in emission intensity as compared to the open-ring isomers **1o**–**3o**. The back irradiation by visible light of appropriate wavelength (λ > 500 nm) regenerated the open-ring isomers **1o**–**3o**, and recovered their original emission intensity. As shown in Figure 6, upon irradiation with UV light, the emission intensity of **1** decreased, and was quenched to ca. 59% in hexane and 35% in a PMMA film, when it arrived at the photostationary state. The fluorescent modulation efficiency in the photostationary state was 41% in hexane and 65% in a PMMA film. Similarly, in the photostationary state, the fluorescence modulation efficiencies of diarylethenes **2** and **3** in hexane were 73 and 78%, and those in PMMA films were 38 and 42%, respectively. The residual fluorescence for **1**–**3** in the photostationary state may be attributed to an incomplete cyclization reaction and the existence of parallel conformations [55,56]. Among the three isomeric derivatives, the fluorescent modulation efficiency of diarylethene **2** was the largest and that of **1** was the smallest in PMMA films, suggesting that the diarylethene **2** is the best candidate for the fluorescence photoswitching material.

Electrochemical properties of diarylethenes 1–3

The electrochemical behaviors of diarylethene derivatives have attracted much attention because of their potential applications in molecular-scale electronic switches [57-62]. The electrochemical properties of **1**–**3** were evaluated by cyclic voltammetry (CV) under the same experimental conditions reported previously [13]. The CV curves of diarylethenes **1**–**3** are shown in Figure 7. The onset potentials (E_{onset}) of oxidation and reduction for **1o** were initiated at +1.79 and −0.89 V, and those of **1c** at +1.76 and −0.91 V, respectively. According to the reported method [63,64], the ionization potential and electron affinities of **1o** were calculated to be −6.59 and −4.09 eV, and those of **1c** were −6.56 and −3.89 eV. Based on the highest occupied molecular orbital (HOMO) and lowest unoccupied molecular orbital (LUMO) energy level, the band gap E_g (E_g = LUMO–HOMO) of **1o** and **1c** can be determined to be +2.50 and +2.67 eV. Similarly, the oxidation potential of **2o** and **3o** is initiated at +1.76 and +1.83 V, and that of **2c** and **3c** is initiated at +1.74 and +1.79 V. The results indicate that the oxidation process for the

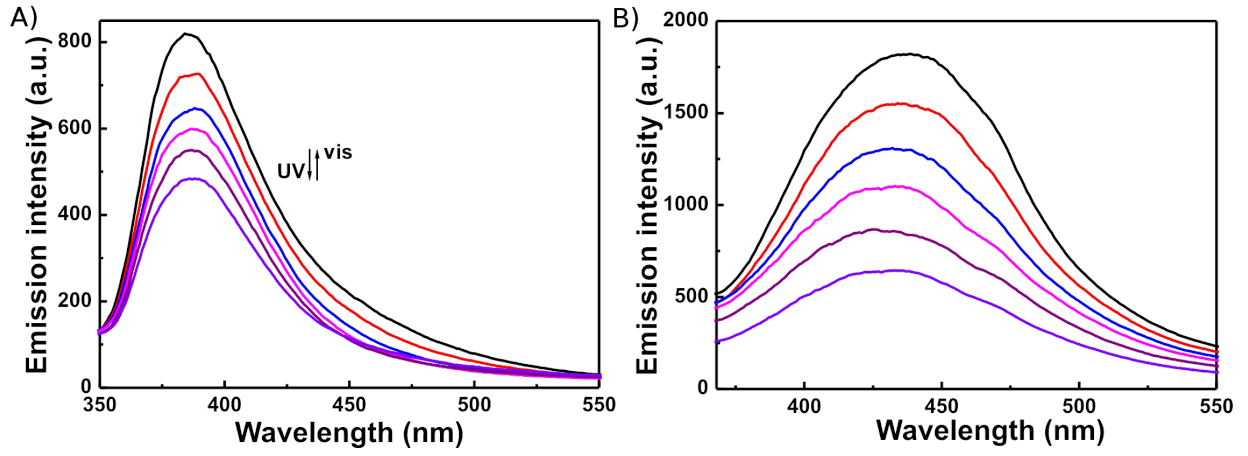

Figure 6: Emission intensity changes of diarylethene **1** upon irradiation with UV light at room temperature: (A) in hexane (excited at 307 nm), (B) in a PMMA film (excited at 324 nm).

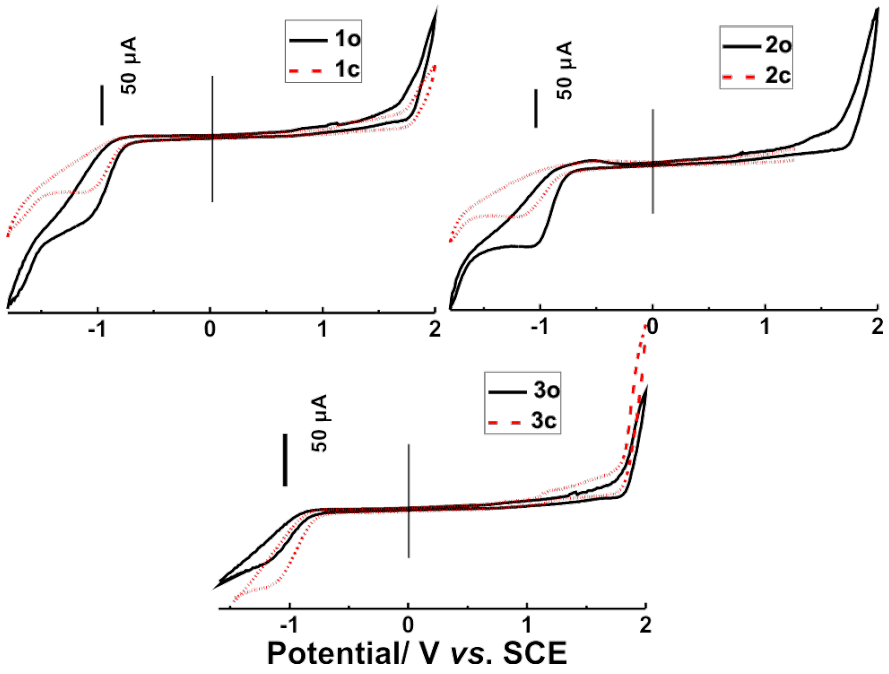

Figure 7: Cyclic voltammetry of diarylethenes **1–3** in acetonitrile with a scanning rate of 50 mV/s.

open-ring isomers **1o–3o** occurs at higher potentials than in the corresponding closed-ring isomers **1c–3c**. This was because the longer conjugation length of the closed-ring isomers generally leads to a less positive potential [62,65]. The cyclization reaction allows the π-conjugation to extend across the perfluorocyclopentene ring causing a lower oxidation onset. As shown in Table 2, for the band gap of diarylethenes **1** and **2**, the values of E_g of the open-ring isomers were lower than those of the closed-ring isomers, with the exception of **3**. Among these compounds, the E_g of **1o** was the smallest, which implies that the charge transfer of **1o** was faster compared to that in others [66]. All these data suggest that the position of the formyl group at the terminal benzene ring has a remarkable effect on the electrochemical behaviors of these diarylethenes, but further work is required to quantify these effects.

Table 2: Electrochemical properties of diarylethenes **1**–**3**.

compound	oxidation		reduction		band gap
	E_{onset} (V)	IP (eV)	E_{onset} (V)	EA (eV)	E_g
1o	+1.79	−6.59	−0.89	−4.09	2.50
1c	+1.76	−6.56	−0.91	−3.89	2.67
2o	+1.76	−6.56	−0.83	−3.97	2.59
2c	+1.74	−6.54	−1.01	−3.79	2.75
3o	+1.83	−6.63	−0.87	−3.93	2.70
3c	+1.79	−6.59	−0.80	−4.00	2.59

Conclusion

Three new asymmetric isomeric diarylethenes containing a formyl group at either the para, meta, or ortho position of the terminal benzene ring were synthesized for the investigation of the effect of substituent position on their optical and electrochemical properties. The results revealed that the formyl group and its position had significant effects on the properties of these isomeric diarylethenes. The electron-withdrawing formyl group endowed these diarylethenes with some new properties, which were different from those of diarylethenes with a methoxy group or halide at the terminal benzene.

Supporting Information

Supporting Information File 1

Experimental procedures and spectral data.
[http://www.beilstein-journals.org/bjoc/content/supplementary/1860-5397-8-114-S1.pdf]

Acknowledgements

This work was supported by the National Natural Science Foundation of China (20962008, 21162011), the Project of Jiangxi Academic and Technological Leader (2009DD00100), the Project of Jiangxi Youth Scientist, and the Project of the Science Funds of Jiangxi Education Office (GJJ10241, GJJ09646).

References

1. Feringa, B. L., Ed. *Molecular Switches;* Wiley-VCH: Weinheim, Germany, 2001. doi:10.1002/3527600329.fmatter_indsub
2. Irie, M. *Chem. Rev.* **2000,** *100,* 1685–1716. doi:10.1021/cr980069d
3. Irie, M. *Diarylethenes with Heterocyclic Aryl Groups*. In *Organic Photochromic and Thermochromic Compounds: Physicochemical Studies, Biological Applications, and Thermochromism;* Crano, J. C.; Guglielmetti, R. J., Eds.; Plenum Press: New York, 1999; Vol. 1, pp 207–222.
4. Luo, Q.; Cheng, H.; Tian, H. *Polym. Chem.* **2011,** *2,* 2435–2443. doi:10.1039/c1py00167a
5. Norsten, T. B.; Branda, N. R. *J. Am. Chem. Soc.* **2001,** *123,* 1784–1785. doi:10.1021/ja005639h
6. Giordano, L.; Jovin, T. M.; Irie, M.; Jares-Erijman, E. A. *J. Am. Chem. Soc.* **2002,** *124,* 7481–7489. doi:10.1021/ja016969k
7. Liddell, P. A.; Kodis, G.; Moore, A. L.; Moore, T. A.; Gust, D. *J. Am. Chem. Soc.* **2002,** *124,* 7668–7669. doi:10.1021/ja026327c
8. Yamaguchi, T.; Irie, M. *J. Org. Chem.* **2005,** *70,* 10323–10328. doi:10.1021/jo051372z
9. Tsivgoulis, G. M.; Lehn, J.-M. *Chem.–Eur. J.* **1996,** *2,* 1399–1406. doi:10.1002/chem.19960021112
10. Pu, S.; Yang, T.; Xu, J.; Chen, B. *Tetrahedron Lett.* **2006,** *47,* 6473–6477. doi:10.1016/j.tetlet.2006.06.073
11. Fan, C.; Pu, S.; Liu, G.; Yang, T. *J. Photochem. Photobiol., A: Chem.* **2008,** *194,* 333–343. doi:10.1016/j.jphotochem.2007.08.032
12. Pu, S.; Yan, L.; Wen, Z.; Liu, G.; Shen, L. *J. Photochem. Photobiol., A: Chem.* **2008,** *196,* 84–93. doi:10.1016/j.jphotochem.2007.11.016
13. Pu, S.; Zheng, C.; Le, Z.; Liu, G.; Fan, C. *Tetrahedron* **2008,** *64,* 2576–2585. doi:10.1016/j.tet.2008.01.025
14. Pu, S.; Fan, C.; Miao, W.; Liu, G. *Dyes Pigm.* **2010,** *84,* 25–35. doi:10.1016/j.dyepig.2009.06.018
15. Goeldner, M.; Givens, R., Eds. *Dynamic Studies in Biology: Phototriggers, Photoswitches and Caged Biomolecules;* Wiley-VCH: Weinheim, Germany, 2005.
16. Gorostiza, P.; Isacoff, E. Y. *Science* **2008,** *322,* 395–399. doi:10.1126/science.1166022
17. Zou, Q.; Li, X.; Zhang, J.; Zhou, J.; Sun, B.; Tian, H. *Chem. Commun.* **2012,** *48,* 2095–2097. doi:10.1039/c2cc16942h
18. Finley, K. R.; Davidson, A. E.; Ekker, S. C. *BioTechniques* **2001,** *31,* 66–72. http://www.biotechniques.com/multimedia/archive/00011/01311st02_11391a.pdf
19. Zheng, Q.; Xu, G.; Prasad, P. N. *Chem.–Eur. J.* **2008,** *14,* 5812–5819. doi:10.1002/chem.200800309
20. Mottram, L. F.; Maddox, E.; Schwab, M.; Beaufils, F.; Peterson, B. R. *Org. Lett.* **2007,** *9,* 3741–3744. doi:10.1021/ol7015093
21. Miller, E. W.; Bian, S. X.; Chang, C. J. *J. Am. Chem. Soc.* **2007,** *129,* 3458–3459. doi:10.1021/ja0668973
22. Tian, H.; Feng, Y. *J. Mater. Chem.* **2008,** *18,* 1617–1622. doi:10.1039/B713216F
23. Willner, I.; Rubin, S.; Wonner, J.; Effenberger, F.; Baeuerle, P. *J. Am. Chem. Soc.* **1992,** *114,* 3150–3151. doi:10.1021/ja00034a078
24. Lion-Dagan, M.; Willner, I. *J. Photochem. Photobiol., A: Chem.* **1997,** *108,* 247–252. doi:10.1016/S1010-6030(97)00083-X
25. Sakata, T.; Yan, Y.; Marriott, G. *Proc. Natl. Acad. Sci. U. S. A.* **2005,** *102,* 4759–4764. doi:10.1073/pnas.0405265102
26. Weston, D. G.; Kirkham, J.; Cullen, D. C. *Biochim. Biophys. Acta* **1999,** *1428,* 463–467. doi:10.1016/S0304-4165(99)00099-9
27. Renner, C.; Moroder, L. *ChemBioChem* **2006,** *7,* 868–878. doi:10.1002/cbic.200500531
28. Volgraf, M.; Gorostiza, P.; Numano, R.; Kramer, R. H.; Isacoff, E. Y.; Trauner, D. *Nat. Chem. Biol.* **2005,** *2,* 47–52. doi:10.1038/nchembio756
29. Willner, I.; Rubin, S.; Riklin, A. *J. Am. Chem. Soc.* **1991,** *113,* 3321–3325. doi:10.1021/ja00009a016
30. Woolley, G. A. *Chem. Res.* **2005,** *38,* 486–493. doi:10.1021/ar040091v
31. Zhang, F.; Zarrine-Afsar, A.; Al-Abdul-Wahid, M. S.; Prosser, R. S.; Davidson, A. R.; Woolley, G. A. *J. Am. Chem. Soc.* **2009,** *131,* 2283–2289. doi:10.1021/ja807938v
32. Zou, Y.; Yi, T.; Xiao, S.; Li, F.; Li, C.; Gao, X.; Wu, J.; Yu, M.; Huang, C. *J. Am. Chem. Soc.* **2008,** *130,* 15750–15751. doi:10.1021/ja8043163
33. Piao, X.; Zou, Y.; Wu, J.; Li, C.; Yi, T. *Org. Lett.* **2009,** *11,* 3818–3821. doi:10.1021/ol9014267
34. Singer, M.; Jäschke, A. *J. Am. Chem. Soc.* **2010,** *132,* 8372–8377. doi:10.1021/ja1024782
35. Wu, Y.; Chen, S.; Yang, Y.; Zhang, Q.; Xie, Y.; Tian, H.; Zhu, W. *Chem. Commun.* **2012,** *48,* 528–530. doi:10.1039/c1cc15824d
36. Tian, H.; Yang, S. *Chem. Soc. Rev.* **2004,** *33,* 85–97. doi:10.1039/B302356G
37. Wang, R.; Pu, S.; Liu, G.; Liu, W.; Xia, H. *Tetrahedron Lett.* **2011,** *52,* 3306–3310. doi:10.1016/j.tetlet.2011.04.063
38. Li, Z.-X.; Liao, L.-Y.; Sun, W.; Xu, C.-H.; Zhang, C.; Fang, C.-J.; Yan, C.-H. *J. Phys. Chem. C* **2008,** *112,* 5190–5196. doi:10.1021/jp711613y
39. Yamamoto, S.; Matsuda, K.; Irie, M. *Org. Lett.* **2003,** *5,* 1769–1772. doi:10.1021/ol034440h
40. Yamamoto, S.; Matsuda, K.; Irie, M. *Angew. Chem., Int. Ed.* **2003,** *42,* 1636–1639. doi:10.1002/anie.200250417
41. Yamamoto, S.; Matsuda, K.; Irie, M. *Chem.–Eur. J.* **2003,** *9,* 4878–4886. doi:10.1002/chem.200304947
42. Kuroki, L.; Takami, S.; Shibata, K.; Irie, M. *Chem. Commun.* **2005,** 6005–6007. doi:10.1039/B512873K
43. Pu, S.; Li, M.; Liu, G.; Le, Z. *Aust. J. Chem.* **2009,** *62,* 464–474. http://www.publish.csiro.au/paper/CH08289
44. Wang, R. J.; Li, W. B.; Liu, W. J.; Liu, G. *Adv. Mater. Res.* **2012,** *393–395,* 381–384. doi:10.4028/www.scientific.net/AMR.393-395.381
45. Liu, G.; Pu, S.; Wang, X. *J. Photochem. Photobiol., A: Chem.* **2010,** *214,* 230–240. doi:10.1016/j.jphotochem.2010.07.001
46. Kawai, S.; Nakashima, T.; Atsumi, K.; Sakai, T.; Harigai, M.; Imamoto, Y.; Kamikubo, H.; Kataoka, M.; Kawai, T. *Chem. Mater.* **2007,** *19,* 3479–3483. doi:10.1021/cm0630340
47. Pu, S.; Li, H.; Liu, G.; Liu, W.; Cui, S.; Fan, C. *Tetrahedron* **2011,** *67,* 1438–1447. doi:10.1016/j.tet.2010.12.041
48. Liu, G.; Pu, S.; Wang, X. *Tetrahedron* **2010,** *66,* 8862–8871. doi:10.1016/j.tet.2010.09.066
49. Pu, S.; Liu, W.; Liu, G. *Dyes Pigm.* **2010,** *87,* 1–9. doi:10.1016/j.dyepig.2010.01.015
50. Pu, S.; Liu, W.; Miao, W. *J. Phys. Org. Chem.* **2009,** *22,* 954–963. doi:10.1002/poc.1545
51. Liu, G.; Pu, S.; Wang, X.; Liu, W.; Fan, C. *Dyes Pigm.* **2011,** *90,* 89–99. doi:10.1016/j.dyepig.2010.12.007
52. Tian, H.; Wang, S. *Chem. Commun.* **2007,** 781–792. doi:10.1039/B610004J
53. Fukaminato, T.; Sasaki, T.; Kawai, T.; Tamai, N.; Irie, M. *J. Am. Chem. Soc.* **2004,** *126,* 14843–14849. doi:10.1021/ja047169n
54. Zhang, J.; Tan, W.; Meng, X.; Tian, H. *J. Mater. Chem.* **2009,** *19,* 5726–5729. doi:10.1039/B908707A

55. Fan, C.; Pu, S.; Liu, G.; Yang, T. *J. Photochem. Photobiol., A: Chem.* **2008,** *197,* 415–425. doi:10.1016/j.jphotochem.2008.02.004
56. Pu, S.; Fan, C.; Miao, W.; Liu, G. *Tetrahedron* **2008,** *64,* 9464–9470. doi:10.1016/j.tet.2008.07.073
57. Bonifazi, D.; Scholl, M.; Song, F.; Echegoyen, L.; Accorsi, G.; Armaroli, N.; Diederich, F. *Angew. Chem., Int. Ed.* **2003,** *42,* 4966–4970. doi:10.1002/anie.200352265
58. Browne, W. R.; de Jong, J. J. D.; Kudernac, T.; Walko, M.; Lucas, L. N.; Uchida, K.; van Esch, J. H.; Feringa, B. L. *Chem.–Eur. J.* **2005,** *11,* 6414–6429. doi:10.1002/chem.200500162
59. Browne, W. R.; de Jong, J. J. D.; Kudernac, T.; Walko, M.; Lucas, L. N.; Uchida, K.; van Esch, J. H.; Feringa, B. L. *Chem.–Eur. J.* **2005,** *11,* 6430–6441. doi:10.1002/chem.200500163
60. Moriyama, Y.; Matsuda, K.; Tanifuji, N.; Irie, S.; Irie, M. *Org. Lett.* **2005,** *7,* 3315–3318. doi:10.1021/ol051149o
61. Zheng, C.; Pu, S.; Xu, J.; Luo, M.; Huang, D.; Shen, L. *Tetrahedron* **2007,** *63,* 5437–5449. doi:10.1016/j.tet.2007.04.049
62. Pu, S.; Yang, T.; Xu, J.; Shen, L.; Li, G.; Xiao, Q.; Chen, B. *Tetrahedron* **2005,** *61,* 6623–6629. doi:10.1016/j.tet.2005.04.044
63. Tsai, F.-C.; Chang, C.-C.; Liu, C.-L.; Chen, W.-C.; Jenekhe, S. A. *Macromolecules* **2005,** *38,* 1958–1966. doi:10.1021/ma048112o
64. Zhan, X.; Liu, Y.; Wu, X.; Wang, S.; Zhu, D. *Macromolecules* **2002,** *35,* 2529–2537. doi:10.1021/ma011593g
65. Perrier, A.; Maurel, F.; Aubard, J. *J. Photochem. Photobiol., A: Chem.* **2007,** *189,* 167–176. doi:10.1016/j.jphotochem.2007.01.030
66. Kim, E.; Kim, M.; Kim, K. *Tetrahedron* **2006,** *62,* 6814–6821. doi:10.1016/j.tet.2006.04.089

License and Terms

Beilstein Journal of Organic Chemistry

Control over molecular motion using the *cis–trans* photoisomerization of the azo group

Estíbaliz Merino*[1] and María Ribagorda[2]

Review

Open Access

Address:
[1]Instituto de Química Orgánica General, Centro Superior de Investigaciones Científicas (CSIC), C/ Juan de la Cierva, 3, 28006, Madrid, Spain and [2]Departmento de Química Orgánica, Facultad de Ciencias, Universidad Autónoma de Madrid, 28049, Madrid, Spain

Email:
Estíbaliz Merino* - estibaliz.merino@iqog.csic.es;
María Ribagorda - maria.ribagorda@uam.es

* Corresponding author

Keywords:
azobenzenes; molecular switches; nanomachines; photoisomerization

Beilstein J. Org. Chem. **2012,** *8,* 1071–1090.
doi:10.3762/bjoc.8.119

Received: 16 March 2012
Accepted: 21 June 2012
Published: 12 July 2012

This article is part of the Thematic Series "Molecular switches and cages".

Guest Editor: D. Trauner

Abstract

Control over molecular motion represents an important objective in modern chemistry. Aromatic azobenzenes are excellent candidates as molecular switches since they can exist in two forms, namely the *cis* (*Z*) and *trans* (*E*) isomers, which can interconvert both photochemically and thermally. This transformation induces a molecular movement and a significant geometric change, therefore the azobenzene unit is an excellent candidate to build dynamic molecular devices. We describe selected examples of systems containing an azobenzene moiety and their motions and geometrical changes caused by external stimuli.

Review

This review is based on an article published in 2009 in *Anales de Química* (Real Sociedad Española de Química) [1]. Azobenzene was described for the first time in 1834 [2] and one century later, in 1937, G. S. Hartley published a study of the influence of light on the configuration of N=N double bonds [3]. The exposure of a solution of azobenzene in acetone to light allowed the discovery of the *cis* isomer. This finding was the starting point of the development of one of the best organic molecular switches described so far. The azobenzenes are organic molecules that present two aromatic rings linked by an azo group (N=N). They have properties that have led to some applications of great importance, mainly for the chemical industry. The azobenzenes are highly coloured compounds and belong to the group of so-called dyes FD&C (food, drug and cosmetics). Nowadays, azobenzene dyes represent approximately 60% of the world production of industrial dyes [4-6].

In recent years, the photochromic properties of azobenzenes have attracted great interest due to the isomerization of the N=N double bonds that occurs readily in the presence of a light source [7-9].

Like a C=C double bond, the azobenzenes have two geometric isomers (*Z*/*E*) around the N=N double bond, the *trans* isomer

(*E*) is ~12 kcal·mol^{-1} more stable than the *cis* isomer (*Z*) [10]. The energy barrier of the photoexcited state is ~23 kcal·mol^{-1}, such that the *trans* isomer is predominant in the dark at room temperature [11].

The *trans*-azobenzene easily isomerizes to the *cis* isomer by irradiation of the *trans* isomer with a wavelength between 320–350 nm. The reaction is reversible and the *trans* isomer is recovered when the *cis* isomer is irradiated with light of 400–450 nm, or heated. For many azobenzenes, the two photochemical conversions occur on the scale of picoseconds, while the thermal relaxation of the *cis* isomer to the *trans* isomer is much slower (milliseconds to days). The photoinduced isomerization of the azobenzenes leads to a remarkable change in their physical properties, such as molecular geometry, dipole moment or absorption spectrum [12-16].

The isomerization process involves a decrease in the distance between the two carbon atoms in position 4 of the aromatic rings of azobenzene, from 9.0 Å in the *trans* form to 5.5 Å in the *cis* form (Figure 1) [17]. The *trans*-azobenzene is almost flat and has no dipole moment, whereas the *cis* isomer presents an angular geometry and a dipole moment of 3.0 D. One of the rings rotates to avoid steric repulsions due to facing of one of the π clouds of one aromatic ring to the other [9]. The arrangement of the aromatic rings is also reflected in the proton nuclear magnetic resonance spectrum (^{1}H NMR). The signals of the *cis* isomer appear at higher field than the signals corresponding to the *trans* isomer, due to the anisotropic effect of the π cloud of the aromatic ring.

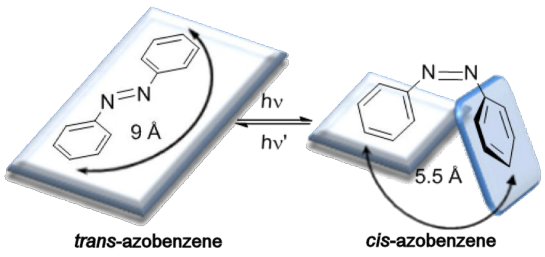

Figure 1: Photoisomerization process of azobenzene.

The UV–vis absorption spectrum of azobenzene presents two characteristic absorption bands corresponding to π→π* and n→π* electronic transitions. The transition π→π* is usually in the near UV region and is common to carbonate systems, such as stilbene [18]. The electronic transition n→π* is usually located in the visible region and is due to the presence of unshared electron pairs of nitrogen atoms [19]. Due to this second electronic transition, the dynamic photoisomerization process of azobenzenes is different to the carbonate compounds [20]. Azobenzene undergoes *trans–cis* isomerization by $S_1 \leftarrow S_0$ and $S_2 \leftarrow S_0$ excitations and *cis–trans* isomerization by exciting into the S_1 or S_2 state [21]. The sum of the quantum yields is different to unity, which indicates multiple pathways for isomerization. In stilbene, the isomerization occurs exclusively by rotation and the quantum yield equals unity [22].

The aromatic azocompounds are classified in three types based on the order of their energetic electronic states π→π* and n→π* [11]. This order depends on the electronic nature of the aromatic rings of azobenzene. Each type of azobenzene also has a predominant colour defined by the wavelength of the maximum absorption band (λ_{max}) (indicated in brackets in each case):

1. Azobenzene type: The π→π* band is very intense in the UV region and there is one n→π* weaker in the visible (yellow colour). The electronic nature of the aromatic rings is very similar to simple azobenzene (Ph–N=N–Ph).
2. Aminoazobenzene type (*o*- or *p*-(X)–C_6H_4–N=N–Ar): The π→π* and n→π* bands are very close or collapsing in the UV–vis region. In this case, the azocompounds have electron-donor substituents (X) in the *ortho* or *para* positions (orange colour).
3. Pseudo-stilbene type [(X)–C_6H_4–N=N–C_6H_4–(Y)]: The absorption band corresponding with π→π* transition is shifted to red, changing the appearance order with respect to the band n→π*. The azocompounds of this type present donor substituents (X) and electron acceptors (Y) at the 4 and 4' positions, respectively (push/pull system) (red colour).

The isomerization process normally involves a colour change to more intense colours. The absorption spectra of both isomers differ mainly in the following aspects (Figure 2) [23]:

Trans isomer: The absorption band π→π* is very intense, with a molar extinction coefficient (ε) ~ 2–3 × 10^4 M^{-1}·cm^{-1}. The second band (n→π*) is much weaker (ε ~ 400 M^{-1}·cm^{-1}) as this transition is not allowed in the *trans* isomer by the symmetry rules.

Cis isomer: The absorption band π→π* is shifted to shorter wavelengths (hypsochromic effect) decreasing significantly in intensity (ε ~ 7–10 × 10^3 M^{-1}·cm^{-1}). The electronic transition n→π* (380–520 nm) is allowed in the *cis* isomer, resulting in

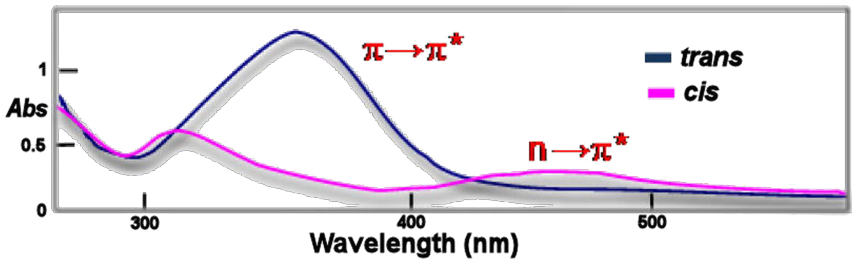

Figure 2: Representative example of an UV spectrum of an azocompound of the azobenzene type (blue line: *trans* isomer; magenta line: *cis* isomer).

an increase in the intensity (ε ~ 1500 $M^{-1}·cm^{-1}$) with respect to the *trans* isomer.

These differences allow carrying out a photochemical interconversion by irradiation with light of a certain wavelength, obtaining different proportions of the *cis* and *trans* photostationary states. The excitation caused by the wavelength is dependent on the nature of the substituents of the aryl groups. In most cases, *trans*→*cis* isomerization is promoted by irradiation with wavelengths between 320–380 nm, while exposures to λ ~ 400–450 nm favor the *cis*→*trans* photoreversion. The mechanism is not well established. Several mechanistic studies have been performed on the isomerization reversal route *cis*→*trans* of azobenzene to investigate the effect of the substituents on the benzene rings as well as the influence of several parameters [24-27]. The available data suggest that the isomerization of azocompounds can proceed through the reversal of one of the N–C bonds or by the rotation of the N=N double bond. The nonbonding electron pair of each nitrogen atom may lead to one n→π* electronic transition (S_0→S_1) with inversion at the nitrogen atom (inversion mechanism) [28,29]. On the other hand, the isomerization can also occur through a rotation mechanism [11,30], which involves a π→π* transition (S_0→S_2) (Figure 3). This mechanism is similar to that produced in the isomerization of stilbene [23].

Azobenzenes as molecular switches

A molecular switch is a molecular system that allows mechanical movements to be carried out when the system is subjected to an external stimulus, such as light, resulting in conformational and environmental changes of the switch.

The basis of a molecular switch is the reversible transformation of chemical species caused by light between two states of a molecule with different absorption spectra.

These photoisomerization processes modify the absorption spectra and can produce variations in different physicochemical properties of molecules, such as ion complexation, refractive index, electrochemical behaviour, and very significant conformational changes in polymers. There may also be variations in the organization of large assemblies of molecules in gels or liquid crystals. When polarized light is used, the photoisomeri-

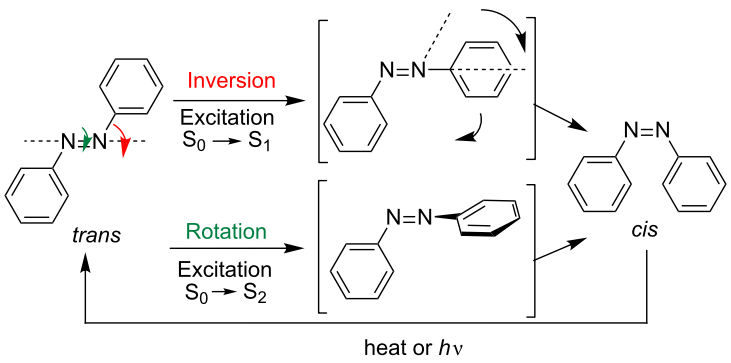

Figure 3: Mechanistic proposals for the isomerization of azobenzenes.

zation often induces a reorganization of chromophores that can be reflected in the circular dichroism spectra.

The basic condition for a molecule to behave as a switch is the existence of two different and stable isomeric forms that interconvert when an external stimulus is applied to it.

The most important requirements for a molecule to behave as a molecular switch are the following [31-35]:

1. The transformation between the two interconvertible structures that comprise the molecular switch must be produced easily and selectively by irradiation with light of a certain wavelength.
2. The thermal interconversion between two isomers should not occur in a wide temperature range, thus allowing the storage of information for an almost infinite length of time.
3. The isomers should have an appreciable resistance to fatigue (number of cycles without decomposition), with the possibility to carry out the cycle of write/erase several times, and should not cause thermal degradation or photochemical side-products.
4. The two structural forms should be easily detectable.
5. An efficient interrupt process. High quantum yields have to be achieved by using short irradiation periods.
6. The response times have to be quick to be also fast interrupting cycles.
7. It is necessary that all properties remain unchanged when the compound used as the photoswitch is a part of a macromolecular structure.

A variety of photosensitive devices, such as smart polymers [36,37], liquid crystals [38,39], intelligent enzymes [40], and various switches and molecular machines [41-48], have been developed by using the photochromic properties of azobenzene and benefiting from its easy synthesis [4,6,49-54]. The molecular motion that occurs in the photoisomerization has allowed the development of azo-structures that have grown in complexity, originality and usefulness [55-58]. This review includes some of the most outstanding examples.

Photoisomerization of azobenzenes: A simple molecular motion

The introduction of an azobenzene fragment in a molecule with biological activity [59-63], such as a protein, can allow the spatial and temporal control of a variety of biological processes through illumination, by means of the direct regulation of enzymatic activity [64-67], peptides, proteins, nucleic acids [68-76], receptors [77-82], or ion channels [83-85], or by modulation of the concentration of several labelled molecules. This strategy is very attractive because it allows control over the conformation and consequently the activity of biomolecules in a reversible way without the addition of any reagent. Structural effects caused by the isomerization can be amplified in the host or initiate a cascade of photophysical and photochemical secondary responses. The first application of an azobenzene in biology was published in the late 1960s and was used to photoregulate the activity of chymotrypsin, a digestive enzyme [86]. Later, a similar strategy was applied in functional and structural studies of the acetylcholine receptor of nicotinic type [87]. The *trans*→*cis* photoisomerization of 4,4'-trimethylammonium methyl substituted azobenzene produced an increase in the concentration of acetylcholine agonists as a result of the specific interaction of both isomers with the acetylcholine receptor that is present in excitable membranes. In this way, it is possible to control the permeability changes, allowing the ion motion during the generation of the bioelectric impulse.

The isomerization of azocompounds has been used as a synthetic tool to control the opening and closing of pores in cellular membranes, essential for the transport of ions. An illustrative example is described by Trauner, Kramer and co-workers to control the K^+ channels in neuronal cells (Figure 4) [88].

The azobenzene **1** is a terminal quaternary ammonium salt, thus when **1** adopts the *trans* configuration, the flow of K^+ ions is blocked. After irradiation with λ = 380 nm, the *cis* isomer brings the aromatic rings closer, shortening its length, and hence the channel blocking is inefficient, allowing the passage of ions. The development of systems capable of photoregulating the activity of ion channels is extremely important in neurobiology. Recently, a maleimide, azobenzene and glutamate derivative (MAG) was used as a photochromic agonist of an ionotropic glutamate receptor (iGluR) (Figure 5a) [89-91]. The chromophore consists of a terminal maleimide unit, which is associated covalently to the protein via a cysteine residue, a central azobenzene unit and a glutamate head. Only the *cis* form of the azobenzene allows the approach of the fragment and the interaction of glutamate with the active site of the protein. When this interaction occurs, the protein folds as a clamshell, triggering the opening of the ion channel (Figure 5b).

Another recent example was described by Woolley et al. [92,93]. They introduced an azobenzene moiety in a polypeptide to control the α-helical conformation and to have a synthetic tool that allows photomodulation of the very important conformation–interaction relationship in biological recognition. Peptides with pairs of cysteine residues were intramolecularly cross-linked with thiol reactive azobenzene-based photoswitches. Photoisomerization of the azobenzene changes the conformation of the peptide depending on the location of the

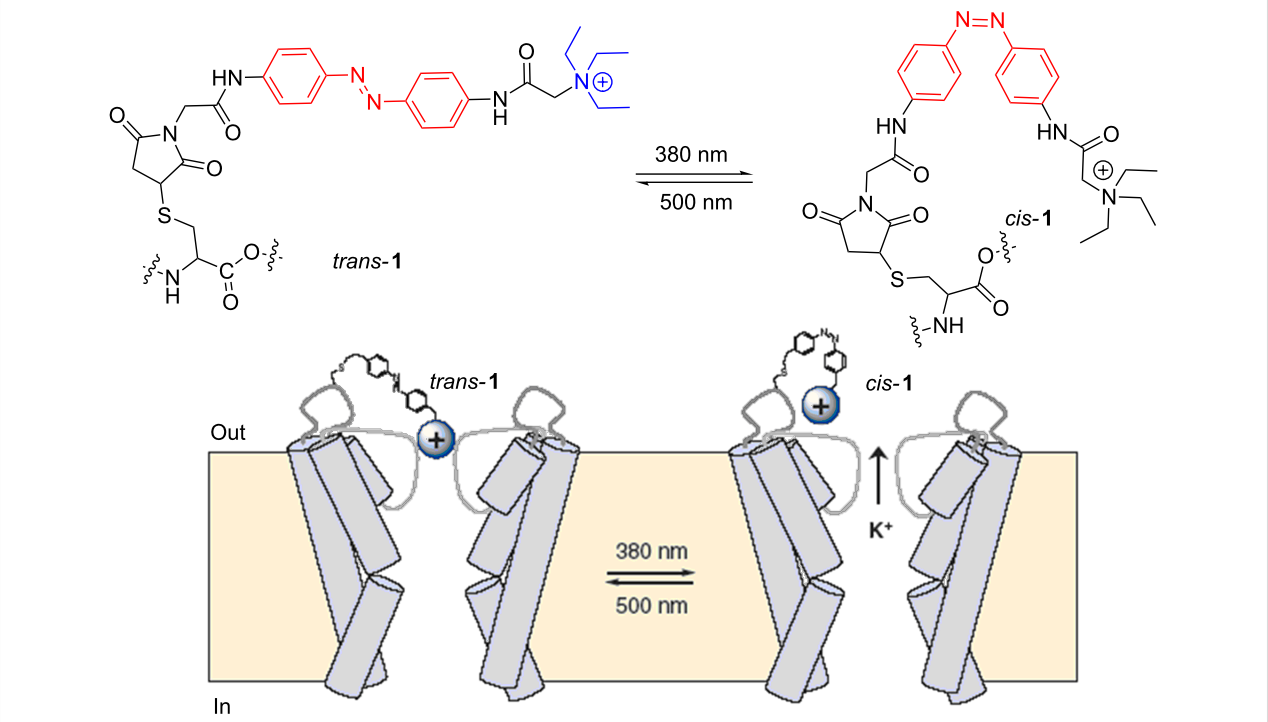

Figure 4: Representation of the photocontrol of a K^+ channel in the cellular membrane based on the isomerization of azocompound **1**. Reprinted (adapted) with permission from Macmillan Publishers Ltd: *Nat. Neurosci.* **2004**, *7*, 1381–1386, copyright (2004).

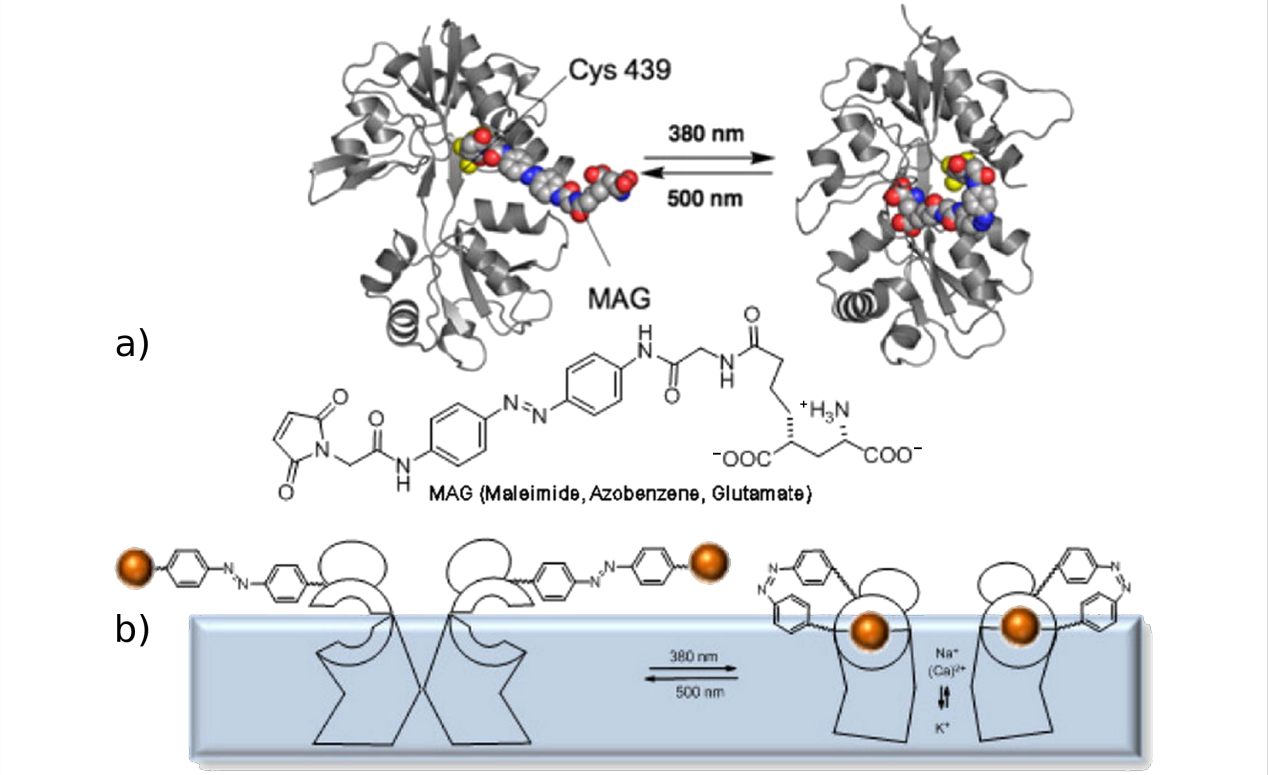

Figure 5: (a) MAG interaction with iGluR; (b) photocontrol of the opening of the ion channel by *trans*–*cis* isomerization of azobenzene. Reprinted with permission from Macmillan Publishers Ltd: *Nat. Chem. Biol.* **2006**, *2*, 47–52, copyright (2006).

cysteine. When the azo group of polypeptide **2** is in its *trans* form, it retains its affinity for DNA and its α-helical conformation. The photoisomerization leads to the *cis* isomer, which disrupts this helicity inhibiting the association with DNA. The photoreversion to the *trans* isomer recovers again the final conformation of the α-helix of DNA. In 2011, the same group carried out the attachment of a fluorescent dye close to the photoswitch giving rise to a fluorescence change upon isomerization. The introduction of azobenzene-modified biomolecules in zebrafish proved that the photochemistry of azobenzenes was similar in vivo and in vitro, and that appropriate azobenzenes could be stable in vivo for days (Figure 6) [94].

The photochromic properties of azobenzenes also find applications in "host–guest" recognition [95,96]. For example, the bis-azo compound **3** behaves as an excellent receptor of guanidinium ions by hydrogen-bonding interactions. The recognition is very effective when the azobenzene adopts the *cis* configuration (Figure 7) [95].

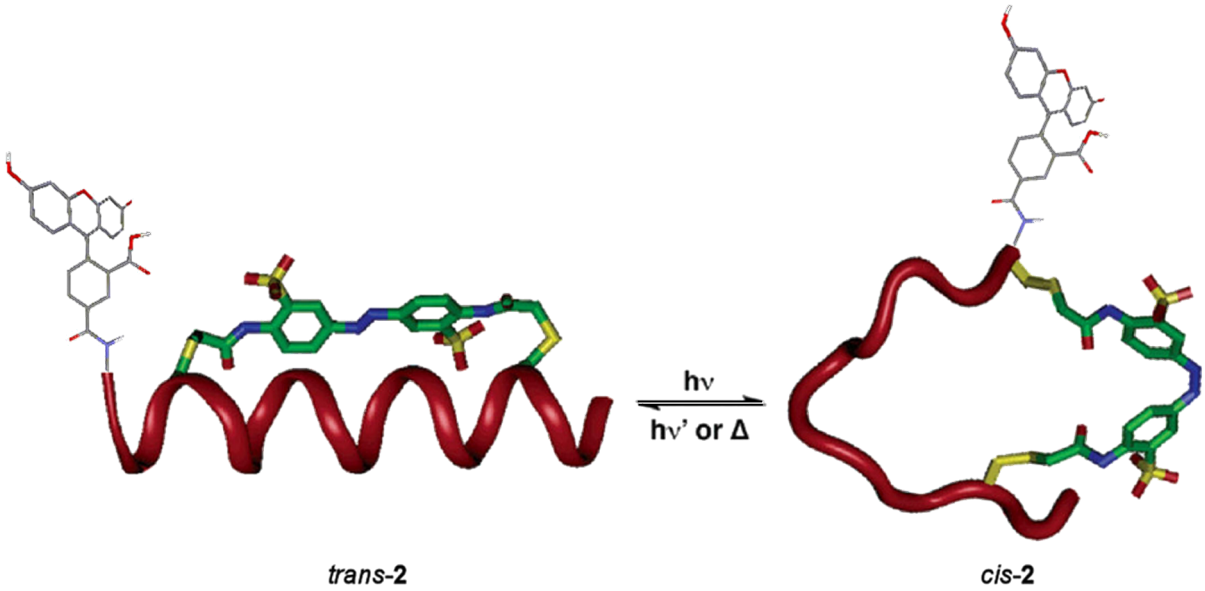

Figure 6: Photocontrol of the structure of the α-helix in the polypeptide azoderivative **2**. Reprinted (adapted) with permission from *J. Am. Chem. Soc.* **2005**, *127*, 15624–15625. Copyright (2005) American Chemical Society.

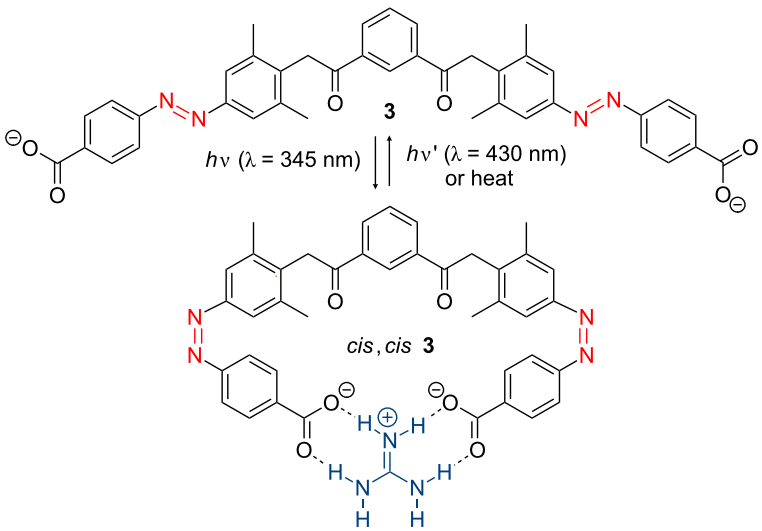

Figure 7: Recognition of a guanidinium ion by a *cis,cis*-bis-azo derivative **3**.

Azobenzene-based molecular devices

Among the systems with the inclusion and complexation properties of ions [97-100], several classes of compounds called azophanes, azocrowns [101-104], azocryptands, azocyclodextrins and azocalixarenes [105-107] have been described. The introduction of an azobenzene in these systems enables the photocontrol of the bonding properties of these molecules. The inclusion and complexation properties of some ions are more selective in one isomer that in the other. For example, the system of azocrown **4** shows a high selectivity for Rb^+ and Cs^+ ions [108]. The photoisomerization yields a similar motion to that of a butterfly, and only in the case of the *cis* isomer are the cations located between the two rings, yielding a "sandwich" structure (Figure 8). The ability of the azo compound **4** to remove cations from an aqueous solution increases in the order $Na^+ < K^+ < Rb^+ < Cs^+$. According to these properties, compound **4** could be used as a selective transport system controlled by light.

The β-cyclodextrin-type structure, schematically represented in Figure 9 as **5**, acknowledges the bipyridinium fragment of diarylazobenzene **6** by formation of an inclusion complex of *trans*-**5**+**6**. This inclusion complex evolves in a reversible way when it is irradiated. The process is especially interesting for

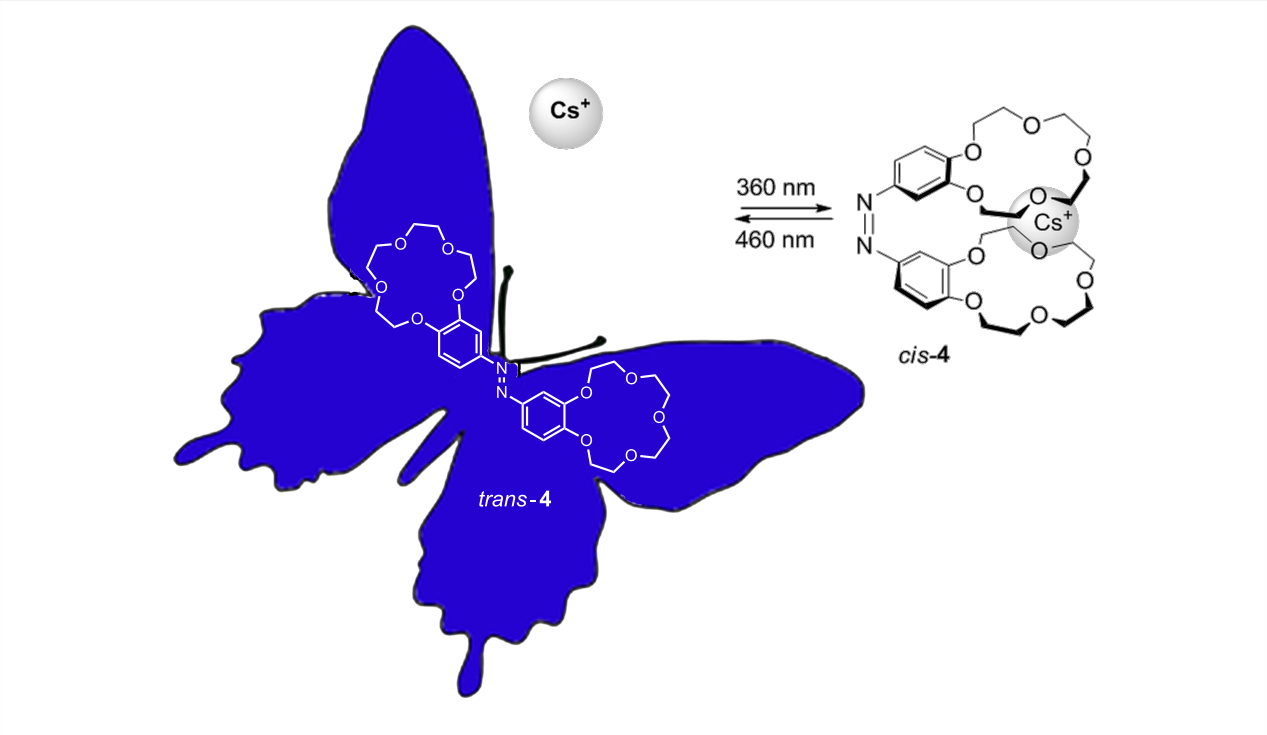

Figure 8: Recognition of cesium ions by *cis*-azo derivative **4**.

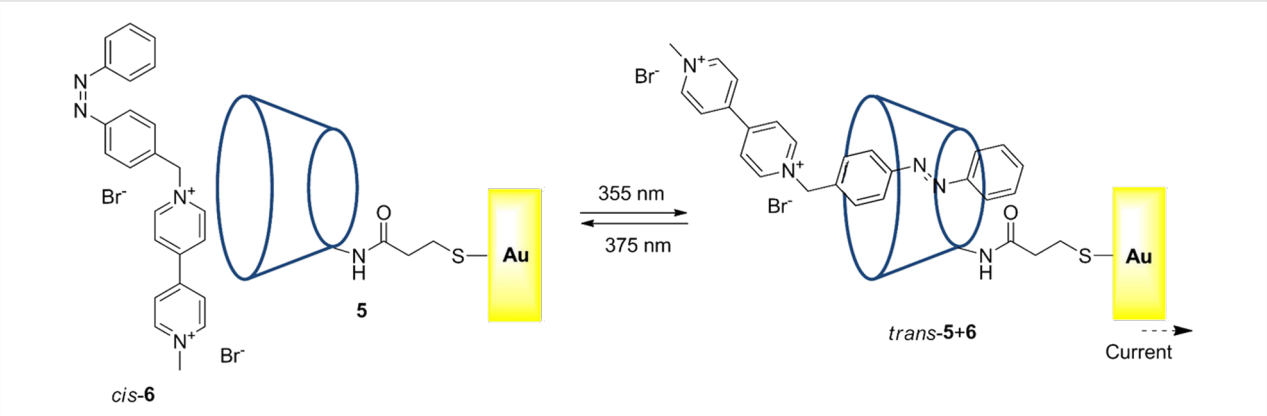

Figure 9: Photocontrolled formation of an inclusion complex of cyclodextrin *trans*-azo **5**+**6**.

the translation of the optical signals recorded by the bipyridinium azobenzene **6** via a β-cyclodextrin single phase prepared on a gold electrode [109].

In 2003, a molecular machine based on a pseudorotaxane was described [110]. Assembly between **7** and **8** occurs only when the azobenzene **7** adopts the *cis* configuration. The pseudorotaxane **7**+**8** is disassembled into its two components when the isomerization to *trans*-azobenzene occurs by an external stimulus (Figure 10).

Hinge molecular

Tamaoki et al. [111] designed a molecular device capable of photo-emulating a hinge motion. This switch consists in two azobenzene units that share a fragment with two coplanar xanthenes (Figure 11). The photoisomerization of the system forces a molecular motion similar to a hinge, in which the two aromatic rings are arranged at an angle of 90°. The photoisomerization process involves three isomeric forms: (*trans*,*trans*), (*trans*,*cis*) and (*cis*,*cis*). The heats of formation of the three isomers were determined by ab initio quantum chemical calculations. The isomers (*trans*,*trans*) and (*cis*,*cis*) are 28 and 2.6 kcal·mol^{-1} more stable than the intermediate isomer, respectively. The large energy difference between (*trans*,*trans*) and (*trans*,*cis*) isomers indicates the ring strain that exists in the (*trans*,*cis*) isomer, and the thermal isomerization from (*cis*,*cis*) to (*trans*,*cis*) is forbidden. The half-life of (*trans*,*cis*)-isomer is only 28 s at 23 °C. In these systems, in which the photochem-

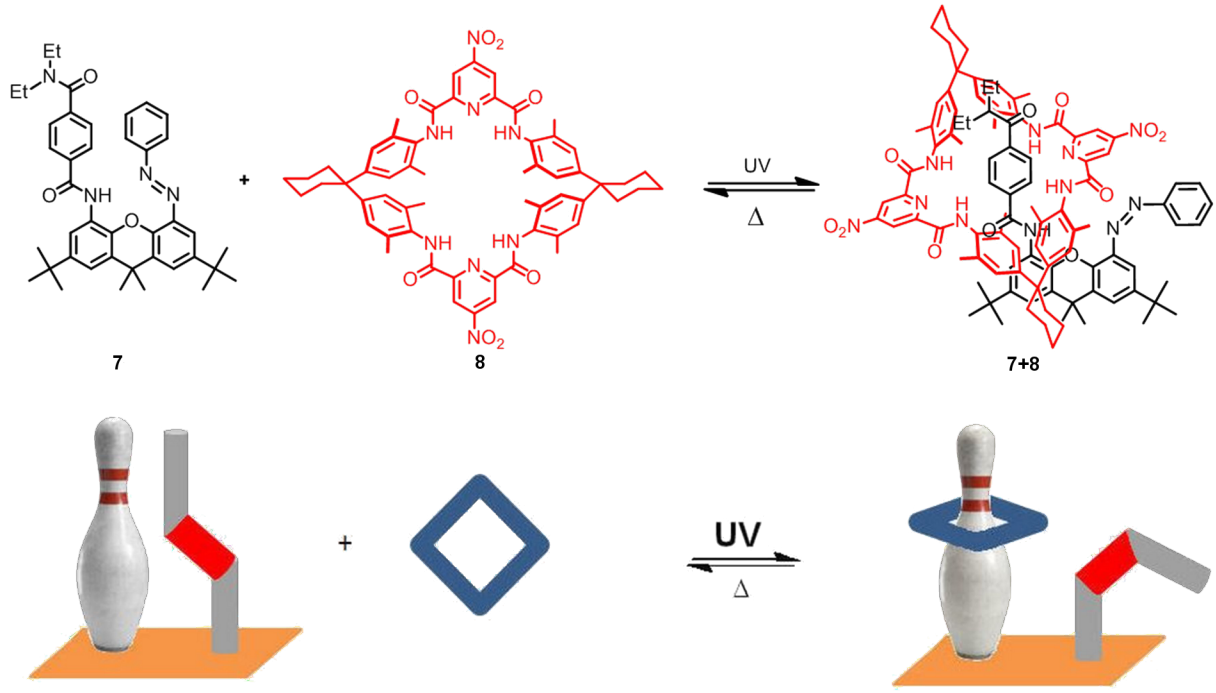

Figure 10: Pseudorotaxane-based molecular machine.

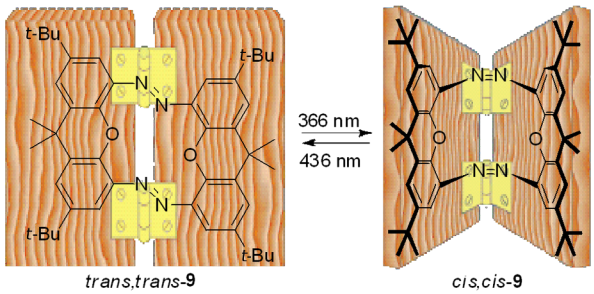

Figure 11: Molecular hinge. Reprinted (adapted) with permission from *Org. Lett.* **2004**, *6*, 2595–2598. Copyright (2004) American Chemical Society.

ical reaction intermediate has a short half-life and the final (*cis*,*cis*)-product is more stable than the intermediate, the photochemical yield is highly dependent on the used light intensity [112-114].

Molecular threader

Stoddart, Balzani et al. [115,116] created an intelligent molecular device (*trans*-**10**·**11**) capable of moving within a cyclophane **11**, as a needle through a buttonhole (Figure 12). The interaction between the two systems is measured on the fluorescence emitted by the pyridinium salt free cyclophane. The azobenzene *trans*-**10** is conveniently replaced with electron donor units, so that when it is associated, as azo-**10**·**11**, the fluorescence is completely inhibited by charge-transfer interactions. The photoexcitation carried out by irradiation with light of λ = 360 nm of a solution of *trans*-**10** and **11** causes a process of "unthreading". The *cis* isomer **10** has a much weaker interaction with cyclophane **11**, and this fact is reflected in the large increase in fluorescence intensity of **11**. The *trans*-isomer **10** is regenerated when the mixture is left in the dark or irradiated with light of λ = 440 nm, and as a result becomes a "thread" in the cyclophane. In this way, the isomerization of the N=N double-bond type triggers a movement of threading/unthreading exclusively governed by light.

Molecular scissors

In 2003, Aida's group described a new generation of optical molecular devices composed of different kinds of organic systems interconnected through an azobenzene unit as the epicentre of the motion. First, a molecular switch was synthesized capable of making a motion similar to the opening and closing of scissors. This switch consists of a central unit of 1,1',3,3'-tetrasubstituted ferrocene, two phenyl groups as scissor blades and two phenylethylene groups as handles linked through an azobenzene [117,118]. The light irradiation of λ = 350 nm (180 min) leads to a mixture of isomers *trans*/*cis* 11:89, while exposure to visible light (λ > 400 nm, 15 min) again enriches 46% of the *trans* isomer. The molecular motion was studied by circular dichroism (CD), ^{1}H NMR and DFT calculations confirming that the change in the configuration of the N=N double bond modifies the initial position of the ferrocene resulting in an opening (*cis*) and closing (*trans*) of the "blades" of the phenyl group (Figure 13). The angle between the two phenyl groups is altered from about 9° upon closing of the "scissors" (*trans*-**12**) to more than 58° when it opens (*cis*-**12**).

Molecular pedals

In 2006 [119,120], the same authors described a more complex system that included two terminal units of porphyrin–Zn noncovalently associated to a host molecule of bis-isoquinoline **13** (Figure 14). The exposure of azo derivative **13** to light of λ = 350 ± 10 nm leads to a mixture of isomers *trans*/*cis* 22:78. Irradiation of this mixture of isomers at λ > 420 nm returns the system to an enrichment of the *trans* isomer (63%).

The study of the photoisomerization process of **13** revealed that the configurational change of the azobenzene unit causes a sequence of molecular motions of the units connected to it. The

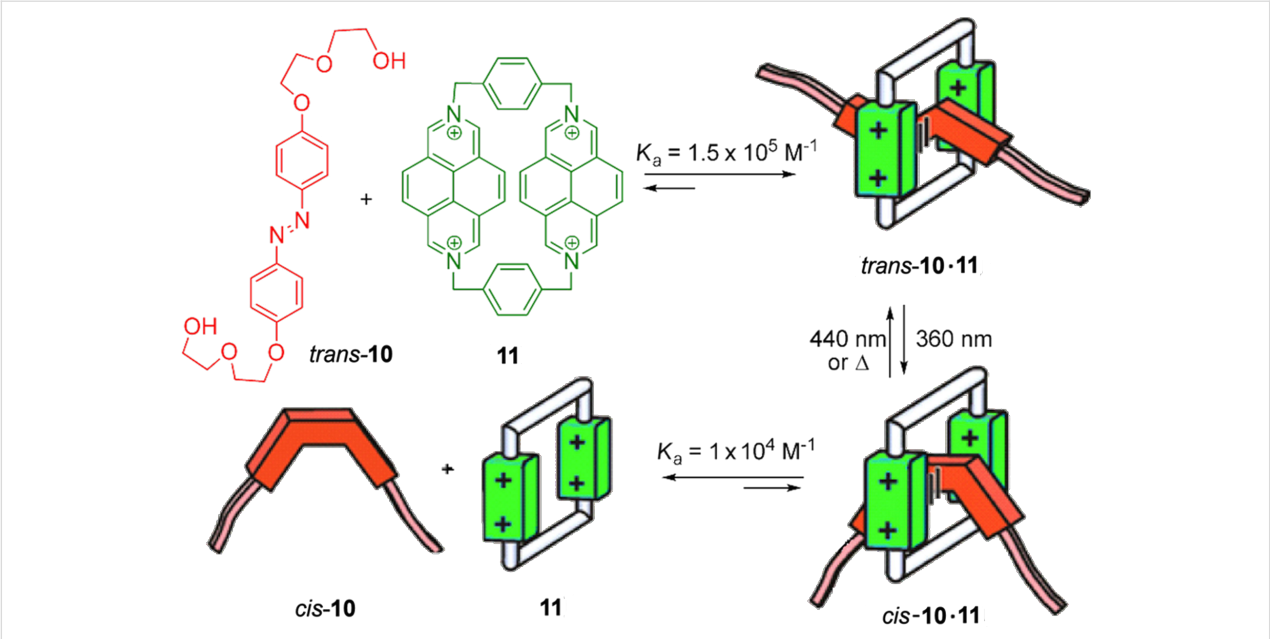

Figure 12: Molecular threader. Reprinted (adapted) with permission from *Acc. Chem. Res.* **2001**, *34*, 445–455. Copyright (2001) American Chemical Society.

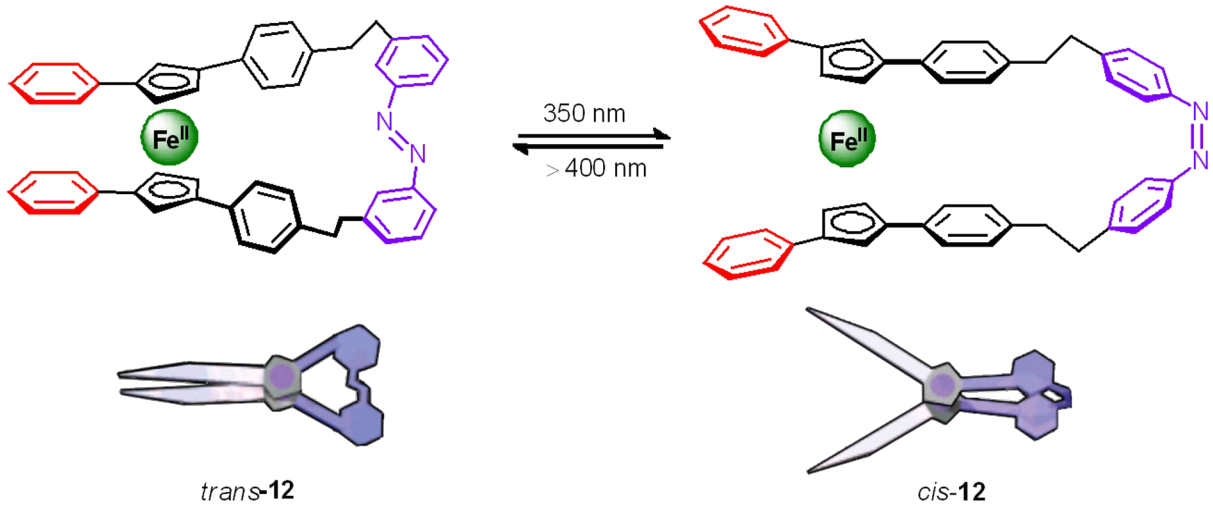

Figure 13: Molecular scissors based on azobenzene **12**. Reprinted (adapted) with permission from *J. Am. Chem. Soc.* **2003**, *125*, 5612–5613. Copyright (2003) American Chemical Society.

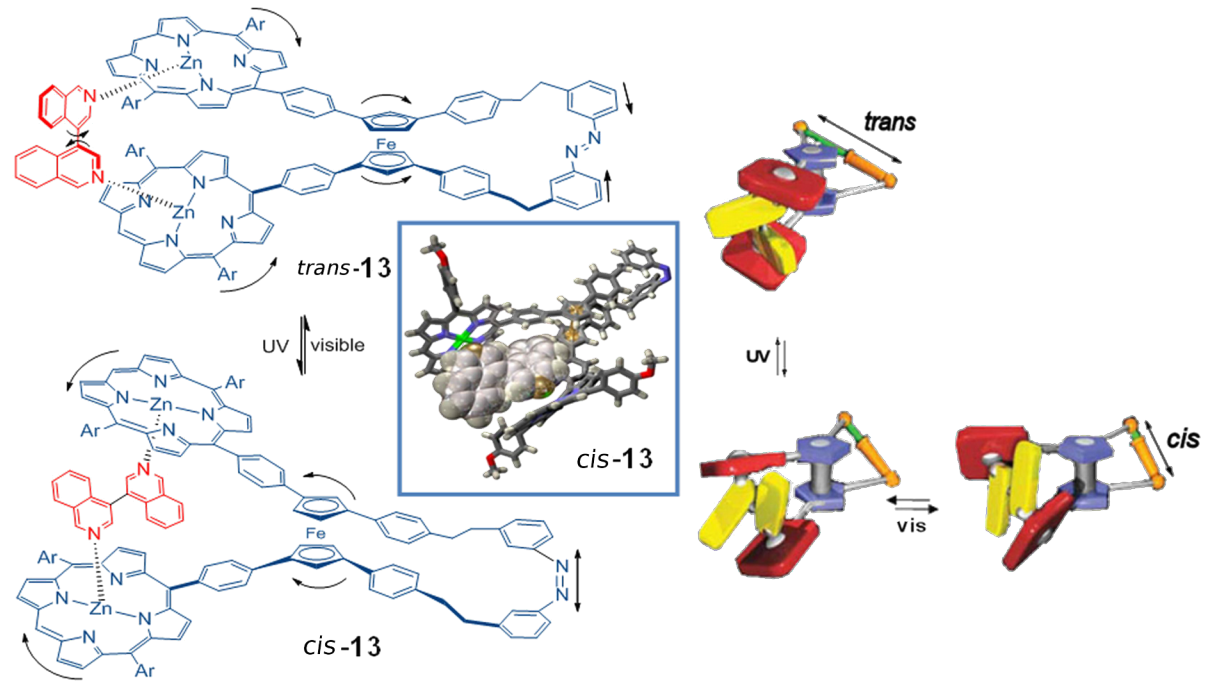

Figure 14: Molecular pedals. Reprinted by permission from Macmillan Publishers Ltd: *Nature*, **2006**, *440*, 512–515, copyright (2006).

ferrocene unit rapidly responds by turning, which in turn induces an opening motion that distances the porphyrin units, causing a mechanical spin rotation in the bis-isoquinoline molecule similar to a pedal. This device is effective if the porphyrin–Zn and bis-isoquinoline units remain associated during the photoisomerization, i.e., the dynamics of dissociation between these units is slower than the photoinduced movement itself. In this case, the dissociation constant is six orders of magnitude slower than the *trans–cis* photoisomerization, which ensures that the bis-isoquinoline unit is coordinated to azocompound **13** during the isomerization process of the azobenzene unit.

Nanovehicle

One proposed mechanism for the isomerization of azobenzene suggests that photoinduced *trans–cis* isomerization passes

through a rotating mechanism, while the thermal *cis–trans* reisomerization follows an inversion mechanism [121]. The combination of both processes (photochemical and thermal) could lead to opening (*trans*) and closing (*cis*) mechanical motion accompanied by a translational motion. Based on this mechanistic hypothesis, Tour et al. created a branched azobenzene structure to realize a nanovehicle able to move like a caterpillar (Figure 15) [122,123].

The system consists of three parts: A central azobenzene, a rigid frame composed of oligo(phenylacetylenes), which in turn are anchored to azobenzene through *para* positions, and wheels based on fullerene C_{60} (azo-**14**) or *p*-carboranes (azo-**15**). Photoisomerization studies suggest that only the azobenzene system with *p*-carborane wheels (azo-**15**) may be useful as a molecular switch, because the photoisomerization of azofullerene **14** leads to only 8% of the *cis*-isomer. Although, the quantum yield obtained for *cis*-**14** is not very high, this proportion is significant, given the speed with which energy transfer to the fullerene unit occurs [124]. In the case of azo-*p*-carborane **15**, irradiation at λ = 365 nm for 10 min leads to 24% of the *cis* isomer. The photochemical (λ > 495 nm, 5 min) or thermal (heating to 40 °C, 15 min) reisomerization recovers the initial state. After these preliminary results it remains to be demonstrated whether the molecular motion of the device **15** achieves the expectations of the authors, to prove the usefulness of the device.

Molecular driving force

One of the more attractive and interesting applications of the isomerization processes of azobenzenes is their use as nanoimpeller-controlled drug release devices. The idea is to anchor a functionalized azobenzene inside the silica nanoparticle, thereby forming light-activated mesostructured silica nanoparticles. The azobenzene **16** is anchored to the particle wall while the other extreme is free (Figure 16) [125-127].

These nanoparticles have pores capable of holding other molecules. The isomerization process of azobenzene generates a molecular flapping and the molecules can be expelled outside in a photoinduced way. The morphology of the light-activated mesostructured silica nanoparticles (LAMs) is evaluated by scanning electron microscopy (SEM), electronic transmission images (TEM), UV–vis and X-ray analysis, setting a pore diameter of 1.9 ± 0.1 nm, a volume of 0.248 $cm^{-3}·g^{-1}$ and a surface area of 621.19 $m^2·g^{-1}$. The nanoparticles, which contain 2.4% by weight of azobenzene, are treated with camptothecin (CPT), a drug used in the treatment of cancer, which is housed inside.

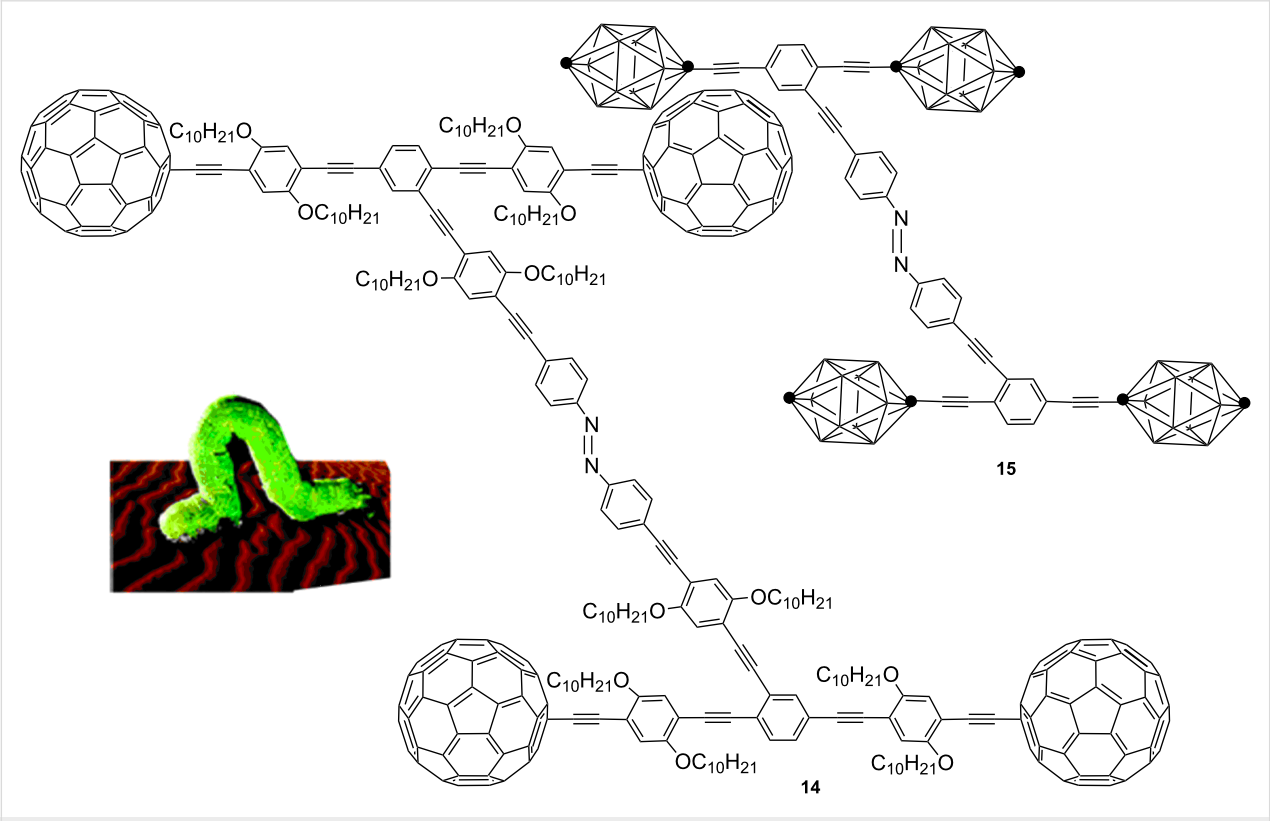

Figure 15: Design of nanovehicles based on azo structures. Reprinted (adapted) with permission from *Org. Lett.* **2008**, *10*, 897–900. Copyright (2008) American Chemical Society.

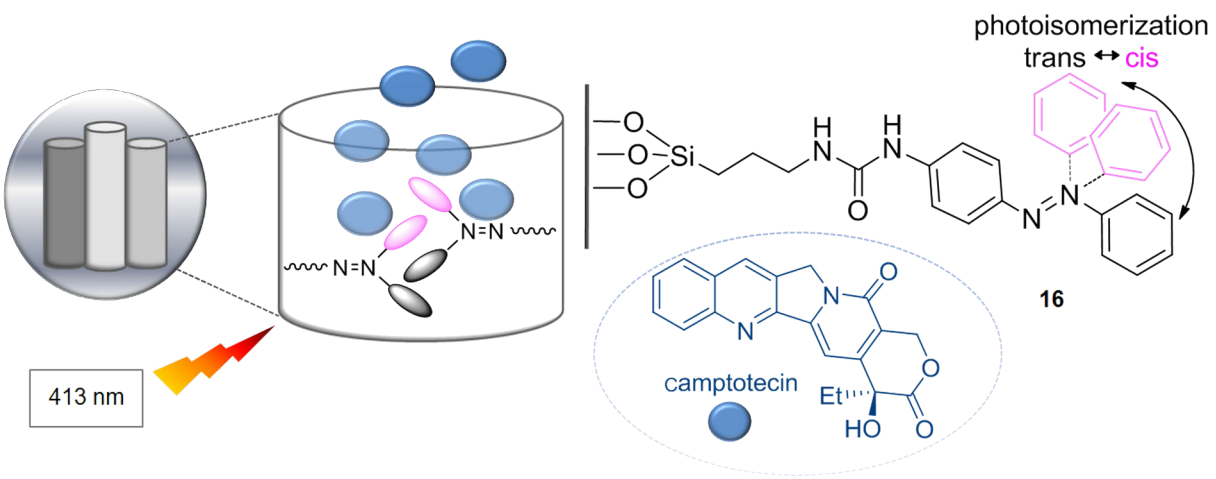

Figure 16: Light-activated mesostructured silica nanoparticles (LAMs).

The LAMs (CPT) were incubated for 3 h with cancer cells in darkness. These cells are irradiated for 5 min at 0.1 W·cm^{-2} at λ = 413 nm, where both isomers have the same extinction coefficient promoting a continuous exchange between both *trans–cis* isomers, and then they were incubated again in the dark for 48 hours. This experiment shows that the azobenzene units located within the LAMs (CPT) act as promoters (Figure 16), releasing the drug (CPT) only after irradiation of the nanoparticle with a light at a certain wavelength, hence resulting in cell death. The number of released molecules can be controlled depending of the light intensity and irradiation time. On the other hand, the camptothecin, in the absence of light, stays inside the nanoparticles and the cells remain intact. Control experiments with cells lacking the nanoparticles revealed that irradiation at 413 nm does not affect cell survival, and similarly irradiation of incubated cells with LAMs not containing CPT, did not lead to cell death, thus confirming the biocompatibility of the LAMs with the cells.

Molecular lift

The individual molecular motion of azobenzene in the *cis–trans* isomerization process can be amplified when the azobenzene is anchored to a more complex system [128]. The cooperative combination of each individual photoisomerization can increase the dynamic response if the azobenzenes are self-assembling, generating an uniform motion [129]. An illustrative example is given in Figure 17, in this case one of the azobenzene rings has a *p*-mercaptophenyl group through which it is associated with an Au(111) layer [130]. All the azobenzenes are oriented and form self-assembled monolayers (SAMs). The *trans–cis* isomerization process of the azobenzene unit placed in the metal layer takes place with excellent yield (88–98% *cis* isomer). This is particularly relevant for future applications in the design of devices for information-storage-based photochromic systems [131]. The photo-reversal of SAMs also proceeds with excellent yield (94–100%). The structural difference (d_{trans}–d_{cis}) between both isomers is approximately 7 Å.

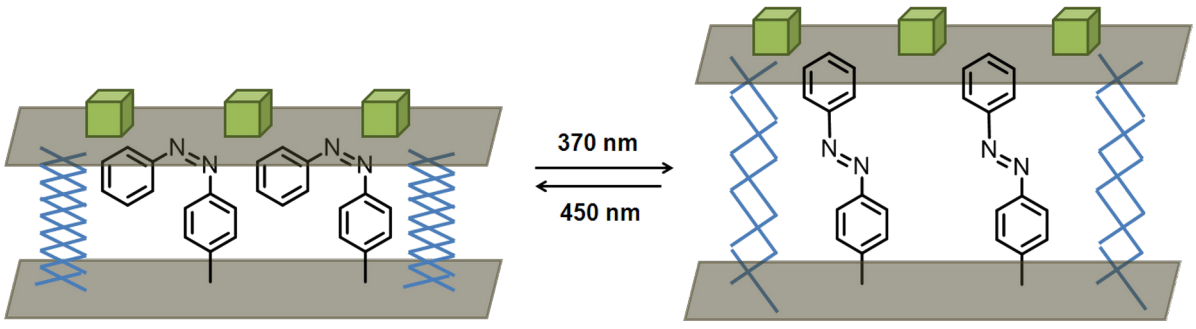

Figure 17: Molecular lift.

By scanning tunnelling microscopy (STM), the authors determined the surface density of SAM_{azo}, and the force exerted in the photoisomerization molecular motion of all the azobenzenes in the SAM_{azo} was calculated. The individual photomovement of each azobenzene results in a collective structural change in a certain direction. This cooperative molecular motion of SAM_{azo} acts as a molecular lift capable of lifting one Hg drop deposited on the monolayer of azobenzenes. Furthermore, this device acts as a photoswitch of the current between the Au(111) layer and the Hg drop. A significant increase of the current density of about one order of magnitude occurs under irradiation at λ = 370 nm, and the corresponding decrease is produced in a reversible way when the azobenzene is irradiated at λ = 450 nm.

Molecular sunflower

When an azobenzene is differently substituted in the *ortho* or *meta* positions, the corresponding *trans* and *cis* isomers can adopt different conformations. A simple example is illustrated in Figure 18 for mono-*ortho*-substituted azobenzene. In the *trans* isomer, the azo group is oriented as far as possible away from the substituent in the *ortho* position (*trans*-**I** form), or placed next to it (*trans*-**II**). Similarly, motion of the aromatic rings accompanying the photoisomerization process can also lead to several *cis* conformers (*cis*-**I** and *cis*-**II**). The electronic nature and steric bulk of the substituents of the aromatic rings can be a key factor in favouring one type of conformation in the azocompounds. Considering the relationship between the molecular conformation and biological recognition, it is particularly interesting to design azo devices that allow control, by an external stimulus, of the configuration of the N=N double bond, and also to define a specific orientation or conformation of each stereoisomer (*trans* or *cis*).

Recently, Carreño et al. [132,133] synthesized different enantiomerically pure sulfinyl azobenzenes. The sulfinyl group is a key component in the design of a molecular sunflower, a device that by means of light can undergo phototropism with a given direction. The enantiomerically pure 2- and 3-sulfinyl azo compounds are obtained with excellent regioselectivities by using a new and simple method for the synthesis of aromatic azobenzenes based on the treatment of quinone bisacetals **17** and **19** with different arylhydrazines **18** [134]. In both cases, the sulfoxide group preferentially adopts a rigid S-*cis* conformation [135], situating the sulfinylic oxygen in 1,3-parallel arrangement with the neighbouring hydrogen (blue arrow, Scheme 1). This arrangement is essential to force a specific final conformation of the azocompound.

Irradiation with light of λ = 365 nm results in 33–75% of *cis*-isomer **20** and 84–99% of *cis*-**21**. The photochemical reisomerization (λ = 436 nm) recovers the initial state in both sets of sulfinyl derivatives. The study of the photochromic properties of enantiopure azocompounds **20** and **21** by using standard techniques (UV–vis, circular dichroism, chiral HPLC and NMR) has established that the chiral optical response differs greatly depending on the position of the sulfoxide group (C-2 or C-3). *Cis* isomers in both *p*-tolylsulfinyl azocompounds show an opposite arrangement of substituents around the N=N group, with an S-shaped structure for *cis*-**20** or a U-shaped structure for *cis*-**21**. The conformational rigidity of the chiral sulfinyl group is the key to controlling the directionality of the molecular

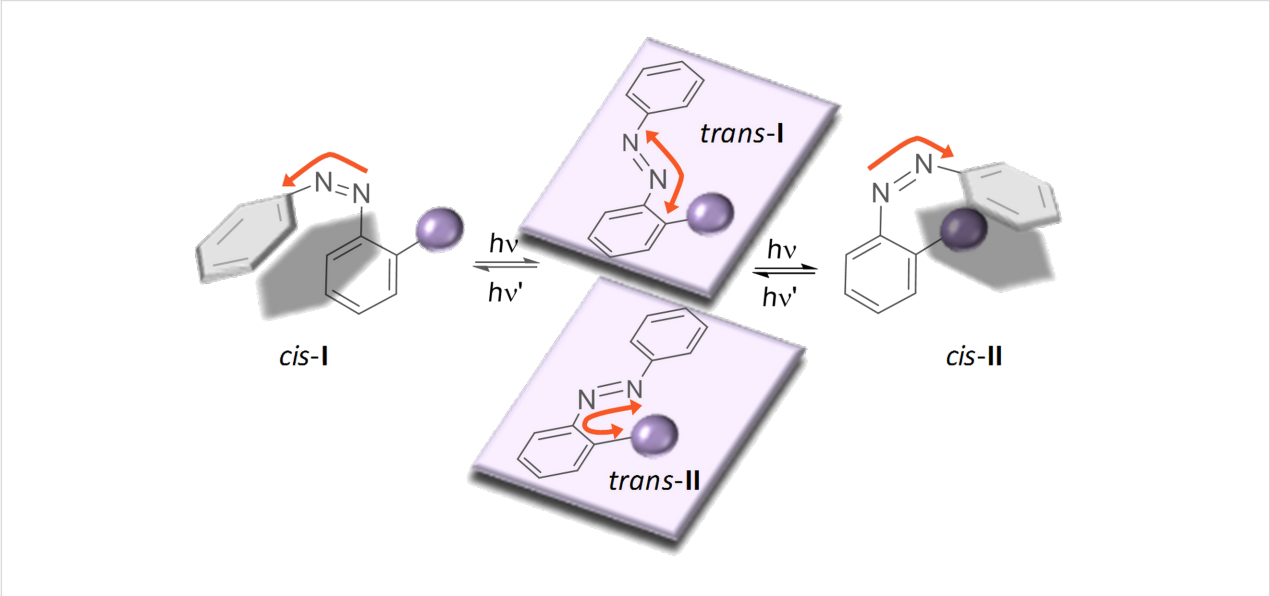

Figure 18: Conformational considerations in mono-*ortho*-substituted azobenzenes.

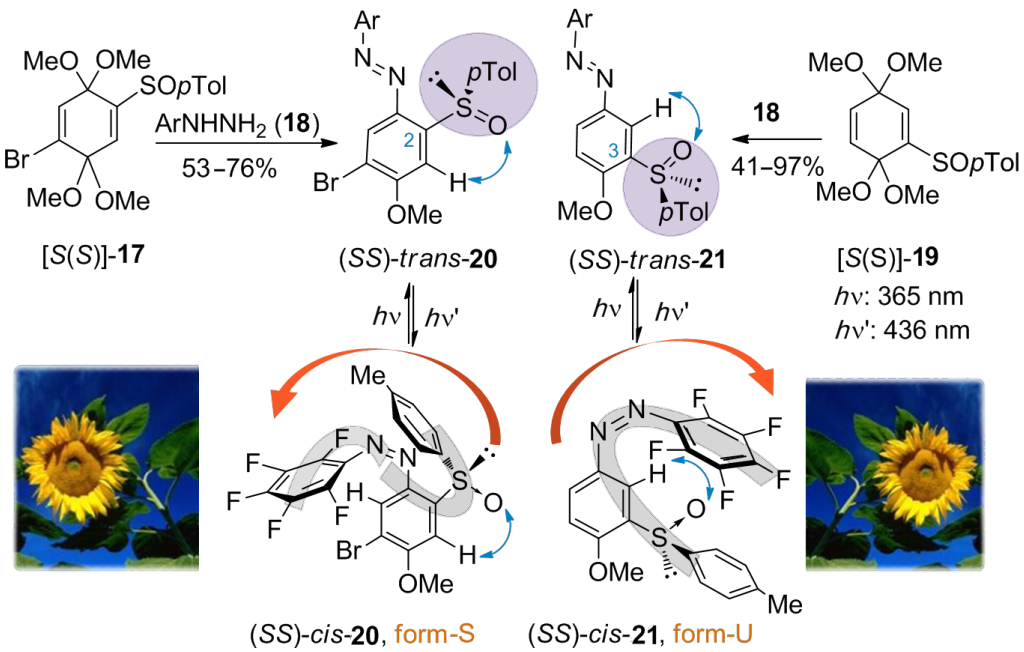

Scheme 1: Synthesis and photoisomerization of sulfinyl azobenzenes. Reprinted (adapted) with permission from *J. Am. Chem. Soc.* **2007**, *129*, 7089–7100. Copyright (2007) American Chemical Society.

motion of photoisomerization. Thus, choosing the position of the sulfoxide group in the azobenzene (*ortho* or *meta* to N=N) by irradiation with light causes a determined geometric, conformational and rigid change, inducing a specific phototropism as in the stem of a sunflower.

Photoactive Brønsted base

The conformation of a molecule can have direct implications for its reactivity. Thus, the control of the conformation is the key to controlling its reactivity. The union of this concept with molecular switches has opened the door to the development of new photoreactive compounds in which the reactivity can be controlled by an external stimulus as a switch (on/off). Recently, Hecht et al. [136,137] designed a Brønsted base whose pK_a changes with light. The study focuses on the azobenzene **22**, which possesses, in an aromatic ring, a spirocyclic lactone fused to a conformationally restricted piperidine (Figure 19).

In the structure of the *trans* isomer **22**, the pair of unshared electrons of nitrogen is inaccessible. The *trans–cis* photoisomerization process changes the disposition of the aromatic rings, unlocking access to the basic center of the piperidine. This switch, of Brønsted base type, has been tested in the Henry reaction between *p*-nitrobenzaldehyde and nitroethane ensuring that only the *cis* isomer is able to catalyze the reaction.

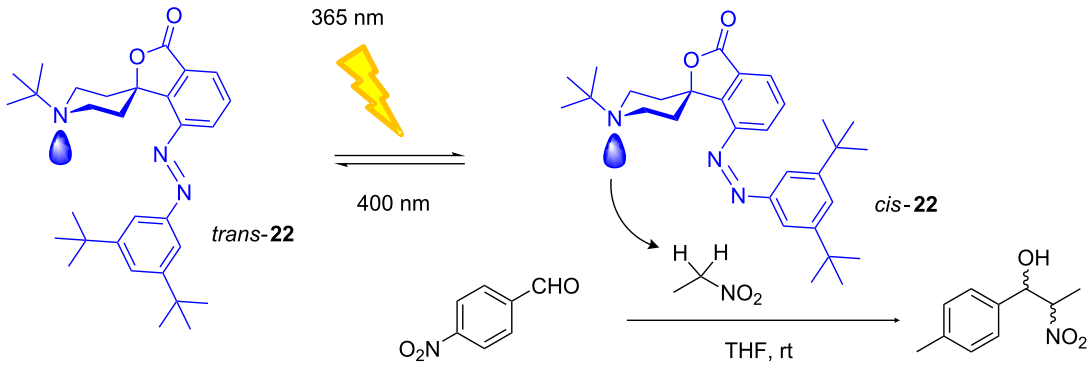

Figure 19: Photoisomerization of azocompound **22** and its application as a photobase catalyst.

Photodirected azo polymers

A spectacular example of the molecular motion of photoisomerization is shown in Figure 20. The irradiation of polymers containing light-sensitive molecules such as azobenzenes can lead to a photocontraction of the polymer, converting luminescent energy to mechanical energy. Ikeda et al. [37] demonstrated how the irradiation of a liquid-crystal elastomer (LCE) of azobenzenes with linearly polarized light is able to collapse and expand the LCE films (yellow sheet in Figure 20) in a certain direction.

The film is obtained by thermal polymerization of the azocompound **23** (monomer), by using the diacrylate derivative **24** as a crosslinking agent. The azo-LCEs comprise a polydomain with the characteristics of a liquid crystal, formed by many micro-sized domains of azobenzene aligned in the same direction. Although macroscopically the direction of alignment is random, under irradiation with linearly polarized light the selective absorption of the light by the azobenzene causes a collective management of all microdomains, such that the orientation of the fold is governed by the direction of the linearly polarized light source (white arrow in Figure 20). The consecutive irradiation with λ = 366 nm at 0°, −45°, −90° or −135° following by irradiation at λ = 540 nm produces the contraction and expansion of the film in the clockwise direction. Recently, this liquid-crystal elastomer was used in developing the first plastic photomechanical motor capable of converting light into mechanical energy without any battery or power source [47].

Bistable memory device

Recently, Stoddart and Venturi's group described a molecular switch using a [2]rotaxane **25**, which undergoes mechanical movements triggered by redox processes and can be switched between two thermodynamically stable conformations [138]. The energy barriers between these conformations can be controlled kinetically by photochemical modulation. The ring component of the [2]rotaxane is cyclobis(paraquat-*p*-phenylene) and the dumbbell is comprised of a tetrathiafulvalene unit and a

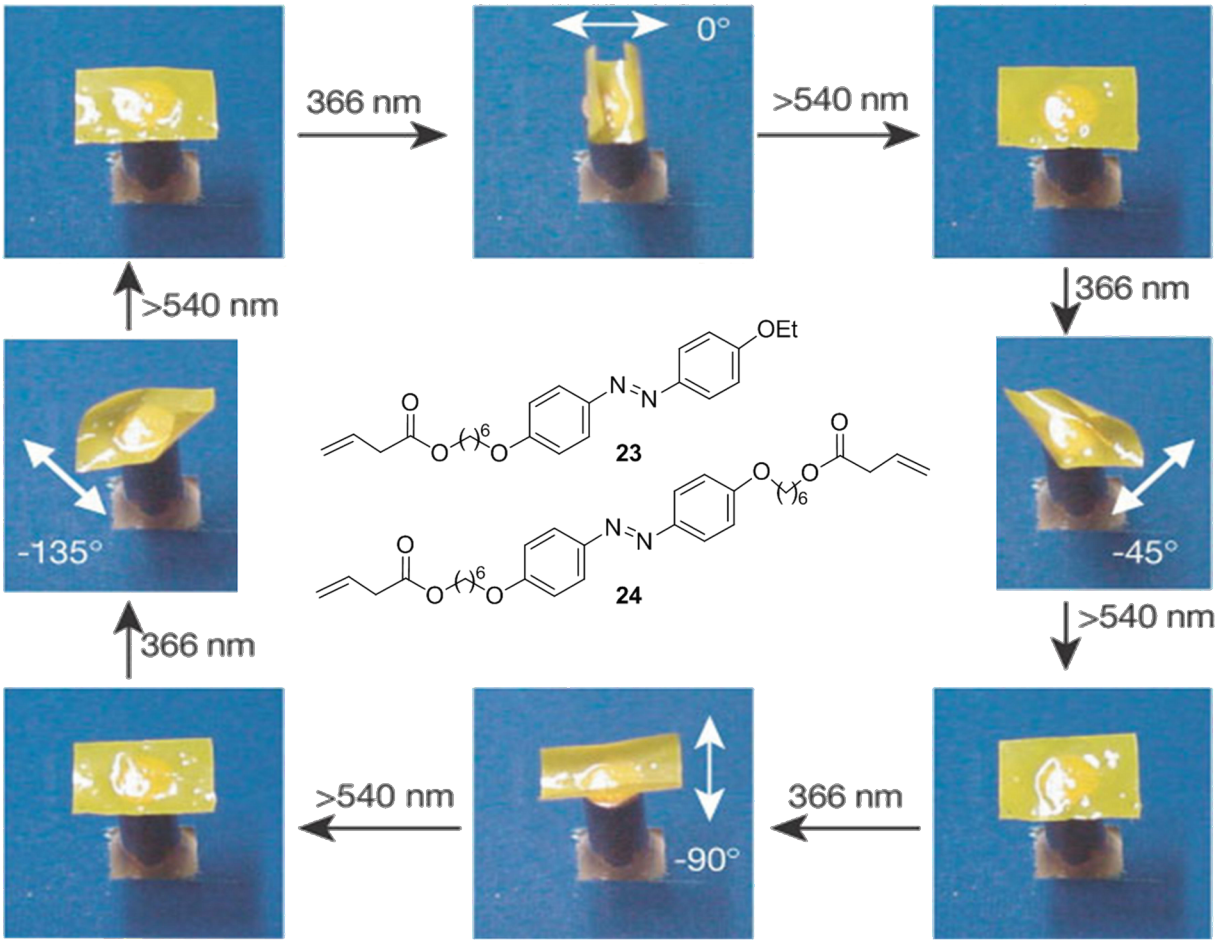

Figure 20: Effect of irradiation with linearly polarized light on azo-LCEs. Reprinted by permission from Macmillan Publishers Ltd: *Nature*, **2003**, *425*, 145–146, copyright (2003).

1,5-dioxynaphthalene as π-electron-donating recognition sites, and a photoactive unit of 3,5,3',5'-tetramethylazobenzene, which by irradiation of light can be switched between its *cis* and *trans* conformations (Figure 21). Probably, this structure is a good candidate for use in the design of engineered test devices. Data can be written on the rotaxane when the units of tetrathiafulvalene are oxidized and then blocked in the *trans–cis* photoisomerization process, on the azobenzene fragment. After writing the information, the oxidized species can be reduced to the original form without loss of data. The data is stored until irradiation of the azobenzene fragment allows the reopening of the azobenzene gate.

Unidirectional photoisomerization

The process, *trans* to *cis* isomerization, generates helicoidal chirality, such that the isomer can adopt a helicoidal geometry with *P* or *M* chirality. The configurational stability of *cis*-azobenzenes depends of the interconversion barrier between the *cis*-(*P*) and *cis*-(*M*) isomers. The size and the electronic nature of the substituents present in the systems are the factors that are more influential on the energetic barrier. Haberhauer et al. described the unidirectional photoisomerization process of azobenzene **26** [139]. The irradiation with light of the achiral *trans* isomer gives rise to the *cis* isomer with *P* helicity. A chiral clamp was synthesized, by anchoring a chiral cyclic imidazole peptide to both aromatic rings of azobenzene. The system is flexible enough to allow the isomerization between the *trans* and *cis* isomer but in turn destabilizes one of the helices of the *cis* isomer, and only one *cis* isomer (*P*) is present in solution (Figure 22).

Conclusion

Azobenzene is one of the most used systems in the design of molecular photoswitches. The synthesis is very easy and their photochromic properties are very interesting. An external stimulus, normally light irradiation at a certain wavelength, causes a fluctuation between the *cis–trans* isomeric species. This isomerization is reversible, photochemically and thermally. The molecular motion that occurs in the isomerization process has facilitated the development of molecular devices. Today, researchers

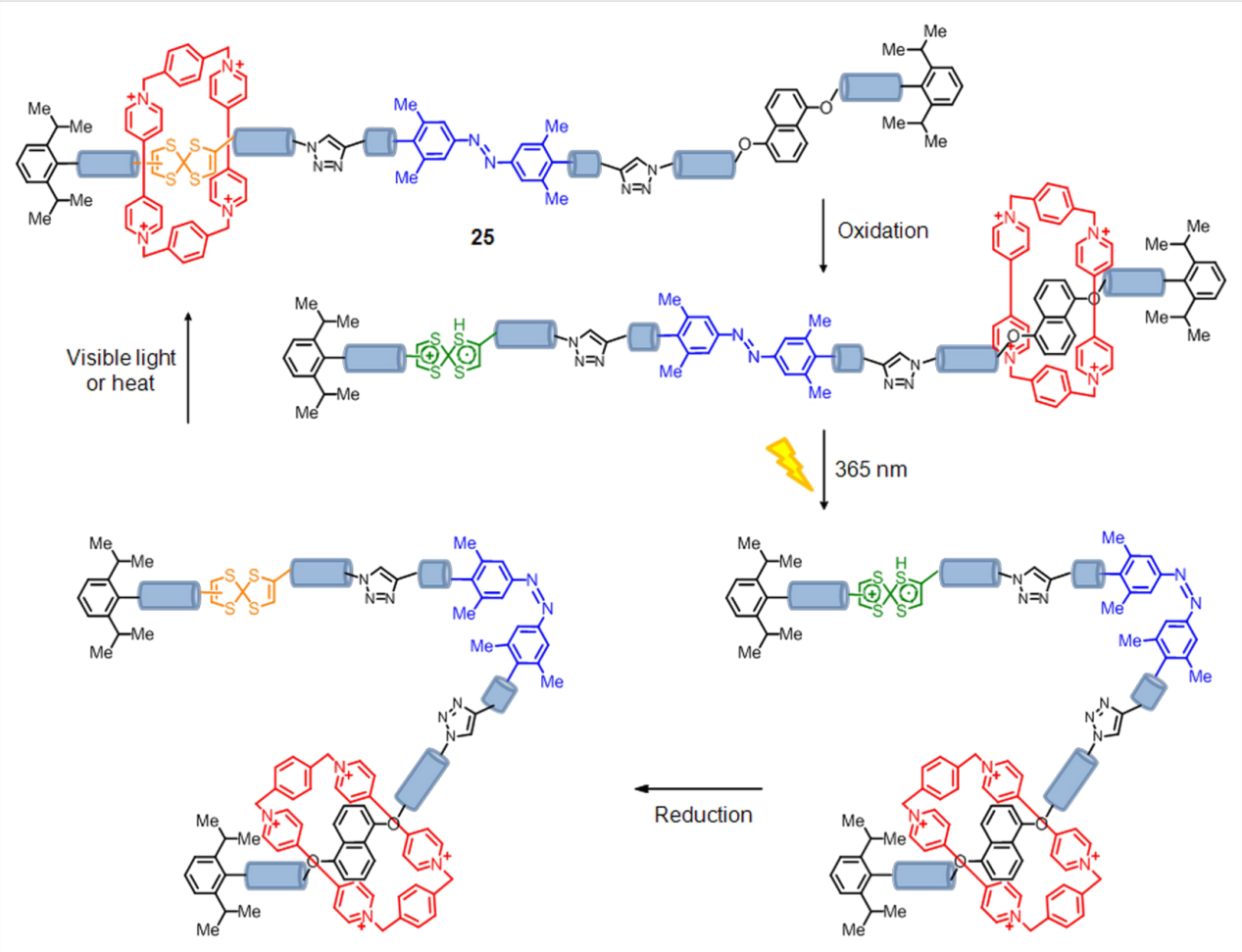

Figure 21: Chemically and photochemically triggered memory switching cycle of the [2]rotaxane **25**.

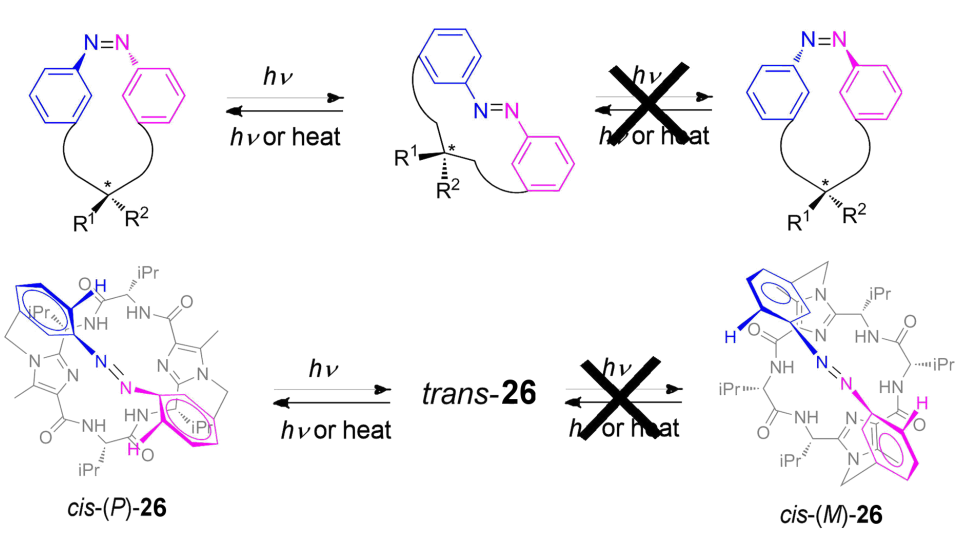

Figure 22: Unidirectional photoisomerization process of the azobenzene **26**.

continue to develop synthetic supplements to improve the properties of azobenzenes towards the development of more efficient devices that control the isomerization and orientation of the azobenzene, shifting the photoisomerization process to other concepts of chemistry, from the development of photoreactive compounds or photomechanical materials and even bioincorporation of azobenzenes, to more complex systems that allow a greater understanding, such as the photocontrol of biological dynamic mechanisms.

Acknowledgements

E.M. thanks Ministerio de Ciencia y Innovación for a contract of "Junta de Ampliación de Estudios" programm (JAEDoc). Financial supports by Ministerio de Ciencia e Innovación (Consolider-Ingenio 2009 (MULTICAT project), MAT2011-29020-C02 and CTQ2011-24783) and European Social Fund (Grant SOLGEMAC-S2009/ENE-1617) are acknowledged.

References

1. Ribagorda, M.; Merino, E. *An. Quim.* **2009,** *105,* 290–299.
2. Mitscherlich, E. *Ann. Pharm.* **1834,** *12,* 311–314. doi:10.1002/jlac.18340120282
3. Hartley, G. S. *Nature* **1937,** *140,* 281–282. doi:10.1038/140281a0
4. Zollinger, H. *Color Chemistry. Syntheses, Properties, and Applications of Organic Dyes and Pigments,* 3rd ed.; Wiley-VCH: Weinheim, Germany, 2003.
5. Hunger, K. *Industrial Dyes: Chemistry, Properties and Applications;* Wiley-VCH: Weinheim, Germany, 2003; pp 14–35.
6. Zollinger, H. *Azo and Diazo Chemistry;* Interscience: New York, 1961.
7. Ross, D. L.; Blanc, J. Photochromism by *cis–trans* Isomerization. In *Photochromism;* Brown, G. H., Ed.; Wiley-Interscience: New York, 1971; pp 471–556.
8. Kumar, G. S.; Neckers, D. C. *Chem. Rev.* **1989,** *89,* 1915–1925. doi:10.1021/cr00098a012
9. Rau, H. Photoisomerization of Azobenzenes. In *Photochemistry and Photophysics;* Rabek, J. F., Ed.; CRC Press: Boca Raton, FL, USA, 1990; Vol. 2, pp 119–142.
10. Rau, H. *Angew. Chem., Int. Ed. Engl.* **1973,** *12,* 224–235. doi:10.1002/anie.197302241
11. Brown, E. V.; Granneman, G. R. *J. Am. Chem. Soc.* **1975,** *97,* 621–627. doi:10.1021/ja00836a025
12. Rau, H. Azo Compounds. In *Photochromism, Molecules and Systems;* Dürr, H.; Bouas-Laurent, H., Eds.; Elsevier: Amsterdam, 2003; Vol. 1, pp 165–192.
13. Suginome, H. In *CRC Handbook of Organic Photochemistry and Photobiology;* Horspool, W. M.; Song, P.-S., Eds.; CRC Press: Boca Raton, FL, USA, 1995; p 824.
14. Morgenstern, K. *Acc. Chem. Res.* **2009,** *42,* 213–223. doi:10.1021/ar800021q
15. Henzl, J.; Mehlhorn, M.; Gawronski, H.; Rieder, K.-H.; Morgenstern, K. *Angew. Chem., Int. Ed.* **2006,** *45,* 603–606. doi:10.1002/anie.200502229
16. Choi, B.-Y.; Kahng, S.-J.; Kim, S.; Kim, H.; Kim, H. W.; Song, Y. J.; Ihm, J.; Kuk, Y. *Phys. Rev. Lett.* **2006,** *96,* 156106. doi:10.1103/PhysRevLett.96.156106
17. Koshima, H.; Ojima, N.; Uchimoto, H. *J. Am. Chem. Soc.* **2009,** *131,* 6890–6891. doi:10.1021/ja8098596
18. Sension, R. J.; Repinec, S. T.; Szarka, A. Z.; Hochstrasser, R. M. *J. Chem. Phys.* **1993,** *98,* 6291–6315. doi:10.1063/1.464824
19. Nägele, T.; Hoche, R.; Zinth, W.; Wachtveitl, J. *Chem. Phys. Lett.* **1997,** *272,* 489–495. doi:10.1016/S0009-2614(97)00531-9
20. Dhammika Bandara, H. M.; Burdette, S. C. *Chem. Soc. Rev.* **2012,** *41,* 1809–1825. doi:10.1039/c1cs15179g
21. Bortolus, P.; Monti, S. *J. Phys. Chem.* **1979,** *83,* 648–652. doi:10.1021/j100469a002
22. Rodier, J. M.; Myers, A. B. *J. Am. Chem. Soc.* **1993,** *115,* 10791–10795. doi:10.1021/ja00076a041
23. Tamai, N.; Miyasaka, H. *Chem. Rev.* **2000,** *100,* 1875–1890. doi:10.1021/cr9800816
24. Chang, C.-W.; Lu, Y.-C.; Wang, T.-T.; Diau, E. W.-G. *J. Am. Chem. Soc.* **2004,** *126,* 10109–10118. doi:10.1021/ja049215p

25. Gegiou, D.; Muszkat, K. A.; Fischer, E. *J. Am. Chem. Soc.* **1968,** *90,* 12–18. doi:10.1021/ja01003a003
26. Malkin, S.; Fischer, E. *J. Phys. Chem.* **1962,** *66,* 2482–2486. doi:10.1021/j100818a038
27. Asano, T.; Yano, T.; Okada, T. *J. Am. Chem. Soc.* **1982,** *104,* 4900–4904. doi:10.1021/ja00382a026
28. Marcandalli, B.; Pellicciari-Di Liddo, L.; Di Fede, C.; Bellobono, I. R. *J. Chem. Soc., Perkin Trans. 2* **1984,** 589–593. doi:10.1039/p29840000589
29. Nishimura, N.; Tanaka, T.; Asano, M.; Sueishi, Y. *J. Chem. Soc., Perkin Trans. 2* **1986,** 1839–1845. doi:10.1039/p29860001839
30. Shin, D. M.; Whitten, D. G. *J. Am. Chem. Soc.* **1988,** *110,* 5206–5208. doi:10.1021/ja00223a058
31. Willner, I.; Rubin, S. *Angew. Chem., Int. Ed. Engl.* **1996,** *35,* 367–385. doi:10.1002/anie.199603671
32. Carter, F. L.; Siatkowski, H.; Wohltgen, H., Eds. *Molecular Electronics Devices;* Elsevier: Amsterdam, 1988.
33. Balzani, V.; Scandola, F., Eds. *Supramolecular Photochemistry;* Ellis Horwood: New York, 1991.
34. Feringa, B. L.; Jager, W. F.; de Lange, B. *Tetrahedron* **1993,** *49,* 8267–8310. doi:10.1016/S0040-4020(01)81913-X
35. Irie, M., Ed. *Photoreactive Materials for Ultrahigh-Density Optical Memory;* Elsevier: Amsterdam, 1994.
36. Yu, Y.; Nakano, M.; Ikeda, T. *Nature* **2003,** *425,* 145–146. doi:10.1038/425145a
37. Yager, K. G.; Barrett, C. J. Azobenzene Polymers as Photomechanical and Multifunctional Smart Materials. In *Intelligent Materials;* Shahinpoor, M.; Schneider, H.-J., Eds.; RSC Publishing: Cambridge, U.K., 2008; pp 424–446.
38. Ikeda, T.; Tsutsumi, O. *Science* **1995,** *268,* 1873–1875. doi:10.1126/science.268.5219.1873
39. Ikeda, T. *J. Mater. Chem.* **2003,** *13,* 2037–2057. doi:10.1039/b306216n
40. Shimoboji, T.; Larenas, E.; Fowler, T.; Kulkarni, S.; Hoffman, A. S.; Stayton, P. S. *Proc. Natl. Acad. Sci. U. S. A.* **2002,** *99,* 16592–16596. doi:10.1073/pnas.262427799
41. Feringa, B. L., Ed. *Molecular Switches;* Wiley-VCH: Weinheim, Germany, 2001.
42. Irie, M., Ed. Photochromism: Memories and Switches. *Chem. Rev.* **2000,** *100,* 1685–1890.
43. Hugel, T.; Holland, N. B.; Cattani, A.; Moroder, L.; Seitz, M.; Gaub, H. E. *Science* **2002,** *296,* 1103–1106. doi:10.1126/science.1069856
44. Balzani, V.; Credi, A.; Ferrer, B.; Silvi, S.; Venturi, M. *Top. Curr. Chem.* **2005,** *262,* 1–27. doi:10.1007/128_008
45. Kinbara, K.; Aida, T. *Chem. Rev.* **2005,** *105,* 1377–1400. doi:10.1021/cr030071r
46. Yamada, M.; Kondo, M.; Mamiya, J.; Yu, Y.; Kinoshita, M.; Barret, C. J.; Ikeda, T. *Angew. Chem., Int. Ed.* **2008,** *47,* 4986–4988. doi:10.1002/anie.200800760
47. Ichimura, K.; Oh, S.-K.; Nakagawa, M. *Science* **2000,** *288,* 1624–1626. doi:10.1126/science.288.5471.1624
48. Browne, W. R.; Pijper, D.; Pollard, M. M.; Feringa, B. L. Switching at the Nanoscale: Chiroptical Molecular Switches and Motors. In *Chirality at the Nanoscale;* Amabilino, D. B., Ed.; Wiley-VCH: Weinheim, Germany, 2009; pp 349–390. doi:10.1002/9783527625345.ch11
49. Merino, E. *Chem. Soc. Rev.* **2011,** *40,* 3835–3853. doi:10.1039/c0cs00183j
50. Zollinger, H. *Diazo Chemistry I. Aromatic and Heteroaromatic Compounds;* VCH: Weinheim, Germany, 1994.
51. Hegarty, A. F. Kinetics and mechanisms of reactions involving diazonium and diazo groups. In *The Chemistry of Diazonium and Diazo Groups, Part 2;* Patai, S., Ed.; Wiley: New York, 1978; pp 511–591.
52. Venkataraman, K., Ed. *The Chemistry of Synthetic Dyes;* Academic Press: New York, 1952; Vol. 1–7.
53. Szele, I.; Zollinger, H. *Top. Curr. Chem.* **1983,** *112,* 1–66. doi:10.1007/3-540-12396-2_5
54. Gordon, P. F.; Gregory, P. *Organic Chemistry in Colour;* Springer: New York, 1983; pp 95 ff.
55. Dugave, C.; Demange, L. *Chem. Rev.* **2003,** *103,* 2475–2532. doi:10.1021/cr0104375
56. El Halabieh, R. H.; Mermut, O.; Barrett, C. J. *Pure Appl. Chem.* **2004,** *76,* 1445–1465. doi:10.1351/pac200476071445
57. Natansohn, A.; Rochon, P. *Chem. Rev.* **2002,** *102,* 4139–4176. doi:10.1021/cr970155y
58. Yitzchaik, S.; Marks, T. J. *Acc. Chem. Res.* **1996,** *29,* 197–202. doi:10.1021/ar9501582
59. Schrader, T. E.; Schreier, W. J.; Cordes, T.; Koller, F. O.; Babitzki, G.; Denschlag, R.; Renner, C.; Löweneck, M.; Dong, S.-L.; Moroder, L.; Tavan, P.; Zinth, W. *Proc. Natl. Acad. Sci. U. S. A.* **2007,** *104,* 15729–15734. doi:10.1073/pnas.0707322104
60. Asanuma, H.; Liang, X.; Nishioka, H.; Matsunaga, D.; Liu, M.; Komiyama, M. *Nat. Protoc.* **2007,** *2,* 203–212. doi:10.1038/nprot.2006.465
61. Srinivas, O.; Mitra, N.; Surolia, A.; Jayaraman, N. *J. Am. Chem. Soc.* **2002,** *124,* 2124–2125. doi:10.1021/ja0173066
62. Guerrero, L.; Smart, O. S.; Weston, C. J.; Burns, D. C.; Woolley, G. A.; Allemann, R. K. *Angew. Chem., Int. Ed.* **2005,** *44,* 7778–7782. doi:10.1002/anie.200502666
63. Caamaño, A. M.; Vázquez, M. E.; Martínez-Costas, J.; Castedo, L.; Mascareñas, J. L. *Angew. Chem., Int. Ed.* **2000,** *39,* 3104–3107. doi:10.1002/1521-3773(20000901)39:17<3104::AID-ANIE3104>3.0.CO;2-0
64. Westmark, P. R.; Kelly, J. P.; Smith, B. D. *J. Am. Chem. Soc.* **1993,** *115,* 3416–3419. doi:10.1021/ja00062a003
65. Hohsaka, T.; Kawashima, K.; Sisido, M. *J. Am. Chem. Soc.* **1994,** *116,* 413–414. doi:10.1021/ja00080a064
66. Nakayama, K.; Endo, M.; Majima, T. *Chem. Commun.* **2004,** 2386–2387. doi:10.1039/b409844g
67. Willner, I.; Rubin, S.; Riklin, A. *J. Am. Chem. Soc.* **1991,** *113,* 3321–3325. doi:10.1021/ja00009a016
68. Dong, S.-L.; Löweneck, M.; Schrader, T. E.; Schreier, W. J.; Zinth, W.; Moroder, L.; Renner, C. *Chem.–Eur. J.* **2006,** *12,* 1114–1120. doi:10.1002/chem.200500986
69. Woolley, G. A.; Jaikaran, A. S. I.; Berezovski, M.; Calarco, J. P.; Krylov, S. N.; Smart, O. S.; Kumita, J. R. *Biochemistry* **2006,** *45,* 6075–6084. doi:10.1021/bi060142r
70. Renner, C.; Kusebauch, U.; Löweneck, M.; Milbradt, A. G.; Moroder, L. *J. Pept. Res.* **2005,** *65,* 4–14. doi:10.1111/j.1399-3011.2004.00203.x
71. Pieroni, O.; Fissi, A.; Angelini, N.; Lenci, F. *Acc. Chem. Res.* **2001,** *34,* 9–17. doi:10.1021/ar990141+
72. Renner, C.; Moroder, L. *ChemBioChem* **2006,** *7,* 868–878. doi:10.1002/cbic.200500531
73. Aaemissegger, A.; Kräutler, V.; van Gunsteren, W. F.; Hilvert, D. *J. Am. Chem. Soc.* **2005,** *127,* 2929–2936. doi:10.1021/ja0442567

74. Beharry, A. A.; Woolley, G. A. *Chem. Soc. Rev.* **2011,** *40,* 4422–4437. doi:10.1039/c1cs15023e
75. Sadovski, O.; Beharry, A. A.; Zhang, F.; Woolley, G. A. *Angew. Chem., Int. Ed.* **2009,** *48,* 1484–1486. doi:10.1002/anie.200805013
76. Beharry, A. A.; Sadovski, O.; Woolley, G. A. *J. Am. Chem. Soc.* **2011,** *133,* 19684–19687. doi:10.1021/ja209239m
77. Cruz, F. G.; Koh, J. T.; Link, K. H. *J. Am. Chem. Soc.* **2000,** *122,* 8777–8778. doi:10.1021/ja001804h
78. Stawski, P.; Sumser, M.; Trauner, D. *Angew. Chem., Int. Ed.* **2012,** *51,* 5748–5751. doi:10.1002/anie.201109265
79. Tochitsky, I.; Banghart, M. R.; Mourot, A.; Yao, J. Z.; Gaub, B.; Kramer, R. H.; Trauner, D. *Nat. Chem.* **2012,** *4,* 105–111. doi:10.1038/nchem.1234
80. Stawski, P.; Janovjak, H.; Trauner, D. *Bioorg. Med. Chem.* **2010,** *18,* 7759–7772. doi:10.1016/j.bmc.2010.09.012
81. Kramer, R. H.; Fortin, D. L.; Trauner, D. *Curr. Opin. Neurobiol.* **2009,** *19,* 544–552. doi:10.1016/j.conb.2009.09.004
82. Fehrentz, T.; Schönberger, M.; Trauner, D. *Angew. Chem., Int. Ed.* **2011,** *50,* 12156–12182. doi:10.1002/anie.201103236
83. Lien, L.; Jaikaran, D. C. J.; Zhang, Z.; Woolley, G. A. *J. Am. Chem. Soc.* **1996,** *118,* 12222–12223. doi:10.1021/ja962217s
84. Mourot, A.; Kienzler, M. A.; Banghart, M. R.; Fehrentz, T.; Huber, F. M. E.; Stein, M.; Kramer, R. H.; Trauner, D. *ACS Chem. Neurosci.* **2011,** *2,* 536–543. doi:10.1021/cn200037p
85. Hilf, R. J. C.; Bertozzi, C.; Zimmermann, I.; Reiter, A.; Trauner, D.; Dutzler, R. *Nat. Struct. Mol. Biol.* **2010,** *17,* 1330–1336. doi:10.1038/nsmb.1933
86. Kaufman, H.; Vratsanos, S. M.; Erlanger, B. F. *Science* **1968,** *162,* 1487–1489. doi:10.1126/science.162.3861.1487
87. Deal, W. J.; Erlanger, B. F.; Nachmansohn, D. *Proc. Natl. Acad. Sci. U. S. A.* **1969,** *64,* 1230–1234. doi:10.1073/pnas.64.4.1230
88. Banghart, M.; Borges, K.; Isacoff, E.; Trauner, D.; Kramer, R. H. *Nat. Neurosci.* **2004,** *7,* 1381–1386. doi:10.1038/nn1356
89. Volgraf, M.; Gorostiza, P.; Numano, R.; Kramer, R. H.; Isacoff, E. Y.; Trauner, D. *Nat. Chem. Biol.* **2006,** *2,* 47–52. doi:10.1038/nchembio756
90. Gorostiza, P.; Volgraf, M.; Numano, R.; Szobota, S.; Trauner, D.; Isacoff, E. Y. *Proc. Natl. Acad. Sci. U. S. A.* **2007,** *104,* 10865–10870. doi:10.1073/pnas.0701274104
91. Volgraf, M.; Gorostiza, P.; Szobota, S.; Helix, M. R.; Isacoff, E. Y.; Trauner, D. *J. Am. Chem. Soc.* **2007,** *129,* 260–261. doi:10.1021/ja067269o
92. Bredenbeck, J.; Helbing, J.; Kumita, J. R.; Woolley, G. A.; Hamm, P. *Proc. Natl. Acad. Sci. U. S. A.* **2005,** *102,* 2379–2384. doi:10.1073/pnas.0406948102
93. Guerrero, L.; Smart, O. S.; Woolley, G. A.; Allemann, R. K. *J. Am. Chem. Soc.* **2005,** *127,* 15624–15629. doi:10.1021/ja0550428
94. Beharry, A. A.; Wong, L.; Tropepe, V.; Woolley, G. A. *Angew. Chem., Int. Ed.* **2011,** *50,* 1325–1327. doi:10.1002/anie.201006506
95. Hunter, C. A.; Togrul, M.; Tomas, S. *Chem. Commun.* **2004,** 108–109. doi:10.1039/b311060e
96. Goodman, A.; Breinlinger, E.; Ober, M.; Rotello, V. M. *J. Am. Chem. Soc.* **2001,** *123,* 6213–6214. doi:10.1021/ja0032475
97. Pedersen, C. J. *J. Am. Chem. Soc.* **1967,** *89,* 2495–2496. doi:10.1021/ja00986a052
98. Pedersen, C. J. *J. Am. Chem. Soc.* **1967,** *89,* 7017–7036. doi:10.1021/ja01002a035
99. Vögtle, F.; Sieger, H.; Müller, W. M. *Top. Curr. Chem.* **1981,** *98,* 107–161. doi:10.1007/BFb0111247
100. Vögtle, F.; Müller, W. M.; Watson, W. H. *Top. Curr. Chem.* **1984,** *125,* 131–164. doi:10.1007/3-540-13569-3_4
101. Shinkai, S.; Manabe, O. *Host Guest Complex Chemistry, Macrocycles;* Springer-Verlag: Berlin, 1983.
102. Kimura, K.; Mizutani, R.; Suzuki, T.; Yokoyama, M. *J. Inclusion Phenom. Mol. Recognit. Chem.* **1998,** *32,* 295–310. doi:10.1023/A:1008075730071
103. Naemura, K.; Ueno, K.; Takeuchi, S.; Tobe, Y.; Kaneda, T.; Sakata, Y. *J. Am. Chem. Soc.* **1993,** *115,* 8475–8476. doi:10.1021/ja00071a078
104. Tamaoki, N.; Wada, M. *J. Am. Chem. Soc.* **2006,** *128,* 6284–6285. doi:10.1021/ja058398s
105. Fujimaki, M.; Matsuzawa, Y.; Hayashi, Y.; Ichimura, K. *Chem. Lett.* **1998,** *27,* 165–166. doi:10.1246/cl.1998.165
106. Kim, J. S.; Shon, O. J.; Lee, J. K.; Lee, S. H.; Kim, J. Y.; Park, K.-M.; Lee, S. S. *J. Org. Chem.* **2002,** *67,* 1372–1375. doi:10.1021/jo0108921
107. Gu, R.; Depraetere, S.; Kotek, J.; Budka, J.; Wagner-Wysiecka, E.; Biernat, J. F.; Dehaen, W. *Org. Biomol. Chem.* **2005,** *3,* 2921–2923. doi:10.1039/b507508d
108. Shinkai, S.; Minami, T.; Kusano, Y.; Manabe, O. *J. Am. Chem. Soc.* **1983,** *105,* 1851–1856. doi:10.1021/ja00345a029
109. Lahav, M.; Ranjit, K. T.; Katz, E.; Willner, I. *Chem. Commun.* **1997,** 259–260. doi:10.1039/a606189c
110. Jeong, K.-S.; Chang, K.-J.; An, Y.-J. *Chem. Commun.* **2003,** 1450–1451. doi:10.1039/b303269h
111. Norikane, Y.; Tamaoki, N. *Org. Lett.* **2004,** *6,* 2595–2598. doi:10.1021/ol049082c
112. Tamaoki, N.; Ogata, K.; Koseki, K.; Yamaoka, T. *Tetrahedron* **1990,** *46,* 5931–5942. doi:10.1016/S0040-4020(01)87918-7
113. Tamaoki, N.; Yamaoka, T. *J. Chem. Soc., Perkin Trans. 2* **1991,** 873–878. doi:10.1039/p29910000873
114. Tamaoki, N.; Yoshimura, S.; Yamaoka, T. *Thin Solid Films* **1992,** *221,* 132–139. doi:10.1016/0040-6090(92)90806-M
115. Asakawa, M.; Ashton, P. R.; Balzani, V.; Brown, C. L.; Credi, A.; Matthews, O. A.; Newton, S. P.; Raymo, F. M.; Shipway, A. N.; Spencer, N.; Quick, A.; Stoddart, J. F.; White, A. J. P.; Williams, D. J. *Chem.–Eur. J.* **1999,** *5,* 860–875. doi:10.1002/(SICI)1521-3765(19990301)5:3<860::AID-CHEM860>3.0.CO;2-K
116. Ballardini, R.; Balzani, V.; Credi, A.; Gandolfi, M. T.; Venturi, M. *Acc. Chem. Res.* **2001,** *34,* 445–455. doi:10.1021/ar000170g
117. Muraoka, T.; Kinbara, K.; Kobayashi, Y.; Aida, T. *J. Am. Chem. Soc.* **2003,** *125,* 5612–5613. doi:10.1021/ja034994f
118. Muraoka, T.; Kinbara, K.; Aida, T. *Chem. Commun.* **2007,** 1441–1443. doi:10.1039/b618248h
119. Muraoka, T.; Kinbara, K.; Aida, T. *Nature* **2006,** *440,* 512–515. doi:10.1038/nature04635
120. Muraoka, T.; Kinbara, K.; Wakamiya, A.; Yamaguchi, S.; Aida, T. *Chem.–Eur. J.* **2007,** *13,* 1724–1730. doi:10.1002/chem.200601098
121. Mitchell, G. R.; King, N. R. *Macromol. Symp.* **1999,** *137,* 155–165. doi:10.1002/masy.19991370116
122. Vives, G.; Tour, J. M. *Acc. Chem. Res.* **2009,** *42,* 473–487. doi:10.1021/ar8002317
123. Sasaki, T.; Tour, J. M. *Org. Lett.* **2008,** *10,* 897–900. doi:10.1021/ol703027h
124. Shirai, Y.; Sasaki, T.; Guerrero, J. M.; Yu, B.-C.; Hodge, P.; Tour, J. M. *ACS Nano* **2008,** *2,* 97–106. doi:10.1021/nn700294m

125. Angelos, S.; Johansson, E.; Stoddart, J. F.; Zink, J. I. *Adv. Funct. Mater.* **2007,** *17,* 2261–2271. doi:10.1002/adfm.200601217
126. Angelos, S.; Choi, E.; Vögtle, F.; De Cola, L.; Zink, J. I. *J. Phys. Chem. C* **2007,** *111,* 6589–6592. doi:10.1021/jp070721l
127. Lu, J.; Choi, E.; Tamanoi, F.; Zink, J. I. *Small* **2008,** *4,* 421–426. doi:10.1002/smll.200700903
128. Schäfer, L. V.; Müller, E. M.; Gaub, H. E.; Grubmüller, H. *Angew. Chem., Int. Ed.* **2007,** *46,* 2232–2237. doi:10.1002/anie.200604595
129. Pace, G.; Ferri, V.; Grave, C.; Elbing, M.; von Hänisch, C.; Zharnikov, M.; Mayor, M.; Rampi, M. A.; Samorì, P. *Proc. Natl. Acad. Sci. U. S. A.* **2007,** *104,* 9937–9942. doi:10.1073/pnas.0703748104
130. Ferri, V.; Elbing, M.; Pace, G.; Dickey, M. D.; Zharnikov, M.; Samorì, P.; Mayor, M.; Rampi, M. A. *Angew. Chem., Int. Ed.* **2008,** *47,* 3407–3409. doi:10.1002/anie.200705339
131. Green, J. E.; Choi, J. W.; Boukai, A.; Bunimovich, Y.; Johnston-Halperin, E.; DeIonno, E.; Luo, Y.; Sheriff, B. A.; Xu, K.; Shin, Y. S.; Tseng, H.-R.; Stoddart, J. F.; Heath, J. R. *Nature* **2007,** *445,* 414–417. doi:10.1038/nature05462
132. Carreño, M. C.; García, I.; Ribagorda, M.; Merino, E.; Pieraccini, S.; Spada, G. P. *Org. Lett.* **2005,** *7,* 2869–2872. doi:10.1021/ol050789o
133. Carreño, M. C.; García, I.; Nuñez, I.; Merino, E.; Ribagorda, M.; Pieraccini, S.; Spada, G. P. *J. Am. Chem. Soc.* **2007,** *129,* 7089–7100. doi:10.1021/ja070163o
134. Carreño, M. C.; Fernández Mudarra, G.; Merino, E.; Ribagorda, M. *J. Org. Chem.* **2004,** *69,* 3413–3416. doi:10.1021/jo0498011
135. Kahn, S. D.; Hehre, W. J. *J. Am. Chem. Soc.* **1986,** *108,* 7399–7400. doi:10.1021/ja00283a040
136. Peters, M. V.; Stoll, R. S.; Kühn, A.; Hecht, S. *Angew. Chem., Int. Ed.* **2008,** *47,* 5968–5972. doi:10.1002/anie.200802050
137. Stoll, R. S.; Peters, M. V.; Kühn, A.; Heiles, S.; Goddard, R.; Bühl, M.; Thiele, C. M.; Hecht, S. *J. Am. Chem. Soc.* **2009,** *131,* 357–367. doi:10.1021/ja807694s
138. Avellini, T.; Li, H.; Coskun, A.; Barin, G.; Trabolsi, A.; Basuray, A. N.; Dey, S. K.; Credi, A.; Silvi, S.; Stoddart, J. F.; Venturi, M. *Angew. Chem., Int. Ed.* **2012,** *51,* 1611–1615. doi:10.1002/anie.201107618
139. Haberhauer, G.; Kallweit, C. *Angew. Chem., Int. Ed.* **2010,** *49,* 2418–2421. doi:10.1002/anie.200906731

License and Terms

Beilstein Journal of Organic Chemistry

Design and synthesis of a photoswitchable guanidine catalyst

Philipp Viehmann and Stefan Hecht*

Full Research Paper

Open Access

Address:
Department of Chemistry, Humboldt-Universität zu Berlin, Brook-Taylor-Str. 2, 12489 Berlin, Germany

Email:
Stefan Hecht* - sh@chemie.hu-berlin.de

* Corresponding author

Keywords:
azobenzenes; guanidines; molecular switches; organocatalysis; photochromism; ring opening polymerization

Beilstein J. Org. Chem. **2012,** *8,* 1825–1830.
doi:10.3762/bjoc.8.209

Received: 11 July 2012
Accepted: 18 September 2012
Published: 24 October 2012

This article is part of the Thematic Series "Molecular switches and cages".

Guest Editor: D. Trauner

Abstract

A novel design as well as a straight-forward synthesis for a photoswitchable guanidine catalyst is reported. Intense studies of the photochromic properties demonstrated the reversible switchability of its photosensitive azobenzene moiety. Its activity in the ring-opening polymerization (ROP) of *rac*-lactide was investigated as well. The obtained results are discussed, and an additional guanidine was synthesized and utilized in the ROP of *rac*-lactide in order to explain the findings.

Introduction

The macroscopic properties of a given polymer, e.g., the glass-transition temperature, morphology, density and tensile strength, are strongly dependent on its microscopic structure. It is well known that this structure, which is characterized by parameters such as molecular weight and distribution, composition, regiochemistry and stereochemistry (tacticity), critically depends on the interaction between catalyst and monomer during the polymerization process. Gaining control over these processes has therefore been the subject of intense research efforts. With this in mind, chemists have recently started to incorporate gates into catalysts to control their action through external stimuli. The use of light as such an external, noninvasive, and well-controlled stimulus perhaps represents the most attractive approach to controlling catalytic activity and selectivity due to the attainable high spatio-temporal resolution [1]. In order to create such photoswitchable catalysts [2], photochromic moieties [3-5] have to be incorporated into the catalyst system [6-13]. To the best of our knowledge, successful examples of photoswitchable catalysts for the ring-opening polymerization (ROP) of lactide have not been reported thus far, although a remarkable example of a photocaged system has been reported [14].

Metal-based catalysts as well as organocatalysts have been widely studied in the ROP of lactide [15]. Guanidines, and especially 1,5,7-triazabicyclo[4.4.0]dec-5-ene (TBD), have

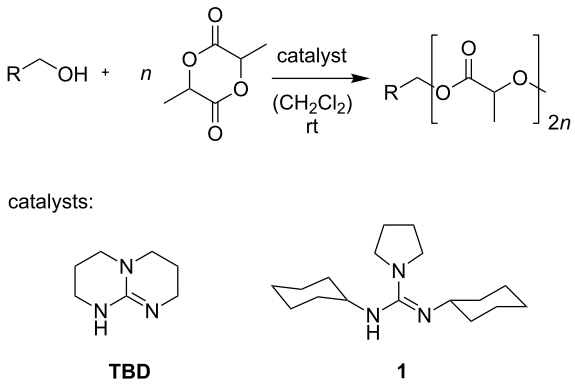

Scheme 1: Ring-opening polymerization (ROP) of lactide with TBD or the acyclic guanidine **1** as catalysts [16,18].

proven to be very powerful in this context (Scheme 1) [16]. However, due to the discussion of several polymerization mechanisms [17], TBD is a difficult target for the incorporation of photoresponsive switches. Recent work indicates that the activation mechanism for acyclic guanidines, such as guanidine **1** (Scheme 1), is strongly dependent on the formation of hydrogen bridges to monomer and initiator [18]. Note that with pyrenebutanol as the initiator, 200 repeat units are grown within 20 s by using TBD as the catalyst, while 1 h is needed with the acyclic guanidine **1** to reach the same average chain length.

Based on this finding it should be possible to create a catalyst that may be deactivated by formation of intramolecular hydrogen bonds to an acceptor (A) and activated by light-triggered dissociation of such intramolecular hydrogen bonds (Scheme 2). Herein, we report the synthesis of the first photoswitchable guanidine, as well as its photochromic behavior.

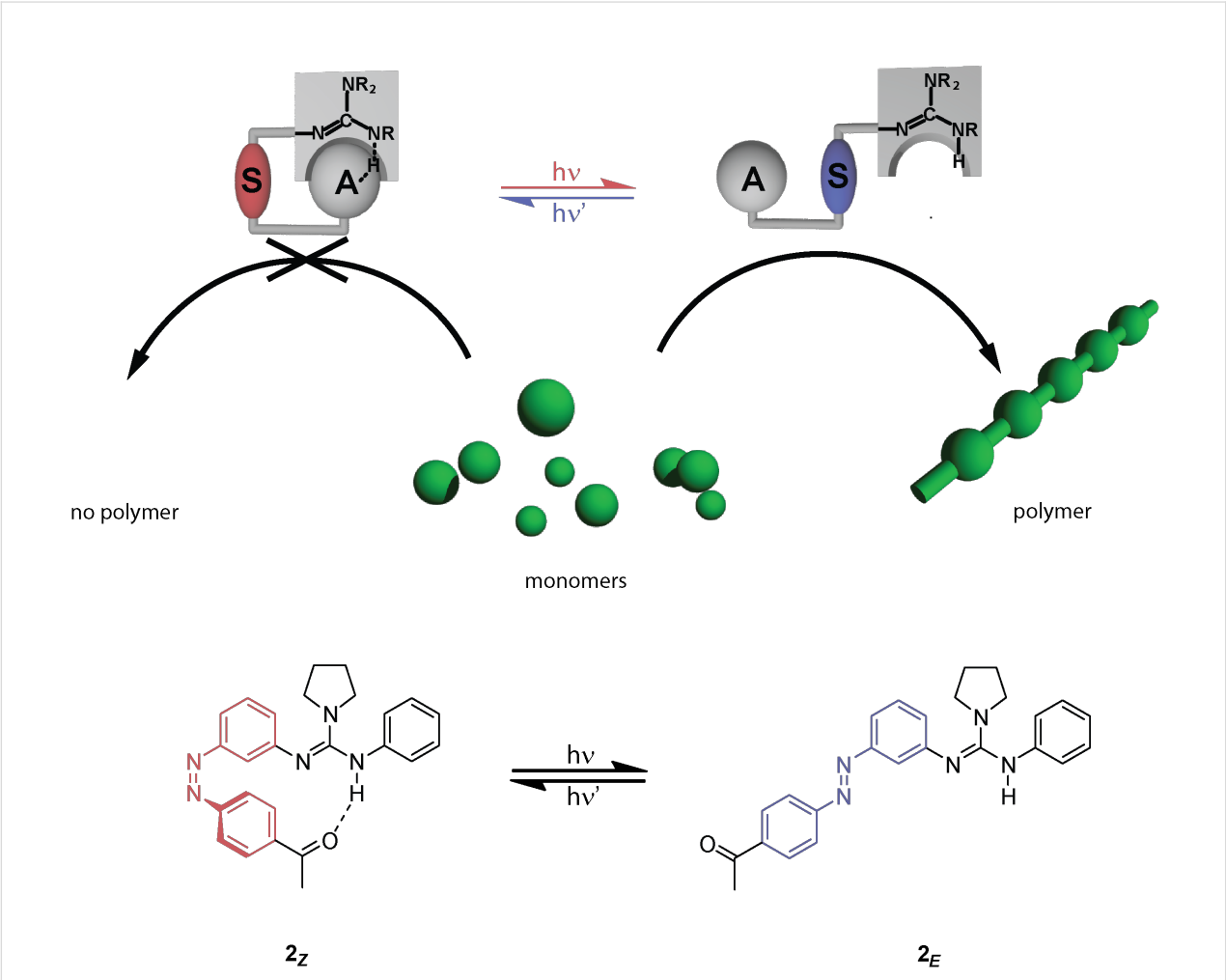

Scheme 2: Illustration of a photoswitchable guanidine catalyst for the ROP of lactide and the corresponding target structures $\mathbf{2}_Z$ and $\mathbf{2}_E$ (S = switching unit, A = H-bond acceptor).

Upon irradiation, the incorporated azobenzene is supposed to undergo photoinduced $E \rightarrow Z$ isomerization, allowing the Brønsted acceptor, in this case a ketone, to form a hydrogen-bridge to the proton of the guanidine.

Results and Discussion

The synthesis of guanidine $\mathbf{2}_{\boldsymbol{E}}$ (Scheme 3) was accomplished starting from phenylisocyanate (**3**) and 3-nitroaniline (**6**). The latter was converted by known procedures into its corresponding nitroso derivative **7** [19], followed by a Mills coupling with 4-aminoacetophenone (**8**) to give azobenzene **9** in 93% yield over two steps. Nitroazobenzene **9** was transformed into its amino derivative **10** by catalytic hydrogenation. Note that under the employed conditions reduction of the azobenzene function of compound **9** was observed, yet the formed hydrazine analogue reoxidized in situ upon being stirred under atmospheric conditions (air). The free amine **10** finally reacts with the in situ prepared Vilsmeyer salt **5** to provide the desired target compound $\mathbf{2}_{\boldsymbol{E}}$. The therefore necessary urea **4** can be obtained from the addition of pyrrolidine to phenylisocyanate (**3**).

The structure of guanidine $\mathbf{2}_{\boldsymbol{E}}$ was proven by NMR spectroscopy, HRMS, as well as by single-crystal X-ray structure analysis (Figure 1). To our knowledge, this is the first example of an X-ray analysis of an acyclic guanidine–methanol adduct, clearly proving the existence of a hydrogen bridge between an alcohol OH function and the nitrogen of the guanidine. This significantly supports the mechanism of alcohol activation in the polymerization process. Additionally, the crystal structure confirms the validity of our concept, illustrating the azobenzene's utilization as a spacer by spatial separation of the guanidine core and carbonyl function.

In order to utilize the incorporated light-sensitive azobenzene functionality, the photochromic behavior of guanidine **2** was

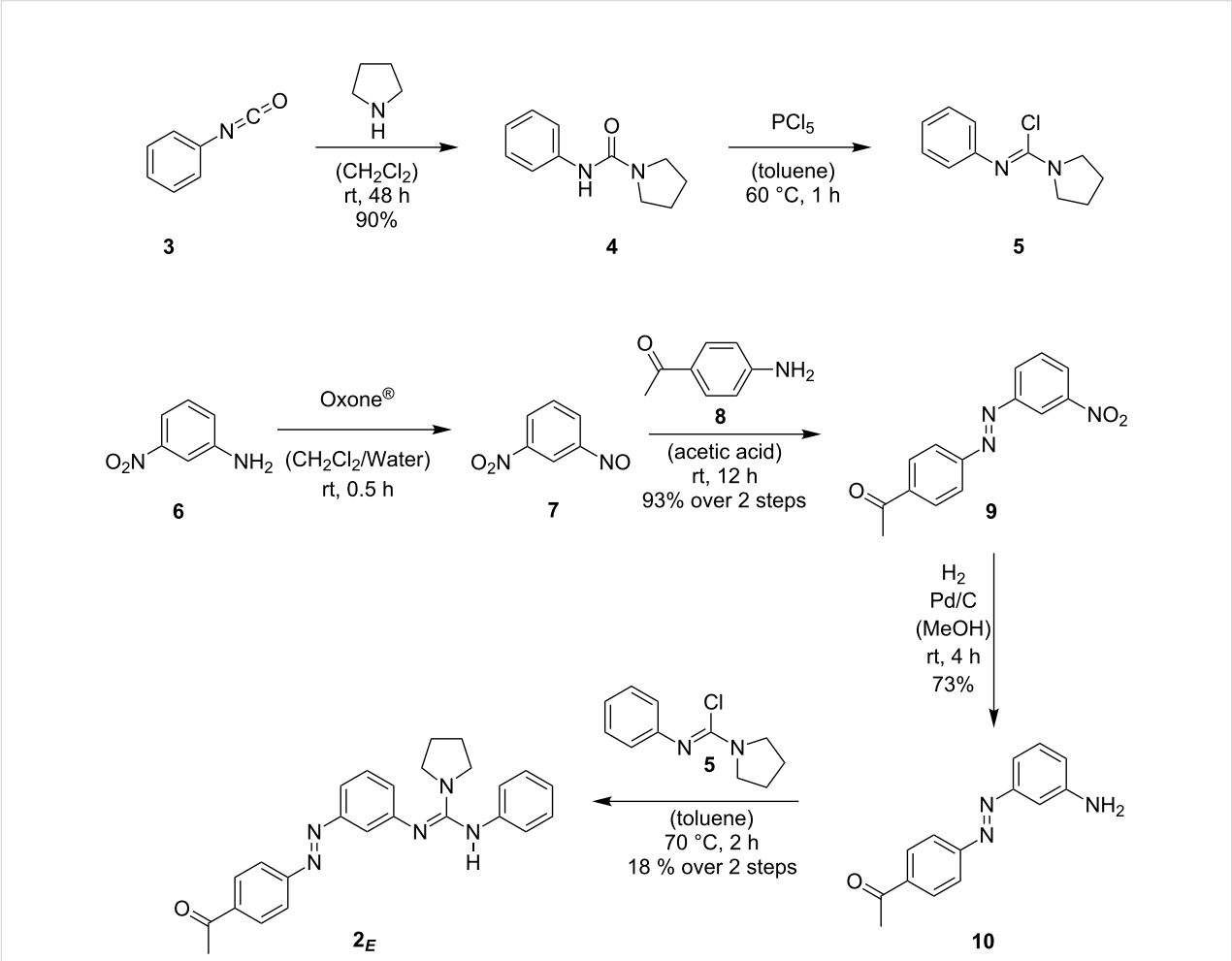

Scheme 3: Synthesis of guanidine $\mathbf{2}_{\boldsymbol{E}}$.

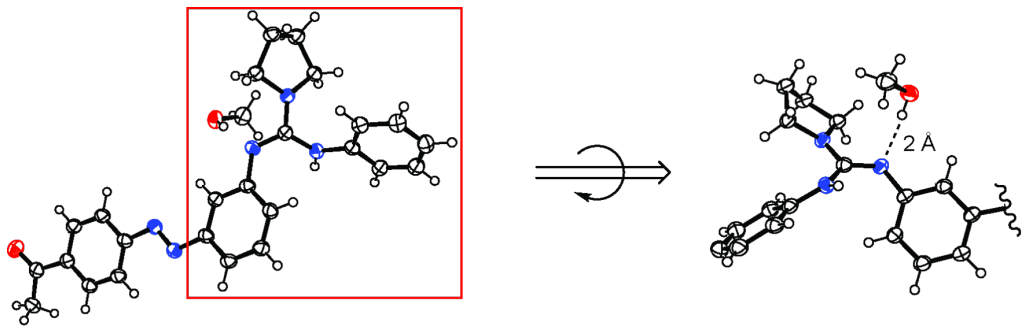

Figure 1: ORTEP image of the single-crystal X-ray structure of guanidine $\mathbf{2}_E$, as well as a rotated close-up of the guanidine moiety, showing 50% thermal ellipsoids (CCDC 891016).

investigated by UV–vis spectroscopy (Figure 2). The UV–vis spectrum of guanidine $\mathbf{2}_E$ in acetonitrile exhibits the expected behavior, similar to the unsubstituted parent azobenzene, i.e., a low intensity n→π* band in the visible region and a much stronger π→π* band in the UV region of the spectrum. Note that the n→π* band partially overlaps with the π→π* band in the (*E*)-isomer. Upon irradiation at 340 nm (Figure 2a), the π→π* band of the isomer $\mathbf{2}_E$ at 326 nm vanishes and the π→π* band of the isomer $\mathbf{2}_Z$ with its blue-shifted maximum at 273 nm appears. The content of isomer $\mathbf{2}_Z$ in the photostationary state (pss) was determined to amount to 61% by UPLC using a detection wavelength on the isosbestic point (290 nm). Based on this

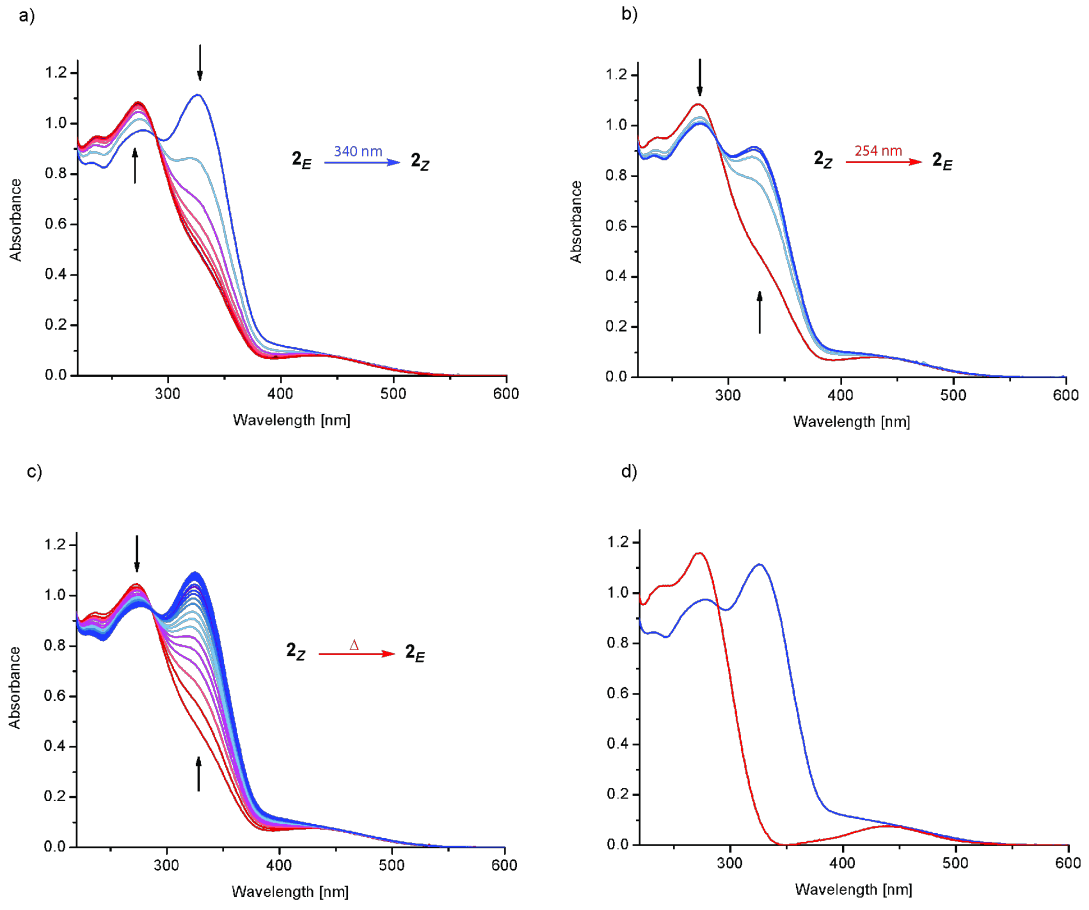

Figure 2: UV–vis spectra of guanidine **2** in acetonitrile, $c = 3.9 \cdot 10^{-5}$ mol/L. (a) *E*→*Z* isomerization with irradiation at 340 nm, 25 °C; (b) *Z*→*E* isomerization with irradiation at 254 nm, 25 °C; (c) thermal *Z*→*E* isomerization at 40 °C; (d) spectra of $\mathbf{2}_E$ (blue) and $\mathbf{2}_Z$ (calculated, red).

data, the UV–vis spectrum of the isomer $\mathbf{2}_{\boldsymbol{Z}}$ was calculated (Figure 2d), assuming that the total absorption is the sum of the partial absorptions. Obviously, the significant hypsochromic shift of the π→π* band leads to a separation of the n→π* and π→π* bands for the (*Z*)-isomer. As expected, an inverse behavior is observed upon irradiation at 254 nm, inducing photoisomerization of guanidine $\mathbf{2}_{\boldsymbol{Z}}$ back to its precursor $\mathbf{2}_{\boldsymbol{E}}$ (Figure 2b). The amount of isomer $\mathbf{2}_{\boldsymbol{E}}$ in the resulting pss was determined to be 94%. The same nearly quantitative *Z*→*E* photoisomerization, giving 92% of $\mathbf{2}_{\boldsymbol{E}}$ in the pss, is obtained upon irradiation at 430 nm.

Related to the supposed function of guanidine as a switchable catalyst, these experiments demonstrate the reversible photoisomerization of the azobenzene moiety. Nevertheless, the switching properties can still be improved, in particular to obtain a pss with higher (*Z*)-content in the *E*→*Z* photoisomerization. Besides the photo-induced *Z*→*E* isomerization, the thermal back-reaction of guanidine $\mathbf{2}_{\boldsymbol{Z}}$ was examined as well (Figure 2c). Based on the measured UV–vis and UPLC data and assuming a first-order rate law, the rate constant of the thermal *Z*→*E* isomerization at 40 °C was determined to be $k_{(40\ °C)} = 6.3{\cdot}10^{-5}\ s^{-1}$ corresponding to a half-life of $\tau_{1/2}$ = 3 h. The measurement at slightly elevated temperature (40 °C) was necessary since at 25 °C the thermal half-life increases significantly (Supporting Information File 1, Figure S-5), leading to distinct difficulties in its determination, e.g., the evaporation of the solvent and the resulting change in concentration. Therefore, the rate constant and thermal half-life at 25 °C could only be estimated by using data points from the first 36 h (Supporting Information File 1, Figure S-6) yielding $k_{(25\ °C)} = 4.2{\cdot}10^{-6}\ s^{-1}$ and $\tau_{1/2}$ = 46 h. Consequently, the half-life significantly exceeds the expected duration of the polymerization reaction [18], rendering guanidine **2** very attractive for this purpose. In summary, the observed photochromic behavior detailed above indicates promising properties for the utilization of guanidine **2** as a photoswitchable catalyst.

In order to determine the activity of the catalyst, the crystal-bound methanol was removed and guanidine $\mathbf{2}_{\boldsymbol{E}}$ was utilized in the ROP of *rac*-lactide with pyrenebutanol as the initiator. In a catalyst/initiator/monomer ratio of 1:1:100 no significant formation of polylactide was observed at rt even after 48 h. The absence of reactivity for guanidine $\mathbf{2}_{\boldsymbol{E}}$ in the ROP of *rac*-lactide may have various origins. First of all, it is obvious that in comparison with catalytically active guanidine **1**, the two cyclohexane substituents on the nitrogen atoms of guanidine are replaced by aromatic residues, which, at least in one case, is necessary for connecting the photochromic azobenzene moiety to the guanidine core. This replacement most likely results in a significant reduction of the basicity of guanidine. Additionally, the acceptor ketone moiety itself may interact with the initiator or the active end of the polymer chain, thereby interfering with catalysis. In order to examine the latter, guanidine **11** was synthesized from Vilsmeyer salt **13** and aniline and tested in the ROP of *rac*-lactide (Scheme 4). The morpholino substituent was introduced to improve the crystallization behavior of guanidine and should not affect the polymerization.

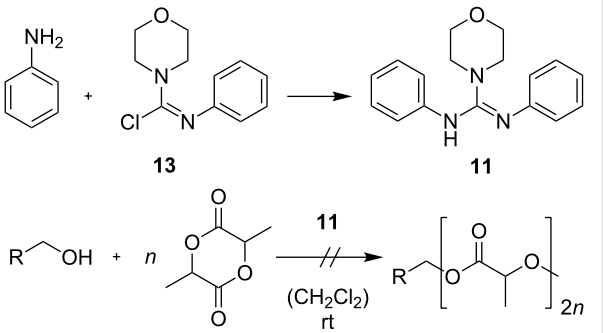

Scheme 4: Guanidine **11** as a catalyst in the ROP of *rac*-lactide (catalyst/initiator/monomer ratio = 10:1:100).

In a catalyst/initiator/monomer ratio of 10:1:100 with pyrenebutanol as initiator no significant formation of polylactide was observed at rt even after 48 h. This indicates that the catalytic inactivity of guanidine $\mathbf{2}_{\boldsymbol{E}}$ is indeed caused by the guanidine core itself. Besides the previously mentioned basicity issue, a possible reason for this behavior may be discerned from the single-crystal X-ray structure analysis of guanidine $\mathbf{2}_{\boldsymbol{E}}$. It can be seen that, in contrast to the supposed polymerization mechanism (Figure 3a) [18], the lone pair of the nitrogen and the hydrogen of the adjacent nitrogen are not arranged in a parallel manner, i.e., unidirectional facing the substrates (Figure 3b). If the observed conformation is not caused by stacking effects in the solid state and prevails in solution, it may substantially lower the catalytic activity of the guanidines $\mathbf{2}_{\boldsymbol{E}}$ and **11**.

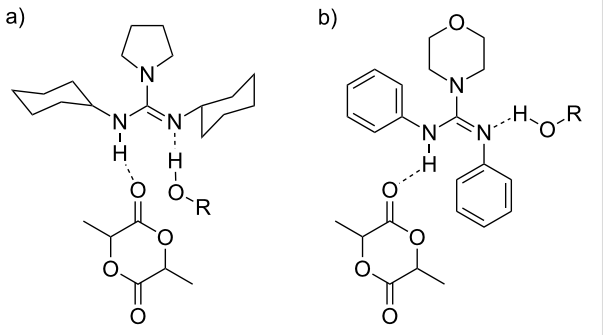

Figure 3: Supposed intermediates resulting from either a cyclohexane-substituted guanidine (a) [18] or an aromatic substituted guanidine (b) with an alcohol and lactide.

Conclusion

In summary, we developed a new approach to the design and synthesis of the novel, photoswitchable guanidine **2**. After detailed investigation of its photochromic properties and demonstrating its reversible, light-induced switchability, we started to investigate the reasons for its inactivity in the ROP of lactide. Our efforts are now directed toward the improvement of the design of the catalyst by exchanging one aromatic residue with an alkyl substituent to improve the basicity of guanidine, as well as by introducing sterically crowded substituents or ring constraints in order to direct the position of the relevant lone pair of guanidine as well as the NH-function.

Supporting Information

The crystal structure has been deposited at the Cambridge Crystallographic Data Centre and allocated the deposition number CCDC 891016.

Supporting Information File 1

Experimental details and spectra.
[http://www.beilstein-journals.org/bjoc/content/supplementary/1860-5397-8-209-S1.pdf]

Acknowledgements

We thank Stefan Mebs (HU Berlin) for carrying out the single-crystal X-ray analysis. Generous support by the German Research Foundation (DFG via SPP 1178) and the European Science Foundation (ESF via P2M) is gratefully acknowledged. We thank BASF AG, Bayer Industry Service, and Sasol Germany for donations of chemicals.

References

1. Russew, M.-M.; Hecht, S. *Adv. Mater.* **2010,** *22,* 3348–3360. doi:10.1002/adma.200904102
2. Stoll, R. S.; Hecht, S. *Angew. Chem., Int. Ed.* **2010,** *49,* 5054–5075. doi:10.1002/anie.201000146
3. Dürr, H.; Bouas-Laurent, H., Eds. *Photochromism: Molecules and Systems,* Revised Edition ed.; Elsevier: Amsterdam, 2003.
4. Feringa, B. L., Ed. *Molecular Switches,* 2nd ed.; Wiley-VCH: Weinheim, Germany, 2001.
5. Crano, J. C.; Guglielmetti, R. J., Eds. *Organic Photochromic and Thermochromic Compounds;* Plenum Publishers: New York, 1999.
6. Peters, M. V.; Stoll, R. S.; Kühn, A.; Hecht, S. *Angew. Chem., Int. Ed.* **2008,** *47,* 5968–5972. doi:10.1002/anie.200802050
7. Stoll, R. S.; Hecht, S. *Org. Lett.* **2009,** *11,* 4790–4793. doi:10.1021/ol902166a
8. Stoll, R. S.; Peters, M. V.; Kuhn, A.; Heiles, S.; Goddard, R.; Bühl, M.; Thiele, C. M.; Hecht, S. *J. Am. Chem. Soc.* **2009,** *131,* 357–367. doi:10.1021/ja807694s
9. Ueno, A.; Takahashi, K.; Osa, T. *J. Chem. Soc., Chem. Commun.* **1981,** 94–96. doi:10.1039/C39810000094
10. Lee, W.-S.; Ueno, A. *Macromol. Rapid Commun.* **2001,** *22,* 448–450. doi:10.1002/1521-3927(20010301)22:6<448::AID-MARC448>3.0.CO;2-W
11. Würthner, F.; Rebek, J., Jr. *Angew. Chem., Int. Ed. Engl.* **1995,** *34,* 446–450. doi:10.1002/anie.199504461
12. Würthner, F.; Rebek, J. *J. Chem. Soc., Perkin Trans. 2* **1995,** 1727–1734. doi:10.1039/P29950001727
13. Cacciapaglia, R.; Di Stefano, S.; Mandolini, L. *J. Am. Chem. Soc.* **2003,** *125,* 2224–2227. doi:10.1021/ja029331x
14. Sun, X.; Gao, J. P.; Wang, Z. Y. *J. Am. Chem. Soc.* **2008,** *130,* 8130–8131. doi:10.1021/ja802816g
15. Dechy-Cabaret, O.; Martin-Vaca, B.; Bourissou, D. *Chem. Rev.* **2004,** *104,* 6147–6176. doi:10.1021/cr040002s
16. Pratt, R. C.; Lohmeijer, B. G. G.; Long, D. A.; Waymouth, R. M.; Hedrick, J. L. *J. Am. Chem. Soc.* **2006,** *128,* 4556–4557. doi:10.1021/ja060662+
17. Chuma, A.; Horn, H. W.; Swope, W. C.; Pratt, R. C.; Zhang, L.; Lohmeijer, B. G. G.; Wade, C. G.; Waymouth, R. M.; Hedrick, J. L.; Rice, J. E. *J. Am. Chem. Soc.* **2008,** *130,* 6749–6754. doi:10.1021/ja0764411
18. Zhang, L.; Pratt, R. C.; Nederberg, F.; Horn, H. W.; Rice, J. E.; Waymouth, R. M.; Wade, C. G.; Hedrick, J. L. *Macromolecules* **2010,** *43,* 1660–1664. doi:10.1021/ma901776x
19. Priewisch, B.; Rück-Braun, K. *J. Org. Chem.* **2005,** *70,* 2350–2352. doi:10.1021/jo048544x

License and Terms

Beilstein Journal of Organic Chemistry

Design and synthesis of quasi-diastereomeric molecules with unchanging central, regenerating axial and switchable helical chirality via cleavage and formation of Ni(II)–O and Ni(II)–N coordination bonds

Vadim A. Soloshonok*[1,2], José Luis Aceña[1], Hisanori Ueki[3] and Jianlin Han[4]

Full Research Paper

Open Access

Address:
[1]Department of Organic Chemistry I, Faculty of Chemistry, University of the Basque Country, 20018 San Sebastián, Spain, [2]IKERBASQUE, Basque Foundation for Science, 48011 Bilbao, Spain, [3]International Center for Materials Nanoarchitectonics (MANA), National Institute for Materials Science (NIMS), 1-1, Namiki, Tsukuba, Ibaraki 305-0044, Japan and [4]School of Chemistry and Chemical Engineering, Nanjing University, Nanjing, 210093, China

Email:
Vadim A. Soloshonok* - vadym.soloshonok@ehu.es

* Corresponding author

Keywords:
axial chirality; central chirality; chiral switches; coordination bonds; functional materials; helical chirality; modular structural design; molecular devices

Beilstein J. Org. Chem. **2012,** *8,* 1920–1928.
doi:10.3762/bjoc.8.223

Received: 09 August 2012
Accepted: 29 October 2012
Published: 13 November 2012

This article is part of the Thematic Series "Molecular switches and cages".

Guest Editor: D. Trauner

Abstract

We describe herein the design and synthesis of asymmetric, pentadentate ligands, which are able to coordinate to Ni(II) cations leading to quasi-diastereomeric complexes displaying two new elements of chirality: stereogenic axis and helix along with configurational stabilization of the stereogenic center on the nitrogen. Due to the stereocongested structural characteristics of the corresponding Ni(II) complexes, the formation of quasi-diastereomeric products is highly stereoselective providing formation of only two, (R_a*,M_h*,R_c*) and (R_a*,P_h*,R_c*), out of the four possible stereochemical combinations. The reversible quasi-diastereomeric transformation between the products (R_a*,M_h*,R_c*) and (R_a*,P_h*,R_c*) occurs by intramolecular trans-coordination of Ni–NH and Ni–O bonds providing a basis for a chiral switch model.

Introduction

The design and synthesis of organic molecules for which the changing of their three-dimensional structure or function can be predicted, is a fast-growing multidisciplinary field of research [1-13]. In particular, organic compounds that can undergo reversible diastereomeric transformations are considered as the most promising models for the development of molecular switches with nondestructive read out of the optical information [14-18]. Taking into account the issue of fatigue resistance

or durability of a potential molecular switch, the newly emerging design strategies make use of the formation and cleavage of metal–ligand coordination bonds as a basis for a chiral conformational switch in the conformationally restricted molecular backbone [19-23]. Here, we would like to describe a new design and synthesis of quasi-diastereomeric molecules with unchanging central, regenerating axial, and switchable helical chirality, through cleavage/formation of Ni(II)–O and Ni(II)–N coordination bonds.

Recently, we introduced a new approach to the design of organic molecules with switchable chirality by simple cleavage and formation of metal–ligand coordination bonds, as a potentially useful and conceptually new model for the development of a new generation of organic chiroptical molecular switches [24,25]. Thus, achiral C_2-symmetric pentadentate ligands **1** were able to coordinate with d^8 metals [Ni(II) or Pd(II)] to form tetra-coordinated diastereomeric complexes (R_a*,P_h*,S_c*)-**2** and (R_a*,M_h*,R_c*)-**3**, which contain at least three elements of chirality, namely stereogenic center, axis and helix (Scheme 1). The structure of these complexes incorporated two five- and one six-membered ring displaying a square-planar geometry. It is worth mentioning that only two out of the four possible diastereomeric complexes were accessed in a highly stereoselective manner, as a result of the intrinsic steric hindrance associated with the design of achiral ligands **1**. In addition, crystallization of the diastereomeric mixtures resulted in the formation of a single diastereomer (R_a*,P_h*,S_c*)-**2** or (R_a*,M_h*,R_c*)-**3** in the solid state, depending on the nature of the chelating metal (Ni or Pd) employed.

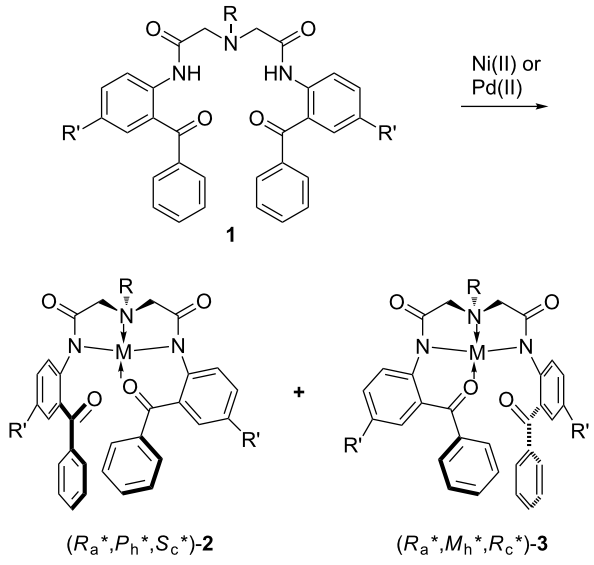

Scheme 1: Previous design of diastereomeric molecules **2** and **3** with switchable chirality starting from achiral, C_2-symmetric pentadentate ligands **1**.

In this context, we subsequently envisioned the design and synthesis of structurally related complexes in which the chiral switch will be based on trans-coordination of nonsymmetric ligands (Scheme 2).

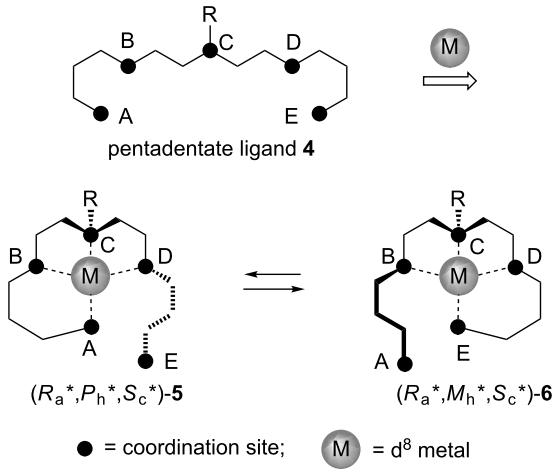

Scheme 2: General design of asymmetric pentadentate ligands **4** and chiroptically switchable quasi-diastereomeric molecules **5** and **6**, possessing elements of central, axial and helical chirality.

The major difference of the general design presented in Scheme 2 with the previously reported models (Scheme 1) is that the starting pentadentate ligand **4** is asymmetric and therefore already possesses the stereogenic center at the coordination site **C**. It is assumed that the pentadentate ligand **4** upon coordination with d^8 metals will give rise to tetra-coordinated square-planar complexes **5** and **6**. The presence of coordinated and noncoordinated groups **A** and **E**, positioned up or down relative to the metal coordination plane, will create an element of axial chirality, directed through the coordination sites **D** in complex **5** and **B** in **6**, and the corresponding adjacent methylenes of the chelating five-membered rings. The second, newly created element of chirality may be provided by steric repulsive interactions in the arms **BA**/**DE**, which will twist the six-membered chelating ring resulting in a screw sense of helical chirality. The transcoordination motion in these complexes is expected to be controlled in a way that noncoordinated sites, i.e., **E** in **5** and **A** in **6**, will move up and down, respectively, resulting in the interconversion of complexes **5** and **6**. This assumed concurrent and unidirectional motion of arms **ED** and **AB** is expected to have the following desired stereochemical consequences: Thus, the axial chirality on the arm **CDE** in **5** will disappear with simultaneous generation of a new chiral axis on the arm **CBA** in **6**, of the same stereochemical sense. Next, this envisioned mode of transcoordination must proceed also with a loss and regeneration of helical chirality, but, in contrast to the loss/regeneration of axial chirality, with the inversion of

the stereochemical sense, providing quasi-diastereomeric relationships between complexes **5** and **6** [26].

As one can expect, these desired structural and stereochemical considerations can be seriously compromised by the presence of central chirality in the starting ligand **4**. For instance, application of racemic ligands **4** will give rise to at least four diastereomeric products rendering the designed diastereomeric intertransformation with switchable chirality simply pointless. Furthermore, application of enantiomerically pure ligands **4** can present a problem of mismatched stereochemical preferences between the existing central and newly generated set of axial and helical chirality. On the other hand, if the stereogenic center in ligands **4** is configurationally flexible (can easily undergo (*S*) to (*R*) transformation) one may expect the opposite trend, as the combined stereochemical preferences of axial and helical chirality will impose the corresponding matching configuration of the stereogenic center. Thus, the geometric difference between the designed quasi-diastereomers **5** and **6** is that the noncoordinated arm **CDE** and the substituent R on the stereogenic coordination site **C** in **5** are on the same side of the metal chelation plane, while in structure of **6** the arm **CBA** and the substituent R are on the opposite sides. In contrast, the geometric relations between the off-plane six-membered chelate rings, giving rise to helical chirality, and the substituent R are the same in both quasi-diastereomers **5** and **6**. Considering these geometric features, one may expect that the actual absolute configuration of the stereogenic center **C**, determined by the stereochemical priority of the groups **A** and **E**, has no importance for the quasi-diastereomeric relationships between **5** and **6**. Consequently, there is a good chance that the geometric position of the substituent R, and therefore the relative configuration of the stereogenic center on **C**, may be efficiently controlled by the matching stereochemical preferences between the axial and helical chirality in the quasi-diastereomers **5** and **6**. However, to realize this possibility the stereogenic center **C** in ligands **4** should be configurationally unstable and easily adaptable to the developing stereochemical environment upon its configurational stabilization in complexes **5** and **6**.

Results and Discussion

To build the real molecules to this design, we explored the preparation of imino–carbonyl ligands **13** (Scheme 3) by desymmetrization of achiral carbonyl–carbonyl ligands **12**. Compounds **12** were prepared in the framework of our recently described methodology for applying a new generation of nucleophilic glycine equivalents [27-32] to a general asymmetric synthesis of α-amino acids [33-38]. In this manner, modular assembly of achiral C_2-symmetric pentadentate ligands **12** was carried out by using three inexpensive and readily available starting structural units. First, the "phenone" modules **7** were reacted [39] with "acid" module **8** to form the corresponding amides **9** in quantitative chemical yield. Application of compounds **9** for bis-alkylation of "amine" module **10** was conducted in two separate steps including isolation and purification of the intermediate products **11**. The undesired formation of the corresponding quaternary ammonium salts was not observed [40] and the target ligands **12** were prepared in high overall yield (96%).

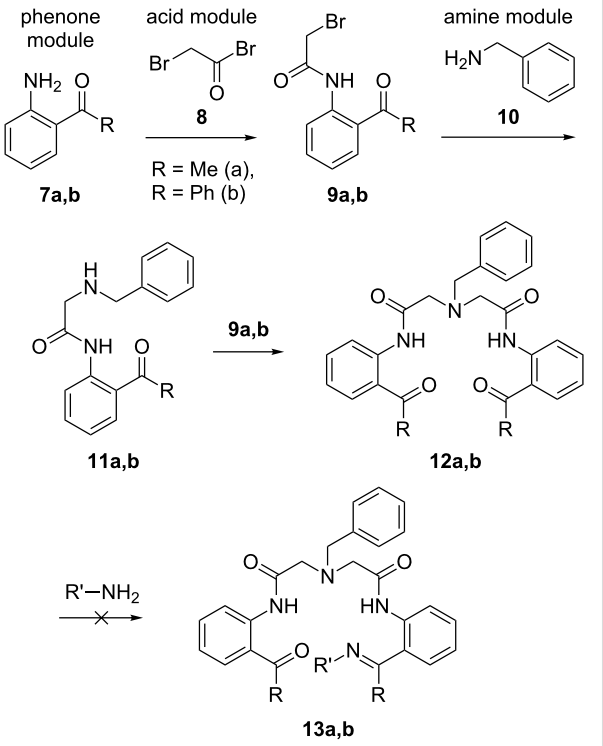

Scheme 3: Preparation of imino–carbonyl ligands **13** by desymmetrization of achiral carbonyl–carbonyl ligands **12**.

Surprisingly, we found that the seemingly simple transformation of **12** to **13** can present a significant synthetic problem. Thus, our attempts to prepare the desired mono-imino ligands **13** from compounds **12**, using one equivalent of various amines, resulted in the formation of complex mixtures of inseparable products. Possible reasons for this outcome are the presence of two potentially reactive amide groups and the multifunctional nature of compounds **12**. In particular, preparation of the most desirable NH-containing (R' = H) derivatives **13**, by reaction of **12** with ammonia or its derivatives, was not possible at all. Modification of the synthetic scheme with installation of the imino functionality on intermediate stages also gave inacceptable results, probably due to hydrolytic liability of the corresponding imino derivatives of, for instance, compounds **9** and **11**.

While these unexpected synthetic obstacles can, probably, be overcome with a more extensive search for optimized conditions, we decided to take advantage of our experience in the chemistry of Ni(II)-chelated amino acid Schiff bases [41-48] and to develop an indirect approach for the preparation of asymmetric ligands of type **13**. To this goal, we studied the reactions of biscarbonyl compounds **12** with glycine.

As shown in Scheme 4, heating of pentadentate ligands **12** in acetonitrile in the presence of a Ni(II) source [$NiCl_2$ or $Ni(NO_3)_2$], glycine and a base, lead to the formation of the quite unusual complexes **14**. In a similar manner, by using $PdCl_2$ instead of Ni(II), the Pd-chelated complex **15** was obtained. As it follows from these results, only one carbonyl group in the starting ligands **12** was involved in the formation of the corresponding Schiff base with glycine, similar to the reactivity observed for tridentate ligands with Ni(II) [49-53]. In the ^1H and ^{13}C NMR spectra of compounds **14** and **15**, resonances of aromatic and aliphatic hydrogens and carbons appear as sharp peaks indicating that the extra bidentate moiety in complexes **14** and **15** acts merely as a substituent and does not compete for coordination with Ni(II). Complexes **14** are red-colored, **15** is yellow, and both are neutral, highly crystalline compounds (mp > 250 °C), good solubility in organic solvents, and can be easily purified by regular column chromatography on SiO_2.

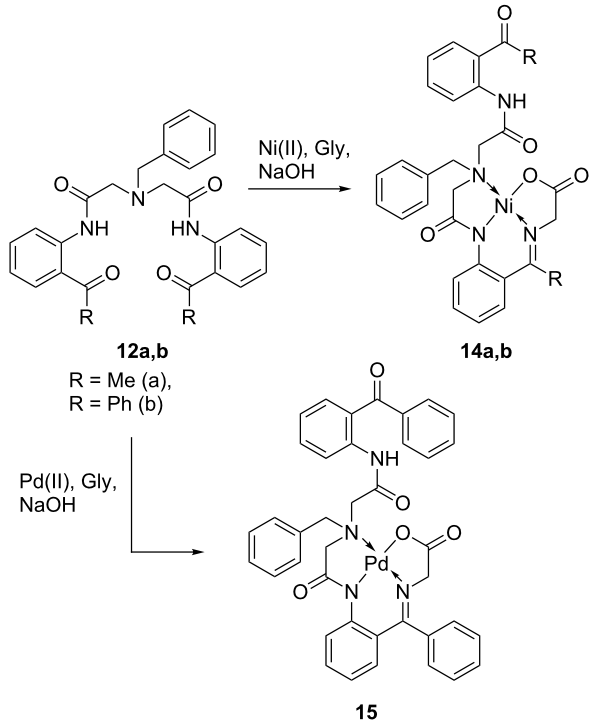

Scheme 4: Preparation of complexes **14a**,**b** and **15** by reactions of ligands **12** with glycine.

To receive more precise data about the structure of complexes **14** and **15** we performed crystallographic analysis of compound **14a** [54] (Figure 1). Quite surprisingly, we found that in the solid state (monoclinic crystal system, space group $P2_1/n$) complex **14a** has three elements of chirality: stereogenic center [N(2)], axis [N(1)–C(8) bond] and helix (off-plane position of the chelate rings). While these three elements of chirality can give up to four possible diastereomeric combinations, only one diastereomer, as a pair of (R_c,R_a,P_h) and (S_c,S_a,M_h) enantiomers, was found in the crystallographic unit cell. This fact clearly suggested that the observed set of stereochemical preferences is a result of a mutual match between these three elements of chirality giving rise to the most stable diastereomeric stereochemistry.

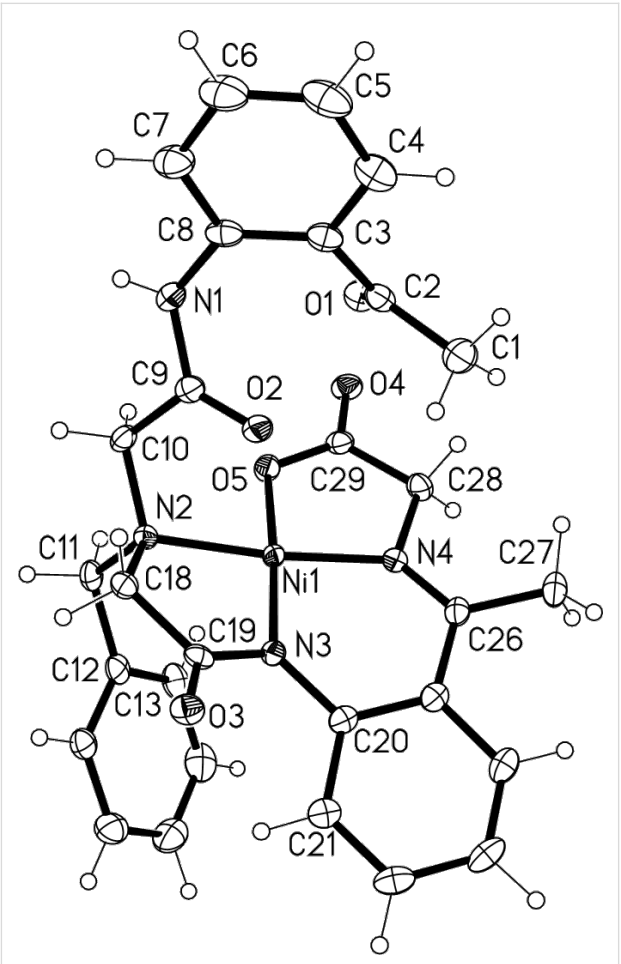

Figure 1: Crystallographic structure of complex **14a**.

The distances of the Ni–O(5) [1.8651(13) Å] and Ni–N(4) [1.8569(16) Å] bonds of the five-membered chelate ring of the glycine Schiff base fragment were relatively similar, while the bonds Ni–N(3) [1.8417(16) Å] and Ni–N(2) [1.9535(16) Å] were noticeably shorter and longer, respectively. The square-

planar structure of compound **14a** is slightly distorted with angles N(4)–Ni–N(2) of 173.48(7)° and N(3)–Ni–O(5) of 175.15(6)°. This deviation from planarity gives compound **14a** a bowl-like shape and renders it inherently chiral. For instance, the torsion angle C(19)–N(3)–C(20)–C(21) of 32.0(3)° sets the element of helical chirality, while the axial chirality is located through the N(1)–C(8) bond with the torsion angle C(9)–N(1)–C(8)–C(7) of −139.5(2)°. The central chirality is located on N(2) as, coordinated to Ni(II), nitrogen is configurationally stable and has four different substituents. As mentioned above, the absorptions of hydrogens and carbons in the NMR spectra, recorded at ambient temperature, are sharp and therefore do not suggest any diastereomeric transformations. Accordingly, one may assume that in $CHCl_3$ solution compounds **14** and **15** also exist in one diastereomeric form possibly stabilized by apical coordination of the amidic carbonyl of the pendent side chain (distance of Ni–O(2) = 2.665 Å).

With complexes **14** and **15** in hand, we next studied the oxidation of **14** as presented in Scheme 5. Formation of the corresponding enolates **16**, in the presence of relatively strong bases (KO*t*-Bu), is an established step in general methods for homologation of the glycine moiety by alkyl halide alkylation [27,50-53], aldol [29,33,36,37] and Michael [28,31,34,35,38,39,43-47] addition reactions. The following oxidation step of the enolates **16** in the presence of atmospheric oxygen, is less studied [48]; however, plausible key transformations can be deduced based on the closely related results on the well-established general oxidation of enolates [55-64] and glycine-derived enolates [65-70], in particular, under similar conditions. Thus, the ionized form of α-hydroxy intermediate **17** can undergo the cleavage of the glycine C–N bond [65,68-70] resulting in the formation of neutral complex **18**. Previously, we demonstrated that in situ formed derivatives of type **18**, without the pendant side chain, undergo further stabilization through dimerization, giving rise to the corresponding binuclear complexes [48]. In this case, the presence of the bidentate substituent allows for a different, intramolecular stabilization mechanism leading to the formation of target complexes **19**/**20**.

It is interesting to note that the acetophenone module-derived compound **14a** gave the expected enolate **16a**; however, its further oxidation lead mostly to decomposition, suggesting higher instability of intermediate derivatives of type **17** and **18** [48]. Also, the benzophenone-derived, Pd(II)-containing analogue **15** (Scheme 4) failed to produce the target complexes of type **19**/**20**, pointing to some limitation of this synthetic alternative. Nevertheless, this oxidative pathway allowed for convenient preparation of otherwise inaccessible complexes **19**/**20** formally derived from asymmetric carbonyl/imine ligands **13** (Scheme 3) and Ni(II). In contrast to typical Ni(II) complexes, such as **14a,b**, compounds **19**/**20** display an unusual dark-brown

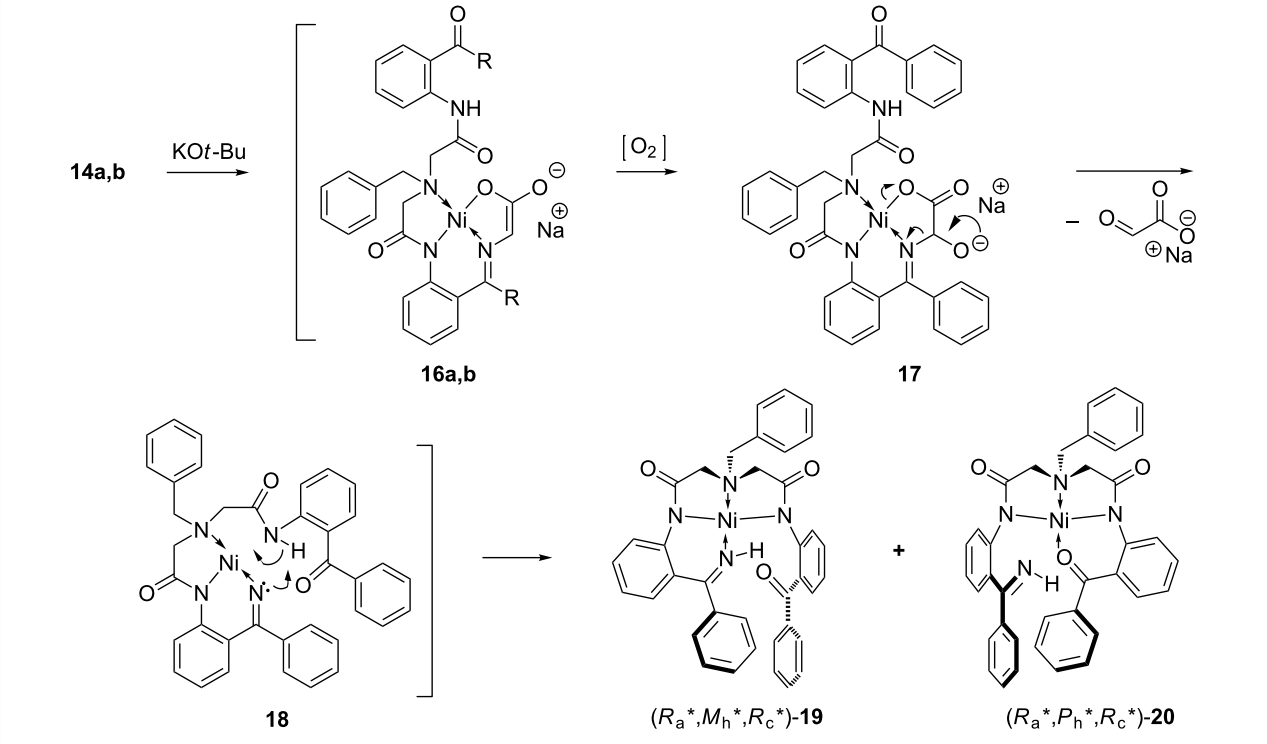

Scheme 5: Oxidation of enolates **16** and formation of complexes **19** and **20**.

color. Nevertheless, their high solubility in polar organic solvents allows for their straightforward purification by column chromatography. Initial assignment of the structures of compounds **19**/**20** by NMR was not possible because of the very fast exchange between Ni–O=C and Ni–NH=C chelation. Thus, due to fast interconversion between compounds **19** and **20**, only broad signals were observed in the ^{1}H NMR spectra recorded at ambient temperature. However, variable temperature experiments (−50 °C) produced a notable sharpening in both aromatic and aliphatic protons. Ultimately, elucidation of their structure was carried out by X-ray analysis, which was feasible due to their high crystallinity [54].

We found that in the solid state, compounds **19** and **20** exist as the sole NH–Ni coordinated quasi-diastereomer (R_a*,M_h*,R_c*)-**19** (Figure 2), containing a pair of (R_a,M_h,R_c) and (S_a,P_h,S_c) enantiomers in the crystallographic unit cell (triclinic, $P\bar{1}$ space group). Surprisingly, the distance of the Ni–NH bond was found to be the shortest [1.8518(15) Å] in the Ni(II)-coordinated plane, followed by the Ni–N(3) [1.8524(14) Å] of the same five-membered chelate ring. Two other Ni–N(1) [1.8760(14) Å] and Ni(1)–N(2) [1.9076(15) Å] were noticeably longer. The square-planar coordination plane in compound **19** was substantially more distorted, as compared with complex **14a** or carbonyl-coordinated analogues **2** and **3** [24,25] (Scheme 1), with the angles N(3)–Ni–N(1) of 171.94(6)° and N(4)–Ni–N(2) of 169.80(6)° rendering it inherently chiral. Consequently, the torsion angle C(24)–N(3)–C(25)–C(26) of 34.4(2)° gives rise to an element of helical chirality in compound **19**. The element of axial chirality is generated by the restricted rotation around the N(1)–C(13) bond with the torsion angle C(14)–N(1)–C(13)–C(12) of −119.59(18)°. The third element of chirality, a stereogenic center, is located on N(2).

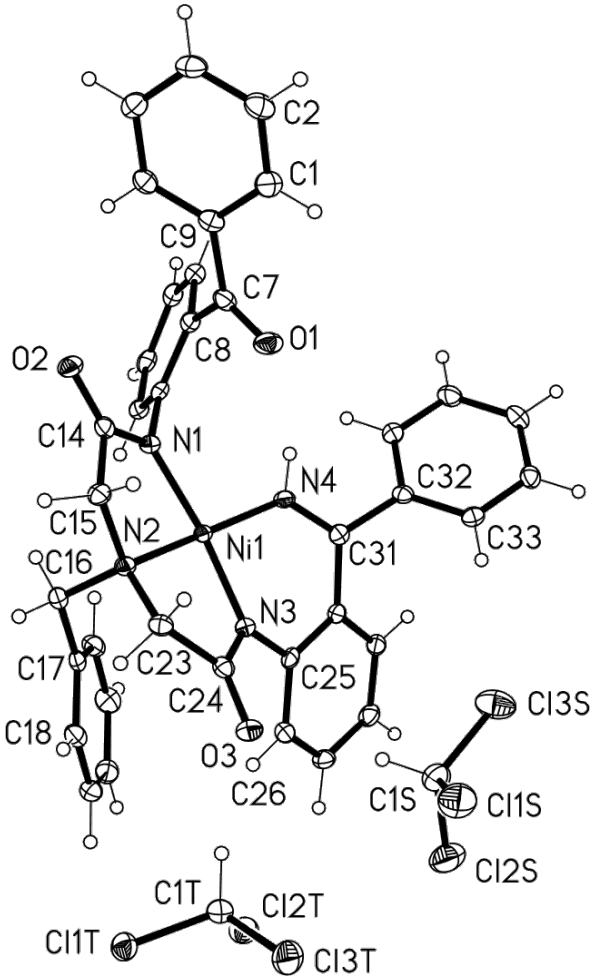

Figure 2: Crystallographic structure of complex **19**.

Conclusion

In conclusion, we have shown that the newly prepared Ni(II) complexes derived from asymmetric, pentadentate ligands exist as quasi-diastereomers, generating two new elements of chirality (stereogenic axis and helix) to the pre-existing configurationally stable stereogenic nitrogen. The stereoselective formation of only two, (R_a*,M_h*,R_c*) and (R_a*,P_h*,R_c*), out of the four possible stereochemical combinations is most remarkable, arising due to the highly stereocongested structural characteristics of these Ni(II) complexes. The quasi-diastereomeric transformation between products (R_a*,M_h*,R_c*) and (R_a*,P_h*,R_c*) occurs by intramolecular transcoordination of Ni–NH and Ni–O bonds. This transcoordination results in the loss and regeneration of axial and helical chirality with retention and inversion, respectively, of the stereochemical sense. The stereogenic center in this case remains unchanged. As it follows from the crystallographic studies, in the solid state there is an obvious preference for Ni–NH over Ni–O coordination. The flexibility of this modular design, in which the three major "phenone", "acid" and "amine" modules can be selected by using many structural modifications, provides a very practical tool for the preparation of a wide variety of Ni(II) complexes, which may result in a higher sensitivity to chemical properties such as temperature, solvent or pH of the reaction medium.

Experimental

General

^{1}H and ^{13}C NMR were performed on Varian Unity-300 (299.94 MHz) and Gemini-200 (199.98 MHz) spectrometers with TMS and $CDCl_3$ as internal standards. High-resolution mass spectra (HRMS) were recorded on a JEOL HX110A instrument. Optical rotations were measured on a JASCO P-1010 polarimeter. Melting points (mp) are uncorrected and were obtained in open capillaries. All reagents and solvents, unless otherwise stated, are commercially available and were used as

received. Unless otherwise stated, yields refer to isolated yields of products of greater than 95% purity as estimated by ^{1}H and ^{13}C NMR spectrometry. All new compounds were characterized by ^{1}H, ^{13}C NMR and HRMS. For preparation of **12a,b** see [25,39].

Synthesis of complexes 14a,b and 15

General procedure. To a suspension of compound **12**, glycine (5 equiv), and MX_2 ($NiCl_2$, $Ni(NO_3)_2$ or $PdCl_2$, 2 equiv) in MeOH, NaOH (7 equiv) was added, and the reaction mixture was stirred at 60–70 °C for 4 h. Then, the reaction mixture was poured over a slurry of ice and 5% AcOH. After complete precipitation, the solid was filtered, washed with water, and dried. The product was purified by silica-gel column chromatography ($CHCl_3$/acetone = 4:1).

Complex 14a (46% yield). Mp 277.2 °C (dec); ^{1}H NMR (300 MHz, $CDCl_3$) δ 2.34 (s, 3H), 2.68 (s, 3H), 2.89 (d, *J* = 15.4 Hz, 1H), 3.30 (d, *J* = 16.5 Hz, 1H), 3.83 (d, *J* = 15.4 Hz, 1H), 3.85 (d, *J* = 16.2 Hz, 1H), 3.86 (d, *J* = 18.8 Hz, 1H), 3.94 (d, *J* = 12.6 Hz, 1H), 4.43 (d, *J* = 19.0 Hz, 1H), 4.54 (d, *J* = 12.8 Hz, 1H), 6.92 (ddd, *J* = 8.30, 7.13, 1.18 Hz, 1H), 7.16–7.24 (m, 2H), 7.30–7.36 (m, 1H), 7.37–7.46 (m, 2H), 7.50 (dd, *J* = 8.30, 1.46 Hz, 1H), 7.64 (ddd, *J* = 8.69, 7.13, 1.56 Hz, 1H), 7.93 (dd, *J* = 8.01, 1.56 Hz, 1H), 8.06 (dd, *J* = 8.59, 1.17 Hz, 1H), 8.09–8.15 (m, 2H), 8.97 (dd, *J* = 8.49, 1.17 Hz, 1H); ^{13}C NMR (75 MHz, $CDCl_3$) δ 18.9, 28.5, 59.8, 60.0, 60.9, 64.4, 121.2, 121.3, 122.1, 123.3, 124.8, 126.8, 128.7, 128.9, 129.4, 131.4, 131.5, 131.7, 132.1, 135.2, 139.9, 141.4, 166.7, 168.8, 176.1, 176.8, 203.2; HRMS–ESI (*m*/*z*): $[M + Na]^+$ calcd for $C_{29}H_{28}N_4NaNiO_5$, 593.1311; found, 593.1321.

Complex 14b (83% yield). Mp 259.3 °C (dec); ^{1}H NMR (300 MHz, $CDCl_3$) δ 2.83 (d, *J* = 16.5 Hz, 1H), 3.37 (d, *J* = 16.4 Hz, 1H), 3.65 (d, *J* = 19.8 Hz, 1H), 3.84 (d, *J* = 12.2 Hz, 1H), 3.88 (d, *J* = 13.2 Hz, 1H), 3.89 (d, *J* = 19.8 Hz, 1H), 4.14 (d, *J* = 12.8 Hz, 1H), 4.70 (d, *J* = 13.1 Hz, 1H), 6.72 (ddd, *J* = 8.30, 6.84, 1.27 Hz, 1H), 6.84 (dd, *J* = 8.20, 1.76 Hz, 1H), 7.00–7.74 (m, 17H), 7.90–8.00 (m, 2H), 8.47 (d, *J* = 8.79 Hz, 1H), 8.83 (d, *J* = 7.91 Hz, 1H), 11.1 (bs, 1H); ^{13}C NMR (75 MHz, $CDCl_3$) δ 59.0, 60.5, 61.2, 63.9, 120.7, 122.6, 123.3, 124.2, 125.1, 125.5, 125.9, 126.3, 128.2, 128.9, 129.1, 129.4, 129.4, 129.6, 129.8, 131.1, 132.0, 132.1, 132.5, 133.0, 133.1, 133.9, 134.7, 138.1, 138.7, 142.4, 166.5, 171.0, 176.7, 177.1, 199.2; HRMS–ESI (*m*/*z*): $[M + H]^+$ calcd for $C_{39}H_{33}N_4NiO_5$, 695.1804; found, 695.1801.

Complex 15 (86% yield). Mp 253.5 °C (dec); ^{1}H NMR (300 MHz, $CDCl_3$): δ 3.77 (d, *J* = 15.8 Hz, 1H), 4.11 (d, *J* = 11.6 Hz, 1H), 4.12 (s, 2H), 4.18 (d, *J* = 11.1 Hz, 1H), 4.30 (d, *J* = 16.4 Hz, 1H), 4.46 (s, 2H), 6.78 (ddd, *J* = 8.20, 7.03, 1.17 Hz, 1H), 6.92–7.01 (m, 2H), 7.13–7.22 (m, 2H), 7.25–7.88 (m, 16H), 8.47 (dd, *J* = 8.79, 1.18 Hz, 1H), 8.58 (dd, *J* = 8.50, 1.18 Hz, 1H), 11.0 (bs, 1H); ^{13}C NMR (75 MHz, $CDCl_3$) δ 61.1, 63.1, 64.0, 65.3, 121.2, 122.4, 123.4, 123.6, 125.0, 126.0, 126.2, 126.4, 128.3, 128.8, 129.4, 129.5, 129.7, 129.7, 129.9, 131.5, 132.3, 132.7, 133.0, 133.1, 133.8, 134.2, 134.9, 137.9, 138.6, 142.2, 165.0, 169.2, 176.6, 177.8, 198.9; HRMS–ESI (*m*/*z*): $[M + H]^+$ calcd for $C_{39}H_{33}N_4O_5Pd$, 743.1436; found, 743.1501.

Complexes 19/20. To a solution of **14b** (1 equiv) in CH_3CN, was added KO*t*-Bu (4 equiv) at rt and the reaction mixture was stirred at rt under aerobic conditions until the starting compound was consumed completely, as confirmed by TLC. After evaporation of the solvent, water and a calculated amount of 5% AcOH aq. (4 equiv) was added and extracted with CH_2Cl_2 three times. The combined organic layers were dried over $MgSO_4$, and the product was purified on a short-path flash silica-gel column. Due to the fast exchange between complexes **19**/**20**, NMR spectra were not properly recorded. Mp 264.5 °C (dec); HRMS–ESI (*m*/*z*): $[M + Na]^+$ calcd for $C_{37}H_{30}N_4NaNiO_3$, 659.1569; found, 659.1547.

Supporting Information

Supporting Information File 1

NMR spectra of compounds **14b** and **19**/**20**.
[http://www.beilstein-journals.org/bjoc/content/supplementary/1860-5397-8-223-S1.pdf]

Acknowledgements

We thank IKERBASQUE, Basque Foundation for Science, for financial support. The crystallographic studies were performed by Dr. D. R. Powell, University of Oklahoma.

References

1. Feringa, B. L.; Koumura, N.; van Delden, R. A.; ter Wiel, M. K. J. *Appl. Phys. A* **2002,** *75,* 301–308. doi:10.1007/s003390201338
2. de Silva, A. P.; Gunaratne, H. Q. N.; Gunnlaugsson, T.; Huxley, A. J. M.; McCoy, C. P.; Rademacher, J. T.; Rice, T. E. *Chem. Rev.* **1997,** *97,* 1515–1566. doi:10.1021/cr960386p
3. Rambidi, N. G. *Microelectron. Eng.* **2003,** *69,* 485–500. doi:10.1016/S0167-9317(03)00337-X
4. Janek, J. *Nat. Mater.* **2009,** *8,* 88–89. doi:10.1038/nmat2364
5. Fukui, M.; Mori, T.; Inoue, Y.; Rathore, R. *Org. Lett.* **2007,** *9,* 3977–3980. doi:10.1021/ol701639u
6. Deng, J.; Song, N.; Zhou, Q.; Su, Z. *Org. Lett.* **2007,** *9,* 5393–5396. doi:10.1021/ol701822u
7. Mori, T.; Inoue, Y. *J. Phys. Chem. A* **2005,** *109,* 2728–2740. doi:10.1021/jp044917m
8. Shie, T.-L.; Lin, C.-H.; Lin, S.-L.; Yang, D.-Y. *Eur. J. Org. Chem.* **2007,** 4831–4836. doi:10.1002/ejoc.200700426

9. Collin, J.-P.; Kern, J.-M.; Raehm, L.; Sauvage, J.-P. Metallo-Rotaxanes and Catenanes as Redox Switches: Towards Molecular Machines and Motors. In *Molecular Switches;* Feringa, B. L., Ed.; Wiley-VCH: Weinheim, Germany, 2001; pp 249–280.
10. Stoddart, J. F.; Colquhoun, H. M. *Tetrahedron* **2008,** *64,* 8231–8263. doi:10.1016/j.tet.2008.06.035
11. Kay, E. R.; Leigh, D. A. *Pure Appl. Chem.* **2008,** *80,* 17–29. doi:10.1351/pac200880010017
12. Kim, Y.-H.; Goddard, W. A., III. *J. Phys. Chem. C* **2007,** *111,* 4831–4837. doi:10.1021/jp065302n
13. Saha, S.; Stoddart, J. F. *Chem. Soc. Rev.* **2007,** *36,* 77–92. doi:10.1039/b607187b
14. Irie, M., Ed. Photochromism: Memories and Switches. *Chem. Rev.* **2000,** *100,* 1683–1890. doi:10.1021/cr980068l
15. Pijper, D.; Jongejan, M. G. M.; Meetsma, A.; Feringa, B. L. *J. Am. Chem. Soc.* **2008,** *130,* 4541–4552. doi:10.1021/ja711283c
16. Geertsema, E. M.; Hoen, R.; Meetsma, A.; Feringa, B. L. *Eur. J. Org. Chem.* **2006,** 3596–3605. doi:10.1002/ejoc.200600280
17. Zheng, J.; Qiao, W.; Wan, X.; Gao, J. P.; Wang, Z. Y. *Chem. Mater.* **2008,** *20,* 6163–6168. doi:10.1021/cm8014644
18. Wang, Z. Y.; Todd, E. K.; Meng, X. S.; Gao, J. P. *J. Am. Chem. Soc.* **2005,** *127,* 11552–11553. doi:10.1021/ja0526721
19. Shinkai, S.; Ikeda, M.; Sugasaki, A.; Takeuchi, M. *Acc. Chem. Res.* **2001,** *34,* 494–503. doi:10.1021/ar000177y
20. Jiang, X.; Lim, Y.-K.; Zhang, B. J.; Opsitnick, E. A.; Baik, M.-H.; Lee, D. *J. Am. Chem. Soc.* **2008,** *130,* 16812–16822. doi:10.1021/ja806723e
21. Li, Y.; Wang, T.; Liu, M. *Soft Matter* **2007,** *3,* 1312–1317. doi:10.1039/b710165a
22. Qiu, Y.; Chen, P.; Guo, P.; Li, Y.; Liu, M. *Adv. Mater.* **2008,** *20,* 2908–2913. doi:10.1002/adma.200801165
23. Canary, J. W.; Zahn, S.; Chiu, Y.-H.; Santos, O.; Liu, J.; Zhu, L. *Enantiomer* **2000,** *5,* 397–403.
24. Soloshonok, V. A.; Ueki, H.; Moore, J. L.; Ellis, T. K. *J. Am. Chem. Soc.* **2007,** *129,* 3512–3513. doi:10.1021/ja067995r
25. Soloshonok, V. A.; Ueki, H. *Synthesis* **2010,** 49–56. doi:10.1055/s-0029-1217090
26. The term “quasi-diastereomer” is used by analogy with “quasi-enantiomer”, as defined by Eliel and Wilen: Eliel, E. L.; Wilen, S. H. *Stereochemistry of Organic Compunds;* Wiley-Interscience: New York, 1994.
27. Ellis, T. K.; Ueki, H.; Soloshonok, V. A. *Tetrahedron Lett.* **2005,** *46,* 941–944. doi:10.1016/j.tetlet.2004.12.050
28. Soloshonok, V. A.; Ueki, H.; Ellis, T. K.; Yamada, T.; Ohfune, Y. *Tetrahedron Lett.* **2005,** *46,* 1107–1110. doi:10.1016/j.tetlet.2004.12.093
29. Ellis, T. K.; Soloshonok, V. A. *Synlett* **2006,** 533–538. doi:10.1055/s-2006-926252
30. Soloshonok, V. A.; Ueki, H.; Ellis, T. K. *Chim. Oggi* **2008,** *26,* 51–54.
31. Yamada, T.; Sakaguchi, K.; Shinada, T.; Ohfune, Y.; Soloshonok, V. A. *Tetrahedron: Asymmetry* **2008,** *19,* 2789–2795. doi:10.1016/j.tetasy.2008.11.036
32. Soloshonok, V. A.; Ueki, H.; Ellis, T. K. *Synlett* **2009,** 704–715. doi:10.1055/s-0028-1087929
33. Soloshonok, V. A.; Belokon, Y. N.; Kuzmina, N. A.; Maleev, V. I.; Svistunova, N. Y.; Solodenko, V. A.; Kukhar, V. P. *J. Chem. Soc., Perkin Trans. 1* **1992,** 1525–1529. doi:10.1039/P19920001525
34. Soloshonok, V. A.; Cai, C.; Hruby, V. J. *Tetrahedron: Asymmetry* **1999,** *10,* 4265–4269. doi:10.1016/S0957-4166(99)00483-8
35. Soloshonok, V. A.; Avilov, D. V.; Kukhar, V. P.; Meervelt, L. V.; Mischenko, N. *Tetrahedron Lett.* **1997,** *38,* 4903–4904. doi:10.1016/S0040-4039(97)01054-X
36. Soloshonok, V. A.; Avilov, D. V.; Kukhar, V. P. *Tetrahedron: Asymmetry* **1996,** *7,* 1547–1550. doi:10.1016/0957-4166(96)00177-2
37. Soloshonok, V. A.; Avilov, D. V.; Kukhar, V. P.; Tararov, V. I.; Saveleva, T. F.; Churkina, T. D.; Ikonnikov, N. S.; Kochetkov, K. A.; Orlova, S. A.; Pysarevsky, A. P.; Struchkov, Y. T.; Raevsky, N. I.; Belokon, Y. N. *Tetrahedron: Asymmetry* **1995,** *6,* 1741–1756. doi:10.1016/0957-4166(95)00220-J
38. Soloshonok, V. A.; Cai, C.; Hruby, V. J. *Org. Lett.* **2000,** *2,* 747–750. doi:10.1021/ol990402f
39. Ellis, T. K.; Ueki, H.; Yamada, T.; Ohfune, Y.; Soloshonok, V. A. *J. Org. Chem.* **2006,** *71,* 8572–8578. doi:10.1021/jo0616198
40. Moore, J. L.; Taylor, S. M.; Soloshonok, V. A. *ARKIVOC* **2005,** No. vi, 287–292.
41. Ueki, H.; Ellis, T. K.; Martin, C. H.; Soloshonok, V. A. *Eur. J. Org. Chem.* **2003,** 1954–1957. doi:10.1002/ejoc.200200688
42. Ueki, H.; Ellis, T. K.; Martin, C. H.; Boettiger, T. U.; Bolene, S. B.; Soloshonok, V. A. *J. Org. Chem.* **2003,** *68,* 7104–7107. doi:10.1021/jo0301494
43. Soloshonok, V. A.; Cai, C.; Hruby, V. J. *Angew. Chem., Int. Ed.* **2000,** *39,* 2172–2175. doi:10.1002/1521-3773(20000616)39:12<2172::AID-ANIE2172>3.0.CO;2-0
44. Soloshonok, V. A.; Cai, C.; Yamada, T.; Ueki, H.; Ohfune, Y.; Hruby, V. J. *J. Am. Chem. Soc.* **2005,** *127,* 15296–15303. doi:10.1021/ja0535561
45. Soloshonok, V. A.; Cai, C.; Hruby, V. J. *Tetrahedron Lett.* **2000,** *41,* 9645–9649. doi:10.1016/S0040-4039(00)01737-8
46. Soloshonok, V. A.; Cai, C.; Hruby, V. J. *Tetrahedron Lett.* **2000,** *41,* 135–139. doi:10.1016/S0040-4039(99)02018-3
47. Yamada, T.; Okada, T.; Sakaguchi, K.; Ohfune, Y.; Ueki, H.; Soloshonok, V. A. *Org. Lett.* **2006,** *8,* 5625–5628. doi:10.1021/ol0623668
48. Soloshonok, V. A.; Ueki, H. *J. Am. Chem. Soc.* **2007,** *129,* 2426–2427. doi:10.1021/ja0671215
49. Qiu, W.; Soloshonok, V. A.; Cai, C.; Tang, X.; Hruby, V. J. *Tetrahedron* **2000,** *56,* 2577–2582. doi:10.1016/S0040-4020(00)00176-9
50. Soloshonok, V. A. *Curr. Org. Chem.* **2002,** *6,* 341–364. doi:10.2174/1385272024605014
51. Soloshonok, V. A.; Tang, X.; Hruby, V. J.; Meervelt, L. V. *Org. Lett.* **2001,** *3,* 341–343. doi:10.1021/ol000330o
52. Ellis, T. K.; Martin, C. H.; Tsai, G. M.; Ueki, H.; Soloshonok, V. A. *J. Org. Chem.* **2003,** *68,* 6208–6214. doi:10.1021/jo030075w
53. Soloshonok, V. A.; Tang, X.; Hruby, V. J. *Tetrahedron* **2001,** *57,* 6375–6382. doi:10.1016/S0040-4020(01)00504-X
54. CCDC 875510 and 875511 contain the supplementary crystallographic data for this paper. These data can be obtained free of charge from The Cambridge Crystallographic Data Centre via http://www.ccdc.cam.ac.uk/data_request/cif.
55. Christoffers, J.; Baro, A.; Werner, T. *Adv. Synth. Catal.* **2004,** *346,* 143–151. doi:10.1002/adsc.200303140 See for a review.
56. Rahman, M. T.; Nishino, H. *Org. Lett.* **2003,** *5,* 2887–2890. doi:10.1021/ol034939b
57. Christoffers, J. *J. Org. Chem.* **1999,** *64,* 7668–7669. doi:10.1021/jo9909094

58. Christoffers, J.; Werner, T.; Unger, S.; Frey, W. *Eur. J. Org. Chem.* **2003,** 425–431. doi:10.1002/ejoc.200390075
59. Christoffers, J.; Werner, T. *Synlett* **2002,** 119–121. doi:10.1055/s-2002-19331
60. Arai, T.; Akazome, M.; Ogura, K. *Chem. Lett.* **1999,** *28,* 107–108. doi:10.1246/cl.1999.107
61. Adam, W.; Cueto, O.; Ehrig, V. *J. Org. Chem.* **1976,** *41,* 370–371. doi:10.1021/jo00864a040
62. Wasserman, H. H.; Lipshutz, B. H. *Tetrahedron Lett.* **1975,** *16,* 1731–1734. doi:10.1016/S0040-4039(00)72245-3
63. Acocella, M. R.; Mancheño, O. G.; Bella, M.; Jørgensen, K. A. *J. Org. Chem.* **2004,** *69,* 8165–8167. doi:10.1021/jo048655w
64. Jefford, C. W.; Currie, J.; Richardson, G. D.; Rossier, J. C. *Helv. Chim. Acta* **1991,** *74,* 1239–1246. doi:10.1002/hlca.19910740612
65. Ooi, T.; Takeuchi, M.; Ohara, D.; Maruoka, K. *Synlett* **2001,** 1185–1187. doi:10.1055/s-2001-15167
66. Bull, S. D.; Davies, S. G.; Garner, A. C.; O'Shea, M. D.; Savory, E. D.; Snow, E. J. *J. Chem. Soc., Perkin Trans. 1* **2002,** 2442–2448. doi:10.1039/B207457P
67. Williams, R. M.; Armstrong, R. W.; Dung, J. S. *J. Am. Chem. Soc.* **1984,** *106,* 5748–5750. doi:10.1021/ja00331a066
68. Garcia-Raso, A.; Deyá, P. M.; Saá, J. M. *J. Org. Chem.* **1986,** *51,* 4285–4287. doi:10.1021/jo00372a033
69. Easton, C. J.; Eichinger, S. K.; Pitt, M. J. *J. Chem. Soc., Chem. Commun.* **1992,** 1295–1296. doi:10.1039/C39920001295
70. Easton, C. J.; Eichinger, S. K.; Pitt, M. J. *Tetrahedron* **1997,** *53,* 5609–5616. doi:10.1016/S0040-4020(97)00216-0

License and Terms

Beilstein Journal of Organic Chemistry

A bisazobenzene crosslinker that isomerizes with visible light

Subhas Samanta, Harris I. Qureshi and G. Andrew Woolley*

Full Research Paper

Open Access

Address:
Department of Chemistry, University of Toronto, 80 St. George St., Toronto, ON, M5S 3H6, Canada; telephone: (416) 978-0675, fax: (416) 978-8775

Email:
G. Andrew Woolley* - awoolley@chem.utoronto.ca

* Corresponding author

Keywords:
azobenzene; molecular switches; switch; photo-control; visible

Beilstein J. Org. Chem. **2012,** *8,* 2184–2190.
doi:10.3762/bjoc.8.246

Received: 24 August 2012
Accepted: 26 November 2012
Published: 14 December 2012

This article is part of the Thematic Series "Molecular switches and cages".

Guest Editor: D. Trauner

Abstract

Background: Large conformational and functional changes of azobenzene-modified biomolecules require longer azobenzene derivatives that undergo large end-to-end distance changes upon photoisomerization. In addition, isomerization that occurs with visible rather than UV irradiation is preferred for biological applications.

Results: We report the synthesis and characterization of a new crosslinker in which a central piperazine unit links two azobenzene chromophores. Molecular modeling indicates that this crosslinker can undergo a large change in end-to-end distance upon *trans*,*trans* to *cis*,*cis* isomerization. Photochemical characterization indicates that it does isomerize with visible light (violet to blue wavelengths). However, the thermal relaxation rate of this crosslinker is rather high ($\tau_{1/2}$ ~ 1 s in aqueous buffer at neutral pH) so that it is difficult to produce large fractions of the *cis*,*cis*-species without very bright light sources.

Conclusion: While cis-lifetimes may be longer when the crosslinker is attached to a biomolecule, it appears the *para*-piperazine unit may be best suited for applications where rapid thermal relaxation is required.

Introduction

Azobenzene derivatives have been used for reversible manipulation of biological targets, including peptide and protein structure and function [1-12], enzyme activities [13-17], oligonucleotide functions [18-20], and ion-channel activities [21-23]. A quantitative analysis of the effects of crosslinkers on protein folding led to the conclusion that photocontrol of folding is best achieved by using rigid crosslinkers that undergo a large change in end-to-end distance upon photoisomerization [6]. Previously, we reported the design and synthesis of the rigid bisazobenzene crosslinker BPDBS, (4,4'-bis(4-(2-chloroacetamido)phenyl)-diazenylbiphenyl-2,2'-disulfonate) (**1**, Scheme 1) [24]. This photoswitch can produce a minimum ~5 Å and a maximum

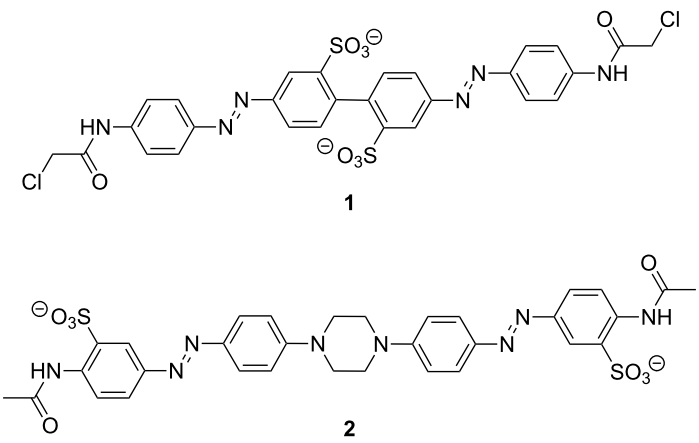

Scheme 1: Bisazobenzene derivatives.

~23 Å end-to-end distance change upon *trans–cis* isomerization. It has a high absorption coefficient (45–60,000 $M^{-1}cm^{-1}$) and can produce up to ~80% *trans–cis* isomerization under favorable conditions. The suitability of this photoswitch for biological systems would be enhanced if the wavelengths required for photoisomerization were longer, so that UV light was not required. UV light is highly scattered by biological samples and can be a toxic stimulus [25,26]. In an attempt to red-shift the switching wavelength while maintaining a large end-to-end distance change upon photoisomerization, we designed compound **2** (Scheme 1). The central piperazine unit in this structure was expected to disconnect the π-delocalization between the two azo chromophores completely, while providing N-centered lone pairs to extend the π-system of each independent azo unit. In this manner, independent photoswitching behavior of the two units at wavelengths shifted towards the visible range was expected to occur.

Results and Discussion

The *p*-diacetamido piperazine-linked bisazobenzene derivative **2** was prepared by a double diazo-coupling reaction between the donor 1,4-diphenylpiperazine (**7**) and the acceptor 4-acetamido-3-sulfobenzenediazonium chloride (**3**), which was synthesized in situ by diazotization of sodium 2-acetamido-5-aminobenzenesulfonate (**4**) using sodium nitrite with HCl (Scheme 2). Compound **4** was prepared by hydrogenation with H_2/Pd-C

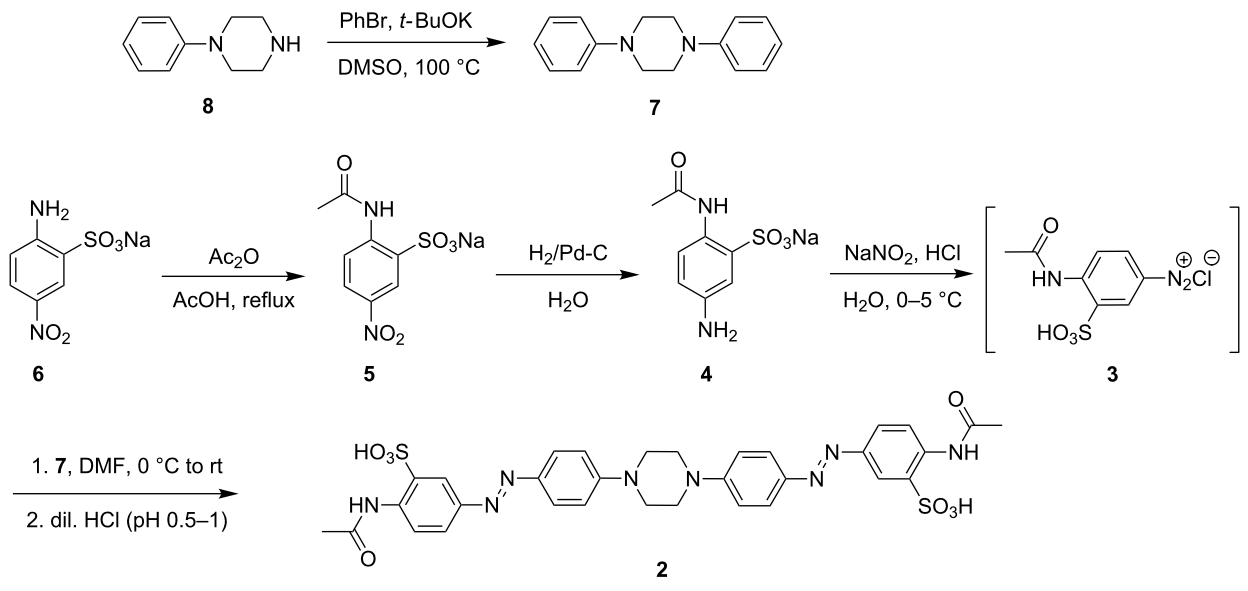

Scheme 2: Synthetic route for the preparation of bisazobenzene derivative **2**.

from sodium 2-acetamido-5-nitrobenzenesulfonate (**5**), which was obtained from commercially available sodium 2-amino-5-nitrobenzenesulfonate (**6**) by acetylation using acetic anhydride. 1,4-Diphenylpiperazine (**7**) was synthesized by a cross-coupling reaction of bromobenzene with 1-phenylpiperazine in the presence of *t*-BuOK.

As with previous crosslinkers, attachment to a target peptide or protein would involve replacement of the two terminal acetamido units with chloro- or iodoacetamide units to enable reaction with Cys residues [24]. The end-to-end distance changes expected upon photoisomerization of the resulting crosslink were estimated by molecular dynamics methods. Figure 1 shows models of compound **2** in *trans*,*trans*, *trans*,*cis*, and *cis*,*cis*-isomeric states. These simulations indicate that the *trans*,*trans* and *cis*,*cis*-states give well-separated end-to-end distance changes. The *trans*,*trans*-isomer has a preferred end-to-end distance of 32.8 Å but some flexibility in the piperazine linkage permits distances between 25 and 35 Å. The *cis*,*cis*-isomer permits distances between ~4 and 25 Å. The *trans*,*cis*-isomers produce an intermediate range of distances between 7 and 30 Å, which overlaps with both *trans*,*trans* and *cis*,*cis*-isomers. This rather large and overlapping range of distances for the *trans*,*cis*-species is problematic from the point of view of photocontrol since a large light-driven change in the end-to-end distribution will require very efficient photoisomerization to the *cis*,*cis*-species. We were, therefore, interested in the photochemical behavior of **2**.

Figure 2 shows UV–vis absorbance spectra of **2** in the dark-adapted *trans*,*trans*-form in various solvents. As expected, the main absorbance band (π–π* transition) is red-shifted compared to BPDBS with a maximum near 420 nm. The molar extinction coefficient for **2** was determined by ^{1}H NMR coupled with UV–vis absorption spectra, to be 66,400 in DMSO at 428 nm, such that on a molar basis, the photoswitch is intensely colored.

The spectra in aqueous solutions are pH dependent below pH 6.0 (Figure 2b). A band corresponding to the azonium species [27] near 600 nm is evident at pH 5 and this does not appear to change upon irradiation. At lower pH values the spectrum undergoes further changes with enhanced absorbance from 530–700 nm consistent with the formation of a doubly protonated bisazonium species. This species is expected to be in equilibrium with the corresponding bisammonium species [27].

Irradiation of **2** in DMSO and in acetonitrile caused only small changes in the spectra indicating rapid thermal reversal. However, switching in aqueous solutions was measurable (Figure 3). The half-life of the irradiated isomers of **2** in phosphate buffer at 4 °C was measured to be 1.5 ± 0.3 s.

Numerous cycles of photoisomerization could be carried out without noticeable photobleaching (Figure 3b). The relatively rapid thermal relaxation, however, means that the overall *trans* versus *cis*-isomer ratio is small, and the fraction of the *cis*,*cis*-species is low. While *cis* lifetimes may be longer when the crosslinker is attached to a biomolecule, it is likely that this crosslink will predominantly cycle between the *trans*,*trans* and *trans*,*cis*-species under low irradiation intensities. These species have overlapping end-to-end distances and would not be expected to drive significant conformational change in a single attached biomolecule [6]. However, high (e.g., pulsed) light intensities may be expected to populate the *cis*,*cis*-state and may permit pulsed-light-driven conformational changes. It is

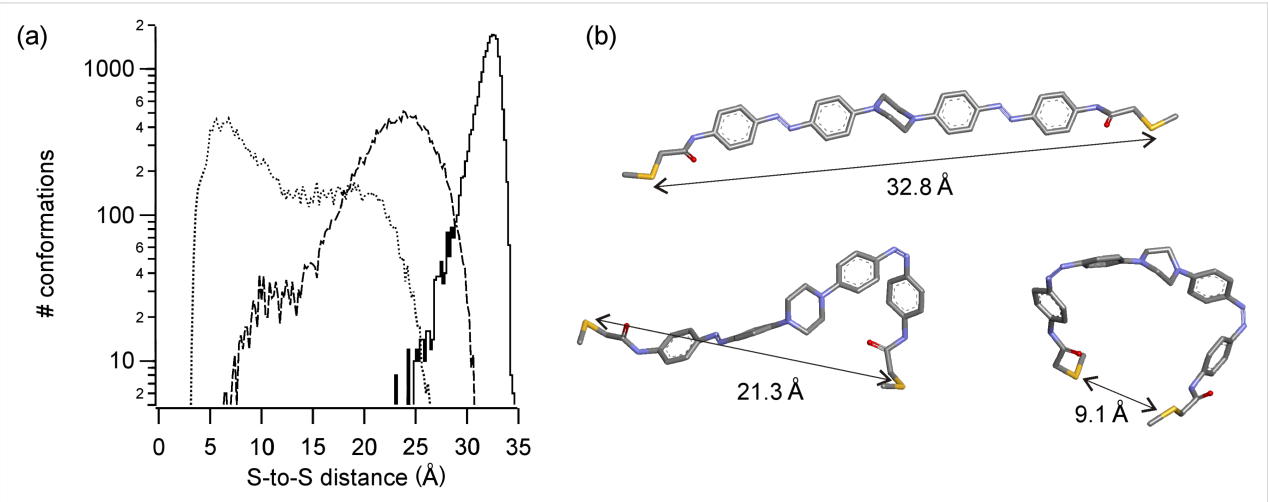

Figure 1: (a) Histograms showing the relative populations of conformations having the sulfur-to-sulfur distances indicated. (b) Examples of *trans*,*trans*, *trans*,*cis* and *cis*,*cis* conformations with the S–S distances indicated.

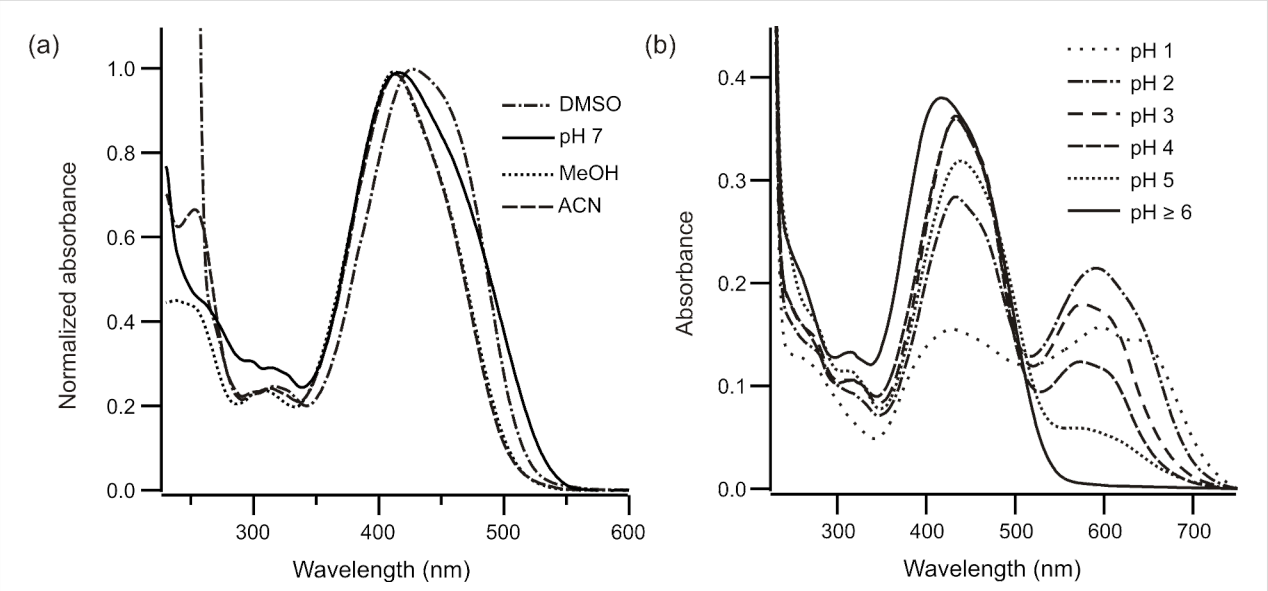

Figure 2: (a) Normalized UV–vis absorption spectra of **2** in DMSO, acetonitrile, MeOH and sodium phosphate buffer (pH 7.0). (b) UV–vis absorption spectra of **2** (~10 μM) in aqueous buffer at different pHs (indicated).

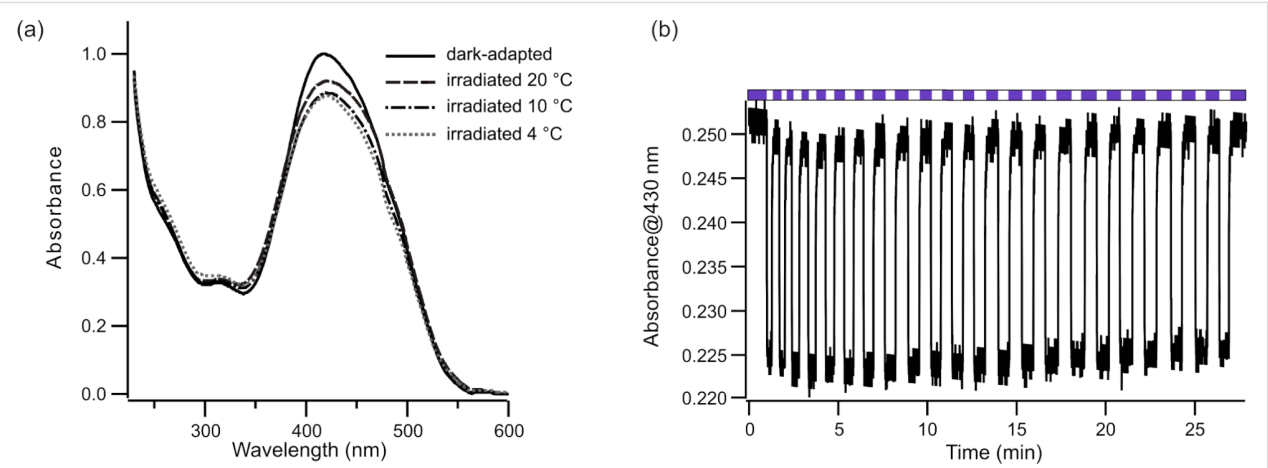

Figure 3: (a) Photoswitching of **2** with violet light (407–410 nm) at different temperatures (4, 10 and 20 °C) in 25 mM sodium phosphate buffer at pH 8. (b) Multiple rounds of photoswitching of **2** with alternating violet light (violet bars) and dark adaption (white bars) in 25 mM phosphate buffer, pH 8, at 10 °C.

possible that further substitution, particularly in positions *ortho* to the azo units may slow down the thermal relaxation rates and make production of a large fraction of the *cis*,*cis*-species possible [28]. Alternatively, azobenzene-based switches with rapid thermal relaxation times are preferred in materials-based applications where they can lead to light-driven changes in polymer properties. Bisazobenzene-based compounds analogous to **2** may be useful in this context [29-33].

Experimental

General aspects: All commercial materials (solvents, reagents and substrates) were used as received. NMR spectra were recorded either on Varian Vnmr-S 400 MHz, Varian Mercury 400 MHz or Agilent DD2 500 MHz spectrometers. Silica gel of particle size 40–63 μm from Silicycle Chemical Division was used for column chromatography.

Synthesis of 1,4-diphenylpiperazine (7) [34]: A mixture of 1-phenylpiperazine (**8**, 2.0 g, 12.3 mmol), bromobenzene (1.9 g, 12.1 mmol) and *t*-BuOK (2.7 g, 24.11 mmol) in anhydrous DMSO (25 mL) was heated at 100 °C for 2 h. The reaction was quenched with water and extracted with dichloromethane. The combined organic layer was dried over anhydrous sodium sulfate and concentrated. The crude oil was subjected to silica-

gel column chromatography to afford 1,4-diphenylpiperazine (**7**, 1.2 g, yield 41%) as a colorless solid. ^{1}H NMR (400 MHz, $CDCl_3$) δ 3.34 (s, 8H), 6.89 (t, J = 7.6 Hz, 2H), 6.99 (d, J = 8.0 Hz, 4H), 7.29 (t, J = 7.6 Hz, 4H) ppm.

Synthesis of sodium 2-acetamido-5-nitrobenzenesulfonate (5): To sodium 2-amino-5-nitrobenzenesulfonate (**6**, 4.0 g, 16.6 mmol) in acetic acid (40 mL) was added acetic anhydride (2.6 g, 24.8 mmol) and the solution was heated under reflux for 4 h. After cooling to rt, the precipitate was filtered, washed with hot acetic acid and then ether, and dried under high vacuum. The crude product was resuspended in hot ethanol, filtered and dried to obtain sodium 2-acetamido-5-nitrobenzenesulfonate (**5**, 4.3 g, yield 90%) as a colorless solid. ^{1}H NMR (400 MHz, DMSO-d_6) δ 2.13 (s, 3H), 8.21 (dd, J_1 = 9.2 Hz, J_2 = 2.8 Hz, 1H), 8.43 (d, J = 2.8 Hz, 1H), 8.55 (d, J = 9.2 Hz, 1H), 10.66 (br s, NH) ppm; ^{13}C NMR (100 MHz, DMSO-d_6) δ 25.7, 120.2, 123.1, 126.2, 135.9, 141.6, 141.8, 169.3 ppm; HRMS–ESI (m/z): $[M - H]^-$ calcd for $C_8H_7N_2O_6S$, 259.2174; found, 259.2172.

Synthesis of sodium 2-acetamido-5-aminobenzenesulfonate (4) [35]: To a solution of sodium 2-acetamido-5-nitrobenzenesulfonate (**5**, 4.2 g, 14.9 mmol) in water (100 mL) contained in a double-necked round-bottom flask was added 10% Pd/C (0.3 g) under nitrogen gas atmosphere. A filled hydrogen balloon was then connected to one neck and the reaction vessel was thoroughly degassed and purged with hydrogen gas. The reaction mixture was vigorously stirred under hydrogen-balloon pressure at rt for 14 h. The reaction mixture was filtered through a celite pad, and the water was removed under vacuum. The crude product was resuspended in hot ethanol, filtered and dried to obtain sodium 2-acetamido-5-aminobenzenesulfonate (**4**, 3.6 g, yield 97%) as a colorless solid. ^{1}H NMR (400 MHz, DMSO-d_6) δ 1.96 (s, 3H), 4.91 (br, NH_2), 6.46 (dd, J_1 = 8.4 Hz, J_2 = 2.8 Hz, 1H), 6.95 (d, J = 2.8 Hz, 1H), 7.88 (d, J = 8.4 Hz, 1H), 9.98 (br, NH) ppm.

Synthesis of *p*-diacetamido piperazine-linked bisazobenzene, 5,5'-((piperazine-1,4-diylbis(4,1-phenylene))bis(diazene-2,1-diyl))bis(2-acetamidobenzenesulfonic acid) (2): An ice-cold mixture of sodium 2-acetamido-5-aminobenzenesulfonate (**4**, 1.6 g, 6.3 mmol) and sodium nitrite (0.47 g, 6.8 mmol) in water (30 mL) was added dropwise to a mixture of concentrated hydrochloric acid (2.8 mL) and ice (30.0 g). The resulting mixture was stirred at 0–5 °C for 1 h. To this diazonium solution was added dropwise an ice-cold solution of 1,4-diphenylpiperazine (**7**, 0.5 g, 2.1 mmol) in DMF (10 mL). After stirring for 2 h at 0–5 °C, it was stirred at room temperature for 24 h. The reaction was made acidic (pH 1 to 0.5), filtered and the residue was washed with cold water. The crude product was subjected to a short silica gel column chromatography to isolate *p*-diacetamido piperazine-linked bisazobenzene **2** (108.0 mg, yield 7%), which was further HPLC purified on a semipreparative SB-C8 column with a linear solvent gradient of 10–75% acetonitrile/H_2O (containing 0.1% trifluoroacetic acid) over a course of 25 min; the product was eluted at 54.5% acetonitrile. ^{1}H NMR (400 MHz, DMSO-d_6) δ 2.08 (s, 6H), 3.54 (s, 8H), 7.11 (d, J = 9.2 Hz, 4H), 7.77–7.81 (m, 6H), 8.09 (d, J = 2.4 Hz, 2H), 8.45 (d, J = 8.8 Hz, 2H), 10.58 (br, NH) ppm; ^{13}C NMR (125 MHz, DMSO-d_6) δ 25.5, 47.0, 114.6, 119.5, 120.1, 124.8, 125.6, 136.2, 137.1, 144.6, 147.1, 152.9, 168.3 ppm; HRMS–ESI (m/z): $[M - H]^-$ calcd for $C_{32}H_{31}N_8O_8S_2$, 719.1711; found, 719.1711.

UV–vis spectra and photoisomerization: UV–vis absorption spectra were obtained using either a Perkin-Elmer Lambda 25 spectrophotometer or using a diode array UV–vis spectrophotometer (Ocean Optics Inc., USB4000) coupled to a temperature-controlled cuvette holder (Quantum Northwest, Inc. Spokane, WA, USA). The latter arrangement was used to measure thermal relaxation rates, and steady-state spectra under UV–vis illumination. For steady-state spectra, typically, a 5–10 μM solution of **2** in 25 mM sodium phosphate buffer (pH 8.0), contained in a 1 cm path length quartz cuvette in the temperature-controlled cuvette holder, was irradiated (at 90° to the measuring beam) with LEDs emitting at 407–410 nm (~460 mW, LEDengin LZ1-10UA05) at 4, 10 and 20 °C for 2 min until no further decrease in absorbance was observed, and under this steady-state-irradiation condition the spectra were recorded.

Rates of thermal reversion of the irradiated samples were measured at 4 °C by monitoring absorbance at 425 nm with time. All curves were fitted to mono-exponential decay kinetics. The light used for the absorbance measurement was of sufficiently low intensity to cause negligible isomerization.

To determine the molar extinction coefficient ^{1}H NMR spectra of a solution of **2** in DMSO-d_6 containing a known concentration of 1,2-dichloroethane (DCE) as an internal reference was recorded. The NMR solution was later diluted in DMSO and the UV–vis spectrum was recorded to calculate the molar extinction coefficient.

Molecular modeling: Models of *trans*,*trans*, *trans*,*cis* and *cis*,*cis*-crosslinkers were built by using HyperChem (v.8, Hypercube Inc.) with the linker terminated with methyl groups representing the β-carbon of Cys in the cross-linked peptide, and minimized by using the Amber99 force field. Restraints were added to the azo-bond for the *trans*,*cis* and *cis*,*cis*-isomers (force constant 16). Molecular dynamics runs were performed

in vacuo, essentially as described previously [36], with a distance-dependent dielectric constant, and 1–4 scale factors of 0.833 for electrostatic and 0.5 for van der Waals interactions, a step size of 1 fs and 300 K as the simulation temperature. Trajectories were analyzed to verify that numerous torsion-angle changes occurred for all single bonds during the course of the simulation to ensure that conformational space was adequately sampled. Histograms of all points were then produced for the S–S distance during the full set of simulations for each isomer.

Supporting Information

Supporting Information File 1

NMR spectra for compounds **2**, **4**, **5** and **7**.
[http://www.beilstein-journals.org/bjoc/content/supplementary/1860-5397-8-246-S1.pdf]

Acknowledgements

We are grateful to the Natural Science and Engineering Research Council of Canada for funding.

References

1. Pieroni, O.; Fissi, A.; Angelini, N.; Lenci, F. *Acc. Chem. Res.* **2001,** *34,* 9–17. doi:10.1021/ar990141+
2. Renner, C.; Moroder, L. *ChemBioChem* **2006,** *7,* 868–878. doi:10.1002/cbic.200500531
3. Zhang, F.; Zarrine-Afsar, A.; Al-Abdul-Wahid, M. S.; Prosser, R. S.; Davidson, A. R.; Woolley, G. A. *J. Am. Chem. Soc.* **2009,** *131,* 2283–2289. doi:10.1021/ja807938v
4. Beharry, A. A.; Woolley, G. A. *Chem. Soc. Rev.* **2011,** *40,* 4422–4437. doi:10.1039/c1cs15023e
5. Woolley, G. A. *Acc. Chem. Res.* **2005,** *38,* 486–493. doi:10.1021/ar040091v
6. Beharry, A. A.; Chen, T.; Al-Abdul-Wahid, M. S.; Samanta, S.; Davidov, K.; Sadovski, O.; Ali, A. M.; Chen, S. B.; Prosser, R. S.; Chan, H. S.; Woolley, G. A. *Biochemistry* **2012,** *51,* 6421–6431. doi:10.1021/bi300685a
7. Zhang, F.; Timm, K. A.; Arndt, K. M.; Woolley, G. A. *Angew. Chem., Int. Ed.* **2010,** *49,* 3943–3946. doi:10.1002/anie.201000909
8. Woolley, G. A.; Jaikaran, A. S.; Berezovski, M.; Calarco, J. P.; Krylov, S. N.; Smart, O. S.; Kumita, J. R. *Biochemistry* **2006,** *45,* 6075–6084. doi:10.1021/bi060142r
9. Guerrero, L.; Smart, O. S.; Woolley, G. A.; Allemann, R. K. *J. Am. Chem. Soc.* **2005,** *127,* 15624–15629. doi:10.1021/ja0550428
10. Guerrero, L.; Smart, O. S.; Weston, C. J.; Burns, D. C.; Woolley, G. A.; Allemann, R. K. *Angew. Chem., Int. Ed.* **2005,** *44,* 7778–7782. doi:10.1002/anie.200502666
11. Kneissl, S.; Loveridge, E. J.; Williams, C.; Crump, M. P.; Allemann, R. K. *ChemBioChem* **2008,** *9,* 3046–3054. doi:10.1002/cbic.200800502
12. Mart, R. J.; Wysoczański, P.; Kneissl, S.; Ricci, A.; Brancale, A.; Allemann, R. K. *ChemBioChem* **2012,** *13,* 515–519. doi:10.1002/cbic.201100800
13. Bose, M.; Groff, D.; Xie, J.; Brustad, E.; Schultz, P. G. *J. Am. Chem. Soc.* **2006,** *128,* 388–389. doi:10.1021/ja055467u
14. Hien, L. T.; Schierling, B.; Ryazanova, A. Yu.; Zatsepin, T. S.; Volkov, E. M.; Kubareva, E. A.; Velichko, T. I.; Pingoud, A.; Oretskaya, T. S. *Russ. J. Bioorg. Chem.* **2009,** *35,* 549–555. doi:10.1134/S1068162009050033
15. Muranaka, N.; Hohsaka, T.; Sisido, M. *FEBS Lett.* **2002,** *510,* 10–12. doi:10.1016/S0014-5793(01)03211-2
16. Nakayama, K.; Endo, M.; Majima, T. *Chem. Commun.* **2004,** 2386–2387. doi:10.1039/b409844g
17. Schierling, B.; Noël, A.-J.; Wende, W.; Hien, L. T.; Volkov, E.; Kubareva, E.; Oretskaya, T.; Kokkinidis, M.; Römpp, A.; Spengler, B.; Pingoud, A. *Proc. Natl. Acad. Sci. U. S. A.* **2010,** *107,* 1361–1366. doi:10.1073/pnas.0909444107
18. Dohno, C.; Uno, S.-n.; Nakatani, K. *J. Am. Chem. Soc.* **2007,** *129,* 11898–11899. doi:10.1021/ja074325s
19. Liang, X.; Takenaka, N.; Nishioka, H.; Asanuma, H. *Chem.–Asian J.* **2008,** *3,* 553–560. doi:10.1002/asia.200700384
20. Liu, Y.; Sen, D. *J. Mol. Biol.* **2004,** *341,* 887–892. doi:10.1016/j.jmb.2004.06.060
21. Banghart, M.; Borges, K.; Isacoff, E.; Trauner, D.; Kramer, R. H. *Nat. Neurosci.* **2004,** *7,* 1381–1386. doi:10.1038/nn1356
22. Lien, L.; Jaikaran, D. C. J.; Zhang, Z.; Woolley, G. A. *J. Am. Chem. Soc.* **1996,** *118,* 12222–12223. doi:10.1021/ja962217s
23. Volgraf, M.; Gorostiza, P.; Numano, R.; Kramer, R. H.; Isacoff, E. Y.; Trauner, D. *Nat. Chem. Biol.* **2006,** *2,* 47–52. doi:10.1038/nchembio756
24. Samanta, S.; Woolley, G. A. *ChemBioChem* **2011,** *12,* 1712–1723. doi:10.1002/cbic.201100204
25. Wang, L. V.; Wu, H.-i. *Biomedical optics: Principles and imaging;* Wiley & Sons, Inc.: Hoboken, New Jersey, 2007.
26. Lin, M. Z.; McKeown, M. R.; Ng, H.-L.; Aguilera, T. A.; Shaner, N. C.; Campbell, R. E.; Adams, S. R.; Gross, L. A.; Ma, W.; Alber, T.; Tsien, R. Y. *Chem. Biol.* **2009,** *16,* 1169–1179. doi:10.1016/j.chembiol.2009.10.009
27. Sanchez, A. M.; Barra, M.; de Rossi, R. H. *J. Org. Chem.* **1999,** *64,* 1604–1609. doi:10.1021/jo982069j
28. Sadovski, O.; Beharry, A. A.; Zhang, F.; Woolley, G. A. *Angew. Chem., Int. Ed.* **2009,** *48,* 1484–1486. doi:10.1002/anie.200805013
29. Hrozhyk, U. A.; Serak, S. V.; Tabiryan, N. V.; White, T. J.; Bunning, T. J. *Opt. Mater. Express* **2011,** *1,* 943–952. doi:10.1364/OME.1.000943
30. Garcia-Amorós, J.; Nonell, S.; Velasco, D. *Chem. Commun.* **2011,** *47,* 4022–4024. doi:10.1039/c1cc10302d
31. Yu, Z.; Hecht, S. *Angew. Chem., Int. Ed.* **2011,** *50,* 1640–1643. doi:10.1002/anie.201006084
32. Khan, A.; Hecht, S. *Chem.–Eur. J.* **2006,** *12,* 4764–4774. doi:10.1002/chem.200501564
33. Khan, A.; Kaiser, C.; Hecht, S. *Angew. Chem., Int. Ed.* **2006,** *45,* 1878–1881. doi:10.1002/anie.200503849
34. Barker, T. J.; Jarvo, E. R. *J. Am. Chem. Soc.* **2009,** *131,* 15598–15599. doi:10.1021/ja907038b
35. Zhang, Z.; Burns, D. C.; Kumita, J. R.; Smart, O. S.; Woolley, G. A. *Bioconjugate Chem.* **2003,** *14,* 824–829. doi:10.1021/bc0340161
36. Chi, L.; Sadovski, O.; Woolley, G. A. *Bioconjugate Chem.* **2006,** *17,* 670–676. doi:10.1021/bc050363u

Beilstein Journal of Organic Chemistry

Amino-substituted diazocines as pincer-type photochromic switches

Hanno Sell[1], Christian Näther[2] and Rainer Herges[*1]

Full Research Paper

Open Access

Address:
[1]Otto-Diels Institut für Organische Chemie, Christian-Albrechts-Universität zu Kiel, Otto-Hahn-Platz 4, 24418 Kiel, Germany and [2]Institut für Anorganische Chemie, Christian-Albrechts-Universität zu Kiel, Max-Eyth-Str. 2, 24418 Kiel, Germany

Email:
Rainer Herges[*] - rherges@oc.uni-kiel.de

* Corresponding author

Keywords:
azobenzene; diazocine; molecular pincer; molecular switches; photochromic compound

Beilstein J. Org. Chem. **2013,** *9,* 1–7.
doi:10.3762/bjoc.9.1

Received: 04 September 2012
Accepted: 26 November 2012
Published: 02 January 2013

This article is part of the Thematic Series "Molecular switches and cages".

Guest Editor: D. Trauner

Abstract

Azobenzenes are robust, reliable, and easy to synthesize photochromic switches. However, their high conformational flexibility is a disadvantage in machine-like applications. The almost free rotation of the phenyl groups can be restricted by bridging two *ortho* positions with a CH_2CH_2 group, as realized in the dihydrodibenzo diazocine framework. We present the synthesis and properties of 3,3'-amino- and 3,3'-acetamido substituted diazocines. Upon irradiation with light of 405 and 530 nm they isomerize from the *cis* to the *trans* configuration and back, and thereby perform a pincer-like motion. In the thermodynamically more stable *cis* isomer the lone pairs of the amino nitrogen atoms point towards each other, and in the *trans* form they point in opposite directions. The distance between the amino nitrogen atoms changes between 8 Å (*cis*) and 11 Å (*trans* isomer).

Introduction

Azobenzenes probably are the most frequently used photochromic switches in chemistry. They are employed as molecular actuators to drive a number of dynamic machine-like functions [1]. To achieve sophisticated engineering tasks such as directed motion at the molecular level [2,3], the geometry change and the force induced during *cis–trans* isomerization has to be coupled to the environment. In the macroscopic world, therefore, machines are made from stiff materials. Azobenzene, however, is a rather floppy molecule. Both phenyl rings can rotate with a low activation barrier, and isomerization of the *trans* form can occur in two different directions, forming two different isomers (enantiomers in the parent system) [4]. Power transmission to neighbouring molecules is inefficient because of energy transfer to internal conformational motion. The first and probably most simple measure to make azobenzene stiffer would be to prevent the phenyl groups from rotating.

Connecting both rings with each other via an alkane bridge is probably the most straightforward way to achieve that. Such a molecule, 5,6-dihydrodibenzo[*c*,*g*][1,2]diazocine (**1**), has been known for more than a hundred years [5]. However, only recently we discovered that the photophysical properties of **1** (quantum yields, photostationary states) are superior to those of parent azobenzene, and most of its derivatives [6-8]. In contrast to azobenzene, diazocine **1** is most stable in its *cis* configuration, which has a boat conformation. The *trans* isomer comes in two conformations: a chair and a twist form, of which the twist is more stable (Figure 1).

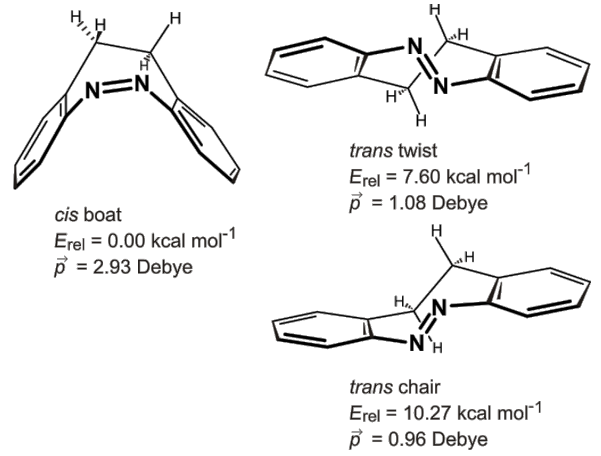

Figure 1: Configurations and conformations of 5,6-dihydrodibenzo[*c*,*g*][1,2]diazocine (**1**), and DFT (B3LYP/6-31G*) calculated energies (kcal mol^{-1}) relative to the most stable *cis* boat form. Dipol moments are given in Debye.

Proper substitution of the diazocine molecular framework is necessary to control the interaction with the environment or with other molecules. Therefore, we explore different approaches to prepare diazocine derivatives. Since the nomenclature is not unambiguous and, hence, potentially confusing, we refer to 5,6-dihydrodibenzo[*c*,*g*][1,2]diazocine derivatives as 2,2'-ethylene-bridged azobenzenes (EBABs).

Results and Discussion

Synthesis

Woolley et al. very recently published the synthesis of a 4,4'-diamino-2,2'-ethylene-bridged azobenzene (4,4'-diamino-EBAB), which exhibits excellent photophysical properties [9]. In planning our synthesis (and not yet being aware of the results of the above authors) we were concerned about the fact that amino substituents in the 4-position with respect to the azo group would impair photochemical conversion, as this is known for 4-amino-substituted azobenzenes [10]. We therefore set out to synthesize 3,3'-diamino-EBAB **4** and derivatives thereof. Key steps of the synthesis are the introduction of the substituents and formation of the azo bond. Several approaches were evaluated, changing the order of the steps and the groups from which the azo unit was generated. The preferred procedure starts from commercially available 1,2-bis(4-aminophenyl)ethane (**2**). Nitration proceeds almost quantitatively in *ortho* position to the ethylene bridge, forming 1,2-bis(2-nitro-4-aminophenyl)ethane (**3**) [11]. Intramolecular reductive coupling of the nitro groups to form the azo unit proceeds with notoriously low yields. The most frequently used procedure using Zn as the reducing agent in $Ba(OH)_2$ [12] or NaOH [13] gives irreproducible and low yields varying from 2% to not more than 19%. Glucose, however, in basic ethanolic solution turned out to furnish the azo compound **4** reproducibly in more than 20% yield. The acetamide derivative **5** is formed by treatment of 3,3'-EBAB **4** with acetic anhydride (Scheme 1).

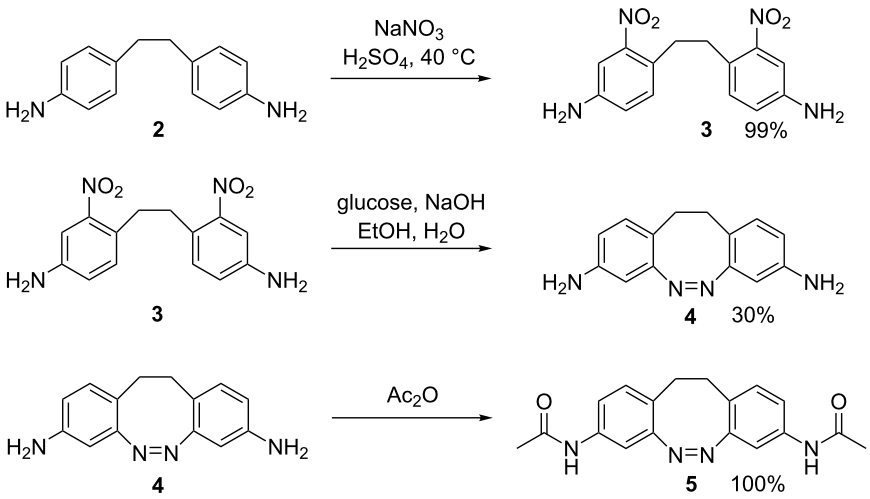

Scheme 1: Synthesis of 3,3'-diamino-EBAB **4** and its acetamide derivative **5**.

The structures of the products were confirmed by ^{1}H and ^{13}C NMR spectroscopy, as well as X-ray crystallography (Figure 2). As in the parent system **1** the amino and acetamido derivates **4** and **5** are thermodynamically most stable in their *cis* form.

Photochromic Properties

trans-Azobenzene exhibits a high-intensity π–π* band at λ_{max} = 316 nm (ε = 22,000 $L \cdot M^{-1} \cdot cm^{-1}$) and a symmetry-forbidden n–π* band at 444 nm with a very low extinction coefficient (ε = 440 $L \cdot M^{-1} \cdot cm^{-1}$) [10]. Irradiation with UV-light of 365 nm converts the *trans* to the *cis* isomer. The n–π* absorption of the nonplanar *cis*-azobenzene is not formally symmetry forbidden. Even though it has a rather low extinction coefficient (1250 $L \cdot M^{-1} \cdot cm^{-1}$), irradiation into the n–π* band leads to complete conversion back to the *trans* isomer [14]. Photoswitching of 5,6-dihydrodibenzo[*c*,*g*][1,2]diazocine (unsubstituted EBAB **1**), however, is performed differently [6]. Conversion of *cis* to *trans*, as well as isomerization of *trans* to *cis*, is achieved by irradiation into the corresponding n–π* bands. This is possible because the n–π* bands appear well separated at different wavelengths (*cis*: 404 nm, *trans*: 490 nm) and the transitions are allowed (albeit weak) in both isomers. Since substituents in the *meta* position are known to interact less efficiently with each other than those in the *ortho* or *para* positions we decided to examine EBABs that are 3,3'-substituted, hoping that the excellent switching properties of the parent system would be retained. For determination of the ratio of isomers in photostationary states we used ^{1}H NMR (for details see Supporting Information File 1).

The UV spectrum of *cis*-3,3'-diamino-EBAB **4** exhibits a π–π* transition at 350 nm, and a shoulder at approximately 400 nm, which arises from the n–π* transition of the azobenzene substructure (Figure 3). Irradiation of a solution of **4** in acetonitrile with light of 405 nm leads to isomerization to the *trans* isomer with 34% *trans* form in the photostationary state (determined by ^{1}H NMR). The rather low conversion rate is probably

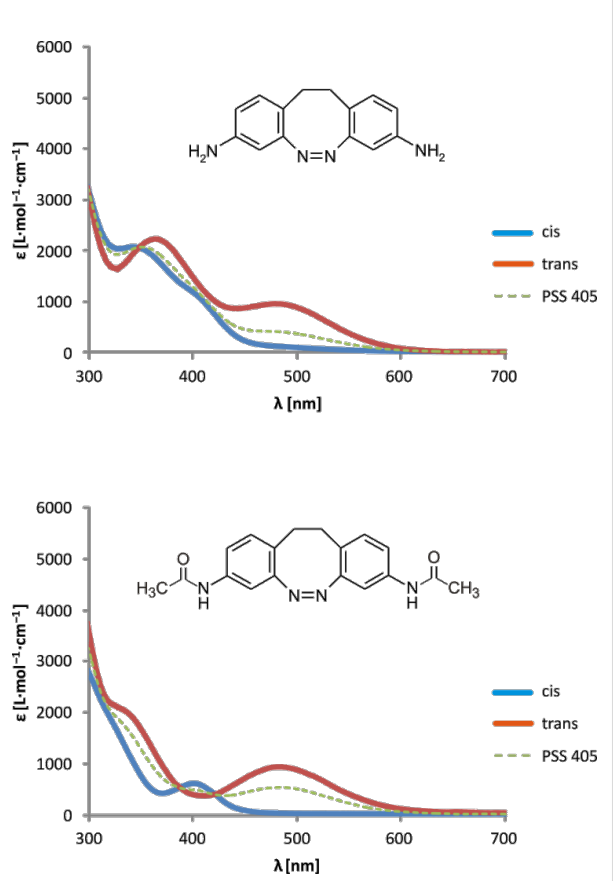

Figure 3: UV–vis spectra of the diazocine derivatives 3,3'-diamino-EBAB **4** and its bisamide derivative **5** in acetonitrile.

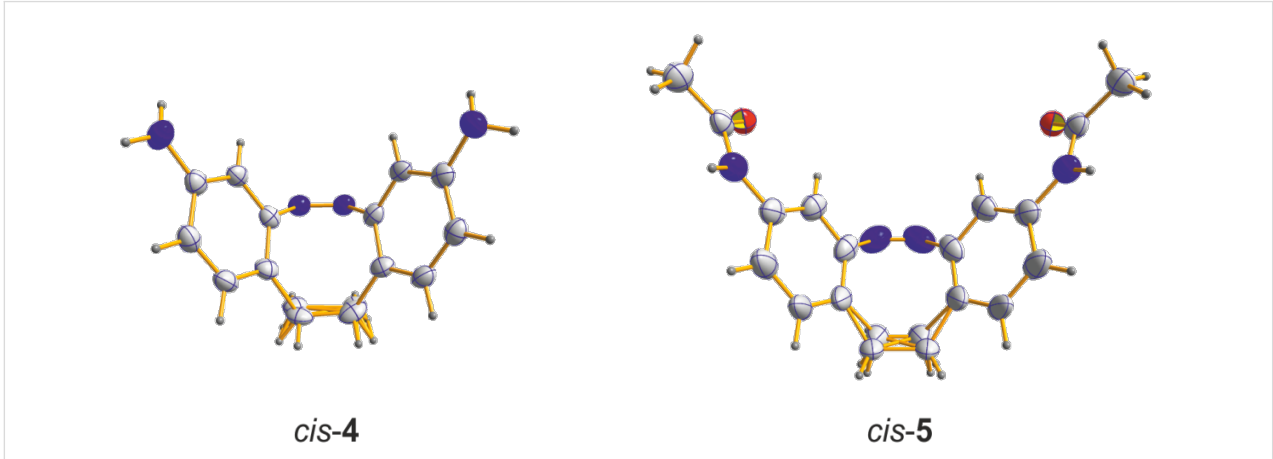

Figure 2: Crystal structures of the *cis* isomers of 3,3'-diamino-EBAB **4** and its acetamide derivative **5**. The atoms of the ethylene bridge are disordered.

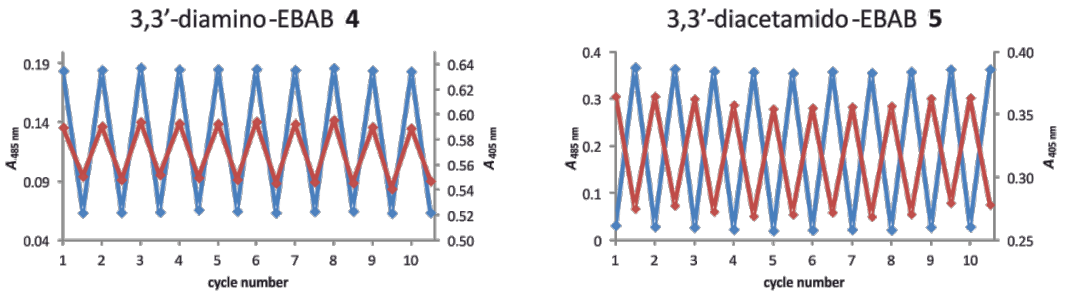

Figure 4: Absorbances of solutions of **4** and **5** in acetonitrile at 405 nm (red) and 485 nm (blue) in the corresponding photostationary states upon alternating irradiation at 405 and 530 nm.

due to the overlap of the π–π* and n–π* transitions in the *cis* form. In the *trans* isomer the n–π* transition is shifted to longer wavelengths (~500 nm) and is clearly separated from any other absorption. Irradiation with light at 450–600 nm therefore converts the *trans* isomer completely back to the *cis* form. As compared to the bisamino-substituted EBAB **4** the π–π* and the n–π* bands of the *cis* isomer of the acetamido derivate **5** are better separated (shoulder at 320 nm and 400 nm) (Figure 3). The photostationary state upon irradiation with 405 nm therefore rises to 54% *trans* form. As in the bisamino-substituted system **4**, conversion of **5** back to the *cis* isomer is quantitative within the error limits of ^{1}H NMR and UV–vis spectroscopy (Figure 4).

Thermal stability of the *trans* isomers

Amino and alkylamino substituents in *para* position to the azo group reduce the lifetime of the *cis* states of azobenzenes [15,16]. A dramatically shortened half-life of an *ortho*-dimethylamino-substituted *cis*-phenylazopyridine (*cis*-4-*N*,*N*-dimethylamino(3-phenylazo)pyridine) has also been observed [17]. The reverse effect was observed in our *meta*-substituted *trans*-3,3'-diamino-EBAB **4**. While the unsubstituted *trans*-EBAB **1** exhibits a half-life of 4.5 h in *n*-hexane solution at room temperature, *trans*-3,3'-EBAB **4** isomerizes to the more stable *cis* form with a half-life of 74 h. The corresponding half-life of *trans*-3,3'-acetamido-EBAB **5** is 46 h (Table 1).

Application as a molecular pincer

In the ^{1}H NMR spectra of *cis*-**4** and *cis*-**5** the four protons of the ethylene bridge yield a centred multiplet. This symmetry of the fine structure shows that they divide into two chemically unequal groups of two chemically equal protons. Hence, there is no boat inversion at room temperature on the NMR time scale. According to the X-ray crystal structures the amino nitrogen lone pairs of *cis*-3,3'-diamino EBAB **4** point towards each other and (if extended to more than 6.5 Å) would intersect with an angle of about 65°. If the acetamido groups in **5** are rotated appropriately, the N–H bonds (extended to 10.5 Å) intersect with an angle of about 45°. Thus, the EBAB derivatives **4** and **5** should be suitable as molecular pincers.

To demonstrate this property we studied the binding of ethylenediamine to the two isomers of the acetamido derivative **5** (Figure 5).

We carried out ^{1}H NMR titrations of *cis*-**5** as well as of the photostationary mixture of *cis*-**5** and *trans*-**5** upon irradiation with light of a wavelength of 405 nm with ethylenediamine in acetonitrile. The spectra showed a significant chemically induced shift (CIS) of the acetamide protons of both isomers upon addition of ethylenediamine. Equilibrium analysis with respect to the CIS binding isotherms by means of nonlinear least-squares methods (for details see Supporting Information

Table 1: Half-life and photostationary states of EBAB **1** and derivatives.

compound	half life [h]	PSS 405 nm % *trans*	PSS 520 nm % *trans*
EBAB **1**	4.5[a]	92%	<1%
3,3'-diamino-EBAB **4**	74[b]	34%	<1%
3,3'-diacetamido-EBAB **5**	46[b]	54%	<1%
4,4'-diacetamido-EBAB	4.8[c]	70%	<1%

[a]300 K, *n*-hexane [6]; [b]300 K, MeCN; [c]293 K, DMSO [9].

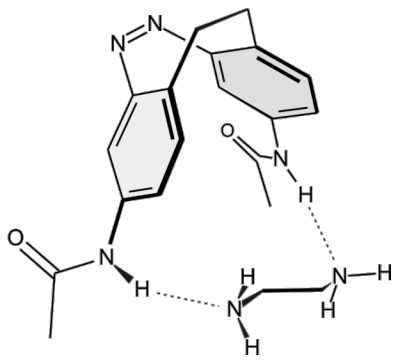

Figure 5: DFT-calculated structure (B3LYP/6-31+G**) of a complex of **5** with ethylenediamine as a conceivable model of the binding mode of 3,3'-diacetamido-EBAB **5**.

File 1) [18,19] yielded a binding constant for the 1:1 ethylenediamine complex of the *cis* isomer of $K_{a,cis}$ = 0.88 ± 0.03 M^{-1}. For the corresponding complex of the *trans* isomer a slightly lower binding constant of $K_{a,trans}$ = 0.61 ± 0.05 M^{-1} was determined in acetonitrile-d_3 at 25 °C.

Conclusion

We prepared ethylene-bridged azobenzene (EBAB) derivatives with amino and acetamido substituents in the *meta* position with respect to the azo group (3,3'-diamino-EBAB **4**, and 3,3'-diacetamido-EBAB **5**). In contrast to azobenzene, and in agreement with the parent EBAB, the *cis* isomer is more stable than the *trans* form. Compared to the parent EBAB, which is a very efficient photoswitch, the conversion from the *cis* to the *trans* isomer upon irradiation with 405 nm is reduced to 34% (diamino derivative **4**) and 54% (diacetamido derivative **5**, cf. 92% in the parent compound). The thermal half-life of the *trans* isomer, however, is drastically increased (3,3'-diamino-EBAB **4**: 74 h, 3,3'-diacetamido-EBAB **5**: 46 h). The EBAB derivatives upon photoisomerization perform a pincer-like motion. Diacetamido derivative **5** binds ethylenediamine better in its *cis* (closed) form than in its *trans* configuration (open form).

Experimental

General remarks

All chemicals were purchased from commercial sources and used without further purification. All NMR spectra were recorded with instruments of the company Bruker (AC 200, DRX 500, and AV 600). The assignments of the NMR signals were confirmed by the evaluation of COSY, HSQC and HMBC spectra. The chemical shifts of the signals were all referenced to residual solvent peaks. The mass spectra were recorded on a Finnigan MAT 8230 instrument. IR spectra were recorded with a Spectrum 100 instrument from Perkin-Elmer equipped with an ATR unit from the company Loriot-Oriel. Melting points were taken without correction. UV–vis spectra were recorded on a Perkin-Elmer Lambda 14 spectrometer.

Synthesis

1,2-Bis(2-nitro-4-aminophenyl)ethane (3): A solution of 5.0 g 1,2-bis(4-aminophenyl)ethane (24.0 mmol) in 40 mL of sulfuric acid was warmed up to 60 °C and a solution of 4.4 g (52.0 mmol) finely grounded sodium nitrate in 45 mL of sulfuric acid was added dropwise. The mixture was stirred at 60 °C for 6 h and afterwards poured into 200 mL of ice–water. The resulting suspension was neutralised by the addition of an aqueous ammonia solution (32%). The red precipitate was filtered off, washed with water and dried in vacuum over $CaCl_2$. Yield: 7.2 g (23.6 mmol, 99%). Mp 247–249 °C; ^{1}H NMR (500 MHz, DMSO-d_6) δ 7.06 (d, $^4J_{6,2}$ = 2.0 Hz, 2H, 6-*H*), 6.99 (d, $^3J_{3,2}$ = 8.3 Hz, 2H, 3-*H*), 6.78 (dd, $^3J_{2,3}$ = 8.3 Hz, $^4J_{2,6}$ = 2.1 Hz, 2H, 2-*H*), 5.58 (s, 4H, 1-NH_2), 2.86 (s, 4H, 7-*H*); ^{13}C NMR (126 MHz, DMSO-d_6) δ 149.90 (C_q, *C*-5), 148.58 (C_q, *C*-1), 132.85 (d, *C*-3), 121.85 (C_q, *C*-4), 119.21 (d, *C*-2), 108.48 (d, *C*-6), 33.25 (t, *C*-7); IR (ATR): 3444 (m), 3363 (s), 3234 (w), 3061 (w), 2947 (w), 2877 (w), 1622 (s), 1513 (vs), 1495 (vs), 1324 (vs), 1272 (s), 1263 (s), 829 (s), 818 (s) cm^{-1}; EIMS (70 eV) m/z (% relative intensity): 302 (16) $[M]^+$, 151 (100); CIMS (isobutane) m/z (% relative intensity): 303 (100) $[M + H]^+$.

(*Z*)-11,12-Dihydrodibenzo[*c*,*g*][1,2]diazocine-3,8-diamine (4): A suspension of 1,2-bis(2-nitro-4-aminophenyl)ethane (**3**) (1.059 g, 3.5 mmol) in a mixture of 140 mL ethanol and a solution of 8.8 g (220 mmol) sodium hydroxide in 35 mL water was heated to 70 °C. A solution of 6.5 g (36 mmol) glucose in 20 mL water was added, and the reaction mixture was stirred overnight. After cooling to room temperature, 500 mL water was added, and the resulting mixture was extracted three times with 100 mL of ethyl acetate. The organic phase was separated and dried over sodium sulfate, and the solvent was evaporated in vacuum. From the obtained residue the product was isolated by flash chromatography (silica gel, cyclohexane/ethyl acetate 1:1) (254 mg, 1.1 mmol, 30%). Mp 193–196 °C; ^{1}H NMR (600 MHz, DMSO-d_6) δ 6.67 (d, $^3J_{6,5}$ = 8.2 Hz, 2H, 6-*H*), 6.24 (dd, $^3J_{5,6}$ = 8.2 Hz, $^4J_{5,3}$ = 2.3 Hz, 2H, 5-*H*), 5.97 (d, $^4J_{3,5}$ = 2.3 Hz, 2H, 3-*H*), 5.15 (br.s, 4H, 4-NH_2), 2.63 (m_c, 4H, 7-H_a, 7-H_b,); ^{13}C NMR (150 MHz, DMSO-d_6) δ 155.87 (C_q, *C*-1), 146.76 (C_q, *C*-2), 130.15 (d, *C*-6), 115.18 (C_q, *C*-4), 112.88 (d, *C*-5), 103.11 (d, *C*-3), 30.44 (t, *C*-7); IR (ATR): 3433 (m), 3344 (m), 3433 (m), 2952 (m), 2850 (m), 1703 (w), 1609 (vs), 1570 (m), 1497 (vs), 1455 (s), 1435 (m), 1303 (s), 1272 (s), 1170 (m), 1142 (m), 1094 (m), 1020 (m), 930 (w), 900 (m), 856 (m), 808 (vs) cm^{-1}; EIMS (70 eV) m/z (% relative intensity): 238 (100) $[M]^+$, 209 (92), 193 (46); CIMS (isobutane) m/z (% relative intensity): 239 (100) $[M + H]^+$.

(*Z*)-N,N'-(11,12-Dihydrodibenzo[*c*,*g*][1,2]diazocine-3,8-diyl)diacetamide (5): In acetic acid anhydride (25 mL), (*Z*)-11,12-dihydrodibenzo[*c*,*g*][1,2]diazocine-3,8-diamine (**4**) (5 mg, 20 mmol) was dissolved. The solution was stirred at room temperature overnight. Afterwards the solvent was evaporated in vacuum, and the product was obtained as a pale yellow solid (7 mg, 20 mmol, 100%). Mp 220–221 °C; ^{1}H NMR (500 MHz, MeCN-d_3) δ 8.25 (s, 2H, 5-N*H*), 7.06 (d, $^4J_{3,5}$ = 2.2 Hz, 2H, 3-*H*), 7.03 (dd, $^3J_{5,6}$ = 8.2 Hz, $^4J_{5,3}$ = 2.2 Hz, 2H, 5-*H*), 6.87 (d, $^3J_{3,5}$ = 2.2 Hz, 2H, 3-*H*), 2.73 (m, 2H, 7-H_a,), 2.70 (m_c, 4H, 7-H_a, 7-H_b), 2.00 (s, 6H, 9-*H*); ^{13}C NMR (125 MHz, MeCN-d_3) δ 168.36 (C_q, *C*-8), 155.27 (C_q, *C*-1), 137.45 (C_q, *C*-2), 129.94 (d, *C*-6), 123.17 (C_q, *C*-4), 117.44 (d, *C*-5), 108.59 (d, *C*-3), 30.29 (t, *C*-7), 22.96 (q, *C*-9); IR (ATR): 3253 (m), 3174 (m), 3102 (m), 3048 (m), 2924 (m), 1711 (m), 1680 (m), 1300 (s), 1260 (s), 1020 (s), 980 (m), 957 (m), 899 (m), 883 (m), 814 (s), 763 (m) cm^{-1}. EIMS (70 eV) m/z (% relative intensity): 322 (50) [M]$^+$, 252 (92), 209 (100); CIMS (isobutane): m/z (% relative intensity) 323 (100) [M + H]$^+$.

Supporting Information

^{1}H NMR spectra of **4** and **5** before and after the irradiation with 405 nm, and ^{1}H NMR binding study of 3,3-acetamido-EBAB (**5**) with ethylenediamine. cif-Files of X-ray crystal structures of *cis*-**4** and *cis*-**5**, and gaussian09 input file of the geometry optimization of the complex of *cis*-**5** and ethylenediamine (DFT B3LYP/6-31+G**).

Supporting Information File 1

Additional NMR spectra and ^{1}H NMR binding study of 3,3-acetamido-EBAB (**5**) with ethylenediamine.
[http://www.beilstein-journals.org/bjoc/content/supplementary/1860-5397-9-1-S1.pdf]

Supporting Information File 2

Crystallographic information file of compound cis-**4**.
[http://www.beilstein-journals.org/bjoc/content/supplementary/1860-5397-9-1-S2.cif]

Supporting Information File 3

Crystallographic information file of compound cis-**5**.
[http://www.beilstein-journals.org/bjoc/content/supplementary/1860-5397-9-1-S3.cif]

Supporting Information File 4

Gaussian09 input file of the geometry optimization of the complex of *cis*-**5** and ethylenediamine.
[http://www.beilstein-journals.org/bjoc/content/supplementary/1860-5397-9-1-S4.gjf]

Acknowledgements

We would like to thank the Deutsche Forschungsgemeinschaft (DFG) for funding through SFB 677 (Function by Switching).

References

1. Merino, E.; Ribagorda, M. *Beilstein J. Org. Chem.* **2012,** *8,* 1071–1090. doi:10.3762/bjoc.8.119
2. Purcell, E. M. *Am. J. Phys.* **1977,** *45,* 3–11. doi:10.1119/1.10903
3. Hänggi, P.; Marchesoni, F. *Rev. Mod. Phys.* **2009,** *81,* 387–442. doi:10.1103/RevModPhys.81.387
4. Haberhauer, G.; Kallweit, C. *Angew. Chem.* **2010,** *122,* 2468–2471. doi:10.1002/ange.200906731
Angew. Chem., Int. Ed. **2010,** *49,* 2418-2421. doi:10.1002/anie.200906731
5. Duval, H. *Bull. Soc. Chim. Fr.* **1910,** *7,* 727.
6. Siewertsen, R.; Neumann, H.; Buchheim-Stehn, B.; Herges, R.; Näther, C.; Renth, F.; Temps, F. *J. Am. Chem. Soc.* **2009,** *131,* 15594–15595. doi:10.1021/ja906547d
7. Jiang, C.-W.; Xie, R.-H.; Li, F.-L.; Allen, R. E. *J. Phys. Chem. A* **2011,** *115,* 244–249. doi:10.1021/jp107991a
8. Böckmann, M.; Doltsinis, N. L.; Marx, D. *Angew. Chem., Int. Ed.* **2010,** *49,* 3382–3384. doi:10.1002/anie.200907039
9. Samanta, S.; Qin, C.; Lough, A. J.; Woolley, G. A. *Angew. Chem.* **2012,** *124,* 6558–6561. doi:10.1002/ange.201202383
Angew. Chem., Int. Ed. **2012,** *51,* 6452–6455. doi:10.1002/anie.201202383
10. Rau, H. In *Azocompounds in Photochromism, Molecules and Systems;* Dürr, H.; Bouas-Laurent, H., Eds.; Elsevier: Amsterdam, 1990; p 165. The *p*-Amino substitution leads to a bathochromic shift of the p–p* transition and thus to an overlap of the p–p* and n–p* transitions.
11. Matei, S. *Rev. Roum. Chim.* **1966,** *11,* 843.
12. Paudler, W. W.; Zeiler, A. G. *J. Org. Chem.* **1969,** *34,* 3237–3239. doi:10.1021/jo01263a004
13. Shine, H. J.; Chamness, J. T. *J. Org. Chem.* **1963,** *28,* 1232–1236. doi:10.1021/jo01040a016
14. Knoll, H. Photoisomerism of Azobenzenes. *CRC Handbook of Organic Photochemistry and Photobiology,* 2nd ed.; CRC Press LLC: Boca Raton, 2004; 89-1–89-16.
15. Schulte-Frohlinde, D. *Justus Liebigs Ann. Chem.* **1958,** *612,* 138–152. doi:10.1002/jlac.19586120115
16. Mourot, A.; Kienzler, M. A.; Banghart, M. R.; Fehrentz, T.; Huber, F. M. E.; Stein, M.; Kramer, R. H.; Trauner, D. *ACS Chem. Neurosci.* **2011,** *2,* 536–543. doi:10.1021/cn200037p
17. Thies, S.; Sell, H.; Bornholdt, C.; Schütt, C.; Köhler, F.; Tuczek, F.; Herges, R. *Chem.–Eur. J.* doi:10.1002/chem.201201698.
18. del Piero, S.; Melchior, A.; Polese, P.; Portanova, R.; Tolazzi, M. *Ann. Chim. (Rome, Italy)* **2006,** *96,* 29–49. doi:10.1002/adic.200690005
19. de Levie, R. *J. Chem. Educ.* **1999,** *76,* 1594–1598. doi:10.1021/ed076p1594

Beilstein Journal of Organic Chemistry

A chemist and biologist talk to each other about caged neurotransmitters

Graham C.R. Ellis-Davies

Commentary

Open Access

Address:
Department of Neuroscience, Mount Sinai School of Medicine, One Gustave Levy Place, New York, NY 10029, USA

Email:
Graham C.R. Ellis-Davies - graham.davies@mssm.edu

Keywords:
caged compounds; cell signaling; electrophysiology; neuronal currents; photolabile neurotransmitters; rates of reaction; receptor antagonism

Beilstein J. Org. Chem. **2013,** *9,* 64–73.
doi:10.3762/bjoc.9.8

Received: 01 September 2012
Accepted: 07 December 2012
Published: 11 January 2013

This article is part of the Thematic Series "Molecular switches and cages".

Guest Editor: D. Trauner

Abstract

Caged compounds are small organic molecules that can be photoactivated with brief pulses of light. They are widely used to study a great variety of biological processes by physiologists, cell biologists and neuroscientists. Initially made and invented by biologists in the late 1970s, they are now made mostly by chemists, often without any dialogue with the end users, the biologists. The idea for this review is to stimulate interaction between the two communities to further the creative development and application of these powerful optical probes.

Introduction

The first biologically active molecules to be synthesized with photochemically protecting groups at their active sites were nucleotides [1,2]. Two reports appeared in 1977 and 1978 describing the synthesis of ortho-nitrobenzyl derivatives of cyclic-AMP [1] and ATP [2]. The photolabile cAMP derivative was one member of a series of phosphate esters made as membrane permeable pronucleotides. Thus, this optical probe arose out of the context of the already developed prodrugs that used thermal chemistry for release of their latent cargo. In contrast, the photolabile ATP molecule was synthesized in a physiology department for rapid photoactivation of a particular enzyme, the Na,K-ATPase. It was the latter group that dubbed such photochemical probes “caged compounds”. This simple term has been adopted by biologists since that time [3-9], perhaps because the photolabile ATP compound was the one that was used in a series of important muscle physiology studies in the 1980s [6,10-13]. Chemists have been much more resistant to embrace the moniker, mostly because the term is used for cagelike structures (e.g., cubane), but also perhaps due to the “lateness of arrival” into the field, which gave rise to attempts to commandeer the field for themselves by using a host of different terms [14-16]. Having expressed this opinion, there is no doubt that chemists were slow to use their great synthetic skills to help biologists develop new caged compounds. It can be seen that in the 1980s all the important new caged compounds were made in biology departments: (1) caged calcium

[17] (molecular biology), (2) caged IP3 [5] (physiology) and carbamoylcholine [9] (biochemistry). The last of these new probes was the beginning of the development of caged neurotransmitters (e.g., glutamate, GABA, sertonin, glycine) and an important collaboration [18-24] between George Hess (a biophysicist) and Barry Carpenter (a chemist).

Why was this collaboration important for this field? The answer has two parts. First, it is rare for one group to encompass all the expertise required for the development of such optical probes, as skills in organic chemistry, photophysics, ion-channel biophysics and neurobiology are ideally all involved in the process. Secondly, the main goal of the team was set by the biological problem [25], and often such problems are not well understood by chemists working in isolation. Thus, to solve the biological problem provided by the biologist (Hess), a newer caging chromophore [18] had to be synthesized by a chemist (Carpenter). Thus, chemists came to play a crucial role in the caged compound field. Chemistry at the service of biology is not unusual or unique, as the pharmaceutical industry is built on this idea. In my view it still remains difficult for organic chemists and neurobiologists to understand the limitations of the others' field, and it is these limitations that are crucial for compound development. In this review I try to take the side of the neurobiologist who is thinking about using a caged transmitter in an experiment. I ask the chemist a series of simple questions about the caged compound(s); some of these questions, we discover, do not have simple answers.

Glutamate is the most important neurotransmitter in the brain, as its release at nerve synapses transfers electrical signals between pre- and postsynaptic cells. Approximately 80% of such signaling is carried out by glutamate binding to AMPA receptors, the major post-synaptic excitatory ionotropic ion channels that bind glutamate. These receptors are blocked specifically by α-amino-3-hydroxy-5-methyl-4-isoxazolepropionic acid, hence their acronym. For this reason the development of caged forms of this neurotransmitter has been the subject of considerable activity by chemists. Furthermore, the vast majority of neurons and all astrocytes have glutamate receptors involved in other types of cellular signaling, and so many biologists are interested in stimulating these receptors. I focus the conversation on caged glutamate probes (Figure 1).

Discussion

Biologist: Is your caged glutamate "biologically inert"?

Chemist: We have several caged glutamate molecules [7,23,26-34], and some are even commercially available [18,26,27,31,33] (Table 1). In order to address your question, we can see that in

Table 1: Properties of various caged glutamate probes[a].

Caged Glu	ε (λ_{max})	Φ (% Glu yield)	ε·Φ	2PuCS (GM/nm)	Commercial	Pharmacology towards GABA-A	Stability in aqueous buffer	Solubility (mM) at pH 7.4 in aqueous buffer
Noc	500 (350)	0.65 (100)	325	NR	none	NR	Stable	>50
CNB	500 (350)	0.14 (100)	60	NR	Invitrogen	Partial agonist	Half-life 17 h rt	>50
MNI	4,300 (330)	0.085 (>95)	357	0.06 (740)	Tocris	SA 10 mM	Stable	400
RuBi	5,600 (450)	0.13 (NQ)	728	0.14 (800)	Tocris	50% inhibition at 0.3 mM	Stable	NR
PMNB	9,900 (317)	0.1 (100)	990	0.45 (800)	none	NR	Stable	Requires 1% DMSO
antMNI	27,000 (300)	0.085 (94)	2295	NR	none	NR	Stable	33
BNSF	64,000 (415)	0.25 (65)	16,000	5 (800)	none	NR	ND	0.1
CDNI	6,400 (330)	0.6 (100)	3,840	0.06 (720)	none	MA 0.4 mM	Stable pH 2	100
DEAC	13,700 (390)	0.11 (NQ)	1507	NR	none	NR	stable	NR
MANI	4,300 (330)	0.1 (100)	430	NR	Sigma	NR	Like MNI	>100
Bhc	43,000 (458)	0.3 (100)	12,900	1 (740)	none	NR	Stable frozen pH 7.4	7.5

[a]Abbreviations and symbols: ε, extinction coefficient; Φ, quantum yield; 2PuCS, 2-photon uncaging cross section; NR, not reported; MA, mild agonist; Noc, *N*-nitrophenethyloxycarbonyl; CNB, carboxynitrobenzyl; MNI, methoxynitroindolinyl; RuBi, ruthenium-bipyridine; PMNB, propylmethoxynitrobiphenyl; antMNI, antennea-methoxynitroindolinyl; BNSF, bisnitropropylstyrylfluorene; CDNI, carboxymethylnitroindolinyl; DEAC, diethylaminocoumarin; MANI, methylacetoxynitroindolinyl; Bhc, bromohydroxycoumarin.

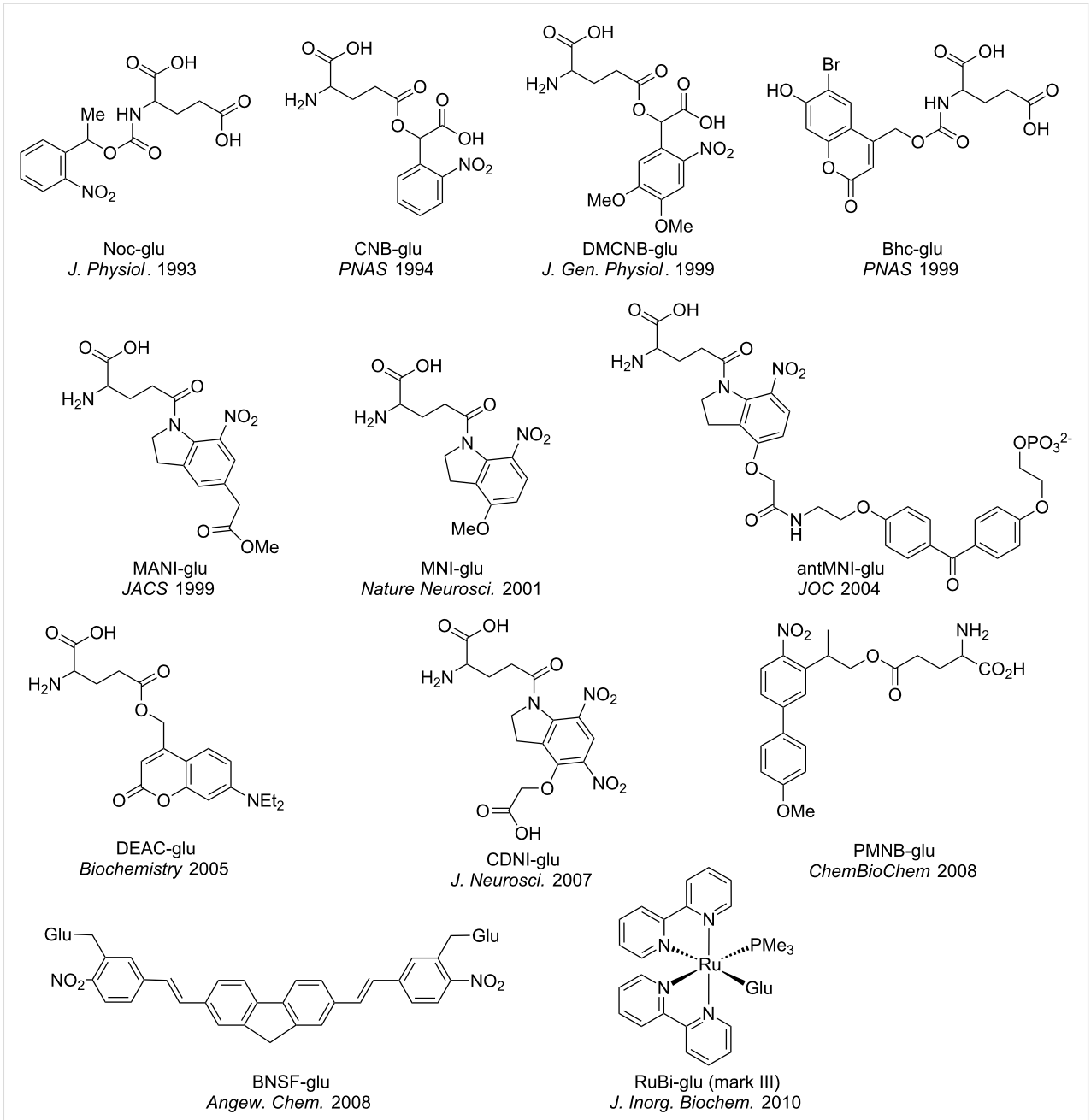

Figure 1: Structures of various caging chromophores. Abbreviations: Noc, *N*-nitrophenethyloxycarbonyl; CNB, carboxynitrobenzyl; DMCNB, dimethoxycarboxynitrobenzyl; Bhc, bromohydroxycoumarin; MANI, methylacetoxynitroindolinyl; MNI, methoxynitroindolinyl; antMNI, antennea-methoxynitroindolinyl; DEAC, diethylaminocoumarin; CDNI, carboxymethylnitroindolinyl; PMNB, propylmethoxynitrobiphenyl; BNSF, bisnitropropyl-styrylfluorene; RuBi, ruthenium-bipyridine.

most of the original papers describing the development of the compounds, detailed pharmacology was described. In one report, the spontaneous miniature excitatory post-synaptic currents (EPSCs) were measured in the presence and absence of a probe when it was puffed at 10 mM concentration onto cultured hippocampal neurons [31]. The histograms of the ensemble averages were indistinguishable. The other examined whether MNI-Glu blocked the current evoked by puffer application of glutamate itself onto neurons [35]. Since these original reports, many other groups have reproduced these results, so they are probably reliable. A recently developed caged glutamate that uses different photochemistry ("RuBi-Glu") is also reported to be inert towards AMPA receptors [33]. This study also noted that MNI-Glu perturbed AMPA spontaneous miniature EPSCs. So it is difficult for us chemists to judge from such reports how to improve the caged compounds any further. In

fact, in our own field we know very well, that the same reagent can give different results under slightly different conditions, or even the same conditions!

Biologist: Neuroscientists most often simply want the technology they buy to "work". So it can be inferred that if many different groups have successively used some piece of technology, it is probably fine.

Chemist: We chemists have a similar appreciation of technology in our own field. For example, in the field of the development of reagents for synthetic methods, there are examples of reagents that have been found to give very reliable and reproducible yields for the transformation that they are designed to accomplish, by many laboratories. In contrast, the literature is full of "single-data-point reports" of chemical transformations. Naturally chemists tend to trust the former.

Biologist: It is well known from work in the pharmaceutical industry that drugs developed to target receptors can have undesirable and surprising side effects, so-called off-target effects. What about these caged Glu probes?

Chemist: It is much harder to give a clear-cut answer to this question. At the high concentrations that are used for two-photon experiments (range 3–12 mM) all classes of caged neurotransmitters are reported to block GABA-A receptors to some extent [33,36,37]. This off-target effect was only discovered relatively recently, as it never occurred to anyone that probes such as MNI-Glu, which were inert toward their target [31], would block another neuroreceptor in the same concentration range [36]. The structure–function relationship for such effects is not fully understood. What is known is that similarly caged Glu and GABA probes (e.g., CDNI-Glu and -GABA) both block GABA-A receptors with the same efficacy, implying that the amino acid is not crucial. Furthermore, the diversity of the structures of caging chromophores (Figure 1) implies that one specific functionality cannot give rise to such undesirable effects. However, at low concentrations (range 5–300 μM) it seems that these off-target effects are significantly reduced [38,39]. For other glutamate receptors, such as amino acid transporters involved in the clearance of glutamate by astrocytes, caged compounds do not block such receptors [40]. The effect of caged transmitters on other membrane receptors, such as voltage-caged ion channels, has not been well studied. The good news is that since the caged transmitters have a relatively low affinity for GABA-A receptors, it turns out that most, if not all, can be overcome by uncaging anyway [36]. Thus, I would like to ask, how important are such off-target effects for your experiments?

Biologist: This is a good question. Perhaps we biologists simply don't like the idea of using probes that slightly perturb the system we study in some way, even if it does not make much difference to the question we are addressing. One type of experiment one could imagine performing where it may be important is the combination of two-photon uncaging of glutamate with optogenetic activation of GABA receptors from genetically selected neurons. In such a paradigm the application of high concentrations of caged Glu would probably block the effects of synaptically released GABA.

A possible advantage of blockade is that it may enhance the spatial restriction of photoreleased transmitter. Certainly, a smart experiment would be to take advantage in some way of the poor pharmacology of caged transmitters towards GABA receptors. Two good examples from another area are the known chloride and pH sensitivity of wild-type GFP fluorescence being used as indicators for these solutes [41,42]. Most fluorescent proteins we use have these properties mutated away; however, the genetically encoded indicators actually use the "weaknesses". Some photolabile neurotransmitters have now been developed and are commercially available without any testing of any sort being performed. Thus, they cannot even really be called "caged".

Biologist: Is your caged transmitter "water soluble"?

Chemist: It is well known in the pharmaceutical industry that water solubility is one of the true challenges for drug development. Often drugs are built up around rigid hydrocarbon scaffolds, such substances are inherently hydrophobic. The same issue applies to caged compounds, as in these we add aromatic rings to produce photosensitivity. The simplest type of caging chromophores are quite water soluble (Table 1), but even modest derivatives can lose water solubility precipitously! With drugs this is often counteracted by adding betacyclodextrin to the formulation, and with caged compounds, a small amount of organic solvent (ca. 1%) is what we chemists typically resort to [28,43,44], but sometimes much larger proportions are required for effective uncaging [45], rendering the method biologically useless. What is acceptable to, or ideal for neurobiologists?

Biologist: Last time I looked there was no organic solvent in the brain. The pH of physiological buffer is in the range of 7.2–7.4 and is set by dissolved CO_2. For obvious reasons, neurobiologists who use acutely isolated brain slices to study neuronal function mimic this buffer. Neurons are the most sensitive cells, so even small amounts of organic solvents can be quite toxic, and thus no one would routinely use any DMSO or methanol in their buffer. Perhaps 0.1% is OK if one is desperate; but ideally no organic solvents should be present in the buffer.

Chemist: We chemists tend not to be too concerned about reagent concentrations in our work, as long as the substrates dissolve, we are fine. All caged neurotransmitters are water soluble to some extent, so how soluble do they have to be?

Biologist: We are very concerned about concentrations! But the exact amounts used always depend on the type of experiment. Routine one-photon uncaging only requires a concentration of 1 mM (maximally), and quite often, much lower concentrations work very well [46-49]. As we have already noted, two-photon uncaging normally requires significantly higher concentrations [30,50-53], so for these experiments solubility becomes more of an issue. It is important for chemists to know that we usually make up stock solutions that are at least 10 times higher than those used, therefore we would look for water solubility in the 50–100 mM range.

Chemist: This can easily be achieved for caged transmitters with simple chromophores such as MNI-Glu and CNB-Glu. But even the addition of one nitro group or aromatic ring to these molecules dramatically reduces their solubility properties making them much more difficult to use [34]. But note the new RuBi-Glu [33] probe is soluble in water up to 20 mM, even though it has many aromatic rings.

Biologist: How water stable are the caged neurotransmitters at physiological pH?

Chemist: Again this varies tremendously. The nature of the chemical bond used for caging defines the aqueous stability. Simple benzyl esters are fairly stable, so CNB-Glu [18] has a decent half-life at pH 7.4. However, more electron-rich molecules tend to be much more unstable. Phosphate esters are more stable than carboxylate esters, but they also suffer from instability. Thus, an electron-deficient NB-caged cAMP is very stable but an electron rich one (DMNB-cAMP) is not [4,54]. The opposite trend is true for nitroindolinyl-caged transmitters [26,27,32,36]. Because of this problem, chemists have resorted to inserting a spacer unit between the caging chromophore and the substrate [7,55-59]. This strategy has been very successful in creating some highly stable caged compounds, but sometimes at the expense of another property, such as the rate of release [7]. For example, GABA caged directly as an ester with coumarin chromophores is photoreleased quickly, but is quite unstable in (frozen) solution [60]. However, when caged via a carbamate, its release is orders of magnitude slower, but the compounds are water stable [56]. When phenols (e.g., serotonin or capsaicin) are caged via the carbonate, they are effectively stable and released quickly [61,62]. It is also important to note that the stability of all these "acid-like" caged compounds depends on the pH of the aqueous solution. All are more stable in the pH range of 2–4, and much less stable above pH 8. Thus, it may be better for long-term storage of solutions to be done at the former, with daily solutions diluted from stocks.

Other caged compounds, due to the chemical bond that is used, are impossible to hydrolyze. For example, all ethers and amines caged with nitrobenzyl groups are completely stable [18]. RuBi-Glu and GABA are also stable [33,38], as these are caged using donation from the amine lone pair of the neurotransmitter into the Ru d-orbital. Finally, it is important to note that many chemists do not study stability at physiological temperatures, nor do they perform long-term stability tests over many months. How important are such details for biological use?

Biologist: In fact this sort of information is really quite important. We often perform experiments with warm buffer (30–37 °C), or even in living animals. Also, for practical purposes we make stock solutions for freezing in aliquots, and only thaw for use at the desired time.

Chemist: Since 1980, the rate of release of the caged compound has been the subject of study by those who develop caged compounds [3]. Since the reaction mechanisms are quite complex, these details have also fascinated many chemists in the field of caged compounds [63]. In fact, we can get quite "distracted" by such arcane studies. Can you help with guidelines for the requirements you have for rates of uncaging?

Biologist: As you noted for chemical stability, such requirements vary a good deal! Our requirements are conditioned by two concerns. First, we are limited by our measurement ability. In terms of imaging or electrophysiology it is very difficult for us to measure anything in a cell faster than a few microseconds. In electrophysiology, we normally apply a digital filter to the signal. These are in the range of a few kilohertz, and such signals would be digitized at tens of kilohertz [64,65]. Imaging is slightly different but it is also relatively slow, and is defined by the ability to collect enough photons from a unit area (a pixel). For standard confocal imaging the dwell time for each pixel is a few microseconds, meaning an image frame takes about 1–2 seconds [66]. This is much slower than electrophysiology. There are several methods that are used to speed up the rate of image acquisition [67,68], but even these are limited to 30–100 Hz for full frame (512 × 512 pixels) imaging. Of course if one takes smaller frame sizes the rate increases. The most widely used method is simply eliminating the frame, by using "line-scan" imaging, in which each line may require only 2 ms. Some modern imaging software allows many "short lines" to be connected, enabling quite fast imaging of selected cellular areas [69,70].

Chemist: So if we uncage in the pico- or nanosecond time range [71,72] is this of any real use for biology?

Biologist: Not really. As mentioned above, because we are constrained by measurement protocols, probably the 1–10 microseconds range is sufficient for most purposes. I have been confused by some reports of "rates of reactions" being given as a time course for steady-state photolysis over many seconds or minutes [45], whereas other reports show rates from laser flash photolysis [3,61]. Can you help clarify this?

Chemist: Only the latter should be called a rate. The former is simply a way of measuring the quantum yield by determining the half-time (hence "rate") of photolysis under some set of defined irradiation conditions. However, even with the former measurement care must be taken. The chemical reactions of release can be quite complex, so the rate of release of product is the key property [3,62,63]. In fact this is one reason why chemists study reaction mechanisms, as there can be several intermediates along the reaction pathway, leading to transmitter release [73]. Unfortunately, there is no easy way to detect glutamate optically, so the other products from uncaging are used as surrogates for the transmitter [61]. For example, protons can often be a reaction product, so pH detection is used [7,8]. If the aromatic side product has a distinctive absorption, the appearance of this species can be measured [3]. However, not all caged compounds have such side products, or their appearance may not be in the rate-limiting step along the reaction pathway.

Biologist: From receptor kinetics in membrane patches from cultured neurons, the estimated half-time of the increase in glutamate concentration is fast [74] (ca. 0.1 ms). The measured postsynaptic rise (10–90%) for excitation [75] is about 0.15–0.70 ms and inhibition [76] about 0.4 ms.

Chemist: Short periods of two-photon excitation (0.05 ms) allow one to mimick such events [31], implying the rate of uncaging of glutamate from MNI-Glu is not rate-limiting for optical stimulation of postsynaptic ionoropic receptors. RuBi-Glu is uncaged in less than 50 ns [77], so this probe may be used with similar confidence. The first fast caged glutamate, CNB-Glu, is photoreleased with a half-time of about 0.03 ms [18].

Chemist: A somewhat neglected property of caged neurotransmitters is their compatibility with biological buffers. This is a different issue from chemical stability and pure solubility. It seems that some phosphate derivatives of polyaromatic chromophores have been reported to precipitate in artificial cerebral spinal fluid [78,79]. This property has not been studied for many other caged transmitters, but probably the lack of difficulties for the most widely used caged compounds suggests that they are well tolerated in physiological buffers.

Biologist: What is the difference between photochemical and chemical efficiency for uncaging reactions?

Chemist: The photochemical efficiency of uncaging involves two completely distinct properties [80]. First, we must consider how well a molecule absorbs light, through the molar extinction coefficient, ε. This property measures how effectively a chromophore absorbs photons. Thus, fluorescein (ε = 80,000/M/cm) absorbs light much better than MNI-Glu [27] (ε = 4,300/M/cm). The second property is the quantum yield of photolysis (chemists use the symbol Φ for this). This measures how many excited molecules give a product, with the normal maximum being 1. Photochemical efficiency is ε·Φ. So, to some extent, a large ε can make up for a poor Φ, but ideally the Φ should be large, to take maximum advantage of the absorbed light. A large ε allows the use of less light, thus potentially avoiding phototoxic side effects from uncaging. However, it has been pointed out that very large ε are not always advantageous for 1-photon uncaging experiments [80,81]. If a solution of 1 mM is applied to a cell and the chromophore has an ε = 4,300/(M·cm), then a 1 mm path length absorbs a fraction 1 − log 0.43, and a 4 mm path length absorbs 1 − log 1.92. Such path lengths are typical for microscope objectives, meaning that much of the light will be absorbed before it reaches the cell [81]. This saturation problem is not an issue for two-photon excitation of caged compounds.

Chemical efficiency is unrelated to ε and Φ. It refers to the basic property of the chemical yield of glutamate compared to the amount of caged glutamate photolyzed. The good news is that most uncaging reactions are quite efficient chemically, with few competing side reactions [80]. One of the caging chromophores has been reported [29] to undergo a significant side reaction that traps the caged compound in a cul-de-sac. However, no reaction is completely "clean", so it is doubtful that 100% release of glutamate can ever come from uncaging.

Biologist: Many really important biological experiments with caged transmitters have been performed with compounds that have relatively poor photochemical efficiency [82]. So why do you chemists continue to make new compounds if the old ones work?

Chemist: This is a good question. Certainly CNB-Glu [18] and CNB-GABA [83] yielded many useful results [82]. For one-photon uncaging the ε·Φ of these is sufficient. However, they

are prone to hydrolysis, so the first nitroindolinyl-caged Glu was a real improvement, as it is much more stable at physiological pH [26]. Thus, for all 1-photon experiments this caged Glu compound is sufficient; however, it is not very sensitive to two-photon excitation. Hence, several other nitroindolinyl-caged transmitters have been made and used [31,32,34,36,39,40,56,84,85]. Since these have been designed for 2-photon uncaging, they have proved useful in many neurophysiological experiments in brain slices, especially those concerning the biochemistry in single spine heads. Note that MNI-Glu was independently made by two groups at the same time [27,86], but only one of them appreciated that the molecule would be useful for this area of optical neuroscience [31]. In reality, I think we chemists need guidance from you biologists as to what is required for the "next phase" of caged transmitter development.

Biologist: Certainly one of the things that would be very helpful for us is that if you make a new caged transmitter, you perform some side-by-side real-world comparison. For example, when the genetically encoded calcium indicators (GECI) are made, it is standard practice to bench-mark them against calcium dyes and earlier GECI [87-93]. The other GE technology based on proteins called "channelrhodopsins" is also rapidly evolving, and this is done in a comparative way [94]. Thus, similar comparisons for each new caged neurotransmitter would be useful. Since one such example has been reported [32] (Figure 2), and several are now commercially available (Table 1) this seems a fairly straightforward task.

Chemist: Since the discovery of the light-gated ion channels called channelrhodopsins (ChR) in 2002 [95] and 2003 [96], a second method for optical activation of neuronal cells has been

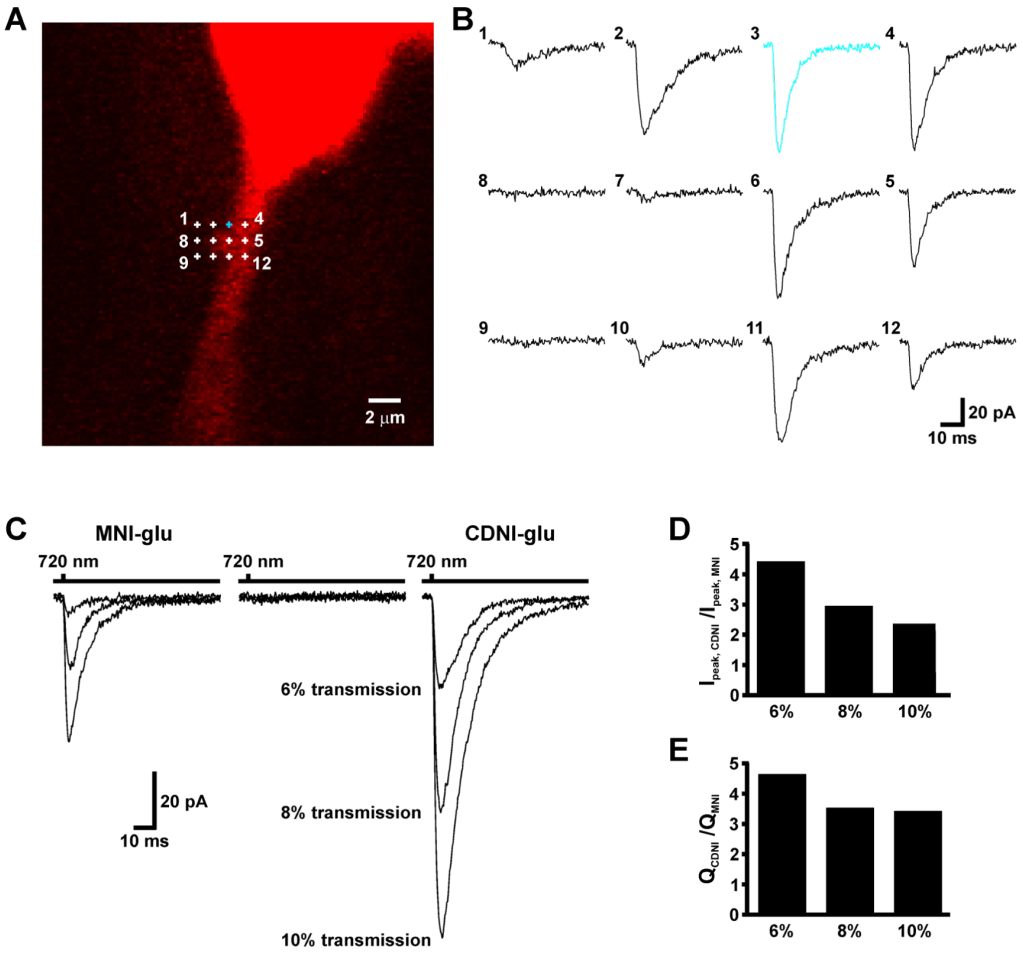

Figure 2: Comparative two-photon uncaging of MNI-Glu and CDNI-Glu on pyramidal neurons in an acutely isolated brain slice. (A) Fluorescent image of a pyramidal neuron filled with red dye. Numbered crosses correspond to the positions of the points of uncaging in B. (B) Currents evoked by two-photon irradiation at points marked in A. (C) Comparative photolysis of MNI-Glu and CDNI-Glu on the same neuron. The caged compound was topically applied from a puffer pipette at a concentration of 10 mM above the brain slice. Current traces are an average of several trials. (D, E) Relative peak currents and charges evoked by CDNI/MNI. Note some receptor saturation from uncaging the more photoactive CDNI decreases the ratio at higher powers. Data courtesy of Martin Paukert and Dwight Bergles (Johns Hopkins School of Medicine). The two caged compounds were applied "blind" during these experiments.

developed. Some think that the massive and expanding popularity of optogenetic stimulation shows that synthetic caged compounds remain a fairly mature niche technology. What do you think is required from chemists to sustain support for uncaging technology?

Biologist: First, it is important to say the obvious, that very clearly channelrhodopsin and caged compounds are complementary methods. But certainly many neuroscientists are using channelrhodopsin who did not use caged compounds. This is because they want to control the behavior of a moving animal [97,98]. Importantly, genetic methods allow ChR to be expressed in cells without any additional cofactors (no chemicals) and to select which cells have the ChR [94,98]. These two properties are very powerful advantages for neuroscience, compared to caged compounds. However, when it comes to other organs, where a firing action potential is not so important, it is not so clear how useful ChR can really be. Secondly, optogenetic control technology is limited to a few signaling cascade molecules [94], whereas caged compounds can be used for virtually any type of molecule [80]. However, all too often the ingenious inventions of organic chemists in this realm do not move beyond the initial proof-of-principle deployment [99-102]. Even in the case of caged glutamate compounds the vast majority of the new probes are not used to do new biological experiments (Table 1). Thus, I think it is vital for chemists to seek out closer collaborations with biologists of all sorts to enable the creative development of truly useful new caged compounds.

Conclusion

Caged compounds have been uniquely powerful optically activated chemical tools for many areas of biological science. In particular, the past 20 years have witnessed an increased refinement in terms of the ability to localize neurotransmitter release. Starting from broad-scale mapping of synaptic connections, by using UV stimulation, to highly local concentration jumps, by two-photon excitation of caged glutamate compounds, caged glutamate probes continue to be widely used by the neuroscience research community. These probes could only have developed in the context of a fruitful dialogue between organic chemists and neurobiologists.

Acknowledgements

My laboratory is supported by grants from the NIH (GM53395 and NS69720). I thank my long-term neuroscience collaborators for many scientific interactions that have stimulated the development of novel caged compounds. I also thank Prof. Matsuzaki for the uncaging data shown in the graphical abstract.

References

1. Engels, J.; Schlaeger, E. J. *J. Med. Chem.* **1977,** *20,* 907–911. doi:10.1021/jm00217a008
2. Kaplan, J. H.; Forbush, B., III; Hoffman, J. F. *Biochemistry* **1978,** *17,* 1929–1935. doi:10.1021/bi00603a020
3. McCray, J. A.; Herbette, L.; Kihara, T.; Trentham, D. R. *Proc. Natl. Acad. Sci. U. S. A.* **1980,** *77,* 7237–7241. doi:10.1073/pnas.77.12.7237
4. Nerbonne, J. M.; Richard, S.; Nargeot, J.; Lester, H. A. *Nature* **1984,** *310,* 74–76. doi:10.1038/310074a0
5. Walker, J. W.; Somlyo, A. V.; Goldman, Y. E.; Somlyo, A. P.; Trentham, D. R. *Nature* **1987,** *327,* 249–252. doi:10.1038/327249a0
6. Goldman, Y. E.; Hibberd, M. G.; McCray, J. A.; Trentham, D. R. *Nature* **1982,** *300,* 701–705. doi:10.1038/300701a0
7. Corrie, J. E.; DeSantis, A.; Katayama, Y.; Khodakhah, K.; Messenger, J. B.; Ogden, D. C.; Trentham, D. R. *J. Physiol.* **1993,** *465,* 1–8.
8. Khan, S.; Castellano, F.; Spudich, J. L.; McCray, J. A.; Goody, R. S.; Reid, G. P.; Trentham, D. R. *Biophys. J.* **1993,** *65,* 2368–2382. doi:10.1016/S0006-3495(93)81317-1
9. Milburn, T.; Matsubara, N.; Billington, A. P.; Udgaonkar, J. B.; Walker, J. W.; Carpenter, B. K.; Webb, W. W.; Marque, J.; Denk, W.; McCray, J. A.; Hess, G. P. *Biochemistry* **1989,** *28,* 49–55. doi:10.1021/bi00427a008
10. Goldman, Y. E.; Hibberd, M. G.; Trentham, D. R. *J. Physiol.* **1984,** *354,* 577–604.
11. Goldman, Y. E.; Hibberd, M. G.; Trentham, D. R. *J. Physiol.* **1984,** *354,* 605–624.
12. Dantzig, J. A.; Higuchi, H.; Goldman, Y. E. *Methods Enzymol.* **1998,** *291,* 307–348. doi:10.1016/S0076-6879(98)91021-7
13. Hibberd, M. G.; Dantzig, J. A.; Trentham, D. R.; Goldman, Y. E. *Science* **1985,** *228,* 1317–1319. doi:10.1126/science.3159090
14. Givens, R. S.; Park, C.-H. *Tetrahedron Lett.* **1996,** *37,* 6259–6262. doi:10.1016/0040-4039(96)01390-1
15. Hagen, V.; Bendig, J.; Frings, S.; Eckardt, T.; Helm, S.; Reuter, D.; Kaupp, U. B. *Angew. Chem., Int. Ed.* **2001,** *40,* 1045–1048. doi:10.1002/1521-3773(20010316)40:6<1045::AID-ANIE10450>3.0.CO;2-F
16. Suzuki, A. Z.; Watanabe, T.; Kawamoto, M.; Nishiyama, K.; Yamashita, H.; Ishii, M.; Iwamura, M.; Furuta, T. *Org. Lett.* **2003,** *5,* 4867–4870. doi:10.1021/ol0359362
17. Tsien, R. Y.; Zucker, R. S. *Biophys. J.* **1986,** *50,* 843–853. doi:10.1016/S0006-3495(86)83525-1
18. Wieboldt, R.; Gee, K. R.; Niu, L.; Ramesh, D.; Carpenter, B. K.; Hess, G. P. *Proc. Natl. Acad. Sci. U. S. A.* **1994,** *91,* 8752–8756. doi:10.1073/pnas.91.19.8752
19. Wieboldt, R.; Ramesh, D.; Carpenter, B. K.; Hess, G. P. *Biochemistry* **1994,** *33,* 1526–1533. doi:10.1021/bi00172a032
20. Breitinger, H.-G. A.; Wieboldt, R.; Ramesh, D.; Carpenter, B. K.; Hess, G. P. *Biochemistry* **2000,** *39,* 5500–5508. doi:10.1021/bi992781q
21. Grewer, C.; Jäger, J.; Carpenter, B. K.; Hess, G. P. *Biochemistry* **2000,** *39,* 2063–2070. doi:10.1021/bi9919652
22. Banerjee, A.; Grewer, C.; Ramakrishnan, L.; Jäger, J.; Gameiro, A.; Breitinger, H.-G. A.; Gee, K. R.; Carpenter, B. K.; Hess, G. P. *J. Org. Chem.* **2003,** *68,* 8361–8367. doi:10.1021/jo0300643
23. Shembekar, V. R.; Chen, Y.; Carpenter, B. K.; Hess, G. P. *Biochemistry* **2005,** *44,* 7107–7114. doi:10.1021/bi047665o
24. Shembekar, V. R.; Chen, Y.; Carpenter, B. K.; Hess, G. P. *Biochemistry* **2007,** *46,* 5479–5484. doi:10.1021/bi700280e

25. Grewer, C.; Hess, G. P. *Biochemistry* **1999,** *38,* 7837–7846. doi:10.1021/bi9827767
26. Papageorgiou, G.; Ogden, D. C.; Barth, A.; Corrie, J. E. T. *J. Am. Chem. Soc.* **1999,** *121,* 6503–6504. doi:10.1021/ja990931e
27. Papageorgiou, G.; Corrie, J. E. T. *Tetrahedron* **2000,** *56,* 8197–8205. doi:10.1016/S0040-4020(00)00745-6
28. Specht, A.; Thomann, J.-S.; Alarcon, K.; Wittayanan, W.; Ogden, D.; Furuta, T.; Kurakawa, Y.; Goeldner, M. *ChemBioChem* **2006,** *7,* 1690–1695. doi:10.1002/cbic.200600111
29. Gug, S.; Bolze, F.; Specht, A.; Bourgogne, C.; Goeldner, M.; Nicoud, J.-F. *Angew. Chem., Int. Ed.* **2008,** *47,* 9525–9529. doi:10.1002/anie.200803964
30. Ellis-Davies, G. C. R. *J. Gen. Physiol.* **1999,** *114,* 1a.
31. Matsuzaki, M.; Ellis-Davies, G. C. R.; Nemoto, T.; Miyashita, Y.; Iino, M.; Kasai, H. *Nat. Neurosci.* **2001,** *4,* 1086–1092. doi:10.1038/nn736
32. Ellis-Davies, G. C. R.; Matsuzaki, M.; Paukert, M.; Kasai, H.; Bergles, D. E. *J. Neurosci.* **2007,** *27,* 6601–6604. doi:10.1523/JNEUROSCI.1519-07.2007
33. Fino, E.; Araya, R.; Peterka, D. S.; Salierno, M.; Etchenique, R.; Yuste, R. *Front. Neural Circuits* **2009,** *3,* 2. doi:10.3389/neuro.04.002.2009
34. Fedoryak, O. D.; Sul, J.-Y.; Haydon, P. G.; Ellis-Davies, G. C. R. *Chem. Commun.* **2005,** 3664–3666. doi:10.1039/b504922a
35. Canepari, M.; Nelson, L.; Papageorgiou, G.; Corrie, J. E. T.; Ogden, D. *J. Neurosci. Methods* **2001,** *112,* 29–42. doi:10.1016/S0165-0270(01)00451-4
36. Matsuzaki, M.; Hayama, T.; Kasai, H.; Ellis-Davies, G. C. R. *Nat. Chem. Biol.* **2010,** *6,* 255–257. doi:10.1038/nchembio.321
37. Maier, W.; Corrie, J. E. T.; Papageorgiou, G.; Laube, B.; Grewer, C. *J. Neurosci. Methods* **2005,** *142,* 1–9. doi:10.1016/j.jneumeth.2004.07.006
38. Rial Verde, E. M.; Zayat, L.; Etchenique, R.; Yuste, R. *Front. Neural Circuits* **2008,** *2,* 2. doi:10.3389/neuro.04.002.2008
39. Alviña, K.; Walter, J. T.; Kohn, A.; Ellis-Davies, G.; Khodakhah, K. *Nat. Neurosci.* **2008,** *11,* 1256–1258. doi:10.1038/nn.2195
40. Huang, Y. H.; Sinha, S. R.; Fedoryak, O. D.; Ellis-Davies, G. C. R.; Bergles, D. E. *Biochemistry* **2005,** *44,* 3316–3326. doi:10.1021/bi048051m
41. Miesenböck, G.; Rothman, J. E. *Proc. Natl. Acad. Sci. U. S. A.* **1997,** *94,* 3402–3407. doi:10.1073/pnas.94.7.3402
42. Kuner, T.; Augustine, G. J. *Neuron* **2000,** *27,* 447–459. doi:10.1016/S0896-6273(00)00056-8
43. Gug, S.; Charon, S.; Specht, A.; Alarcon, K.; Ogden, D.; Zietz, B.; Léonard, J.; Haacke, S.; Bolze, F.; Nicoud, J.-F.; Goeldner, M. *ChemBioChem* **2008,** *9,* 1303–1307. doi:10.1002/cbic.200700651
44. Donato, L.; Mourot, A.; Davenport, C. M.; Herbivo, C.; Warther, D.; Léonard, J.; Bolze, F.; Nicoud, J.-F.; Kramer, R. H.; Goeldner, M.; Specht, A. *Angew. Chem., Int. Ed.* **2012,** *51,* 1840–1843. doi:10.1002/anie.201106559
45. Pirrung, M. C.; Dore, T. M.; Zhu, Y.; Rana, V. S. *Chem. Commun.* **2010,** *46,* 5313–5315. doi:10.1039/c0cc00782j
46. Eder, M.; Becker, K.; Rammes, G.; Schierloh, A.; Azad, S. C.; Zieglgansberger, W.; Dodt, H. U. *J. Neurosci.* **2003,** *23,* 6660–6670.
47. Shepherd, G. M. G.; Svoboda, K. *J. Neurosci.* **2005,** *25,* 5670–5679. doi:10.1523/JNEUROSCI.1173-05.2005
48. Callaway, E. M.; Katz, L. C. *Proc. Natl. Acad. Sci. U. S. A.* **1993,** *90,* 7661–7665. doi:10.1073/pnas.90.16.7661
49. Bendels, M. H. K.; Beed, P.; Leibold, C.; Schmitz, D.; Johenning, F. W. *J. Neurosci. Methods* **2008,** *175,* 44–57. doi:10.1016/j.jneumeth.2008.08.010
50. Sobczyk, A.; Scheuss, V.; Svoboda, K. *J. Neurosci.* **2005,** *25,* 6037–6046. doi:10.1523/JNEUROSCI.1221-05.2005
51. Carter, A. G.; Sabatini, B. L. *Neuron* **2004,** *44,* 483–493. doi:10.1016/j.neuron.2004.10.013
52. Araya, R.; Eisenthal, K. B.; Yuste, R. *Proc. Natl. Acad. Sci. U. S. A.* **2006,** *103,* 18799–18804. doi:10.1073/pnas.0609225103
53. Nikolenko, V.; Poskanzer, K. E.; Yuste, R. *Nat. Methods* **2007,** *4,* 943–950. doi:10.1038/nmeth1105
54. Wang, L.; Corrie, J. E. T.; Wootton, J. F. *J. Org. Chem.* **2002,** *67,* 3474–3478. doi:10.1021/jo020040g
55. Rossi, F. M.; Margulis, M.; Tang, C.-M.; Kao, J. P. Y. *J. Biol. Chem.* **1997,** *272,* 32933–32939. doi:10.1074/jbc.272.52.32933
56. Kantevari, S.; Matsuzaki, M.; Kanemoto, Y.; Kasai, H.; Ellis-Davies, G. C. R. *Nat. Methods* **2010,** *7,* 123–125. doi:10.1038/nmeth.1413
57. Cürten, B.; Kullmann, P. H. M.; Bier, M. E.; Kandler, K.; Schmidt, B. F. *Photochem. Photobiol.* **2005,** *81,* 641–648. doi:10.1111/j.1751-1097.2005.tb00238.x
58. Furuta, T.; Wang, S. S.-H.; Dantzker, J. L.; Dore, T. M.; Bybee, W. J.; Callaway, E. M.; Denk, W.; Tsien, R. Y. *Proc. Natl. Acad. Sci. U. S. A.* **1999,** *96,* 1193–1200. doi:10.1073/pnas.96.4.1193
59. Wilcox, M.; Viola, R. W.; Johnson, K. W.; Billington, A. P.; Carpenter, B. K.; McCray, J. A.; Guzikowski, A. P.; Hess, G. P. *J. Org. Chem.* **1990,** *55,* 1585–1589. doi:10.1021/jo00292a038
60. Senda, N.; Momotake, A.; Arai, T. *Bull. Chem. Soc. Jpn.* **2007,** *80,* 2384–2388. doi:10.1246/bcsj.80.2384
61. Zhao, J.; Gover, T. D.; Muralidharan, S.; Auston, D. A.; Weinreich, D.; Kao, J. P. Y. *Biochemistry* **2006,** *45,* 4915–4926. doi:10.1021/bi052082f
62. Gilbert, D.; Funk, K.; Dekowski, B.; Lechler, R.; Keller, S.; Möhrlen, F.; Frings, S.; Hagen, V. *ChemBioChem* **2007,** *8,* 89–97. doi:10.1002/cbic.200600437
63. Pelliccioli, A. P.; Wirz, J. *Photochem. Photobiol. Sci.* **2002,** *1,* 441–458. doi:10.1039/b200777k
64. Sigworth, F. J. *J. Neurosci. Methods* **1995,** *56,* 195–202. doi:10.1016/0165-0270(94)00128-4
65. Sigworth, F. J.; Affolter, H.; Neher, E. *J. Neurosci. Methods* **1995,** *56,* 203–215. doi:10.1016/0165-0270(94)00129-5
66. Conchello, J.-A.; Lichtman, J. W. *Nat. Methods* **2005,** *2,* 920–931. doi:10.1038/nmeth815
67. Roorda, R. D.; Hohl, T. M.; Toledo-Crow, R.; Miesenböck, G. J. *J. Neurophysiol.* **2004,** *92,* 609–621. doi:10.1152/jn.00087.2004
68. Bacskai, B. J.; Wallen, P.; Lev-Ram, V.; Grillner, S.; Tsien, R. Y. *Neuron* **1995,** *14,* 19–28. doi:10.1016/0896-6273(95)90237-6
69. Nguyen, Q.-T.; Tsai, P. S.; Kleinfeld, D. *J. Neurosci. Methods* **2006,** *156,* 351–359. doi:10.1016/j.jneumeth.2006.03.001
70. Katona, G.; Kaszás, A.; Turi, G. F.; Hájos, N.; Tamás, G.; Vizi, E. S.; Rózsa, B. *Proc. Natl. Acad. Sci. U. S. A.* **2011,** *108,* 2148–2153. doi:10.1073/pnas.1009270108
71. Hagen, V.; Dekowski, B.; Nache, V.; Schmidt, R.; Geißler, D.; Lorenz, D.; Eichhorst, J.; Keller, S.; Kaneko, H.; Benndorf, K.; Wiesner, B. *Angew. Chem., Int. Ed.* **2005,** *44,* 7887–7891. doi:10.1002/anie.200502411
72. Hagen, V.; Frings, S.; Wiesner, B.; Helm, S.; Kaupp, U. B.; Bendig, J. *ChemBioChem* **2003,** *4,* 434–442. doi:10.1002/cbic.200300561
73. Il'ichev, Y. V.; Schwörer, M. A.; Wirz, J. *J. Am. Chem. Soc.* **2004,** *126,* 4581–4595. doi:10.1021/ja039071z

74. Clements, J. D.; Lester, R. A.; Tong, G.; Jahr, C. E.; Westbrook, G. L. *Science* **1992,** *258,* 1498–1501. doi:10.1126/science.1359647
75. Gardner, S. M.; Trussell, L. O.; Oertel, D. *J. Neurosci.* **1999,** *19,* 8721–8729.
76. Nusser, Z.; Cull-Candy, S.; Farrant, M. *Neuron* **1997,** *19,* 697–709. doi:10.1016/S0896-6273(00)80382-7
77. Salierno, M.; Marceca, E.; Peterka, D. S.; Yuste, R.; Etchenique, R. *J. Inorg. Biochem.* **2010,** *104,* 418–422. doi:10.1016/j.jinorgbio.2009.12.004
78. Papageorgiou, G.; Ogden, D.; Corrie, J. E. T. *J. Org. Chem.* **2004,** *69,* 7228–7233. doi:10.1021/jo049071x
79. Papageorgiou, G.; Ogden, D.; Corrie, J. E. T. *Photochem. Photobiol. Sci.* **2008,** *7,* 423–432. doi:10.1039/b800683k
80. Ellis-Davies, G. C. R. *Nat. Methods* **2007,** *4,* 619–628. doi:10.1038/nmeth1072
81. Trigo, F. F.; Corrie, J. E. T.; Ogden, D. *J. Neurosci. Methods* **2009,** *180,* 9–21. doi:10.1016/j.jneumeth.2009.01.032
82. Eder, M.; Zieglgänsberger, W.; Dodt, H.-U. *Rev. Neurosci. (Berlin, Ger.)* **2004,** *15,* 167–183. doi:10.1515/REVNEURO.2004.15.3.167
83. Gee, K. R.; Wieboldt, R.; Hess, G. P. *J. Am. Chem. Soc.* **1994,** *116,* 8366–8367. doi:10.1021/ja00097a054
84. Matsuzaki, M.; Ellis-Davies, G. C. R.; Kasai, H. *J. Neurophysiol.* **2008,** *99,* 1535–1544. doi:10.1152/jn.01127.2007
85. Matsuzaki, M.; Ellis-Davies, G. C. R.; Kanemoto, Y.; Kasai, H. *Neural Syst. Circuits* **2011,** *1,* 2. doi:10.1186/2042-1001-1-2
86. Matsuzaki, M.; Ellis-Davies, G. C. R.; Miyashita, Y.; Iino, M.; Kasai, H. *Soc. Neurosci. Abstr.* **2000,** *426,* 12.
87. Mao, T.; O'Connor, D. H.; Scheuss, V.; Nakai, J.; Svoboda, K. *PLoS One* **2008,** *3,* e1796. doi:10.1371/journal.pone.0001796
88. Tian, L.; Hires, S. A.; Mao, T.; Huber, D.; Chiappe, M. E.; Chalasani, S. H.; Petreanu, L.; Akerboom, J.; McKinney, S. A.; Schreiter, E. R.; Bargmann, C. I.; Jayaraman, V.; Svoboda, K.; Looger, L. L. *Nat. Methods* **2009,** *6,* 875–881. doi:10.1038/nmeth.1398
89. Zhao, Y.; Araki, S.; Wu, J.; Teramoto, T.; Chang, Y.-F.; Nakano, M.; Abdelfattah, A. S.; Fujiwara, M.; Ishihara, T.; Nagai, T.; Campbell, R. E. *Science* **2011,** *333,* 1888–1891. doi:10.1126/science.1208592
90. Hendel, T.; Mank, M.; Schnell, B.; Griesbeck, O.; Borst, A.; Reiff, D. F. *J. Neurosci.* **2008,** *28,* 7399–7411. doi:10.1523/JNEUROSCI.1038-08.2008
91. Mank, M.; Griesbeck, O. *Chem. Rev.* **2008,** *108,* 1550–1564. doi:10.1021/cr078213v
92. Borghuis, B. G.; Tian, L.; Xu, Y.; Nikonov, S. S.; Vardi, N.; Zemelman, B. V.; Looger, L. L. *J. Neurosci.* **2011,** *31,* 2855–2867. doi:10.1523/JNEUROSCI.6064-10.2011
93. Pologruto, T. A.; Yasuda, R.; Svoboda, K. *J. Neurosci.* **2004,** *24,* 9572–9579. doi:10.1523/JNEUROSCI.2854-04.2004
94. Mattis, J.; Tye, K. M.; Ferenczi, E. A.; Ramakrishnan, C.; O'Shea, D. J.; Prakash, R.; Gunaydin, L. A.; Hyun, M.; Fenno, L. E.; Gradinaru, V.; Yizhar, O.; Deisseroth, K. *Nat. Methods* **2012,** *9,* 159–172. doi:10.1038/nmeth.1808
95. Nagel, G.; Ollig, D.; Fuhrmann, M.; Kateriya, S.; Musti, A. M.; Bamberg, E.; Hegemann, P. *Science* **2002,** *296,* 2395–2398. doi:10.1126/science.1072068
96. Nagel, G.; Szellas, T.; Huhn, W.; Kateriya, S.; Adeishvili, N.; Berthold, P.; Ollig, D.; Hegemann, P.; Bamberg, E. *Proc. Natl. Acad. Sci. U. S. A.* **2003,** *100,* 13940–13945. doi:10.1073/pnas.1936192100
97. Nagel, G.; Brauner, M.; Liewald, J. F.; Adeishvili, N.; Bamberg, E.; Gottschalk, A. *Curr. Biol.* **2005,** *15,* 2279–2284. doi:10.1016/j.cub.2005.11.032
98. Gradinaru, V.; Thompson, K. R.; Zhang, F.; Mogri, M.; Kay, K.; Schneider, M. B.; Deisseroth, K. *J. Neurosci.* **2007,** *27,* 14231–14238. doi:10.1523/JNEUROSCI.3578-07.2007
99. Mayer, G.; Heckel, A. *Angew. Chem., Int. Ed.* **2006,** *45,* 4900–4921. doi:10.1002/anie.200600387
100. Lawrence, D. S. *Curr. Opin. Chem. Biol.* **2005,** *9,* 570–575. doi:10.1016/j.cbpa.2005.09.002
101. Fehrentz, T.; Schönberger, M.; Trauner, D. *Angew. Chem., Int. Ed.* **2011,** *50,* 12156–12182. doi:10.1002/anie.201103236
102. Givens, R. S.; Rubina, M.; Wirz, J. *Photochem. Photobiol. Sci.* **2012,** *11,* 472–488. doi:10.1039/c2pp05399c

License and Terms

Beilstein Journal of Organic Chemistry

Synthesis and testing of the first azobenzene mannobioside as photoswitchable ligand for the bacterial lectin FimH

Vijayanand Chandrasekaran, Katharina Kolbe, Femke Beiroth and Thisbe K. Lindhorst*

Full Research Paper

Open Access

Address:
Christiana Albertina University of Kiel, Otto Diels Institute of Organic Chemistry, Otto-Hahn-Platz 3/4, D-24098 Kiel, Germany, Fax: +49 431 8807410

Email:
Thisbe K. Lindhorst* - tklind@oc.uni-kiel.de

* Corresponding author

Keywords:
azobenzene glycosides; bacterial adhesion; *E*/*Z* photoisomerisation; FimH antagonists; mannobiosides; molecular switches; sweet switches

Beilstein J. Org. Chem. **2013,** *9,* 223–233.
doi:10.3762/bjoc.9.26

Received: 08 November 2012
Accepted: 18 January 2013
Published: 01 February 2013

This article is part of the Thematic Series "Molecular switches and cages".

Guest Editor: D. Trauner

Abstract

In order to allow spatial and temporal control of carbohydrate-specific bacterial adhesion, it has become our goal to synthesise azobenzene mannosides as photoswitchable inhibitors of type 1 fimbriae-mediated adhesion of *E. coli*. An azobenzene mannobioside **2** was prepared and its photochromic properties were investigated. The *E*→*Z* isomerisation was found to be highly effective, yielding a long-lived (*Z*)-isomer. Both isomers, *E* and *Z*, show excellent water solubility and were tested as inhibitors of mannoside-specific bacterial adhesion in solution. Their inhibitory potency was found to be equal and almost two orders of magnitude higher than that of the standard inhibitor methyl mannoside. These findings could be rationalised on the basis of computer-aided docking studies. The properties of the new azobenzene mannobioside have qualified this glycoside to be eventually employed on solid support, in order to fabricate photoswitchable adhesive surfaces.

Introduction

Adhesion of bacteria to surfaces can be a severe problem both in vivo and in vitro. Hence, inhibition of bacterial adhesion by powerful antagonists is highly desirable, however, ideally on demand, that is, in a specific and spatially as well as temporally resolved way. Often bacterial adhesion depends on the interaction of adhesive organelles called fimbriae. They project from the surface of bacteria and contain lectin domains to attach to certain carbohydrate ligands of a glycosylated surface such as the glycocalyx of eukaryotic target cells (Figure 1A) [1-4]. This offers the possibility to inhibit bacterial adhesion by designed

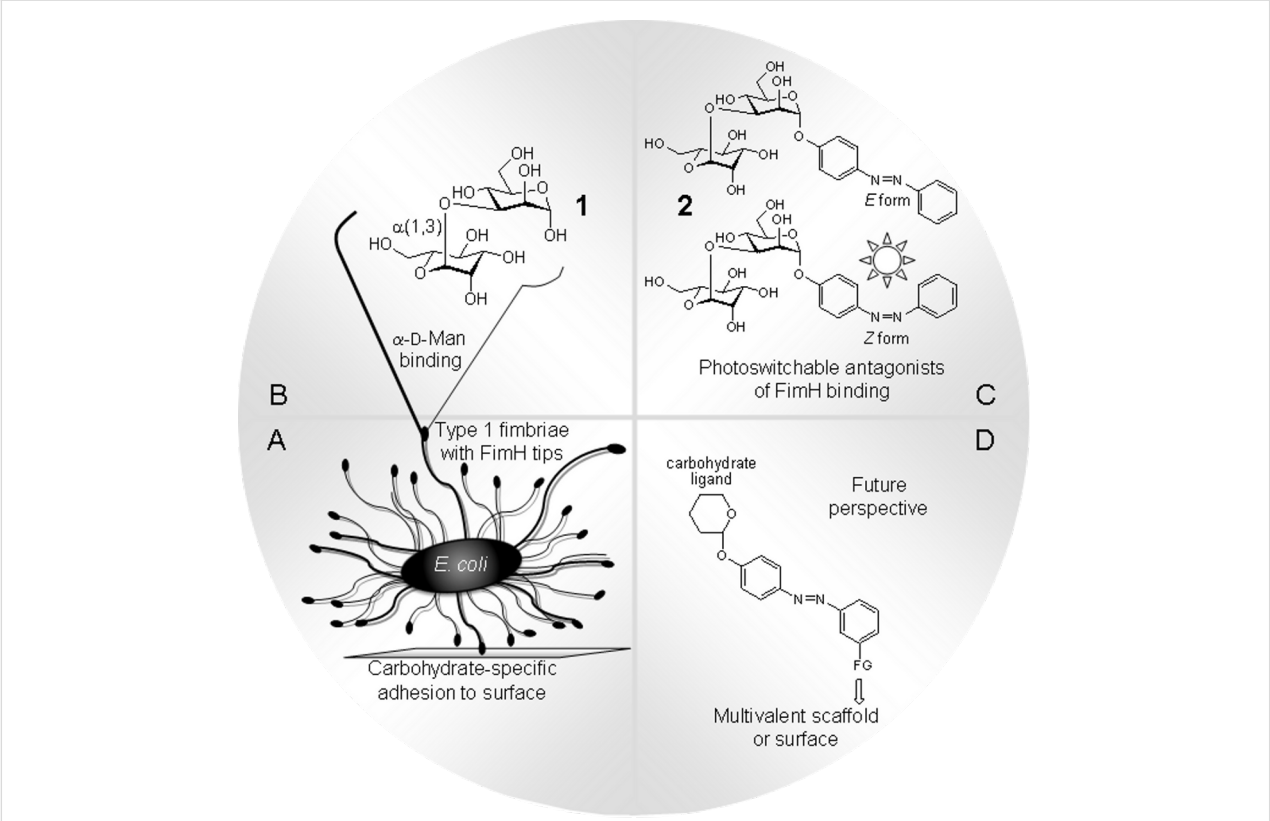

Figure 1: The α-(1→3)-linked mannobioside α-D-Man-(1→3)-D-Man **1** (B) is a potent disaccharide ligand for the bacterial lectin FimH and can thus inhibit type 1 fimbriae-mediated bacterial adhesion to glycosylated surfaces (A). Introduction of an azobenzene aglycone moiety turns glycoside **1** into a putative photoswitchable antagonist **2** of mannose-specific bacterial adhesion, displaying an (*E*)-, as well as a (*Z*)-form (C). In a future perspective azobenzene glycosides such as **2** can be further functionalised to be attached to oligofunctional core molecules or immobilised on surfaces (D).

antagonists of the respective carbohydrate-specific bacterial lectins [5]. In order to expand the scope of carbohydrate-based antiadhesives, it has become our goal to make photoswitchable ligands of bacterial lectins to allow blocking of bacterial adhesion in a photocontrolled manner.

One of the best-known fimbriae are the type 1 fimbriae of uropathogenic *E. coli* (UPEC), which comprise the α-D-mannosyl-specific lectin FimH at the tip of the fimbrial shaft. FimH antagonists are currently considered as new therapeutics for the treatment of urinary tract infections [6]. The carbohydrate specificity of FimH has been investigated in great detail [7] and its structure is well-known from several X-ray studies [8-11]. It has turned out that the 1,3-linked mannobioside α-D-Man-(1→3)-D-Man (**1**, Figure 1B) is an ideal disaccharide ligand for FimH [3,12]. All other isomeric mannobiosides do not bind favourably to FimH. Therefore, we have designed the respective azobenzene mannobioside **2** (Figure 1C) in order to make a photoswitchable FimH antagonist available. Photoirradiation of azobenzene glycosides at ~365 nm effects *E*→*Z* isomerisation of the N=N double bond, and thermal relaxation or irradiation at ~450 nm leads to *Z*→*E* back isomerisation [13,14]. In the case that the *E*→*Z* isomerisation process is high-yielding and the lifetime of the (*Z*)-form of the azobenzene glycoside is long enough, it can be employed in bacterial adhesion assays independently from the more stable (*E*)-isomer. Eventually, this type of azobenzene mannobioside can be further functionalised to be attached to various supports such as oligofunctional core molecules [15] or surfaces, to achieve switchable adhesive surfaces in continuation of our work on glycoarrays [16-18] (Figure 1D).

In this account, we describe the synthesis of the azobenzene mannobioside **2** as well as of mannoside **6**, investigation of their photochromic properties, and testing of mannobioside **2** as an inhibitor of type 1 fimbriae-mediated bacterial adhesion. Interpretation of the test results was supported by computer-aided docking studies.

Results

Synthesis of azobenzene mannobioside **2**

For the preparation of azobenzene mannobioside **2**, the azobenzene mannoside **6** was prepared first. Thus, mannosylation of the hydroxy-functionalised azobenzene **4** by using the mannosyl

trichlororacetimidate **3** [19] led to the respective azobenzene α-mannosides **5** in 81% yield (Scheme 1). Treatment of **5** under Zemplén conditions [20] furnished the deprotected mannoside **6** in a basically quantitative reaction. Then, a standard protecting-group strategy was employed to allow the synthesis of the 3-OH unprotected mannoside **10**, which is a key intermediate serving as the glycosyl acceptor in the following disaccharide synthesis. First, regioselective protection of the primary 6-hydroxy group in **6** was accomplished by using TBDMS chloride in pyridine to yield **7**. Then, triethylorthoacetate was employed to make the orthoester **8**, which, without intermediate purification steps, could be carried on in a sequence of silyl ether-deprotection leading to the intermediate **9**, acetylation of the 4- and 6-hydroxy groups, and then acid-mediated regioselective ring opening of the 2,3-orthoester in the same pot to yield the free 3-OH azobenzene mannoside **10** in an overall yield of 43%. Thus, the required protecting group pattern was obtained in a highly efficient way, based on the regioselective opening of orthoacetates to yield a vicinal arrangement of equatorial OH and axial O-acetyl groups [21,22]. The acetylation pattern was

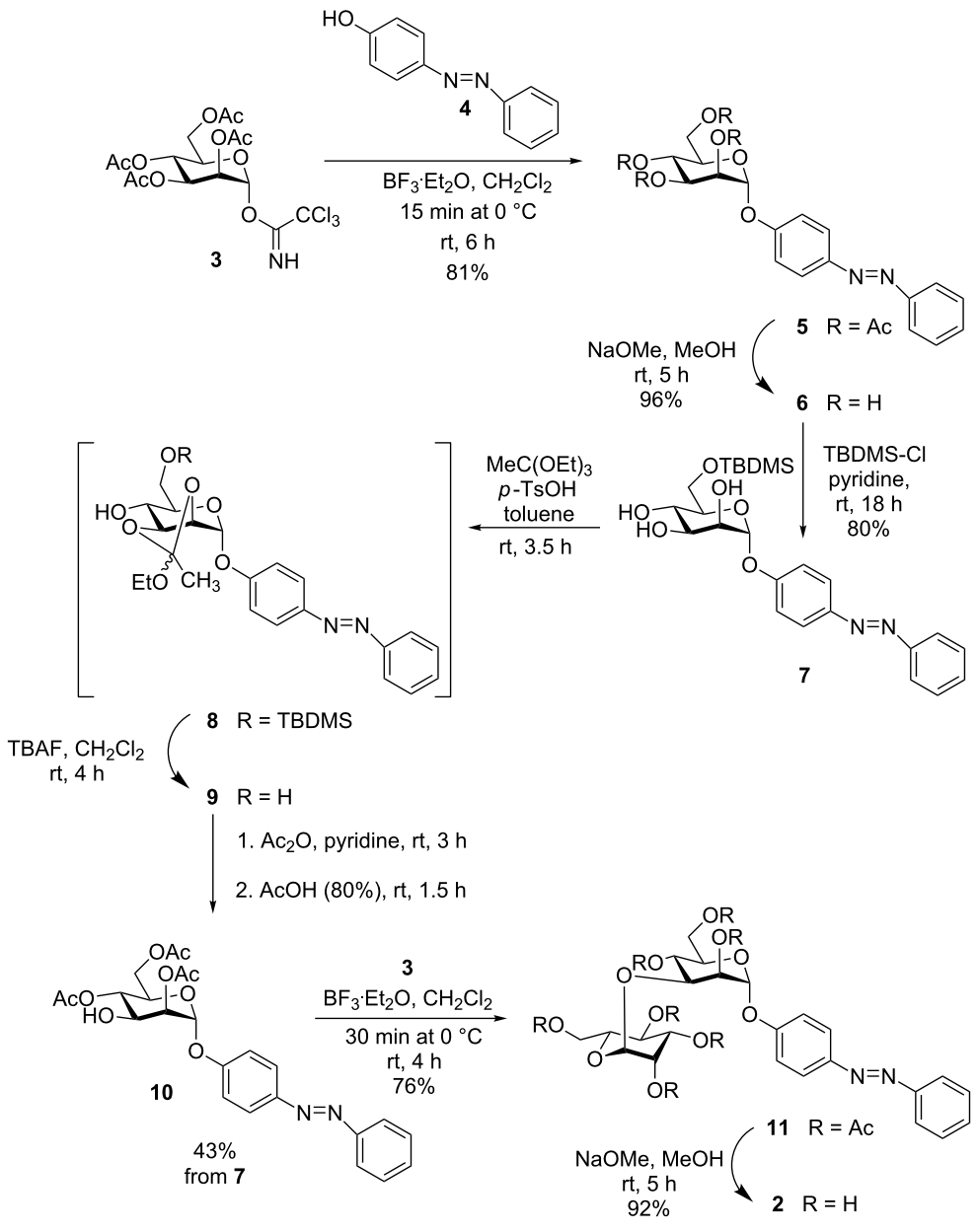

Scheme 1: Synthesis of azobenzene mannoside **6** and azobenzene mannobioside **2** by glycosylation.

clearly confirmed by ^{1}H NMR spectroscopy showing the expected downfield shift for the H-3 signal resonating at 4.32 ppm (H-2: 5.30 ppm, H-4: 5.17 ppm).

Next, glycosylation of the key intermediate **10** by using the mannosyl donor **3** gave the desired mannobioside **11** in 76% yield. Finally, removal of the *O*-acetyl groups according to Zemplén led to the unprotected 1,3-linked target mannobioside α-D-Man-(1→3)-D-Man (**2**).

With the two azobenzene glycosides **6** and **2** at hand, their solubility and photochromic properties were then investigated and compared. Mannoside **6** showed only poor solubility in most organic solvents, except for DMSO. Unfortunately, it was also not soluble in water, or in water/DMSO mixtures, which would allow biological testing. Mannobioside **2**, on the other hand, showed good solubility in polar organic solvents as well as in pure water. Thus, it was amenable to biological testing in aqueous buffer.

E→*Z* photoisomerisation of azobenzene mannoside **6** was studied in DMSO, while isomerisation of azobenzene mannobioside **2** was performed in water. Photoirradiation was carried out in the dark at room temperature by employing a 365 nm LED. Photostationary states (PSS) were reached after 10 minutes of irradiation for both compounds. *E*→*Z* isomerisation was observed by both ^{1}H NMR and UV–vis spectroscopy. The *E*/*Z* ratios of the ground state (GS) as well as of the photostationary state were determined on the basis of the integration of the anomeric H-1 protons in the ^{1}H NMR spectrum. Half-life were determined by UV–vis spectroscopic observation of the thermal *Z*→*E* relaxation process (Supporting Information File 1). The respective data are collected in Table 1.

Fortunately, the mannobioside **2** is ideally suited for biological testing as it is soluble in water and aqueous buffer, respectively. Photoirradiation of the (*E*)-isomer leads to almost quantitative isomerisation, and the life time of the resulting (*Z*)-isomer is long enough to test this isomer independently from the more stable (*E*)-form.

Biological testing of azobenzene mannobioside **2**

As a test system for mannose-specific bacterial adhesion, fluorescent GFP-transfected *E. coli* bacteria (pPKL1162) [23] were employed and tested on a mannan-coated polystyrene microtiter plate surface. In this setup the amount of bacterial adhesion correlates with fluorescence intensity and can be quantified by using a standard microtiter plate reader. For inhibition of bacterial adhesion, two sets of serially diluted solutions of **2** were prepared to inhibit adhesion of fluorescing *E. coli* to the mannan surface. In one case, a stock solution of (*E*)-**2** was serially diluted, in the second case, this stock solution of (*E*)-**2** was irradiated for 15 minutes to obtain the pure (*Z*)-**2** isomer for subsequent serial dilution. The effect of both isomers as inhibitors of mannose-specific bacterial adhesion was then measured in a concentration-dependent way. From the testing results sigmoidal inhibition curves were obtained (Supporting Information File 1) from which IC_{50} values for every individual inhibitor were deduced. The IC_{50} value reflects the concentration at which a compound inhibits 50% of bacterial adhesion to a mannan-coated surface. The determined IC_{50} values were referenced to the inhibitory potency of methyl α-D-mannoside (MeMan) and *p*-nitrophenyl α-D-mannoside (*p*NPMan), respectively, each tested on the same plate. Thus, relative inhibitory potencies (RIP values) were obtained, which allow comparison of inhibitory potencies of different inhibitors, even when they were not tested in the same experiment. The testing results collected in Table 2 show that the inhibitory power of mannobioside **2** is roughly the same, regardless of whether its (*E*)- or (*Z*)-form was employed. Inspection of their relative inhibitory potencies reveals that both isomers of **2** are equally potent inhibitors of type 1 fimbriae-mediated bacterial adhesion, similar to the power of the well-known mannoside *p*NPMan.

Table 1: Characterisation of the (*E*)- and (*Z*)-isomers of azobenzene glycosides **6** and **2**.

azobenzene glycoside	*E*/*Z*[a] (GS)	*E*/*Z*[a] (PSS)	H-1 (ppm) (*E*)-isomer	H-1 (ppm) (*Z*)-isomer	UV–vis absorption maxima (nm) $\lambda_{max}(E)$, $\lambda_{max}(Z)$	half-life, $\tau_{1/2}$ (h)
6	99:1	3:97	5.54[b]	5.34[b]	347, 440[c]	89
2	95:5	4:96	5.65[d]	5.52[d]	339, 429[e]	178.5

[a]according to the integration ratio of H-1(*E*) and H-1(*Z*) in the ^{1}H NMR spectrum;
[b]10 mM concentration in DMSO-d_6;
[c]50 μM concentration in DMSO;
[d]8 mM concentration in D_2O;
[e]65 μM concentration in H_2O.

Table 2: Inhibition of adhesion of *E. coli* to a mannan-coated surface. The inhibitory potencies of (*E*)- and (*Z*)-**2** are compared to the standard inhibitors MeMan and *p*NPMan. [a]

	MeMan	*p*NPMan	(*E*)-**2**	(*Z*)-**2**
IC_{50} ± SD (mM)	5.205 ± 0.416		0.064 ± 0.018	0.073 ± 0.001
		0.073 ± 0.003	0.078 ± 0.006	0.084 ± 0.002
RIP (MeMan) ± SD	IP ≡ 1		81 ± 25	71 ± 1
RIP (*p*NPMan) ± SD		IP ≡ 1	0.94 ± 0.07	0.87 ± 0.02

[a]Average values from duplicate results; SD: standard deviation (from one assay); RIP: relative inhibitory potency referenced to either MeMan or *p*NPMan, each tested on the same microtiter plate.

In order to support the interpretation of the obtained test results, binding of (*E*)-**2** and (*Z*)-**2** to the bacterial lectin FimH was investigated by computer-aided docking studies to get an idea of their interactions with the carbohydrate-recognition domain (CRD) of the lectin.

Docking of azobenzene mannobioside **2** into the carbohydrate binding site of FimH

To visualise complexation of the (*E*)- and (*Z*)-isomers of azobenzene mannobioside **2** within the CRD of FimH FlexX [24-26], flexible docking and consensus scoring [27,28], as implemented in Sybyl 6.9 [29], was employed. Docking was based on two different X-ray structures of FimH. They differ in the conformation of the so-called tyrosine gate at the entrance of the CRD, formed by the side chains of Y48 and Y137. One structure is crystallised in an "open-gate" conformation [9], another in the "closed-gate" conformation [10]. Affinity of any FimH ligand is improved when it exerts favourable interactions with the tyrosine gate of FimH. Thus, this substructure is an important feature of the rim of the carbohydrate binding site of this lectin.

Before minimisation of the ligands, the bond angle of the N=N double bond of the azobenzene moiety was manually set as 180° for (*E*)-**2** and as 90° for (*Z*)-**2** [30]. Then docking was performed holding the FimH CRD fixed whereas the ligands were allowed to change their conformations under the influence of the force field. A FlexX scoring value has been attributed to each of the 30 obtained conformations (Table 3). This value correlates with the binding affinity of the ligand for the FimH CRD, more negative values suggesting higher binding affinity than less negative ones.

Docking gave very similar results for both isomers of mannobioside **2**, (*E*)-**2** and (*Z*)-**2**. Scoring values based on the open-gate structure of FimH are almost equal (−28.8 and −28.7), and also the scoring values obtained with the closed-gate structure do not differ significantly (−20.4 and −21.6). Interestingly, the predictions for *p*NPMan and also MeMan are the opposite, suggesting better binding to the closed-gate conformation of FimH, as described earlier [31]. Representative snapshots as depicted in Figure 2 show that both isomers have the terminal mannoside complexed within the CRD of the lectin, as expected, and furthermore, that in both cases the azobenzene moiety exerts effective interactions with the tyrosine gate involving both benzene rings.

Table 3: FlexX scoring values for the (*E*)- and the (*Z*)-isomer of **2** based on two different crystal structures in comparison to MeMan and *p*NPMan.

Ligand	"open-gate" structure [9]	"closed-gate" structure [10]
MeMan	−22.5	−23.3
*p*NPMan	−24.9	−27.4
(*E*)-**2**	−28.8	−20.4
(*Z*)-**2**	−28.7	−21.6

Regardless of whether the (*E*)- or the (*Z*)-form of **2** is complexed with FimH, favourable π–π interactions can be formed between the azobenzene moiety and the tyrosine gate at the entrance of the CRD, though in different ways. The only difference that is seen is that, apparently, the interactions of mannobioside **2** with the open-gate conformation of FimH are advantageous over those with the closed-gate form. From the bioassay in solution phase it can certainly not be decided, which conformation the bacterial lectin adopts to interact with compound **2**; however, our test results confirm that both isomers of the azobenzene mannobioside **2** have the same power as inhibitors of FimH-mediated bacterial adhesion.

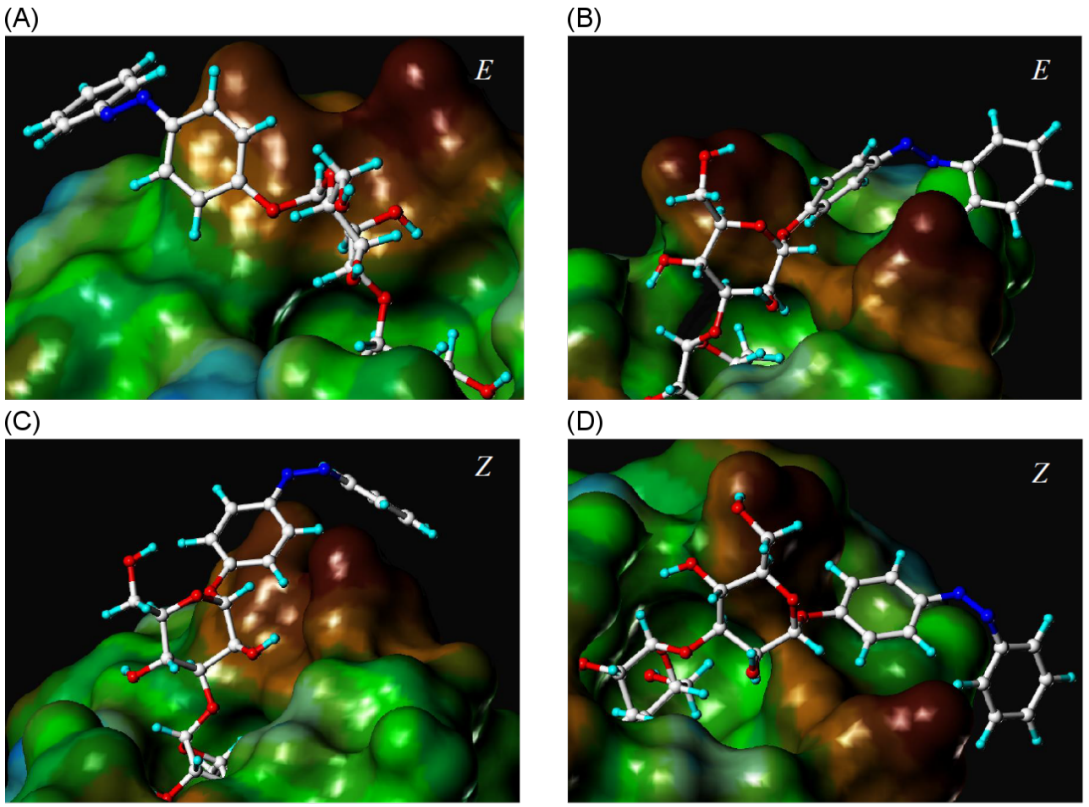

Figure 2: Connolly [32,33] descriptions of the FimH CRD with the docked azobenzene mannobioside **2**. Top: (*E*)-isomer (A, closed-gate; B, open-gate conformation). Bottom: (*Z*)-isomer (C, closed-gate; D, open-gate conformation).

Discussion

The azobenzene mannobioside **2** was selected as a photoswitchable inhibitor of the bacterial lectin FimH based on earlier findings about the inhibitory potency of several mannobiosides [34,35]. Its synthesis was straightforward and high-yielding. It has very convenient photochromic properties as the $E \rightarrow Z$ isomerisation is almost quantitative and the resulting (*Z*)-isomer is especially long-lived. Both isomers are very well water-soluble and could be independently tested as inhibitors of mannose-specific bacterial adhesion and showed an equal and high inhibitory potency in the range of the well-known high-affinity inhibitor *p*-nitrophenyl α-D-mannoside (*p*NPMan). This result can be rationalised by computer docking, showing that regardless of the configuration of the N=N double bond of the azobenzene moiety in **2**, favourable interactions can be formed with the tyrosine gate of the FimH CRD. While the terminal mannoside portion is complexed in the carbohydrate binding site, the first mannoside does not add significantly to the affinity and this is in accordance with other studies on the complexation of oligosaccharides by FimH [11]. However, this mannose ring acts as a spacer moiety, sticking out straight from the CRD and placing the azobenzene portion in an orientation that allows flexible interactions with the tyrosine gate at the entrance of the carbohydrate binding site of the lectin.

Apparently, the affinity of **2** to the open-gate form of FimH is higher than to the closed-gate conformation, a finding that differs from many other docked FimH ligands. Here, the higher affinity for the open-gate FimH can be explained by strong π–π stacking of the first aromatic ring of the azobenzene unit with the tyrosine gate.

As both isomers of **2** interact equally well with FimH, they can't be used to switch type 1 fimbriae-mediated bacterial adhesion in solution. On the other hand, the obtained results support the idea to immobilise the azobenzene mannobioside on a solid support to photocontrol the adhesive properties of the resulting surface. In this approach the azobenzene N=N double bond can be used as a hinge region to bend down the terminal mannose moiety of the compound, which is critical for specific bacterial

adhesion. Thus, upon $E \rightarrow Z$ isomerisation, the ligand will no longer be available for the interaction with the FimH-terminated type 1 fimbriae that mediate adhesion. In this approach, the second mannose moiety of the mannobioside is important both to mediate hydrophilicity and to intensify the steric effect that photoswitching has on the exposition of the terminal mannoside.

Conclusion

The azobenzene mannosides presented herein resemble a structure quite similar to biaryl mannosides, which have been introduced lately and shown to be of medical relevance as FimH antagonists [6]. Thus, our novel "sweet switches" [15] appear to be highly promising FimH ligands, with the additional feature of a photoswitchable moiety. The biomedicinal potential of azobenzene glycosides seems even higher when their favourable physiological properties are considered, such as low toxicity [36] and receptor specificity of the azobenzene aglycon [37]. It will be our next goal to employ derivatives of azobenzene mannobioside **2** for immobilisation to test the photoswitching of adhesion on surfaces.

Experimental

Materials and general methods

p-Hydroxyazobenzene was purchased from Sigma Aldrich and used without further purification. Moisture-sensitive reactions were carried out under nitrogen in dry glassware. Thin-layer chromatography was performed on silica-gel plates (GF 254, Merck). Detection was effected by UV and/or charring with 10% sulfuric acid in EtOH followed by heat treatment at ~180 °C. Flash chromatography was performed on silica gel 60 (Merck, 230–400 mesh, particle size 0.040–0.063 mm) by using distilled solvents. Optical rotations were measured with a Perkin-Elmer 241 polarimeter (sodium D-line: 589 nm, length of cell: 1 dm) in the solvents indicated. ^{1}H and ^{13}C NMR spectra were recorded on Bruker DRX-500 and AV-600 spectrometers at 300 K. Chemical shifts are reported relative to internal tetramethylsilane (δ = 0.00 ppm) or D_2O (δ = 4.76 ppm). Full assignment of the peaks was achieved with the aid of 2D NMR techniques (^{1}H/^{1}H COSY and ^{1}H/^{13}C HSQC). IR spectra were measured with a Perkin Elmer FT-IR Paragon 1000 (ATR) spectrometer. ESI mass spectra were recorded on an Esquire-LC instrument from Bruker Daltonics. MALDI-TOF mass spectra were recorded on a Bruker Biflex III instrument with 19 kV acceleration voltage, and 2,5-dihydroxybenzoic acid (DHB) was used as the matrix. UV–vis absorption spectra were performed on Perkin-Elmer Lambda-241 or Varian Cary-5000 at a temperature of 18 ± 1 °C. Photoirradiaton was carried out by using a LED (emitting 365 nm light) from the Nichia Corporation (NC4U133A) with a FWHM of 9 nm and an optical power output (P_o) ~ 1 W.

For NMR assignments the following numbering was used:

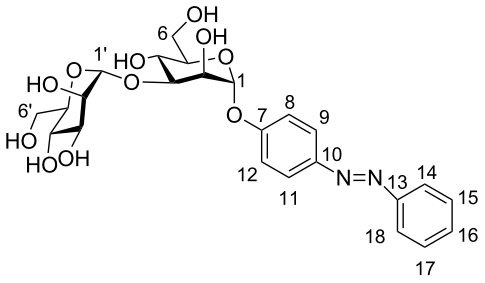

(*E*)-*p*-(Phenylazo)phenyl 2,3,4,6-tetra-*O*-acetyl-α-D-mannopyranoside (5). To a solution of the mannosyl donor **3** (5.00 g, 10.2 mmol) and *p*-hydroxyazobenzene (**4**, 2.01 g, 10.2 mmol) in dry CH_2Cl_2 (100 mL) BF_3·etherate (1.88 mL, 15.2 mmol) was added at 0 °C under N_2 atmosphere, and the reaction mixture was stirred at this temperature for 15 min. Then, stirring was continued at rt for about 6 h, and then the reaction was quenched by the addition of satd. aq. $NaHCO_3$ solution (50 mL). The phases were separated, the aqueous phase was extracted with CH_2Cl_2 (2 × 150 mL), and the combined organic phases were dried over $MgSO_4$. This was filtered, and the filtrate was concentrated under reduced pressure. Purification of the crude product by column chromatography (cyclohexane/ethyl acetate, 3:1) gave the title glycoside **5** as an orange crystalline solid (4.33 g, 8.19 mmol, 81%). Mp 53–55 °C; R_f 0.35 (cyclohexane/ethyl acetate 2:1); $[\alpha]^{20}_D$ +0.86 (*c* 0.9, DMSO); ^{1}H NMR (500 MHz, $CDCl_3$) δ 7.92 (d, J = 9.0 Hz, 2H, H-9, H-11), 7.89 (d, J = 8.5 Hz, 2H, H-14, H-18), 7.53–7.45 (m, 3H, H-15, H-16, H-17), 7.23 (d, J = 9.0 Hz, 2H, H-8, H-12), 5.62 (d, $J_{1,2}$ = 1.8 Hz, 1H, H-1), 5.58 (dd, $J_{2,3}$ = 3.6 Hz, $J_{3,4}$ = 10.1, 1H, H-3), 5.49 (dd, $J_{1,2}$ = 1.8 Hz, $J_{2,3}$ = 3.6 Hz, 1H, H-2), 5.39 (dd~t, $J_{3,4} = J_{4,5}$ = 10.0 Hz, 1H, H-4), 4.30 (dd, $J_{5,6a}$ = 5.4 Hz, $J_{6a,6b}$ = 12.0 Hz, 1H, H-6a), 4.14–4.07 (m, 2H, H-5, H-6b), 2.21, 2.06, 2.05, 2.03 (each s, each 3H, 4 OAc); ^{13}C NMR (125 MHz, $CDCl_3$) δ 170.5, 169.9, 169.9, 169.7 (4 C=O), 157.6 (C-7), 152.6 (C-13), 148.4 (C-10), 130.8 (C-16), 128.9 (C-15, C-17), 124.6 (C-9, C-11), 123.1 (C-14, 18), 116.8 (C-8, C-12), 95.7 (C-1), 69.4 (C-5), 69.3 (C-2), 68.8 (C-3), 65.9 (C-4), 62.1 (C-6), 20.9, 20.7, 20.7, 20.6 (4 CO$\underline{C}$H$_3$); IR (ATR) $\tilde{\nu}$: 2929, 1743, 1598, 1496, 1366, 1209, 1029 cm^{-1}; ESIMS (*m*/*z*): $[M + Na]^+$ calcd for $C_{26}H_{28}N_2O_{10}$, 551.5; found, 551.1.

(*E*)-*p*-(Phenylazo)phenyl α-D-mannopyranoside (6). To a solution of the acetyl-protected glycoside **5** (600 mg, 1.14 mmol) in dry MeOH (6 mL), a catalytic amount of solid NaOMe was added under N_2 atmosphere, and the reaction mixture was stirred for 5 h at rt. Then it was neutralized with Amberlite IR 120 ion-exchange resin and filtered. The filtrate was evaporated under reduced pressure to yield the deprotected

mannoside **6** as a pale yellow solid (393 mg, 1.09 mmol, 96%). Mp 183–185 °C; R_f 0.34 (ethyl acetate/MeOH 4:1); $[\alpha]^{20}_D$ +1.40 (*c* 1.0, DMSO); ^{1}H NMR (500 MHz, DMSO-d_6) δ 7.86 (d, *J* = 8.7 Hz, 2H, H-9, H-11), 7.82 (d, *J* = 7.7 Hz, 2H, H-14, H-18), 7.53–7.45 (m, 3H, H-15, H-16, H-17), 7.26 (d, *J* = 8.7 Hz, 2H, H-8, H-12), 5.53 (bs, 1H, H-1), 3.89 (dd~bs, 1H, H-2), 3.73 (dd, $J_{3,4}$ = 9.2 Hz, $J_{3,2}$ = 3.0 Hz, 1H, H-3), 3.58–3.47 (m, 3H, H-6a, H-4, H-6b), 3.38 (m_c, 1H, H-5); ^{13}C NMR (125 MHz, DMSO-d_6) δ 158.9 (C-7), 155.5 (C-13), 151.9 (C-10), 130.9 (C-16), 129.4 (C-15, C-17), 124.3 (C-9, C-11), 122.3 (C-14, C-18), 117.1 (C-8, C-12), 98.7 (C-1), 75.2 (C-5), 70.6 (C-3), 69.9 (C-2), 66.6 (C-4), 60.9 (C-6); UV, λ_{max}: 347 nm; ε = 25907 ± 529 L × mol^{-1} × cm^{-1}; IR (ATR) $\tilde{\nu}$: 3337, 2920, 1599, 1584, 1496, 1227 cm^{-1}; MALDI-TOFMS (*m*/*z*): $[M + H]^+$ calcd for 361.36; found, 361.21; anal. calcd for $C_{18}H_{20}N_2O_6$: C, 59.99; H, 5.59; N, 7.77; found: C, 61.07; H, 5.80; N, 8.07.

NMR spectroscopic data for (*Z*)-6. ^{1}H NMR (500 MHz, DMSO-d_6) δ 7.32 (t, *J* = 7.8 Hz, 2H, H-15, H-17), 7.18 (t, *J* = 7.4 Hz, 1H, H-16), 6.97 (d, *J* = 8.9 Hz, 2H, H-9, H-11), 6.82 (dd, *J* = 8.2 Hz, *J* = 6.7 Hz, 4H, H-8, H-12, H-14, H-18), 5.32 (d, $J_{1,2}$ = 1.6 Hz, 1H, H-1), 3.77 (dd, $J_{2,3}$ = 3.1 Hz, $J_{1,2}$ = 1.9 Hz, 1H, H-2), 3.62 (dd, $J_{3,4}$ = 9.3 Hz, $J_{3,2}$ = 3.3 Hz, 1H, H-3), 3.52 (dd, $J_{5,6a}$ = 2.1 Hz, $J_{6a,6b}$= 11.8 Hz, 1H, H-6a), 3.48–3.36 (m, 2H, H-4, H-6b), 3.31 (ddd, $J_{4,5}$ = 9.4 Hz, $J_{5,6a}$ = 5.8 Hz, $J_{5,6b}$ = 2.1 Hz, 1H, H-5); ^{13}C NMR (125 MHz, DMSO-d_6) δ 155.4 (C-7), 153.8 (C-13), 147.3 (C-10), 129.1 (C-15, C-17), 127.0 (C-16), 122.5 (C-8, C-12), 119.4 (C-14, C-18), 116.7 (C-9, C-11), 98.7 (C-1), 74.8 (C-5), 70.3 (C-3), 69.7 (C-2), 66.3 (C-4), 60.7 (C-6); UV, λ_{max}: 440 nm, ε = 2635 ± 76 L × mol^{-1} × cm^{-1}.

(*E*)-*p*-(Phenylazo)phenyl 6-*O*-*tert*-butyldimethylsilyl-α-D-mannopyranoside (7). To a solution of the azobenzene mannoside **6** (3.00 g, 8.33 mmol) in pyridine (30.0 mL) *tert*-butyldimethylchlorosilane (1.38 g, 9.17 mmol) was added and the reaction mixture was stirred at rt for 18 h, after which TLC showed complete consumption of the starting material. The reaction was quenched with MeOH (2.0 mL) and further diluted with ethyl acetate (150 mL). Then it was washed with satd. aq. $NaHCO_3$ solution (30 mL) and the aqueous phase extracted with ethyl acetate (2 × 50 mL). The combined organic phases were dried over $MgSO_4$ and filtered, and the filtrate concentrated under reduced pressure to obtain the crude product. Purification by flash column chromatography (CH_2Cl_2/MeOH 3:7) gave the title compound as a dark orange solid (3.16 g, 6.66 mmol, 80%). Mp 74 °C; R_f 0.59 (CH_2Cl_2/MeOH 7:1); $[\alpha]^{20}_D$ +73 (*c* 0.97, MeOH); ^{1}H NMR (500 MHz, MeOH-d_4) δ 7.94–7.88 (m, 4H, H-9, H-11, H-14, H-18), 7.57–7.49 (m, 3H, H-15, H-16, H-17), 7.30 (d, *J* = 9.0 Hz, 2H, H-8, H-12), 5.62 (d, $J_{1,2}$ = 1.7 Hz, 1H, H-1), 4.08 (dd, $J_{1,2}$ = 1.8 Hz, $J_{2,3}$ = 3.4 Hz, 1H, H-2), 3.98 (dd, $J_{5,6a}$ = 1.8 Hz, $J_{6a,6b}$ = 11.2 Hz, 1H, H-6a), 3.94 (dd, $J_{2,3}$ = 3.5 Hz, $J_{3,4}$ = 9.1 Hz, 1H, H-3), 3.82 (dd, $J_{5,6b}$ = 6.5 Hz, $J_{6a,6b}$ = 11.3 Hz, 1H, H-6b), 3.71 (t, *J* = 9.4 Hz, 1H, H-4), 3.65 (m_c, 1H, H-5), 0.83 (s, 9H, *tert*-butyl), 0.04, 0.05 (each s, each 3H, 2 Si-CH_3) ppm; ^{13}C NMR (125 MHz, MeOH-d_4) δ 160.4 (C-7), 154.1 (C-13), 149.18 (C-10), 131.8 (C-16), 130.2 (C-15), 125.5 (C-17), 123.6 (C-9), 118.2 (C-11), 100.0 (C-1), 76.2 (C-5), 72.3 (C-2), 71.7 (C-3), 68.6 (C-4), 64.4 (C-6), 26.4 (C($\underline{C}H_3)_3$), 19.1 ($\underline{C}(CH_3)_3$), −5.13 (2 Si-CH_3) ppm; IR (ATR) $\tilde{\nu}$: 3337, 2928, 1599, 1498, 1229, 1006, 685 cm^{-1}; ESIMS (*m*/*z*): $[M + Na]^+$ calcd for $C_{24}H_{34}N_2O_6Si$, 497.1; found, 497.2;.

(*E*)-*p*-(Phenylazo)phenyl 6-*O*-*tert*-butyldimethylsilyl-2,3-*O*-(ethylorthoacetyl)-α-D-mannopyranoside (8). To a solution of mannoside **7** (500 mg, 1.05 mmol) in toluene (8.0 mL), triethylorthoacetate (773 µL, 4.22 mmol) and a catalytic amount of *p*-toluenesulfonic acid were added at rt, and the reaction mixture was stirred for 3.5 h, after which TLC showed complete consumption of the starting material. Then, it was neutralised with triethylamine (100 µL), and the solution was diluted with water (10 mL). It was extracted with toluene (2 × 20 mL), and the extract was concentrated under reduced pressure to get crude **8** (600 mg) as a red viscous syrup, which was used in the next reaction step without further purification.

(*E*)-*p*-(Phenylazo)phenyl 2,3-*O*-(ethylorthoacetyl)-α-D-mannopyranoside (9). The crude intermediate **8** (600 mg) was dissolved in CH_2Cl_2 (6.0 mL), tetrabutylammonium fluoride (1 M solution in THF, 1.68 mL) was added, and the reaction mixture was stirred at rt for 4 h, after which TLC showed complete consumption of the starting material. Then, it was concentrated under reduced pressure to obtain crude **9** as a dark red viscous syrup (594 mg), which was used in the next reaction step without further purification.

(*E*)-*p*-(Phenylazo)phenyl 2,4,6-tri-*O*-acetyl-α-D-mannopyranoside (10). The crude orthoester-protected mannoside **9** (594 mg) was dissolved in pyridine (2.5 mL), and acetic anhydride (1.26 mL) was added for O-acetylation. The reaction mixture was stirred at rt for 3 h. Then, pyridine was removed under reduced pressure, and the residue was dissolved in ethyl acetate (20 mL) and washed with satd. aq. $NaHCO_3$ solution (10 mL). The aqueous phase was extracted with ethyl acetate (2 × 25 mL), the combined organic phases were dried over Na_2SO_4 and filtered, and the filtrate concentrated was under reduced pressure to obtain a syrupy intermediate. It was dissolved in 80% acetic acid (2.5 mL), and the mixture was stirred at rt for 1.5 h to effect regioselective cleavage of the orthoester. Then, ethyl acetate (50 mL) was added and the

organic layer was washed with water (5 mL) and dried over $MgSO_4$. It was filtered, and the filtrate was evaporated to obtain the crude product, which purified by column chromatography (cyclohexane/ethyl acetate 2:1) to yield the free 3-OH title mannoside **10** as a bright orange solid (220 mg, 0.453 mmol, 43% over three steps). Mp 144–146 °C; R_f 0.21 (cyclohexane/ethyl acetate); $[\alpha]^{20}_D$ +70 (*c* 0.96, CH_2Cl_2); ^{1}H NMR (500 MHz, $CDCl_3$) δ 7.92 (d, *J* = 8.9 Hz, 2H, H-9, H-11), 7.89 (d, *J* = 7.9 Hz, 2H, H-14, H-18), 7.53–7.44 (m, 3H, H-15, H-16, H-17), 7.19 (d, *J* = 8.9 Hz, 2H, H-8, H-12), 5.69 (d, $J_{1,2}$ = 1.4 Hz, 1H, H-1), 5.30 (dd, $J_{1,2}$ = 1.7 Hz, $J_{2,3}$ = 3.8 Hz, 1H, H-2), 5.17 (t, *J* = 10.0 Hz, 1H, H-4), 4.32 (m, 2H, H-3, H-6a), 4.11 (dd, $J_{5,6b}$ = 2.2 Hz, $J_{6a,6b}$ = 12.4 Hz, 1H, H-6b), 4.05 (m_c, 1H, H-5), 2.23, 2.15, 2.03 (each s, each 3H, 3 OAc), 1.62 (bs, OH) ppm; ^{13}C NMR (150 MHz, $CDCl_3$) δ 171.3, 170.6, 170.4 (3 $\underline{C}OCH_3$), 157.7 (C-7), 152.6 (C-13), 148.3 (C-10), 130.8 (C-16), 129.1 (C-15, C-17), 124.6 (C-9, C-11), 122.7 (C-14, C-18), 116.7 (C-8, C-12), 95.42 (C-1), 71.99 (C-2), 69.14 (C-5), 69.04 (C-4), 68.47 (C-3), 62.15 (C-6), 20.97, 20.91, 20.69 (3 CO$\underline{C}H_3$) ppm; IR (ATR) $\tilde{\nu}$: 3453, 2961, 1737, 1228, 1023, 798 cm^{-1}; ESIMS (*m*/*z*): [M + H]+ calcd for $C_{24}H_{26}N_2O_9$, 509.1; found, 509.2.

(*E*)-*p*-(Phenylazo)phenyl 3-*O*-(2,3,4,6-tetra-*O*-acetyl-α-D-mannopyranosyl)-2,4,6-tri-*O*-acetyl-α-D-mannopyranoside (11). The 3-OH unprotected mannoside **10** (50 mg, 103 µmol) and the mannosyl donor **3** (101 mg, 206 µmol) were dissolved in dry CH_2Cl_2 (10 mL), and the mixture was cooled to −10 °C under N_2 atmosphere. To this ice-cooled solution BF_3·etherate (13 µL, 108 µmol) was added and the mixture was stirred at 0 °C for about 30 min. Then, the reaction mixture was allowed to warm to rt and stirred for another 4 h. The reaction mixture was then quenched by the addition of a catalytic amount of solid $NaHCO_3$ and concentrated under reduced pressure to obtain the crude product as a dark reddish-brown syrup. Purification by column chromatography (CH_2Cl_2/ethyl acetate 8:2) gave the acetyl-protected mannobioside **11** as a pale yellow solid (64 mg, 78 µmol, 76%). Mp 84–85 °C; R_f 0.57 (CH_2Cl_2/ethyl acetate 8:2); $[\alpha]^{20}_D$ +103 (*c* 0.86, CH_2Cl_2); ^{1}H NMR (500 MHz, $CDCl_3$) δ 7.92 (d, *J* = 9.0 Hz, 2H, H-9, H-11), 7.89 (d, *J* = 7.1 Hz, 2H, H-14, H-18), 7.46–7.38 (m, 3H, H-15, H-16, H-17), 7.18 (d, *J* = 9.0 Hz, 2H, H-8, H-12), 5.65 (d, $J_{1,2}$ = 1.7 Hz, 1H, H-1), 5.46 (dd, $J_{1,2}$ = 1.8 Hz, $J_{2,3}$ = 3.5 Hz, 1H, H-2), 5.40 (t, *J* = 10.1 Hz, 1H, H-4′), 5.30 (m_c, 1H, H-3′), 5.26 (m_c, 1H, H-4), 5.09 (d, $J_{1,2}$ = 1.7 Hz 1H, H-1′), 5.06 (dd, $J_{1,2}$ = 1.9 Hz, $J_{2,3}$ = 2.9 Hz, 1H, H-2′), 4.41 (dd, $J_{2,3}$ = 3.5 Hz, $J_{3,4}$ = 9.9 Hz, 1H, H-3), 4.30 (dd, $J_{5,6b}$ = 6.3 Hz, $J_{6a,6b}$ = 12.7 Hz, 1H, H-6a), 4.24 (dd, $J_{5',6b'}$ = 5.8 Hz, $J_{6a',6b'}$ = 12.3 Hz, 1H, H-6a′), 4.14–4.10 (m, H-5′, H-6b), 4.08 (dd, $J_{5,6a}$ = 2.4 Hz, $J_{6a,6b}$ = 12.3 Hz, 1H, H-6b), 3.99 (ddd, $J_{4,5}$ = 10.2 Hz, $J_{5,6a}$ = 2.3 Hz, $J_{6a,6b}$ = 5.8 Hz, 1H, H-5), 2.20, 2.09, 2.08, 2.03, 2.00, 1.97, 1.94 (each s, each 3H, 7 OAc) ppm; ^{13}C NMR (125 MHz, $CDCl_3$) δ 170.6, 170.5, 170.4, 170.0, 169.9, 169.8, 169.6 (7 $\underline{C}OCH_3$), 157.4 (C-7), 152.6 (C-13), 148.4 (C-10), 130.8 (C-16), 129.1 (C-15, C-17), 124.6 (C-9, C-11), 122.71 (C-14, C-18) 116.7 (C-8, C-12), 99.1 (C-1′), 95.6 (C-1), 74.8 (C-3), 70.8 (C-2), 69.9 (C-2′), 69.9, 69.6 (C-5, C-5′), 68.3 (C-4), 67.4 (C-4′), 65.9 (C-3′), 62.5, 62.7 (C-6, C-6′), 20.9, 20.8, 20.7, 20.7, 20.7, 20.6, 20.6 (7 CO$\underline{C}H_3$) ppm; IR (ATR) $\tilde{\nu}$: 1743, 1213, 1032, 838 cm^{-1}; ESIMS (*m*/*z*): [M + Na]$^+$ calcd for $C_{38}H_{44}N_2O_{18}$, 839.3; found, 839.2.

(*E*)-*p*-(Phenylazo)phenyl 3-*O*-(α-D-mannopyranosyl)-α-D-mannopyranoside (2). The acetyl-protected disaccharide **11** (50 mg, 61.2 µmol) was dissolved in dry MeOH (2 mL) and a catalytic amount of solid NaOMe was added under N_2 atmosphere. The reaction mixture was stirred for 5 h at rt, and then it was neutralized with Amberlite IR 120 ion-exchange resin. It was then filtered and thoroughly washed with MeOH (2 × 20 mL), and the filtrate was evaporated to obtain the crude product, which after purification by flash column chromatography (CH_2Cl_2/methanol 9:1) gave the final mannobioside **2** as a pale yellow solid (29.3 mg, 56.1 µmol, 92%). Mp 107–109 °C; R_f 0.08 (CH_2Cl_2/MeOH 9:1); $[\alpha]^{20}_D$ +18.4 (*c* 0.48, MeOH); ^{1}H NMR (500 MHz, D_2O) δ 7.81 (d, *J* = 8.2 Hz, 2H, H-9, H-11), 7.75 (d, *J* = 7.4 Hz, 2H, H-14, H-18), 7.53–7.49 (m, 3H, H-15, H-16, H-17), 7.24 (d, *J* = 8.3 Hz, 2H, H-8, H-12), 5.65 (s, 1H, H-1), 5.16 (s, 1H, H-1′), 4.29 (m_c, 1H, H-2), 4.14 (dd, $J_{2,3}$ = 3.1 Hz, $J_{3,4}$ = 10.3 Hz, 1H, H-3′), 4.06 (m_c, 1H, H-2′), 3.89–3.81 (m, 3H, H-3, H-4, H-4′), 3.79–3.62 (m, 6H, H-6a, H-6b, H-5, H-5′, H-6a′, H-6b′) ppm; ^{13}C NMR (125 MHz, D_2O) δ 158.2 (C-7), 151.3 (C-13), 148.2 (C-10), 131.4 (C-16), 129.6 (C-15, C-17), 124.4 (C-9, C-11), 122.2 (C-14, C-18), 117.3 (C-8, C-12), 102.4 (C-1′), 97.8 (C-1), 77.9 (C-3′), 73.8 (C-5), 73.5 (C-3), 70.5 (C-4′), 70.1 (C-2′), 69.5 (C-2), 66.9 (C-5′), 65.9 (C-4), 61.1 (C-6), 60.6 (C-6′) ppm; IR (ATR) $\tilde{\nu}$: 3318, 2927, 1599, 1231, 1007, 685 cm^{-1}; MALDI-TOFMS (*m*/*z*): [M + Na]$^+$ calcd for $C_{24}H_{30}N_2O_{11}$, 545.18; found, 545.17; UV, λ_{max}: 339 nm, ε = 14776 ± 729 L × mol^{-1} × cm^{-1}; anal. calcd for $C_{24}H_{30}N_2O_{11}$ × 1.1 H_2O: C, 52.11; H, 6.09; N, 5.07; found: C, 52.04; H, 5.79; N, 5.06.

NMR-spectroscopic data for (*Z*)-2. ^{1}H NMR (500 MHz, D_2O) δ 7.32 (t, *J* = 7.1 Hz, 2H, H-15, H-17), 7.24 (t, 1H, H-16), 7.00 (dd, *J* = 1.9 Hz, *J* = 8.9 Hz, 2H, H-9, H-11), 6.95 (dd, *J* = 1.9 Hz, *J* = 8.9 Hz, 2H, H-8, H-12), 6.91 (dd, *J* = 1.3 Hz, *J* = 7.8 Hz, 2H, H-14, H-18), 5.52 (s, 1H, H-1), 5.12 (s, 1H, H-1′), 4.22 (m_c, 1H, H-2), 4.07 (m_c, 1H, H-3′), 4.03 (dd, $J_{1,2}$ = 1.7 Hz, $J_{2,3}$ = 3.2 Hz, 1H, H-2′), 3.85–3.82 (m, 2H, H-3, H-4), 3.79–3.59 (m, 7H, H-4′, H-6a, H-6b, H-5, H-5′, H-6a′, H-6b′) ppm; ^{13}C NMR (125 MHz, D_2O) δ 155.3 (C-7), 153.5 (C-13), 146.9 (C-10), 129.2 (C-15, C-17), 128.2 (C-16), 123.4 (C-8,

C-12), 120.3 (C-14, C-18), 116.9 (C-9, C-11), 102.4 (C-1′), 97.8 (C-1), 77.8 (C-3′), 73.7 (C-5), 73.4 (C-3), 70.4 (C-4′), 70.1 (C-2′), 69.4 (C-2), 66.8 (C-5′), 65.9 (C-4), 61.0 (C-6), 60.6 (C-6′) ppm; UV, λ_{max}: 429 nm, ε = 1699 ± 68 L × mol^{-1} × cm^{-1}.

Supporting Information

Supporting Information File 1

Photoisomerization studies, UV–vis spectra, NMR spectra, bioassay and docking results.
[http://www.beilstein-journals.org/bjoc/content/supplementary/1860-5397-9-26-S1.pdf]

Acknowledgements

Financial support by the DFG (collaborative network SFB677) and FCI (Fonds der Chemischen Industrie) is gratefully acknowledged. We thank Max Britz for technical assistance.

References

1. Ohlsen, K.; Oelschlaeger, T. A.; Hacker, J.; Khan, A. S. *Top. Curr. Chem.* **2009,** *288,* 17–65. doi:10.1007/128_2008_10
2. Klemm, P.; Schembri, M. A. *Int. J. Med. Microbiol.* **2000,** *290,* 27–35. doi:10.1016/S1438-4221(00)80102-2
3. Mulvey, M. A. *Cell. Microbiol.* **2002,** *4,* 257–271. doi:10.1046/j.1462-5822.2002.00193.x
4. Kau, A. L.; Hunstad, D. A.; Hultgren, S. J. *Curr. Opin. Microbiol.* **2005,** *8,* 54–59. doi:10.1016/j.mib.2004.12.001
5. Hartmann, M.; Lindhorst, T. K. *Eur. J. Org. Chem.* **2011,** 3583–3609. doi:10.1002/ejoc.201100407
See for a review.
6. Scharenberg, M.; Schwardt, O.; Rabbani, S.; Ernst, B. *J. Med. Chem.* **2012,** *55,* 9810–9816. doi:10.1021/jm3010338
7. Knight, S. D.; Bouckaert, J. *Top. Curr. Chem.* **2009,** *288,* 67–107. doi:10.1007/128_2008_13
8. Choudhury, D.; Thompson, A.; Stojanoff, V.; Langerman, S.; Pinkner, J.; Hultgren, S. J.; Knight, S. D. *Science* **1999,** *285,* 1061–1066. doi:10.1126/science.285.5430.1061
9. Hung, C.-S.; Bouckaert, J.; Hung, D.; Pinkner, J.; Widberg, C.; Defusco, A.; Auguste, C. G.; Strouse, R.; Langermann, S.; Waksman, G.; Hultgren, S. J. *Mol. Microbiol.* **2002,** *44,* 903–918. doi:10.1046/j.1365-2958.2002.02915.x
10. Bouckaert, J.; Berglund, J.; Schembri, M.; Genst, E. D.; Cools, L.; Wuhrer, M.; Hung, C.-S.; Pinkner, J.; Slättegård, R.; Zavialov, A.; Choudhury, D.; Langermann, S.; Hultgren, S. J.; Wyns, L.; Klemm, P.; Oscarson, S.; Knight, S. D.; Greve, H. D. *Mol. Microbiol.* **2005,** *55,* 441–455. doi:10.1111/j.1365-2958.2004.04415.x
11. Wellens, A.; Garofalo, C.; Nguyen, H.; Van Gerven, N.; Slättegård, R.; Hernalsteens, J. P.; Wyns, L.; Oscarson, S.; De Greve, H.; Hultgren, S.; Bouckaert, J. *PLoS One* **2008,** *3,* e2040. doi:10.1371/journal.pone.0002040
12. Dubber, M.; Sperling, O.; Lindhorst, T. K. *Org. Biomol. Chem.* **2006,** *4,* 3901–3912. doi:10.1039/b610741a
13. Russew, M.-M.; Hecht, S. *Adv. Mater.* **2010,** *22,* 3348–3360. doi:10.1002/adma.200904102
14. Kramer, R. H.; Fortin, D. L.; Trauner, D. *Curr. Opin. Neurobiol.* **2009,** *19,* 544–552. doi:10.1016/j.conb.2009.09.004
15. Chandrasekaran, V.; Lindhorst, T. K. *Chem. Commun.* **2012,** *48,* 7519–7521. doi:10.1039/c2cc33542e
16. Weissenborn, M. J.; Castangia, R.; Wehner, J. W.; Šardzík, R.; Lindhorst, T. K.; Flitsch, S. *Chem. Commun.* **2012,** 4444–4446. doi:10.1039/c2cc30844d
17. Grabosch, C.; Kolbe, K.; Lindhorst, T. K. *ChemBioChem* **2012,** *13,* 1874–1879. doi:10.1002/cbic.201200365
18. Wehner, J. W.; Weissenborn, M. J.; Hartmann, M.; Gray, C. J.; Šardzík, R.; Eyers, C. E.; Flitsch, S. L.; Lindhorst, T. K. *Org. Biomol. Chem.* **2012,** *10,* 8919–8926. doi:10.1039/c2ob26118a
19. Jung, K.-H.; Hoch, M.; Schmidt, R. R. *Liebigs Ann. Chem.* **1989,** 1099–1106. doi:10.1002/jlac.198919890276
20. Zemplén, G.; Pacsu, E. *Ber. Dtsch. Chem. Ges. B* **1929,** *62,* 1613–1614. doi:10.1002/cber.19290620640
21. Lindhorst, T. K.; Bruegge, K.; Fuchs, A.; Sperling, O. *Beilstein J. Org. Chem.* **2010,** *6,* 801–809. doi:10.3762/bjoc.6.90
22. Oscarson, S.; Tidén, A.-K. *Carbohydr. Res.* **1993,** *247,* 323–328. doi:10.1016/0008-6215(93)84266-9
23. Hartmann, M.; Horst, A. K.; Klemm, P.; Lindhorst, T. K. *Chem. Commun.* **2010,** *46,* 330–332. doi:10.1039/b922525k
24. Rarey, M.; Kramer, B.; Lengauer, T.; Klebe, G. *J. Mol. Biol.* **1996,** *261,* 470–489. doi:10.1006/jmbi.1996.0477
25. Rarey, M.; Kramer, B.; Lengauer, T. *J. Comput.-Aided Mol. Des.* **1997,** *11,* 369–384. doi:10.1023/A:1007913026166
26. Kramer, B.; Rarey, M.; Lengauer, T. *Proteins: Struct., Funct., Genet.* **1999,** *37,* 228–241. doi:10.1002/(SICI)1097-0134(19991101)37:2<228::AID-PROT8>3.0.CO;2-8
27. Clark, R. D.; Strizhev, A.; Leonard, J. M.; Blake, J. F.; Matthew, J. B. *J. Mol. Graphics Modell.* **2002,** *20,* 281–295. doi:10.1016/S1093-3263(01)00125-5
28. Charifson, P. S.; Corkery, J. J.; Murcko, M. A.; Walters, W. P. *J. Med. Chem.* **1999,** *42,* 5100–5109. doi:10.1021/jm990352k
29. *SYBYL,* Version 6.9; Tripos, Inc.: St. Louis, MO.
30. Dokić, J.; Gothe, M.; Wirth, J.; Peters, M. V.; Schwarz, J.; Hecht, S.; Saalfrank, P. *J. Phys. Chem. A* **2009,** *113,* 6763–6773. doi:10.1021/jp9021344
31. Sperling, O.; Fuchs, A.; Lindhorst, T. K. *Org. Biomol. Chem.* **2006,** *4,* 3913–3922. doi:10.1039/b610745a
32. Connolly, M. L. *Science* **1983,** *221,* 709–713. doi:10.1126/science.6879170
33. Connolly, M. L. *J. Appl. Crystallogr.* **1983,** *16,* 548. doi:10.1107/S0021889883010985
34. Sharon, N. *FEBS Lett.* **1987,** *217,* 145–157. doi:10.1016/0014-5793(87)80654-3
35. Lindhorst, T. K. Ligands for FimH. In *Synthesis and Biological Applications of Glycoconjugates;* Renaudet, O.; Spinelli, N., Eds.; Bentham Science e-Books, 2011; pp 12–35.
36. Hartmann, M.; Papavlassopoulos, H.; Chandrasekaran, V.; Grabosch, C.; Beiroth, F.; Lindhorst, T. K.; Röhl, C. *FEBS Lett.* **2012,** *586,* 1459–1465. doi:10.1016/j.febslet.2012.03.059
37. Garcia-Amorós, J.; Díaz-Lobo, M.; Nonell, S.; Velasco, D. *Angew. Chem., Int. Ed.* **2012,** *51,* 12820–12823. doi:10.1002/anie.201207602

Beilstein Journal of Organic Chemistry

Spin state switching in iron coordination compounds

Philipp Gütlich*[1], Ana B. Gaspar[2] and Yann Garcia[3]

Review

Open Access

Address:
[1]Institut für Anorganische Chemie und Analytische Chemie, Johannes Gutenberg-Universität, Staudingerweg 9, 55099 Mainz, Germany, [2]Institut de Ciència Molecular (ICMOL)/Departament de Química Inorgànica, Universitat de València, Edifici de Instituts de Paterna, Apartat de Correus 22085, 46071 València, Spain and [3]Institute of Condensed Matter and Nanosciences, MOST – Inorganic Chemistry, Université Catholique de Louvain, Place L. Pasteur 1, 1348 Louvain la Neuve, Belgium

Email:
Philipp Gütlich* - guetlich@uni-mainz.de

* Corresponding author

Keywords:
cages; iron(II) coordination compounds; physical techniques; polyfunctional materials; spin crossover

Beilstein J. Org. Chem. **2013,** *9,* 342–391.
doi:10.3762/bjoc.9.39

Received: 24 October 2012
Accepted: 18 January 2013
Published: 15 February 2013

This article is part of the Thematic Series "Molecular switches and cages". Dedicated to Professor Horst Elias on the occasion of his 80th birthday.

Guest Editor: D. Trauner

Abstract

The article deals with coordination compounds of iron(II) that may exhibit thermally induced spin transition, known as spin crossover, depending on the nature of the coordinating ligand sphere. Spin transition in such compounds also occurs under pressure and irradiation with light. The spin states involved have different magnetic and optical properties suitable for their detection and characterization. Spin crossover compounds, though known for more than eight decades, have become most attractive in recent years and are extensively studied by chemists and physicists. The switching properties make such materials potential candidates for practical applications in thermal and pressure sensors as well as optical devices.

The article begins with a brief description of the principle of molecular spin state switching using simple concepts of ligand field theory. Conditions to be fulfilled in order to observe spin crossover will be explained and general remarks regarding the chemical nature that is important for the occurrence of spin crossover will be made. A subsequent section describes the molecular consequences of spin crossover and the variety of physical techniques usually applied for their characterization. The effects of light irradiation (LIESST) and application of pressure are subjects of two separate sections. The major part of this account concentrates on selected spin crossover compounds of iron(II), with particular emphasis on the chemical and physical influences on the spin crossover behavior. The vast variety of compounds exhibiting this fascinating switching phenomenon encompasses mono-, oligo- and polynuclear iron(II) complexes and cages, polymeric 1D, 2D and 3D systems, nanomaterials, and polyfunctional materials that combine spin crossover with another physical or chemical property.

Introduction

Coordination compounds of transition-metal ions may, under certain conditions, exhibit a switching phenomenon, whereby the central metal ion changes the spin state upon a change of temperature, application of pressure, irradiation with light, or in a magnetic field. This phenomenon is known as *spin transition* (ST) or *spin crossover* (SCO). The change of spin state is accompanied by a change of electronic structure of the central ion and the complex molecule on the whole, which changes markedly the physical and chemical properties of the substance. Most spectacular is the change of magnetic behavior and color, which has made such SCO substances very attractive because of their potential for practical applications, e.g., as switching devices and sensors.

A thermally induced change of spin state (spin transition, spin crossover) was first reported some eighty years ago by Cambi and co-workers. They prepared a great variety of dithiocarbamato complexes of iron(III), by varying the substituents at the dithiocarbamate ligands, and investigated their magnetic properties. From magnetic susceptibility measurements at room temperature they found that some of the samples showed magnetic moments corresponding to five unpaired electrons (later on denoted as *high-spin state,* HS) and others with different substituents showed magnetic moments corresponding to only one unpaired electron (*low-spin state,* LS). A third class of such complexes exhibited very unusual magnetic properties: they showed HS behavior at room temperature, but changed more or less gradually to LS behavior on cooling [1-6]. Many more SCO complex compounds of iron(III) have been synthesized thereafter and extensively investigated [7-13].

More than thirty years after the discovery of thermal ST by Cambi et al. the first iron(II) coordination compound, viz. $[Fe(phen)_2(NCS)_2]$ (phen = 1,10-phenanthroline), was observed to show also thermally induced ST between HS and LS states: the spin transition takes place very abruptly near to 175 K [14,15]. Since then, many further examples of iron(II) SCO compounds have been published [7-13,16-28], and other coordination compounds of 3d transition elements such as cobalt(II) [29,30], and to a much lesser extent cobalt(III), chromium(II), manganese(II), manganese(III), and nickel were found to exhibit thermal ST phenomena [31-33]. But practically no example of thermal ST with coordination compounds of the 4d and 5d transition metal series has been reported up to now, which is well understood on the basis of ligand field theory [34,35].

The purpose of this article is to introduce researchers, mainly from the vast field of organic chemistry, to the fascinating SCO switching phenomenon occurring in inorganic coordination compounds of transition-metal ions. In the first part we shall describe the principle of thermal spin crossover and methods of physical characterization, and demonstrate with a selection of typical examples, mainly SCO compounds of iron(II), the variety of chemical and physical influences on the spin transition behavior. The second part will be devoted to a brief overview of selected SCO compounds of iron(II) including mono-, di-, oligonuclear and higher nuclearity complexes, polymeric 1D, 2D and 3D systems, 1D chain compounds and 2D and 3D networks, SCO in nanomaterials, and soft matter, such as metallomesogens, as examples for the main current objectives in SCO research, viz. synthesizing so-called multifunctional materials, which combine the SCO switching phenomenon with other functionalities. The limited scope of the present account has not enabled us to present a rigorous quantitative review aimed at researchers actively working in this field. We extend our sincere apologies to all those who have contributed and published excellent SCO work, which, because of limited space, we were not able to include here.

The article concludes with an outlook, emphasizing on the one hand the current activities in SCO research towards arriving at a better understanding of the molecular processes and cooperative interactions during the spin transition, which is of utmost importance for eventual practical applications of SCO materials; and on the other hand, the necessity and usefulness of close cooperation between organic and inorganic chemists will be pointed out in view of the nature and rich variety of SCO compounds, where (often sophisticated) organic ligand molecules are coordinated to transition-metal ions stimulating and controlling the electronic switching phenomenon.

Review

Occurrence of spin transition

The occurrence of ST in coordination compounds of transition-metal ions is governed by the relationship between the strength of the ligand field (the electrostatic field acting at the central metal ion) and the mean spin-pairing energy [34,35]. Octahedral complexes of d^{4-7} ions may be either HS or LS, depending on whether the ligand field strength is weaker or stronger, respectively, than the spin pairing energy. In order for thermally induced ST to occur the difference in the Gibb's free energies for the two spin states involved must be on the order of thermal energy, k_BT [23]. An increase in temperature favors the HS state, while lowering the temperature favors the LS state. The condition for thermal ST to occur and the consequences of ST are depicted in Figure 1 [23].

Thermal spin transition occurs nearly exclusively with coordination complexes of 3d metal ions. This is not expected for 4d

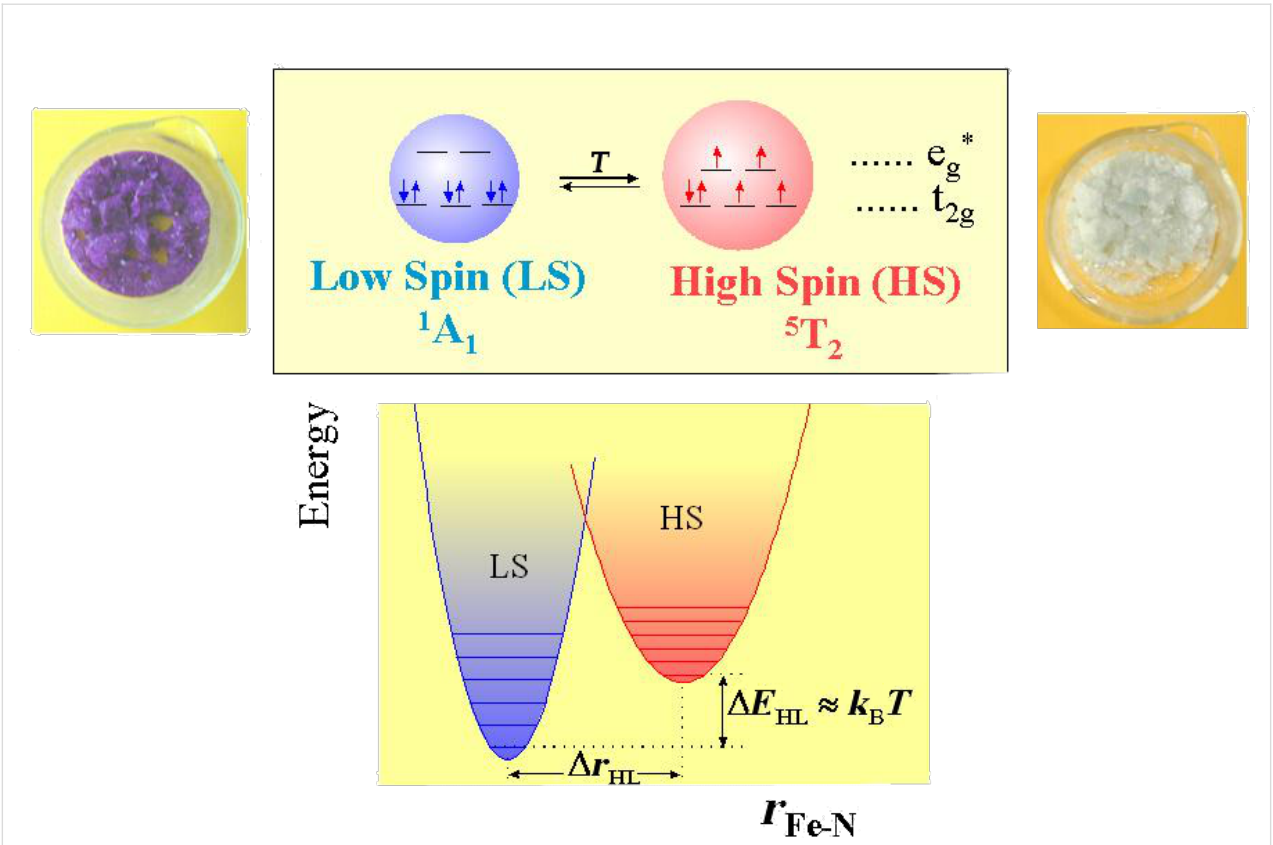

Figure 1: Change of electron distribution between HS and LS states of an octahedral iron(II) coordination compound exhibiting thermal spin crossover. The orbitals e_g^* and t_{2g} arise from splitting of the 3d orbitals in an octahedral ligand field. Depletion of charge in the antibonding e_g^* orbitals during HS to LS transition shortens the metal-to-ligand bond distances and reduces the molecular volume. SCO is mostly accompanied by a color change, e.g., in the present case, from white in the HS state to violet in the LS state. The condition to fulfil in order to observe thermal spin crossover is $\Delta E_{HL} \approx k_B T$. Increasing the temperature favors the HS state, decreasing it favors the LS state [23]. (Reproduced with permission from [36]. Copyright 2012 Wiley-VCH Verlag GmbH & Co. KGaA).

and 5d transition element compounds on the basis of ligand field theory, because the strength of the ligand field increases notably (by ca. 50% from 3d to 4d and also from 4d to 5d) relative to analogous 3d compounds and is generally much greater than the spin pairing energy; hence virtually all 4d and 5d transition metal complexes show LS behavior.

Spin transition seems to occur predominantly for six-coordinate iron(II) complexes with the following change of electron configurations and ligand field states:

$$t_{2g}^6 e_g^0 \left(^1A_{1g}, \text{LS}\right) \leftrightarrow t_{2g}^4 e_g^2 \left(^5T_{2g}, \text{HS}\right). \quad (1)$$

SCO complexes of iron(II) have been most extensively characterized and explored; the field has been reviewed many times [7-13,16-28]. Most of the iron(II) SCO compounds known possess an $[N_6]$ donor atom set, i.e., an $[FeN_6]$ chromophor with N-coordinated ligands of variable denticity. A few examples with other donor-atom sets, e.g., N_4O_2 [37-40], P_4Cl_2, have also been reported [41]. $[FeN_6]$ systems of iron(II) involve, for instance, $[Fe(diimine)_2(NCS)_2]$ complexes, among them the *classical* complexes with 1,10-phenanthroline (phen) and 2,2'-bipyridine (bipy) as bisdentate diimine ligands, which were among the first SCO compounds of iron(II) reported in the literature [14,15]. An example of $[FeN_6]$ complexes with tris-dentate N-donor ligands is bis[hydro-tris(pyrazolyl-borato)]iron(II) [42,43] and related systems.

Thermal SCO has been observed with $[Fe(diimine)_2(NCS)_2]$ complexes employing a large variety of diimine ligands and also with iron(II) complexes containing derivatives of unidentate pyridine [44], bridging diimine and bis(unidentate) ligand components. The anionic groups X in $[Fe(diimine)_2X_2]$ complexes, where X is directly coordinated to the central metal ion, can be varied too, and SCO has been reported for $[Fe(diimine)_2X_2]$ systems with $X^- = NCSe^-$ [14,15], $[NCBH_3]^-$ [45], $TCNQ^-$ [46], $[N(CN)_2]^-$ [47], and $2X^- = [WS_4]^{2-}$ [48].

Many $[FeN_6]^{2+}$ systems are based on the cationic LS [Fe(2,2”-bipyridine)$_3$]$^{2+}$ or [Fe(2,2":2',6'-terpyridine)$_2$]$^{2+}$ ions, where the critical field strength to reach the crossover condition is fulfilled by introducing sterically hindering groups adjacent to the donor atoms or by replacing the pyridine rings by five-membered heterocycles [25,26]. Examples are the SCO systems tris(6-methyl-2,2'-bipyridine)iron(II) and bis(2,4-bis(pyridin-2-yl)thiazole)iron(II) ions [49]. The $[FeN_6]$ system can also exhibit SCO behavior when six monodentate N-donating ligand molecules are involved. The best known examples are the [Fe(N-alkyl-tetrazole)$_6$]X$_2$ complexes, which are nearly regular octahedral [50]. Another possibility to fulfill the condition for thermal spin crossover to occur is the coordination of a hexadentate system, such as the mixed aliphatic/heterocyclic tetrakis(2-pyridylmethyl)ethylenediamine) [51] or the completely saturated, encapsulating hexadentate donor system as described by Martin et al. [52].

Through extensive synthetic work one has learned that *cooperative interactions* between the spin-state-changing complex molecules are of utmost importance for the ST behavior in solid SCO compounds. There are essentially three synthetic strategies that have been developed to create and strengthen cooperativity, i.e., (i) incorporation of a hydrogen-bonded network; (ii) incorporation of π-stacking moieties; and (iii) coordination of bridging ligands. The thermal ST behavior is commonly expressed in terms of the molar fraction of HS molecules, $\gamma_{HS}(T)$, as a function of temperature denoted as the ST function. Spin transitions have been categorized into the types depicted in Figure 2, i.e., gradual (a), abrupt (b), with hysteresis (c), stepwise (d) and incomplete (e). Gradual spin transitions (type a) appear in solution, where practically no cooperative interactions exist and the ST curve follows a simple Boltzmann distribution over all energy levels involved. In solid material, however, the electronic and structural changes accompanying the ST propagate throughout the solid through short and long range interactions and influence markedly the ST function $\gamma_{HS}(T)$.

Thermal spin transition in iron(II) compounds: Consequences and physical characterization

LS↔HS conversions are accompanied by profound changes in all properties that depend on the distribution of the 3d valence electrons, predominantly optical, vibrational, magnetic and structural properties. These molecular changes enable one to detect the occurrence of thermal SCO and monitor the temperature dependence of a ST, as sketched in Figure 2, employing various physical methods, primarily magnetic susceptibility measurements, optical and vibrational spectroscopy, Mössbauer spectroscopy, crystal-structure determination and heat-capacity

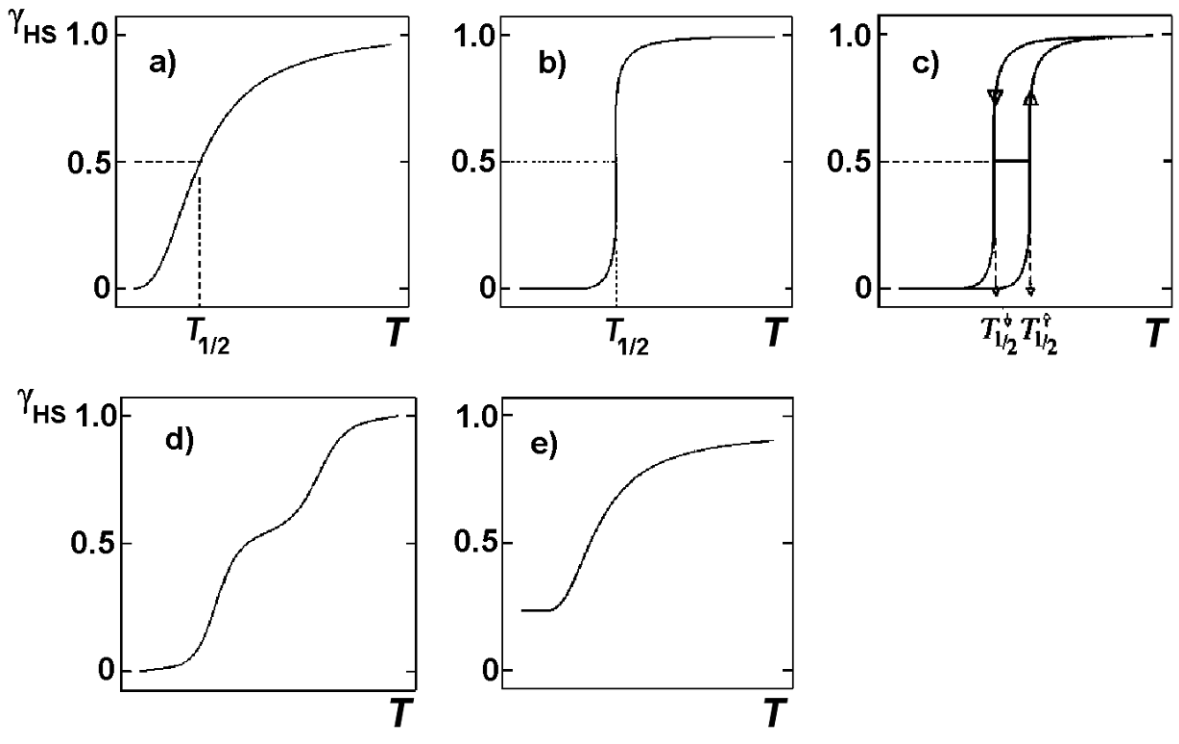

Figure 2: Types of spin transition curves in terms of the molar fraction of HS molecules, $\gamma_{HS}(T)$, as a function of temperature [23]. (Reproduced with permission from [27]. Copyright 2003 Wiley-VCH Verlag GmbH & Co. KGaA).

measurements [23,27,28]. In the following we shall briefly discuss the main molecular changes that accompany LS↔HS conversions in iron(II) compounds and their detection with suitable physical methods. As will be shown in many examples, Mössbauer spectroscopy has proven to be a particularly elegant microscopic tool for the characterization of iron-containing SCO systems. It has been invaluable in detailed studies.

Magnetic susceptibility measurements

From the very beginning of experimental SCO research, measuring the magnetic susceptibility of a sample as a function of temperature, $\chi(T)$, and, if required, deriving the magnetic moment thereof has always been the main characterization method. The different number of unpaired electrons in the HS and LS states, e.g., in the case of iron(II) with four unpaired electrons in the strongly paramagnetic HS state and no unpaired electrons in the diamagnetic LS state, is readily signalized by a drastic change in the magnetic susceptibility. $\chi(T)$ can then be calculated by using Equation 2:

$$\chi(T) = \gamma_{HS}(T) \cdot \chi_{HS} + (1-\gamma_{HS}(T)) \cdot \chi_{LS}, \qquad (2)$$

where γ_{HS} is the molar fraction of HS molecules, and χ_{HS} and χ_{LS} refer to the magnetic susceptibilities of the sample in the pure HS and LS states, which can be measured at sufficiently high and low temperatures, respectively, in the case of a complete spin state transition. The ST curve $\gamma_{HS}(T)$ can be readily obtained with these quantities. One can also derive the effective magnetic moment $\mu_{eff} = 2.83\ \sqrt{\chi T}$ [34,53,54] and plot it as a function of temperature. However, because of certain complications, e.g., orbital contribution and zero-field splitting effects, it has become common practice to study the ST behavior by plotting the $\gamma_{HS}(T)$ function rather than the magnetic moment $\mu_{eff}(T)$.

Techniques for magnetochemical studies of solid material (Faraday balance, Foner type magnetometer, SQUID and AC devices) as well as solutions (Evans' NMR method) are described in [55,56].

Optical spectroscopy

Thermochromism is a typical feature that goes along with thermal ST in nearly all SCO compounds. The color change can be easily monitored by temperature-dependent optical spectroscopy in the UV–vis region. The electric dipole (E1) ligand field transitions (d–d transitions) involved are parity-forbidden but spin-allowed and can give rise to rather intense coloration, particularly in the LS state. For example, SCO complexes of iron(II) with tetrazole and triazole ligands are generally weakly colored or nearly white in the HS state but purple in the LS state. If such ligand field transitions are well resolved and not hidden by more intense parity- and spin-allowed charge-transfer bands, the optical spectrum recorded in the UV–visible region distinguishes well the two spin states involved and can therefore be employed to follow the ST phenomenon qualitatively and quantitatively. From the temperature-dependent area fractions of the absorption bands one can construct the ST curve $\gamma_{HS}(T)$. An example is displayed in Figure 3, where optical spectra (UV–vis) of a single crystal of the SCO compound $[Fe(ptz)_6](BF_4)_2$ (ptz = 1-propyltetrazole), recorded at 300 K and 80 K, are shown [57-60].

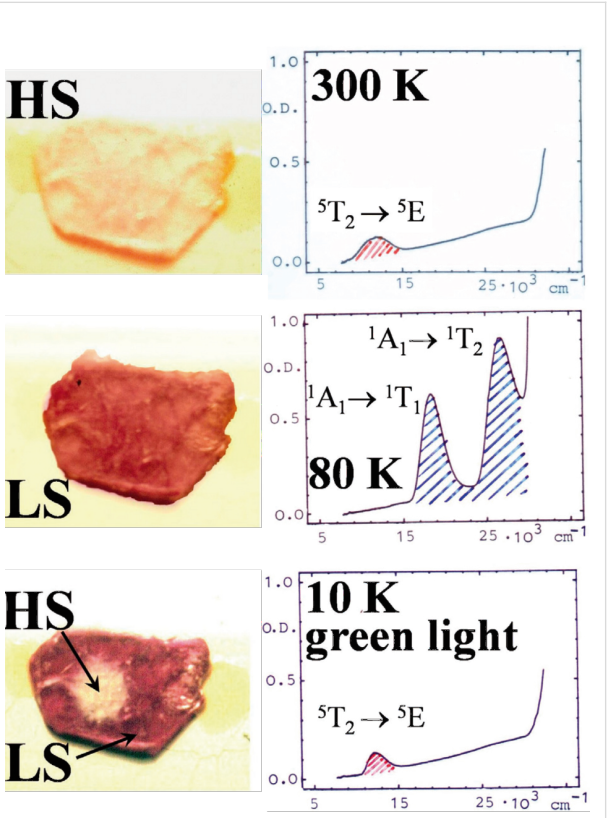

Figure 3: Single crystal UV–vis spectra of the spin crossover compound $[Fe(ptz)_6](BF_4)_2$ (ptz = 1-propyltetrazole). At 300 K, the crystal is white and in the HS state. The spectrum shows a weak $^5T_2 \rightarrow {}^5E$ band at ca. 12000 cm^{-1}. At ca. 135 K, a spin transition takes place to the deeply colored LS state. At 80 K the crystal is red–purple, and the spectrum shows two spin-allowed d–d bands, $^1A_1 \rightarrow {}^1T_1$ and $^1A_1 \rightarrow {}^1T_2$ above 20000 cm^{-1}. The LS state can be switched back to the long-lived metastable HS state by irradiation with green light. The optical spectrum recorded at 10 K shows the typical HS band again. This observation, known as the LIESST effect, is described in more detail below. (Reproduced with permission from [36]. Copyright 2012 Wiley-VCH Verlag GmbH & Co. KGaA).

Vibrational spectroscopy

As discussed above and shown in Figure 1 for the case of SCO in iron(II) compounds, thermal spin state conversion from HS to LS states is connected with depletion of charge in the anti-

bonding e_g orbitals and simultaneous increase of charge in the lower lying slightly bonding t_{2g} orbitals on lowering of the temperature. This results in strengthening of the metal–donor-atom bonds and can be observed in the vibrational spectrum recorded in the far-infrared (FIR) region between ~250 and ~500 cm^{-1}, where the central metal–donor-atom stretching frequencies of transition metal compounds generally appear [61-63]. Detailed and often tedious band assignment is not necessary. With temperature-dependent FIR or Raman spectroscopy, one can readily recognize the vibrational bands characteristic of the HS and the LS species as those with decreasing and increasing intensity, respectively, on cooling of the sample [64-70]. Although not often practiced, one can also derive the spin state conversion curve $\gamma_{HS}(T)$ (Figure 2) by plotting the normalized area fractions of characteristic HS or LS bands as a function of temperature.

A new method of studying vibrational properties has been developed based on *nuclear resonance scattering (NRS) with synchrotron radiation,* also denoted as *Mössbauer spectroscopy in the time domain* in comparison to classical *Mössbauer spectroscopy in the energy domain* [71-73]. NRS experiments are carried out in two ways: nuclear inelastic scattering (NIS) and nuclear forward scattering (NFS) of synchrotron radiation. The NIS technique has proven to be an excellent tool to identify typical HS and LS vibrational bands. One recognizes them as bands with temperature intensity arising in the near neighborhood of Mössbauer-active nuclides (e.g., ^{57}Fe). They give information on the local densities of HS and LS vibrational states [74-76].

Spin state conversion can also affect certain ligand vibrations and can therefore be used to trace the spin state conversion curve $\gamma_{HS}(T)$. Examples are the N-coordinated ligands NCS^- and $NCSe^-$, for instance in the "classical" systems $[Fe(phen)_2(NCS)_2]$ and $[Fe(phen)_2(NCSe)_2]$ [61-63]. The C–N stretching bands of NCS^- and $NCSe^-$ are seen as a strong doublet near 2060–2070 cm^{-1} in the HS state. Upon cooling of $[Fe(phen)_2(NCS)_2]$ to below the transition temperature (175 K), this doublet decreases in intensity, favoring the appearance of a new doublet at 2100–2110 cm^{-1}, which obviously stems from the LS state [61-63]. One has also found that certain vibrational modes of lattice constituents, such as non-coordinating anions or solvent molecules, interconnecting the spin state changing metal complexes via hydrogen bonds, van der Waals or other interactions, can "feel" spin state changes at the metal centers and can therefore be made use of to study ST phenomena. As an example, one has found for the SCO compound $[Fe(ptz)_6](BF_4)_2$ that certain B–F vibrations of the tetrafluoroborato anion show temperature-dependent intensity in agreement with results from magnetic measurements [59].

Mössbauer spectroscopy

^{57}Fe Mössbauer spectroscopy [36,77-81] has proved to be a most powerful tool in probing the oxidation and spin states of iron in coordination compounds. Two of the most important parameters derived from a Mössbauer spectrum, i.e., the *isomer shift* δ and the *quadrupole splitting* ΔE_Q, vary significantly between iron(II)-HS and iron(II)-LS. The area fractions of the resonance signals are proportional to the concentrations of the coexisting spin states, and in most cases the ST curve $\gamma_{HS}(T)$ can be obtained by plotting the area fraction of one of the spin states, usually the HS state, as a function of temperature. Examples are displayed in Figure 4 and Figure 5. ^{57}Fe Mössbauer spectra of the SCO compound $[Fe(ptz)_6](BF_4)_2$ recorded at three different temperatures are displayed in Figure 4. The quadrupole doublet shown in red is characteristic of the HS state, being the only one present in the region above the critical ST temperature $T_{1/2}$ at ca. 135 K; $T_{1/2}$ is the temperature where both spin states HS and LS are present at 50% each. Below $T_{1/2}$, the compound is in the LS state, and the resonance signal (blue) has changed dramatically. Details about the different isomer shift values and the origin and size of the quadrupole splitting of the two spin states of iron(II) are explained elsewhere [36,77-81].

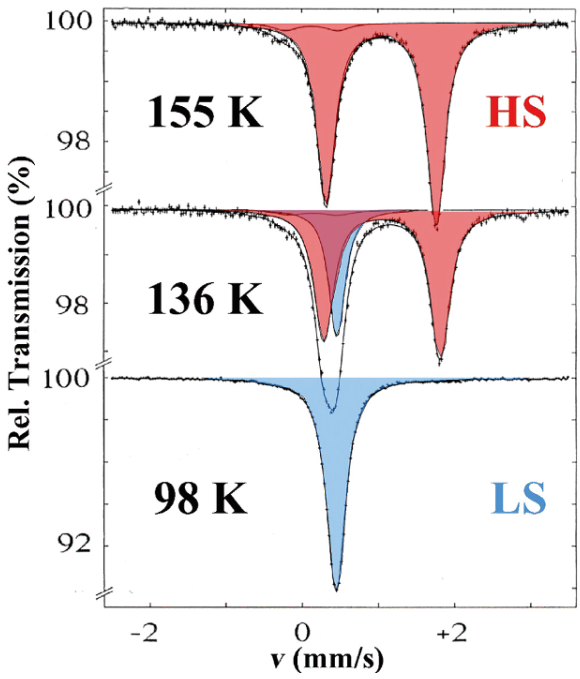

Figure 4: Thermal spin crossover in $[Fe(ptz)_6](BF_4)_2$ (ptz = 1-propyltetrazole) recorded at three different temperatures. The spin transition temperature $T_{1/2}$ is ca. 135 K. The ^{57}Fe Mössbauer spectra demonstrate the transition between the HS phase (quadrupole doublet shown in red) and the LS phase (singlet shown in blue) at the spin transition temperature $T_{1/2}$ of ca. 135 K [59] (Reproduced with permission from [36]. Copyright 2012 Wiley-VCH Verlag GmbH & Co. KGaA).

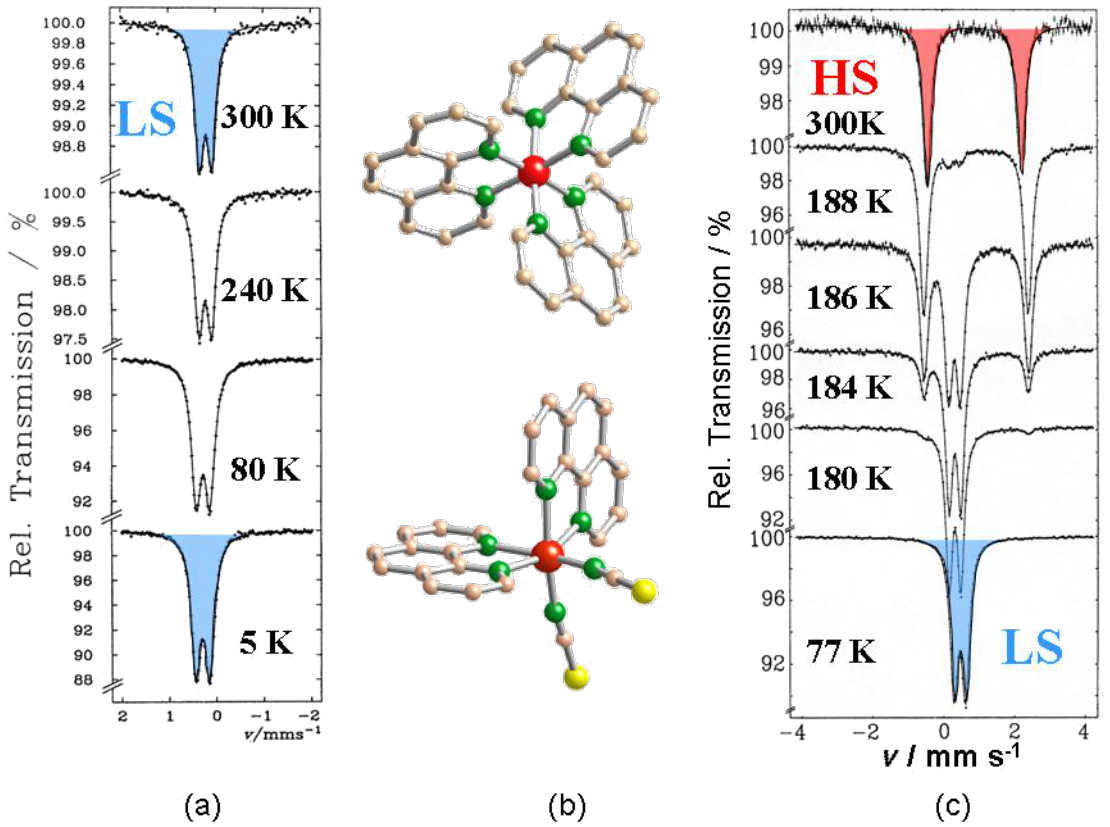

Figure 5: (a) Mössbauer spectra of the LS compound $[Fe(phen)_3]X_2$ recorded over the temperature range 300–5 K. (b) Perspective crystal structures of $[Fe(phen)_3]^{2+}$ (top) and $[Fe(phen)_2(NCS)_2]$ (bottom). (c) Temperature-dependent Mössbauer spectra of $[Fe(phen)_2(NCS)_2]$ indicating the thermally induced HS↔LS spin transition around 175 K [79] (Reproduced with permission from [36]. Copyright 2012 Wiley-VCH Verlag GmbH & Co. KGaA).

Another instructive example is the study of the classical iron(II) SCO compound $[Fe(phen)_2(NCS)_2]$ with ^{57}Fe Mössbauer spectroscopy, which was first reported by Dézsi et al. [82]. This compound is derived from $[Fe(phen)_3]X_2$, which displays LS behavior over the entire temperature range from 300 to 5 K as confirmed by temperature-dependent Mössbauer spectroscopy (Figure 5a).

On replacement of one phen ligand by two weaker isothiocyanato anions the strength of the average ligand field acting at the central iron atom is weakened such that the condition for thermal SCO to occur is now fulfilled. This is corroborated by the temperature-dependent Mössbauer spectra presented in Figure 5c. The quadrupole doublet (marked in red) observed at room temperature, shows a large splitting of ca. 3 mm s^{-1}, which is typical for HS Fe(II) compounds [79,82]. Upon cooling, a very abrupt spin state conversion (within a few Kelvin) to the LS state takes place near the spin transition temperature of ca. 175 K, signalized by the disappearance of the HS doublet in favor of a new doublet (blue) with considerably smaller quadrupole splitting energy of ca. 0.5 mm s^{-1}, which is typical for LS Fe(II) compounds. The very sharp ST agrees well with data from magnetic susceptibility measurements [83].

It is worth noting that for iron(II) SCO compounds the HS↔LS fluctuation rate is on the order of $\leq 10^7$ s^{-1}. This estimate is derived from the time window of ^{57}Fe Mössbauer spectroscopy, which is determined by the mean life time τ_N of ca. 140 ns of the first excited nuclear state of ^{57}Fe. Since the subspectra arising from HS and LS states appear as sharp signals, their life times must be longer than τ_N, and thus, the spin state fluctuation rate is $1/\tau_N \leq 10^7$ s^{-1}.

Calorimetry

Studies of SCO compounds often require a knowledge of thermodynamic quanitities such as the changes of enthalpy $\Delta H = H_{HS} - H_{LS}$ and entropy $\Delta S = S_{HS} - S_{LS}$ because of their valuable information regarding the ST properties, in particular cooperative interactions and the order of the ST transition. Enthalpy changes $\Delta H = H_{HS} - H_{LS}$ are typically 10 to 20 kJ mol^{-1}, and entropy changes $\Delta S = S_{HS} - S_{LS}$ are on the order of 50 to 80 J mol^{-1} K^{-1} [22]. The thermally induced ST is

an entropy-driven process because the degree of freedom is much higher in the HS state than in the LS state, which is schematically shown in Figure 1 by the narrower distances between the vibrational levels in the HS state as compared to the LS state. Approximately 25% of the total entropy gain on going from LS to HS is of magnetic origin, viz., it arises from the change in spin multiplicity, $\Delta S_{mag} = R[\ln(2S + 1)_{HS} - \ln(2S + 1)_{LS}]$, ≈ 13 cal mol^{-1} K^{-1}, and the major part originates from changes in the intramolecular, and to a much lesser extent, intermolecular vibrations [84,85].

The first precise heat capacity measurements on a SCO compound were performed by Sorai and Seki on the classical iron(II) SCO compounds $[Fe(phen)_2(NCX)_2]$ with X = S, Se [84,85]. Other SCO compounds of Fe(II) [86,87], Fe(III) [88] and Mn(III) [89,90] have been studied down to liquid-helium temperature. Such measurements are very tedious. For qualitative information on enthalpy change ΔH, entropy change ΔS, transition temperature $T_{1/2}$, and occurrence of hysteresis, DSC measurements down to liquid-nitrogen temperatures are sufficient in most cases [91-94].

Diffraction Methods

The rearrangement of the valence electrons among the antibonding e_g *orbitals* and the slightly bonding t_{2g} orbitals (in the case of octahedral symmetry) during thermal ST is always associated with more or less strong changes in the crystal lattice. Continuous spin transitions only ever show changes in metal–ligand bond angles and lengths (*displacive* transitions), but do not display changes in the space groups. Discontinuous spin transitions with hysteresis in the ST curve $\gamma_{HS}(T)$ curves typically occur alongside a change in the space group, i.e., a crystallographic phase change of first order with a major reorganization of the lattice *(reconstructive* transitions). Thus, it is obvious that the determination of crystal structure at various temperatures around the ST temperature $T_{1/2}$ is highly desirable in studies of ST phenomena in solids. Even temperature-dependent X-ray powder diffraction data from temperature-dependent studies can be extremely useful in the characterization of the type of ST (continuous or discontinuous) and for determining changes of the lattice parameters [95].

Extensive structural investigations have been carried out on many SCO compounds, mostly by X-ray diffraction [18,22,96-99]. As expected, one has found that in all cases the metal–ligand bond length is longer in the HS state than in the LS state due to the above-described charge reorganization. The change of metal–ligand bond lengths is particularly large for SCO compounds of iron(II), viz. ca. 10% ($\Delta r_{HL} = r_{HS} - r_{LS}$ ~ 200–220 pm). This generally causes a change of 3–4% in elementary cell volumes [22,99,100]. For comparison, bond-length changes in octahedral iron(III) SCO compounds, also with $\Delta S = 2$ transitions, are less dramatic with only Δr_{HL} = 10–13 pm, because the LS state contains one electron hole in the t_{2g} orbitals as can be seen from the electron configurations $t_{2g}^5e_g^0$ ($^2T_{2g}$, LS)↔$t_{2g}^3e_g^2$ ($^6A_{1g}$, HS). Δr_{HL} is even less pronounced in cobalt(II) SCO compounds ($\Delta r_{HL} \leq 10$ pm) with $\Delta S = 1$ transitions between the electron configurations $t_{2g}^6e_g^1$ (^2E_g, LS)↔$t_{2g}^5e_g^2$ ($^4T_{1g}$, HS), because only one electron is transferred from antibonding e_g^* to t_{2g} orbitals. The size of Δr_{HL} is important for the build-up of cooperative interactions.

Structural investigations of SCO compounds at variable temperatures are of outmost importance for the development of theoretical approaches [23,24,101,102] to understand the detailed steps in ST processes in solids. For this purpose it is extremely helpful that with single-crystal structure studies one can unravel the structures of existing networks of hydrogen bonding or specific orderings of π-stacking. Although they are not a prerequisite for thermal ST to take place, such features take part or at least aid in the cooperative interactions involved in the spin transition. This has been demonstrated experimentally, e.g., by examining the effect of ^{1}H/D or ^{14}N/^{15}N isotope exchange on the properties of the $\gamma_{HS}(T)$ conversion curves [103].

Other physical methods for spin crossover studies

The techniques described in the above sections are commonly employed in most SCO studies. Other techniques are used in special cases, e.g., where further valuable information about a SCO phenomenon can be obtained, which is otherwise not accessible, or where certain material properties (size, susceptibility) require special instrumentation or sample handling. A brief survey of such methods employed less frequently is given in the following.

X-ray absorption spectroscopy *(XAS*) can help in obtaining structural information in cases where the material under study is highly dispersed and no single crystal is available. It is usually carried out in two variants: X-ray absorption near edge structure (XANES) and extended X-ray absorption fine structure (EXAFS). XANES provides information essentially about molecular geometry and oxidation states. EXAFS yields information about very local electronic and molecular properties, such as coordination number, ligand denticity, and isomerism [104]. In addition, structures have been derived from EXAFS spectroscopy, e.g., for iron(II)-1,2,4-triazole polymeric chain compounds [105-109], which, however, is possible in some cases only by comparative studies of analogous Cu compounds.

Positron annihilation spectroscopy (PAS) was first applied to investigate the SCO compound $[Fe(phen)_2(NCS)_2]$ [110] and

later on to study the SCO behavior of single crystals of $[Fe(ptz)_6](BF_4)_2$ and zinc-diluted mixed crystals thereof [111]. Although one has observed changes of specific PAS parameters (Doppler broadening of the annihilation peak, lifetime of the ortho-positronium) in different spin states, the technique will probably not attain the status of a widely employed method in SCO research.

Magnetic resonance spectroscopy *(NMR, EPR).* Proton NMR measurements (Evans method) have been carried out to follow a temperature-dependent ST phenomenon in solution [82,112-117]. The paramagnetic peak changes position with varying temperature relative to a standard reference signal, which in favorable cases can be part of the SCO compound (e.g., the anion) [113-118], and this reflects the ST process. In studies of the solid state, however, the NMR spectrum of SCO compounds has been of little value. The various different protons typically present in the ligand molecules give rise to broad lines, which are difficult or impossible to analyze.

EPR spectroscopy has been more successfully employed in SCO research than has NMR. SCO compounds of iron(III), iron(II), and cobalt(II), which are the 3d transition metal elements most actively studied with EPR, typically reveal characteristic spectra that are sufficiently well resolved in both HS and LS states. There is no spin–orbit coupling in SCO compounds of iron(III) in the HS (^{6}S) state and, hence, the relaxation times are long. EPR signals appear at characteristic g values and provide information about characteristic parameters of the zero-field-splitting (ZFS), D for axial and E for rhombic distortions. In the LS state of iron(III) ($^2T_2$) spin–orbit coupling does occur, but at low temperatures the vibrations are slowed down and electron–phonon coupling becomes weak and therefore relaxation times are long, and hence, the EPR spectrum of the LS state of iron(III) exhibits a single line near to $g \sim 2$, typical for the presence of one unpaired electron, for a polycrystalline sample. In a single-crystal study, anisotropy effects usually play an important role and can be observed through the g-value components g_x, g_y, g_z. EPR spectroscopy is a highly valuable tool to decipher the structural information of a SCO system, which is otherwise barely or not at all accessible.

EPR spectroscopy of paramagnetic iron(II) is impossible at higher temperatures, because spin–orbit coupling within the $^5T_2$ state produces short spin-lattice relaxation times. EPR spectra can only be measured at 20 K or lower, at which the relaxation times are longer due to a slowing down of the vibrations. The resolution of EPR signals can be improved significantly on doping of the Fe(II) SCO complex with appropriate EPR probes, such as Mn(II) or Cu(II), as was reported first by McGarvey et al. [119] with $[Fe(phen)_2(NCS)_2]$ and $[Fe(2\text{-pic})_3]Cl_2{\cdot}EtOH$ (2-pic = 2-picolylamine) doped with 1% Mn(II) and later by Haasnoot et al. [120] with $[Fe(btr)_2(NCS)_2]{\cdot}H_2O$ (btr = 4,4'-bis-1,2,4-triazole) doped with ca. 10% Cu(II). Employing this technique, McGarvey et al. also measured excellent quality EPR spectra of single crystals of $[Fe(ptz)_6](BF_4)_2$ doped with 1% Mn(II) [121]. They determined the D and E values for both spin states and verified the existence of two structurally different LS phases, which are formed by fast or slow cooling. This method of doping SCO systems with Cu(II) and Mn(II) as EPR probes has proven to be very informative and easy to apply to spin crossover studies [122-126].

Muon spin relaxation *(μSR)* has only recently been applied to the study of SCO in iron(II) complexes [127-140], while this technique is widely used for the study of organic radicals [141,142]. Spin-polarized positive muons μ^+ implanted into a sample act as probes of local magnetization. Information about magnetic fluctuations is obtained in a time window covering the range of 10^{-9}–10^{-5} s, which complements the time windows of other physical techniques for studying dynamic phenomena [143-148]. The thermally induced SCO in $[Fe(ptz)_6](ClO_4)_2$ was followed by recording the temperature dependence of the initial asymmetry in zero field, a_0 [129,130]. This measurement reflected the fraction of muons interacting with unpaired spins and, thus, the fraction of HS molecules at any temperature [135,136]. The possibility of investigating spin fluctuation rates was established with the classical iron(II) complex $[Fe(phen)_2(NCS)_2]$, polymorph I [135,136]. In another case, fast dynamics have been revealed in the HS regime of the ST coordination polymer $[Fe(NH_2trz)_3](NO_3)_2$ (NH_2trz = 4-amino-1,2,4-triazole) [138,139].

Nuclear resonance scattering of synchrotron radiation *(NRS)* began with the pioneering work of Gerdau et al. in 1985 [71-73] who proposed an unconventional Mössbauer spectroscopy technique based on the possibility of using synchrotron radiation for nuclear resonance experiments in two ways, i.e., *nuclear forward scattering (NFS) and nuclear inelastic scattering (NIS)* of synchrotron radiation. Whereas conventional Mössbauer spectroscopy can be considered as "spectroscopy in the energy domain", NFS has been successfully employed as a time-differential technique. NFS allows one to study hyperfine interactions to obtain the Mössbauer parameters isomer shift, electric quadrupole and magnetic dipole splitting, as can be obtained by conventional Mössbauer spectroscopy, albeit with much smaller samples and shorter measuring times. Of even greater importance, Mössbauer isotopes that have not been accessible with conventional Mössbauer spectroscopy can be used. NIS allows the investigation of vibrational modes and the partial density of states (PDOS) locally, i.e., in the close neighborhood of the

Mössbauer probe nucleus. Compared, for instance, to Raman spectroscopy, NIS allows measurements with higher resolution without perturbation from surrounding vibrations.

Light-induced spin transition in iron(II) compounds

An unusual photophysical phenomenon was discovered with the SCO compound $[Fe(ptz)_6](BF_4)_2$ by the Mainz group [57] in 1984. $[Fe(ptz)_6](BF_4)_2$ undergoes thermal ST as clearly demonstrated by the temperature-dependent Mössbauer spectra shown in Figure 4 as well as the color change of a single crystal and the optical spectra depicted in Figure 3. The phase change occurs at a ST temperature $T_{1/2}$ of ca. 135 K with hysteresis of ca. 7 K width [58,59]. In a temperature-dependent study of the optical spectra of this compound it was observed for the first time that a LS to HS conversion in a solid SCO compound can also be induced by irradiating the crystals with (preferentially green) light, leading to a metastable long-lived HS state, which can have very long lifetimes on the order of days at temperatures below ca. 20 K [57,59]. This photophysical phenomenon has been termed *Light-Induced Excited Spin State Trapping* (LIESST).

Figure 6 recapitulates the discovery of the LIESST phenomenon [60]. A single crystal of $[Fe(ptz)_6](BF_4)_2$ (size ca. 3 × 3 cm^2) was mounted in a cryostat for optical spectroscopy at variable temperatures down to that of liquid helium. The crystal is white in the HS phase and displays only a weak absorption band at 12000 cm^{-1} of the spin-allowed but parity-forbidden $^5T_2 \rightarrow {}^5E$ transition. At 80 K, the crystal changed to the LS state by thermal SCO and the $^5T_2 \rightarrow {}^5E$ transition is no longer observable. In the LS state the crystal is red and absorbs (more strongly than in the HS phase due to stronger oscillator strength) at 18000 and 26000 cm^{-1} arising from the spin-allowed LS absorption bands $^1A_1 \rightarrow {}^1T_1$ and $^1A_1 \rightarrow {}^1T_2$. Irradiation of the crystal at ca. 10 K with green light (514 nm from Ar^+ laser) leads to convertion of the LS state to the metastable HS state. The optical spectrum of the white spot (ca. 1 mm in diameter) is virtually identical to that measured at 300 K.

Mössbauer spectroscopy is ideally suited to follow the light-induced spin state conversion, as demonstrated for $[Fe(ptz)_6]BF_4)_2$ in Figure 6. The advantage of using Mössbauer spectroscopy is that the sample under study may be polycrystalline material; it does not require a single crystal as with optical spectroscopy. The ^{57}Fe Mössbauer spectra shown in Figure 6 were recorded with a polycrystalline sample of $[Fe(ptz)_6](BF_4)_2$, which was first cooled to 15 K, at which the sample is in the LS state (upper left). Irradiating the sample with green light (ca. 500 nm from an argon ion laser) at 15 K converts the LS state (resonance signal shown in blue) quantitatively to the long-lived metastable HS state (middle left, quadrupole doublet shown in red). Thermal relaxation occurs at 50 K on a 15 minute timescale; the HS doublet disappears in favor of the reappearance of the thermodynamically stable LS state (lower left and upper right: the sample was heated for 15 minutes at 50 K and then cooled down quickly to the measuring temperature of 15 K in two runs). As indicated by

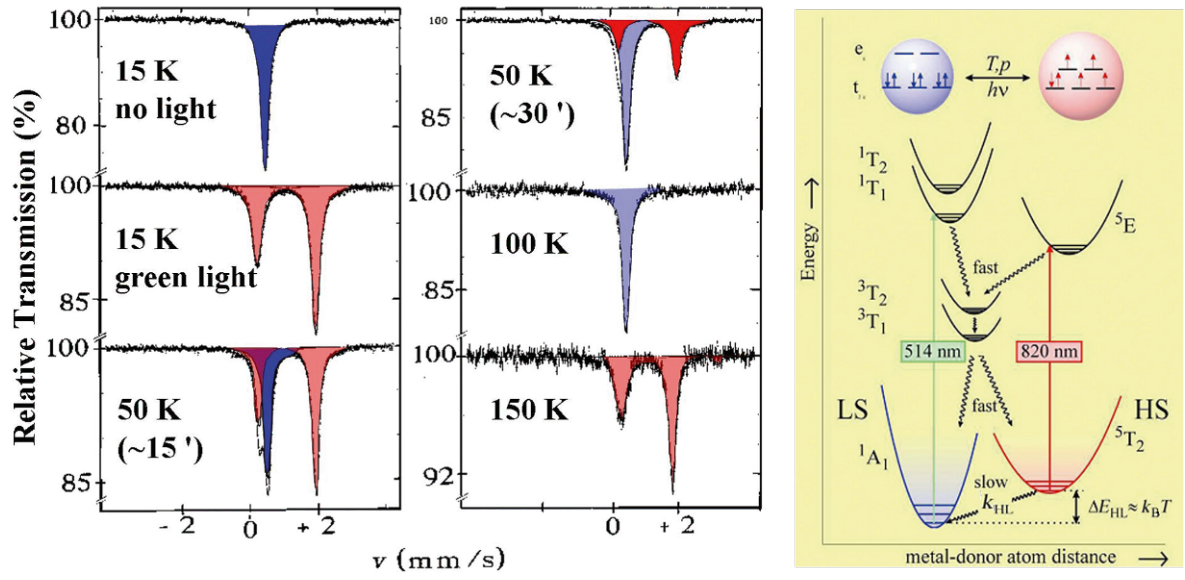

Figure 6: (left) Demonstration of light-induced spin state trapping (LIESST) in $[Fe(ptz)_6]BF_4)_2$ with ^{57}Fe Mössbauer spectroscopy (for details see text). (right) Jablonski diagram showing the photophysical processes of the LIESST and reverse-LIESST effects [23]; details are described in the text (Reproduced with permission from [36]. Copyright 2012 Wiley-VCH Verlag GmbH & Co. KGaA).

the spectrum shown in Figure 6 (middle right), thermal relaxation of the metastable HS (LIESST) state to the stable LS state is complete at 100 K. Further heating to 150 K converts the sample thermally at ca. 135 K from the LS to the HS state.

The LIESST phenomenon is well understood on the basis of ligand field theory [23,149]. The photophysical processes involved in the LIESST phenomenon are depicted in the Jablonski diagram in Figure 6 (right). Note that the two potential wells for the LS and HS ground states are displaced due to the fact that the metal-ion–donor-atom distance in the HS state is weaker and therefore longer compared to the stronger and therefore shorter bond distance in the LS state (Figure 1). Green light (514 nm from an Argon ion laser) excites the LS state ($^1A_1$) by the spin-allowed but parity-forbidden transition to the $^1T_1$ and $^1T_2$ ligand field states. These decay fast in two consecutive intersystem crossing processes, to the spin triplet states $^3T_{1,2}$ and finally to the $^5T_2$ state. Two factors are favorable for the occurrence of LIESST: (i) The spin triplet states $^3T_{1,2}$ are placed energetically lower than the $^1T_1$ and $^1T_2$ ligand field states; (ii) The *double intersystem crossing* decay path is favored by spin–orbit coupling and therefore faster than the direct decay path back to $^1A_1$. The decay of the $^5T_2$ state to the $^1A_1$ state is highly spin- and parity-forbidden; the long-lived metastable HS state is trapped until radiationless thermal relaxation (heat is transferred to lattice vibrations) sets in by non-adiabatic multiphonon processes [23,149]. Light-induced back conversion (reverse-LIESST) of the metastable LIESST state is effected by irradiating the sample with red light (820 nm from a Krypton laser), whereby the metastable $^5T_2$ state ("LIESST state") is excited to the ^5E_g state, which decays fast – again favored by spin–orbit coupling – by double intersystem crossing via $^3T_{1,2}$ states to the LS ($^1A_1$) state [149]. The LIESST effect has mostly been observed with SCO compounds of iron(II), but a few examples of SCO compounds of iron(III) exhibiting LIESST have recently been reported [150].

The HS→LS relaxation kinetics of decaying metastable LIESST states was examined experimentally by Hauser [151]. He interpreted the results on the basis of a nonadiabatic multiphonon relaxation model proposed earlier by Buhks, Jortner et al. [152]. As an essential feature, it was found that the lifetime t_{HL}^0, i.e., the low temperature tunneling rate $k_{HL}^0 = (t_{HL}^0)^{-1}$ of the LIESST state, is governed by the energy difference ΔE_{HL}^0 between the lowest vibronic energy levels of the HS and LS states involved; this has become known as *inverse energy gap law*. The energy gap ΔE_{HL}^0 increases with increasing ligand field strength. This means that, at comparable temperatures, the metastable LIESST state lives longer the weaker the ligand field strength is [149,151]. Typical lifetimes of photoexcited LIESST states in SCO complexes have been found to be on the order of minutes to hours, or even days, below ca. 20 K. In the case of LS complexes with considerably stronger ligand field strength, LIESST states decay much faster (within micro- to nanoseconds). However, an exception was reported for which the authors observed that in the case of the system $[Fe_{0.02}Mn_{0.98}(terpy)_2](ClO_4)_2$, where 2% of ^{57}Fe enriched $[^{57}Fe(terpy)_2]^{2+}$ complex molecules embedded in the host matrix of the corresponding Mn compound are in the LS state even in the room-temperature region, the inverse-energy-gap law was not obeyed. In this case mean lifetimes of the LIESST state in photo-excited $[^{57}Fe(terpy)_2]^{2+}$ complex molecules with LS behavior were expected to be roughly on the order of microseconds at 20 K or below [153]. Surprisingly, the measurements yielded lifetimes on the order of several days. The authors have named this phenomenon the *strong-field LIESST* effect.

Later it was found that photo-induced excited spin state trapping similar to LIESST is also possible with hard X-rays as the excitation source [154]. Moreover, *light-induced perturbation of thermal hysteresis* (LIPTH) was observed as a possible consequence of LIESST in a SCO compound of iron(II) [155].

Zarembowitch and Boillot et al. [156,157] have proposed and successfully verified another strategy, denoted as *ligand-driven light-induced spin change* (LD-LISC), to induce spin state switching in iron(II) complexes. The primary step of LD-LISC is a photochemical reaction on the ligand molecules, for instance a photo-induced *cis*/*trans*-isomerization on 4-styrylpyridine (stpy) as a ligand, e.g., in $[Fe(II)(stpy)_4(NCS)_2]$, which modulates the ligand field strength at the metal center and eventually leads to spin state switching. The occurrence of the LD-LISC effect was observed in several iron(II) and iron(III) complexes. On changing the composition of the sample, the working temperature and excitation wavelengths are modulated so that the effect may be observed at room temperature upon irradiation of the sample with visible light. Experiments so far were performed on compounds either in solution or embedded in polymeric matrices.

Effect of pressure on thermal spin crossover

Application of pressure shortens the metal–donor-atom distances of SCO complex molecules and increases the ligand field strength at the metal center. It is therefore expected that application of pressure favors the LS state. This was already experimentally confirmed by Ewald et al. in their studies of pressure effects on solutions of iron(III) complexes [158]. They found that the temperature dependent thermal equilibrium between $^2T_2 \leftrightarrow {}^6A_1$ was shifted under pressure in favor of the LS state $^2T_2$. It is indeed the large difference in the metal–donor-atom bond lengths, $\Delta r_{HL} = r_{HS} - r_{LS} \approx 0.1$ and 0.2 Å, for Fe(III)

and Fe(II) SCO molecules, respectively, that stabilizes the LS state under application pressure. Figure 7 schematizes the effect of pressure on the SCO behavior in the case of SCO complexes of iron(II).

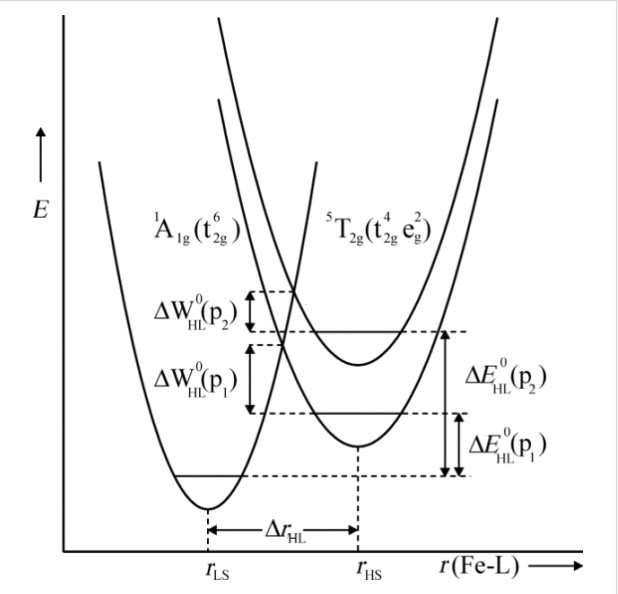

Figure 7: Schematic representation of the pressure influence ($p_2 > p_1$) on the LS and HS potential wells of an Fe(II) spin crossover compound (Reproduced with permission from [159]. Copyright 2005 Elsevier B. V.).

Application of pressure ($p_2 > p_1$) increases the relative vertical displacement of the potential wells and thus stabilizes the LS state; the additional minor decrease of the relative horizontal displacement of the potential wells under pressure is neglected in this picture. As a consequence, the zero-point energy difference ΔE^0_{HL} increases by the work term $p\Delta V^0_{HL}$, which in turn decreases the activation energy ΔW^0_{HL} and finally favors the LS state.

Extensive high-pressure experiments on SCO compounds by using diamond anvil cells have been reported by H. G. Drickamer [160] and later by other research groups [161-163]. One has realized that the SCO properties are very susceptible to the application of pressure and that it is more favorable and meaningful for studies of the mechanisms of thermal ST and LIESST state relaxation in solids, to perform such experiments with hydrostatic pressure cells working in relatively low pressure regions (up to ca. 1.5 GPa). Such experiments were first carried out by using hydrostatic gas pressure cells in conjunction with Mössbauer spectroscopy [97,164] and optical spectroscopy [165]. More recently, special hydrostatic pressure cells for magnetic and Mössbauer measurements have been developed, in which silicon oil is used as the pressure-transmitting medium [166,167].

The influence of pressure on SCO properties, for instance the critical ST temperature and shape and position of hysteresis loops (condition for bistability), has potential for practical applications, e.g., as a pressure sensor in remote locations. ST curves $\gamma_{HS}(T)$ or, more often used, $\chi_M T$ (χ_M = molar magnetic susceptibility) are recorded as a function of the applied pressure. From a series of such curves a calibration plot $\gamma_{HS}(p)_T$ or $(\chi_M T)(p)_T$ can be constructed, preferentially at room temperature. The ST curves at different pressures may be recorded with a convenient method, e.g., magnetic, optical or Mössbauer measurements. Although the primary focus here is on studies of pressure effects on SCO coordination compounds, we should like to point out that similar studies have been carried out by several research groups on oxidic phases of transition elements in natural materials, e.g., in the earth's mantle, as well as in synthetic materials, and it has been found that indeed SCO phenomena may occur in such compounds under the influence of pressure [168-172]. Of the many studies of pressure effects on SCO compounds carried out so far [23,160,168-175], only a few selected examples will now be discussed.

In Figure 8 are plotted the $\chi_M T$ versus T curves of $[Fe(phen)_2(NCS)_2]$ (Polymorph II) measured at different pressures [176]. Thermal ST at ambient pressure occurs near 175 K. With increasing pressure the transition curves are shifted to higher temperatures, due to stabilization of the LS state, and become slightly more gradual. At the highest pressure applied in this study, viz. 0.57 GPa, the paramagnetic HS state is nearly suppressed in the room-temperature region. On release of pressure, the ST behavior is practically the same as before under ambient pressure.

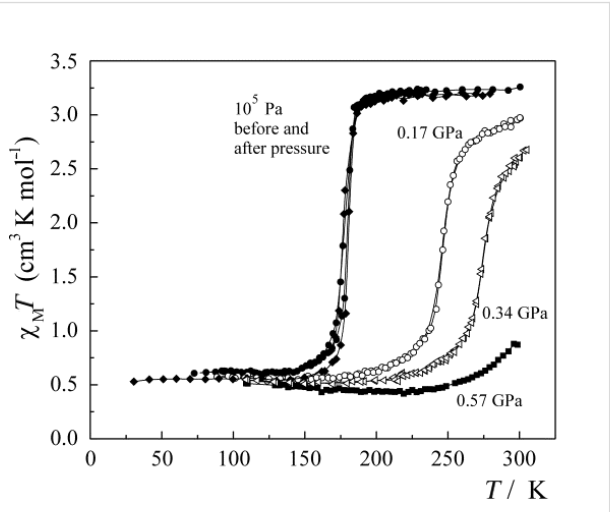

Figure 8: $\chi_M T$ versus T curves at different pressures for $[Fe(phen)_2(NCS)_2]$, polymorph II. (Reproduced with permission from [159]. Copyright 2005 Elsevier B. V.).

Very similar results were obtained from a pressure-effect study on the SCO compound $[Cr(II)I_2(depe)_2]$ (depe = diethylphosphino-ethane), which undergoes at ambient pressure a sharp $^3T_{1g}$ (S = 1)↔^5E_g (S = 2) thermal ST at 169 K [176]. In this case, the ST curves become considerably more gradual with increasing pressure than in the former case but are also shifted to higher temperatures until, at the highest pressure applied, the HS (S = 2) state has entirely been suppressed in the room-temperature region (Figure 9).

Figure 10 shows the results of a pressure-effect study on $[Fe(phy)_2](BF_4)_2$ (phy = 1, 10-phenanthroline-2-carbaldehyde-phenylhydrazone) [167]. This system exhibits hysteresis during the thermal ST. The occurrence of hysteresis is known to be a prerequisite for bistability, i.e., within the hysteresis loop the compound shows two different $\gamma_{HS}(T)$ values at the very same temperature, one each on temperature decrease and increase. It is clearly seen that the hysteresis loop is sensitive to the application of pressure.

In addition, polymeric SCO compounds of iron(II) have been comprehensively studied [177-180]. An example is given by the system $[Fe(hyptrz)_3](4\text{-chlorophenylsulfonate})_2{\cdot}H_2O$, in which hyptrz = 4-(3'-hydroxpropyl)-1,2,4-triazole, which displays a very steep and complete ST around 180 K with thermal hysteresis of 6 K in width as supported by magnetic susceptibility measurements at ambient pressure (Figure 11b) [178]. Application of pressure causes a shift of the transition curve to room temperature and even higher but retains the original steepness and shape. The sharp HS→LS transition is accompanied by an easily detectable color change from white (HS) to deep purple (LS). This material holds the potential for application as a pressure sensor [181].

Selected spin crossover compounds of iron(II)

As stated above, SCO research began around 1930 with the first observations of thermally induced spin state conversion in iron(III) compounds [1-6]. Exploration of this field was intensified ca. thirty years later with the first documentations of thermal SCO phenomena in iron(II) compounds [7-15]. With the advent of Mössbauer spectroscopy in the early sixties an excellent microscopic tool became available for the characterization, predominantly of iron compounds, regarding their valence electron structure and the resulting physical properties. In many cases this hyperfine interaction technique has enabled one to gain insight into details of SCO phenomena that are not accessible with other techniques.

The early observations of thermal SCO phenomena were all made on mononuclear compounds of iron(III) [1-6] and iron(II) [7-13]. One had soon realized that the SCO behavior, i.e., the shape of the ST function $\gamma_{HS}(T)$, as sketched in Figure 2, may change considerably from one compound to another and that this may be largely caused by cooperative interactions between the spin state changing complex molecules. From then on up to the present stage, cooperative interactions have been one of the most important aspects in SCO research. Questions concerning

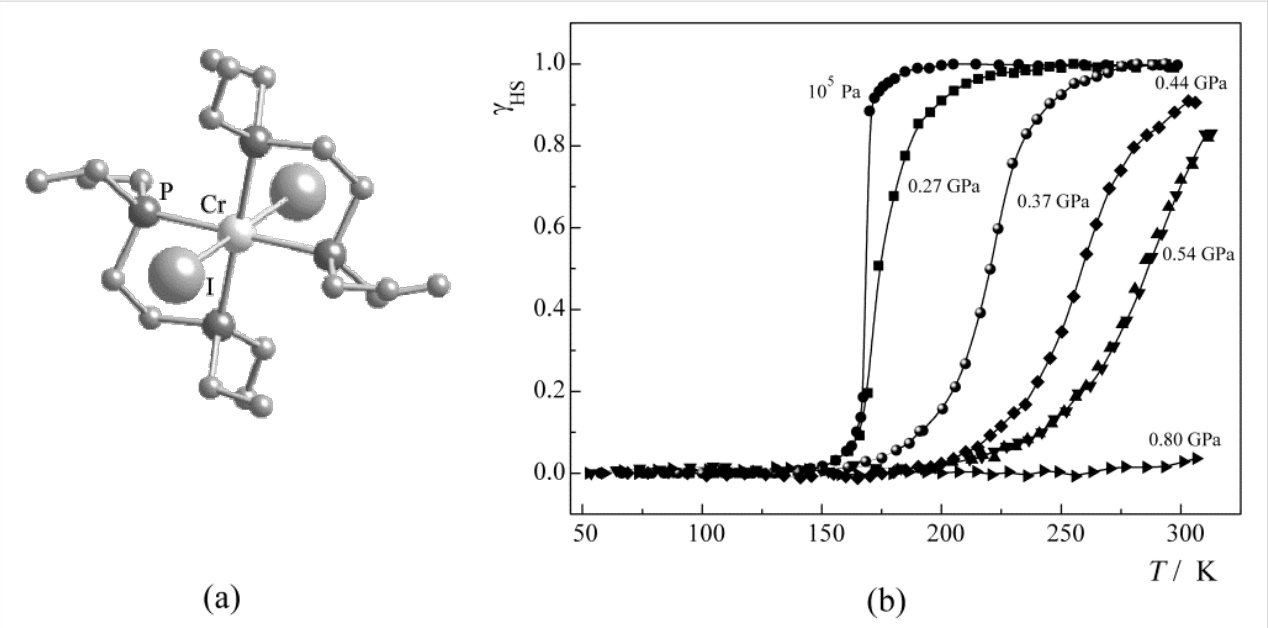

Figure 9: Molecular structure (a) and $\gamma_{HS}(T)$ curves at different pressures for $[CrI_2(depe)_2]$ (b) (Reproduced with permission from [159]. Copyright 2005 Elsevier B. V.).

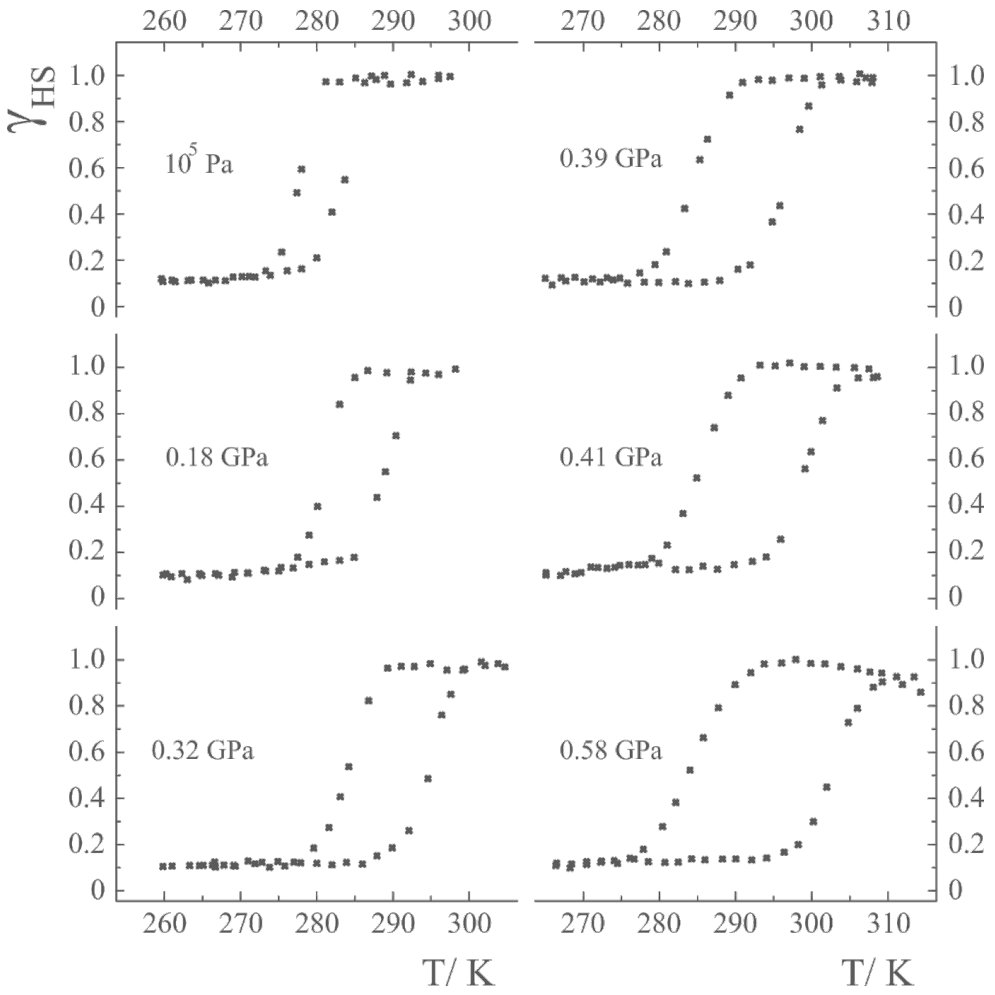

Figure 10: HS molar fraction γ_{HS} versus T at different pressures for $[Fe(phy)_2](BF_4)_2$. The hysteresis loop broadens with increasing pressure. (Reproduced with permission from [167]. Copyright 1999 Elsevier B. V.).

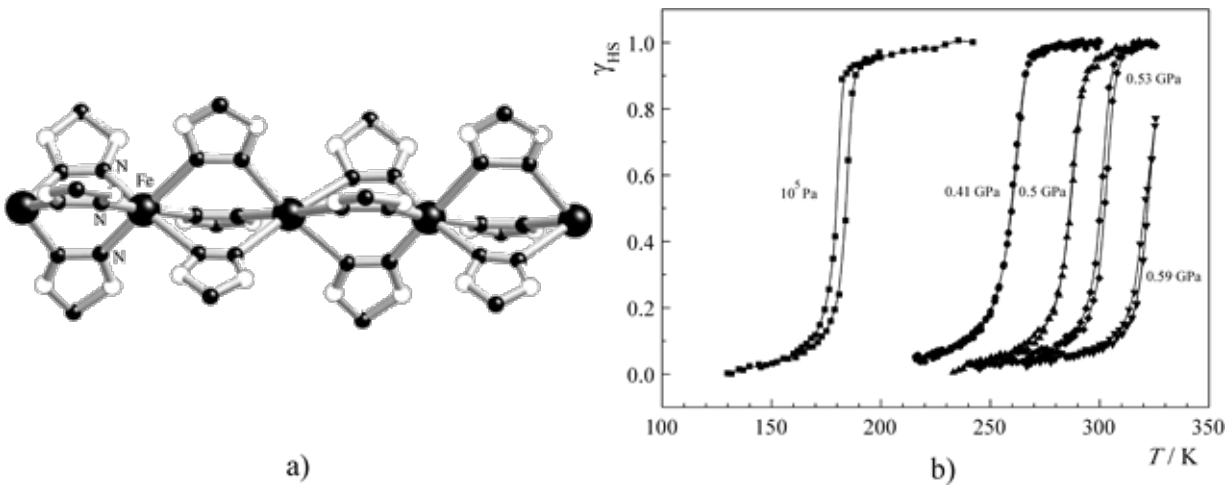

Figure 11: Proposed structure of the polymeric $[Fe(4R\text{-}1,2,4\text{-triazole})_3]^{2+}$ spin crossover cation (a) and plot of γ_{HS} versus T at different pressures for $[Fe(hyptrz)_3](4\text{-chlorophenylsulfonate})_2 \cdot H_2O$ (b). (Reproduced with permission from [159]. Copyright 2005 Elsevier B. V.).

the creation, nature, strength and mechanism of cooperative interactions have been the main objectives of nearly all experimental and theoretical SCO projects. Work has been performed on a large variety of SCO materials, from simple mononuclear and oligonuclear compounds with zero-dimensional lattices, to polymeric systems with 1D, 2D and 3D lattices. In the case of mononuclear SCO compounds various influences on the SCO behavior have been studied in detail. Examples will be described in the next section.

Influences on SCO behavior in mononuclear SCO compounds of iron(II)

Mononuclear SCO compounds with zero-dimensional lattices, such as the classical SCO compound $[Fe(II)(phen)_2(NCS)_2]$, the picolylamine complexes $[Fe(II)(2\text{-pic})_3]X_2{\cdot}Sol$ (X = Cl, Br, I; Sol = EtOH, MeOH, H_2O, $2H_2O$) and the alkyltetrazole complexes of iron(II), e.g., $[Fe(II)(ptz)_6](BF_4)_2$, have been extensively studied regarding chemical and physical influences on the SCO behavior ([23] and references therein).

Replacement of ligand: An example for the effect of replacement of a ligand in the complex molecule is shown in Figure 5. The compound $[Fe(phen)_3]X_2$ is in the LS state, because the ligand field strength is too strong to meet the critical SCO condition. Replacement of one bifunctional phen ligand by two monofunctional NCS^- ligands weakens the ligand field strength sufficiently to induce a thermal spin transition.

Intraligand substitution: A similar effect may be observed when the ligand field strength is modulated by substitution inside the ligand molecule. This has been illustrated with the group of $[Fe(Y\text{-phen})_3]X_2$ complexes [182]. Exchange of H for CH_3 in either the 2- or 9-position of the three phen ligands weakens the ligand field strength due to steric hindrance (whereby the metal–donor-atom distance is elongated) and the LS behavior of $[Fe(phen)_3]X_2$ turns to SCO behavior of the tris(2-CH_3-phen) complex. If both the 2- and 9-positions of the three phen ligands are substituted by CH_3 the steric hindrance is even stronger and weakens the ligand field strength further, yielding HS behavior of the tris[2,9-$(CH_3)_2$] complex down to very low temperatures. It was found that a combination of steric hindrance due to bulkiness and an electronic influence of the substituent on the basicity of the coordinating N-atom is responsible for the influence on the SCO behavior. The paramagnetic property of the complex (given by the molar fraction of HS molecules, γ_{HS}, at a given temperature), increases in the order Y = H < CH_3O < CH_3 < Cl. One has also found that a change of the substituents at positions not adjacent to the coordinating N-atom in the phen ligand does not influence the spin state in comparison to the unsubstituted $[Fe(phen)_3]X_2$ complex.

Influence of metal dilution: The occurrence of thermal SCO in the picolylamine complexes $[Fe(II)(2\text{-pic})_3]X_2{\cdot}Sol$ (X = Cl^-, Br^-, I^-; Sol = EtOH, MeOH, H_2O, $2H_2O$) was first reported by Renovitch and Baker [183]. Determination of the crystal structure of $[Fe(II)(2\text{-pic})_3]Cl_2{\cdot}EtOH$ [96,97] above and below the ST temperature pointed to the existence of hydrogen bonding, which was believed to cause, through cooperative interactions, the marked differences in the ST curves $\gamma_{HS}(T)$ of the halides [183] and, as found later with Mössbauer spectroscopy [184], also in the various solvates. A detailed study of the ST behavior in the mixed-crystal series $[Fe(II)_xZn_{1-x}(2\text{-pic})_3]Cl_2{\cdot}EtOH$ using Mössbauer spectroscopy showed that the ST curve was strongly influenced by substitution of Fe by Zn (Figure 12) [185]. Zinc was chosen in this "metal dilution" study because it has the same crystal structure as the analogous iron(II) complex. Most important is the result that, with decreasing iron concentration, the ST curves become more gradual and are shifted to lower temperatures, until at very high dilution the ST curve resembles that of a SCO phenomenon occurring in liquid solution, where practically no cooperative interactions exist. Clearly, the existence of cooperative interactions in solid SCO compounds has been proven in this study. The effect of metal dilution was later studied in other SCO complexes [23] and supported the earlier results. These observations were most important for the development of the so-called *Mainz Model* [23,101,102], a theoretical approach based on a pure mechanical "communication" mode between the spin state changing complex molecules featuring elasticity and lattice expansion.

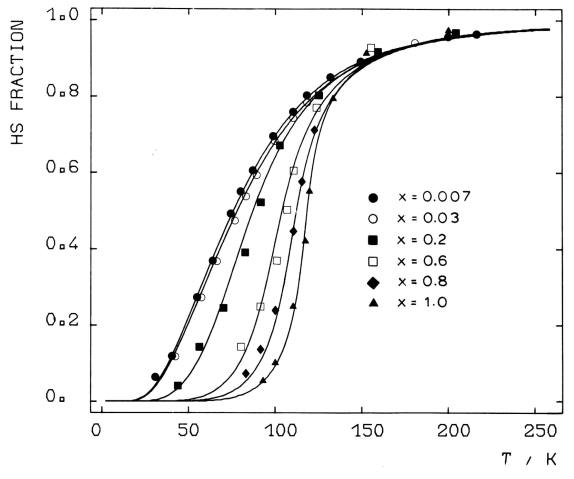

Figure 12: Temperature dependence of the HS fraction $\gamma_{HS}(T)$, determined from Mössbauer spectra of $[Fe(II)_xZn_{1-x}(2\text{-pic})_3]Cl_2{\cdot}EtOH$ for different iron concentrations x. The ST curves become more gradual with increasing x due to weakening of the strength of the cooperative interactions. (Reproduced with permission from [27]. Copyright 2003 Wiley-VCH Verlag GmbH & Co. KGaA).

Influence of noncoordinated anions: In the case of the SCO compound $[Fe(II)(phen)_2(NCS)_2]$ the NCS^- anions are coordinated directly to the Fe^{2+} center, i.e., the NCS^- anion is in this case a direct codeterminant of the ligand field strength at the metal center. In ionic lattices with cationic SCO complex molecules and uncoordinated counterions in lattice positions remote from the metal center, the anion can nevertheless exercise a strong influence on the SCO behavior through cooperative interactions. Examples are the halides of the series $[Fe(II)(2\text{-pic})_3]X_2{\cdot}EtOH$ for which the ST characteristics was found to depend strongly on the nature of the anion X = Cl^-, Br^-, I^- (Figure 13) [186,187].

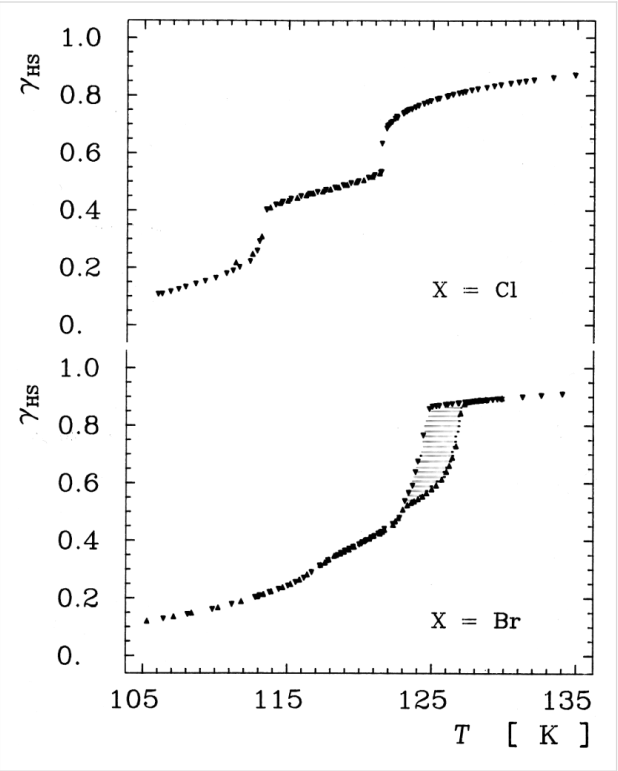

Figure 13: Influence of the noncoordinated anion on the spin transition curve $\gamma_{HS}(T)$ near the transition temperature $T_{1/2}$ in $[Fe(II)(2\text{-pic})_3]X_2{\cdot}EtOH$ (X = Cl, Br). (Reproduced with permission from [27]. Copyright 2003 Wiley-VCH Verlag GmbH & Co. KGaA).

Influence of noncoordinated solvents molecules: The various solvates of the SCO complexes $[Fe(II)(2\text{-pic})_3]Cl_2{\cdot}Solv$ with Solv = EtOH, MeOH, H_2O, $2H_2O$ were studied with Mössbauer spectroscopy to explore the influence of the noncoordinated solvent molecules on the SCO behavior (Figure 14) [184]. The ethanolate shows a rather steep transition near 115 K; the methanolate shows a more gradual ST near 150 K; the monohydrate exhibits a very broad hysteresis loop with transition temperatures $T_{1/2}{}^{\downarrow}$ near 200 K and $T_{1/2}{}^{\uparrow}$ near 290 K; and the dehydrated sample exhibits no ST at all but remains in the LS state. This is clear evidence for the existence of hydrogen bonding as the communication pathways for the cooperative interactions propagating through the lattice.

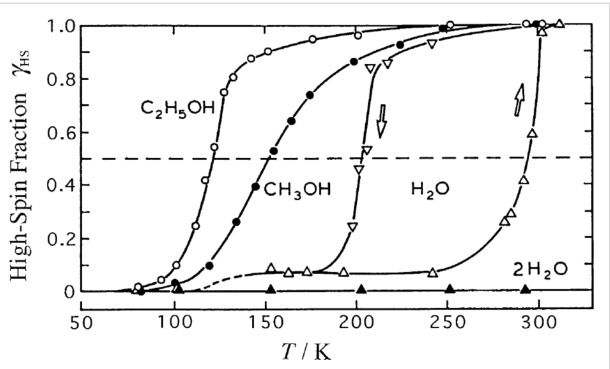

Figure 14: Spin transition curves $\gamma_{HS}(T)$ for different solvates of the SCO complexes. $[Fe(II)(2\text{-pic})_3]Cl_2{\cdot}Solv$ (Solv = EtOH, MeOH, H_2O, $2H_2O$) [184]. Differences in the hydrogen bonding network are responsible for the different spin crossover behaviours in these solvates. (Reproduced with permission from [23]. Copyright 1994 Wiley-VCH Verlag GmbH & Co. KGaA).

Stepwise spin transition: In the early stage of SCO research the observed ST curves have always been of the more or less gradual, continuous type (Figure 2). In the case of the SCO system $[Fe(II)(2\text{-pic})_3]Cl_2{\cdot}EtOH$ it was observed for the first time that thermal ST may also proceed in steps [187]. Earlier studies of this compound with magnetic and Mössbauer measurements always showed a continuous trend of the ST curve $\gamma_{HS}(T)$ curve in the region of 110–125 K (ca. 50% spin state conversion). A detailed Mössbauer effect study of this region by Köppen et al. revealed that ST in this system occurs in two steps, as is clearly seen in Figure 13 and Figure 15. It was found later by low-temperature crystal structure determination that the stepwise ST in this SCO system is due to an order–disorder phase transition with formation of an intermediate phase [188]. Such stepwise spin transitions have later also been reported for a number of other SCO systems (e.g., [189,190]).

Isotope effects: A Mössbauer spectroscopy study was performed to investigate the influence of deuteration, in various positions of the solvent molecules, on the SCO behavior of $[Fe(II)(2\text{-pic})_3]Cl_2{\cdot}Solv$ (Solv = EtOH, MeOH). Temperature-dependent Mössbauer spectra were recorded of the solvates with Sol = C_2D_5OH and C_2H_5OD/ND_2 and compared with that of the nondeuterated ethanolate $[Fe(II)(2\text{-pic})_3]Cl_2{\cdot}C_2H_5OH$. The ST curves for the three solvates are displayed in Figure 15 [97].

The ST curve of the nondeuterated ethanolate shows the "two-step" spin transition first observed in this system [103,191]. The solvate with C_2D_5OH is only slightly affected by the deutera-

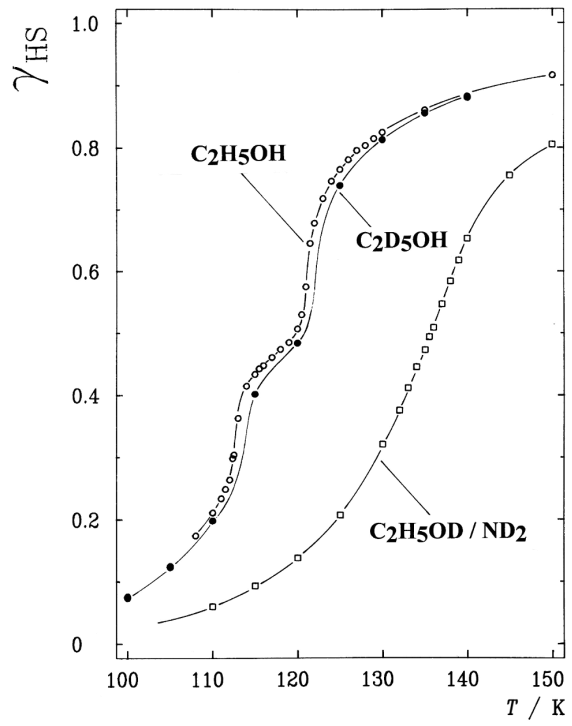

Figure 15: ST curves $\gamma_{HS}(T)$ of the deuterated solvates of [Fe(II)(2-pic)$_3$]Cl$_2$·Solv with Solv = C_2D_5OH and C_2H_5OD/ND_2 compared with that of the nondeuterated solvate [Fe(II)(2-pic)$_3$]Cl$_2$·C_2H_5OH derived from Mössbauer spectra [103,191]. Deuteration affects the ST behavior in those cases where isotope exchange occurs in positions that are actively involved in the hydrogen-bonding network. (Reproduced with permission from [23]. Copyright 1994 Wiley-VCH Verlag GmbH & Co. KGaA).

tion. The reason is that the H/D isotope exchange takes place in a position that is not a constituent of the hydrogen bonding as can be seen from the crystal structure [95,96]. In the case of the system denoted as C_2H_5OD/ND_2, however, deuteration occurs at the OH group, which is a building element of the hydrogen bonding. Simultaneously deuteration occurs also at the acidic NH_2 group, which is also directly involved in the hydrogen-bonding chain [95,96]. As a consequence, deuteration affects this system much more strongly than in the former case. This is reflected in Figure 15 by a drastic shift of the ST curve to higher temperature and the disappearance of the step. These results clearly underline the importance of hydrogen bonding for cooperative interactions between spin state changing complex molecules. It also evidences that intra- and intermolecular vibrations play an important role in the communication of spin state changes through the lattice. Similar observations have been made for the deuterated methanolate (Solv = CH_3OH) [103] and also for [Fe(II)(2-pic)$_3$]Cl$_2$·C_2H_5OH with H/D exchange in the CD_2NH_2 substituent and at the 3,4,5-positions of the pyridine ring [191]. An isotope effect study was also performed with $^{14}N/^{15}N$ exchange at the amino group [191]. Despited the fact that the coordinating N atom is an important constituent of the hydrogen-bonding chain, the ST curve maintained the step in this case and was shifted only slighty to higher temperature, very similar to the effect observed on the C_2D_5OH system. A minor influence on the SCO curve is expected in the case of $^{14}N/^{15}N$ exchange because of the relatively small change of reduced mass as compared to that of H/D exchange.

***Influence of a magnetic field**:* Since different spin states with different magnetic properties are involved in ST phenomena, one should expect that the SCO behavior responds to an applied magnetic field and indicates a change of the ST curve $\gamma_{HS}(T)$. An estimate using a simple formula [192] shows that the effect on the ST temperature $T_{1/2}$ is expected to be very small. An experiment with a sample of [Fe(phen)$_2$(NCS)$_2$] placed in a magnetic field of 5 Tesla showed indeed a small effect; $T_{1/2}$ was shifted by −0.11 K [192]. Later, similar experiments were carried out with samples placed in high magnetic fields [89,90,193]. The results were in agreement with those of the earlier study [192], though correspondingly larger because of the six-times higher magnetic field used in the latter case.

***Influence of sample preparation**:* It was found that the way of treating an SCO compound may influence strongly the SCO behavior. For instance, ball milling or crushing crystals in a mortar often increases the residual HS fraction in the low-temperature region and tends to make the ST curve more gradual [194,195]. The explanation is still rather speculative. It has been proposed that these effects are mainly caused by crystal defects introduced by mechanical treatment (ball milling, crushing in mortar) or by rapid precipitation. The particle size has also been reported to play a role [196]. In any case, the sample preparation for physical characterization of a SCO compound is very crucial and should be done with great care.

Dinuclear systems

The possibility of combining two properties such as magnetic coupling and SCO in the same molecule was the original motivation for undertaking the study of such Fe(II) dinuclear molecules [197], as well as the possibility of investigating new cooperative behavior through covalent bonding of active sites compared to mononuclear complexes dealt with in the previous section.

Dinuclear SCO molecules can adopt three different spin-pair states: A fully diamagnetic state, [LS–LS], with both iron(II) atoms in the LS state; a paramagnetic mixed spin-pair state [LS–HS]; and an antiferromagnetically coupled [HS–HS] state. Stabilization of the [LS–HS] state depends on a subtle balance between intra- and intermolecular interactions in the solid state

[198]. Consequently, the thermal dependence of the physical and structural properties can present one-step or two-step spin transitions. The former case involves the [LS–LS]↔[HS–HS] transformation, while in the latter case the intermediate stage responsible for the plateau, at 50% conversion between the two steps, is observed. This may be due to the formation of a 50% mixture of [HS–HS] and [LS–LS] or to the existence of 100% [LS–HS] species. In some cases, switching between the three spin-pair states has been observed upon the action of temperature, pressure or light, which implies competition between magnetic coupling and SCO phenomena (Figure 16).

{[Fe(bpym)$(NCS)_2]_2$bpym}(bpym = 2,2'-bipyrimidine) [199] was the first example of a series of compounds designed to this end. Its magnetic behavior is that of two iron(II) atoms in the HS state displaying intramolecular antiferromagnetic (AF) coupling ($J = -4.1$ cm^{-1}). In the search for new dinuclear SCO complexes the ligand field strength was fine-tuned by varying the peripheral ligands. Thus, the formal substitution of the peripheral bpym ligands with organic ligands such as bromazepam (bzp) [199], 2,2'-bithiazoline (bt) [200,201], dipyridylamine (dpa) [202] and 6-methyl-2,2-bipyridine (Mebipy) [203] and phen [204] afforded the first evidence of spin crossover. The ligand field strength could also be tuned by changing the coordinated pseudohalide, namely NCS^- and $NCSe^-$. The crystal structures of the centrosymmetric {[Fe(bpym)$(NCS)_2]_2$bpym}, {[Fe(bt)$(NCS)_2]_2$bpym} and {[Fe(Mebipy)$(NCS)_2]_2$bpym} derivatives are known [197].

bzp and dpa derivatives undergo smooth spin conversions, being rather incomplete in the case of the bzp derivative, while the Mebipy derivative is HS. The most interesting observations have been made with the compounds {[Fe(L)$(NCX)_2]_2$bpym}, where L = bpym or bt and X = S or Se, which have been extensively investigated. The magnetic behavior of these four compounds is depicted in Figure 17. The derivative with bpym and NCS^- as peripheral ligands (denoted [bpym, NCS^-]) seems to fulfill the necessary conditions to observe SCO, however, as mentioned above, this derivative remains in the [HS–HS] state and displays intramolecular AF coupling but not SCO. The substitution of the NCS^- with an $NCSe^-$ group increases the ligand field strength around the iron atoms and the resulting dinuclear species [bpym, $NCSe^-$] undergo a sharp ST around 120 K, which involves 50% of the iron(II) atoms. The [bt, NCS^-] compound, formally derived from the replacement of bpym with the stronger ligand bt, displays two spin transitions separated by a plateau at 50% conversion and centered at 175 K. The first and second steps take place at ca. $T_{1/2}{}^1 = 163$ K and $T_{1/2}{}^2 = 197$ K, respectively. Finally, when the NCS^- group is replaced with the $NCSe^-$ group in the latter compound, the ligand field increases and the resulting [bt, $NCSe^-$] derivative shows a similar two-step ST at higher temperatures, $T_{1/2}{}^1 = 223$ K and $T_{1/2}{}^2 = 265$ K.

Because the SCO ion is larger in the HS state than in the LS state, an alternative way to induce SCO is to pressurize the sample at constant or variable temperature. Applying external pressure is also an efficient way to tune the ligand field strength in HS complexes that are not far from the crossing point of the HS and LS states. Figure 18 displays the thermal variation of the magnetic susceptibility, recorded at constant hydrostatic pressure at different increasing/decreasing pressures, for the dinuclear systems [bpym, NCS^-] and [bpym, $NCSe^-$]. Between ambient pressure (10^3 hPa) and ca. 0.4 GPa the compound [bpym, NCS^-] does not undergo SCO [205]. However, for pressures higher than 0.6 GPa this compound shows the onset of a very incomplete SCO, which coexists with the magnetic exchange. At 0.9 GPa the compound undergoes a ST involving 50% of the iron(II) atoms with $T_{1/2} = 150$ K. A further increase of pressure up to 1.1 GPa does not alter the spin transition; it is similar to that observed for [bpym, $NCSe^-$] at ambient pressure [206]. In addition, the latter dinuclear species experiences a

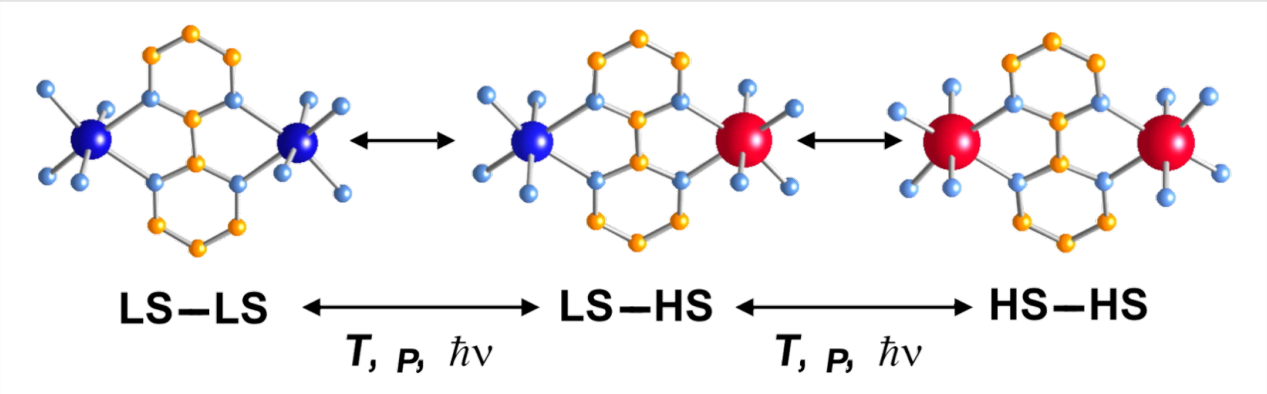

Figure 16: Sketch of the two-step spin transition; [LS–LS] pair is diamagnetic, [LS–HS] is paramagnetic and the [HS–HS] pair is antiferromagnetically coupled.

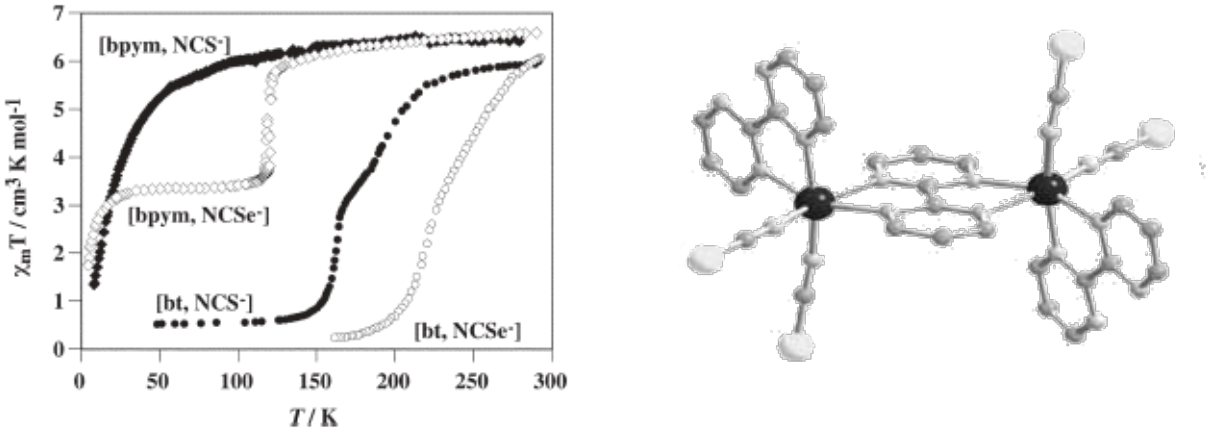

Figure 17: (left) Temperature dependence of $\chi_M T$ for {[Fe(L)(NCX)$_2$]$_2$bpym}(L = bpym or bt and X = S or Se). (right) Crystal structure of {[Fe(bpym)(NCS)$_2$]$_2$bpym}.

two-step ST for pressures higher than 0.45 GPa (Figure 18 right). This behavior resembles that observed for [bt, NCS^-] and [bt, $NCSe^-$] at ambient pressure.

The existence of [HS–HS], [LS–HS] and [LS–LS] spin-pair states and the nature of plateaus in ST curves was the subject of conjecture for a long time. However, their unambiguous identification was achieved by using Mössbauer spectroscopy. Standard zero-field Mössbauer spectroscopy reflects the total amount of LS and HS species but cannot distinguish between the spin pairs involved. As an example, Figure 19a shows the zero-field Mössbauer spectrum of [bpym, $NCSe^-$] measured at 4.2 K. From the area fractions of the quadrupole doublet of HS-Fe(II) (outer two lines) and that of the LS-Fe(II) (inner two lines) one arrives at an estimate of 50% each in the HS and LS state. No distinction can be made between the presence of a mixture of [HS–HS] and [LS–LS] spin-pair states on the one hand, and 100% of [LS–HS] on the other hand. However, it was realized that at sufficiently low temperature, Mössbauer spectroscopy could identify them by placing the sample in an intense magnetic field [207,208]. The Mössbauer spectrum of [bpym, $NCSe^-$] measured at 4.2 K in a magnetic field of 5 T (50 kOe) is shown in Figure 19b. The analysis of the spectrum [207] yields the presence of three components. One corre-

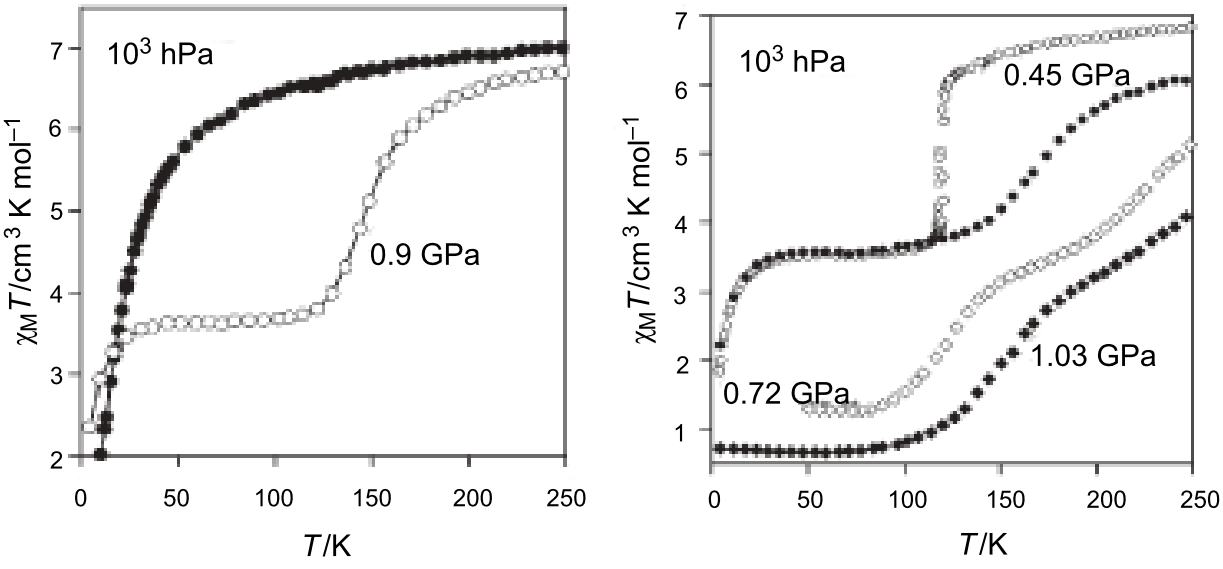

Figure 18: Temperature dependence of $\chi_M T$ for [bpym, NCS^-] (left) and [bpym, $NCSe^-$] (right) at different pressures (Reproduced with permission from [206]. Copyright 2001 American Chemical Society).

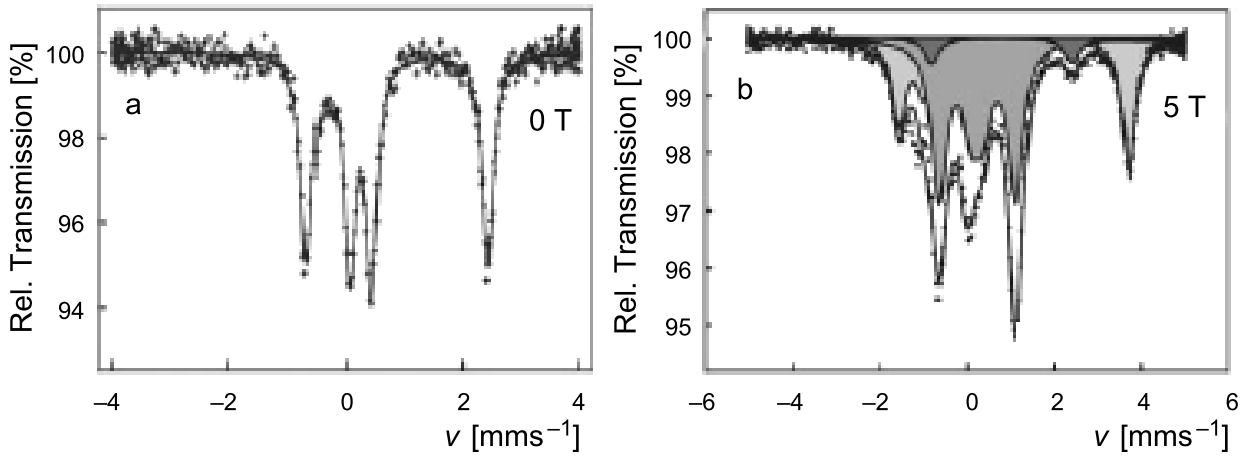

Figure 19: ^{57}Fe Mössbauer spectra of [bpym, $NCSe^-$] measured at 4.2 K at zero field (a) and at 5 T (b) (see text) [207,208] .

sponds to LS-Fe(II) (52%, grey component) assignable to [LS–LS] and [LS–HS] pairs. The second component [dark grey] is minor, ca. 4%, and arises from [HS–HS] pairs. The third component (light grey), 44%, corresponds to the magnetically split Mössbauer sextet spectrum of an uncoupled iron(II) atom in the HS state. Clearly, the two major components represent the uncoupled paramagnetic [LS–HS] spin pair state (88%) while the remainder corresponds to 8% and 4% of [LS–LS] and [HS–HS] spin pairs, respectively.

Observation of the LIESST effect in dinuclear compounds has been limited for a long time to the [bpym, $NCSe^-$] [205,209,210], [bt, NCS^-] [201,209] and [bt, $NCSe^-$] [211] derivatives. These experiments showed, for the first time, the interplay between SCO and antiferromagnetic coupling in the same molecule. The combination of magnetic-field Mössbauer with the LIESST effect has given deeper insight into the dynamics of conversion between the different spin-pair states and at the same time has given support to the hypothesis of the occurrence of three spin-pair states and their transformation by means of temperature, pressure or light [212,213].

Once the existence of the [LS–LS], [LS–HS] and [HS–HS] spin pairs had been proven, the next important step in this research concerned the possibility of photo-switching between them selectively. Initial evidence arose from photomagnetic experiments performed on the [bt, NCS^-] compound by using different wavelengths [214]. Raman studies have confirmed that the nature of the plateau in the two-step transition of [bt, NCS^-] is not a 1:1 mixture of [LS–LS] and [HS–HS] species but corresponds to the mixed-spin species [214]. Furthermore, the [LS–LS] state can be selectively switched at low temperatures to the [HS–HS] state and to the [LS–HS] state by using red light (647.1 nm) or infra-red light (1342 nm) [212,213].

The series of new dinuclear iron(II) SCO compounds reported recently by the groups of Real, Gütlich, Murray, Brooker, Kaizaki, Matouzenko, and Garcia, among others, have added new interesting results to this topic [215-235].

The triple helicate dinuclear iron(II) complex, $[Fe_2(L)_3](ClO_4)_4{\cdot}2H_2O$ [217], presents an unusual two-step spin conversion on cooling, proceeding very smoothly at $T_{1/2}^{(1)}$ ~ 240 K and $T_{1/2}^{(2)}$ ~ 120 K (Figure 20). This thermochromic material does not switch its spin state on cooling further below 20 K, as demonstrated by zero-field Mössbauer spectroscopy despite the steep decrease of $\chi_M T$, which is due to both weak

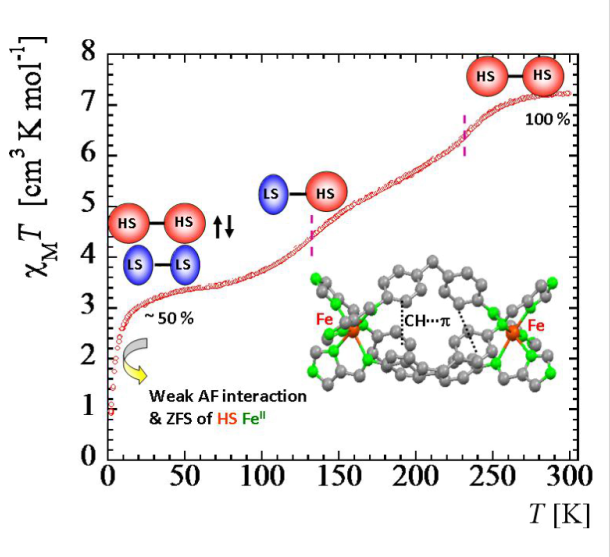

Figure 20: Temperature dependence of $\chi_M T$ for $[Fe_2(L)_3](ClO_4)_4{\cdot}2H_2O$ showing a complete two-step spin conversion from 100% [HS–HS] pairs to 50/50% [HS–HS] and [LS–LS] pairs as discussed in the text. The triple helicate dinuclear unit with intramolecular CH···π interactions is shown in insert [230].

AF coupling and zero-field splitting of HS Fe(II) ions [230]. As revealed by applied-field ^{57}Fe Mössbauer spectroscopy carried out at 4.2 K, the thermal spin conversion for one half of the Fe(II) active sites is complete. The existence of a plateau tracked in the spin conversion curve at ~200 K and identified through the variation of hyperfine parameters of an uncoupled iron(II) site indicates the presence of an [LS–HS] intermediate spin state [230]. Interestingly, spin pairs can also be revealed without the need for an external magnetic field [221]. Very recently, the first crystal structures in the HS and LS states of a dinuclear iron(II) complex with three *N*1,*N*2-1,2,4-triazole bridges, which is considered as a structural model of 1,2,4-triazole iron(II) 1D chains, was reported. The abrupt change in the magnetic properties of $[Fe_2(Hsaltrz)_5(NCS)_4]\cdot 4MeOH$ (Hsaltrz = *N*-salicylidene-4-amino-1,2,4-triazole), at $T_{1/2} \sim 150(1)$ K, from [HS–HS] to [LS–LS] pairs results from the cooperative manifestation of the ST process thanks to intra- and intermolecular interactions mediated by 1,2,4-triazole and supramolecular interactions, respectively (Figure 21) [235]. A similar cooperative situation was found within the pentanuclear assembly $[Fe_2(totrz)_5(NCS)_4]_2[Fe(totrz)_2(NCS)_2(H_2O)_2]\cdot nH_2O$ with totrz = 4-(*p*-tolyl)-1,2,4-triazole, which also includes similar binuclear iron(II) entities that are linked to a non-SCO mononuclear unit by hydrogen bonding [236]. As a result, a very sharp ST is observed. However, the cooperativity is not sufficient to induce a hysteretic effect.

Such investigations have pointed out two different SCO processes occurring in dinuclear iron(II) units, namely stepwise [LS–LS]↔[LS–HS]↔[HS–HS] and direct [LS–LS]↔[HS–HS] transformations. Moreover, it has been evidenced that the plateau observed between two separate spin transitions can be associated with the existence of the mixed spin state [LS–HS], or with a 1:1 mixture of the [HS–HS] and [LS–LS] states [197,213]. In addition, the mixed spin state [LS–HS] has been structurally characterized for dinuclear entities of different chemical coordination sphere. Considerable progress has been made in understanding both SCO processes, although the factors that determine the preference of each SCO mechanism have not yet been elucidated.

Systems with higher nuclearity and cages

Ranging between dinuclear units and coordination polymers, a few systems of higher nuclearity have been reported. The series of iron(II) linear trinuclear complexes of formula $[Fe_3(4\text{-}R\text{-}1,2,4\text{-triazole})_{12-y}(H_2O)_y](anion)_6\cdot nH_2O$ have revealed gradual spin conversions, as expected with the switch of a single iron atom isolated from its two counterparts [98,237-246]. Indeed, their crystal structures reveal a central FeN_6 SCO site, which is bridged by three 1,2,4-triazole ligands to peripheral HS iron sites, which are coordinated by water molecules, as shown, for instance, for $[Fe_3(hyetrz)_6(H_2O)_6](CF_3SO_3)_6$ (hyetrz = 4-(2'-hydroxyethyl)-1,2,4-triazole) (Figure 22) [98]. Interestingly, this complex presents a 50% LS/HS spin population at room temperature ($T_{1/2}$ = 290 K), with pale mauve, thermochromic, hexagonal crystals. This material was suggested for the purpose of imaging spin domains at the nanoscale using a coating layer by AFM [239].

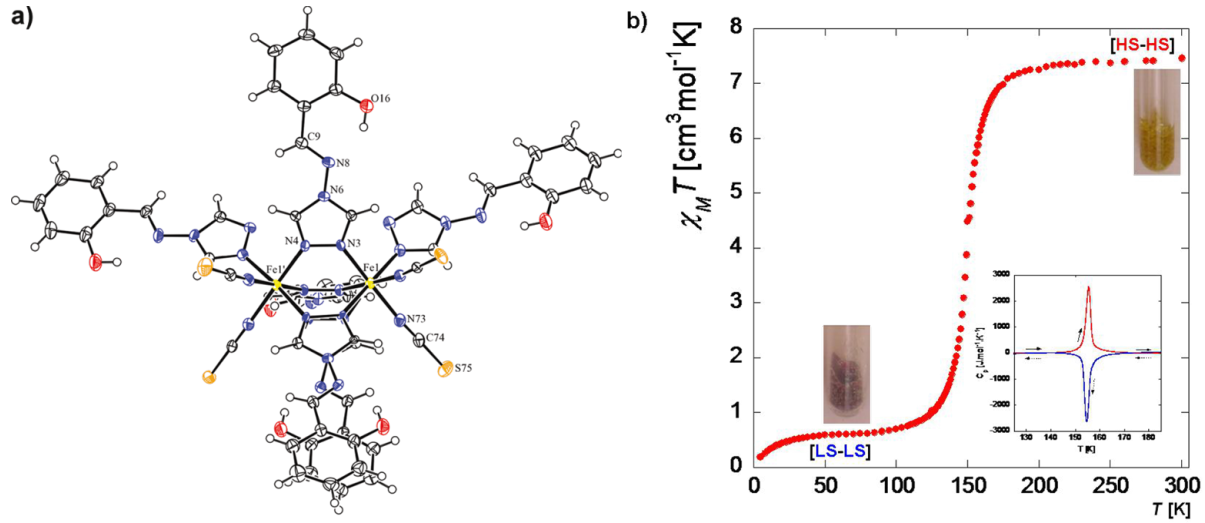

Figure 21: (a) View of the dinuclear unit in the crystal structure of $[Fe_2(Hsaltrz)_5(NCS)_4]\cdot 4MeOH$. (b) Temperature dependence of $\chi_M T$ versus T revealing a steep spin transition from [HS–HS] to [LS–LS] pairs. The tubes show the color change from yellow at room temperature to burgundy at liquid nitrogen temperature. The DSC response, shown in the inset, confirms that a first-order phase transition takes place on cooling and warming [235].

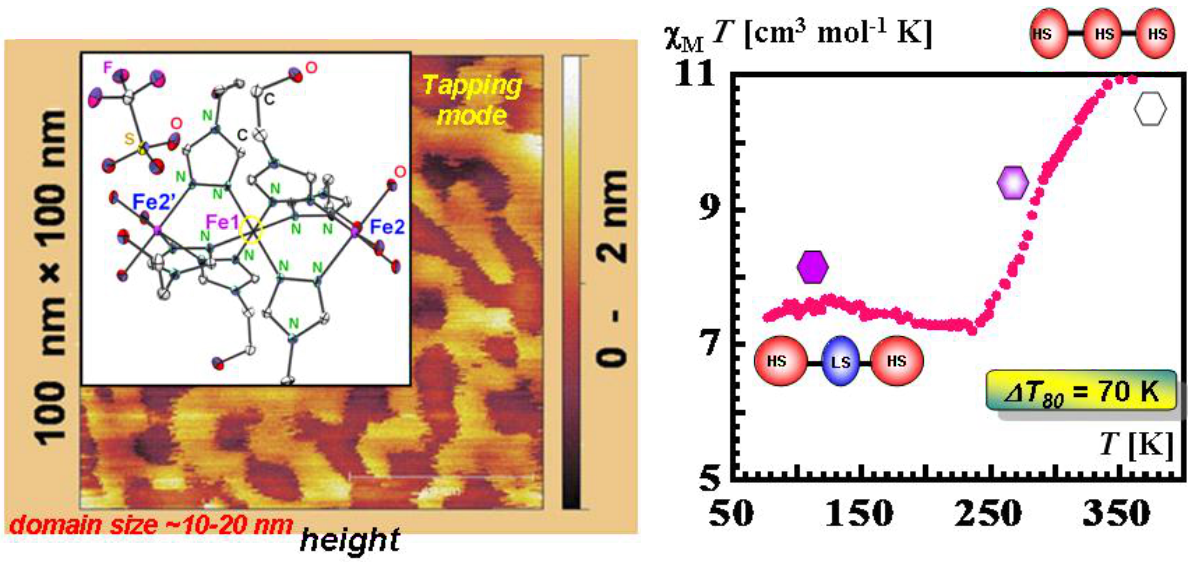

Figure 22: (left) AFM pattern recorded in tapping mode at room temperature on hexagonal single crystals of $[Fe_3(hyetrz)_6(H_2O)_6](CF_3SO_3)_6$. A domain size of ~10–20 nm was identified [239]. The insert shows the crystal structure of the trinuclear unit as well as the noncoordinated anion [98]. (right) $\chi_M T$ versus T showing a gradual spin conversion from [HS–LS–HS] trimers below ~250 K to [HS–HS–HS] trimers above ~350 K. The color of the crystals is shown as well as ΔT_{80}, which represents the temperature interval for which 80% of ions have switched [98].

More recently, the first triangular SCO trinuclear complex, $[Fe_3L_2(NCS)_4(H_2O)]$ with L = 1,3-bis[(2-pyridylmethyl)imino]propan-2-ol, was reported [247]. The magnetic behavior is similar to the 1,2,4-triazoles trinuclear complexes discussed above with two external HS iron(II) ions and one central SCO center, but with a different donor set (N_4O_2) [247]. While an iron(II) trinuclear complex with three SCO sites is still awaited, several tetranuclear iron(II) complexes have been communicated.

Compartmental polypyridyl ligands are considered as key components to induce the formation of grid-type complexes by self assembly [248]. The first iron(II) tetranuclear complexes, $[Fe_4L_4]A_4$ (A = BF_4^-, ClO_4^-, PF_6^-) with pyrimidine-derived compartmental ligand strands were described by Lehn et al. [249-251]. $[Fe_4L_4](BF_4)_4$ exhibits a continuous and incomplete SCO between three magnetic levels [249]. Interestingly, intramolecular cooperative effects, which were expected from the tetranuclear arrangement of spin carriers, are not evident from temperature-dependent magnetic measurements, which revealed a very smooth spin conversion (Figure 23, right). However, Mössbauer measurements under permanent green-light irradiation revealed hidden cooperative effects thanks to the detection of a light-induced thermal hysteresis (LITH) loop (Figure 23, left).

Supramolecular [2 × 2] grid-type complexes constructed from the same ligand system and arranged either in a 1D columnar superstructure or in a wall-like 2D layer, also exhibit a gradual spin conversion [252], which was also found for another grid based on a pyrazolate binucleating bpy ligand [248].

Cyanide bridged ferrous tetranuclear squares exhibiting smooth spin conversion have attracted recent interest. The spin state switching of $[Fe_4(\mu\text{-}CN)_4(L)_4(tpa)_2](PF_6)_4$ (tpa = tris(2-pyridylmethyl)amine) occurs in two steps at ~160 K and ~380 K for the L = bpy derivative [253,254] and around room temperature for the L = phen complex [255]. Above room temperature, spin state conversion is reached for the tetranuclear $[Fe_4(\mu\text{-}CN)_4(bpy)_4(bpym)_4](PF_6)_4{\cdot}6CH_3OH{\cdot}4H_2O$ [256]. Other tetranuclear square iron(II) complexes constructed on tpa and dca [257] or with oxo bridged ligands were also reported [258,259]. DFT studies of these systems, which all display gradual spin state conversion, have just started [260,261].

SCO complexes with higher nuclearity have not yet been reported except for a heptanuclear mixed valence iron(III) complex [262] and a discrete porous iron(II) nanoball made on Cu(I) building blocks presenting a gradual spin state conversion, which can also be switched by light irradiation at liquid He temperatures (Figure 24) [263,264].

Polymeric 1D, 2D and 3D systems

The number of polymeric iron(II) SCO compounds has rapidly increased in the context of the booming interest on coordination polymers (CPs) [265] and metal organic frameworks

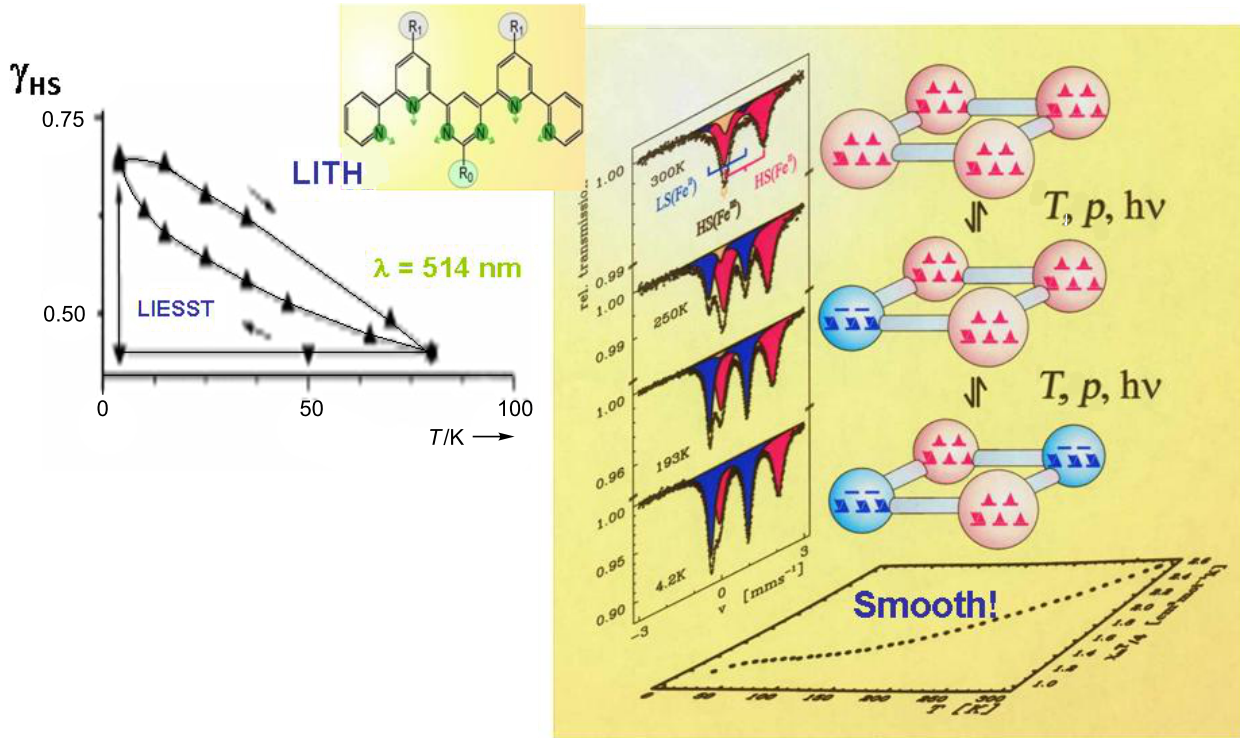

Figure 23: (right) Stepwise SCO in an Fe_4 [2 × 2] grid, which reveals a smooth magnetic profile under ambient and applied pressure. ^{57}Fe Mössbauer spectra are also shown. (left) This material is also switchable by light (LIESST). A LITH loop is observed during continuous irradiation with green light. The ligand system used for the self assembly process is also depicted [249].

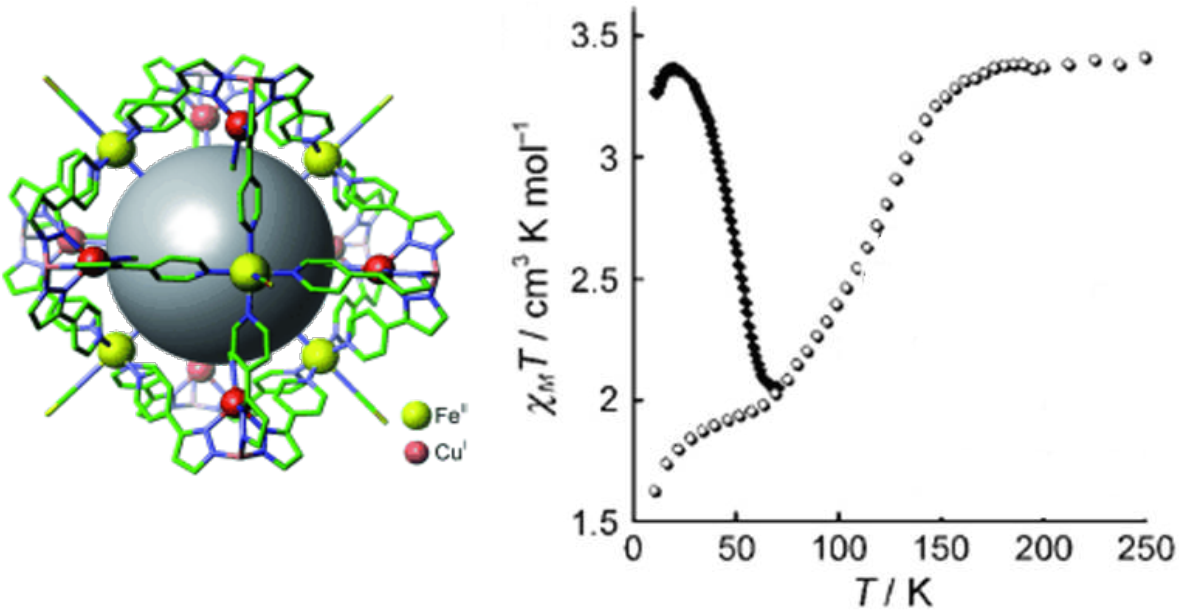

Figure 24: (left) View of the discrete nanoball made of Fe(II) SCO units as well as Cu(I) building blocks. (right) $\chi_M T$ versus T for the nanoball cluster showing both a thermally induced spin state conversion with $T_{1/2}$ ~125 K as well a thermal HS to LS relaxation after LIESST [263]. (Reproduced with permission from [263]. Copyright 2009 Wiley-VCH Verlag GmbH & Co. KGaA).

(MOFs) [266]. Most of these materials incorporate multidentate *N*-donor heterocyclic bridging ligands, such as 1,2,4- or 1,2,3-triazole, 1-R or 2-R-tetrazole, and polypyridine-like derivatives, as well as tetra- and dicyanometallate, polynitrile anions, and tetradentate Schiff bases [13,267-271]. These coordination complexes usually exhibit thermally induced spin conversions of a gradual nature. In certain cases, abrupt spin transitions with hysteresis effects, whose width is strongly dependent on the type of molecular bridge between iron(II) sites as well as on crystal packing considerations, are observed. A few examples of iron(III) and cobalt(II) SCO CPs have also been described [272-275]. In this section, we review prototype materials as well as highlight recent examples of CPs and MOFs constructed from ligands based on organic molecules.

1D chain compounds: 4-R-1,2,4-triazole based iron(II) chain compounds have been widely studied, due to their tremendous potential for practical applications based on their thermochromic effect (memory devices, displays, sensors) [276-280], and are currently the topic of intense miniaturization efforts [281-287]. [Fe(4-R-1,2,4-triazole)$_3$]A$_2$·Solv are composed of linear chains in which the iron(II) ions are connected by three *N*1,*N*2-1,2,4-triazole ligands (Figure 11a). Noncoordinated species, such as counteranions (A) and solvent molecules (very often water) are confined between the chains. The coordination linker in these polymeric compounds is rigid enough to allow an efficient transmission of elastic cooperative effects leading to a hysteresis loop of width ranging from ~2–20 K [268]. Inspired by the systematic parallel shift of ST curves under hydrostatic pressure that is discussed above [177,178,180], several synthetic approaches have been successfully developed to reach the room temperature region by making use of internal pressure provided by anion (Figure 25), solvent and ligand substitution in the crystal lattice [159,268,288]. In a few cases, the hysteresis width could be increased up to ~35–50 K, when noncoordinated anions were connected to 1D chains by hydrogen bonds [139,180,289-293]. Consequently, abrupt spin transitions with broad thermal hysteresis loops along with a color change from pink/purple (LS) to white (HS) have been observed (Figure 25, right) [276-280]. Remarkably, a few examples of this family of materials can also be switched by light [181,294-297].

[Fe(1,2-bis(tetrazol-1-yl)propane)$_3$](ClO$_4$)$_2$ represents the first SCO chain whose crystal structure has been determined by X-ray diffraction, both in the HS and LS states (Figure 26). Despite its polymeric nature, the spin conversion is very gradual. The virtual absence of cooperativity, also noted in the isostructural tetrafluoroborate derivative, has been attributed to the flexibility of the bridging network, as well as the absence of intermolecular contacts between 1D chains that cannot transmit efficiently the structural changes associated with the spin change in the crystal lattice. This compound exhibits, in addition, the LIESST effect, which was observed for this substance class for the first time [298]. A similar gradual SCO behavior was revealed for other 1D iron(II) chains with triply [299,300] and doubly bridging bis-tetrazole ligands [301]. The situation differs for [Fe(μ-btzmp)$_2$(btzmp)$_2$](ClO$_4$)$_2$ (btzmp = 1,2-

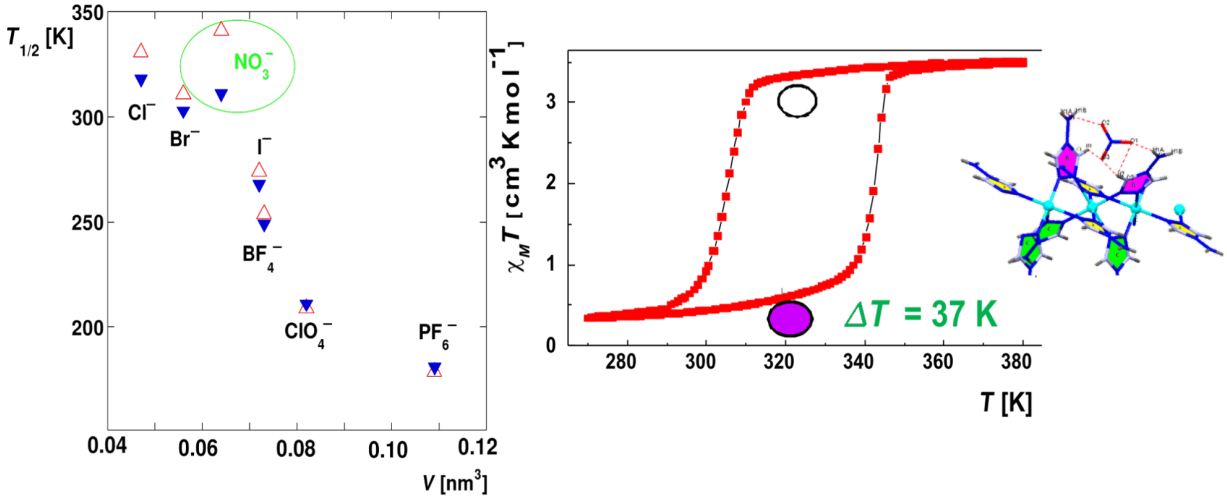

Figure 25: (left) Linear dependency between $T_{1/2}$ in the heating (Δ) and cooling (▽) modes versus the anion volume for the series [Fe(NH$_2$trz)$_3$]A$_2$. The circle highlights the case of the nitrate derivative that displays a larger hysteresis width. (right) $\chi_M T$ versus T of [Fe(NH$_2$trz)$_3$](NO$_3$)$_2$ showing a hysteretic ST slightly above the room-temperature region. The nitrate anion is hydrogen-bonded to NH$_2$trz (in pink) coordinated to two metal centers, thus acting as a supramolecular link in addition to the bridge made by triple *N*1,*N*2-1,2,4-triazoles [293].

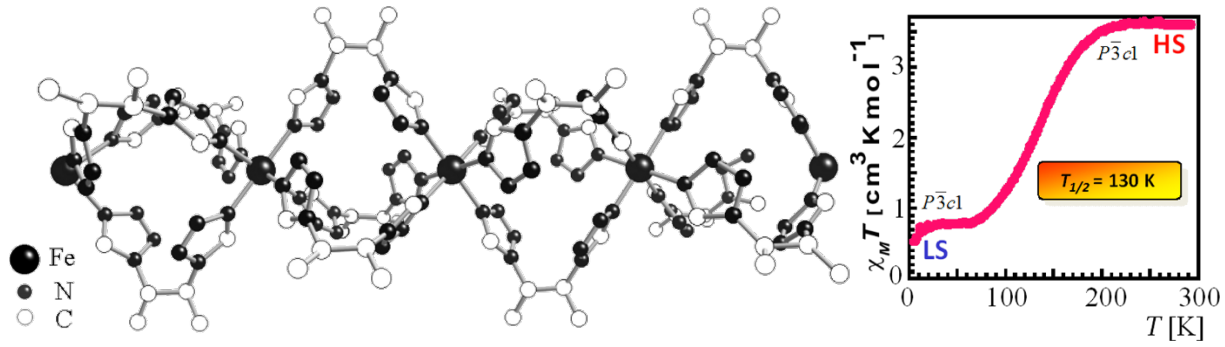

Figure 26: (left) View of the linear chain structure of $[Fe(1,2\text{-bis(tetrazol-1-yl)propane})_3]^{2+}$ along the *a* axis. (right) $\chi_M T$ versus T showing a gradual spin conversion for the perchlorate derivative, with $T_{1/2}$ = 130 K [298].

bis(tetrazol-1-yl)-2-methylpropane), which displays a steep and hysteretic spin transition, partly attributed to an anion order/disorder phenomenon [302]. Other 1D iron(II) chains made of two bridges that cushion elastic interactions [303] were also reported [304-307].

Noticeably, numerous examples of 1D chains made of flexible single bridge spacers systematically reveal a gradual spin conversion as noted for 1,2-bis(4-pyridyl)etha(e)ne [308], 4,4'-bpy [309,310], substituted triazine/pyrimidine [307,311-313], pyrazine [314], dca [315] and tcpd anions [316]. Some other very interesting 1D chains were recently prepared by Weber et al. using tetradentate Schiff bases allowing them to set up a N_4O_2 core and to observe a variety of magnetic behavior including gradual, hysteretic, complete, incomplete and even double-step spin conversions [317-324]. We anticipate that further 1D SCO chains will be reported with both rigid linkers as well as with predesigned modules suitable for supramolecular contacts to enhance communication between spin centers throughout the crystal lattice.

2D and 3D networks: A crystal-engineering strategy towards obtaining polymeric systems of higher dimensionality makes use of multidentate organic ligands (that are suitable for SCO) connected by different spacers, which boosts the possibilities to increase the dimensionality. The first ones can potentially coordinate several metals whereas the second ones can increase the degrees of liberty/flexibility of the coordinating groups in order to promote coordination in several directions [27].

$[Fe(btr)_2(NCX)_2]\cdot H_2O$ (X = S, Se) represent the first 2D ST compounds [325,326]. The sulfur derivative displays on cooling a square-shape hysteresis loop of width 21 K, associated with an extremely abrupt and completely thermally induced ST, free of any structural phase transition (Figure 27). Its crystal structure consists of iron(II) ions linked by btr in two orthogonal directions establishing a grid. The isothiocyanate anions, coordinated in the *trans* position, prevent the formation of a 3D lattice. The layers are connected by means of van der Waals forces and weak hydrogen bond bridges involving the water molecules, which are also H-bonded to peripheral nitrogen atoms of the triazole. In fact, the water molecule is crucial to maintain spin state switching [325]. The Se derivative displays, as expected with the increase of ligand field strength, a ST at higher temperature but with a narrower hysteresis (~6 K) [326]. A similar 2D ST grid was found for $[Fe(baztrz)(pyz)(NCS)_2]\cdot 4H_2O$ (baztrz = *trans*-4,4′-azo-1,2,4-triazole) with the replacement of one btr by pyrazine [327]. Using only one bridging bis-tetrazole afforded another 2D SCO grid but with a less cooperative behavior [328,329].

Several complexes of formula $[FeL_2(NCS)_2]\cdot$Solv show a similar layered, stacked structure with bis-monodentate pyridine-like ligands instead of btr [267-270]. This includes bispyridylethylene (bpe, Solv = MeOH) [331], *trans*-4,4'-azopyridine (azpy, Solv = MeOH, EtOH and PrOH) [332,333], and 1,4-bis(4-pyridylbutadiyne) (bpb, Solv = 0.5 MeOH) [334]. The larger size of bpe and azpy allow interpenetration of two equivalent sets of layers, whereas for the bpb a framework made up of three different arrays of mutually perpendicular, interlocked 2D networks was obtained (Figure 28). A gradual and incomplete SCO behavior is observed due to the flexible link between the iron(II) ions within a single layer, despite the interlocked character of the material.

The first ST grid with a 1-R-tetrazole was discovered for $[Fe\{N(entz)_3\}_2](BF_4)_2$ with a tripodal ligand, N(entz)$_3$ = tris[2-(tetrazol-1-yl)ethyl]amine by Rudolf et al. [335,336].

The coordination occurs through the *N*4 nitrogen atoms of the tetrazole rings that are brought by N(entz) (Figure 29) [335,336]. An extremely abrupt ST with thermal hysteresis was observed ($T_{1/2}^{\uparrow}$ = 176 K and $T_{1/2}^{\downarrow}$ = 167 K). Recently, a honeycomb-like pattern with cages occupied by disordered anions

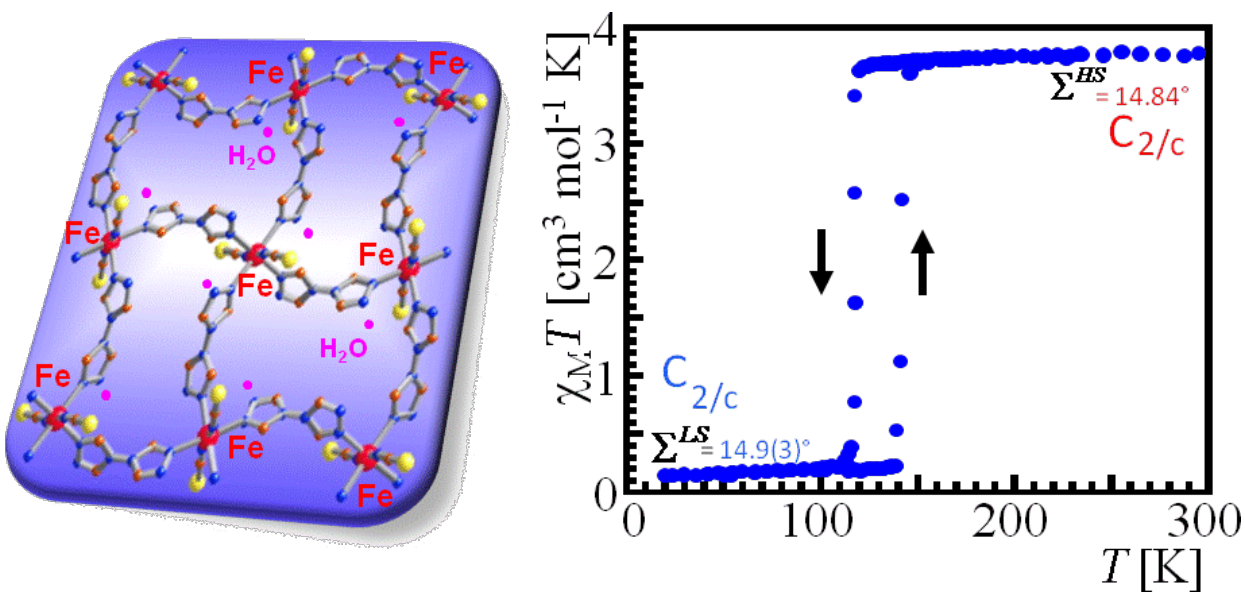

Figure 27: (left) View of the 2D layered structure of $[Fe(btr)_2(NCS)_2]\cdot H_2O$ (at 293 K). The water molecules (in violet) are located between the layers and H-bonded to triazole ligands [325]. (right) $\chi_M T$ versus T showing a square-shaped hysteresis loop on cooling. The structural distortion parameter Σ remains the same in the HS and LS states revealing that the local symmetry is not modified by the spin state change [330].

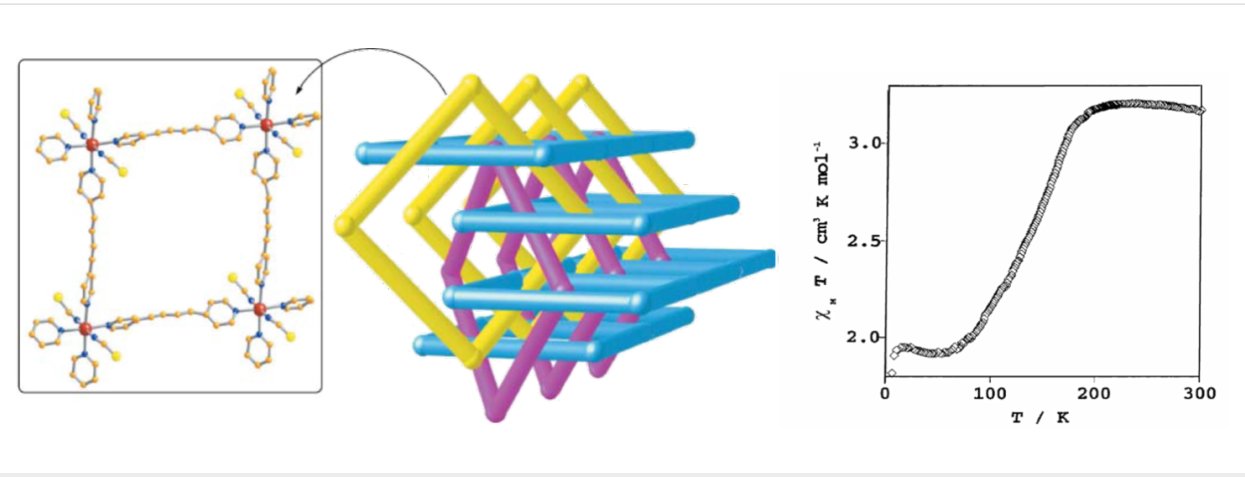

Figure 28: (left) Three interpenetrated square networks for $[Fe(bpb)_2(NCS)_2]\cdot MeOH$. (right) $\chi_M T$ versus T plot shows a gradual and incomplete spin conversion [334].

was discovered for $[Fe\{C(mtz)_3\}_2]A_2$, (A = ClO_4^-, BF_4^-) built from another spider-like ligand, $C(mtz)_3$ = tris(tetrazol-1-ylmethyl)methane. These 2D materials both display a sharp ST at $T_{1/2}$ = 193 K (BF_4^-) and $T_{1/2}$ = 176 K (ClO_4^-) [337]. $[Fe(trptrz)_2](BF_4)_2\cdot 5H_2O$ with trptrz = tris-3-[1,2,4]triazol-4-ylpropyl phloroglucinol, obtained thanks to a Mitsonubu coupling, is another example of 2D SCO CP based on a tripodal ligand. It reveals a gradual spin conversion due to the flexible propyl group attached to the triazole ligand, which cushions elastic interactions [338]. $[Fe(bbtr)_3]A_2$, where A = ClO_4^- [339,340] or BF_4^- [340,341] (bbtr = 1,4-di(1,2,3-triazol-1-yl)butane), are other 2D CPs with a (3,6) network topology presenting a hexagonal sheet structure. While the perchlorate derivative displays an abrupt hysteretic ST around 100 K, the tetrafluoroborate stays in the HS state. Both materials are currently the topic of extensive optical investigations [342-345].

Very recently, highly robust 2D neutral Fe(II) MOFs have been reported for $[FeL_2]$ with L = 3-(2-pyridyl)-5-(3-pyridyl)-1,2,4-triazole or 3-(3-methyl-2-pyridyl)-5-(3-pyridyl)-1,2,4-triazole. These materials display two-step SCO at remarkably high temperatures (the highest step is above 500 K) [346], which would make them good candidates for CVD deposition of thin films.

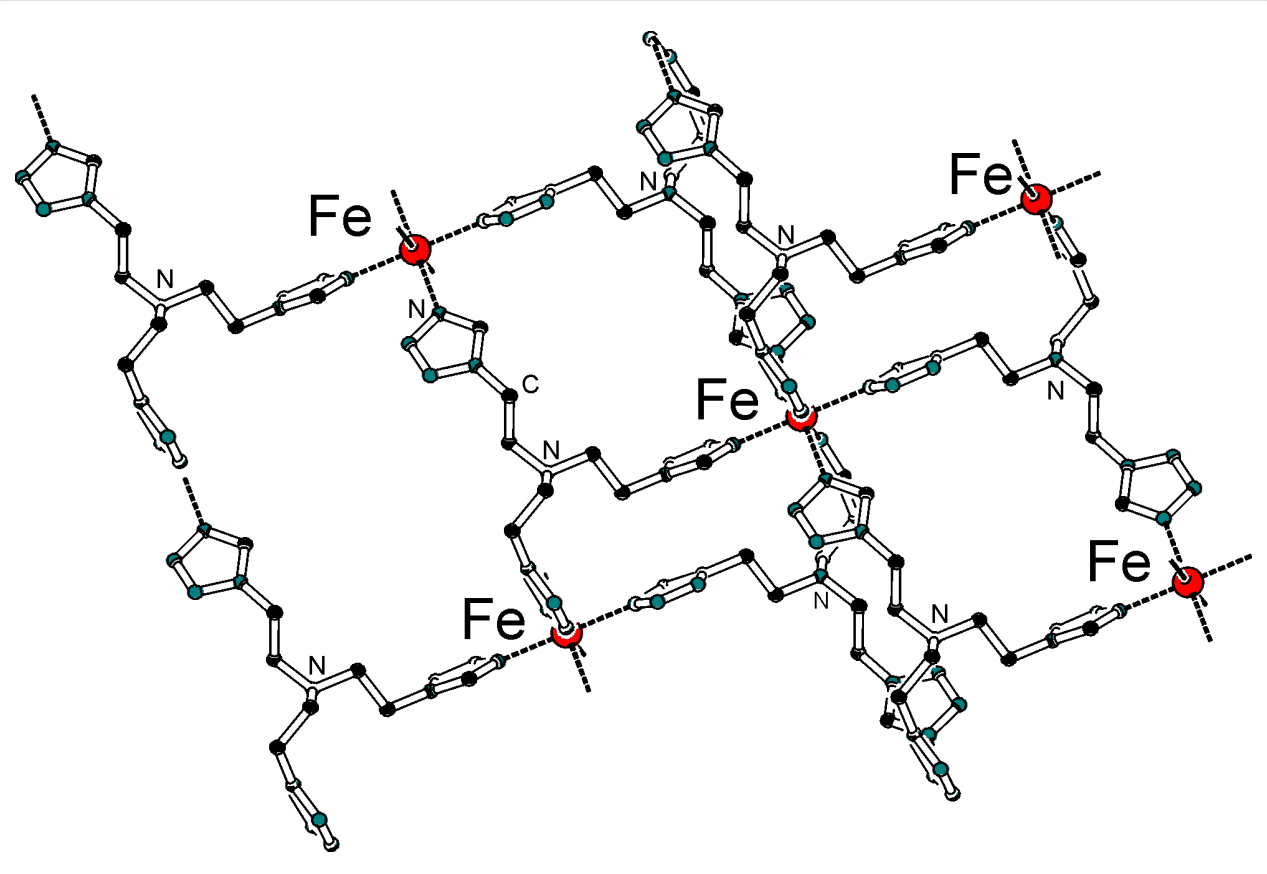

Figure 29: Part of the crystal structure of $[Fe\{N(entz)_3\}](BF_4)_2$ (T = 293 K) [335,336]. (Reproduced with permission from [23]. Copyright 1994 Wiley-VCH Verlag GmbH & Co. KGaA).

$[Fe(btr)_3](ClO_4)_2$ is the first 3D ST compound [347]. Its crystal structure (Figure 30) is made of iron(II) ions connected by btr ligands at the nitrogen atoms that occupy the 1 and 1' positions. The noncoordinated perchlorate anions are to be seen in the voids of the 3D architecture. A spin conversion proceeding in two steps was detected by magnetic susceptibility, Mössbauer spectroscopy, and differential scanning calorimetry upon cooling. Temperature-dependent ^{57}Fe Mössbauer spectroscopy and a detailed single-crystal X-ray analysis have together demonstrated that the formation of a plateau around ~200 K was due to a consecutive spin conversion occuring at two crystallographically inequivalent iron sites [347]. The narrow hysteresis that can be seen in the lower branch of the spin conversion curve by magnetic susceptibility measurements (not shown in Figure 30), is free of any crystallographic phase transition, and is associated with a higher variation of the dihedral angle δ between the triazole moieties, compared to the higher branch of the SCO curve, which is smoother (Figure 30). A similar 3D network was observed for [Fe(1,3-bis(tetrazol-2-yl)propane)$_3$](ClO$_4$)$_2$·2EtOH that revealed a smooth spin conversion again caused by the flexibility of the spacer between tetrazole molecules [348].

A 3D coordination network constructed from two interlocked cube units was observed for the complexes $[Fe(baztrz)_3]A_2{\cdot}2H_2O$ (A = ClO_4^-, BF_4^-), which both display an abrupt transition around room temperature [328]. Such an interlocked architecture was first reported for the 3D CPs $[Fe(btzb)_3]A_2{\cdot}Solv$, (A = ClO_4^-, PF_6^-; Solv = MeOH, H_2O) (btzb = 1,2-bis(tetrazole-1-yl)butane) [349-351]. An abrupt SCO behavior is observed in contrast to the 3D bis-tetrazolate SCO polymer $[Fe_2(H_{0.67}bdt)_3]{\cdot}13H_2O$ with H_2bdt = 5,5′-(1,4-phenylene)bis(1*H*-tetrazole) [352,353]. Another bidentate ligand based on a pyridine conjugated Schiff base, afforded a CP with a diamond-like 3D network made of FeN_4O_2 sites and displaying a gradual spin conversion [354].

An alternative strategy to bis-organic ligands makes use of cyanometallates [270], and to a minor extent cyanide [267], which afforded a large series of fascinating single or interpenetrated 2D and 3D lattices of various topologies and which are covered in review articles from Real et al. [267-270]. Porous materials based on this category as well as Hofmann-like cyanide compounds and other systems are reviewed below. At this stage, many more examples of bis-triazole iron(II) SCO

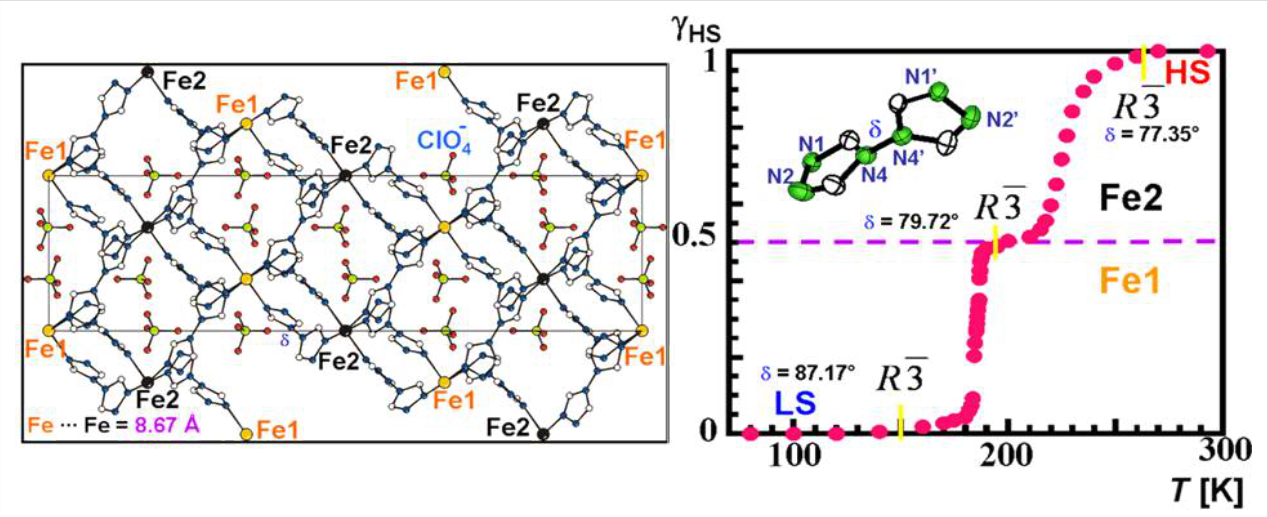

Figure 30: (left) Projection of the crystal structure of $[Fe(btr)_3](ClO_4)_2$ along the *c* axis revealing a 3D structure with Fe1 and Fe2 sites. The perchlorate anions occupy the voids. (right) HS molar fraction determined by ^{57}Fe Mössbauer spectroscopy. Note the variation of the dihedral angle δ between triazole moieties accompanying the spin conversion, which is greater in the lower branch that shows the steeper spin conversion. The space group is also given at three temperatures [347].

CPs are anticipated after the communication of a revised one-step synthesis of btr and derivatives thanks to a simplified transamination method reducing the reaction time, increasing the yield and avoiding tedious chromatographic separations [355] and which has already afforded numerous CPs and MOFs.

SCO in nanomaterials

A rational control of the growth of SCO materials at the nanometric scale and the study of the size-dependent SCO properties is crucial for their successful integration in functional devices [356-358]. In fact, determination of the critical particle size or film thickness that preserves a complete ST with hysteretic behavior is a vital factor in the nanominiaturization of a SCO material. Recent studies have involved the preparation of nanocrystals [359,360] and thin films [361,362] of the 3D coordination polymer $[Fe(pz)Pt(CN)_4]$ (pz = pyrazine) [363] exhibiting size-dependent ST characteristics. Bulk microcrystalline samples undergo very cooperative ST with $T_{1/2}^{\downarrow} = 285$ K and $T_{1/2}^{\uparrow} = 309$ K. The corresponding nanocrystals of average dimensions 200 × 200 × 60 nm and 60 × 60 × 30 nm display practically complete spin transitions, demonstrating a decrease of the critical temperatures and hysteresis widths with decreasing size of the crystallites (Figure 31) [359]. This effect is even more pronounced for 10–20 nm sized nanoparticles,

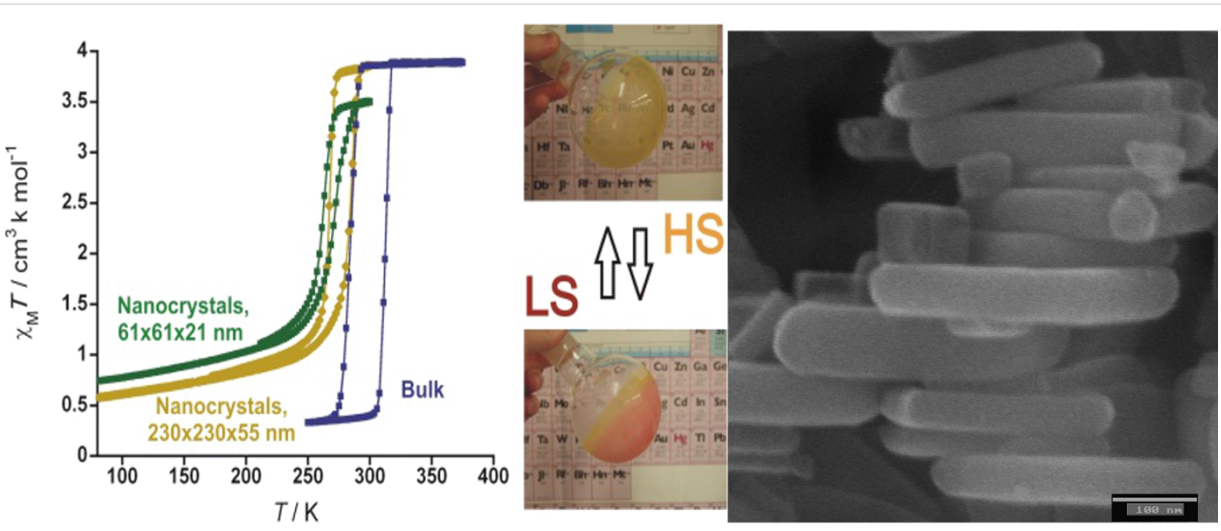

Figure 31: Size-dependent SCO properties in $[Fe(pz)Pt(CN)_4]$ (left), change of color upon spin state transition (middle) and image of the nanocrystals (right) [359].

where only around 1/3 of the Fe(II) ions undergo ST characterized by a very narrow thermal hysteresis loop [360]. A similar situation was found for $[Fe(pz)Ni(CN)_4]$ nanoparticles of about 4 nm coated with Chitosan polymer [364].

The 2D coordination polymers $[Fe(3\text{-}Fpy)_2M(CN)_4]$ (M(II) = Ni, Pd, Pt), and 3-Fpy = 3-fluoropyridine) [365] have also been the subject of study. Surfactant-free nanocrystals of average dimensions 400 × 400 × 30 nm were synthesized from water-in-oil microemulsions (w/o) and nanoparticles of 200 × 100, 100 × 60, and 70 × 30 nm were prepared by using the coating polymer poly(vinylpyrrolidone) (PVP). The nanocrystals exhibit virtually complete first-order spin transitions centered in the interval 200–225 K, while PVP-coated nanoparticles undergo a continuous second-order ST at much lower temperatures (ca. 160 K) [366].

The dependence of the hysteresis width on particle size in these polymers corresponds well to the behavior predicted by Monte Carlo simulations for cubic or spherical SCO nanoparticles [367]. However, these simulations predict a much weaker (almost negligible) dependence of the transition temperature on particle size than that observed. This discrepancy may reflect the oversimplified nature of the model employed, in which only short-range elastic interactions [368] have been taken into account. Indeed, a significant influence of long-range interactions on the cooperativity of the SCO process was inferred from infrared and Raman studies of the $[Fe(pz)M(CN)_4]$ and $[Fe(pyridine)M(CN)_4]$ series [369,370].

A different behavior was observed for surfactant-coated nanoparticles of the triazole-based 1D SCO polymers $[Fe(Htrz)_2(trz)]BF_4$ (Htrz = 1,2,4-4*H*-triazole) and $[Fe(4\text{-}NH_2trz)_3]Br_2$. Twenty-nanometer size nanoparticles of the former display a strong cooperative ST with a large hysteresis loop just like the one observed for the bulk material [281], while in the latter, the abruptness of the ST and the hysteresis width diminish as the particle size decreases with minimal displacement of $T_{1/2}{}^{\uparrow}$ [371-373].

The puzzling results reported for 1D triazole based SCO nanoparticles makes difficult any comparison with those results found for 2D and 3D Hofmann Clathrate analogue SCO nanocrystals/nanoparticles.

Thin films of SCO materials were first obtained by using the Langmuir–Blodgett [374] technique or by evaporation of solutions on substrates [375-377]. More recently deposition by sublimation under high vacuum [378-381] or layer-by-layer epitaxial growth techniques were employed (Figure 32)

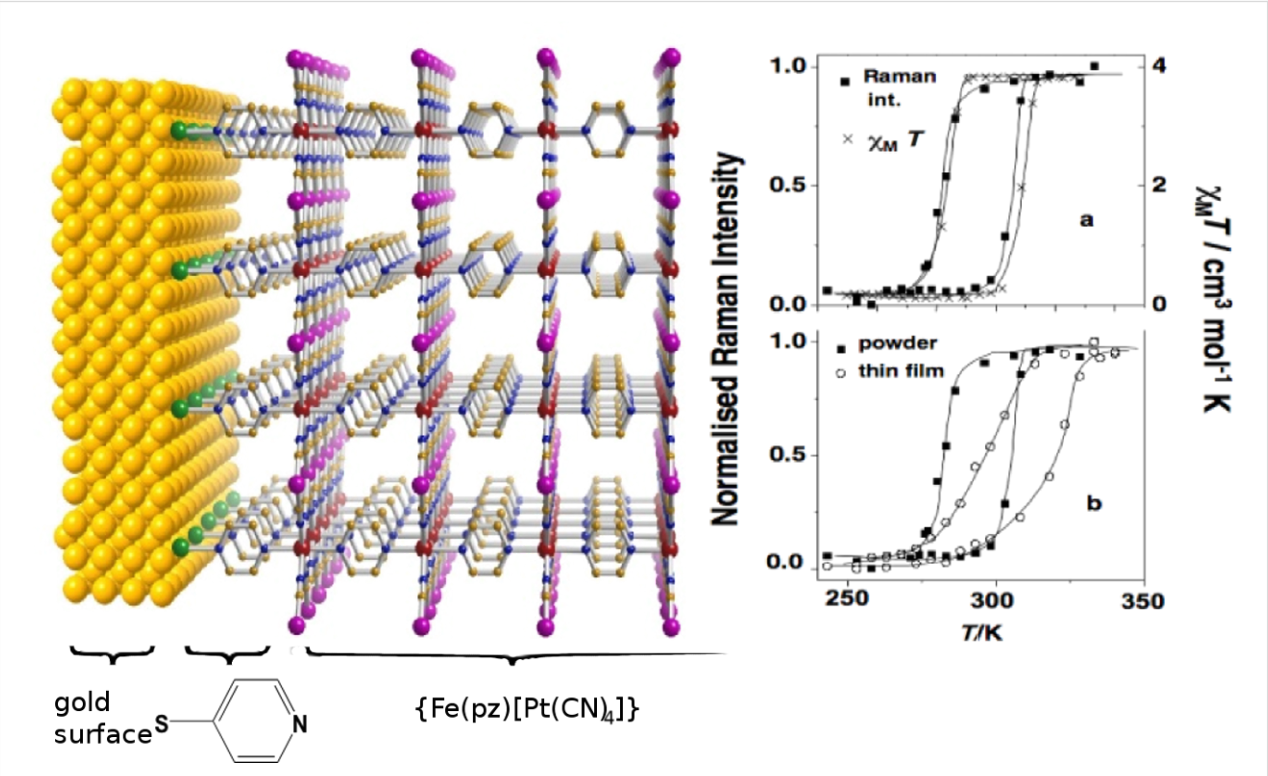

Figure 32: Schematic showing the epitaxial growth of polymer $\{Fe(pz)[Pt(CN)_4]\}$ and the spin transition properties of thin films studied by Raman spectroscopy [361].

[361,362,382,383]. The ST dependence on film thickness was investigated as well as the LIESST effect in several 3D Hofmann-like polymers and mononuclear compounds.

A bio-inspired approach was recently introduced to produce $[Fe(ptz)_6](BF_4)_2$ thin films on a *Alium cepa* membrane [384]. The size of the deposited crystals ranges from nano- to micrometers, and can be controlled depending on nucleation and growth rate, as shown by scanning electron microscopy, which also revealed morphogenesis. The thin films show a thermochromic SCO, which was detected by both UV–vis and ^{57}Fe Mössbauer measurements [384,385]. Most interestingly, printed membranes could be used as a natural stencil in soft lithography to produce nanodots of the SCO complex of 30–55 nm size on a Si-wafer and glass supports (Figure 33). This transfer method opens perspectives to study nanoparticles awayfrom their natural confinement and directly on selected supports [384].

Polyfunctional SCO materials (SCO combined with other functions, e.g., LC, gel and porous properties, electrical conductivity and fluorescence)

In recent years research on solid-state SCO materials has also been directed towards the combination of SCO with other functions, e.g., liquid-crystalline (LC) behaviour, gel and porous properties, electrical conductivity, fluorescence, etc. The idea is to make use of spin state switching in combination with another physical or chemical property that eventually opens pathways to a new generation of multifunctional materials.

Spin crossover in Fe(II) metallomesogens

Metallomesogens are metal-containing-liquid crystals [386]. A number of advantages in practical applications may be realized through the combination of SCO and liquid-crystalline behavior, for example, switching and sensing in different temperature regimes, the achievement of thermochromism or photochromism in liquid crystals, external electric- and possibly magnetic-field-based modulation of the SCO properties, and the facile processibility of materials into thin films. In the field of liquid crystals, color change is certainly a phenomenon of interest due to the necessity of color change in a number of applications of liquid crystals, such as laser-addressed devices, passive blocking filters, polarizers based on dichroic effects, or the use of thermochromism.

An initial step aimed at achieving a material combining SCO and LC properties has led to an iron(III) metallomesogen in which both properties are not simultaneously apparent but are seen in different temperature intervals [387]. Subsequently, Co(II) and Fe(II) metallomesogens were synthesized displaying similar properties [388-390]. Recently, the synchronization of spin state and liquid-crystal transitions in Fe(II) metallomesogens was shown to be achievable by selecting a suitable parent SCO system and attaching it to the liquid-crystal moiety,

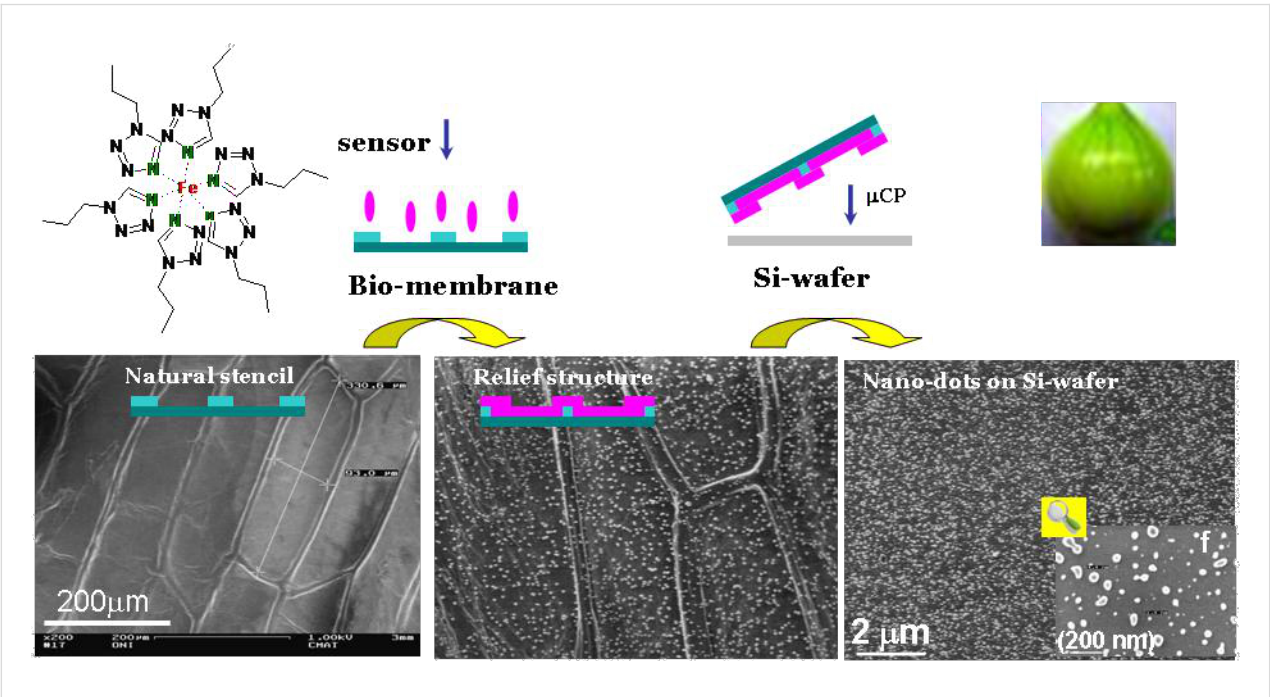

Figure 33: Microcontact printing (μCP) of nanodots on Si-wafer of $[Fe(ptz)_6](BF_4)_2$ after deposition of crystals on *Allium cepa* membrane [384,385].

with the aim of reaching the LS state or SCO properties at the temperature where the solid–liquid-crystal transition is expected (275–400 K) [391].

Although the number of examples of Fe(II) metallomesogens reported so far is small, the interplay/synergy between ST and liquid-crystal phase transitions has been seen to be very rich and the behaviors may be summarized as follows [358]:

1. systems with coupled phase transitions, subdivided into three groups: (a) where the structural changes associated with the Cr↔LC phase change drive the spin transition; (b) where the structural changes influence the spin state of the metallic centers but are not the driving force for the spin state transition; (c) where the vitrification of the material inhibits the SCO properties [375,392-394];
2. systems where both transitions coexist in the same temperature region but are not coupled [375,394,395];
3. systems with uncoupled phase transitions [358,394].

Presented below are some of the most representative examples of the Fe(II) metallomesogens where the Cr↔LC phase change drives the spin state transition (type 1) [394] and those metallomesogens for which the preparation of thin films was possible [375].

The ligand tris[3-aza-4-((5-C_n)(6-H)(2-pyridyl))but-3-enyl]amine (C_n-trenH) has been reacted with $FeCl_2{\cdot}sH_2O$ salts to afforded a family of complexes with the general formula $[Fe(C_n\text{-trenH})]Cl_2{\cdot}0.5H_2O$ where n = 16, 18 and 20 [394]. A similar structure to that found for the derivative $[Fe(C_6\text{-trenH})](ClO_4)_2$ was obtained from analysis of the XPRD patterns at 293 K. Figure 34 (left) illustrates the molecular structure of this system. A pseudo-octahedral symmetry is adopted by the iron atoms, and they are surrounded by six nitrogen atoms belonging to imino groups and pyridines of the trifurcated ligand C_n-trenH. Self-assembly to a bilayered composite results due to the amphiphilic nature of the alkylated molecules, with one layer being made up of polar head groups together with perchlorate anions (Figure 34 right). The nonpolar chains from oppositely oriented molecules meet together forming a hydrocarbon layer. The almost fully stretched alkyl chains are only distorted by the *gauche* conformation of some of the methylene groups and are tilted towards the *ac* plane, but they do not intertwine with chains of adjacent layers.

As a consequence of the melting between 340 and 350 K for $[Fe(C_{16}\text{-trenH})]Cl_2{\cdot}0.5H_2O$ the temperature variation of the interlayer distances d presents an abrupt increase (Figure 35a). For derivatives with n = 16, 18 and 20 the melting was found at 296, 311 and 328 K, respectively. DSC and optical polarizing microscopy (OPM) further confirmed the temperature of melting. A smectic mesophase S_A has been identified based on these findings, with layered structures similar to $[Fe(C_6\text{-trenH})](ClO_4)_2$ [394].

Figure 35c displays the $\chi_M T$ versus T plots for $[Fe(C_n\text{-trenH})]Cl_2{\cdot}0.5H_2O$ (n = 16, 18 and 20). Also shown is the Mössbauer spectrum measured for the derivative with n = 16 at 80 K (Figure 35b). The compounds are in the LS state in the temperature range of 4.2–290 K in which the Mössbauer spectra highlight the presence of a small residual HS fraction. For each of these derivatives a variation accompanied by a narrow hysteresis is seen in the $\chi_M T$ versus T between 400 and 296 K

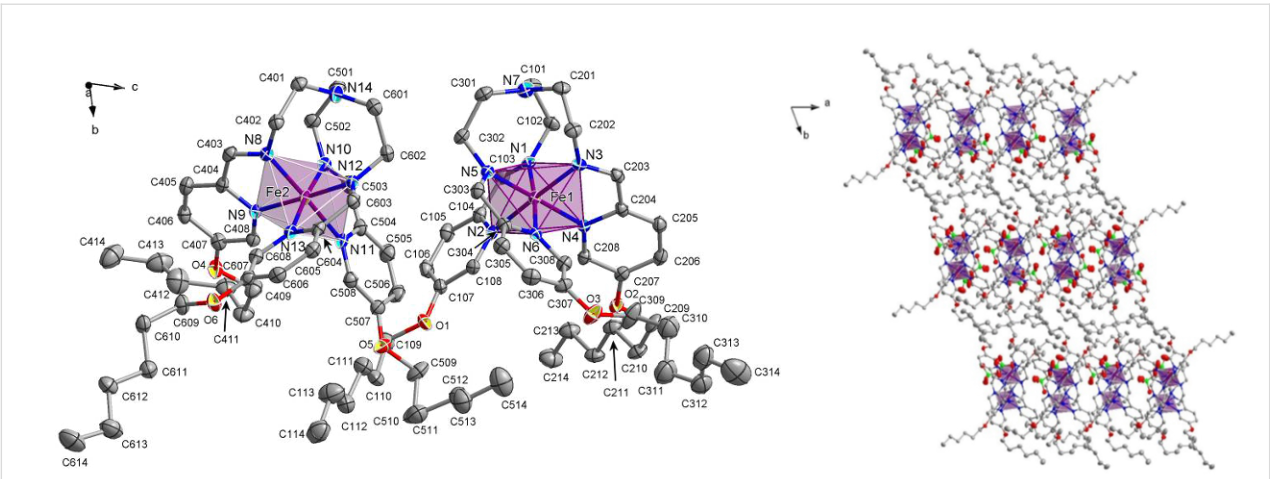

Figure 34: (left) Projection of the two independent cations of $[Fe(C_6\text{–trenH})]^{2+}$ with atom numbering scheme (150 K). (right) Projection of the molecular packing of the same complex along the *c* axis. Displacement ellipsoids are shown at 50% probability level. Hydrogen atoms and perchlorate anions are omitted for clarity. (Reproduced with permission from [394]. Copyright 2008 American Chemical Society).

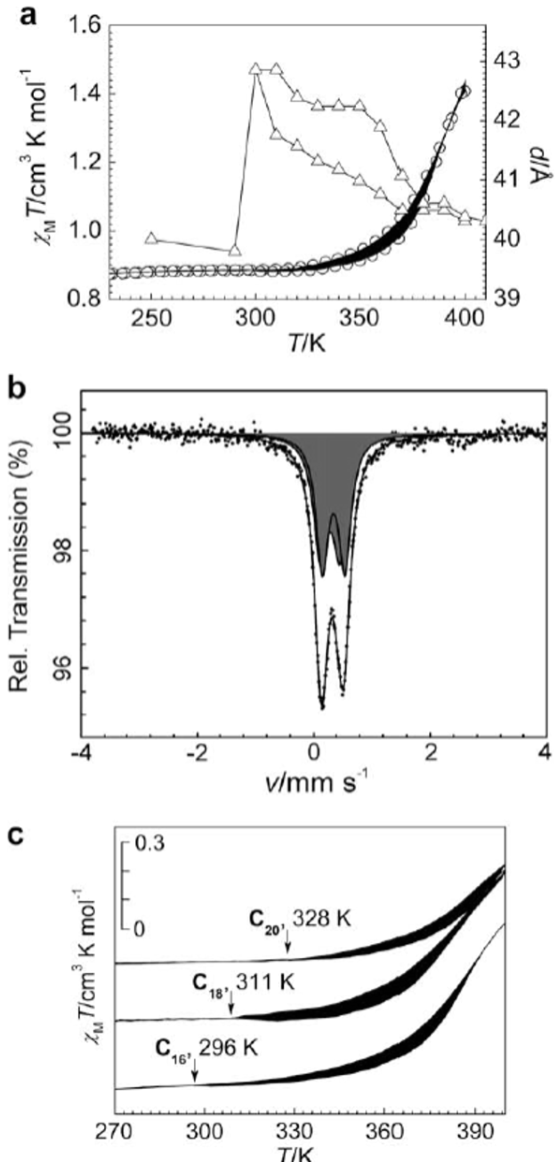

Figure 35: (a) $\chi_M T$ versus T for [Fe(C_{16}-trenH)]Cl_2·0.5H_2O and variation of the distance d with temperature (T) deduced from XPRD profiles after following the sequence 310–410–230–410 K. (b) Mössbauer spectra of [Fe(C_{16}-trenH)]Cl_2·0.5H_2O measured at 80 K (HS doublet: light grey; LS doublet: dark grey). (c) $\chi_M T$ versus T for [Fe(C_n-trenH)]Cl_2·0.5H_2O (n = 16, 18 and 20), arrows indicate the temperatures at which the heating and cooling curves diverge. The black areas indicate the hysteresis loops. (Reprinted with permission from [394]. Copyright 2008 American Chemical Society).

(Figure 35c). Below 296 K, $\chi_M T$ stays almost constant up to 10 K at which point it sharply decreases due to the zero-field splitting of the Fe(II) ions that remain in the HS state [394]. The thermally induced ST in [Fe(C_n-trenH)]Cl_2·0.5H_2O begins immediately after the onset of the first-order phase transition (Cr↔S_A). One can conclude that, since the ST is blocked below the temperature at which the compounds solidify, the spin transition is driven by the melting process in these metallomesogens. The hysteresis accompanying the ST in the S_A mesophase is due to the reorganization of the metallomesogen structure upon Cr↔S_A transition. It is worthy of mention that the ST temperature is dependent on the melting temperature, which is higher for the derivatives with longer alkyl chains (Figure 35c). In the LS state these compounds are dark purple, becoming light purple-brown in the HS state.

An interesting and important feature is the possibility to obtain these materials in the form of thin films by exploiting their fluid nature. Thin films of a few micrometers thick have been formed by solvent evaporation for metallomesogens that exhibit Colh mesophase at room temperature. Examples are [Fe(C_n-tba)$_3$]A_2 [C_n-tba = 3,5-bis(alkoxy)-N-(4*H*-1,2,4-triazol-4-yl)benzamide, A = $CF_3SO_3^-$, 4-$MeC_6H_4SO_3^-$ and n = 8, 10, 12] [375,392]. Reversible color change of the films by heating or cooling around 300 K, between violet (LS state) and white (HS state), was observed without fatigue (Figure 36).

SCO in gels

The transfer of SCO properties into a soft-matter phase, such as a gel, has been accomplished by functionalizing the polymeric Fe(II)/4-R-1,2,4-triazole system with long alkyl chains on the 4-substituent [396-399]. By dissolution of these SCO materials in organic solvents, hybrid gels have been obtained, and their thermo-reversible magnetic, optical and rheological properties could be studied. It was shown that T_{melt} and $T_{1/2}$ can be tuned by using mixtures of solvents and by changing the counter-anions, respectively (Figure 37) [396].

Compared to references dealing with nongelling aromatic solvents, a quick thermal response is characteristic of SCO physical gels, due to a rapid restoration of the H-bonding network, possibly a result of dynamic structural ordering through an enhanced lipophilic interaction of the self-assembling components in hydrocarbon solvents [397].

Spin crossover in porous coordination polymers

Porous coordination polymers (PCPs), also known as MOFs, represent a new class of functional molecular materials [400-407], which are able to mimic and even improve the functions of zeolites [408], i.e., storage [409,410], separation [411,412], sensing [413] and catalysis [414-416]. The vast majority of their applications are related to pore sizes, shapes, flexibility and structures/environments. Particularly interesting are those PCPs where the solid-state properties of the framework (magnetism [417], luminescence [418], conductivity [419,420], charge transport [421], etc.) change upon sorption/desorption of guest molecules. This new generation of PCPs acts in a sensory way expressing the host–guest interactions.

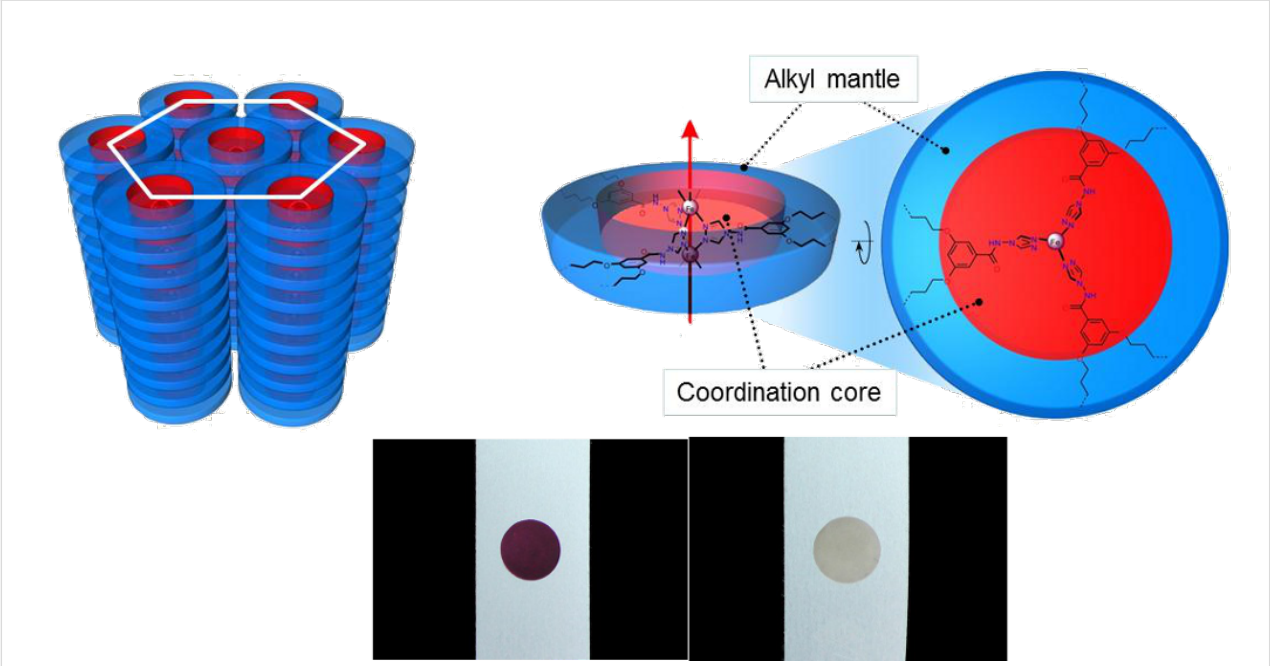

Figure 36: Schematic illustration of the structure of compounds $[Fe(C_n\text{-tba})_3]X_2$ adopting a columnar mesophase (top). Change of color in the SCO LC films around 60 °C (bottom). (Reprinted with permission from [375]. Copyright 2006 American Chemical Society).

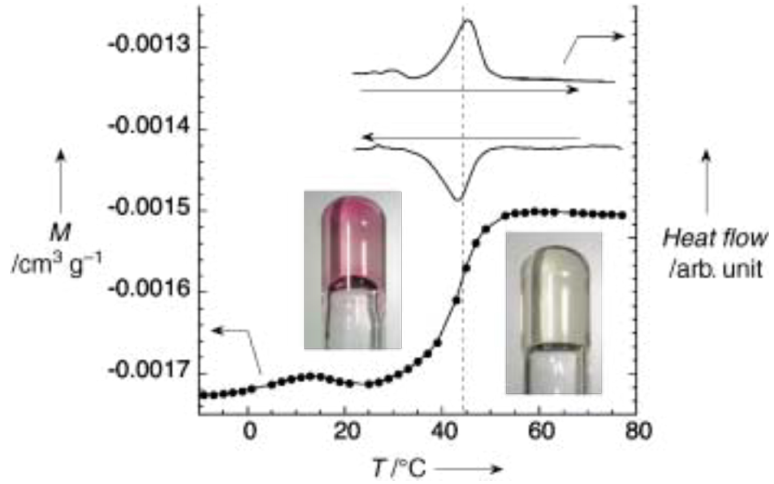

Figure 37: Temperature dependence of the magnetic moment (M) at 1000 Oe and DSC profiles (inset; 5 °C/min) of a 5 wt % of [Fe(II)(4-octadecyl-1,2,4-triazole)$_3$](tosylate)$_2$·2H$_2$O in decane gel. The dotted line corresponds to the $T_{1/2}$ = 44 °C deduced from DSC and magnetic measurements. The anomalies observed on the magnetic moment curve below 25 °C correspond to the solid–liquid first-order transition in pure decane [279]. (Reproduced with permission from [396]. Copyright 2004 Wiley-VCH Verlag GmbH & Co. KGaA).

Among PCPs incorporating both porous and magnetic properties, it is noteworthy that these porous polymers are made up of bi-stable Fe(II) building units. The guest inclusion in the SCO framework can provoke the stabilization of the Fe(II) ions in the HS or LS state or has no effect at all. The resulting effect relies on the chemical nature and size of the guest molecules that occupy the pores. Detection of the sorption/desorption of guest molecules in the framework is performed by analyzing magnetic and optical outputs (the temperature dependence of the magnetic susceptibility and/or by the change of color at a

given temperature). In principal, a fingerprint in the form of a magnetic response pattern may be attainable for distinct analytes.

Examples of Fe(II) SCO-PCPs reported up to date are still scarce. The first report on a microporous coordination polymer was based on the ligand dpe (1,2-di(4-pyridyl)ethylene)(*trans* isomer) [331] and dates back to 1995. Almost a decade later, a detailed investigation was published of the guest influence on the SCO properties in analogous frameworks with composition $[Fe(L)(NCS)_2]\cdot G$ (L = azpy and bped (1,2-bis(4-pyridyl)-1,2-ethanediol)) [227]. In these SCO-PCPs the adsorption of guest molecules induces some stabilization of the framework in the LS state. Typically they show gradual SCO in the temperature region 10–200 K.

More recently a drastic influence of the guest inclusion on $T_{1/2}$ and cooperativity has been reported for the 3D Hofmann-like SCO-PCPs $\{Fe(L)[M(CN)_4]\}\cdot G$ [L = pz [363,422-425]; azpy [382]; bpac (bis(4-pyridyl)acetylene) [426]; dpe (*trans* isomer) [300] M(II) = Ni, Pd, Pt)]. This type of framework provides two guest interactive sites, one between the organic bridges (site A) and another between the four-coordinate M centers (site B) (Figure 38).

Particularly interesting are the results obtained with the SCO-PCP $\{Fe(pz)[M(CN)_4]\}$. In fact, this represents a new generation of functional materials responding to their environment since the framework can allow reversible control of the magnetic and optical outputs through the chemical response at room temperature [363,422-425]. The reversible spin state transition at the Fe(II) sites occurs concomitantly with the uptake of guest molecules. Hydroxy solvents, five- and six-membered aromatic molecules, stabilize the HS state (yellow color) while CS_2 (for M = Pt) [422] or CH_3CN (for M = Ni) [423] favor the LS state (red color). Desorption of guest molecules under vacuum produces the guest-free framework in the induced spin state. The initial HS or LS state is not recovered by the system after release of the guest molecules within the bistable temperature region. Information about adsorption of the guest molecules in the form of the spin state, magnetism, color, and structure are retained by this memory function; information that can be erased by using the appropriate operator (i.e., by applying either $\Delta T - \Delta T$ or $-\Delta T + \Delta T$, from room temperature) (Figure 38).

Moreover, the occurrence of coordinative unsaturated metal centers M(II) provided enhanced adsorptive selectivity for dihalogen molecules. Indeed, an associative oxidation of Pt(II) to Pt(IV) and reduction of the dihalogen to the corresponding halide to give $\{Fe(pz)[Pt(CN)_4(X)]\}$ ($X = Cl^-$, Br^- and I^-) has been demonstrated (Figure 39) [424]. Particularly, successful control of the $T_{1/2}$ value from 300 to 400 K while maintaining bistability (25 K wide thermal hysteresis) has been achieved for $\{Fe(pz)[Pt(CN)_4(I)_n]\}$ ($n = 0–1$) [425].

Inclusion of thiourea molecules capable of interacting with the organic pillar ligands and the unsaturated metal coordination sites through weak intermolecular interactions leads to the clarthrate compounds formulated as $\{Fe(pz)[Pt(CN)_4]\}\cdot 0.5(CS(NH_2)_2)$ and $\{Fe(pz)[Pd(CN)_4]\}\cdot 1.5H_2O\cdot 0.5(CS(NH_2)_2)$ [428]. These 3D porous coordination polymers exhibit unprecedented ST accompanied by large thermal hysteresis cycles of ca. 60 K wide. Apparently, this strong cooperative ST arises from the fact that multiple significant intermolecular interactions have to be reorganized upon the

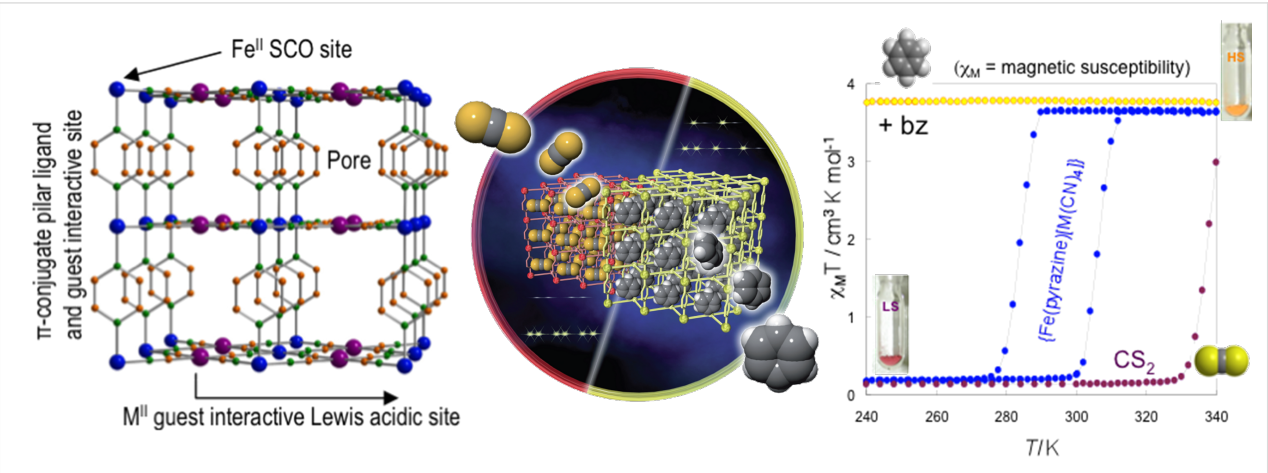

Figure 38: Porous structure of the SCO-PMOFs $\{Fe(pz)[M(II)(CN)_4]\}$ (left), representation of the host–guest interaction (middle) and change of the spin state upon guest adsorption (right) [paramagnetic, yellow (C_6H_6); diamagnetic, red CS_2]. (Reproduced with permission from [422]. Copyright 2009 Wiley-VCH Verlag GmbH & Co. KGaA).

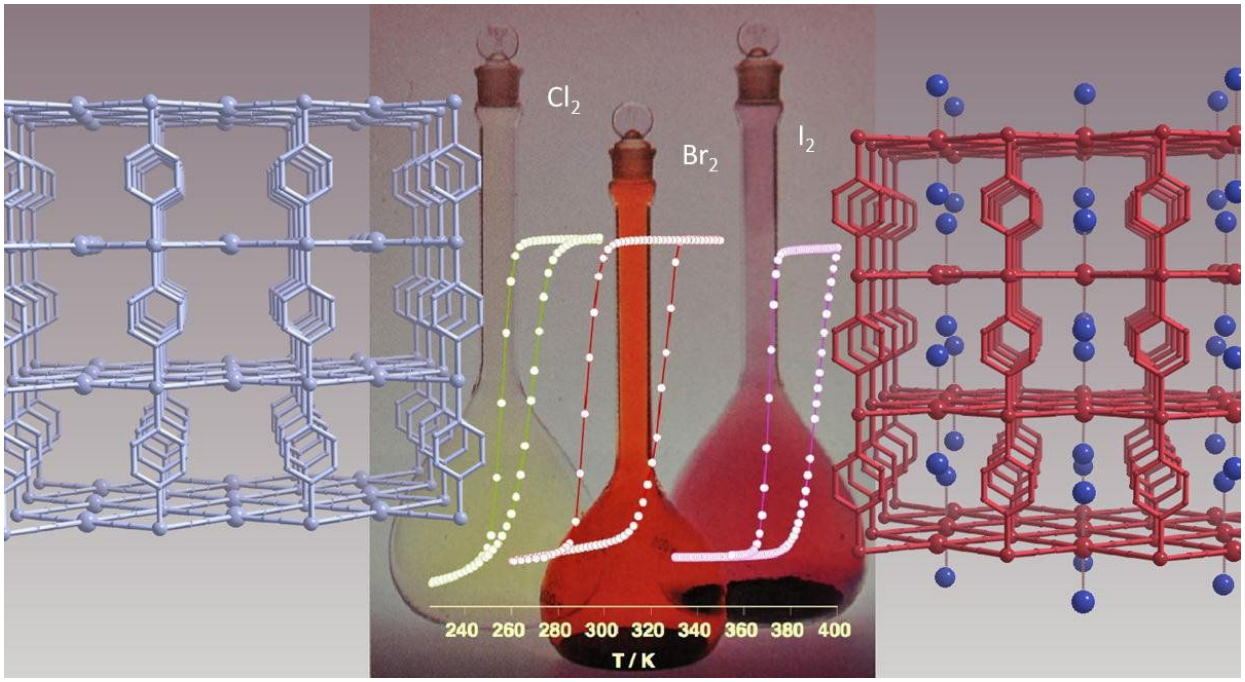

Figure 39: Porous structure of the guest-free SCO-PMOF's {Fe(pz)[M(II)(CN)$_4$]} (left), magnetic properties of the {Fe(pz)[Pt(CN)$_4$(X)]} (X = Cl^-, Br^- and I^-) compounds (middle) and crystal structure of compound {Fe(pz)[Pt(CN)$_4$(I)]}. (Reproduced with permission from [424]. Copyright 2009 Wiley-VCH Verlag GmbH & Co. KGaA).

SCO process, since the dimensions of the pores are different in the LS and HS states (Figure 40).

Current development of this topic points at increasing the pore size and inner pore functionality of the SCO-PCPs. The goals are twofold: (i) develop novel SCO-PCPs for sensing the uptake/release of aromatic guest molecules in solution or air; and (ii) to study selective adsorption and separation of aromatic molecules on SCO-PCPs. In comparison with gas storage investigations on PCPs, systematic studies of guest adsorption and separation on PCPs for which single-crystal information is available are scarce, particularly for aromatic molecules [425]. However, the separation and capture of aromatic molecules is very important in industry and for the development of green environments [415,416].

In this respect, a novel Hoffman-like 3D CP {Fe(dpe)[Pt(CN)$_4$]}·0.5(dpe) (**3**) based on the organic pillar ligand dpe (1,2-di(4-pyridyl)ethylene) (trans isomer) has been recently reported. This compound is commonly crystallized in

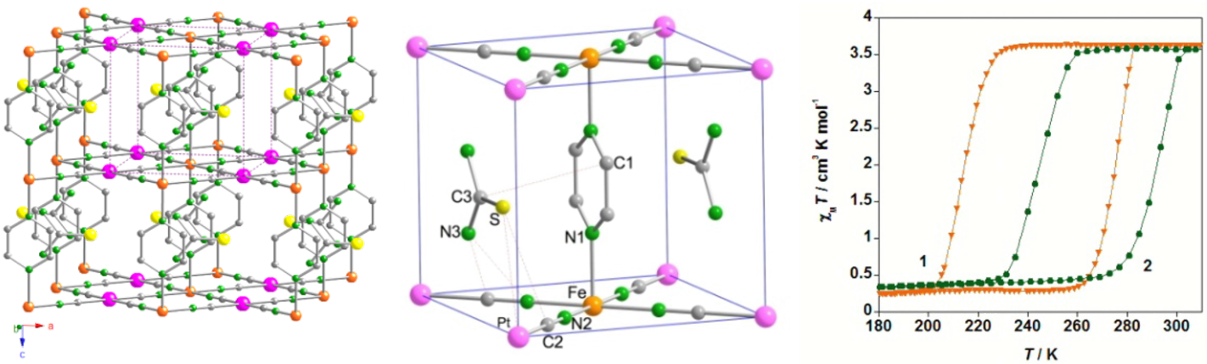

Figure 40: (left) The 3D porous structure of {Fe(pz)[Pt(CN$_4$]]·0.5(CS(NH$_2$)$_2$) (**1**) and {Fe(pz)[Pd(CN$_4$]]·1.5H$_2$O·0.5(CS(NH$_2$)$_2$) (**2**) in a direction close to [101]. Atom code: Fe (orange), Pt (pink), N (green), and C (grey). (right) Magnetic properties of **1** and **2** in the form of $\chi_M T$ versus T. (Reproduced with permission from [428]. Copyright 2012 Royal Society of Chemistry).

its monohydrate form {[Fe(dpe)[Pt(CN)$_4$]}·0.5(dpe)·H$_2$O (**4**). The water molecule can be reversibly sorbed/desorbed while maintaining crystallinity. The guest-free framework undergoes strong cooperative ST located at $T_{1/2}^{\downarrow}$ = 135 K and $T_{1/2}^{\uparrow}$ = 150 K while the water-containing framework exhibits a two-step ST in the interval of 275–240 K. Interestingly, clathrates formulated as {Fe(dpe)[Pt(CN)$_4$]}·*n*G (*n* = 1; G = phenazine (**5**), anthracene (**6**) and naphthalene (**7**)) are obtained when the guest molecules are present during the crystallization process (Figure 41) [427]. Detection of the phenazine, anthracene or naphthalene encapsulation in the framework can be done by recording the magnetic susceptibility at a given temperature

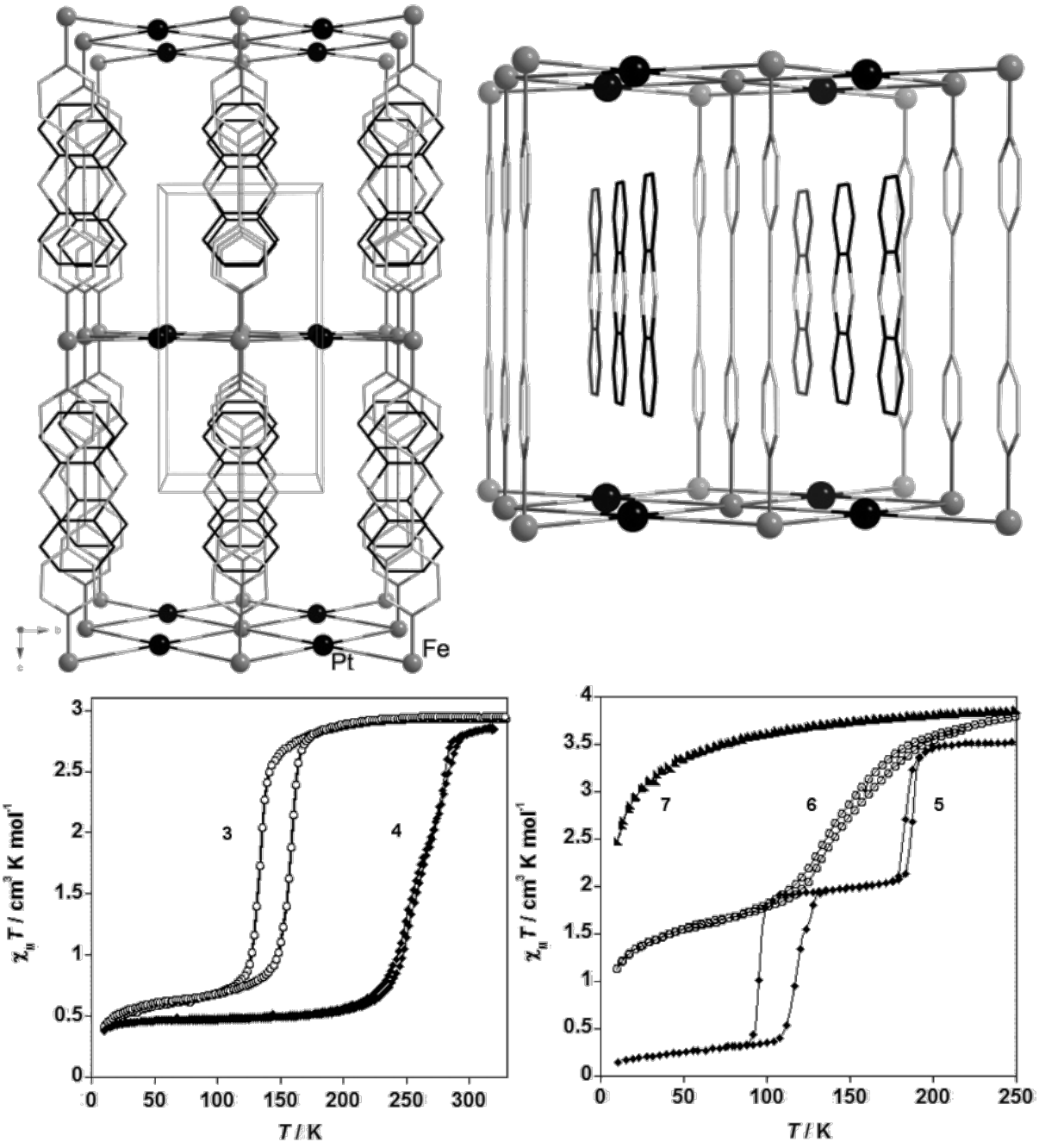

Figure 41: Top: The 3D porous structure of {Fe(dpe)[Pt(CN)$_4$]}·phenazine in a direction close to [101] emphasizing the guest inclusion in the framework. Bottom: Magnetic properties of {Fe(dpe)[Pt(CN)$_4$]}·0.5(dpe) (**3**), {[Fe(dpe)[Pt(CN)$_4$]}·0.5(dpe)·H$_2$O (**4**), and {Fe(dpe)[Pt(CN)$_4$]}·nG (n = 1; G = phenazine (**5**), anthracene (**6**) and naphthalene (**7**)) in the form of $\chi_M T$ versus *T*. (Reproduced with permission from [300]. Copyright 2008 Wiley-VCH Verlag GmbH & Co. KGaA).

since the magnetic properties of the clathrate compounds are very different. The fact that the clathrates present abrupt, incomplete or two-step ST or paramagnetic behavior is related to their size, shape, location and interaction with the framework. In general, it is observed that clathration of phenazine, anthracene or naphthalene leads to the stabilization of the frameworks in the HS state. In the case of **6** and **7** the guest molecules would be most probably located between the dpe pillar ligands in analogy with **5**. However, the particular stabilization of the HS state seems to be regarded with a possible tilt of the guest molecules with respect to the pillar ligands dpe, as observed for the clathrate $\{Fe(pz)[M(CN)_4]\}\cdot pz$ [422]. This particular location of guest molecules prevents the intrinsic contraction–expansion of the framework associated with the spin transition.

Combination of SCO and electrical conductivity

In molecular science, the fundamental property of electrical conductivity is currently being investigated. Spurred on by finding of electrical conductivity in perylene bromide, researchers have been working hard to produce high T_c superconductors based on organic and organometallic charge-transfer complexes and radical-ion salts [429]. Currently, the field of molecular conductors tends towards the design of hybrid materials in which a second interesting physical property is incorporated.

Two different synthetic approaches can be outlined with regard to the combination of SCO and electrical conductivity properties. First, a recently proposed strategy is the assembly of switchable molecular SCO building blocks with radical ionic salts, to tune (switch on/off) the conducting properties by acting on the bistable cation. A separate strategy involves the covalent linkage of paramagnetic metal ions to redox-active ligands. By associating redox-active moieties and heteroatom-based ligands capable of coordinating to the metallic center, a novel approach toward the modulation of the collective electronic properties of the resulting bifunctional material is realized.

The former strategy has led to the compounds $\{[Fe(sal_2\text{-}trien)][Ni(dmit)_2]_3\}$ [430], $[Fe(qsal)_2][Ni(dmit)_2]_3\cdot CH_3CN\cdot H_2O$ [431] and $[Fe(qnal)_2][Pd(dmit)_2]_5\cdot(CH_3)_2CO$ [432]. These materials exhibit a structural arrangement typical of $[M(dmit)_2]^x$ (M = Ni, Pd) fractional-oxidation-state compounds, where the $[Ni(dmit)_2]^-$ or $[Pd(dmit)_2]^x$ units interact through S···S short contacts, defining layers, which alternate with layers of $[Fe(L)]^+$ (Figure 42). The cationic units undergo cooperative SCO behavior and the layers of $[M(dmit)_2]^x$ enables the occurrence of electronic transport. At room temperature the electrical conductivity of these hybrid complexes is in the range of 0.1–2.0 S cm^{-1}. Interplay between SCO and electrical conductivity has been observed for $[Fe(qnal)_2][Pd(dmit)_2]_5\cdot(CH_3)_2CO$ [432]. The cooperative SCO phenomenon is considered to induce a chemical uniaxial strain effect on the conducting layer. Such a cooperativity based on supramolecular interactions is crucial for controlling or switching the electronic properties of a molecular solid by external stimuli.

The second approach has as yet been less developed due to the difficulties implicit in the organic synthesis of ligands containing redox-active moieties and heteroatom-based ligands. Figure 43 illustrates two examples of Fe(II) coordination compounds derived from this approach [433,434]. In both cases, the magnetic and electrical resistivity measurements suggested an interaction of ST and electrical conductivity, since the electrical conductivity shows an anomaly around the critical ST temperature.

Combination of SCO and fluorescence properties

Combining SCO and fluorescence in a single material dates back to the first report on a Ni(II) tetraaza-macrocyclic complex [435] followed by iron(II) SCO complexes studied as thin films [436]. In general, fluorescence quenching was observed in one spin state, as found for the heterodinuclear triple helicate iron(II) complex including a luminescent ion (Eu) [437] or for the 1D-1,2,4-triazole iron(II) chain including pyrene [438]. When this later fluorophore was decorated on a ligand of an Fe(II) mononuclear complex [439], temperature-dependent studies of the photophysical properties did not reveal any obvious correlation between the fluorescence of the pyrene group and the spin state of the Fe(II) ion.

The celebrated 1D polymeric iron(II) chain system provided hybrid materials showing fluorescent properties tuned by the spin state transition. Hybrid nanoparticles containing SiO_2 and $[Fe(Htrz)_2(trz)]BF_4$ were coated with the fluorophore 3-(dansylamido)propyltrimethoxysilane (dansyl) [286]. The hybrid nanoparticles preserve the magnetic bistability and, as a new property resulting from the hybrid material, the luminescence is coupled with the spin state transition showing bistability as well. Similar synergy between spin state transition and luminescence has been observed in solution in nanoparticles of $[Fe(NH_2trz)_3](tos)_2$ coated with rhodamine-110 chloride (9-(2-carboxyphenyl)-3,6-diamino-3*H*-xanthylium chloride). This multiproperty material has been proposed as a prototype for fluorescent thermometry [440].

The first observation of the tracking of a ST by fluorescence in the crystalline state has recently been made for the dinuclear Fe(II) complex $[Fe_2(Hsaltrz)_5(NCS)_4]\cdot 4MeOH$ [235]. In this complex, a fluorophore tag whose fluorescence is due to different prototropic forms of a *N*-salicylidene aniline (enol*

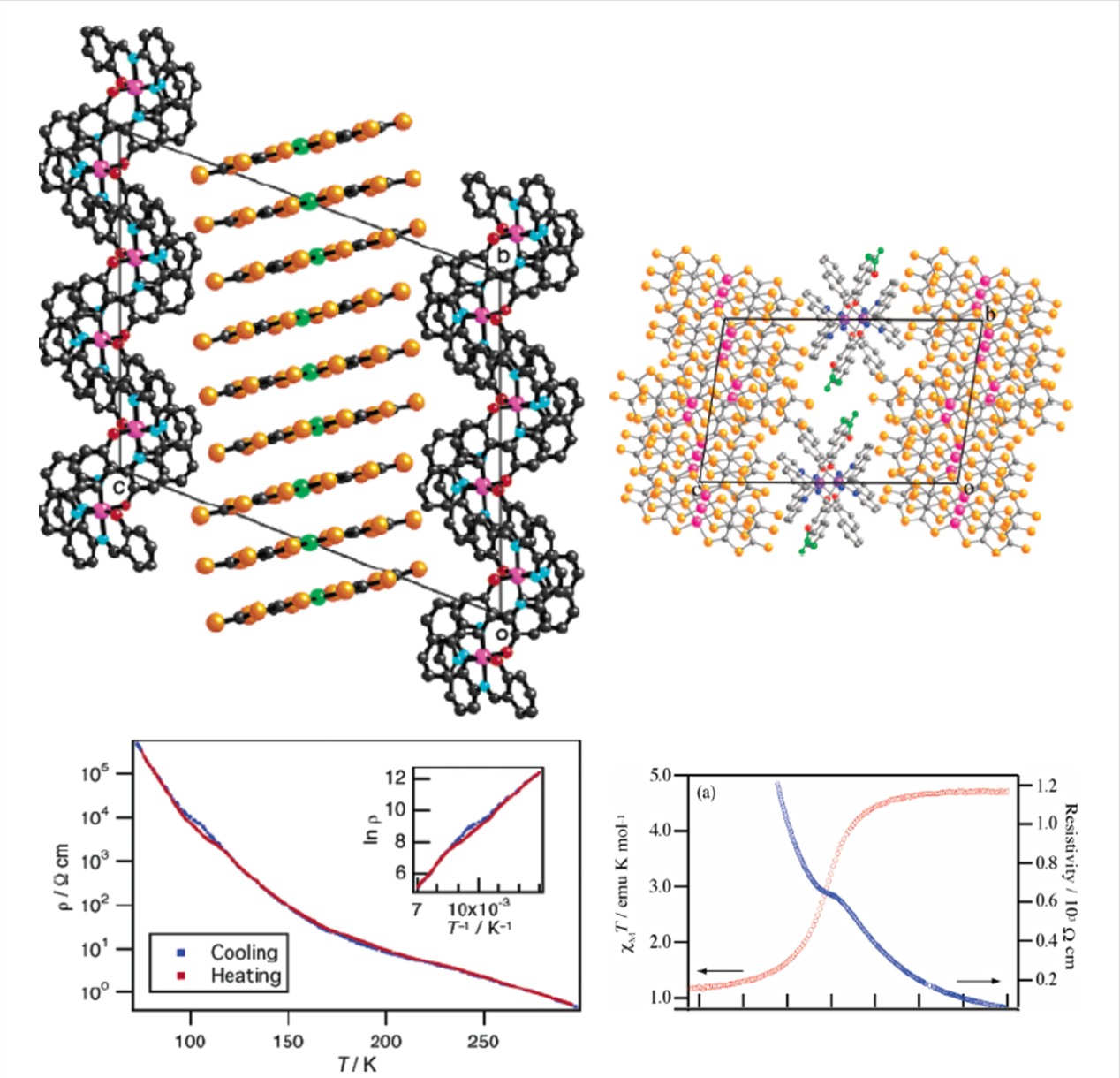

Figure 42: View of the segregated stacking of $[Ni(dmit)_2]^-$ and $[Fe(sal_2\text{-trien})]^+$ in $[Fe(qsal)_2][Ni(dmit)_2]_3{\cdot}CH_3CN{\cdot}H_2O$ (left) and in $[Fe(qnal)_2][Pd(dmit)_2]_5{\cdot}(CH_3)_2CO$ (right) together with magnetic and resistivity plots. [430]. (Reproduced with permission from [431] and [432]. Copyright 2006 & 2008 American Chemical Society).

and *cis*-keto* forms) [441] was directly grafted on to the 1,2,4-triazole ligand (Figure 21). The wavelength emission maximum of the enol* band (λ_{max} enol*) could be used as a marker to track the SCO event by fluorescence spectroscopy. As shown in Figure 44, a drastic jump of 20 nm was observed over the temperature range of 135–179 K, from ~395 nm below 150 K to 415 nm above 200 K. Remarkably, such a dramatic increase in the wavelength precisely follows the temperature dependence of γ_{HS} derived by SQUID measurements, and the transition temperature, $T_{1/2}$ = 157(1) K, is in good agreement with the one obtained by DSC [T^{max} = 155(1) K] [235].

Conclusion

In this article we have described a special class of molecular switches based on a dynamic electronic-structure phenomenon known as *spin crossover*. The principle of the molecular switching is a change of the spin state of a transition metal ion that is located in the center of complex molecules and coordinated to ligand atoms or molecules. Depending on the strength of the ligand field, i.e., the electrostatic field exerted at the central metal ion, the valence electron configuration of the metal can switch between two stable electron arrangements, one with maximum spin multiplicity, known as the high spin (HS) state,

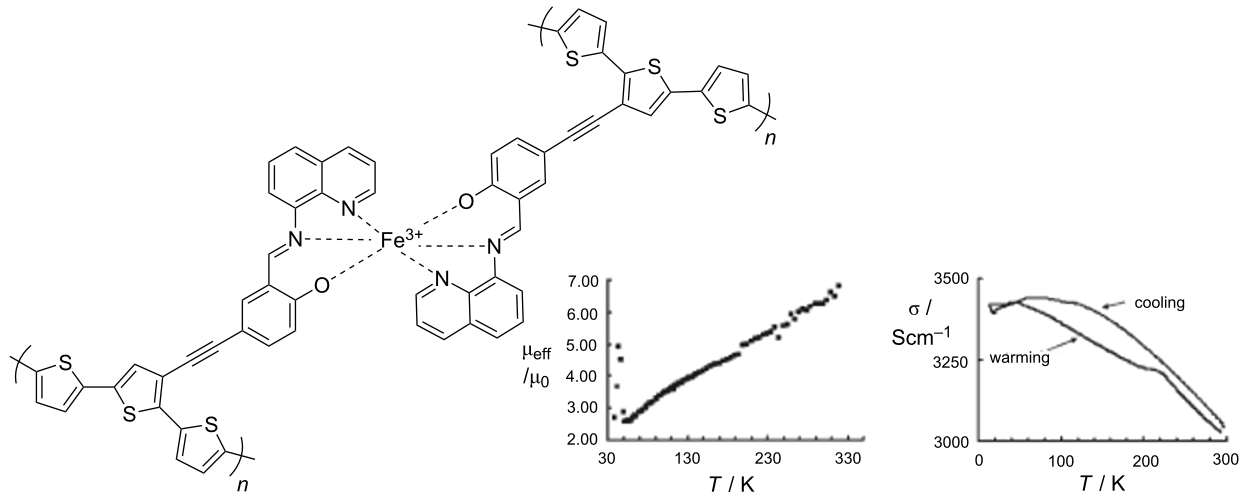

Figure 43: Thin films based on Fe(III) compounds coordinated to Terthienyl-substituted QsalH ligands [434] together with magnetic and resistivity plots. (Reproduced with permission from [434]. Copyright 2009 American Chemical Society).

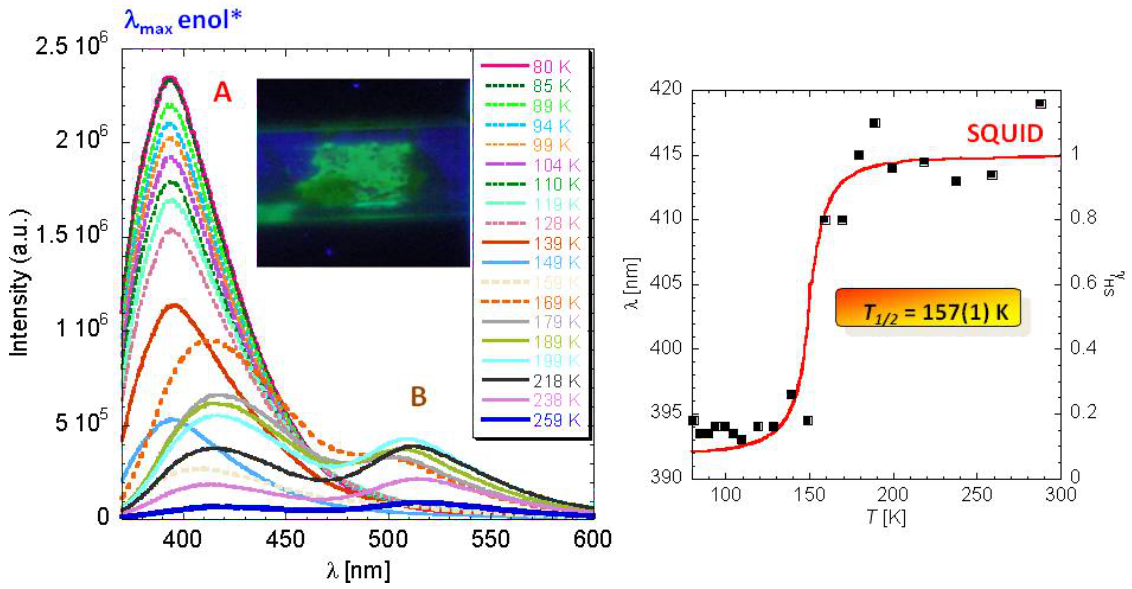

Figure 44: Left: Temperature-dependent emission spectra for $[Fe_2(Hsaltrz)_5(NCS)_4]\cdot 4MeOH$ at λ^{ex} = 350 nm over the range 80–259 K. The inset shows the fluorescence at 293 K produced by continuous irradiation at 254 nm. Right: Temperature dependence of λ_{max} enol* in the emission spectrum (■), which follows γ_{HS} derived from SQUID data (solid line) [235].

and one with minimum spin multiplicity, the low spin (LS) state. This switching can be stimulated by variation of temperature, application of pressure, light irradiation, and other external stimuli. The two phases involved have drastically different magnetic and optical properties, which provide the means for detection of the spin state phases. The spin crossover phenomenon occurs in numerous classes of coordination compounds; by far the majority of them are coordination compounds containing iron(II), iron(III) or cobalt(II). We have presented a selection of spin crossover compounds of iron(II) classified as mono-, di- and oligonuclear systems as well as 1D, 2D and 3D coordination polymers. As the latest developments in this area, preparation and studies of materials on the nanoscale have been illustrated. Likewise, systems combining spin crossover and other physical or chemical properties, such as liquid-crystalline and gel behavior, electric conductivity, fluorescence and porous

properties, have been covered. In nearly all these classes of spin crossover compounds it is important and necessary to go beyond the borderline of classical coordination chemistry and make use of strategies for the synthesis of new organic ligands and of organic synthesis techniques that would provide novel systems and functionalities.

Spin crossover compounds bear the potential for practical applications. Molecular electronics, data storage, display devices and sensors are objectives currently under consideration.

References

1. Cambi, L.; Cagnasso, A. *Atti R. Accad. Naz. Lincei* **1931,** *13,* 809.
2. Cambi, L.; Szegö, L. *Ber. Dtsch. Chem. Ges. B* **1931,** *64,* 2591–2598.
3. Cambi, L.; Szegö, L.; Cagnasso, A. *Atti. R. Accad. Naz. Lincei* **1932,** *15,* 266.
4. Cambi, L.; Szegö, L.; Cagnasso, A. *Atti. R. Accad. Naz. Lincei* **1932,** *15,* 329.
5. Cambi, L.; Szegö, L. *Ber. Dtsch. Chem. Ges. B* **1933,** *66,* 656–661. doi:10.1002/cber.19330660508
6. Cambi, L.; Malatesta, L. *Ber. Dtsch. Chem. Ges. B* **1937,** *70,* 2067–2078. doi:10.1002/cber.19370701006
7. Ewald, A. H.; Martin, R. L.; Ross, I. G.; White, A. H. *Proc. R. Soc. London, Ser. A* **1964,** *280,* 235–257. doi:10.1098/rspa.1964.0143
8. König, E. *Coord. Chem. Rev.* **1968,** *3,* 471–495. doi:10.1016/S0010-8545(00)80097-1
9. van Koningsbruggen, P. J.; Maeda, Y.; Oshio, H. Iron(III) Spin Crossover Compounds. *Spin Crossover in Transition Metal Compounds I;* Top. Curr. Chem., Vol. 233; Springer-Verlag: Berlin, Heidelberg, New York, 2004; pp 259–324. doi:10.1007/b95409
10. Murray, K. S. *Eur. J. Inorg. Chem.* **2008,** 3101–3121. doi:10.1002/ejic.200800352
11. Larionov, S. V. *Russ. J. Coord. Chem.* **2008,** *34,* 237–250. doi:10.1134/S1070328408040015
12. Krüger, H.-J. *Coord. Chem. Rev.* **2009,** *253,* 2450–2459. doi:10.1016/j.ccr.2009.06.004
13. Weber, B.; Jäger, E.-G. *Eur. J. Inorg. Chem.* **2009,** 465–477. doi:10.1002/ejic.200800891
14. Madeja, K.; König, E. *J. Inorg. Nucl. Chem.* **1963,** *25,* 377–385. doi:10.1016/0022-1902(63)80188-8
15. Baker, W. A., Jr.; Bobonich, H. M. *Inorg. Chem.* **1964,** *3,* 1184–1188. doi:10.1021/ic50018a027
16. Goodwin, H. A. *Coord. Chem. Rev.* **1976,** *18,* 293–325. doi:10.1016/S0010-8545(00)80430-0
17. Gütlich, P. *Struct. Bonding* **1981,** *44,* 83.
18. König, E. *Prog. Inorg. Chem.* **1987,** *35,* 527. doi:10.1002/9780470166369.ch6
19. Beattie, J. K. *Adv. Inorg. Chem.* **1988,** *32,* 1–53. doi:10.1016/S0898-8838(08)60230-5
20. Toftlund, H. *Coord. Chem. Rev.* **1989,** *94,* 67–108. doi:10.1016/0010-8545(89)80045-1
21. Gütlich, P.; Hauser, A. *Coord. Chem. Rev.* **1990,** *97,* 1–22. doi:10.1016/0010-8545(90)80076-6
22. König, E. *Struct. Bonding* **1991,** *76,* 51.
23. Gütlich, P.; Hauser, A.; Spiering, H. *Angew. Chem., Int. Ed. Engl.* **1994,** *33,* 2024–2054. doi:10.1002/anie.199420241
24. Gütlich, P.; Spiering, H.; Hauser, A. In *Inorganic Electronic Structure and Spectroscopy;* Solomon, E. I.; Lever, A. B. P., Eds.; Wiley: New York, 1999; Vol. 2, pp 575 ff.
25. Gütlich, P.; Garcia, Y.; Goodwin, H. A. *Chem. Soc. Rev.* **2000,** *29,* 419–427. doi:10.1039/b003504l
26. Gütlich, P.; Goodwin, H. A. Electronic Spin Crossover. In *Comprehensive Coordination Chemistry II;* McCleverty, J. A.; Meyer, T. J., Eds.; Elsevier, 2004; pp 421–426. doi:10.1016/B0-08-043748-6/01096-3
27. Gütlich, P.; Garcia, Y.; Spiering, H. Spin Transition Phenomena. In *Magnetism: Molecules to Materials IV;* Miller, J. S.; Drillon, M., Eds.; Wiley-VCH Verlag: Weinheim, Germany, 2003; pp 271–344.
28. Gütlich, P.; Goodwin, H. A., Eds. *Spin Crossover in Transition Metal Compounds I–III;* Top. Curr. Chem., Vol. 233, 234, 235; Springer-Verlag: Berlin, Heidelberg, New York, 2004.
29. Rao, C. N. R.; Seikh, M. M.; Narayana, C. Spin-State Transition in $LaCoO_3$ and Related Materials. *Spin Crossover in Transition Metal Compounds II;* Top. Curr. Chem., Vol. 234; Springer-Verlag: Berlin, Heidelberg, New York, 2004; pp 1–21. doi:10.1007/b95410
30. Goodwin, H. A. Spin Crossover in Cobalt(II) Systems. *Spin Crossover in Transition Metal Compounds II;* Top. Curr. Chem., Vol. 234; Springer-Verlag: Berlin, Heidelberg, New York, 2004; pp 23–47. doi:10.1007/b95411
31. Garcia, Y.; Gütlich, P. Thermal Spin Crossover in Mn(II), Mn(II), Cr(II) and Co(II) Coordination Compounds. *Spin Crossover in Transition Metal Compounds II;* Top. Curr. Chem., Vol. 234; Springer-Verlag: Berlin, Heidelberg, New York, 2004; pp 49–62. doi:10.1007/b95412
32. Thies, S.; Bornholdt, C.; Köhler, F.; Sönnichsen, F. D.; Näther, C.; Tuczek, F.; Herges, R. *Chem.–Eur. J.* **2010,** *16,* 10074–10083. doi:10.1002/chem.201000603
33. Venkataramani, S.; Jana, U.; Dommaschk, M.; Sönnichsen, F. D.; Tuczek, F.; Herges, R. *Science* **2011,** *331,* 445–448. doi:10.1126/science.1201180
34. Schläfer, H. L.; Gliemann, G. *Einführung in die Ligandenfeldtheorie;* Akademische Verlagsgesellschaft: Wiesbaden, Germany, 1980.
35. Shriver, D. F.; Atkins, P. W.; Langford, C. H. *Inorganic Chemistry,* 2nd ed.; Oxford University Press: Oxford, Melbourne, Tokyo, 1994.
36. Gütlich, P. *Z. Anorg. Allg. Chem.* **2012,** *638,* 15–43. doi:10.1002/zaac.201100416
37. Boinnard, D.; Bousseksou, A.; Dworkin, A.; Savariault, J. M.; Varret, F.; Tuchagues, J. P. *Inorg. Chem.* **1994,** *33,* 271–281. doi:10.1021/ic00080a015
38. Bousseksou, A.; Salmon, L.; Varret, F.; Tuchagues, J.-P. *Chem. Phys. Lett.* **1998,** *282,* 209–214. doi:10.1016/S0009-2614(97)01229-3
39. Weber, B.; Kaps, E.; Weigand, J.; Carbonera, C.; Letard, J.-F.; Achterhold, K.; Parak, F. G. *Inorg. Chem.* **2008,** *47,* 487–496. doi:10.1021/ic070067o
40. Klingele, J.; Kaase, D.; Hilgert, J.; Steinfeld, G.; Klingele, M. H.; Lach, J. *Dalton Trans.* **2010,** *39,* 4495–4507. doi:10.1039/b925107c
41. König, E.; Ritter, G.; Kulshreshtha, S. K.; Waigel, J.; Sacconi, L. *Inorg. Chem.* **1984,** *23,* 1241–1246. doi:10.1021/ic00177a015
42. Jesson, J. P.; Trofimenko, S.; Eaton, D. R. *J. Am. Chem. Soc.* **1967,** *89,* 3158–3164. doi:10.1021/ja00989a015
43. Hannay, C.; Hubin-Franskin, M.-J.; Grandjean, F.; Briois, V.; Itié, J.-P.; Polian, A.; Trofimenko, S.; Long, G. J. *Inorg. Chem.* **1997,** *36,* 5580–5588. doi:10.1021/ic970506r
44. Roux, C.; Zarembowitch, J.; Gallois, B.; Granier, T.; Claude, R. *Inorg. Chem.* **1994,** *33,* 2273–2279. doi:10.1021/ic00088a033

45. Edwards, M. P.; Hoff, C. D.; Curnutte, B.; Eck, J. S.; Purcell, K. F. *Inorg. Chem.* **1984,** *23,* 2613–2619. doi:10.1021/ic00185a015
46. Kunkeler, P. J.; van Koningsbruggen, P. J.; Cornelissen, J. P.; van der Horst, A. N.; van der Kraan, A. M.; Spek, A. L.; Haasnoot, J. G.; Reedijk, J. *J. Am. Chem. Soc.* **1996,** *118,* 2190–2197. doi:10.1021/ja943960s
47. Moliner, N.; Gaspar, A.; Muñoz, M. C.; Niel, V.; Cano, J.; Real, J. A. *Inorg. Chem.* **2001,** *40,* 3986–3991. doi:10.1021/ic0100976
48. Czernuszewicz, R. S.; Nakamoto, K.; Strommen, D. P. *Inorg. Chem.* **1980,** *19,* 793–797. doi:10.1021/ic50206a001
49. Childs, B. J.; Craig, D. C.; Scudder, M. L.; Goodwin, H. A. *Inorg. Chim. Acta* **1998,** *274,* 32–41. doi:10.1016/S0020-1693(97)05987-2
50. Wiehl, L. *Acta Crystallogr., Sect. B* **1993,** *49,* 289–303. doi:10.1107/S0108768192009042
51. Chang, H.-R.; McCusker, J. K.; Toftlund, H.; Wilson, S. R.; Trautwein, A. X.; Winkler, H.; Hendrickson, D. N. *J. Am. Chem. Soc.* **1990,** *112,* 6814–6827. doi:10.1021/ja00175a012
52. Martin, L. L.; Martin, R. L.; Murray, K. S.; Sargeson, A. M. *Inorg. Chem.* **1990,** *29,* 1387–1394. doi:10.1021/ic00332a021
53. Carlin, R. L.; van Duyneveldt, A. J. *Magnetic Properties of Transition Metal Compounds;* Springer: New York, 1977. doi:10.1007/978-3-642-87392-8
54. Kahn, O. *Molecular Magnetism;* Wiley-VCH: New York, 1993; pp 53 ff.
55. O'Connor, C. J. Magnetic-Susceptibility Measurement Techniques. *Molecule Based Magnetic Materials; ACS Symp. Ser.*, Vol. 644; 1996; pp 44–66. doi:10.1021/bk-1996-0644.ch004
56. Palacio, F. Magnetic Phenomena in Molecular Materials. In *Localized and itinerant molecular magnetism. From molecular assemblies to the devices;* Coronado, E.; Delhaès, P.; Gatteschi, D.; Miller, J. S., Eds.; NATO ASI Series C, Vol. 321; Kluwer Acadamic Publishers, 1996; pp 5–63.
57. Decurtins, S.; Gütlich, P.; Köhler, C. P.; Spiering, H.; Hauser, A. *Chem. Phys. Lett.* **1984,** *105,* 1–4. doi:10.1016/0009-2614(84)80403-0
58. Franke, P. L.; Haasnoot, J. G.; Zuur, A. P. *Inorg. Chim. Acta* **1982,** *59,* 5–9. doi:10.1016/S0020-1693(00)87299-0
59. Müller, E. W.; Ensling, J.; Spiering, H.; Gütlich, P. *Inorg. Chem.* **1983,** *22,* 2074–2078. doi:10.1021/ic00156a027
60. Decurtins, S.; Gütlich, P.; Hasselbach, K. M.; Hauser, A.; Spiering, H. *Inorg. Chem.* **1985,** *24,* 2174–2178. doi:10.1021/ic00208a013
61. Takemoto, J. H.; Hutchinson, B. *Inorg. Nucl. Chem. Lett.* **1972,** *8,* 769–772. doi:10.1016/0020-1650(72)80152-1
62. Takemoto, J. H.; Hutchinson, B. *Inorg. Chem.* **1973,** *12,* 705–708. doi:10.1021/ic50121a049
63. Takemoto, J. H.; Streusand, B.; Hutchinson, B. *Spectrochim. Acta, Part A* **1974,** *30,* 827–834. doi:10.1016/0584-8539(74)80199-6
64. Baker, W. A., Jr.; Long, G. J. *Chem. Commun.* **1965,** 368–369. doi:10.1039/c19650000368
65. König, E.; Madeja, K. *Inorg. Chem.* **1967,** *6,* 48–55. doi:10.1021/ic50047a011
66. König, E.; Madeja, K. *Spectrochim. Acta, Part A* **1967,** *23,* 45–54. doi:10.1016/0584-8539(67)80206-X
67. Herber, R.; Casson, L. M. *Inorg. Chem.* **1986,** *25,* 847–852. doi:10.1021/ic00226a025
68. Herber, R. H. *Inorg. Chem.* **1987,** *26,* 173–178. doi:10.1021/ic00248a034
69. Figg, D. C.; Herber, R. H. *Inorg. Chem.* **1990,** *29,* 2170–2173. doi:10.1021/ic00336a026
70. Bousseksou, A.; McGarvey, J. J.; Varret, F.; Real, J. A.; Tuchagues, J.-P.; Dennis, A. C.; Boillot, M. L. *Chem. Phys. Lett.* **2000,** *318,* 409–416. doi:10.1016/S0009-2614(00)00063-4
71. Gerdau, E.; Rüffer, R.; Winkler, H.; Tolksdorf, W.; Klages, C. P.; Hannon, J. P. *Phys. Rev. Lett.* **1985,** *54,* 835–838. doi:10.1103/PhysRevLett.54.835
72. Gerdau, E.; de Waard, H., Eds. *Nuclear resonant scattering of synchrotron radiation (Part A); Hyperfine Interact.*, Vol. 123–124; 1999.
73. Gerdau, E.; de Waard, H., Eds. *Nuclear resonant scattering of synchrotron radiation (Part B); Hyperfine Interact.*, Vol. 125; 2000.
74. Grünsteudel, H.; Paulsen, H.; Meyer-Klaucke, W.; Winkler, H.; Trautwein, A. X.; Grünsteudel, H. F.; Baron, A. Q. R.; Chumakov, A. I.; Rüffer, R.; Toftlund, H. *Hyperfine Interact.* **1998,** *113,* 311–317. doi:10.1023/A:1012641614937
75. Böttger, L. H.; Chumakov, A. I.; Grunert, C. M.; Gütlich, P.; Kusz, J.; Paulsen, H.; Ponkratz, U.; Rusanov, V.; Trautwein, A. X.; Wolny, J. A. *Chem. Phys. Lett.* **2006,** *429,* 189–193. doi:10.1016/j.cplett.2006.08.004
76. Ronayne, K. L.; Paulsen, H.; Höfer, A.; Dennis, A. C.; Wolny, J. A.; Chumakov, A. I.; Schünemann, V.; Winkler, H.; Spiering, H.; Bousseksou, A.; Gütlich, P.; Trautwein, A. X.; McGarvey, J. J. *Phys. Chem. Chem. Phys.* **2006,** *8,* 4685–4693. doi:10.1039/b610634j
77. Greenwood, N. N.; Gibb, T. C. *Mössbauer Spectroscopy;* Chapman and Hall: London, 1971. doi:10.1007/978-94-009-5697-1
78. Gütlich, P.; Bill, E.; Trautwein, A. X., Eds. *Mössbauer Spectroscopy and Transition Metal Chemistry – Fundamentals and Applications;* Springer-Verlag: Berlin, Heidelberg, 2011. doi:10.1007/978-3-540-88428-6
79. Gütlich, P. Spin Transition in Iron Compounds. In *Chemical Mössbauer Spectroscopy;* Herber, R. H., Ed.; Plenum: New York, 1984; pp 27–64. doi:10.1007/978-1-4613-2431-7_2
80. Gütlich, P. Spin Transition in Iron Complexes. In *Mössbauer Spectroscopy Applied to Inorganic Chemistry;* Long, G. J., Ed.; Plenum: New York, 1984; Vol. 1, pp 287–338.
81. Gütlich, P.; Garcia, Y. *J. Phys.: Conf. Ser.* **2010,** *217,* 012001. doi:10.1088/1742-6596/217/1/012001
82. Dészi, I.; Molnár, B.; Tarnóczi, T.; Tompa, K. *J. Inorg. Nucl. Chem.* **1967,** *29,* 2486–2490. doi:10.1016/0022-1902(67)80307-5
83. König, E.; Madeja, K. *Chem. Commun.* **1966,** 61–62. doi:10.1039/c19660000061
84. Sorai, M.; Seki, S. *J. Phys. Soc. Jpn.* **1972,** *33,* 575. doi:10.1143/JPSJ.33.575
85. Sorai, M.; Seki, S. *J. Phys. Chem. Solids* **1974,** *35,* 555–570. doi:10.1016/S0022-3697(74)80010-7
86. Kaji, K.; Sorai, M. *Thermochim. Acta* **1985,** *88,* 185–190. doi:10.1016/0040-6031(85)85426-5
87. Jakobi, R.; Romstedt, H.; Spiering, H.; Gütlich, P. *Angew. Chem., Int. Ed. Engl.* **1992,** *31,* 178–180. doi:10.1002/anie.199201781
88. Conti, A. J.; Kaji, K.; Nagano, Y.; Sena, K. M.; Yumoto, Y.; Chadha, R. K.; Rheingold, A. L.; Sorai, M.; Hendrickson, D. N. *Inorg. Chem.* **1993,** *32,* 2681–2693. doi:10.1021/ic00064a018
89. Garcia, Y.; Kahn, O.; Ader, J.-P.; Buzdin, A.; Meurdesoif, Y.; Guillot, M. *Phys. Lett. A* **2000,** *271,* 145–154. doi:10.1016/S0375-9601(00)00346-7
90. Martinho, P. N.; Gildea, B.; Harris, M. M.; Lemma, T.; Naik, A. D.; Müller-Bunz, H.; Keyes, T. E.; Garcia, Y.; Morgan, G. G. *Angew. Chem., Int. Ed.* **2012,** *50,* 12597–12601. doi:10.1002/anie.201205573

91. König, E.; Ritter, G.; Kulshreshta, S. K.; Waigel, J.; Goodwin, H. A. *Inorg. Chem.* **1984,** *23,* 1896–1902. doi:10.1021/ic00181a022
92. Kulshreshta, S. K.; Iyer, R. M.; König, E.; Ritter, G. *Chem. Phys. Lett.* **1984,** *110,* 201–204. doi:10.1016/0009-2614(84)80175-X
93. Kulshreshta, S. K.; Sasikala, R.; König, E. *Chem. Phys. Lett.* **1986,** *123,* 215–217. doi:10.1016/0009-2614(86)80015-X
94. Kulshreshta, S. K.; Iyer, R. M. *Chem. Phys. Lett.* **1987,** *134,* 239–244. doi:10.1016/0009-2614(87)87128-2
95. Neville, S. M.; Halder, G. J.; Chapman, K. W.; Duriska, M. B.; Moubaraki, B.; Murray, K. S.; Kepert, C. J. *J. Am. Chem. Soc.* **2009,** *131,* 12106–12108. doi:10.1021/ja905360g
96. Mikami, M.; Konno, M.; Saito, Y. *Chem. Phys. Lett.* **1979,** *63,* 566–569. doi:10.1016/0009-2614(79)80715-0
97. Köhler, C. P.; Jakobi, R.; Meissner, E.; Wiehl, L.; Spiering, H.; Gütlich, P. *J. Phys. Chem. Solids* **1990,** *51,* 239–247. doi:10.1016/0022-3697(90)90052-H
98. Garcia, Y.; Guionneau, P.; Bravic, G.; Chasseau, D.; Howard, J. A. K.; Kahn, O.; Ksenofontov, V.; Reiman, S.; Gütlich, P. *Eur. J. Inorg. Chem.* **2000,** 1531–1538. doi:10.1002/1099-0682(200007)2000:7<1531::AID-EJIC1531>3.0.CO;2-C
99. Kusz, J.; Gütlich, P.; Spiering, H. Structural Investigations of Tetrazole Complexes of Iron(II). In *Spin Crossover in Transition Metal Compounds II;* Gütlich, P.; Goodwin, H. A., Eds.; *Top. Curr. Chem.*, Vol. 234; Springer-Verlag: Berlin, Heidelberg, 2004; pp 129–153.
100. Guionneau, P.; Marchivie, M.; Bravic, G.; Létard, J.-F.; Chasseau, D. Structural Aspects of Spin Crossover. Example of the $[Fe^{II}L_n(NCS)_2]$ Complexes. In *Spin Crossover in Transition Metal Compounds II;* Gütlich, P.; Goodwin, H. A., Eds.; *Top. Curr. Chem.*, Vol. 234; Springer-Verlag: Berlin, Heidelberg, 2004; pp 97–128.
101. Spiering, H.; Willenbacher, N. *J. Phys.: Condens. Matter* **1989,** *1,* 10089–10105. doi:10.1088/0953-8984/1/50/011
102. Willenbacher, N.; Spiering, H. *J. Phys. C: Solid State Phys.* **1988,** *21,* 1423–1440. doi:10.1088/0022-3719/21/8/017
103. Gütlich, P.; Köppen, H.; Steinhäuser, H. G. *Chem. Phys. Lett.* **1980,** *74,* 475–480. doi:10.1016/0009-2614(80)85256-0
104. Penner-Hahn, J. E. *Coord. Chem. Rev.* **1999,** *190,* 1101–1123. doi:10.1016/S0010-8545(99)00160-5
105. Michalowicz, A.; Moscovici, J.; Ducourant, B.; Cracco, D.; Kahn, O. *Chem. Mater.* **1995,** *7,* 1833–1842. doi:10.1021/cm00058a013
106. Michalowicz, A.; Moscovici, J.; Kahn, O. *J. Phys. IV* **1997,** *7,* C2-633–C2-635. doi:10.1051/jp4/1997124
107. Garcia, Y.; van Koningsbruggen, P. J.; Bravic, G.; Guionneau, P.; Chasseau, D.; Cascarano, G. L.; Moscovici, J.; Lambert, K.; Michalowicz, A.; Kahn, O. *Inorg. Chem.* **1997,** *36,* 6357–6365. doi:10.1021/ic970895p
108. Michalowicz, A.; Moscovici, J.; Garcia, Y.; Kahn, O. *J. Synchrotron Radiat.* **1999,** *6,* 231–232. doi:10.1107/S090904959900093X
109. Michalowicz, A.; Moscovici, J.; Charton, J.; Sandid, F.; Benamrane, F.; Garcia, Y. *J. Synchrotron Radiat.* **2001,** *8,* 701–703. doi:10.1107/S0909049500018057
110. Kajcsos, Z.; Vértes, A.; Szeles, C.; Burger, K.; Spiering, H.; Gütlich, P.; Abbe, J. C.; Haissler, H.; Brauer, C. P.; Köhler, C. P. In *Positron Annihilation;* Jain, P. C.; Singru, R. M.; Gopinathan, K. P., Eds.; World Scientific: Singapore, 1985; pp 195 ff.
111. Vértes, A.; Süvegh, K.; Hinek, R.; Gütlich, P. *Hyperfine Interact.* **1994,** *84,* 483–489. doi:10.1007/BF02060698
112. Chum, H. L.; Vanin, J. A.; Holanda, M. I. D. *Inorg. Chem.* **1982,** *21,* 1146–1152. doi:10.1021/ic00133a053
113. Kläui, W. *J. Chem. Soc., Chem. Commun.* **1979,** 700. doi:10.1039/C39790000700
114. Gütlich, P.; McGarvey, B. R.; Kläui, W. *Inorg. Chem.* **1980,** *19,* 3704–3706. doi:10.1021/ic50214a026
115. Eberspach, W.; Murr, N. E.; Kläui, W. *Angew. Chem., Int. Ed. Engl.* **1982,** *21,* 915–916. doi:10.1002/anie.198209151
116. Navon, G.; Kläui, W. *Inorg. Chem.* **1984,** *23,* 2722–2725. doi:10.1021/ic00185a036
117. Kläui, W.; Eberspach, W.; Gütlich, P. *Inorg. Chem.* **1987,** *26,* 3977–3982. doi:10.1021/ic00271a004
118. Janiak, C.; Scharmann, T. G.; Bräuniger, T.; Holubová, J.; Nádvornik, M. *Z. Anorg. Allg. Chem.* **1998,** *624,* 769–774. doi:10.1002/(SICI)1521-3749(199805)624:5<769::AID-ZAAC769>3.0.CO;2-#
119. Rao, P. S.; Reuveni, A.; McGarvey, B. R.; Ganguli, P.; Gütlich, P. *Inorg. Chem.* **1981,** *20,* 204–207. doi:10.1021/ic50215a041
120. Vreugdenhil, W.; Haasnoot, J. G.; Kahn, O.; Thuéry, P.; Reedijik, J. *J. Am. Chem. Soc.* **1987,** *109,* 5272–5273. doi:10.1021/ja00251a038
121. Ozarowski, A.; McGarvey, B. R. *Inorg. Chem.* **1989,** *28,* 2262–2266. doi:10.1021/ic00311a005
122. Cantin, C.; Kliava, J.; Servant, Y.; Sommier, L.; Kahn, O. *Appl. Magn. Reson.* **1997,** *12,* 87–93. doi:10.1007/BF03161994
123. Cantin, C.; Daubric, H.; Kliava, J.; Kahn, O. *Solid State Commun.* **1998,** *108,* 17–22. doi:10.1016/S0038-1098(98)00304-4
124. Cantin, C.; Daubric, H.; Kliava, J.; Servant, Y.; Sommier, L.; Kahn, O. *J. Phys.: Condens. Matter* **1998,** *10,* 7057. doi:10.1088/0953-8984/10/31/021
125. Daubric, H.; Cantin, C.; Thomas, C.; Kliava, J.; Létard, J.-F.; Kahn, O. *Chem. Phys.* **1999,** *244,* 75–88. doi:10.1016/S0301-0104(99)00093-2
126. Daubric, H.; Kliava, J.; Guionneau, P.; Chasseau, D.; Letard, J. F.; Kahn, O. *J. Phys.: Condens. Matter* **2000,** *12,* 5481–5494. doi:10.1088/0953-8984/12/25/312
127. Shioyasu, N.; Kagetsu, K.; Mishima, K.; Kubo, M. K.; Tominaga, T.; Nishiyama, K.; Nagamine, K. *Hyperfine Interact.* **1994,** *84,* 477–481. doi:10.1007/BF02060697
128. Kubo, M. K. *Anal. Sci.* **2001,** *17,* i653–i656.
129. Campbell, S. J.; Ksenofontov, V.; Garcia, Y.; Lord, J. S.; Reiman, S.; Gütlich, P. *Hyperfine Interact. (C)* **2002,** *5,* 363–366. doi:10.1007/978-94-010-0281-3_90
130. Campbell, S. J.; Ksenofontov, V.; Garcia, Y.; Lord, J. S.; Boland, Y.; Gütlich, P. *J. Phys. Chem. B* **2003,** *107,* 14289–14295. doi:10.1021/jp036078u
131. Blundell, S. J.; Pratt, F. L.; Lancaster, T.; Marshall, I. M.; Steer, C. A.; Heath, S. L.; Létard, J.-F.; Sugano, T.; Mihailovic, D.; Omerzu, A. *Polyhedron* **2003,** *22,* 1973–1980. doi:10.1016/S0277-5387(03)00257-2
132. Blundell, S. J.; Pratt, F. L.; Lancaster, T.; Marshall, I. M.; Steer, C. A.; Hayes, W.; Sugano, T.; Létard, J.-F.; Caneshi, A.; Gatteschi, D.; Heath, S. L. *Physica B* **2003,** *326,* 556–562. doi:10.1016/S0921-4526(02)01688-5
133. Blundell, S. J.; Pratt, F. L.; Steer, C. A.; Marshall, I. M.; Létard, J.-F. *J. Phys. Chem. Solids* **2004,** *65,* 25–28. doi:10.1016/j.jpcs.2003.08.017
134. Blundell, S. J.; Lancaster, T.; Pratt, F. L.; Steer, C. A.; Brooks, M. L.; Létard, J.-F. *J. Phys. IV* **2004,** *114,* 601–605. doi:10.1051/jp4:2004114143
135. Garcia, Y.; Ksenofontov, V.; Campbell, S. J.; Lord, J. S.; Boland, Y.; Gütlich, P. *Phys. Status Solidi A* **2004,** *201,* 3309–3313. doi:10.1002/pssa.200405458

136. Garcia, Y.; Ksenofontov, V.; Campbell, S. J.; Lord, J. S.; Boland, Y.; Gütlich, P. *J. Phys. Chem. B* **2004,** *108,* 17838–17844. doi:10.1021/jp046695y
137. Roubeau, O.; Gubbens, P. C. M.; Visser, D.; Blaauw, M.; Dalmas de Réotier, P.; Yaouanc, A.; Haasnoot, J. G.; Reedijk, J.; Sakarya, S.; Jayasooriya, U. A.; Cottrell, S. P.; King, P. J. C. *Chem. Phys. Lett.* **2004,** *395,* 177–181. doi:10.1016/j.cplett.2004.07.016
138. Ksenofontov, V.; Garcia, Y.; Campbell, S. J.; Boland, Y.; Lord, J. S.; Gütlich, P. *Physica B* **2006,** *374–375,* 126–129. doi:10.1016/j.physb.2005.11.032
139. Garcia, Y.; Campbell, S. J.; Lord, J. S.; Boland, Y.; Ksenofontov, V.; Gütlich, P. *J. Phys. Chem. B* **2007,** *111,* 11111–11119. doi:10.1021/jp072399k
140. Garcia, Y.; Campbell, S. J.; Lord, J. S.; Gütlich, P. *Inorg. Chim. Acta* **2008,** *361,* 3577–3585. doi:10.1016/j.ica.2008.03.034
141. Roduner, E. *Chem. Soc. Rev.* **1993,** *22,* 337–346. doi:10.1039/cs9932200337
142. Roduner, E. Aspects of muon chemistry. In *Muon Science: Muons in Physics, Chemistry and Materials;* Lee, S. L.; Kilcoyne, S. H.; Cywinski, R., Eds.; Institute of Physics Publishing: London, Philadelphia, 1999; pp 173–209.
143. Cox, S. F. J. *J. Phys. C: Solid State Phys.* **1987,** *20,* 3187. doi:10.1088/0022-3719/20/22/005
144. Blundell, S. J. *Contemp. Phys.* **1999,** *40,* 175–192. doi:10.1080/001075199181521
145. Blundell, S. J. *Philos. Trans. R. Soc. London, Ser. A* **1999,** *357,* 2923–2937. doi:10.1098/rsta.1999.0474
146. Lee, S. L.; Kilcoyne, S. H.; Cywinski, R., Eds., Muon Science: Muons in Physics, Chemistry and Materials, Proceedings of the 50th Scottish University Summer School in Physics, vol. 51, A Nato Advanced Study Institute, Institute of Physics, 1999.
147. Blundell, S. J. *Chem. Rev.* **2004,** *104,* 5717–5736. doi:10.1021/cr030632e
148. Yaouanc, A.; Dalmas de Réotier, P. *Muon spin rotation, relaxation and resonance - Applications to Condensed Matter;* Oxford University Press: Oxford, 2011.
149. Hauser, A. Light-Induced Spin Crossover and the High-Spin→Low-Spin Relaxation. In *Spin Crossover in Transition Metal Compounds II;* Gütlich, P.; Goodwin, H. A., Eds.; *Top. Curr. Chem.*, Vol. 234; Springer-Verlag: Berlin, Heidelberg, 2004; pp 155–198.
150. Hayami, S.; Hiki, K.; Kawahara, T.; Maeda, Y.; Urakami, D.; Inoue, K.; Ohama, M.; Kawata, S.; Sato, O. *Chem.–Eur. J.* **2009,** *15,* 3497–3508. doi:10.1002/chem.200802395
151. Hauser, A. *Comments Inorg. Chem.* **1995,** *17,* 17–40. doi:10.1080/02603599508035780 And references therein.
152. Buhks, E.; Navon, G.; Bixon, M.; Jortner, J. *J. Am. Chem. Soc.* **1980,** *102,* 2918–2923. doi:10.1021/ja00529a009
153. Renz, F.; Oshio, H.; Ksenofontov, V.; Waldeck, M.; Spiering, H.; Gütlich, P. *Angew. Chem., Int. Ed.* **2000,** *39,* 3699–3700. doi:10.1002/1521-3773(20001016)39:20<3699::AID-ANIE3699>3.0.CO;2-Z
154. Vankó, G.; Renz, F.; Molnár, G.; Neisius, T.; Kárpáti, S. *Angew. Chem., Int. Ed.* **2007,** *46,* 5306–5309. doi:10.1002/anie.200604432
155. Renz, F.; Spiering, H.; Goodwin, H. A.; Gütlich, P. *Hyperfine Interact.* **2000,** *126,* 155–158. doi:10.1023/A:1012609231853
156. Boillot, M.-L.; Zarembowitch, J.; Sour, A. Ligand-Driven Light-Induced Spin Change (LD-LISC): A Promising Photomagnetic Effect. In *Spin Crossover in Transition Metal Compounds II;* Gütlich, P.; Goodwin, H. A., Eds.; *Top. Curr. Chem.*, Vol. 234; Springer-Verlag: Berlin, Heidelberg, 2004; pp 261–276. doi:10.1007/b95419
157. Gütlich, P.; Garcia, Y.; Woike, Y. *Coord. Chem. Rev.* **2001,** *219–221,* 839–879. doi:10.1016/S0010-8545(01)00381-2
158. Ewald, A. H.; Martin, R. L.; Sinn, E.; White, A. H. *Inorg. Chem.* **1969,** *8,* 1837–1846. doi:10.1021/ic50079a006
159. Gütlich, P.; Ksenofontov, V.; Gaspar, A. B. *Coord. Chem. Rev.* **2005,** *249,* 1811–1829. doi:10.1016/j.ccr.2005.01.022
160. Drickamer, H. G.; Frank, C. W. *Electronic Transitions and the High Pressure Chemistry and Physics of Solids;* Chapman and Hall: London, 1973.
161. Pebler, J. *Inorg. Chem.* **1983,** *22,* 4125–4128. doi:10.1021/ic00168a059
162. Long, G. J.; Hutchinson, B. B. *Inorg. Chem.* **1987,** *26,* 608–613. doi:10.1021/ic00251a023
163. Konno, M.; Mikami-Kido, M. *Bull. Chem. Soc. Jpn.* **1991,** *64,* 339–345. doi:10.1246/bcsj.64.339
164. Meissner, E.; Köppen, H.; Köhler, C. P.; Spiering, H.; Gütlich, P. *Hyperfine Interact.* **1987,** *36,* 1–12. doi:10.1007/BF02396844
165. Romstedt, H.; Hauser, A.; Spiering, H. *J. Phys. Chem. Solids* **1998,** *59,* 265–275. doi:10.1016/S0022-3697(97)00142-X
166. Baran, M.; Dyakonov, V. P.; Gladczuk, L.; Levchenko, G.; Piechota, S.; Shymchak, G. *Physica C* **1995,** *241,* 383–388. doi:10.1016/0921-4534(94)02359-X
167. Ksenofontov, V.; Spiering, H.; Schreiner, A.; Levchenko, G.; Goodwin, H. A.; Gütlich, P. *J. Phys. Chem. Solids* **1999,** *60,* 393–399. doi:10.1016/S0022-3697(98)00259-5
168. McCammon, C. *J. Mineral. Petrol. Sci.* **2006,** *101,* 130–144. doi:10.2465/jmps.101.130
169. Speziale, S.; Milner, A.; Lee, V. E.; Clark, S. M.; Pasternak, M. P.; Jeanloz, R. *Proc. Natl. Acad. Sci. U. S. A.* **2005,** *102,* 17918–17922. doi:10.1073/pnas.0508919102
170. Xu, W. M.; Pasternak, M. P.; Rozenberg, G. K.; Taylor, R. D. *Hyperfine Interact.* **2002,** *141–142,* 243–247. doi:10.1023/A:1021243128644
171. Lyubutin, I. S.; Gavriliuk, A. G. *Phys.-Usp.* **2009,** *52,* 989–1018. doi:10.3367/UFNe.0179.200910b.1047
172. Lyubutin, I. S.; Ovchinnikov, S. G. *J. Magn. Magn. Mater.* **2012,** *324,* 3538–3541. doi:10.1016/j.jmmm.2012.02.084
173. Ksenofontov, V.; Gaspar, A. B.; Gütlich, P. Pressure Effect Studies on Spin Crossover and Valence Tautomeric Systems. In *Spin Crossover in Transition Metal Compounds III;* Gütlich, P.; Goodwin, H. A., Eds.; *Top. Curr. Chem.*, Vol. 235; Springer-Verlag: Berlin, Heidelberg, 2004; pp 23–64.
174. Gütlich, P.; Gaspar, A. B.; Ksenofontov, V.; Garcia, Y. *J. Phys.: Condens. Matter* **2004,** *16,* S1087. doi:10.1088/0953-8984/16/14/019
175. Gütlich, P.; Gaspar, A. B.; Garcia, Y.; Ksenofontov, V. *C. R. Chim.* **2007,** *10,* 21–36. doi:10.1016/j.crci.2006.09.011
176. Ksenofontov, V.; Gaspar, A. B.; Levchenko, G.; Fitzsimmons, B.; Gütlich, P. *J. Phys. Chem. B* **2004,** *108,* 7723–7727. doi:10.1021/jp049512g
177. Garcia, Y.; van Koningsbruggen, P. J.; Lapouyade, R.; Fournès, L.; Rabardel, L.; Kahn, O.; Ksenofontov, V.; Levchenko, G.; Gütlich, P. *Chem. Mater.* **1998,** *10,* 2426–2433. doi:10.1021/cm980107+
178. Garcia, Y.; Ksenofontov, V.; Levchenko, G.; Gütlich, P. *J. Mater. Chem.* **2000,** *10,* 2274–2276. doi:10.1039/b003794j

179. Garcia, Y.; Ksenofontov, V.; Levchenko, G.; Schmitt, G.; Gütlich, P. *J. Phys. Chem. B* **2000,** *104,* 5045–5048. doi:10.1021/jp0004922
180. Garcia, Y.; Moscovici, J.; Michalowicz, A.; Ksenofontov, V.; Levchenko, G.; Bravic, G.; Chasseau, D.; Gütlich, P. *Chem.–Eur. J.* **2002,** *8,* 4992–5000. doi:10.1002/1521-3765(20021104)8:21<4992::AID-CHEM4992>3.0.CO;2-8
181. Garcia, Y.; Ksenofontov, V.; Gütlich, P. *Hyperfine Interact.* **2002,** *139–140,* 543–551.
182. Fleisch, J.; Gütlich, P.; Hasselbach, K. M.; Müller, W. *J. Phys., Colloq.* **1974,** *6,* 659–662.
183. Renovitch, G. A.; Baker, W. A., Jr. *J. Am. Chem. Soc.* **1967,** *89,* 6377–6378. doi:10.1021/ja01000a083
184. Sorai, M.; Ensling, J.; Hasselbach, K. M.; Gütlich, P. *Chem. Phys.* **1977,** *20,* 197–208. doi:10.1016/0301-0104(77)85023-4
185. Sorai, M.; Ensling, J.; Gütlich, P. *Chem. Phys.* **1976,** *18,* 199–209. doi:10.1016/0301-0104(76)87047-4
186. Wiehl, L.; Kiel, G.; Köhler, C. P.; Spiering, H.; Gütlich, P. *Inorg. Chem.* **1986,** *25,* 1565–1571. doi:10.1021/ic00230a012
187. Köppen, H.; Müller, E. W.; Köhler, C. P.; Spiering, H.; Meissner, E.; Gütlich, P. *Chem. Phys. Lett.* **1982,** *91,* 348–352. doi:10.1016/0009-2614(82)83298-3
188. Chernyshov, D.; Hostettler, M.; Törnroos, K.; Bürgi, H.-B. *Angew. Chem., Int. Ed.* **2003,** *42,* 3825–3830. doi:10.1002/anie.200351834
189. Kepenekian, M.; Sánchez Costa, J.; Le Guennic, B.; Maldivi, P.; Bonnet, S.; Reedijk, J.; Gamez, P.; Robert, V. *Inorg. Chem.* **2010,** *49,* 11057–11061. doi:10.1021/ic101669b
190. Klingele, J.; Kaase, D.; Klingele, M. H.; Lach, J.; Demeshko, S. *Dalton Trans.* **2010,** *39,* 1689–1691. doi:10.1039/b924223f
191. Köppen, H. Ph.D. Thesis, University of Mainz, Mainz, Germany, 1985.
192. Qi, Y.; Müller, E. W.; Spiering, H.; Gütlich, P. *Chem. Phys. Lett.* **1983,** *101,* 503–505. doi:10.1016/0009-2614(83)87521-6
193. Bousseksou, A.; Varret, F.; Goiran, M.; Boukheddaden, K.; Tuchagues, J.-P. The Spin Crossover Phenomenon Under High Magnetic Field. In *Spin Crossover in Transition Metal Compounds III;* Gütlich, P.; Goodwin, H. A., Eds.; Top. Curr. Chem., Vol. 235; Springer-Verlag: Berlin, Heidelberg, New York, 2004; pp 65–84.
194. Haddad, M. S.; Federer, W. D.; Lynch, M. W.; Hendrickson, D. N. *J. Am. Chem. Soc.* **1980,** *102,* 1468–1470. doi:10.1021/ja00524a065
195. Müller, E. W.; Spiering, H.; Gütlich, P. *Inorg. Chem.* **1984,** *23,* 119–120. doi:10.1021/ic00169a026
196. Wei, H. H.; Jean, Y. C. *Chem. Phys. Lett.* **1984,** *106,* 523–526. doi:10.1016/0009-2614(84)85375-0
197. Gaspar, A. B.; Muñoz, M. C.; Real, J. A. *J. Mater. Chem.* **2006,** *16,* 2522–2533. doi:10.1039/b603488h
198. Zein, S.; Borshch, S. A. *J. Am. Chem. Soc.* **2005,** *127,* 16197–16201. doi:10.1021/ja054282k
199. Real, A.; Zarembowitch, J.; Kahn, O.; Solans, X. *Inorg. Chem.* **1987,** *26,* 2939–2943. doi:10.1021/ic00265a005
200. Real, J. A.; Castro, I.; Bousseksou, A.; Verdaguer, M.; Burriel, R.; Castro, M.; Linares, J.; Varret, F. *Inorg. Chem.* **1997,** *36,* 455–464. doi:10.1021/ic960509o
201. Gaspar, A. B.; Ksenofontov, V.; Reiman, S.; Gütlich, P.; Thompson, A. L.; Goeta, A. E.; Muñoz, M. C.; Real, J. A. *Chem.–Eur. J.* **2006,** *36,* 9289–9298. doi:10.1002/chem.200600559
202. Létard, J.-F.; Real, J. A.; Moliner, N.; Gaspar, A. B.; Capes, L.; Cador, O.; Kahn, O. *J. Am. Chem. Soc.* **1999,** *121,* 10630–10631. doi:10.1021/ja991476p
203. Gaspar, A. B.; Ksenofontov, V.; Real, J. A.; Gütlich, P. *Chem. Phys. Lett.* **2003,** *373,* 385–391. doi:10.1016/S0009-2614(03)00560-8
204. Gaspar, A. B.; Ksenofontov, V.; Martínez, V.; Muñoz, M. C.; Real, J. A.; Gütlich, P. *Eur. J. Inorg. Chem.* **2004,** 4770–4773. doi:10.1002/ejic.200400586
205. Batten, S. R.; Bjernemose, J.; Jensen, P.; Leita, B. A.; Murray, K. S.; Moubaraki, B.; Smith, J. P.; Toftlund, H. *Dalton Trans.* **2004,** 3370–3375. doi:10.1039/B410425K
206. Ksenofontov, V.; Gaspar, A. B.; Real, J. A.; Gütlich, P. *J. Phys. Chem. B* **2001,** *105,* 12266–12271. doi:10.1021/jp0116961
207. Ksenofontov, V.; Spiering, H.; Reiman, S.; Garcia, Y.; Gaspar, A. B.; Moliner, N.; Real, J. A.; Gütlich, P. *Chem. Phys. Lett.* **2001,** *348,* 381–386. doi:10.1016/S0009-2614(01)01114-9
208. Ksenofontov, V.; Spiering, H.; Reiman, S.; Garcia, Y.; Gaspar, A. B.; Real, J. A.; Gütlich, P. *Hyperfine Interact.* **2002,** *141–142,* 47–52.
209. Chastanet, G.; Gaspar, A. B.; Real, J. A.; Létard, J.-F. *Chem. Commun.* **2001,** 819–820. doi:10.1039/b100426n
210. Chastanet, G.; Carbonera, C.; Mingotaud, C.; Létard, J.-F. *J. Mater. Chem.* **2004,** *14,* 3516–3523. doi:10.1039/b408079c
211. Real, J. A.; Gaspar, A. B.; Muñoz, M. C.; Gütlich, P.; Ksenofontov, V.; Spiering, H. Bipyrimidine-Bridged Dinuclear Iron(II) Spin Crossover Compounds. In *Spin Crossover in Transition Metal Compounds I;* Gütlich, P.; Goodwin, H. A., Eds.; *Top. Curr. Chem.*, Vol. 233; Springer-Verlag: Berlin, Heidelberg, 2004; pp 167–193.
212. Moussa, N. O.; Molnár, G.; Bonhommeau, S.; Zwick, A.; Mouri, S.; Tanaka, K.; Real, J. A.; Bousseksou, A. *Phys. Rev. Lett.* **2005,** *94,* 107205. doi:10.1103/PhysRevLett.94.107205
213. Bousseksou, A.; Molnár, G.; Real, J. A.; Tanaka, K. *Coord. Chem. Rev.* **2007,** *251,* 1822–1833. doi:10.1016/j.ccr.2007.02.023
214. Ksenofontov, V.; Gaspar, A. B.; Niel, V.; Reiman, S.; Real, J. A.; Gütlich, P. *Chem.–Eur. J.* **2004,** *10,* 1291–1298. doi:10.1002/chem.200305275
215. Ortega-Villar, N.; Thompson, A. L.; Muñoz, M. C.; Ugalde-Saldívar, V. M.; Goeta, A. E.; Moreno-Esparza, R.; Real, J. A. *Chem.–Eur. J.* **2005,** *11,* 5721–5734. doi:10.1002/chem.200500171
216. Klingele, M. H.; Moubaraki, B.; Cashion, J. D.; Murray, K. S.; Brooker, S. *Chem. Commun.* **2005,** 987–989. doi:10.1039/b415891a
217. Tuna, F.; Lees, M. R.; Clarkson, G. J.; Hannon, M. J. *Chem.–Eur. J.* **2004,** *10,* 5737–5750. doi:10.1002/chem.200400518
218. Nakano, K.; Kawata, S.; Yoneda, K.; Fuyuhiro, A.; Yagi, T.; Nasu, S.; Morimoto, S.; Kaizaki, S. *Chem. Commun.* **2004,** 2892–2893. doi:10.1039/b411190g
219. Yoneda, K.; Adachi, K.; Hayami, S.; Maeda, Y.; Katada, M.; Fuyuhiro, A.; Kawata, S.; Kaizaki, S. *Chem. Commun.* **2006,** 45–47. doi:10.1039/b512266j
220. Nakano, K.; Suemura, N.; Yoneda, K.; Kawata, S.; Kaizaki, S. *Dalton Trans.* **2005,** 740–743. doi:10.1039/b416986g
221. Grunert, C. M.; Reiman, S.; Spiering, H.; Kitchen, J. A.; Brooker, S.; Gütlich, P. *Angew. Chem., Int. Ed.* **2008,** *47,* 2997–2999. doi:10.1002/anie.200705778
222. Archer, R. J.; Hawes, C. S.; Jameson, G. N. L.; McKee, V.; Moubaraki, B.; Chilton, N.; Murray, K. S.; Schmitt, W.; Kruger, P. E. *Dalton Trans.* **2011,** *40,* 12368–12373. doi:10.1039/c1dt11381j
223. Kaiba, A.; Shepherd, H. J.; Fedaoui, D.; Rosa, P.; Goeta, A. E.; Rebbani, N.; Létard, J.-F.; Guionneau, P. *Dalton Trans.* **2010,** *39,* 2910–2918. doi:10.1039/b914841h

224. Verat, A. Yu.; Ould-Moussa, N.; Jeanneau, E.; Le Guennic, B.; Bousseksou, A.; Borshch, S. A.; Matouzenko, G. S. *Chem.–Eur. J.* **2009,** *15,* 10070–10082. doi:10.1002/chem.200900921
225. Matouzenko, G. S.; Jeanneau, E.; Verat, A. Yu.; Bousseksou, A. *Dalton Trans.* **2011,** *40,* 9608–9618. doi:10.1039/c1dt10312a
226. Matouzenko, G. S.; Jeanneau, E.; Verat, A. Yu.; de Gaetano, Y. *Eur. J. Inorg. Chem.* **2012,** 969–977. doi:10.1002/ejic.201101178
227. Weber, B.; Kaps, E. S.; Obel, J.; Achterhold, K.; Parak, F. G. *Inorg. Chem.* **2008,** *47,* 10779–10787. doi:10.1021/ic801388a
228. Kitchen, J.; White, N. G.; Jameson, G. N. L.; Tallon, J. L.; Brooker, S. *Inorg. Chem.* **2011,** *50,* 4586–4597. doi:10.1021/ic200308k
229. Amoore, J. J. M.; Neville, S. M.; Moubaraki, B.; Iremonger, S. S.; Létard, J.-F.; Kepert, C. J. *Chem.–Eur. J.* **2010,** *16,* 1973–1982. doi:10.1002/chem.200901809
230. Garcia, Y.; Grunert, M.; Reiman, S.; van Campenhoudt, O.; Gütlich, P. *Eur. J. Inorg. Chem.* **2006,** 3333–3339. doi:10.1002/ejic.200600365
231. Pelleteret, D.; Clérac, R.; Mathonière, C.; Harté, E.; Schmitt, W.; Kruger, P. E. *Chem. Commun.* **2009,** 221–223. doi:10.1039/b816196h
232. Fujita, K.; Kawamoto, R.; Tsubouchi, R.; Sunatsuki, Y.; Kojima, M.; Iijima, S.; Matsimoto, N. *Chem. Lett.* **2007,** *36,* 1284–1285. doi:10.1246/cl.2007.1284
233. Sunatsuki, Y.; Maruyama, H.; Fujita, K.; Suzuki, T.; Kojima, M.; Matsumoto, N. *Bull. Chem. Soc. Jpn.* **2009,** *82,* 1497–1505. doi:10.1246/bcsj.82.1497
234. Roubeau, O.; Gamez, P.; Teat, S. J. *Eur. J. Inorg. Chem.* **2013**. doi:10.1002/ejic.201201126
235. Garcia, Y.; Robert, F.; Naik, A. D.; Zhou, G.; Tinant, B.; Robeyns, K.; Michotte, S.; Piraux, L. *J. Am. Chem. Soc.* **2011,** *133,* 15850–15853. doi:10.1021/ja205974q
236. Kolnaar, J. J. A.; de Heer, M. L.; Kooijman, H.; Spek, A. L.; Schmitt, G.; Ksenofontov, V.; Gütlich, P.; Haasnoot, J. G.; Reedijk, J. *Eur. J. Inorg. Chem.* **1999,** 881–886. doi:10.1002/(SICI)1099-0682(199905)1999:5<881::AID-EJIC881>3.0.CO;2-Q
237. Vos, G.; Le Fêbre, R. A.; de Graaff, R. A. G.; Haasnoot, J. G.; Reedijk, J. *J. Am. Chem. Soc.* **1983,** *105,* 1682–1683. doi:10.1021/ja00344a060
238. Vos, G.; de Graaff, R. A. G.; Haasnoot, J. G.; van der Kraan, A. M.; de Vaal, P.; Reedijk, J. *Inorg. Chem.* **1984,** *23,* 2905–2910. doi:10.1021/ic00186a038
239. Chong, C.; Berini, B.; Boukheddaden, K.; Codjovi, E.; Linarès, J.; Garcia, Y.; Naik, A. D.; Varret, F. *Phys. Status Solidi A* **2010,** *207,* 1227–1231. doi:10.1002/pssa.200925502
240. Wolny, J. A.; Rackwitz, S.; Achterhold, K.; Garcia, Y.; Muffler, K.; Naik, A. D.; Schünemann, V. *Phys. Chem. Chem. Phys.* **2010,** *12,* 14782–14788. doi:10.1039/c0cp01108h
241. Kolnaar, J. J. A.; van Dijk, G.; Kooijman, H.; Spek, A. L.; Ksenofontov, V. G.; Gütlich, P.; Haasnoot, J. G.; Reedijk, J. *Inorg. Chem.* **1997,** *36,* 2433–2440. doi:10.1021/ic9612010
242. Thomann, M.; Kahn, O.; Guilhem, J.; Varret, F. *Inorg. Chem.* **1994,** *33,* 6029–6037. doi:10.1021/ic00104a010
243. Kahn, O.; Codjovi, E. *Philos. Trans. R. Soc. London, A* **1996,** *354,* 359–379. doi:10.1098/rsta.1996.0012
244. Dîrtu, M. M.; Rotaru, A.; Gillard, D.; Linares, J.; Codjovi, E.; Tinant, B.; Garcia, Y. *Inorg. Chem.* **2009,** *48,* 7838–7852. doi:10.1021/ic900814b
245. Robert, F.; Naik, A. D.; Garcia, Y. *J. Phys.: Conf. Ser.* **2010,** *217,* 012031. doi:10.1088/1742-6596/217/1/012031
246. Savard, D.; Cook, C.; Enright, G. D.; Korobkov, I.; Burchell, T. J.; Murugesu, M. *CrystEngComm* **2011,** *13,* 5190–5197. doi:10.1039/c1ce05275f
247. Psomas, G.; Bréfuel, N.; Dahan, F.; Tuchagues, J.-P. *Inorg. Chem.* **2004,** *43,* 4590–4594. doi:10.1021/ic049877f
248. Schneider, B.; Demeshko, S.; Dechert, S.; Meyer, F. *Angew. Chem., Int. Ed.* **2010,** *49,* 9274–9277. doi:10.1002/anie.201001536
249. Breuning, E.; Ruben, M.; Lehn, J.-M.; Renz, F.; Garcia, Y.; Ksenofontov, V.; Gütlich, P.; Wegelius, E.; Rissanen, K. *Angew. Chem., Int. Ed.* **2000,** *39,* 2504–2507. doi:10.1002/1521-3773(20000717)39:14<2504::AID-ANIE2504>3.3.CO;2-2
250. Ruben, M.; Breuning, E.; Lehn, J.-M.; Ksenofontov, V.; Renz, F.; Gütlich, P.; Vaughan, G. B. M. *Chem.–Eur. J.* **2003,** *9,* 4422–4429. doi:10.1002/chem.200304933
251. Ruben, M.; Breuning, E.; Lehn, J.-M.; Ksenofontov, V.; Gütlich, P.; Vaughan, G. *J. Magn. Magn. Mater.* **2004,** *272–276,* E715–E717. doi:10.1016/j.jmmm.2003.12.1423
252. Ruben, M.; Ziener, U.; Lehn, J.-M.; Ksenofontov, V.; Gütlich, P.; Vaughan, G. B. M. *Chem.–Eur. J.* **2005,** *11,* 94–100. doi:10.1002/chem.200400584
253. Nihei, M.; Ui, M.; Yokota, M.; Han, L.; Maeda, A.; Kishida, H.; Okamoto, H.; Oshio, H. *Angew. Chem.* **2005,** *117,* 6642–6645. doi:10.1002/ange.200502216
254. Nishihara, T.; Nihei, M.; Oshio, H.; Tanaka, K. *J. Phys.: Conf. Ser.* **2009,** *148,* 012033. doi:10.1088/1742-6596/148/1/012033
255. Boldog, I.; Muñoz-Lara, F. J.; Gaspar, A. B.; Muñoz, M. C.; Seredyuk, M.; Real, J. A. *Inorg. Chem.* **2009,** *48,* 3710–3719. doi:10.1021/ic802306r
256. Nihei, M.; Ui, M.; Oshio, H. *Polyhedron* **2009,** *28,* 1718–1721. doi:10.1016/j.poly.2008.10.051
257. Wei, R.-J.; Huo, Q.; Tao, J.; Huang, R.-B.; Zheng, L.-S. *Angew. Chem., Int. Ed.* **2011,** *50,* 8940–8943. doi:10.1002/anie.201103648
258. Wu, D.-Y.; Sato, O.; Einaga, Y.; Duan, C.-Y. *Angew. Chem., Int. Ed.* **2009,** *48,* 1475–1478. doi:10.1002/anie.200804529
259. Shuvaev, K. V.; Dawe, L. N.; Thompson, L. K. *Dalton Trans.* **2010,** *39,* 4768–4776. doi:10.1039/b915595c
260. Zueva, E. M.; Ryabikh, E. R.; Kuznetsov, A. M.; Borshch, S. A. *Inorg. Chem.* **2011,** *50,* 1905–1913. doi:10.1021/ic102387x
261. Borshch, S. A.; Zueva, E. M. *Eur. J. Inorg. Chem.* **2013**. doi:10.1002/ejic.201201074
262. Boča, R.; Šalitroš, I.; Kožišek, J.; Linares, J.; Moncol, J.; Renz, F. *Dalton Trans.* **2010,** *39,* 2198–2200. doi:10.1039/b919120h
263. Duriska, M. B.; Neville, S. M.; Moubaraki, B.; Cashion, J. D.; Halder, G. J.; Chapman, K. W.; Balde, C.; Létard, J. F.; Murray, K. S.; Kepert, C. J.; Batten, S. R. *Angew. Chem., Int. Ed.* **2009,** *48,* 2549–2552. doi:10.1002/anie.200805178
264. Duriska, M. B.; Neville, S. M.; Moubaraki, B.; Murray, K. S.; Balde, C.; Létard, J. F.; Kepert, C. J.; Batten, S. R. *ChemPlusChem* **2012,** *77,* 616–623. doi:10.1002/cplu.201200123
265. Janiak, C. *Dalton Trans.* **2003,** 2781–2804. doi:10.1039/b305705b
266. Naik, A. D.; Dîrtu, M. M.; Railliet, A. P.; Marchand-Brynaert, J.; Garcia, Y. *Polymers (Basel, Switz.)* **2011,** *3,* 1750–1775. doi:10.3390/polym3041750
267. Real, J. A.; Gaspar, A. B.; Niel, V.; Muñoz, M. C. *Coord. Chem. Rev.* **2003,** *236,* 121–141. doi:10.1016/S0010-8545(02)00220-5
268. Garcia, Y.; Niel, V.; Muñoz, M. C.; Real, J. A. Spin Crossover in 1D, 2D, 3D Polymeric Fe(II) Networks. In *Spin Crossover in Transition Metal Compounds I;* Gütlich, P.; Goodwin, H. A., Eds.; *Top. Curr. Chem.*, Vol. 233; Springer-Verlag: Berlin, Heidelberg, 2004; pp 229–257. doi:10.1007/b95408

269. Real, J. A.; Gaspar, A. B.; Muñoz, M. C. *Dalton Trans.* **2005,** 2062–2079. doi:10.1039/b501491c
270. Muñoz, M. C.; Real, J. A. *Coord. Chem. Rev.* **2011,** *255,* 2068–2093. doi:10.1016/j.ccr.2011.02.004
271. Weber, B. *Coord. Chem. Rev.* **2009,** *253,* 2432–2449. doi:10.1016/j.ccr.2008.10.002
272. Fukuya, M.; Ohba, M.; Motoda, K.-I.; Matsumoto, N.; Ôkawa, H.; Maeda, Y. *J. Chem. Soc., Dalton Trans.* **1993,** 3277–3281. doi:10.1039/DT9930003277
273. Imatomi, S.; Kitashima, R.; Hamamastu, T.; Okeda, M.; Ogawa, Y.; Matsumoto, M. *Chem. Lett.* **2006,** *35,* 502–503. doi:10.1246/cl.2006.502
274. Hayami, S.; Hashiguchi, K.; Juhász, G.; Ohba, M.; Okawa, H.; Maeda, Y.; Kato, K.; Osaka, K.; Takata, M.; Inoue, K. *Inorg. Chem.* **2004,** *43,* 4124–4126. doi:10.1021/ic049509b
275. Bhar, K.; Khan, S.; Costa, J. S.; Ribas, J.; Roubeau, O.; Mitra, P.; Ghosh, B. K. *Angew. Chem., Int. Ed.* **2012,** *51,* 2142–2145. doi:10.1002/anie.201107116
276. Kahn, O.; Kröber, J.; Jay, C. *Adv. Mater.* **1992,** *4,* 718–728. doi:10.1002/adma.19920041103
277. Kahn, O.; Jay-Martinez, C. *Science* **1998,** *279,* 44–48. doi:10.1126/science.279.5347.44
278. Kahn, O.; Codjovi, E. *Philos. Trans. R. Soc., A* **1996,** *354,* 359–379. doi:10.1098/rsta.1996.0012
279. Kahn, O.; Codjovi, E.; Garcia, Y.; van Koningsbruggen, P. J.; Lapouyade, R.; Sommier, L. Spin-Transtion Molecular Materials for Display and Data Processing. In *Molecule-Based Magnetic Materials;* Turnbull, M. M.; Sugimoto, T.; Thompson, L. K., Eds.; *ACS Symp. Ser.*, Vol. 644; 1996; pp 298–310.
280. Linares, J.; Codjovi, E.; Garcia, Y. *Sensors* **2012,** *12,* 4479–4492. doi:10.3390/s120404479
281. Coronado, E.; Galán-Mascarós, J. R.; Monrabal-Capilla, M.; García-Martínez, J.; Pardo-Ibáñez, P. *Adv. Mater.* **2007,** *19,* 1359–1361. doi:10.1002/adma.200700559
282. Galán-Mascarós, J. R.; Coronado, E.; Forment-Aliaga, A.; Monrabal-Capilla, M.; Pinilla-Cienfuegos, E.; Ceolin, M. *Inorg. Chem.* **2010,** *49,* 5706–5714. doi:10.1021/ic100751a
283. Mader, D.; Pillet, S.; Carteret, C.; Stébé, M.-J.; Blin, J.-L. *J. Dispersion Sci. Technol.* **2011,** *32,* 1771–1779. doi:10.1080/01932691.2011.616173
284. Roubeau, O. *Chem.–Eur. J.* **2012,** *18,* 15230–15244. doi:10.1002/chem.201201647
285. Tokarev, A.; Salmon, L.; Guari, Y.; Nicolazzi, W.; Molnár, G.; Bousseksou, A. *Chem. Commun.* **2010,** 8011–8013. doi:10.1039/c0cc02606a
286. Titos-Padilla, S.; Herrera, J. M.; Chen, X.-W.; Delgado, J. J.; Colacio, E. *Angew. Chem., Int. Ed.* **2011,** *50,* 3290–3293. doi:10.1002/anie.201007847
287. Faulmann, C.; Chahine, J.; Malfant, I.; de Caro, D.; Cormary, B.; Valade, L. *Dalton Trans.* **2011,** *40,* 2480–2485. doi:10.1039/c0dt01586e
288. Garcia, Y.; Ksenofontov, V.; Mentior, S.; Dîrtu, M. M.; Gieck, C.; Bhatthacharjee, A.; Gütlich, P. *Chem.–Eur. J.* **2008,** *14,* 3745–3758. doi:10.1002/chem.200701305
289. Kröber, J.; Audière, J.-P.; Claude, R.; Codjovi, E.; Kahn, O.; Haasnoot, J. G.; Grolière, F.; Jay, C.; Bousseksou, A.; Linarès, J.; Varret, F.; Gonthier-Vassal, A. *Chem. Mater.* **1994,** *6,* 1404–1412. doi:10.1021/cm00044a044
290. Verelst, M.; Sommier, L.; Lecante, P.; Mosset, A.; Kahn, O. *Chem. Mater.* **1998,** *10,* 980–985. doi:10.1021/cm970375s
291. Grosjean, A.; Négrier, P.; Bordet, P.; Etrillard, C.; Mondieig, D.; Pechev, S.; Lebraud, E.; Létard, J.-F.; Guionneau, P. *Eur. J. Inorg. Chem.* **2013**. doi:10.1002/ejic.201201121
292. Lavrenova, L. G.; Ikorskii, V. N.; Varnek, V. A.; Oglezneva, I. M.; Larionov, S. V. *Koord. Khim.* **1986,** *12,* 207.
293. Dîrtu, M. M.; Neuhausen, C.; Naik, A. D.; Rotaru, A.; Spinu, L.; Garcia, Y. *Inorg. Chem.* **2010,** *49,* 5723–5736. doi:10.1021/ic100667f
294. Liu, X. J.; Moritomo, Y.; Makamura, A.; Hirao, T.; Toyazaki, S.; Kojima, N. *J. Phys. Soc. Jpn.* **2001,** *70,* 2521–2524. doi:10.1143/JPSJ.70.2521
295. Mitsuoka, T.; Nakagawa, M.; Iyoda, T.; Einaga, Y. *J. Nucl. Radiochem. Sci.* **2007,** *8,* 1–3.
296. Nakamoto, A.; Ono, Y.; Kojima, N.; Matsumura, D.; Yokoyama, T.; Liu, X. J.; Moritomo, Y. *Synth. Met.* **2003,** *137,* 1219–1220. doi:10.1016/S0379-6779(02)01058-5
297. Moussa, N. O.; Ostrovskii, D.; Martinez Garcia, V.; Molnár, G.; Tanaka, K.; Gaspar, A. B.; Real, J. A.; Bousseksou, A. *Chem. Phys. Lett.* **2009,** *477,* 156–159. doi:10.1016/j.cplett.2009.06.065
298. van Koningsbruggen, P. J.; Garcia, Y.; Kahn, O.; Kooijman, H.; Spek, A. L.; Haasnoot, J. G.; Moscovici, J.; Provost, K.; Michalowicz, A.; Renz, F.; Gütlich, P. *Inorg. Chem.* **2000,** *39,* 1891–1900. doi:10.1021/ic991118n
299. Schweifer, J.; Weinberger, P.; Mereiter, K.; Boca, M.; Reichl, C.; Wiesinger, G.; Hilscher, G.; van Koningsbruggen, P. J.; Kooijman, H.; Grunert, M.; Linert, W. *Inorg. Chim. Acta* **2002,** *339,* 297–306. doi:10.1016/S0020-1693(02)00934-9
300. Quesada, M.; Prins, F.; Bill, E.; Kooijman, H.; Gamez, P.; Roubeau, O.; Spek, A. L.; Haasnoot, J. G.; Reedijk, J. *Chem.–Eur. J.* **2008,** *14,* 8486–8499. doi:10.1002/chem.200800990
301. Bialońska, A.; Bronisz, R.; Weselski, M. *Inorg. Chem.* **2008,** *47,* 4436–4438. doi:10.1021/ic8002993
302. Quesada, M.; Kooijman, H.; Gamez, P.; Sánchez Costa, J.; van Koningsbruggen, P. J.; Weinberger, P.; Reissner, M.; Spek, A. L.; Haasnoot, J. G.; Reedijk, J. *Dalton Trans.* **2007,** 5434–5440. doi:10.1039/b709460d
303. van Konginsbruggen, P. J. Special Classes of Iron(II) Azole Spin Crossover Compounds. In *Spin Crossover in Transition Metal Compounds I;* Gütlich, P.; Goodwin, H. A., Eds.; *Top. Curr. Chem.*, Vol. 233; Springer: Berlin, Heidelberg, 2004; pp 123–149. doi:10.1007/b13531
304. Galet, A.; Muñoz, M. C.; Real, J. A. *Inorg. Chem.* **2006,** *45,* 4583–4585. doi:10.1021/ic060247i
305. Yang, F.-L.; Li, B.; Hanajima, T.; Einaga, Y.; Huang, R.-B.; Zheng, L.-S.; Tao, J. *Dalton Trans.* **2010,** *39,* 2288–2292. doi:10.1039/b917518k
306. Yang, F.-L.; Tao, J.; Huang, R.-B.; Zheng, L.-S. *Inorg. Chem.* **2011,** *50,* 911–917. doi:10.1021/ic101490a
307. Ross, T. M.; Moubaraki, B.; Batten, S. R.; Murray, K. S. *Dalton Trans.* **2012,** *41,* 2571–2581. doi:10.1039/c1dt10818b
308. Matouzenko, G. S.; Perrin, M.; Le Guennic, B.; Genre, C.; Molnár, G.; Bousseksou, A.; Borshch, S. A. *Dalton Trans.* **2007,** 934–942. doi:10.1039/b615410g
309. Matouzenko, G. S.; Molnar, G.; Bréfuel, N.; Perrin, M.; Bousseksou, A.; Borshch, S. A. *Chem. Mater.* **2003,** *15,* 550–556. doi:10.1021/cm021307v
310. Genre, C.; Matouzenko, G. S.; Jeanneau, E.; Luneau, D. *New J. Chem.* **2006,** *30,* 1669–1674. doi:10.1039/b608679a

311. Neville, S. M.; Leita, B. A.; Offermann, D. A.; Duriska, M. B.; Moubaraki, B.; Chapman, K. W.; Halder, G. J.; Murray, K. S. *Eur. J. Inorg. Chem.* **2007,** 1073–1085. doi:10.1002/ejic.200601034
312. Ross, T. M.; Moubaraki, B.; Turner, D. R.; Halder, G. J.; Chastanet, G.; Neville, S. M.; Cashion, J. D.; Létard, J.-F.; Batten, S. R.; Murray, K. S. *Eur. J. Inorg. Chem.* **2011,** 1395–1417. doi:10.1002/ejic.201000876
313. Neville, S. M.; Leita, B. A.; Halder, G. J.; Kepert, C. J.; Moubaraki, B.; Létard, J.-F.; Murray, K. S. *Chem.–Eur. J.* **2008,** *14,* 10123–10133. doi:10.1002/chem.200800886
314. Białońska, A.; Bronisz, R.; Darowska, K.; Drabent, K.; Kusz, J.; Siczek, M.; Weselski, M.; Zubko, M.; Ozarowski, A. *Inorg. Chem.* **2010,** *49,* 11267–11269. doi:10.1021/ic102040y
315. Genre, C.; Jeanneau, E.; Bousseksou, A.; Luneau, D.; Borshch, S. A.; Matouzenko, G. S. *Chem.–Eur. J.* **2008,** *14,* 697–705. doi:10.1002/chem.200700998
316. Dupouy, G.; Triki, S.; Marchivie, M.; Cosquer, N.; Gómez-García, C. J.; Pillet, S.; Bendeif, El-E.; Lecomte, C.; Asthana, S.; Létard, J.-F. *Inorg. Chem.* **2010,** *49,* 9358–9368. doi:10.1021/ic101038z
317. Weber, B.; Tandon, R.; Himsl, D. *Z. Anorg. Allg. Chem.* **2007,** *633,* 1159–1162. doi:10.1002/zaac.200700092
318. Weber, B.; Kaps, E. S.; Desplanches, C.; Létard, J.-F. *Eur. J. Inorg. Chem.* **2008,** 2963–2966. doi:10.1002/ejic.200800391
319. Bauer, W.; Pfaffeneder, T.; Achterhold, K.; Weber, B. *Eur. J. Inorg. Chem.* **2011,** 3183–3192. doi:10.1002/ejic.201100224
320. Bauer, W.; Scherer, W.; Altmannshofer, S.; Weber, B. *Eur. J. Inorg. Chem.* **2011,** 2803–2818. doi:10.1002/ejic.201001363
321. Pfaffeneder, T. M.; Thallmair, S.; Bauer, W.; Weber, B. *New J. Chem.* **2011,** *35,* 691–700. doi:10.1039/c0nj00750a
322. Bauer, W.; Dîrtu, M. M.; Garcia, Y.; Weber, B. *CrystEngComm* **2012,** *14,* 1223–1231. doi:10.1039/c2ce06253d
323. Bauer, W.; Schlamp, S.; Weber, B. *Chem. Commun.* **2012,** *48,* 10222–10224. doi:10.1039/c2cc35109a
324. Nowak, R.; Bauer, W.; Ossiander, T.; Weber, B. *Eur. J. Inorg. Chem.* **2013**. doi:10.1002/ejic.20120105
325. Vreugdenhil, W.; van Diemen, J. H.; de Graaff, R. A. G.; Haasnoot, J. G.; Reedijk, J.; van der Kraan, A. M.; Kahn, O.; Zarembowitch, J. *Polyhedron* **1990,** *9,* 2971–2979. doi:10.1016/S0277-5387(00)84209-6
326. Ozarowski, A.; Shunzhong, Y.; McGarvey, B. R.; Mislankar, A.; Drake, J. E. *Inorg. Chem.* **1991,** *30,* 3167–3174. doi:10.1021/ic00016a013
327. Chuang, Y.-C.; Liu, C.-T.; Sheu, C.-F.; Ho, W.-L.; Lee, G.-H.; Wang, C.-C.; Wang, Y. *Inorg. Chem.* **2012,** *51,* 4663–4671. doi:10.1021/ic202626c
328. Białońska, A.; Bronisz, R. *Inorg. Chem.* **2010,** *49,* 4534–4542. doi:10.1021/ic9024603
329. Quesada, M.; Prins, F.; Roubeau, O.; Gamez, P.; Teat, S. J.; van Koningsbruggen, P. J.; Haasnoot, J. G.; Reedijk, J. *Inorg. Chim. Acta* **2007,** *360,* 3787–3796. doi:10.1016/j.ica.2006.12.010
330. Garcia, Y.; Bravic, G.; Gieck, C.; Chasseau, D.; Tremel, W.; Gütlich, P. *Inorg. Chem.* **2005,** *44,* 9723–9730. doi:10.1021/ic050971l
331. Real, J. A.; Andrés, E.; Muñoz, M. C.; Julve, M.; Granier, T.; Bousseksou, A.; Varret, F. *Science* **1995,** *268,* 265–267. doi:10.1126/science.268.5208.265
332. Halder, G. J.; Kepert, C. J.; Moubaraki, B.; Murray, K. S.; Cashion, J. D. *Science* **2002,** *298,* 1762–1765. doi:10.1126/science.1075948
333. Neville, S. M.; Halder, G. J.; Chapman, K. W.; Duriska, M. B.; Southon, P. D.; Cashion, J. D.; Lètard, J.-F.; Moubaraki, B.; Murray, K. S.; Kepert, C. J. *J. Am. Chem. Soc.* **2008,** *130,* 2869–2876. doi:10.1021/ja077958f
334. Moliner, N.; Muñoz, M. C.; Létard, S.; Solans, X.; Menendez, N.; Goujon, A.; Varret, F.; Real, J. A. *Inorg. Chem.* **2000,** *39,* 5390–5393. doi:10.1021/ic0005588
335. Bronisz, R.; Ciunik, Z.; Drabent, K.; Rudolf, M. F. In *Conference Proceedings;* Ortalli, I., Ed.; ICAME-95, Vol. 50; SIF: Bologna, Italy, 1996; pp 15 ff.
336. Bronisz, R. Ph.D. Thesis, University of Wroclaw, Wroclaw, Poland, 1999.
337. Białońska, A.; Bronisz, R.; Rudolf, M. F.; Weselski, M. *Inorg. Chem.* **2012,** *51,* 237–245. doi:10.1021/ic201535x
338. Boland, Y.; Herstens, P.; Marchand-Brynaert, J.; Garcia, Y. *Synthesis* **2006,** 1504–1512. doi:10.1055/s-2006-926439
339. Bronisz, R. *Inorg. Chem.* **2005,** *44,* 4463–4465. doi:10.1021/ic050449z
340. Kusz, J.; Bronisz, R.; Zubko, M.; Bednarek, G. *Chem.–Eur. J.* **2011,** *17,* 6807–6820. doi:10.1002/chem.201100394
341. Chakraborty, P.; Bronisz, R.; Besnard, C.; Guénée, L.; Pattison, P.; Hauser, A. *J. Am. Chem. Soc.* **2012,** *134,* 4049–4052. doi:10.1021/ja211897t
342. Krivokapic, I.; Enachescu, C.; Bronisz, R.; Hauser, A. *Chem. Phys. Lett.* **2008,** *455,* 192–196. doi:10.1016/j.cplett.2008.02.088
343. Krivokapic, I.; Enachescu, C.; Bronisz, R.; Hauser, A. *Inorg. Chim. Acta* **2008,** *361,* 3616–3622. doi:10.1016/j.ica.2008.03.064
344. Chong, C.; Slimani, A.; Varret, F.; Boukheddaden, K.; Collet, E.; Ameline, J.-C.; Bronisz, R.; Hauser, A. *Chem. Phys. Lett.* **2011,** *504,* 29–33. doi:10.1016/j.cplett.2011.01.041
345. Slimani, A. Doctoral Thesis, University of Versailles Saint Quentin en Yvelines, France, 2012.
346. Bao, X.; Guo, P.-H.; Liu, W.; Tucek, J.; Zhang, W.-X.; Leng, J.-D.; Chen, X.-M.; Gural'skiy, I.; Salmon, L.; Bousseksou, A.; Tong, M.-L. *Chem. Sci.* **2012,** *3,* 1629–1633. doi:10.1039/c2sc00924b
347. Garcia, Y.; Kahn, O.; Rabardel, L.; Chansou, B.; Salmon, L.; Tuchagues, J.-P. *Inorg. Chem.* **1999,** *38,* 4663–4670. doi:10.1021/ic990511q
348. Bronisz, R. *Inorg. Chem.* **2007,** *46,* 6733–6739. doi:10.1021/ic070223r
349. van Koningsbruggen, P. J.; Garcia, Y.; Kooijman, H.; Spek, A. L.; Haasnoot, J. G.; Kahn, O.; Linares, J.; Codjovi, E.; Varret, F. *J. Chem. Soc., Dalton Trans.* **2001,** 466–471. doi:10.1039/B008073J
350. Grunert, C. M.; Schweifer, J.; Weinberger, P.; Linert, W.; Mereiter, K.; Hilscher, G.; Müller, M.; Wiesinger, G.; van Koningsbruggen, P. J. *Inorg. Chem.* **2004,** *43,* 155–165. doi:10.1021/ic034452z
351. Bartel, M.; Absmeier, A.; Jameson, G. N. L.; Werner, F.; Kato, K.; Takata, M.; Boca, R.; Hasegawa, M.; Mereiter, K.; Caneschi, A.; Linert, W. *Inorg. Chem.* **2007,** *46,* 4220–4229. doi:10.1021/ic070173q
352. Liu, W.-T.; Li, J.-Y.; Ni, Z.-P.; Bao, X.; Ou, Y.-C.; Leng, J.-D.; Liu, J.-L.; Tong, M.-L. *Cryst. Growth Des.* **2012,** *12,* 1482–1488. doi:10.1021/cg201569m
353. Yan, Z.; Li, M.; Gao, H.-L.; Huang, X.-C.; Li, D. *Chem. Commun.* **2012,** *48,* 3960–3962. doi:10.1039/c2cc18140a
354. Li, L.; Clarkson, G. J.; Evans, D. J.; Lees, M. R.; Turner, S. S.; Scott, P. *Chem. Commun.* **2011,** *47,* 12646–12648. doi:10.1039/c1cc15574a
355. Naik, A. D.; Marchand-Brynaert, J.; Garcia, Y. *Synthesis* **2008,** 149–154. doi:10.1055/s-2007-983896

356. Ozin, G. A.; Arsenault, A. C. *Nanochemistry: A Chemical Approach to Nanomaterials;* The Royal Society of Chemistry: Cambridge, 2005.
357. Burda, C.; Chen, X.; Narayanan, R.; El-Sayed, M. A. *Chem. Rev.* **2005,** *105,* 1025–1102. doi:10.1021/cr030063a
358. Gaspar, A. B.; Seredyuk, M.; Gütlich, P. *J. Mol. Struct.* **2009,** *924–926,* 9–19. doi:10.1016/j.molstruc.2008.11.021
359. Boldog, I.; Gaspar, A. B.; Martínez, V.; Pardo-Ibañez, P.; Ksenofontov, V.; Bhattacharjee, A.; Gütlich, P.; Real, J. A. *Angew. Chem., Int. Ed.* **2008,** *47,* 6433–6437. doi:10.1002/anie.200801673
360. Volatron, F.; Catala, L.; Rivière, E.; Gloter, A.; Stéphan, O.; Mallah, T. *Inorg. Chem.* **2008,** *47,* 6584–6586. doi:10.1021/ic800803w
361. Cobo, S.; Molnár, G.; Real, J. A.; Bousseksou, A. *Angew. Chem., Int. Ed.* **2006,** *45,* 5786–5789. doi:10.1002/anie.200601885
362. Molnár, G.; Cobo, S.; Real, J. A.; Carcenac, F.; Daran, E.; Vieu, C.; Bousseksou, A. *Adv. Mater.* **2007,** *19,* 2163–2167. doi:10.1002/adma.200700448
363. Niel, V.; Martínez-Agudo, J. M.; Muñoz, M. C.; Gaspar, A. B.; Real, J. A. *Inorg. Chem.* **2001,** *40,* 3838–3839. doi:10.1021/ic010259y
364. Larionova, J.; Salmon, L.; Guari, Y.; Tokarev, A.; Molvinger, K.; Molnar, G.; Bousseksou, A. *Angew. Chem., Int. Ed.* **2008,** *47,* 8236–8240. doi:10.1002/anie.200802906
365. Martínez, V.; Gaspar, A. B.; Muñoz, M. C.; Bukin, G. V.; Levchenko, G.; Real, J. A. *Chem.–Eur. J.* **2009,** *15,* 10960–10971. doi:10.1002/chem.200901391
366. Martínez, V.; Boldog, I.; Gaspar, A. B.; Ksenofontov, V.; Bhattacharjee, A.; Gütlich, P.; Real, J. A. *Chem. Mater.* **2010,** *22,* 4271–4281. doi:10.1021/cm101022u
367. Kawamoto, T.; Abe, S. *Chem. Commun.* **2005,** 3933–3935. doi:10.1039/b506643c
368. Spiering, H. Elastic Interaction in Spin Crossover Compounds. In *Spin Crossover in Transition Metal Compounds III;* Gütlich, P.; Goodwin, H. A., Eds.; *Top. Curr. Chem.*, Vol. 235; Springer-Verlag: Berlin, Heidelberg, 2004; pp 171–196.
369. Tayagaki, T.; Galet, A.; Molnár, G.; Muñoz, M. C.; Zwick, A.; Tanaka, K.; Real, J. A.; Bousseksou, A. *J. Phys. Chem. B* **2005,** *109,* 14859–14867. doi:10.1021/jp0521611
370. Molnár, G.; Niel, V.; Real, J. A.; Dubrovinsky, L.; Bousseksou, A.; McGarvey, J. J. *J. Phys. Chem. B* **2003,** *107,* 3149–3155. doi:10.1021/jp027550z
371. Létard, J.-F.; Nguyen, O.; Daro, N. Nanoparticles of a spin transition compound. WO Patent WO2007065996, June 14, 2007; p 31.
372. Forestier, T.; Mornet, S.; Daro, N.; Nishihara, T.; Mouri, S.; Tanaka, K.; Fouché, O.; Freysz, E.; Létard, J.-F. *Chem. Commun.* **2008,** 4327–4329. doi:10.1039/B806347H
373. Forestier, T.; Kaiba, A.; Pechev, S.; Denux, D.; Guionneau, P.; Etrillard, C.; Daro, N.; Freysz, E.; Létard, J.-F. *Chem.–Eur. J.* **2009,** *15,* 6122–6130. doi:10.1002/chem.200900297
374. Armand, F.; Badoux, C.; Bonville, P.; Ruaudel-Teixier, A.; Kahn, O. *Langmuir* **1995,** *11,* 3467–3472. doi:10.1021/la00009a032
375. Seredyuk, M.; Gaspar, A. B.; Ksenofontov, V.; Reiman, S.; Galyametdinov, Y.; Haase, W.; Rentschler, E.; Gütlich, P. *Chem. Mater.* **2006,** *18,* 2513–2519. doi:10.1021/cm052632w
376. Alam, M. S.; Stocker, M.; Gieb, K.; Müller, P.; Haryono, M.; Student, K.; Grohmann, A. *Angew. Chem., Int. Ed.* **2010,** *49,* 1159–1163. doi:10.1002/anie.200905062
377. Naik, A. D.; Dîrtu, M. M.; Garcia, Y. *J. Phys.: Conf. Ser.* **2010,** *217,* 012032. doi:10.1088/1742-6596/217/1/012032
378. Shi, S.; Schmerber, G.; Arabski, J.; Beaufrand, J. B.; Kim, D. J.; Boukari, S.; Bowen, M.; Kemp, N. T.; Viart, N.; Rogez, G.; Beaurepaire, E.; Aubriet, H.; Petersen, J.; Becker, C.; Ruch, D. *Appl. Phys. Lett.* **2009,** *95,* 043303. doi:10.1063/1.3192355
379. Naggert, H.; Bannwarth, A.; Chemnitz, S.; von Hofe, T.; Quandt, E.; Tuczek, F. *Dalton Trans.* **2011,** *40,* 6364–6366. doi:10.1039/c1dt10651a
380. Gopakumar, T. G.; Matino, F.; Naggert, H.; Bannwarth, A.; Tuczek, F.; Berndt, R. *Angew. Chem., Int. Ed.* **2012,** *51,* 6262–6266. doi:10.1002/anie.201201203
381. Palamarciuc, T.; Oberg, J. C.; El Hallak, F.; Hirjibehedin, C. F.; Serri, M.; Heutz, S.; Létard, J.-F.; Rosa, P. *J. Mater. Chem.* **2012,** *22,* 9690–9695. doi:10.1039/c2jm15094h
382. Agustí, G.; Cobo, S.; Gaspar, A. B.; Molnár, G.; Moussa, N. O.; Szilágyi, P. A.; Palfi, V.; Vieu, C.; Muñoz, M. C.; Real, J. A.; Bousseksou, A. *Chem. Mater.* **2008,** *20,* 6721–6732. doi:10.1021/cm8019878
383. Bartual-Murgui, C.; Akou, A.; Salmon, L.; Molnár, G.; Thibault, C.; Real, J. A.; Bousseksou, A. *Small* **2011,** *7,* 3385–3391. doi:10.1002/smll.201101089
384. Naik, A. D.; Stappers, L.; Snauwaert, J.; Fransaer, J.; Garcia, Y. *Small* **2010,** *6,* 2842–2846. doi:10.1002/smll.201001527
385. Naik, A. D.; Garcia, Y. *Hyperfine Interact.* **2012,** *206,* 7–11. doi:10.1007/s10751-011-0436-z
386. Serrano, J. L., Ed. *Metallomesogens;* VCH: Weinheim, Germany, 1996.
387. Galyametdinov, Y.; Ksenofontov, V.; Prosvirin, A.; Ovchinnikov, I.; Ivanova, G.; Gütlich, P.; Haase, W. *Angew. Chem., Int. Ed.* **2001,** *40,* 4269–4271. doi:10.1002/1521-3773(20011119)40:22<4269::AID-ANIE4269>3.0.CO;2-8
388. Hayami, S.; Danjobara, K.; Inoue, K.; Ogawa, T.; Matsumoto, N.; Maeda, Y. *Adv. Mater.* **2004,** *16,* 869–872. doi:10.1002/adma.200306632
389. Hayami, S.; Motokawa, N.; Shuto, A.; Masuhara, N.; Someya, T.; Ogawa, Y.; Inoue, K.; Maeda, Y. *Inorg. Chem.* **2007,** *46,* 1789–1794. doi:10.1021/ic061646g
390. Hayami, S.; Moriyama, R.; Shuto, A.; Maeda, Y.; Ohta, K.; Inoue, K. *Inorg. Chem.* **2007,** *46,* 7692–7694. doi:10.1021/ic700754s
391. Gaspar, A. B.; Seredyuk, M.; Gütlich, P. *Coord. Chem. Rev.* **2009,** *253,* 2399–2413. doi:10.1016/j.ccr.2008.11.016
392. Seredyuk, M.; Gaspar, A. B.; Ksenofontov, V.; Galyametdinov, Y.; Verdaguer, M.; Villain, F.; Gütlich, P. *Inorg. Chem.* **2008,** *47,* 10232–10245. doi:10.1021/ic8006266
393. Seredyuk, M.; Gaspar, A. B.; Ksenofontov, V.; Galyametdinov, Y.; Kusz, J.; Gütlich, P. *Adv. Funct. Mater.* **2008,** *18,* 2089–2101. doi:10.1002/adfm.200800049
394. Seredyuk, M.; Gaspar, A. B.; Ksenofontov, V.; Galyametdinov, Y.; Kusz, J.; Gütlich, P. *J. Am. Chem. Soc.* **2008,** *130,* 1431–1439. doi:10.1021/ja077265z
395. Fujigaya, T.; Jiang, D. L.; Aida, T. *J. Am. Chem. Soc.* **2003,** *125,* 14690–14691. doi:10.1021/ja038088e
396. Roubeau, O.; Colin, A.; Schmitt, V.; Clérac, R. *Angew. Chem., Int. Ed.* **2004,** *43,* 3283–3286. doi:10.1002/anie.200454050
397. Fujigaya, T.; Jiang, D.-L.; Aida, T. *Chem.–Asian J.* **2007,** *2,* 106–113. doi:10.1002/asia.200600371
398. Rubio, M.; López, D. *Eur. Polym. J.* **2009,** *45,* 3339–3346. doi:10.1016/j.eurpolymj.2009.10.013
399. Grondin, P.; Roubeau, O.; Castro, M.; Saadaoui, H.; Colin, A.; Clérac, R. *Langmuir* **2010,** *26,* 5184–5195. doi:10.1021/la903653d

400. Kitagawa, S.; Kitaura, R.; Noro, S. *Angew. Chem., Int. Ed.* **2004,** *43,* 2334–2375. doi:10.1002/anie.200300610
401. Maspoch, D.; Ruiz-Molina, D.; Veciana, J. *Chem. Soc. Rev.* **2007,** *36,* 770–818. doi:10.1039/b501600m
402. Kitagawa, S.; Matsuda, R. *Coord. Chem. Rev.* **2007,** *251,* 2490–2509. doi:10.1016/j.ccr.2007.07.009
403. Férey, G. *Chem. Soc. Rev.* **2008,** *37,* 191–214. doi:10.1039/b618320b
404. Czaja, A. U.; Trukhan, N.; Müller, U. *Chem. Soc. Rev.* **2009,** *38,* 1284–1293. doi:10.1039/b804680h
405. Horike, S.; Shimomura, S.; Kitagawa, S. *Nat. Chem.* **2009,** *1,* 695–704. doi:10.1038/nchem.444
406. Lin, W.; Rieter, W. J.; Taylor, K. M. L. *Angew. Chem., Int. Ed.* **2009,** *48,* 650–658. doi:10.1002/anie.200803387
407. Jiang, H. L.; Xu, Q. *Chem. Commun.* **2011,** *47,* 3351–3370. doi:10.1039/c0cc05419d
408. Cundy, C. S.; Cox, P. A. *Chem. Rev.* **2003,** *103,* 663–702. doi:10.1021/cr020060i
409. Hu, Y. H..; Zhang, L. *Adv. Mater.* **2010,** *22,* E117–E130. doi:10.1002/adma.200902096
410. Yang, S.; Lin, X.; Blake, A. J.; Walker, G. S.; Hubberstey, P. N.; Champness, N. R.; Schröder, M. *Nat. Chem.* **2009,** *1,* 487–493. doi:10.1038/nchem.333
411. Chen, B.; Liang, C.; Yang, J.; Conteras, D. S.; Clancy, Y. L.; Lobkovsky, E. B.; Yaghi, O. M.; Dai, S. *Angew. Chem., Int. Ed.* **2006,** *45,* 1390–1393. doi:10.1002/anie.200502844
412. Couck, S.; Denayer, J. F. M.; Baron, G. V.; Rémy, T.; Gascon, J.; Kapteijn, F. *J. Am. Chem. Soc.* **2009,** *131,* 6326–6327. doi:10.1021/ja900555r
413. McManus, G. J.; Perry, J. J., IV; Perry, M.; Wagner, B. D.; Zaworotko, M. J. *J. Am. Chem. Soc.* **2007,** *129,* 9094–9101. doi:10.1021/ja071271d
414. Tonigold, M.; Lu, Y.; Bredenkötter, B.; Rieger, B.; Bahnmüller, S.; Hitzbleck, J.; Langstein, G.; Volkmer, D. *Angew. Chem., Int. Ed.* **2009,** *48,* 7546–7550. doi:10.1002/anie.200901241
415. Corma, A.; García, H.; Llabrés i Xamena, F. X. *Chem. Rev.* **2010,** *110,* 4606–4655. doi:10.1021/cr9003924
416. Farrusseng, D.; Aguado, S.; Pinel, C. *Angew. Chem., Int. Ed.* **2009,** *48,* 7502–7513. doi:10.1002/anie.200806063
417. Dechambenoit, P.; Long, J. R. *Chem. Soc. Rev.* **2011,** *40,* 3249–3265. doi:10.1039/c0cs00167h
418. Rocha, J.; Carlos, L. D.; Almeida Paz, F. A.; Ananias, D. *Chem. Soc. Rev.* **2011,** *40,* 926–940. doi:10.1039/c0cs00130a
419. Avendano, C.; Zhang, Z.; Ota, A.; Zhao, H.; Dunbar, K. R. *Angew. Chem., Int. Ed.* **2011,** *50,* 6543–6547. doi:10.1002/anie.201100372
420. Shimomura, S.; Kitagawa, S. *J. Mater. Chem.* **2011,** *21,* 5537–5546. doi:10.1039/c1jm10208g
421. Shigematsu, A.; Yamada, T.; Kitagawa, H. *J. Am. Chem. Soc.* **2011,** *133,* 2034–2036. doi:10.1021/ja109810w
422. Ohba, M.; Yoneda, K.; Agustí, G.; Muñoz, M. C.; Gaspar, A. B.; Real, J. A.; Yamasaki, M.; Ando, H.; Nakao, Y.; Sakaki, S.; Kitagawa, S. *Angew. Chem., Int. Ed.* **2009,** *48,* 4767–4771. doi:10.1002/anie.200806039
423. Southon, P. D.; Liu, L.; Fellows, E. A.; Price, D. J.; Halder, G. J.; Chapman, K. W.; Moubaraki, B.; Murray, K. S.; Létard, J.-F.; Kepert, C. J. *J. Am. Chem. Soc.* **2009,** *131,* 10998–11009. doi:10.1021/ja902187d
424. Agustí, G.; Ohtani, R.; Yoneda, K.; Gaspar, A. B.; Ohba, M.; Sánchez-Royo, J. F.; Muñoz, M. C.; Kitagawa, S.; Real, J. A. *Angew. Chem., Int. Ed.* **2009,** *48,* 8944–8947. doi:10.1002/anie.200904379
425. Ohtani, R.; Yoneda, K.; Furukawa, S.; Horike, N.; Kitagawa, S.; Gaspar, A. B.; Muñoz, M. C.; Real, J. A.; Ohba, M. *J. Am. Chem. Soc.* **2011,** *133,* 8600–8605. doi:10.1021/ja111674c
426. Bartual-Murgui, C.; Ortega-Villar, N. A.; Shepherd, H. J.; Muñoz, M. C.; Salmon, L.; Molnár, G.; Bousseksou, A.; Real, J. A. *J. Mater. Chem.* **2011,** *21,* 7217–7222. doi:10.1039/c0jm04387g
427. Muñoz-Lara, F. J.; Gaspar, A. B.; Muñoz, M. C.; Arai, M.; Kitagawa, S.; Ohba, M.; Real, J. A. *Chem.–Eur. J.* **2012,** *18,* 8013–8018. doi:10.1002/chem.201200377
428. Muñoz Lara, F. J.; Gaspar, A. B.; Aravena, D.; Ruiz, E.; Muñoz, M. C.; Ohba, M.; Ohtani, R.; Kitagawa, S.; Real, J. A. *Chem. Commun.* **2012,** *48,* 4686–4688. doi:10.1039/C2CC31048A
429. Akamatu, H.; Inokuchi, H.; Matsunaga, Y. *Nature* **1954,** *173,* 168–169. doi:10.1038/173168a0
430. Dorbes, S.; Valade, L.; Real, J. A.; Faulmann, C. *Chem. Commun.* **2005,** 69–71. doi:10.1039/b412182a
431. Takahashi, K.; Cui, H.-B.; Okano, Y.; Kobayashi, H.; Einaga, Y.; Sato, O. *Inorg. Chem.* **2006,** *45,* 5739–5741. doi:10.1021/ic060852l
432. Takahashi, K.; Cui, H.-B.; Okano, Y.; Kobayashi, H.; Mori, H.; Tajima, H.; Einaga, Y.; Sato, O. *J. Am. Chem. Soc.* **2008,** *130,* 6688–6689. doi:10.1021/ja801585r
433. Nihei, M.; Nobukazu, T.; Nishikawa, H.; Oshio, H. *Dalton Trans.* **2011,** *40,* 2154–2156. doi:10.1039/c0dt01092h
434. Djukic, B.; Lemaire, M. T. *Inorg. Chem.* **2009,** *48,* 10489–10491. doi:10.1021/ic9015542
435. Engeser, M.; Fabbrizzi, L.; Licchelli, M.; Sacchi, D. *Chem. Commun.* **1999,** 1191–1192. doi:10.1039/a901931f
436. Hasegawa, M.; Renz, F.; Hara, T.; Kichuki, Y.; Fukada, Y.; Okubo, J.; Hoshi, T.; Linert, W. *Chem. Phys.* **2002,** *277,* 21–30. doi:10.1016/S0301-0104(01)00706-6
437. Edder, C.; Piguet, C.; Bünzli, J.-C. G.; Hopfgartner, G. *Chem.–Eur. J.* **2001,** *7,* 3014–3024. doi:10.1002/1521-3765(20010716)7:14<3014::AID-CHEM3014>3.0.CO;2-D
438. Matsukizono, H.; Kuroiwa, K.; Kimizuka, N. *Chem. Lett.* **2008,** *37,* 446–447. doi:10.1246/cl.2008.446
439. González-Prieto, R.; Fleury, B.; Schramm, F.; Zoppellaro, G.; Chandrasekar, R.; Fuhr, O.; Lebedkin, S.; Kappes, M.; Ruben, M. *Dalton Trans.* **2011,** *40,* 7564–7570. doi:10.1039/c1dt10420a
440. Salmon, L.; Molnár, G.; Zitouni, D.; Quintero, C.; Bergaud, C.; Micheau, J.-C.; Bousseksou, A. *J. Mater. Chem.* **2010,** *20,* 5499–5503. doi:10.1039/c0jm00631a
441. Robert, F.; Naik, A. D.; Hidara, F.; Tinant, B.; Robiette, R.; Wouters, J.; Garcia, Y. *Eur. J. Org. Chem.* **2010,** 621–637. doi:10.1002/ejoc.200901175

License and Terms